

4. SITE 645¹

Shipboard Scientific Party²

HOLE 645A

Date occupied: 4 September 1985, 0400 AST
Date departed: 5 September 1985, 1625 AST
Time on hole: 1 day, 12.25 hr
Position: 70°27.43'N, 64°39.26'W
Water depth (sea level; corrected m, echo-sounding): 2005.8
Water depth (rig floor; corrected m, echo-sounding): 2016.3
Bottom felt (rig floor, m; drill-pipe measurement): 2017.6
Distance between rig floor and sea level (m): 10.5
Total depth (rig floor; m): 2022.6
Penetration (m): 4.94
Number of cores (including cores with no recovery): 1 (APC)
Total length of cored section (m): 4.94
Total core recovered (m): 4.94
Core recovery (%): 100

Oldest sediment cored:

Depth sub-bottom (m): 4.94
Nature: silty mud to muddy sand
Age: late Pleistocene
Measured velocity (km/s): 1.5

HOLE 645B

Date occupied: 5 September 1985, 1625 AST
Date departed: 10 September 1985, 0425 AST
Time on hole: 4 days, 12 hr
Position: 70°27.43'N, 64°39.26'W
Water depth (sea level; corrected m, echo-sounding): 2001
Water depth (rig floor; corrected m, echo-sounding): 2011.5
Bottom felt (rig floor, m; drill-pipe measurement): 2018.7
Distance between rig floor and sea level (m): 10.5
Total depth (rig floor, m): 2317.6
Penetration (m): 298.9
Number of cores (including cores with no recovery): 32 (XCB)
Total length of cored section (m): 298.9
Total core recovered (m): 171.9
Core recovery (%): 57.5
Oldest sediment cored:
Depth sub-bottom (m): 298.9
Nature: pebbly, silty to sandy mud, olive green to gray
Age: Pliocene (dinoflagellates, paleomagnetism)
Measured velocity (km/s): 1.7

HOLE 645C

Date occupied: 10 September 1985, 0425 AST
Date departed: 10 September 1985, 0900 AST
Time on hole: 4.4 hr
Position: 70°27.43'N, 64°39.26'W
Water depth (sea level; corrected m, echo-sounding): 2001
Water depth (rig floor; corrected m, echo-sounding): 2011.5
Bottom felt (rig floor, m; drill-pipe measurement): 2018.2
Distance between rig floor and sea level (m): 10.5
Total depth (rig floor, m): 2041.5
Penetration (m): 23.3
Number of cores (including cores with no recovery): 3 (APC)
Total length of cored section (m): 23.3
Total core recovered (m): 10.9
Core recovery (%): 46.8
Oldest sediment cored:
Depth sub-bottom (m): 23.3
Nature: pebbly, sandy mud and muddy sand, olive green, gray
Age: late Pleistocene
Measured velocity (km/s): 1.5

¹ Srivastava, S. P., Arthur, M., Clement, B., et al., 1987. *Proc., Init. Repts. (Pt. A), ODP*, 105.

² Ali Aksu, Earth Sciences Department, Memorial University of Newfoundland, St. John's, Newfoundland A1B 3X5, Canada; Michael Arthur (Co-Chief Scientist), Graduate School of Oceanography, University of Rhode Island, Narragansett, RI 02882; Jack Baldauf, Ocean Drilling Program, 1000 Discovery Drive, College Station, TX 77840; Gerhard Bohrmann, Geologisch-Palaeontologisches Institut und Museum der CAU, Olshausenstr. 40, 2300 Kiel, Federal Republic of Germany; William Busch, Department of Geology and Geophysics, University of New Orleans, New Orleans, LA 70148; Tommy Cederberg, University of Copenhagen, Geological Institute, Oester Voldgade 10, DK-1350, Copenhagen, Denmark; Bradford Clement (Co-Chief Scientist), Ocean Drilling Program, 1000 Discovery Drive, College Station, TX 77840; Michel Cremer, Département de Géologie et Océanographie, UA 197, Université de Bordeaux I, Avenue des Facultés, 33405 Talence Cedex, France; Kathleen Dadey, Graduate School of Oceanography, University of Rhode Island, Narragansett, RI 02882; Anne De Vernal, GEOTOP, Sciences de la Terre, Université du Québec à Montréal, L.P. 8888, Succ "A," Montréal, Québec H3C 3P8, Canada; John Firth, Department of Geology, Florida State University, Tallahassee, FL 32306; Frank Hall, Graduate School of Oceanography, University of Rhode Island, Narragansett, RI 02882; Martin Head, Department of Geology, University of Toronto, Toronto M5A 1A1, Canada; Richard Hiscott, Earth Sciences Department, Memorial University, St. John's, Newfoundland A1B 3X5, Canada; Rich Jarrard, Lamont-Doherty Geological Observatory, Palisades, NY 10964; Michael Kaminski, WHOI/MIT Joint Program in Oceanography, Woods Hole Oceanographic Institution, Clark 1, Woods Hole, MA 02543; David Lazarus, Woods Hole Oceanographic Institution, Department of Geology and Geophysics, Woods Hole, MA 02543; Anne-Lise Monjanel, Université de Bretagne Occidentale, G.I.S. Océanologie et Géodynamique, 6, Av. Victor le Gorgeu, 29283 Brest Cedex, France; Ole Bjorslev Nielsen, Department of Geology, Aarhus University, DK-8000 Aarhus C, Denmark; Surat P. Srivastava (Co-Chief Scientist), Atlantic Geoscience Centre, Geological Survey of Canada, P.O. Box 1006, Dartmouth, Nova Scotia B2Y A42, Canada; Ruediger Stein, Institute of Petroleum and Organic Geochemistry, KFA Julich, P.O. Box 1913, 5170 Julich, Federal Republic of Germany (current address: Institut fuer Geowissenschaften und Lithosphaeren Forschung, Universitaet Giessen, Senckenbergstr. 3, 6300 Giessen, Federal Republic of Germany); François Thiebault, Lab. Dynamique Sédimentaire et Structurale, UA 713 UER Sciences de la Terre, Université de Lille I, 59655 Villeneuve D'Ascq Cedex, France; James Zachos, Graduate School of Oceanography, University of Rhode Island, Narragansett, RI 02882; Herman Zimmerman, Department of Geology, Union College, Schenectady, NY 12308 (current address: Division of Polar Programs, National Science Foundation, Washington, D.C. 20550).

HOLE 645D

Date occupied: 10 September 1985, 1500 AST
Date departed: 14 September 1985, 0000 AST
Time on hole: 3 days, 9 hr
Position: 70°27.43' N, 64°39.37' W
Water depth (sea level; corrected m, echo-sounding): 2005.8
Water depth (rig floor; corrected m, echo-sounding): 2016.3
Bottom felt (rig floor, m; drill-pipe measurement): 2018
Distance between rig floor and sea level (m): 10.5
Total depth (rig floor; m): 2480.8
Penetration (m): 465.8
Number of cores (including cores with no recovery): 20 (rotary)
Total length of cored section (m): 200.1
Total core recovered (m): 106.6
Core recovery (%): 53.3
Oldest sediment cored:
 Depth sub-bottom (m): 465.8
 Nature: silty muddy sand
 Age: Pliocene

HOLE 645E

Date occupied: 14 September 1985, 0000 AST
Date departed: 27 September 1985, 2330 AST
Time on hole: 13 days, 23.5 hr
Position: 70°27.48' N, 64°39.30' W
Water depth (sea level; corrected m, echo-sounding): 2005.8
Water depth (rig floor; corrected m, echo-sounding): 2016.3
Bottom felt (rig floor, m; drill-pipe measurement): 2018.8
Distance between rig floor and sea level (m): 10.5
Total depth (rig floor; m): 3165.9
Penetration (m): 1147.1
Number of cores (including cores with no recovery): 78 (rotary)
Total length of cored section (m): 846
Total core recovered (m): 535.7
Core recovery (%): 63.3
Oldest sediment cored:
 Depth sub-bottom (m): 846
 Nature: muddy sandstone and silty mudstone
 Age: early Miocene

HOLE 645F

Date occupied: 28 September 1985, 0000 AST
Date departed: 28 September 1985, 0930 AST
Time on hole: 9.5 hr
Position: 70°27.48' N, 64°39.29' W
Water depth (sea level; corrected m, echo-sounding): 2005.8
Water depth (rig floor; corrected m, echo-sounding): 2016.3
Bottom felt (rig floor, m; drill-pipe measurement): 2018.8
Distance between rig floor and sea level (m): 10.5
Total depth (rig floor; m): 2041.8
Penetration (m): 23.0
Number of cores (including cores with no recovery): 3 (APC)

Total length of cored section (m): 23.0
Total core recovered (m): 12.3
Core recovery (%): 53.5
Oldest sediment cored:
 Depth sub-bottom (m): 23.0
 Nature: silty clay
 Age: late Pleistocene

HOLE 645G

Date occupied: 28 September 1985, 0945 AST
Date departed: 28 September 1985, 1200 AST
Time on hole: 2.25 hr
Position: 70°27.48' N, 64°39.29' W
Water depth (sea level; corrected m, echo-sounding): 2005.8
Water depth (rig floor; corrected m, echo-sounding): 2016.3
Bottom felt (rig floor, m; drill-pipe measurement): 2018
Distance between rig floor and sea level (m): 10.5
Total depth (rig floor; m): 2035
Penetration (m): 17.0
Number of cores (including cores with no recovery): 2 (APC)
Total length of cored section (m): 16.0
Total core recovered (m): 8.5
Core recovery (%): 51.1
Oldest sediment cored:
 Depth sub-bottom (m): 17.0
 Nature: silty
 Age: late Pleistocene

Principal results: Major lithologic units drilled at Site 645 are as follows:

Unit I. (Cores 105-645A-1H, 105-645B-1X to 105-645B-18X, 105-645C-1H to 105-645C-3H, 105-645F-1H to 105-645F-3H, and 105-645G-1H to 105-645G-2H) 0–168.1 mbsf. Age: late Pleistocene–Holocene. Description: subdivided into two units as follows:

Subunit IA (Cores 105-645A-1H, 105-645B-1X to 105-645B-8X, 105-645C-1H to 105-645C-3H, 105-645F-1H to 105-645F-3H, and 105-645G-1H to 105-645G-2H) 0–71.6 mbsf. Age: Pleistocene to Holocene. Description: alternating beds of light-tan to gray, gravel-bearing detrital carbonate sand and silty mud, scattered dropstones grading to cobble size; carbonate content (detrital), 30%–40%. Cyclicity of lithofacies on scale of tens of centimeters to 1–2 m; bioturbation is slight.

Subunit IB (Cores 105-645B-9X to 105-645B-18X) 71.6–168.1 mbsf. Age: Pleistocene. Description: alternating beds of gray detrital carbonate silty clay to dark olive-gray silty mud, dropstones grading to cobble size. Carbonate content (detrital), 30%–40%, but dolomite/calcite ratio, about 2:1; distinct to subtle cyclicity of lithofacies and slight bioturbation.

Unit II (Cores 105-645B-19X to 105-645B-32X, 105-645D-1R to 105-645D-6R, and 105-645E-1R to 105-645E-3R) 168.1–335 mbsf. Age: Pliocene–early Pleistocene. Description: noncarbonate silty mud, clayey silt, and silty clay and dropstones grading to cobble size. Carbonate content, 5%–10%, predominantly dolomite. Cyclicity similar to that of Unit I, bioturbated to faintly laminated in places. A 5-m-thick homogeneous fine sand layer occurs near base of Unit II. In the basal 30-m interval of low recovery, gravel predominates (we attempted to core this interval at three different holes and had little success). Precise definition of the lower boundary of Unit II was, therefore, difficult, but logs constrain the boundary to 332–336 mbsf.

Unit III (Cores 105-645D-8R to 105-645D-20R and 105-645E-4R to 105-645E-78R) 335–1147.1 mbsf. Age: early Miocene–Pliocene. Description: subdivided into three units as follows:

Subunit IIIA (Cores 105-645D-8R to 105-645D-20R and 105-645E-4R to 105-645E-36R) 335–753.4 mbsf. Age: late Miocene–Pliocene. Description: poorly sorted olive-gray muddy sandstone and sand-

bearing silty mudstone with scattered pebbles; predominantly shale clasts in coarser beds. Maximum quartz grain size is as large as granule. Homogeneous to slightly bioturbated textures and few primary structures. Variations in grain size on scale of meters with gradational boundaries. Some sharp-based graded beds, ranging in thickness from 20 to 100 cm, are interbedded in unit.

Subunit IIIB (Cores 105-645E-37R to 105-645E-54R) 753.4–916.8 mbsf. Age: middle to late Miocene. Description: olive-gray muddy sandstone and dark-gray silty mudstone, interbedded with well-laminated medium-gray calcareous silty claystones with organic carbon contents as high as 3% (abundant wood fragments) and moderate to strong bioturbation.

Subunit IIIC (Cores 105-645E-55R to 105-645E-78R) 916.8–1147.1 mbsf. Age: early to middle Miocene. Description: predominantly fine- to medium-grained muddy sandstone and silty mudstone; glauconite-bearing sandstone (>10%) in part. Moderate to strong bioturbation of coarser facies, but some interbedded fine-grained intervals are well stratified. A few horizons show features of soft-sediment deformation.

Summary of Interpretation

The sequence recovered at Site 645 has a pronounced terrigenous character and surprisingly sparse planktonic biota. The average sedimentation rate for the sequence is about 60 m/m.y. (6 cm/k.y.), but it ranges from 40 to 130 m/m.y. (4 to 13 cm/k.y.). The sparse siliceous and calcareous planktonic assemblages and evidence of reworking make precise age assignments difficult. We primarily depend on dinocyst and benthic foraminifer age picks and a few tie points from calcareous nannofossils and diatoms. Magnetostratigraphy from the pass-through cryogenic data and the discrete-sample record is helpful down to 900 m, below which the section is badly remagnetized. Further shore-based studies of fairly abundant dinocysts will undoubtedly provide better stratigraphic control. The following conclusions concerning timing of events are based on our preliminary stratigraphy and should be considered highly tentative.

Recovery in Unit I with HPC and XCB tools was poor, probably because of unusual firmness and abundant dropstones. Piecing together recovery from Holes 645A, 645B, 645C, 645F, and 645G of the upper 25 m of HPC/XCB-cored material and carefully correlating distinctive lithologic units gives a nearly complete sequence (upper part of upper Pleistocene), enabling high-resolution studies of glacial-interglacial changes in the paleoenvironment. Rhythmic sedimentation is evident throughout Units I and II (late Pliocene–Pleistocene), but, unfortunately, the recovery in the uppermost 170 m is insufficient for tests of orbital forcing over long time series in Baffin Bay.

In Unit I, the most characteristic pattern is interbedded dark-gray and light brownish to grayish brown calcareous silty clay or mud. Contacts between each lithology are sharp, and bioturbation is minor. The light-colored intervals contain a greater portion of coarser detritus, including silt-sized detrital carbonate. Pebbles and cobbles, interpreted as ice-rafted detritus, are apparently randomly distributed in both lithologies. The cycles average about 1 m in thickness, which is equivalent to about 8 k.y., given the average depositional rate of 130 m/m.y. in the upper 470 m of this section. Such a period is much shorter than the 41 k.y.-period reported by Aksu (1983) from his studies of the oxygen-isotope stratigraphy of shallow piston cores from Baffin Bay. Thus, either a major change in sedimentation rate occurs between 10 and 95 mbsf or Aksu's correlations are incorrect. Detailed shore-based studies are required to check this further, but our preliminary results strongly suggest that the melting of sea ice and the advance and retreat of glacial ice on the margins of the Baffin Bay region occurred on a much shorter time scale than expected.

The onset of major glacial ice rafting in Baffin Bay, recorded by the first abundant dropstones and other coarse sediment, was at least as early as 2.5 Ma (340 mbsf) and probably as early as 3.4 Ma (465 mbsf). The beginning of major glacial activity in this region, therefore, preceded evidence of ice rafting in the North Atlantic by at least 1 m.y. However, isolated pebbles and granules in strata as old as late Miocene (605 mbsf) could indicate the presence of at least seasonal sea ice in Baffin Bay as early as 8 Ma. A major unconformity (reflector R1), observed in a regional multichannel seismic net, probably represents a change in depositional style near the early/late

Pliocene boundary and is overlain by a thick wedge of upper Pliocene–Pleistocene “glacial” sediment that prograded westward from the West Greenland margin. The upper 160 m of upper Pleistocene sediment is predominantly ice rafted.

Interpretation of regional seismic lines and of sedimentary textures and structures at Site 645 suggests an unexpectedly pronounced but variable influence of deep “contour-following” currents during deposition of Units II and III (early Miocene to Pliocene) in western Baffin Bay. These features and the nearly complete absence of planktonic biota indicating incursions of warmer North Atlantic waters into the basin suggest possible southward-directed flow of Arctic water masses to the Labrador Sea beginning at least from the middle Miocene to the Holocene. Calcareous microfossils, having North Atlantic warm-temperate affinities, occurred in some intervals of the early Miocene at Site 645, possibly indicating the waning influence of relatively warmer northward flow from the North Atlantic to Baffin Bay at that time. Reflector R2 is an erosional unconformity over at least part of the region, particularly on the Baffin Island shelf and slope. Middle Miocene, partly bottom-current-deposited strata overlie R2, suggesting that this reflector and unconformity mark the onset of vigorous southward-directed circulation in the basin, coincident with dominance of faunal and floral assemblages indicating mainly cooler climatic conditions after 16 Ma. Evidence of a middle Miocene climatic amelioration observed elsewhere in the circum-North Atlantic region is not immediately obvious at Site 645 although some evidence signifies a relatively high-productivity event during that interval.

The paucity of siliceous and calcareous biota, the neritic aspect suggested by diatom and dinocyst occurrences, the dominance of organic matter of terrestrial derivation (even though organic carbon contents in some intervals were as great as 3%), and pollen denoting a cool-temperate to boreal climate indicate predominance of cool, nutrient-poor surface waters characterized by generally low productivity for most of the Miocene to Holocene. However, dissolution and/or diagenesis cannot be ruled out as at least a partial explanation of the poor preservation or absence of calcareous and siliceous faunal/floral remains.

Although, contrary to plans, we did not reach as deep as reflector R3 at about 1565 mbsf, the drilling results provide constraints on the earlier evolution of this basin. Extrapolation of sedimentation rates gives an approximate Eocene/Oligocene boundary age to reflector R3. This reflector extends across Baffin Bay and, therefore, confirms that cessation of seafloor spreading probably occurred by the end of the Eocene in the Baffin Bay region. Subsidence at the site follows a path expected for thinned or thermally disturbed crust, which began subsiding between 63 and 55 Ma. Correlation of drilling results, measurements of physical properties, and seismic data at the site will allow correlation of events across much of the basin. Geophysical logs were obtained only for just over 200 m of the sequence because of hole problems. A detailed set of organic and inorganic geochemical analyses is providing a good understanding of diagenesis of this terrigenous sequence.

BACKGROUND AND OBJECTIVES

Baffin Bay forms a link between the Arctic Ocean to the north and the Labrador Sea and North Atlantic Ocean to the south. Before separation of Eurasia from Greenland in the late Paleocene to early Eocene, Baffin Bay may have formed the main conduit for the exchange of water between these two oceans. Scant paleontological data from marine outcrops on land and from deep exploratory wells drilled on West Greenland and South Baffin Island shelves, when combined with the paleogeographic reconstructions of this region, suggest that a narrow seaway may have existed through this region, allowing such an exchange of surface-water masses (Fig. 9, “Introduction” chapter, this volume; Gradstein and Srivastava, 1980). Considering that the Davis Straits may have been a barrier at that time, other pathways, such as adjacent submerged land areas, are possible. The nature of this water exchange can be ascertained only by establishing the subsidence history of Baffin Bay and Davis Strait regions as well as by studying the planktonic and benthic faunas and floras from these regions. No seismic strati-

graphic control exists in these regions to constrain subsidence history.

Furthermore, the origin of Baffin Bay has been a subject of much debate; a divergence of opinion revolves around whether Baffin Bay formed by seafloor spreading (Keen and Barrett, 1972; Srivastava et al., 1981) or by foundering and thinning of continental crust (Kerr, 1967; Grant, 1980). The prime reason for the lack of consensus as discussed in the "Introduction" chapter (this volume) has been the absence of clearly recognizable seafloor-spreading magnetic anomalies as well as the absence of crustal structure resembling typical oceanic regions in this area. Yet indirect evidence, such as the presence of a deep graben in the center of Baffin Bay recognized in seismic-reflection and gravity data, the presence of a very thin crust under the Bay (Fig. 6, "Introduction" chapter, this volume), and the small amount of opening required in this region by plate kinematic solutions for the adjoining regions (Srivastava and Tapscott, 1986), highly suggest a seafloor-spreading origin for this region. Drilling in Baffin Bay was designed to establish its tectonic history and the timing of rifting as well as to provide data to study paleocirculation in and through this region.

Site 645 lies on the continental slope off southern Baffin Island in water depths of about 2020 m (Fig. 1). Gravity (Fig. 3, "Introduction" chapter, this volume) and magnetic data (Figs. 7 and 8, "Introduction" chapter, this volume) near the site together with seismic-refraction measurements north of the site (Figs. 6 and 7, "Introduction" chapter, this volume) suggest that the site lies near the continental/oceanic crust boundary. A number of multichannel seismic-reflection profiles were shot in this region by Petro-Canada (Fig. 2), and these show the presence of down-faulted basement blocks covered by a substantial amount of Cretaceous and younger sediments west of the site. Site 645 is located on Petro-Canada multichannel line 74-51 at shotpoint 511 (Fig. 2). Examination of this and several other lines that lie in this region (Fig. 3) reveals the presence of many prominent seismic reflectors. These have been divided into four seismic units according to their regional uniformity and seismic characteristics, as described in the "Seismic Stratigraphy" section (this chapter).

Tectonic and Sedimentary Framework

Our greatest objective at Site 645 was penetration and recovery of strata from below the R3 reflector (Fig. 60, "Seismic Stratigraphy" section, this chapter). This reflector was thought to be middle Eocene or older, on the basis of a preliminary interpretation of seismic data supplied by Petro-Canada; however, this age was not well constrained. The depth to this reflector is estimated at between 1470 and 1700 mbsf, using an average velocity of about 2.1 km/s. Assuming that the section spans about 50 m.y., the average sedimentation rates would be between 30 and 35 m/m.y., not accounting for the presence of hiatuses. This rate is the same magnitude as the late Quaternary rates suggested by the oxygen-isotopic stratigraphy from 10-m piston cores in central Baffin Bay (Aksu, 1983). Such high rates of sedimentation are typical of hemipelagic environments, and we expected the sediments to be dominated by terrigenous (detrital) input, particularly in the glacial Pliocene-Pleistocene section. Because Baffin Bay is a relatively young (active spreading continued until the middle Oligocene) and narrow basin, it is probable that both the Baffin Island margin and the Greenland margin were relatively high standing and a source of much clastic material throughout the depositional history of the basin. These margins have now subsided, and the glacial ice sheets have further eroded and loaded (isostatic subsidence) the continental surfaces. Thicknesses of 3–5 km of sediment in most of Baffin Bay attest to the significant removal of mass from the adjacent continental blocks (Fig. 4).

Thick, prograding deltaic sequences of Paleocene through at least Miocene age on the margins of West Greenland and southern Baffin Island are seen in seismic sections and recovered in exploratory wells on the shelf (Henderson et al., 1981; Klose et al., 1982). Strong progradation and influx of coarse clastic material from the east on the West Greenland margin suggests accelerated uplift of crystalline basement on East Greenland during the Eocene-Oligocene (Henderson et al., 1981). We suggest that this episode of uplift and high rates of sediment supply may be the result of westward tilting of Greenland associated with the early rifting and opening of the Norwegian Sea. These prograding deltaic sequences are underlain by middle to upper Paleocene basalt flows and pillow breccias over part of the West Greenland margin (Clarke and Pederson, 1976; Henderson et al., 1981; Rolle, 1985). We similarly interpret the high-amplitude reflectors under the inshore parts of our seismic lines on the Baffin Island side as being Paleogene-age basalt flows. Most of the Upper Cretaceous-middle Eocene strata in the exploratory wells are marine prodeltaic muds, whereas the upper Eocene and younger sediments are primarily marginal marine to marine (deltaic to prodeltaic), consisting of predominantly coarse-grained deposits, which contain relatively little biogenic material (Rolle, 1985). These deposits are mineralogically and texturally immature, suggesting rapid denudation and little sedimentary recycling of basement rocks.

Current interpretation of the seismic lines in western Baffin Bay provides no firm conclusions whether the lateral equivalents of the Paleogene deposits on the West Greenland margin were derived from West Greenland or from some other region. Seismic units 2 through 4 (Fig. 53, "Seismic Stratigraphy" section, this chapter) do not noticeably thicken toward Greenland. A pronounced basement high west of the site (Fig. 3) may have blocked much of the direct input of sediment to the site from Baffin Island before deposition of seismic unit 2 (perhaps Miocene and younger). Sediment of Paleocene and older age was probably trapped in grabens between tilted basement blocks along part of the Baffin margin west of Site 645 (Fig. 3); therefore, the thick sequences of Paleogene (and older?) sediment, more than 2 s thick, were probably derived from a direction along basin strike or perhaps from the east.

Apparently, the sediment composing seismic unit 1 was derived more or less from the east, according to our seismic interpretations. These seismic lines show that reflectors at the base of seismic unit 1 progressively onlap reflector R1 (top of seismic unit 2) from east to west and that seismic unit 1 thickens drastically in an eastward direction (Figs. 5 and 6). The age span of seismic unit 1 was poorly known, but we suspected it to be Pliocene-Pleistocene and composed predominantly of material transported by glacial ice to the west margin of Greenland and redeposited to the deeper Baffin Bay basin by turbidity currents and debris flows. We therefore expected very high sedimentation rates in seismic unit 1, particularly in the eastern part of the region where rates may be > 300 m/m.y. (> 30 cm/k.y.), assuming that the base of the unit is about 3 Ma old.

Although the presence of relatively high-velocity deep currents was unexpected, we detected signs in the multichannel seismic records that such currents have affected sedimentation in the western part of Baffin Bay. Reflector R2 (Fig. 5) is an obvious erosional unconformity on the Baffin Island shelf and upper slope, cutting into a substantial thickness of older strata. Although R2 could be interpreted as being the lower surface of a substantial slide block or as an unconformity that represents uplift, subaerial exposure, and erosion of the sedimentary sequence followed by renewed subsidence and sedimentation, we favor the hypothesis that R2 represents a prolonged episode of submarine erosion along at least part of the Baffin Island margin. The amount of vertical motion required by the uplift/ero-

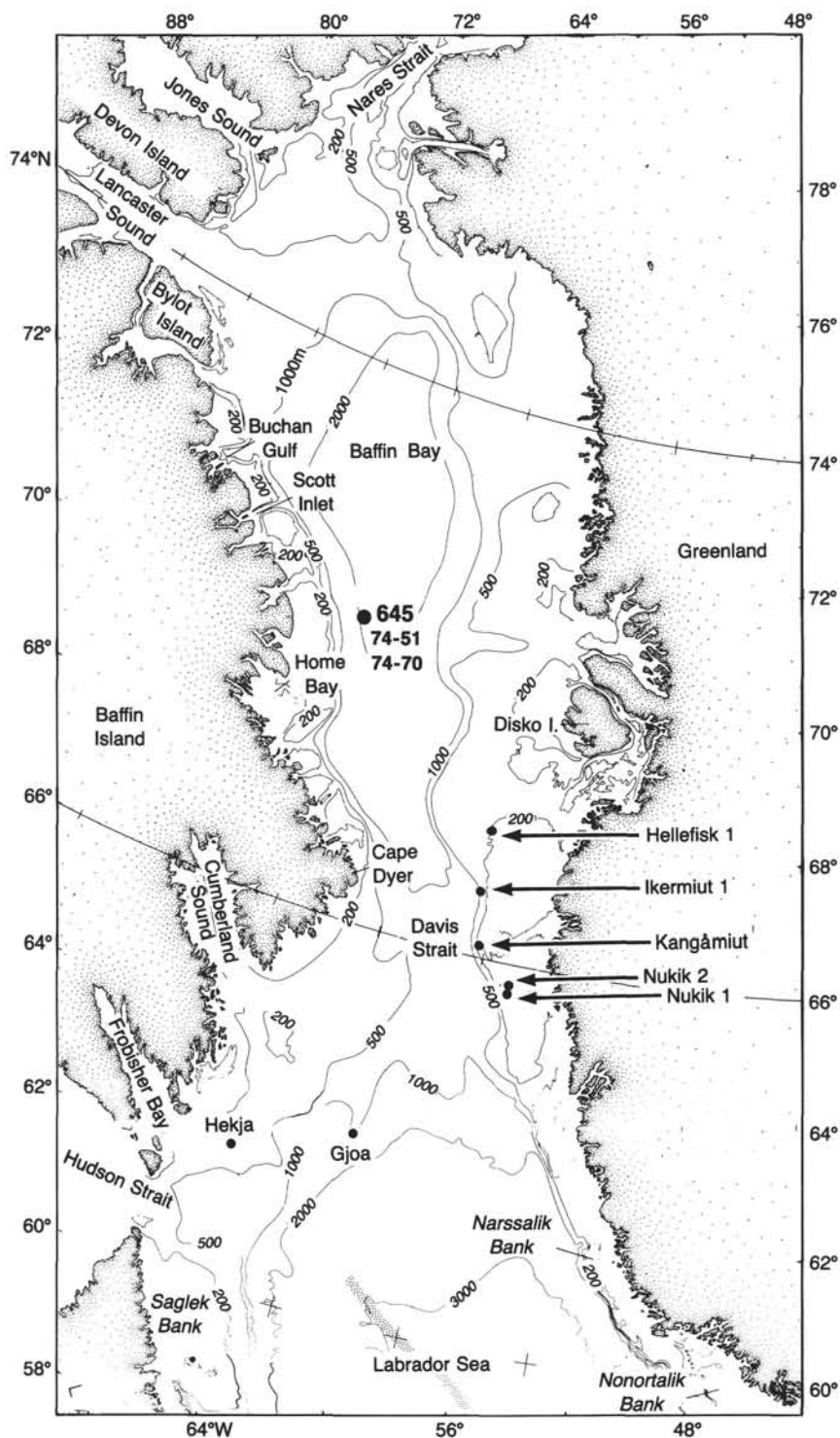


Figure 1. Bathymetric map of Baffin Bay. Location of Site 645 is shown in southern part of region and also shown are the locations of exploratory wells (Hekja, Gjoa, Kangamiut, Nukik, Ikermiut, and Hellefisk). Locations of two multichannel lines, 74-51 and 74-70, shot by Petro-Canada are also shown. Depth contours are in meters.

sion hypothesis seems unreasonable given the available time. The internal structure and lack of a pronounced toe also argue against the slide hypothesis. In addition, the deposits of seismic units 1 and 2 above the unconformity landward of Site 645 on line 74-51 (Fig. 50, "Seismic Stratigraphy" section, this chapter) strongly resemble contour-current-influenced depositional ridges having sigmoidal internal reflections that bend down and then

up in a troughlike feature adjacent to their onlap onto R2. Similar features are also seen, though a bit subdued, on other seismic lines (e.g., 74-70, Fig. 2) in the region. The constructional ridges appear to have built up and migrated progressively landward through time. These seismic data suggest onset of strong erosive bottom currents near the end of seismic unit 3 deposition and a gradual increase in sediment supply or diminishing

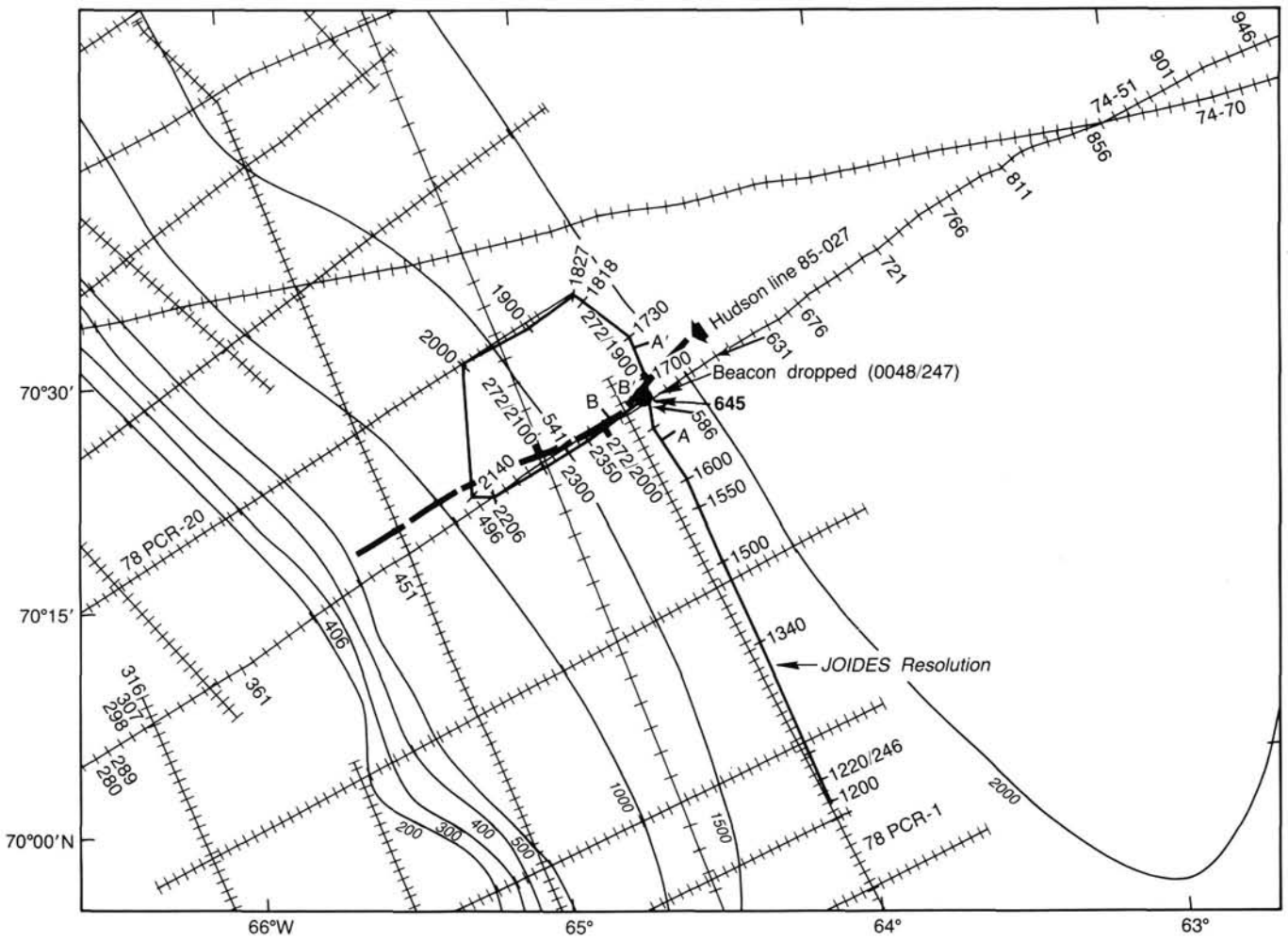


Figure 2. Multichannel tracklines shot by Petro-Canada in area of Site 645, with shotpoint grid. Note location of Site 645 and Resolution trackline.

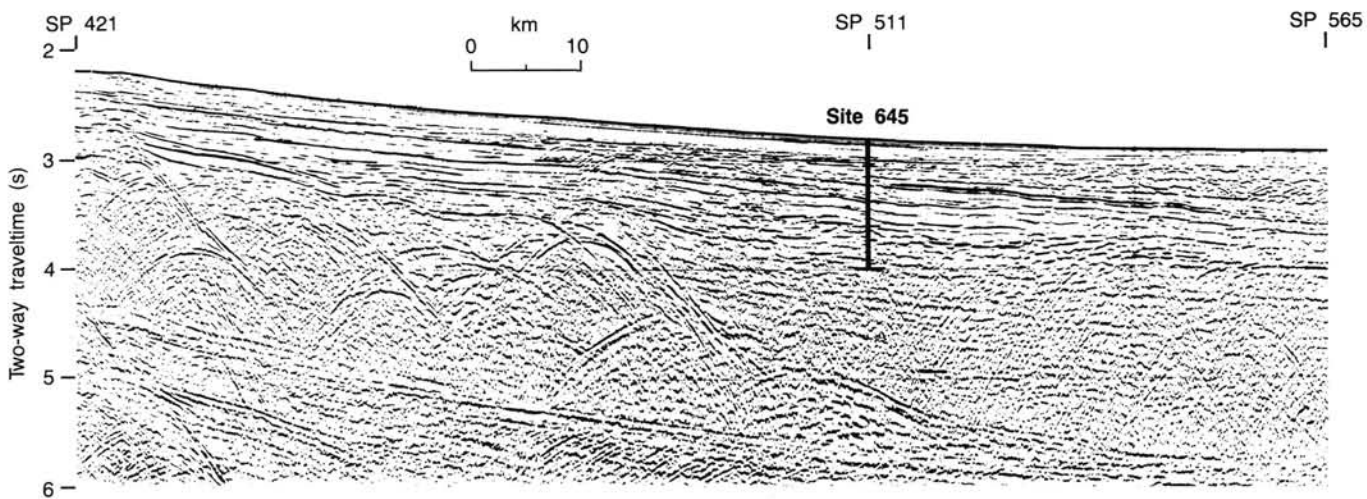


Figure 3. Part of uninterpreted multichannel line 74-51 from shotpoint 421 to shotpoint 565, showing nature of reflectors and location of Site 645.

current strength throughout deposition of seismic units 2 and 1, which allowed net, current-influenced sedimentation. The transparent deposits of seismic unit 1A (Fig. 53, "Seismic Stratigraphy" section, this chapter) appear to evenly drape the seafloor, even on the slope and outer shelf, suggesting that the influence

of submarine currents waned significantly during deposition of that unit. Seismic unit 1A may consist primarily of ice-rafted detritus, which we would expect to more or less evenly drape seafloor topography and have rather homogeneous seismic character.

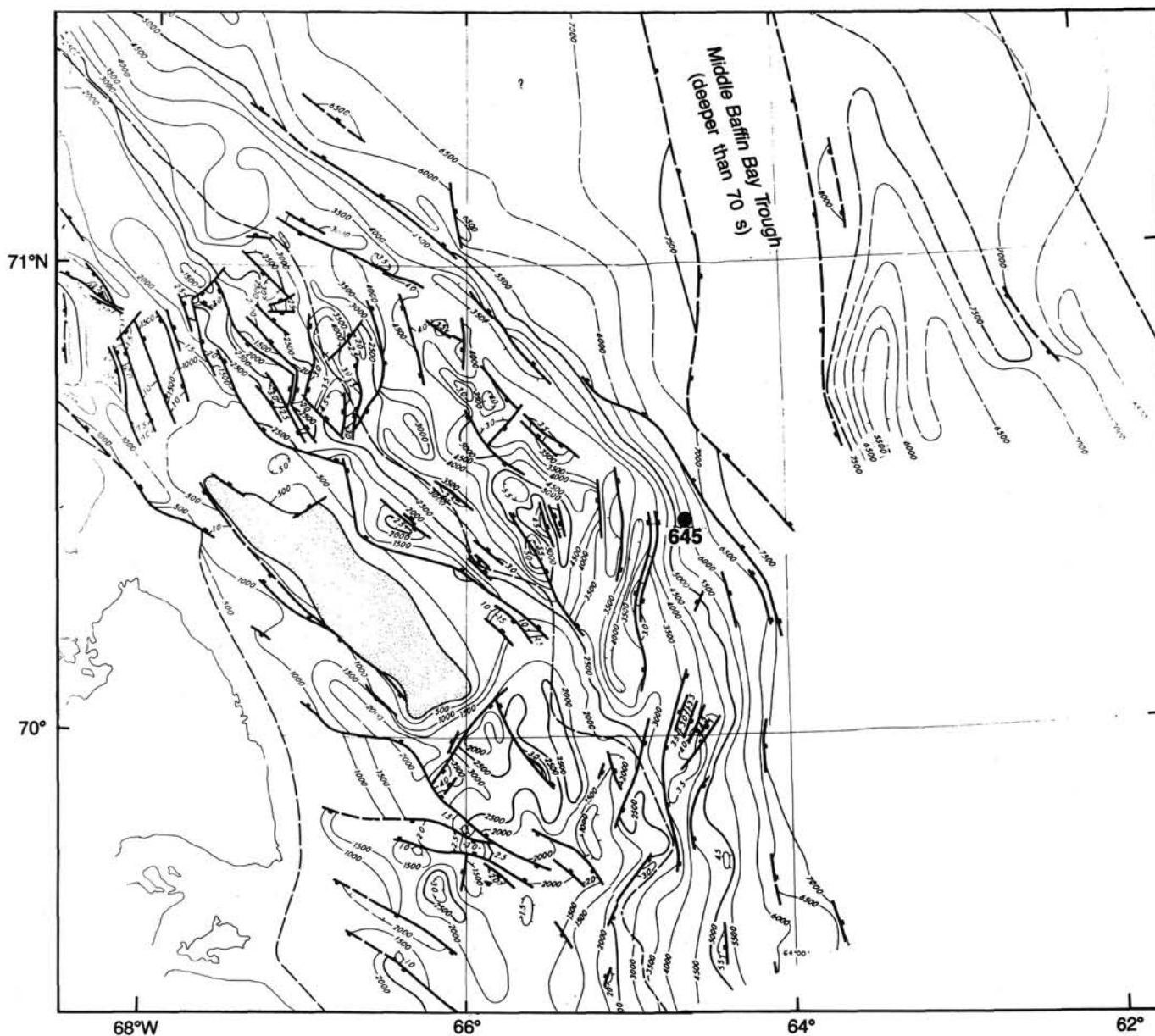


Figure 4. Depth to basement in meters below sea level near Site 645, constructed on the basis of multichannel seismic net by Petro-Canada using interval velocities derived from multichannel stacking exercise. Bathymetry in meters.

The margins of Baffin Bay, particularly the relative widths of the Baffin Island and West Greenland shelves, may provide a further indication of both the relative importance of sediment supply from the two regions and the influence of contour-following deep currents. West Greenland shelf is a relatively wide feature, possessing an irregular, lobate outline. Pronounced lobes occur in front of the major glacial drainages, now marked by incised canyons, suggesting major point sources of sediment associated with the canyons. The Baffin Island margin, on the other hand, has a narrow shelf and a relatively smooth slope, suggesting less buildup of the shelf sedimentary prism. This is perhaps because of the lower sediment supply from land as well as the erosion and sediment redistribution by contour currents. No distinct canyons cut the shelf/slope boundary. The seismic data also show that the shelf sedimentary prism is thinner (mostly

0–2 s thick) off southern Baffin Island than on the West Greenland side (mostly 2–3 s thick).

Extensional faulting disrupts the section between reflectors R1 and R3 in the western part of Baffin Bay, but we cannot definitely state that the faults offset R3 because of the generally poor resolution on the multichannel lines deeper in the sequence. We tentatively interpret the faulting as being compaction related rather than tectonically induced. Growth faults might be expected in high-sedimentation-rate environments. Further study of the multichannel net will be necessary to resolve the growth fault versus tectonic origins of the faulting.

Our intent in drilling at Site 645 was to determine the age of major reflectors and seismic units, thus enabling constraint of ages of the circulation and sedimentation events inferred from the seismic records.

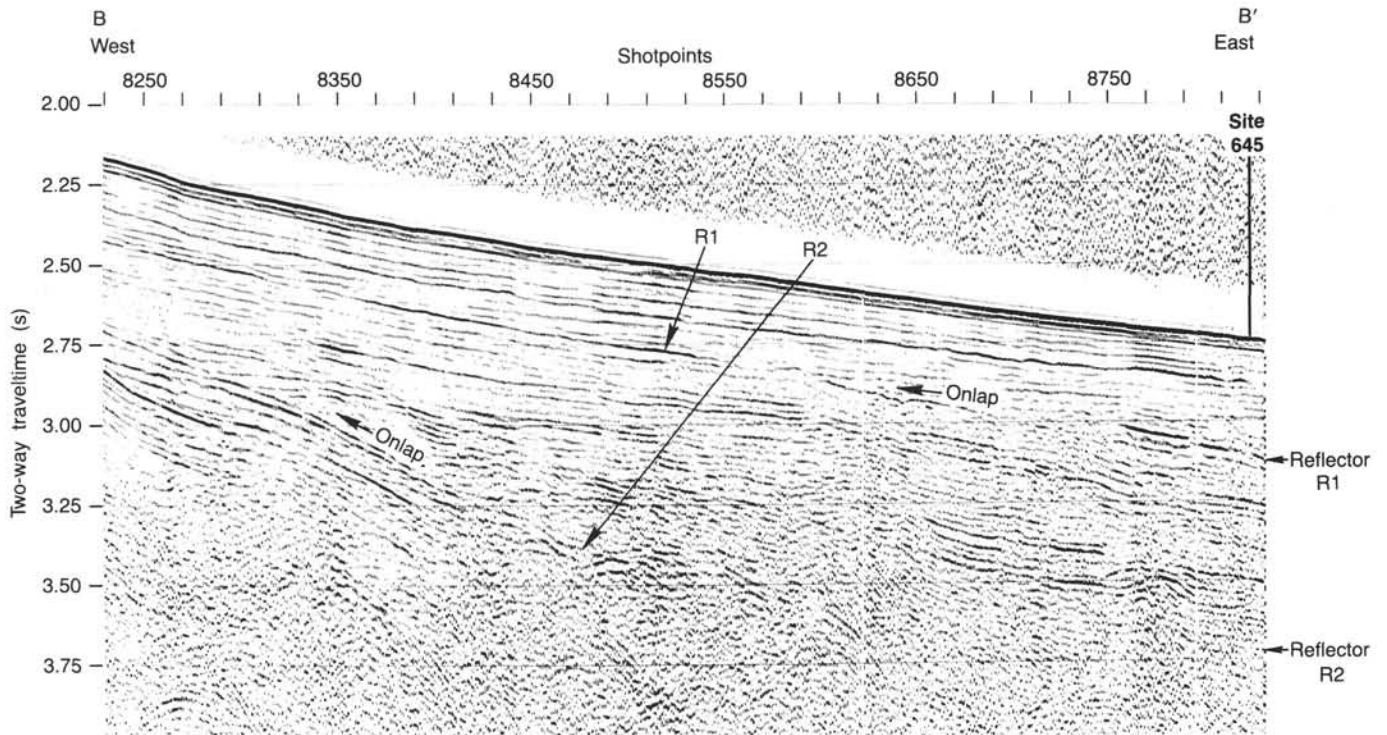


Figure 5. Single-channel seismic line (B-B' on Fig. 2) shot by *JOIDES Resolution* (with 80-in.³ water guns) normal to slope of Site 645 along approximate trace of multichannel line 74-51. Reflections visible to about 3.75 s (about 1.5 s penetration). Note that onlap of seismic unit 2 (between R1 and R2) on unit 3 is pronounced in western part of section. Onlap of bases of seismic unit 1 on R1 is also highly visible.

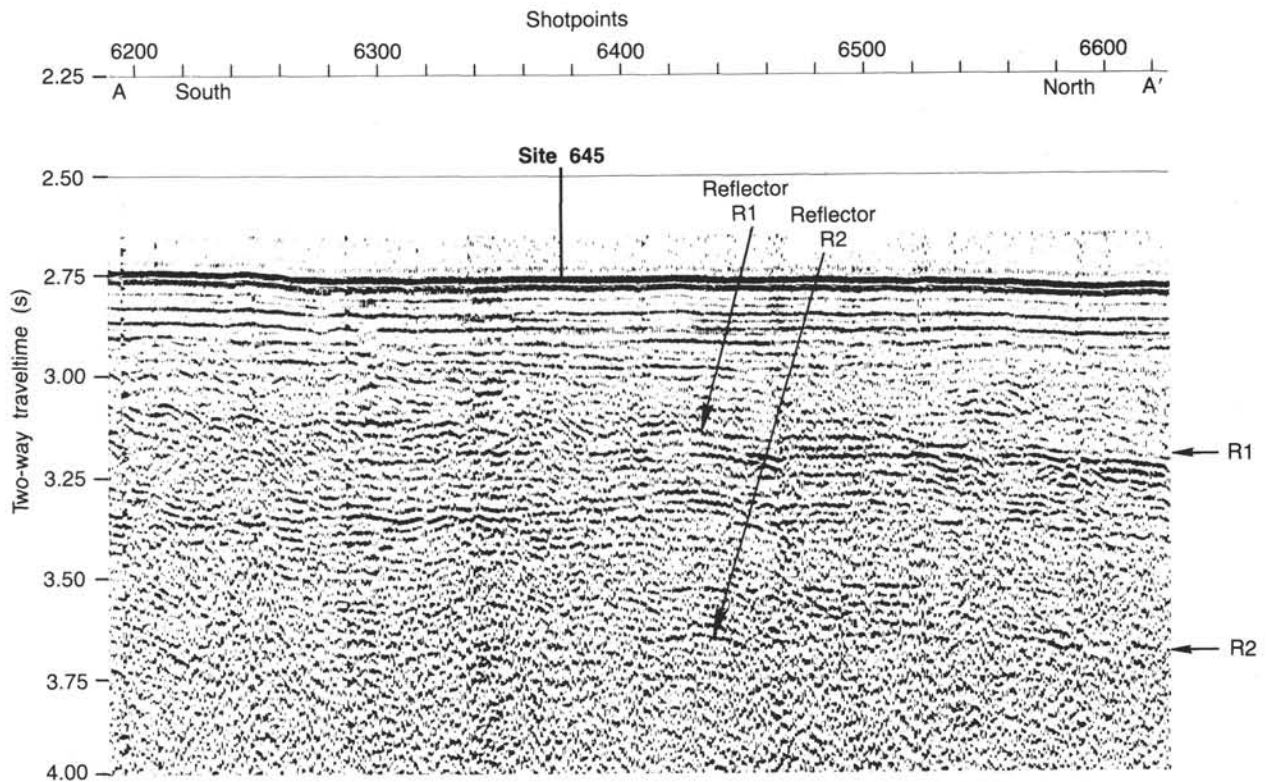


Figure 6. Single-channel line shot by *JOIDES Resolution*. Line runs roughly north-south (A-A' on Fig. 2). Note that the sequence above R1 (seismic unit 1) appears to thicken toward the north and between R1 and R2 to the south.

Summary of Main Objectives at Site 645

Sedimentary and Tectonic History

Baffin Bay is a piece of the history puzzle of tectonic events in the northern North Atlantic–Arctic region. Although some well log data and high-quality seismic and other geophysical readings are available from the region and reasonable models of the timing and nature of plate movements have been presented, drilling at Site 645 was proposed to test some of the hypotheses for the timing of rifting and possible seafloor spreading (see “Introduction” chapter, this volume). In particular, adequate ages of the major reflectors were needed to provide a proper understanding of the implications of the seismic data for timing of tectonic events, subsidence, and sedimentation events in Baffin Bay and to place them in a global context. The implications of strong, deep currents in the basin and the age of the prograding wedge of sediments of seismic unit 1 were especially needed. Likewise, we were interested in correlating certain sedimentation and climate episodes or events with those elucidated by our proposed drilling in the Labrador Sea.

Paleogene Climate and Circulation

One of the major objectives of Leg 105 was to develop a better understanding of Paleogene climate and circulation in and through Baffin Bay during and following its Late Cretaceous–Paleogene opening. Of particular interest was possible evidence of warm climatic conditions over the anticipated recovery interval of Paleogene strata at the site in the form of subtropical calcareous plankton assemblages in the sediments. Such faunal and floral remains were expected, on the basis of earlier studies of exploratory wells drilled on shelves in Labrador and West Greenland and of outcrops on West Greenland. From the faunal and floral assemblages and the other data, we had hoped to reconstruct the paleotemperatures of surface- and deep-water masses and to assess the nature and importance of possible connections between the Arctic and the North Atlantic during the early stages of rifting, subsidence, and formation of Baffin Bay. Such a connection may have been important in maintaining a warm Arctic region during the Paleogene. Unfortunately, we were unable to penetrate below the lower Miocene because of time limitations, and this objective was, therefore, not achieved.

Eocene–Oligocene Events and Climate Deterioration

The drilling in Baffin Bay also presented an opportunity to observe the events at the Eocene/Oligocene boundary at high latitudes. We expected that the overall high sedimentation rates presumed to exist at the site would provide a detailed record of the Eocene/Oligocene transition, a time of apparent global cooling and hiatus formation in much of the world's oceans. In addition, we hoped to monitor the pace of global climatic differentiation between high and low latitudes through the Oligocene–Miocene and perhaps a superimposed episode of warming in the middle Miocene. We were aware of a possible complication being that the regional imprint on oceanography of Baffin Bay could dampen out the global paleoclimatic signal. We expected to depend greatly on pollen and dinoflagellate assemblages for both stratigraphic control and information on the paleoenvironment in Baffin Bay and the surrounding regions. However, we hoped that siliceous microfossils and the occasional incursion of warm-water calcareous plankton into Baffin Bay would provide better biostratigraphic control. Unfortunately, we were unable to penetrate below the lower Miocene because of time limitations, and this objective was, therefore, not achieved.

Onset of Glaciation

Prevailing models call for the major development of northern hemisphere continental ice sheets to begin at about 2.4–2.5

Ma (Roberts, Schnitker, et al., 1984). However, major cooling began earlier, and ice buildup in continental regions at high latitudes could also have begun earlier, thus explaining some, as yet poorly understood, positive events in the oxygen-isotopic record. We thought that the Baffin Bay record would allow us to recognize perhaps the earliest development of marginal marine glaciers in a region of high continentality. The signal of major cooling and/or connections with the Arctic would have been heralded by the predominance of Arctic plankton and the beginning of glaciation, at least in those glaciers having calved icebergs to Baffin Bay surface waters, and by the first signs of ice-rafted debris.

Glacial Cycles

A high-amplitude Quaternary paleoenvironmental signal was recognized in Baffin Bay (Aksu, 1983; Mudie and Aksu, 1984); the amplitude is related to the relatively small size of Baffin Bay and the location at the outlets of Greenland and Innuitian ice sheets. We hoped to obtain long, continuous, and relatively undisturbed HPC sequences to continue studies of the driving force of glacial advances and retreats at high latitudes and to test whether the dominant periodicity is 41 k.y. north of 60°N, as predicted by the orbital control hypothesis (Berger, 1978). The rate of buildup and retreat of glacial ice sheets is particularly important because of the disparity between models based on interpretation of oxygen-isotopic profiles from many areas of the world's oceans (Ruddiman and MacIntyre, 1981a) and those based on study of glacial stratigraphy in the Baffin Bay region (Andrews et al., 1983). The first type of model calls for gradual buildup of the ice sheets and somewhat more rapid deglaciation, whereas the latter requires rapid glacial advances and retreats. Within the limitations of the potential oxygen-isotope stratigraphy, magnetostratigraphy, and biostratigraphy in Baffin Bay, we hoped to be able to distinguish between the two models.

OPERATIONS

Leg 105 was originally scheduled to begin in Stavanger, Norway, on 16 August 1985, but because of the long transit time between Stavanger and our first drill site in Baffin Bay, we decided to start this leg from St. John's instead. *JOIDES Resolution* arrived in St. John's, Newfoundland, Canada, on Friday, 22 August 1985, at 2130 hr UTC. The ship was scheduled to depart on the morning of 26 August 1985 to begin Leg 105, but departure was delayed until 29 August 1985 because two of the rods needed for the heave compensator had not arrived in time for installation. It was essential to have the heave compensator working for this leg, particularly in the Labrador Sea, where high seas were expected; thus, ODP decided to delay *JOIDES Resolution's* departure. The compensator rods were flown from Holland to St. John's and arrived on 27 August. They were installed in the heave compensator, and the whole unit was tested before *JOIDES Resolution's* departure from St. John's at 1035 hr UTC on 29 August. As soon as we were outside the harbor, we were greeted by strong easterly winds that very gently rolled the ship.

Except for the first 2 days when light to moderate winds prevailed, the weather throughout the transit from St. John's to Baffin Bay Site 645 remained relatively calm and sunny. *JOIDES Resolution* steamed during this period at an average speed of 11.6 kt, except on the night before arriving at the site, when slower speeds of 4 kt were required because of fog and the danger of running into growlers. Only a few icebergs were seen during the entire transit to the site. No underway geophysical data were collected until we were about 8 hr from the site because the steaming rate of between 5 and 8 kt necessary for collecting seismic data would have significantly lengthened the transit time.

Site 645 Approach

Site 645 was proposed for a 70°27'N, 64°39'W location on multichannel seismic line BE 74-51 (Fig. 1) at about shotpoint (SP) 511 at a water depth of about 2090 m. Our plan for the approach to this site was first to obtain single-channel seismic-reflection profile and precision depth recorder (PDR) records along depositional strike (roughly north-south) in western Baffin Bay along the approximate trace of multichannel line 78 PCR-1 (Fig. 2), which crosses line BE 74-51 just about 3 km west of the proposed location of Site 645. At the same time, we intended to obtain a sonobuoy record extending to the vicinity of the site to check interval velocities obtained during stacking of multichannel records and to aid us in calculating the depths to major reflectors. We started towing our system, which consisted of a Teledyne streamer, a 400-in.³ water gun, and a magnetometer, at 5 kt at about 1000 hr UTC on 3 September 1985. This was done to allow enough time to check the system and to collect some wide-angle seismic-reflection data near the proposed site before dropping the beacon. Unfortunately, neither the large water gun (400 in.³) nor the 300-in.³ air gun, which were deployed about 64 km before crossing the site and towed at an average speed of just over 5 kt, functioned properly. Instead, operation with two 80-in.³ water guns became necessary. The two sonobuoys released at shotpoints at 4 and 2 hr before crossing the site also failed to function and/or gave weak returns that were not received by *JOIDES Resolution's* system; we were therefore unable to run a velocity survey. However, the two water guns and a 500-m streamer provided reasonably good single-channel records for a depth of 2 s sub-bottom (Fig. 5).

After crossing near the proposed site and obtaining a number of good satellite fixes (about 1/30 min) on this north-south line, we turned and ran approximately along multichannel line 78 PCR-20 on a heading of about 235° (Fig. 2). Most of the basement structural relief occurs to the west of the proposed site, and we were able to correlate our single-channel record closely with the multichannel line at adequate sub-bottom penetration. Thus, we were fairly confident of our location and were able to turn south at about SP 500 to intersect line 74-51 near SP 388. Upon reaching line 74-51, we turned northeast and ran along it. Again, we were able to compare our single-channel seismic and precision depth recorder (PDR) records with the multichannel lines and to select the site on the basis of a close correspondence between the dead-reckoned (with satellite corrections) and seismic locations. The beacon was dropped at 0048 hr UTC on 4 September. Site 645 is at 70°27.43'N and 64°39.26'W in 2018 m of water. The single-channel record allows us to adequately correlate between the drilling results and the multichannel seismic record (for details see "Seismic Stratigraphy" section, this chapter). The towed seismic gear and magnetometer were retrieved, and we returned to the place where the beacon was dropped at about 0230 hr UTC on 4 September.

The order of drilling and cores obtained in each hole are summarized in Table 1. The details of operations at each hole are described as follows.

Hole 645A

The precision depth recorder (PDR) reading was interpreted as being 2074 m (corrected for variation of sound velocity in this northern latitude by using Matthews' tables [Matthews, 1939]) from the dual elevator stool (DES) of the rig. A standard advanced-piston-corer/extended-core-barrel (APC/XCB)/bottom-hole-assembly (BHA) tool having the required number of drill pipes was lowered to a depth of 2060.5 m below sea level (mbsl). The APC was lowered on the sand line, and it stopped at a depth of 1979.5 mbsl. We retrieved the core barrel twice in an attempt to determine the cause of this resistance. When the sys-

Table 1. Coring summary, Site 645.

Core no.	Date (Sept. 1985)	Time (UTC)	Sub-bottom depths (m)	Length cored (m)	Length recovered (m)	Recovery (%)
Hole 645A						
105-645A-1H	5	1700	0.0-4.9	4.9	4.9	100.0
Hole 645B						
105-645B-1X	7	0630	0.0-4.0	4.0	4.0	100.8
105-645B-2X	7	0825	4.0-13.5	9.5	5.1	54.1
105-645B-3X	7	1000	13.5-22.8	9.3	4.1	44.5
105-645B-4X	7	1115	22.8-32.2	9.4	0.6	6.5
105-645B-5X	7	1245	32.2-42.6	10.4	4.3	41.3
105-645B-6X	7	1415	42.6-52.3	9.7	1.0	10.0
105-645B-7X	7	1530	52.3-62.0	9.7	0.2	1.5
105-645B-8X	7	1645	62.0-71.6	9.6	3.7	38.3
105-645B-9X	7	1800	71.6-81.3	9.7	5.0	51.1
105-645B-10X	7	1930	81.3-90.9	9.6	4.7	48.9
105-645B-11X	7	2045	90.9-100.6	9.7	4.9	50.2
105-645B-12X	7	2215	100.6-110.3	9.7	0.1	0.7
105-645B-13X	7	2330	110.3-119.9	9.6	6.3	65.3
105-645B-14X	8	0100	119.9-129.5	9.6	5.1	52.9
105-645B-15X	8	0230	129.5-139.1	9.6	1.1	11.0
105-645B-16X	8	0345	139.1-148.8	9.7	0.5	5.1
105-645B-17X	8	0530	148.8-158.4	9.6	6.2	64.7
105-645B-18X	8	0715	158.4-168.1	9.7	2.2	22.6
105-645B-19X	8	0930	168.1-177.1	9.0	8.9	99.0
105-645B-20X	8	1300	177.1-187.4	9.7	5.3	54.3
105-645B-21X	8	1515	187.4-196.8	9.4	10.0	106.0
105-645B-22X	8	1730	196.8-206.6	9.8	9.8	100.4
105-645B-23X	8	2000	206.6-216.2	9.6	9.6	100.2
105-645B-24X	8	2200	216.2-225.9	9.7	8.1	83.4
105-645B-25X	9	0030	225.9-235.6	9.7	0.0	0.0
105-645B-26X	9	0230	235.6-245.2	9.6	10.1	105.4
105-645B-27X	9	0530	245.2-254.9	9.7	9.8	101.0
105-645B-28X	9	0830	254.9-264.6	9.7	5.5	56.2
105-645B-29X	9	1030	264.6-274.2	9.6	8.1	84.1
105-645B-30X	9	1330	274.2-283.8	9.6	9.7	100.8
105-645B-31X	9	1900	283.8-293.5	9.7	8.2	84.7
105-645B-32X	9	2215	293.5-298.9	5.4	9.7	180.2
Hole 645C						
105-645C-1H	10	0600	0.0-4.5	4.5	4.5	99.3
105-645C-2H	10	0715	4.5-14.0	9.5	0.3	3.5
105-645C-3H	10	0830	14.0-23.3	9.3	6.1	65.5
Hole 645D						
105-645D-1R	12	0100	265.7-272.9	7.2	5.6	78.0
105-645D-2R	12	0230	272.9-282.5	9.6	8.9	92.6
105-645D-3R	12	0400	282.5-292.2	9.7	0.1	1.0
105-645D-4R	12	0545	292.2-301.8	9.6	0.1	0.7
105-645D-5R	12	0715	301.8-311.4	9.6	0.0	0.0
105-645D-6R	12	0930	311.4-321.1	9.7	0.4	3.7
105-645D-7R	12	1130	321.1-330.7	9.6	0.0	0.0
105-645D-8R	12	1530	340.4-350.0	9.6	4.0	41.1
105-645D-9R	12	1700	350.0-359.7	9.7	9.3	95.3
105-645D-10R	12	1830	359.7-369.4	9.7	5.4	55.7
105-645D-11R	12	2000	369.4-379.0	9.6	9.6	100.4
105-645D-12R	12	2145	379.0-388.6	9.6	2.2	22.8
105-645D-13R	12	2330	388.6-398.3	9.7	9.1	93.5
105-645D-14R	13	0115	398.3-407.9	9.6	7.2	74.6
105-645D-15R	13	0300	407.9-417.6	9.7	9.3	95.8
105-645D-16R	13	0430	417.6-427.2	9.6	4.5	47.0
105-645D-17R	13	0615	427.2-436.9	9.7	9.6	99.2
105-645D-18R	13	0745	436.9-446.5	9.6	4.6	48.0
105-645D-19R	13	0930	446.5-456.2	9.7	9.1	93.3
105-645D-20R	13	1100	456.2-465.8	9.6	7.6	79.3
Hole 645E						
105-645E-1R	16	2000	301.1-310.8	9.7	0.1	0.7
105-645E-2R	16	2330	310.8-320.4	9.6	1.7	18.1
105-645E-3R	17	0115	320.4-330.1	9.7	0.1	0.5
105-645E-4R	17	0845	455.2-464.9	9.7	5.3	54.1
105-645E-5R	17	1030	464.9-474.5	9.6	0.0	0.0
105-645E-6R	17	1200	474.5-484.1	9.6	8.7	90.5
105-645E-7R	17	1330	484.1-493.7	9.6	7.4	76.5
105-645E-8R	17	1430	493.7-503.4	9.7	8.4	86.8
105-645E-9R	17	1545	503.4-513.0	9.6	8.7	91.0
105-645E-10R	17	1715	513.0-522.6	9.6	4.1	42.8
105-645E-11R	17	1830	522.6-532.2	9.6	8.2	85.4
105-645E-12R	17	2000	532.2-541.8	9.6	7.0	73.1
105-645E-13R	17	2130	541.8-551.5	9.7	8.6	88.1
105-645E-14R	17	2300	551.5-561.1	9.6	10.2	106.1
105-645E-15R	17	0030	561.1-570.8	9.7	8.2	84.8
105-645E-16R	18	0215	570.8-580.5	9.7	10.2	105.2
105-645E-17R	18	0400	580.5-590.1	9.6	8.4	87.5
105-645E-18R	18	0530	590.1-599.8	9.7	2.2	22.5
105-645E-19R	18	0700	599.8-609.3	9.5	6.9	72.6
105-645E-20R	18	0800	609.3-618.9	9.6	4.7	48.8

Table 1 (continued).

Core no.	Date (Sept. 1985)	Time (UTC)	Sub-bottom depths (m)	Length cored (m)	Length recovered (m)	Recovery (%)
Hole 645E (cont.)						
105-645E-21R	18	1015	618.9-624.4	5.5	1.8	33.1
105-645E-22R	18	1200	624.4-628.4	4.0	3.4	86.0
105-645E-23R	18	1315	628.4-638.0	9.6	4.7	49.1
105-645E-24R	18	1445	638.0-647.7	9.7	3.6	37.2
105-645E-25R	18	1615	647.7-657.1	9.4	3.0	31.7
105-645E-26R	18	1815	657.1-666.7	9.6	4.8	50.4
105-645E-27R	18	1945	666.7-676.4	9.7	8.6	88.7
105-645E-28R	18	2130	676.4-686.0	9.6	2.8	28.9
105-645E-29R	18	2330	686.0-695.6	9.6	9.7	101.0
105-645E-30R	19	0115	695.6-705.3	9.7	2.4	24.3
105-645E-31R	19	0245	705.3-709.7	4.4	0.4	10.0
105-645E-32R	19	0430	709.7-714.7	5.0	6.1	121.8
105-645E-33R	19	0615	714.7-724.4	9.7	9.3	96.2
105-645E-34R	19	0815	724.4-734.0	9.6	5.4	56.1
105-645E-35R	19	1030	734.0-743.7	9.7	5.6	57.9
105-645E-36R	19	1200	743.7-753.4	9.7	3.0	31.0
105-645E-37R	19	1400	753.4-763.0	9.6	9.0	93.3
105-645E-38R	19	1530	763.0-772.7	9.7	9.7	99.6
105-645E-39R	19	1730	772.7-782.3	9.6	7.0	72.4
105-645E-40R	19	1930	782.3-792.0	9.7	9.1	93.8
105-645E-41R	19	2145	792.0-801.6	9.6	9.6	100.2
105-645E-42R	19	0230	801.6-811.2	9.6	9.4	98.3
105-645E-43R	21	1930	811.2-820.8	9.6	9.7	100.8
105-645E-44R	21	2215	820.8-830.5	9.7	9.7	100.1
105-645E-45R	22	0030	830.5-840.1	9.6	6.9	71.8
105-645E-46R	22	0245	840.1-849.7	9.6	5.9	61.8
105-645E-47R	22	0530	849.7-859.4	9.7	0.1	0.8
105-645E-48R	22	0830	859.4-868.6	9.2	5.2	56.1
105-645E-49R	22	1115	868.6-878.2	9.6	8.9	92.8
105-645E-50R	22	1430	878.2-884.9	6.7	6.7	100.6
105-645E-51R	22	1615	884.9-887.9	3.0	3.1	103.7
105-645E-52R	22	1800	887.9-897.6	9.7	6.7	69.5
105-645E-53R	22	2030	897.6-907.2	9.6	9.5	98.6
105-645E-54R	22	2230	907.2-916.8	9.6	9.3	97.2
105-645E-55R	23	0115	916.8-926.6	9.8	9.9	100.9
105-645E-56R	23	0330	926.6-936.2	9.6	9.2	96.0
105-645E-57R	23	0600	936.2-945.9	9.7	8.8	90.6
105-645E-58R	23	0915	945.9-955.6	9.7	7.7	79.5
105-645E-59R	23	1130	955.6-965.3	9.7	9.9	102.1
105-645E-60R	23	1430	965.3-974.9	9.6	9.4	97.6
105-645E-61R	23	1715	974.9-984.5	9.6	9.2	95.5
105-645E-62R	23	1915	984.5-994.2	9.7	8.7	89.5
105-645E-63R	23	2115	994.2-1003.9	9.7	9.3	95.4
105-645E-64R	23	2315	1003.9-1013.6	9.7	7.4	75.8
105-645E-65R	24	0115	1013.6-1023.3	9.7	9.8	101.2
105-645E-66R	24	0315	1023.3-1032.9	9.6	8.6	90.0
105-645E-67R	24	0645	1032.9-1042.6	9.7	8.8	90.3
105-645E-68R	24	0845	1042.6-1052.2	9.6	9.4	98.3
105-645E-69R	24	1200	1052.2-1061.9	9.7	9.1	94.0
105-645E-70R	24	1430	1061.9-1071.1	9.2	8.2	88.9
105-645E-71R	24	1600	1071.1-1080.7	9.6	6.3	65.8
105-645E-72R	24	1800	1080.7-1090.4	9.7	9.4	97.1
105-645E-73R	24	2045	1090.4-1099.8	9.4	7.1	75.9
105-645E-74R	24	2230	1099.8-1109.3	9.5	9.3	98.3
105-645E-75R	25	0000	1109.3-1118.8	9.5	5.7	59.5
105-645E-76R	25	0145	1118.8-1128.2	9.4	9.1	96.8
105-645E-77R	25	0415	1128.2-1137.7	9.5	7.9	82.8
105-645E-78R	25	0645	1137.7-1147.1	9.4	8.3	87.7
Hole 645F						
105-645F-1H	28	0515	0.0-4.0	4.0	4.0	101.0
105-645F-2H	28	0700	4.0-13.5	9.5	1.1	11.6
105-645F-3H	28	0800	13.5-23.0	9.5	7.2	75.8
Hole 645G						
105-645G-1H	28	1030	1.0-7.5	6.5	6.4	98.0
105-645G-2H	28	1130	7.5-17.0	9.5	2.1	22.3

tem appeared normal, we advanced the APC to a depth of 2040 mbsl and tried, with little success, to fire it by increasing the hydraulic pressure. Then we decided to trip out the entire drill string to find the cause of this resistance. When the last section of the drill string arrived on board, we discovered that the BHA had broken off and one of the pipes was badly bent. This could only have been caused by a mistake in calculating the water depth. Furthermore, the driller had failed to identify bottom by a change in the weight indicator. On close inspection, we found that a mistake had been made in calculating the water depth from the DES because of a misreading of the Matthews tables.

The correct depth was then calculated to be 2016 m from the DES.

A new BHA was made up and, together with the drill string, was lowered to a depth of 2013 m from the DES. An APC having soft shear pins was lowered, but when the shear pins could not be fired even at 3000 psi, an overshot device was lowered to retrieve the core barrel. It too failed to retrieve the core barrel. Finally, the entire drill string was tripped out to retrieve the barrel and to inspect the BHA. We found that the core barrel was shot and fully extended, but upon retrieval, it jammed at the pen end of the seal bore of the drilling collar. A 4.9-m-long core was recovered from this core barrel (Hole 645A). Tests were then carried out by lowering the drill string with the same BHA to a depth of 130 m below the DES and shooting the APC at 1600 psi. The APC was found to be properly seated but stuck.

Another BHA was assembled and tested with XCB at a depth of 150 m below DES. When everything looked satisfactory, the drill string was lowered to a depth of 2017 m below the DES with XCB in place. The drill string was circulated at a pressure of 1600 psi, followed by a pressure of 300 psi. We again tried to core the mud line (from 2017 to 2022 m [DES]). Upon retrieving the core barrel (CB), we found that the lower part of the barrel had dropped off on the seafloor. This failure was caused by a nut stripping off the shaft mandrel. We then offset the ship 50 ft to the east and dropped a new XCB but were unable to circulate even at 3000 psi. An attempt was made to core the mud line, but the XCB was retrieved with no core.

We again tripped out the drill string and disassembled the BHA from the bit upward to find the cause of this failure. The problem was resolved when we discovered an eccentric bore (0.5 in.) through the head sub (0L1010-5), causing the APC and XCB barrels to stop before seating. Once the head sub was replaced, the core barrel passed through it and seated properly.

Hole 645B

We tripped in and started coring Hole 645B at 0830 hr UTC, 7 September 1985 with the XCB corer. Core recovery for the first 168 mbsf was only 35%. Glacial rocks and boulders were encountered through the first 200 mbsf. Recovery to total depth at 298 mbsf increased to about 90%. Hole conditions were good to 260 mbsf, where some drag was encountered and the bit was partly plugged. We dropped the core barrel with bit plugged and increased pressure to 2500 psi. The pressure dropped to 200 psi at 40 strokes. On retrieving the core barrel, we found that the pressure drop occurred when the nut again stripped off the core barrel mandrel, leaving the bottom part of the XCB barrel inaccessible at the bottom of the hole. This was the second failure of the drive mandrel within 2 days. The hole was filled with 11.5 parts per gallon (ppg) mud to comply with safety regulations. The lowest C1/C2 gas ratio of 560 was in Core 105-645B-21X. Meanwhile, a large iceberg had arrived within 0.5 mi from the danger zone. If the core barrel had not stopped us, this iceberg would have. The string was tripped out to clear the mud line.

Hole 645C

While waiting for the iceberg to move away from the drill ship, we decided to collect a few more APC cores. After offsetting 16 m to the north, we positioned the bit at 2002 mbsl, and the first APC was shot from the mud line. Two soft pins were sheared at 1700 psi, and we recovered 4.4 m of ooze. The second APC core resulted in 0.3 m of recovery and a shattered core liner. The last core recovered 6 m and a collapsed liner. We tripped out the drill string to the mud line when the large iceberg entered the danger zone. The trip was completed at 1800 hr UTC, 10 September 1985. The ship had to move 1500 ft (500 m) while the large iceberg passed within 0.25 mi of our site.

Hole 645D

On Hole 645D, we decided to try rotary coring rather than XCB coring because the formation was beginning to get harder and we wanted to ensure that rotary coring could be carried out to target depth if we decided to try setting a reentry cone. A new BHA for rotary coring (RCB) was made and lowered to 150-m depth to check for proper seating of the core barrel into the new BHA. When we found that it was correctly seated, the core barrel was retrieved, and we continued tripping the pipe into the mud line at 2008 mbsl. At this point, a center bit was lowered and used for drilling. The bit encountered something hard (probably a boulder) at 22 mbsf. Because only 25% of the BHA was below the mud line, intense danger of breaking the BHA by drilling through this boulder layer caused us to decide to move the ship to a new location. We cleared the mud line, offset the ship 75 ft (25 m) east, and respudded Hole 645D. We drilled to 2273 mbsl, losing about 1.5 hr as a result of a power-supply failure to the coring winch. During drilling to 2273 mbsl, three multishots were taken, one at 2097 mbsl showing 2.75° deviation, another at 2213 mbsl showing 2.25° deviation, and the last at 2273 mbsl showing 2.75° deviation.

We commenced rotary-core-barrel (RCB) coring at 2283 m and cored silty sandy clay having glacial dropstones. Cores 105-645D-3R through 105-645D-7R taken from 2290 mbsl (282 mbsf) to 2338 mbsl (330 mbsf) resulted in recovery of only 0.5 m of core. Gas samples, which had been collected routinely from all the core samples as soon as they were pulled from the core barrel, showed an increase in ethane/methane ratio at this level. For this reason we felt it essential to have better recovery in this interval. The drill string continued to rotate, giving no indication of extra torque or drag. The poor recovery was thought to have been caused by a small boulder lodged in the throat of the bit. To dislodge this obstruction, a center bit was deployed, and we drilled from 2338 to 2348 mbsl. Core 105-645D-8H produced 4 m of very dark, hard core. Drilling continued normally to Core 105-645D-20H at 2473-mbsl depth (462 mbsf), when two icebergs, which had been about 1–2 mi away from the danger zone (2.5-m radius), moved into the danger zone. At this time we decided to stop drilling, fill the hole with 11.5 ppg mud, and perform a jet-in test for deploying a reentry cone.

The pipe was then tripped out until the bit cleared the mud line. The ship moved 200 ft east, and the entire drill string was circulated with seawater to wash out some ice, which had apparently formed in the drill pipe as the result of relatively fresh water circulated through the string at low bottom-water temperatures (about 0.5°C). This was discovered during the tripping-out operation, when long cylinders of frozen mud slid out onto the rig floor as stands of pipe were removed from the drill string. We jetted in (without rotating the drill pipe) from the mud line at 2008–2023 mbsl, encountered positive resistance at 15 mbsf, and decided to move 50 ft east of this site for another test. We jetted in from the mud line to 2029 mbsl (21 mbsf) and again encountered firm resistance from 12 to 15 mbsf and another interval at 20 mbsf. At this point, we decided to terminate the test because the two icebergs were still in the danger zone and to trip out the pipe to begin assembly of a reentry cone.

Hole 645E

Once the reentry cone was ready (partly assembled during port call at St. John's), it was moved over the moonpool doors under the rotary table for testing. Seventeen meters of 16-in. casing were run and landed above the cone throat. A 14¾-in. bit with a jetting BHA (without the bumper subs) was made up. After some adjustments, which took about 10 hr, the double-J running tool function was tested. Three icosahedrons and one ODP-design reflector were mounted on the cone, and the entire

reentry cone assembly was lowered through the moonpool at 1200 hr UTC, 14 September.

During this operation, the icebergs had moved out of the danger zone, the closest iceberg being 3 mi from the drill site. Since the reentry cone with 21 m of casing could be raised above the mud line quickly in case the iceberg moved near the drill site, we decided to try jetting in the reentry assembly. Jetting in took much longer than anticipated because of the resistance encountered at 14–20 mbsf. After lowering the double-J tool, we drilled to 2050 mbsl (42 mbsf), then released the reentry cone and continued the trip out to change the bit and remove the double-J running tool.

Penetration rates for Holes 645B, 645D, and 645E are shown in Figure 7.

Reentry 1

The drill string together with a rotary-coring BHA was tripped into 1098 mbsl. Then we lowered the Mesotech sonar and scanned for reentry starting at 1800 hr UTC, 15 September. We scanned for 1.5 hr but failed to locate the cone. We then retrieved the Mesotech, ran the Edo tool, and scanned for 1 hr, but the signal was still too weak to pick up reflectors. Thus, we retrieved the Edo tool to check the system and replaced a PC board in the Edo sonar display. The same Edo was re-run, but the signal remained too weak to identify reflectors. It was then replaced by the Mesotech tool. We ran the Mesotech tool and made reentry after scanning 20 min at 0815 hr UTC, 16 September.

Then we drilled (washed) from 2050 to 2309 mbsl and cored from 2309 to 2338 m because we missed this section in Hole 645D, and still we recovered very little. We drilled from 2338 to

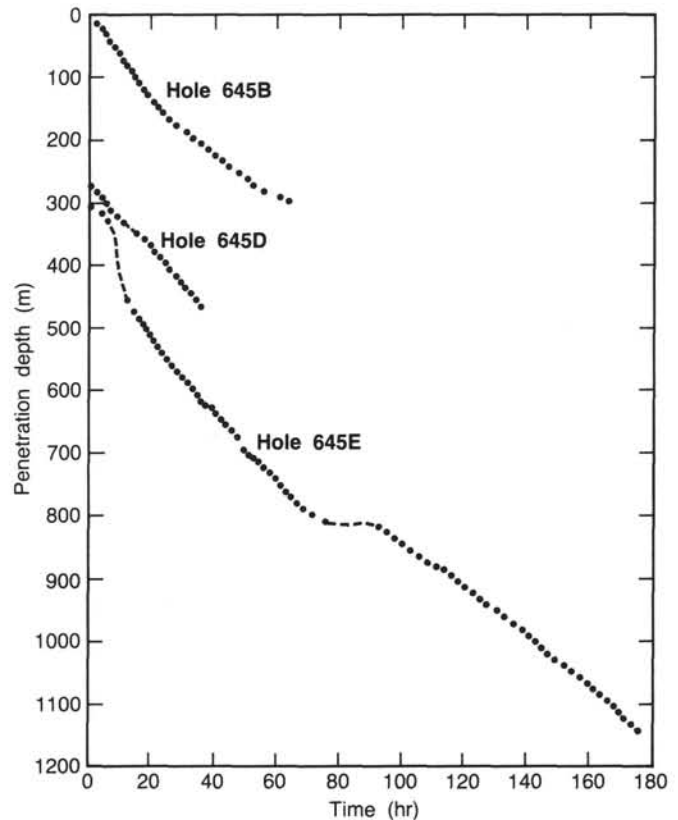


Figure 7. Penetration rates in Holes 645D and 645E.

2463 mbsl and cored silty clay from 2463 to 2819 mbsl. Rather than lose time waiting on an iceberg that had moved into the danger zone, we decided to trip out and change the bit because the bit appeared to be showing signs of wear. We cored 385 m and recovered 348 m for a 64% recovery.

Reentry 2

The drill string was tripped in with a new bit to 1098 mbsl. The plan was to reenter before waiting for the iceberg to leave the danger zone. The Mesotech tool was lowered and a reentry attempted after scanning 1.75 hr starting at 2115 UTC, 20 September. We retrieved the sonar tool and lowered the drill string to 2021 mbsl; a change in weight indicated a "mis-stab." We raised the bit above the cone and attempted another reentry after scanning for 0.75 hr. Apparently, we had another mis-stab. Then we lost the signal from the sonar tool. After retrieving the Mesotech tool, we lowered the Edo tool, and this time reentered after scanning for 1.5 hr at 0800 UTC, 21 September.

After having spent 24 hr in the danger zone, the iceberg moved into the yellow zone. By the time we had drilled 450 mbsf, two growlers were spotted 0.5 mi from the rig. We set back the top drive, pulled out of the hole to 2213 mbsl, and offset the ship 500 ft (165 m) east. After 1.5 hr, the growlers had passed. We positioned the ship over the reentry cone and resumed drilling.

We cored silty gray clay (shale) from 2819 to 3155 mbsl. The hole conditions were good. We cored 336 m and recovered 288 m, resulting in an 85% recovery. We suspended coring operations at 3155 mbsl at 0645 UTC on 25 September to prepare for logging because our schedule required departure from the site within 48 hr. Seawater was circulated for 0.5 hr. After spending 3.5 hr trying unsuccessfully to release the hydraulic bit release (HBR), we pulled out of the hole to remove the BHA and core bit. The drill string was tripped out to remove the HBR and rotary core bit. A logging BHA was made up and tripped into 1098 mbsl.

Reentry 3

We lowered the Edo tool (0845 UTC, 26 September), and when it did not seat properly, we retrieved it. We discovered that the landing ring was oversized, causing the sonar tool to seat too high. We changed its landing shoulder and lowered it again. We started scanning for reentry at 0100 hr UTC, 26 September, and reentered the hole after scanning for 2.75 hr. We retrieved the sonar tool and lowered the drill string to logging depth at 194 mbsf.

The logging tools, consisting of DIL, LSS, GR, and MCD, were rigged and lowered down the drill string. A bridge was encountered at 2250 mbsl. The logging tools were retrieved, and the drill string was lowered to 2250 mbsl to clean out a 3-m bridge. The drill string was tripped in 2490 mbsl, and no evidence of additional obstructions was found. By the time the string was tripped out to 2305 mbsl, a huge iceberg had started drifting into the danger zone. We decided to trip to the bottom (3149 mbsl) and fill the hole with weighted polymer mud because small amounts of gas had been measured in the lower 700 m of the hole. The hole was then filled with 11 ppg polymer mud, and the drill pipe was tripped out to 2083 mbsl. By this time, the iceberg had drifted past the ship at a distance of 2.5 mi.

The same logging tool was lowered down the drill string. Another bridge was encountered at 2359 mbsl. We retrieved the logging tools and lowered a clean-out bit to free the bridge. A solid bridge encountered at 2359 mbsl was cleaned at 1500 psi. The string was tripped out to 2308 mbsl, and the same logging tools were lowered after a minor mishap, which damaged neither equipment nor personnel. We logged to a depth of 2450 mbsl, where another bridge was encountered that could not be

cleared without retrieving tools. At this point, we decided to end the logging operation and retrieve all the equipment. Operations finished at this hole (0230 hr UTC, 28 September) after the hole was filled with 11 ppg polymer mud. Altogether, we devoted 68 hr to logging and made every attempt to clear sediment bridges to obtain at least one continuous log with the sonic-caliper-GR-resistivity tool, perhaps at the cost of not reaching our deep R3 reflector objective at about 1500 mbsf.

Holes 645F and 645G

Because of the poor recovery in the upper part of the section on previous holes, we decided to use the APC on the upper 50 m, again with limited time remaining. Another BHA was made up for the APC, and three APC cores were collected between 2018 and 2041 m from the DES. On the fourth APC run, when a rock was encountered, we decided to trip out to the mud line and try for two more cores, which were recovered at this site (Hole 645G) before operations ended. By 1845 hr UTC, 28 September, all equipment was secured on board, and *JOIDES Resolution* departed for Site 646 in the Labrador Sea, towing seismic gear and a magnetometer at 8 kt and following the ice-surveillance boat, *Chester*.

In addition to the numerous technical difficulties, operations at this site were hindered by the movements of icebergs and growlers. Forty-three icebergs were observed within a radius of 20 mi of the drill ship. Many of these passed us within a radius of 5 mi. On three occasions, the drill ship had to move from its position to avoid a collision. A composite chart (Fig. 8) shows the movements of these icebergs during the time the drill ship occupied Site 645. Whether the drilling program would have suffered greatly without the ice-surveillance boat, *Chester*, is uncertain, but its presence allowed for operation with much more confidence and ease.

SEDIMENTOLOGY

Three lithological units are recognized at Site 645 (Table 2; Fig. 9A). Relatively poor sorting, a dominance of subangular to subrounded grains, and poorly developed primary physical sedimentary structures generally characterize the sediments. Gravel is present in both Units I and II, is minor in Subunit IIIA, and is rare in Subunits IIIB and IIIC. The sediments are also mineralogically immature, suggesting low-intensity chemical weathering of source rocks.

Unit I (0–168.1 mbsf) is dominated in its upper part (Subunit IA) by lithologic cycles of detriticarbonate muddy sands and gravel-bearing muddy sands, detriticarbonate silty muds, and silty clays (Fig. 9B) having a mean carbonate content of about 20% (Fig. 10). The carbonate component is entirely detrital (eroded from older rocks) and consists of about twice as much dolomite as calcite (Fig. 10). All parts of Unit I contain large pebbles and cobbles, ranging in size up to at least the diameter of the plastic core liner (6 cm). Some larger cobbles were cored or were able to enter the core liner with their long axis (>6 cm) aligned vertically. The upper part, Subunit IA (0–71.6 mbsf), is coarser than the lower part, Subunit IB (71.6–168.1 mbsf). Subunit IA has a mean sand content of about 50% (smear slide data). Subunit IB (71.6–168.1 mbsf) averages <10% sand and consists predominantly of detriticarbonate silty muds and silty clays.

Unit II (168.1–335 mbsf) contains an average of only about 5% detrital carbonate and is generally coarser grained than Subunit IB but finer grained than Subunit IA (Fig. 9). Major lithologic compositions are silty mud, clayey silt, and silty clay (Fig. 9) and scattered large pebbles and cobbles of igneous, metamorphic, and carbonate (limestone and dolostone) rocks. Burrows and evidence of bioturbation, black iron sulfide particles, and streaks are common. Near the base of Unit II (274–284 mbsf) is

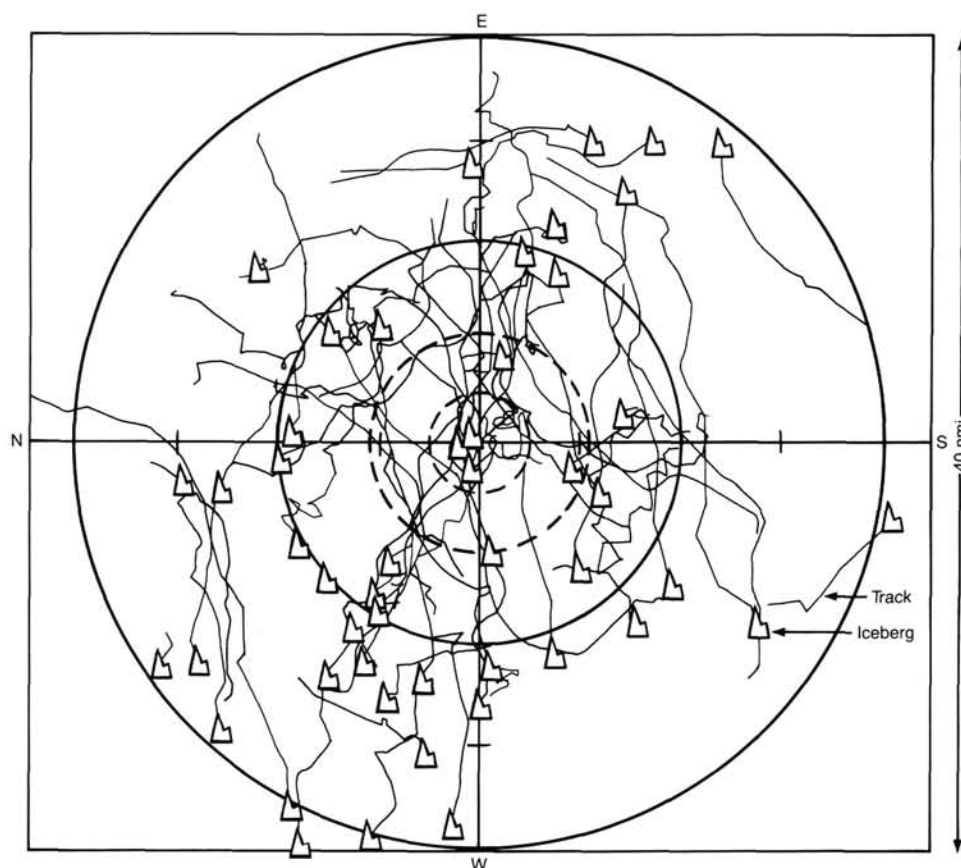


Figure 8. Mims ice map showing iceberg and growler tracks at Site 645, 3 through 28 September 1985.

Table 2. Lithostratigraphy summary, Site 645.

Unit/ subunit	Lithology	Sedimentary structures	Interval (mbsf)	Age	Occurrence
IA	Alternating beds of detrital muddy sand and silty mud, with scattered dropstones to cobble size. Carbonate content = 30%-40%. Dolomite/calcite = about 2:1.	Cyclicality of lithofacies on scale of tens of centimeters to 1-2 m. Dropstones. Slight bioturbation.	0-71.6	Pleistocene-Holocene	105-645A-1H; 105-645B-1X to -8X; 105-645C-1H to -3H; 105-645F-1H, to -3H; 105-645G-1H to -2H
IB	Alternating beds of detrital silty clay to silty mud, with dropstones to cobble size. Carbonate content = 30%-40%. Dolomite/calcite = about 2:1.	Cyclicality of lithofacies on scale of tens of centimeters to 1-2 m. Dropstones. Slight bioturbation.	71.6-168.1	Pleistocene	105-645B-9X to -18X
II	Noncarbonate silty mud, clayey silt, and silty clay, with dropstones to cobble size. Scattered iron sulfides. Carbonate content = 5%-10%, almost entirely dolomite.	Cyclicality of lithofacies on scale of tens of cms to meters. Dropstones. Locally laminated. A homogeneous layer of fine sand (about 5 m thick) occurs near base of unit.	168.1-335	Pliocene-early Pleistocene	105-645B-19X to -32X, 105-645D-1R to -6R, 105-645E-1R to -3R
IIIA	Poorly sorted muddy sand and sand-bearing silty mud, with scattered, predominantly shale, pebbles in coarser beds. Maximum quartz grain size ranges to granules.	Homogeneous, slightly bioturbated silty muds with few primary structures. Variations in grain size are on the scale of meters, with gradational boundaries. Interspersed are sharp-based graded beds, ranging in thickness from about 20 cm to 1 m.	335-753.4	late Miocene-Pliocene	105-645D-8R to -20R, 105-645E-4R to -36R
IIIB	Muddy sandstone and silty mudstone, interbedded with well-laminated carbonate-rich silty claystones. Organic carbon content to about 3%. Scattered pyrite and wood fragments.	Moderate to strong bioturbation of various burrow types, spreiten filled. Silty claystones are well-laminated in cm-thick layers.	753.4-916.8	Middle-late Miocene	105-645E-37R to -54R
IIIC	Fine- to medium-grained muddy sandstone and silty mudstone. Sandstone occasionally glauconite-bearing (as much as 10%).	Moderate to strong bioturbation in coarser facies. Some fine-grained intervals are well stratified. A few horizons show features of soft-sediment deformation.	916.8-1147.1	Early-middle Miocene	105-645E-55R to -78R

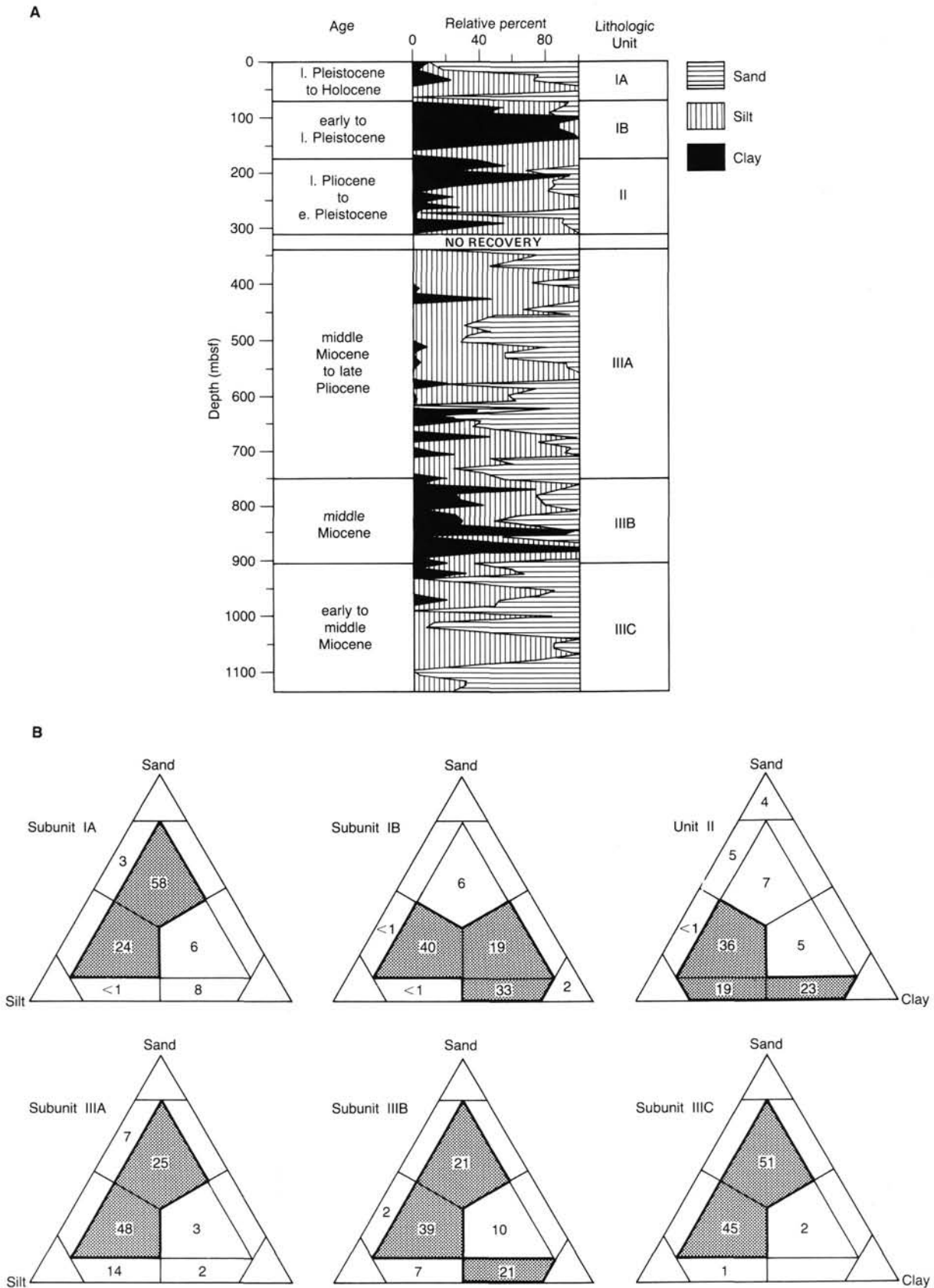


Figure 9. A. Summary of lithologic variations with depth in Holes 645A through 645G, showing percentage in single cores of clay-rich lithologies (clay, silty clay, sandy clay, clayey mud—solid pattern), silty lithologies (silt, clayey silt, sandy silt, silty mud—vertical pattern), and sandy lithologies (sand, silty sand, clayey sand, muddy sand—horizontal rule). Boundaries of Lithologic Units I, II, and III, as well as subunit boundaries, are indicated. General attributes of these units are summarized in Table 2. B. Percentages of lithologies in units and subunits. The major lithologies are outlined in black and stippled.

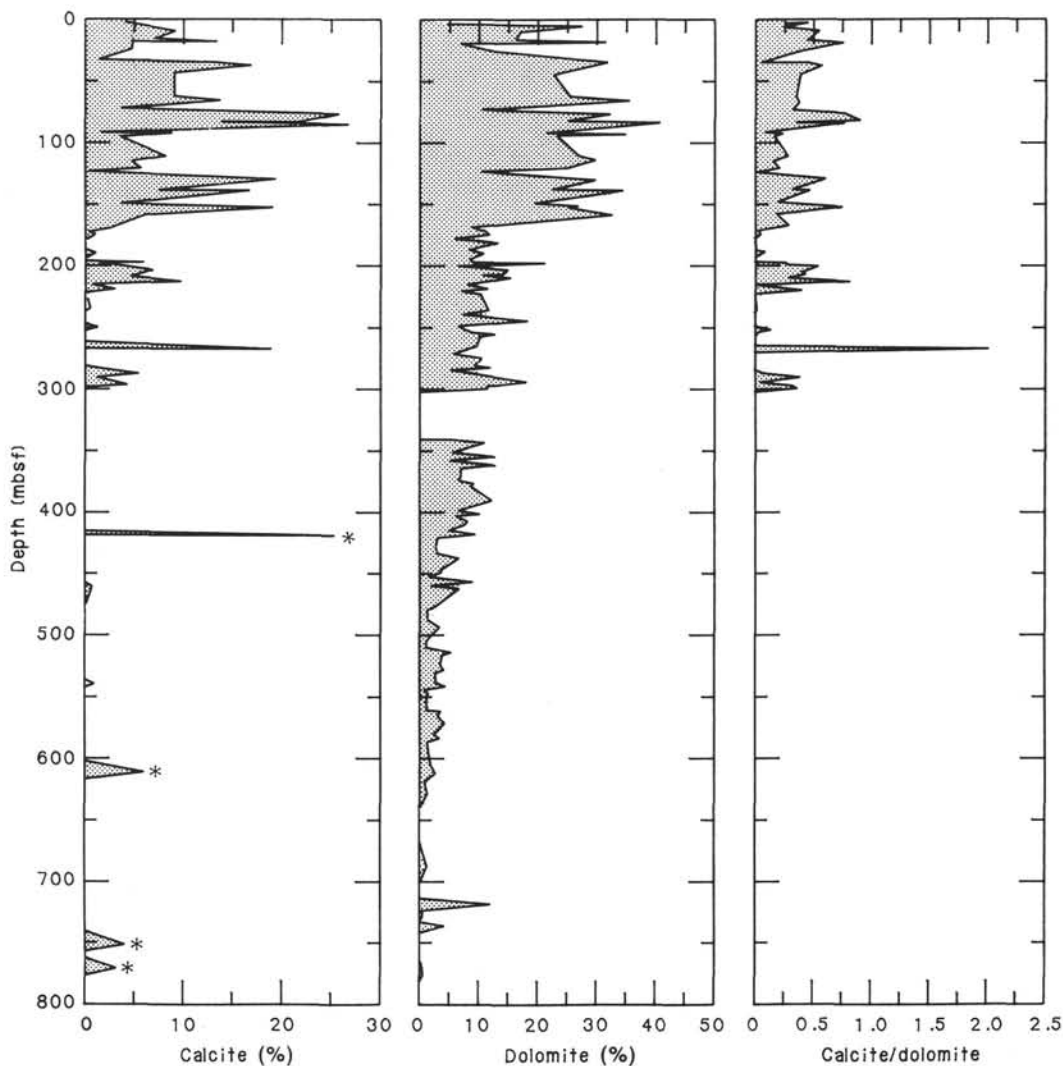


Figure 10. Abundances of carbonate minerals with depth, approximately to the top of Subunit IIIB, based on XRD data. Note that the ratio of calcite/dolomite is consistently < 1 and eventually approaches zero. Peaks on the "calcite" plot marked by an asterisk (*) are not calcite but rather mixtures of siderite and rhodocrosite.

an interval of moderately sorted, fine-grained sand and silty sand.

The contact between Units II and III occurs within a 40-m interval of poor recovery but is more tightly constrained to a 4-m interval (332–336 mbsf) by downhole logs (see "Downhole Logging" section, this chapter). The progress and style of drilling, as well as the poor recovery, suggest an interval of sediment characterized by abundant gravel, although no dramatic lithologic change appears in the 40-m interval ("Downhole Logging" section).

Unit III (335–1147.1 mbsf) is devoid of large pebble and cobble clasts (> 2 –3 cm) and is divided into three parts, Subunits IIIA, IIIB, and IIIC (Fig. 9A), the transitional passages between the subunits being somewhat arbitrarily placed between Cores 105-645E-36R and 105-645E-37R (753.4 mbsf) and between Cores 105-645E-54R and 105-645E-55R (916.8 mbsf). Subunit IIIA is characterized by scattered pebble-sized clasts, predominantly black shales, and minor amounts of pebbles of friable sandstones, carbonates, and granitic rocks. These occurrences decrease downsection. Major lithologic compositions are homogeneous, poorly sorted muddy sands and sand-bearing silty

muds (Fig. 9B) having few primary physical structures; the sediments are commonly bioturbated. The features of some interspersed muddy sands suggest a density-current origin. These sand units have relatively sharp bases, are apparently free of bioturbation, show a poorly developed, delayed grading (i.e., most of the grading being at the top of the bed), and occur in units approximately 50–100 cm thick. Except for the sharp-based muddy sands, the boundaries between lithologic units are very gradational. Subunit IIIB is dominated by fine-grained to very fine grained muddy sandstones, silty mudstones, and carbonate-rich silty claystones (Fig. 9B). Faint lamination and moderate to strong bioturbation (e.g., *Zoophycos* type) are characteristic. Small gastropods and black woody fragments are present but rare. Subunit IIIC is almost entirely composed of muddy sandstones and silty mudstones (Fig. 9), bioturbated except for small intervals having distinct parallel lamination in some of the muddy sandstones. Glauconite grains are locally prominent in the sand fraction, at a few places forming a major constituent. Soft-sediment slide folds occur in Core 105-645E-66R.

Five samples of clay-size sediment were analyzed using the shipboard X-ray diffractometer (XRD). Sample preparation was

simple (see "Explanatory Notes" chapter, this volume), and only a few samples were analyzed; therefore, only general conclusions are possible.

Dissolved components, mainly Na^+ and Cl^- in the pore water, precipitated on the surface of the preparation; consequently all samples contain halite. Except for a sample at 459.7 mbsf, which was taken from the central part of a burrow, all samples contain kaolinite, chlorite, illite, feldspars, and a broad band ranging from 5 to 7.5 Å, indicating the presence of expandable lattice elements (Table 3). Whether their elements are incorporated in mixed-layer minerals or they represent discrete smectitic minerals is impossible to demonstrate using this method. Pyrite is present in two samples, whereas carbonates are in three samples, dolomite being the most abundant phase in two of these samples. The sample from the burrow differs highly from the other four samples. Chlorite and expandable lattice elements are absent, and pyrite is abundant.

The presence of kaolinite probably indicates the reworking of older sediments containing kaolinite. Kaolinite is not likely to have formed under the relatively cold climatic conditions that prevailed during deposition of the upper parts of the cored interval from which the clay samples were obtained.

In addition to the analyses of clay-size material, approximately 200 samples were analyzed using the X-ray diffraction (XRD) method for bulk mineralogy. Unfortunately, it was possible to obtain an XRD record down to only about 800 mbsf (Hole 645E, Core 105-645E-41R) because the X-ray diffractometer failed to function properly.

Results of the XRD analyses are summarized in Figures 11 and 12, showing the percentages of clay (illite + kaolinite + chlorite), quartz, feldspar (K-feldspar + plagioclase), and carbonates (calcite + dolomite).

The general trend in amount of clay minerals indicates a continuous increase with depth. The clay minerals are less important in the upper 300 m (i.e., in Lithologic Units I and II), ranging between 0% and 30%. In Subunit IIIA, clay minerals range between 15% and >50%. The maximum values are recorded between 680 and 800 mbsf, i.e., near the boundary of Subunits IIIA and IIIB.

Quartz is the dominant mineral phase throughout the entire sediment section of the upper 800 m (Fig. 11). Most of the sediments have a quartz content of about 40%–60%. Somewhat lower abundances (20%–50%) occur in Unit I. In most samples, the quartz/feldspar ratio fluctuates between 2 and 7 (Fig. 12). Near the boundary of Units I and II, a distinct maximum occurs, quartz/feldspar ratios being >15.

Feldspar contents are generally 10%–25% (Fig. 11). Intervals with dominantly low values occur in Subunit IB and near the boundary of Subunits IIIA and IIIB. Units II and III are characterized by the occasional occurrence of feldspar bursts of >45%. K-feldspar/plagioclase ratios (Fig. 12) indicate that pla-

gioclase content increases in the upper 400 m. Below 400 m, K-feldspar becomes more abundant. The distinct feldspar spikes observed in Figure 11 are caused by a sharp increase in K-feldspar, shown by distinctly higher K-feldspar/plagioclase ratios, reaching values of 4–10 (Fig. 12).

The amount of carbonate minerals (i.e., calcite + dolomite) shown in Figure 11 agrees well with the results of the carbonate-bomb analysis (Fig. 56, "Summary and Conclusions" section, this chapter). Carbonate minerals are important components only to 170 mbsf (i.e., in Unit I) and range from 10% to 60% (Fig. 56). The dolomite/calcite ratio is about 2:1 (Fig. 10). In Unit II, carbonate varies between 10% and 20%, followed by a continuous decrease toward 0% in Subunit IIIA, mainly caused by a decrease of dolomite (see following discussion). The calcite content distinctly decreases below 170 mbsf, reaching 0% at about 300 mbsf (Fig. 10). The spikes below 300 mbsf (marked in Fig. 10 by asterisks) indicate the amount of siderite and rhodocrosite determined in those samples. Dolomite values are relatively constant at about 10% in Unit II. Subunit IIIA is characterized by a continuous decrease of dolomite to 0% at the bottom of this subunit.

Description of Units

Unit I: Hole 645A (Core 105-645A-1H), Hole 645B (Cores 105-645B-1X to 105-645B-18X), Hole 645C (Cores 105-645C-1H to 105-645C-3H), Hole 645F (Cores 105-645F-1H to 105-645F-3H), Hole 645G (Cores 105-645G-1H to 105-645G-2H); Holocene-Pleistocene; 0–168.1 mbsf

The uppermost unit extends from the seafloor to a depth of 168.1 mbsf and is characterized by alternating beds of gravel-bearing muddy sand and silty mud. The base of this unit is clearly defined in smear slides and in carbonate-bomb (Fig. 56, "Summary and Conclusions" section, this chapter) and XRD data (Fig. 10) by an abrupt decrease in carbonate content from approximately 40%–50% to 5%–10%. An increase in pyrite content with an associated darkening in color also marks the lower boundary.

Unit I is subdivided into two subunits defined by the varying importance of sand and detrital carbonate particles (Fig. 9A). Both subunits contain scattered pebbles and cobbles in roughly equal amounts (Fig. 13). Subunit IA, predominantly a muddy sand with interbedded silty muds and silty clays, however, is generally a coarse sediment having a mean sand content of about 50% (smear slide data). Subunit IA extends from the seafloor to 71.6 mbsf; Subunit IB extends from the base of Subunit IA to the contact with the underlying unit at 168.1 mbsf. Subunit IB contains <10% sand. Silty muds and clays predominate, interbedded by clayey muds (Fig. 9B). An additional distinguishing characteristic is the organic carbon content (Fig.

Table 3. Mineral percentages of the <2- μm fraction.

	Depth (mbsf)				
	194.0	311.6	321.0	457.0	459.7 burrow
Site 645 core section interval (cm)	105-645B-21X-5 61	105-645D-6R-1 23	105-645D-6R-CC 2	105-645E-4R-2 33	105-645E-4R-4 3
Illite (%)	51	49	45	36	27
Kaolinite + chlorite (%)	25	21	39	43	23
Quartz (%)	9	9	8	15	17
K-feldspar (%)	12	7	trace	7	24
Plagioclase (%)	3	12	7	0	0
Calcite (%)	0	trace	0	0	3
Dolomite (%)	0	2	1	0	0
Pyrite (%)	0	trace	0	0	6

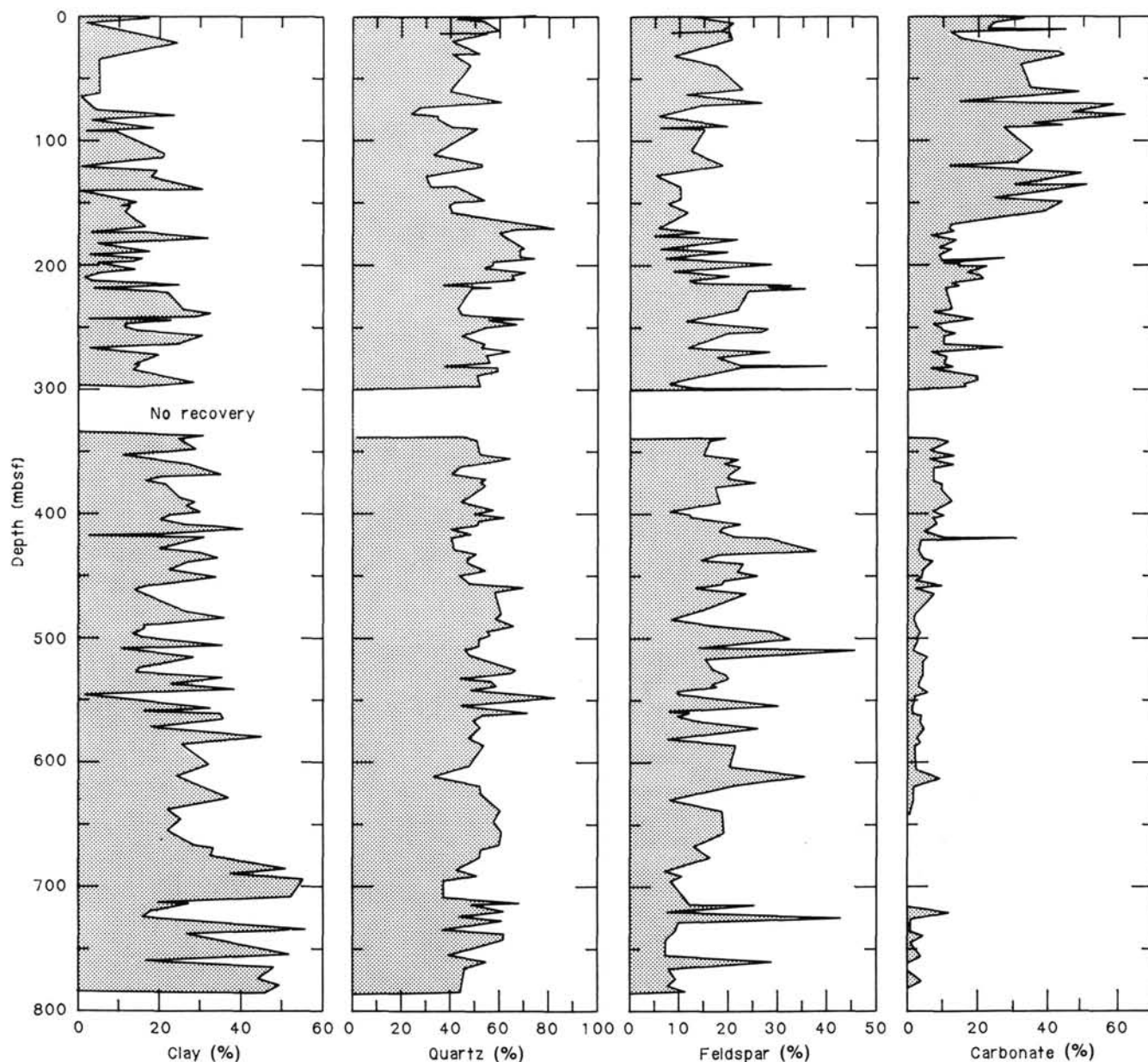


Figure 11. Stratigraphic variation of mineralogical composition, according to XRD data, to about the top of Subunit IIIB.

56), which averages about 0.5% in the sediments of Subunit IA but increases to an average of about 0.9% in Subunit IB. Organic carbon content peaks at 1.5% in Core 105-645B-13X (110–120 mbsf).

Five holes penetrated Subunit IA. The longest section was cored by XCB in Hole 645B, which reached the base of the subunit. Recovery averaged only 35% of the section. A variable amount of drilling disturbance occurred. Hole 645B and the shallow cores taken at Holes 645A, 645C, 645F, and 645G were successfully correlated by visual comparison of archive halves after abandonment of the site (Fig. 14). This correlation suggests that recovery of the uppermost 22 m was complete, except a 2.5-m-thick interval at a depth of about 10–13 mbsf.

Throughout Subunit IA, its most striking characteristics are the cyclicity of lithofacies, the presence of detrital carbonate, and the general paucity of microfossils (for paleontological details, see “Biostratigraphy” section, this chapter). Overall, the unit consists of distinct lithofacies in alternating layers, varying

in thickness from 10 cm to approximately 1 m. A sketch depicting the essential features of a typical cycle is presented in Figure 15. These layers consist of detrital carbonate muddy sands and silty muds, generally gravel bearing, which are lighter (pale gray and grayish brown to olive gray), interbedded with silty and clayey muds, which are generally darker (dark greenish gray and olive gray). The contacts between layers are sharp and distinct, although somewhat bioturbated (Fig. 16). The dark silty and clayey muds locally are slightly bioturbated and may contain 1–3-cm-thick, sharp-based, graded and laminated detrital carbonate silt layers (Fig. 17). In general, the detrital carbonate, light-colored beds are thicker than the dark clay/silt beds (see visual core-description forms).

In the upper part of Subunit IA (from 0 to about 40 mbsf), some layers are separated by a reddish zone, 3–10 cm thick, at the base of the gravel-bearing, lighter muddy sand or silty mud layers (Fig. 18). These zones consist of coarse iron-stained sand, containing discrete particles of iron-oxides; some quartz grains

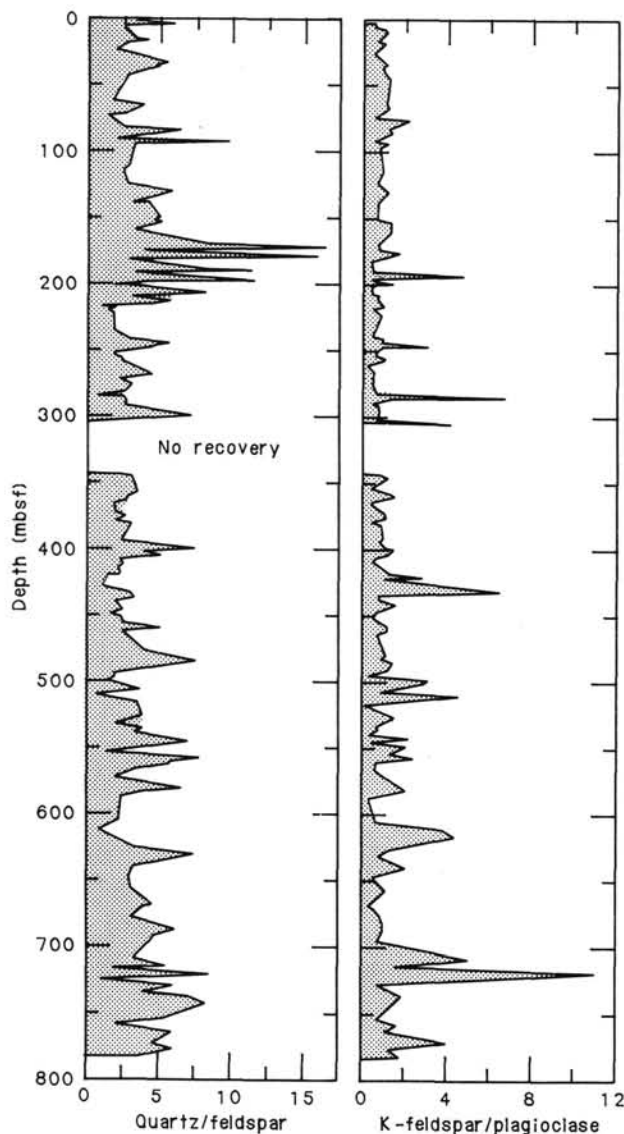


Figure 12. Stratigraphic variation of silicate mineral ratios to about the top of Subunit IIIB. Note the peak in the ratio of quartz/feldspar at the top of Unit II (168.1 mbsf).

are well rounded. Deeper in the sequence, these reddish zones disappear, and the lighter detriticarbonate muddy sands contact sharply with the darker clayey muds. Scattered cobbles and large pebbles are distributed throughout the unit, their occurrence apparently not being confined to any particular facies. The detriticarbonate muddy sands, however, contain more granules and fine pebbles of sedimentary origin and more coarse sand grains than do other lithofacies. Some dark clayey muds contain a coarse central zone with granules and cobbles of granitic and gneissic rocks. The unit is slightly bioturbated and mottled; otherwise these sediments are relatively featureless, having few distinct primary structures.

The correlation of cores from Holes 645A, 645B, 645C, 645F, and 645G (Fig. 14) revealed that some units, particularly the gravel-bearing detriticarbonate muddy sands and gravel-bearing silty muds, vary over short lateral distances (i.e., from tens to hundreds of meters) in maximum clast size, apparent thickness, and in some places degree of iron-oxide coloration.

Subunit IB consists mainly of interbedded detriticarbonate silty mud, detriticarbonate silty clay, and detriticarbonate clayey mud

(Fig. 9), having individual bed thicknesses of tens of centimeters. Some layers are a few centimeters thick. Detriticarbonate muddy sand and detriticarbonate clay are only rarely present. All contacts between lithofacies are gradational. Pebbles and cobbles are uniformly scattered in all lithofacies. The carbonate content varies from <10% to >50% and averages about 40% (Fig. 56). The most carbonate-rich layers are generally olive gray to light brownish gray, whereas the less carbonate-rich layers are dark gray and dark grayish brown. Primary sedimentary structures are rarely observed. Indistinct laminations occur in some intervals, whereas burrows were described only from one interval, which is <1 m thick.

Unit I consists almost entirely of terrigenous components (Figs. 11 and 12), including carbonate grains, and a small component of authigenic dolomite; scattered microfossils are only in the upper few sections. The carbonate component is primarily in the form of detrital particles showing the entire range of grain size from cobble to clay size. According to visual smear slide estimates, the lighter-shade layers in Subunit IA consist of about 40%–50% carbonate, whereas the darker clays contain only about 10% carbonate. Biogenic particles and authigenic minerals (e.g., pyrite) are rare, although pyrite is more abundant in Subunit IB than in Subunit IA. The carbonate particles in Subunit IB are commonly dominant in the silt fraction and probably also form a large part of the clay fraction. In both subunits, dolomite is approximately twice as abundant as calcite (Fig. 10).

Visual smear slide estimates show that biogenic opal skeletons constitute about 5% of the bulk surface sediment, which is predominantly in the form of diatom frustules with lesser amounts of sponge spicules and rare silicoflagellates and radiolaria. Examination at closely spaced intervals shows that these constituents disappear at the 15–20-cm level; only trace amounts of biogenic silica, entirely sponge spicules, occur beneath that depth.

In both subunits, the major sedimentary components are identical; lithofacies are distinguished only on the basis of different ratios between components. Muddy sands of Subunit IA consist of 30%–60% quartz, 10%–20% feldspar, 20%–35% carbonate, and 5%–20% clay minerals. Interbedded silty muds and clays consist of 20%–30% quartz, 5%–10% feldspar, 30%–60% carbonate, and 35%–40% clay minerals. In Subunit IB, silty muds consist of 20%–40% quartz, 5%–10% feldspar, 40%–60% carbonate, and 15%–20% clay minerals; whereas clayey muds and silty clays contain less quartz and feldspar grains but greater amounts of clay minerals. Mica, amphibole, pyrite, sphene, garnet, and epidote were identified in trace amounts as accessory minerals in this unit.

Unit II: Hole 645B (Cores 105-645B-19X to 105-645B-32X), Hole 645D (Cores 105-645D-1R to 105-645D-6R), Hole 645E (Cores 105-645E-1R to 105-645E-3R); early Pleistocene–Pliocene; 168.1–335 mbsf

Unit II is distinguished from Unit I primarily on the basis of carbonate content, which drops sharply from a mean of about 30% above 170 mbsf to <10% below that depth (Fig. 56). Silts and muds at the top of Unit II also reveal a distinct increase in the quartz/feldspar ratio (Fig. 14), indicating an enhanced mineralogical maturity and probable change in source area. The boundary between the units is placed at the top of Core 105-645B-19X. The average recovery for Unit II was 68%, in contrast to 35% for Unit I. The age of Unit II is not well constrained; its top is older than the youngest normal event within the generally reversed magnetic-polarity Matuyama Chronozone (i.e., older than 0.73 Ma; for details, see "Paleomagnetism" section, this chapter). The base of Unit II was not observed because of failure in three attempts (Holes 645B, 645D, and 645E)

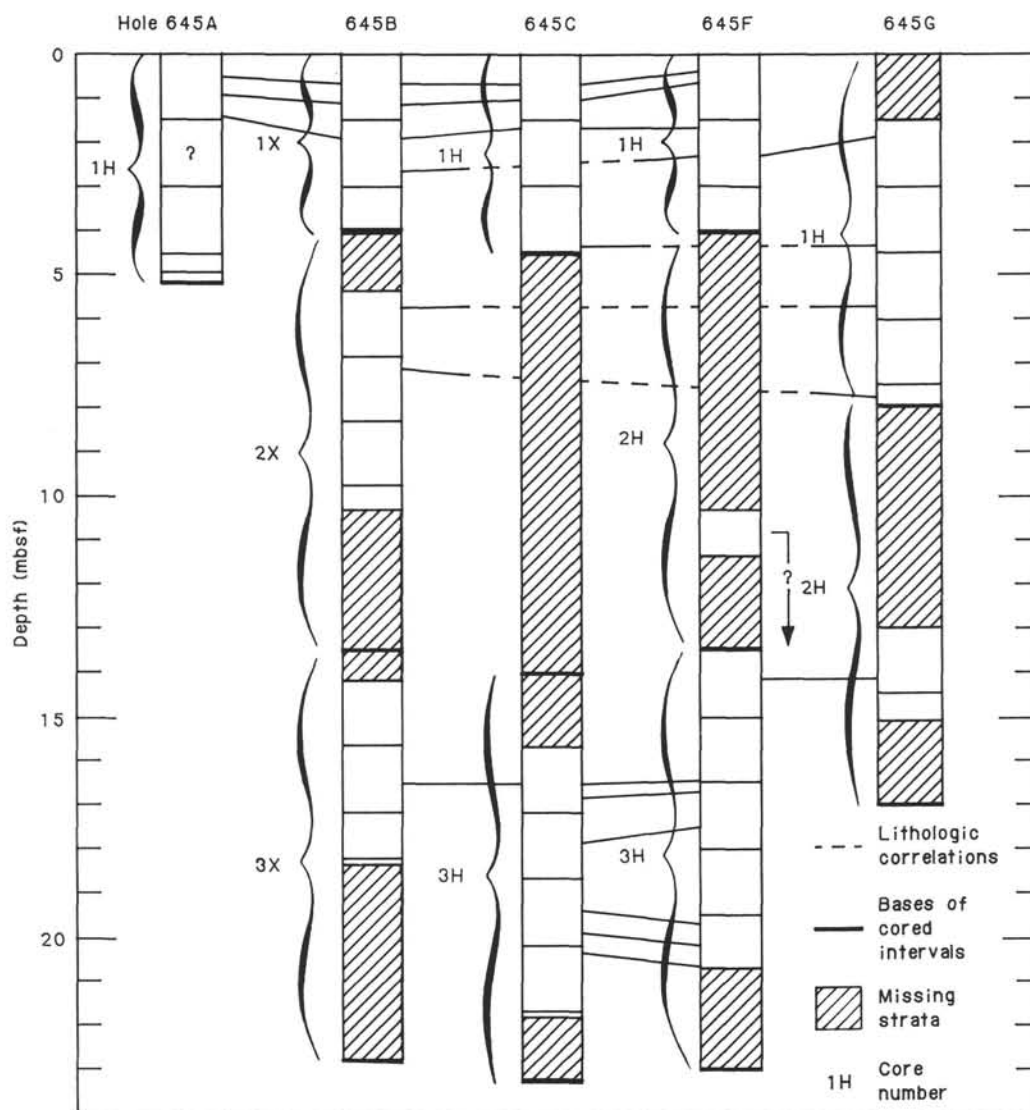


Figure 14. Correlation diagram of the upper parts of Holes 645A, 645B, 645C, 645F, and 645G, based on direct shipboard visual comparison of archive halves of cores and aided by correlation of plots of GRAPE data and magnetic susceptibility. Hole 645G did not core the mud line. The position of the single section of Core 105-645F-2H is constrained only by the observation that it shows no obvious overlap with either of Cores 105-645B-1X or 105-645G-2H. Solid tie lines indicate positive correlation between adjacent cores, whereas dashed tie lines indicate that correlation was not made with the core in the dashed interval.

to recover sediment from the interval at 320–340 mbsf. Analysis of well logs (see “Downhole Logging” section, this chapter) places the base between 332 and 336 mbsf. Drilling progress within the interval at 320–340 mbsf and our failure to recover these sediments suggest a relatively high gravel content, although downhole logs indicate no major lithologic changes.

Unit II consists mainly of gray, greenish gray to reddish gray silty mud (36% of the recovered sediments), gray to greenish gray clayey silt (19%), and dark-gray to dark greenish gray silty clay (23%) (Fig. 9B). Minor lithofacies are dark grayish brown to dark-gray muddy sand (7%), greenish gray silty sand (5%), dark greenish gray clayey mud (5%), and dark-gray sand (4%). Individual lithofacies form layers from tens of centimeters to a few meters thick and have gradational upper and lower contacts. A dark-gray, fine-grained sand forms a distinct 5.5-m-thick layer near the base of Unit II (Hole 645B, Core 105-645B-30X). This sand is relatively rich in heavy minerals (as much as 10%), foraminifers, and rare sponge spicules and diatoms, all

characteristic of neritic environments (see “Biostratigraphy” section, this chapter).

Upward-fining sequences on the scale of single sections (1.5 m), from muddy sand to silty mud, were observed in several cores (105-645B-21X, 105-645B-22X, 105-645B-29X, 105-645D-1R, and 105-645D-2R); however, the basal contacts of the muddy sands are gradational in thin upward-coarsening sequences. Visual observation failed to identify clearly defined sedimentary structures. In some cores, regularly spaced dark laminae probably result from smearing of iron sulfides along the margins of drilling biscuits rather than from the presence of primary sedimentary structures. The mottled aspect of some sediments is interpreted as being the result of bioturbation.

On the basis of smear slide examination and XRD analysis (Fig. 11; see preceding discussion of XRD), the nonclay fraction of the sediment consists mainly of detrital quartz (35%–85%), fresh feldspars (about 15% plagioclase and microcline), and detrital carbonate (about 10%). Bulk XRD analyses also indicate

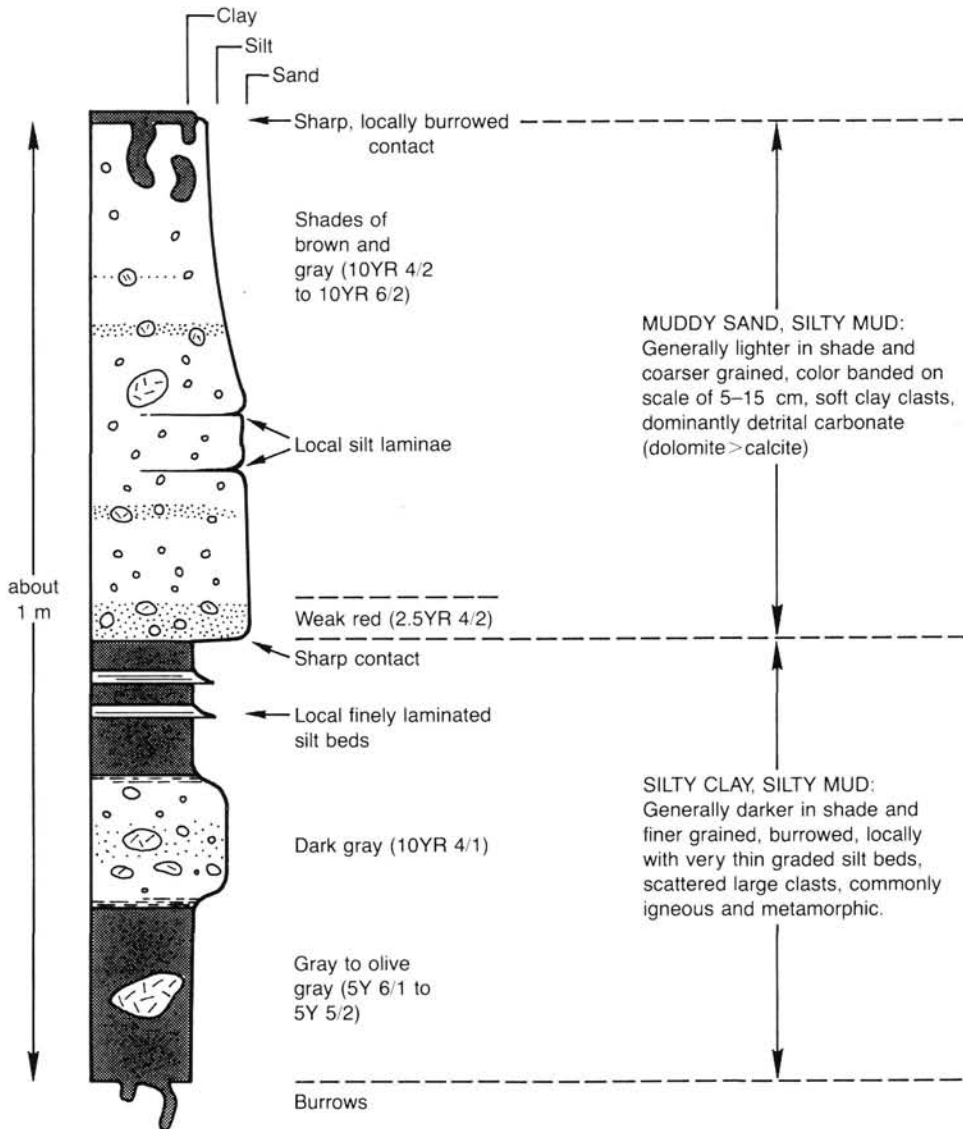


Figure 15. Composite sketch of the general features of a “typical” lithologic cycle in Subunit IA. These cycles vary greatly, and all units depicted may not be present. In particular, the thin, graded, silt/mud couplets in the darker, fine-grained interval were observed only in a few cycles.

that the carbonate is essentially entirely dolomite (Fig. 10). Accessory minerals in sand and silty sand layers include green or colorless amphibole, tourmaline, garnet, and epidote; volcanic glass is rare. Iron sulfide grains and granules may constitute as much as 10% of the sediment. In general, biogenic components are absent or rare in smear slides. Organic carbon contents (Fig. 56) are somewhat less than those in Subunit IB and average about 0.5%.

Granules, sand lenses and irregular sandy pockets, and pebbles and cobbles, some cored during drilling, as much as 7 cm in diameter, are scattered in all facies. According to observations on two thin sections (washed gravel from core catchers of Cores 105-645B-22X and 105-645B-26X), the pebbles consist of fine-grained limestone (15%–35%), fine-grained or subhedral granular dolostone (0%–20%), and granitic and gneissic rocks (10%–45%). Smaller sand- to granule-sized grains of quartz, feldspar, quartzarenite, and other sandstones were also noted.

The percentage of gravel (granule size and coarser) decreases downsection from 5%–20% in Cores 105-645B-19X to 105-645B-22X to 0%–5% in Cores 105-645B-23X to 105-645B-30X of

Hole 645B but slightly increases near the base of the unit (0%–10% in Cores 105-645B-31X, 105-645B-32X, 105-645D-1R, and 105-645D-2R). This same variation is indicated by the number of large pebbles per meter of recovered core (Fig. 15).

Unit III: Hole 645D (Cores 105-645D-8R to 105-645D-20R), Hole 645E (Cores 105-645E-4R to 105-645E-78R); Pliocene–early Miocene; 335–1147.1 mbsf

The total thickness of Unit III cored at Holes 645D and 645E is 812.1 m. Average recovery was 73%. The unit is divided into three subunits (Table 2). Subunit IIIA (335–753.4 mbsf) is generally homogeneous and consists of poorly sorted muddy sands and silty muds (Fig. 9), including scattered coarse sand grains and granules in some units. This subunit contains scattered pebbles mainly of black shale (Fig. 13). Lamination is slight. Subunit IIIA also contains at least 22 sharp-based, graded muddy sand beds, constituting < 10% of the recovered section (Table 4), although in general most contacts between units of different grain size are gradational. Subunit IIIB (753.4–916.8 mbsf) is characterized by silty mudstones, carbonate-rich silty

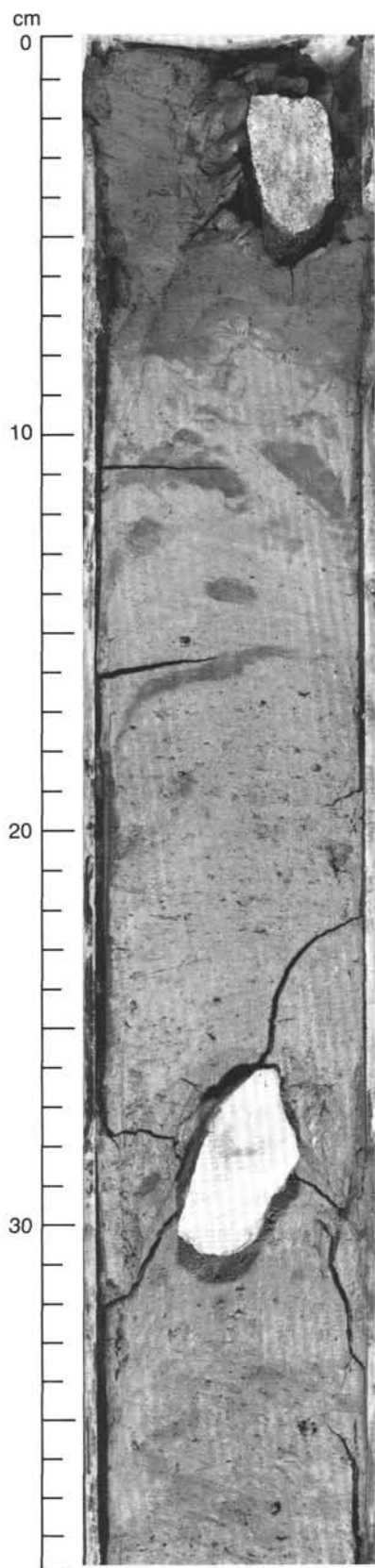


Figure 16. Bioturbated contact (8–15 cm) between (1) dark-gray silty mud (0–8 cm) and clayey mud (8–15 cm), and (2) light brownish gray, gravel-bearing, detritic muddy sand (15–38 cm). Interval shown is Sample 105-645C-3H-5, 0–39 cm.

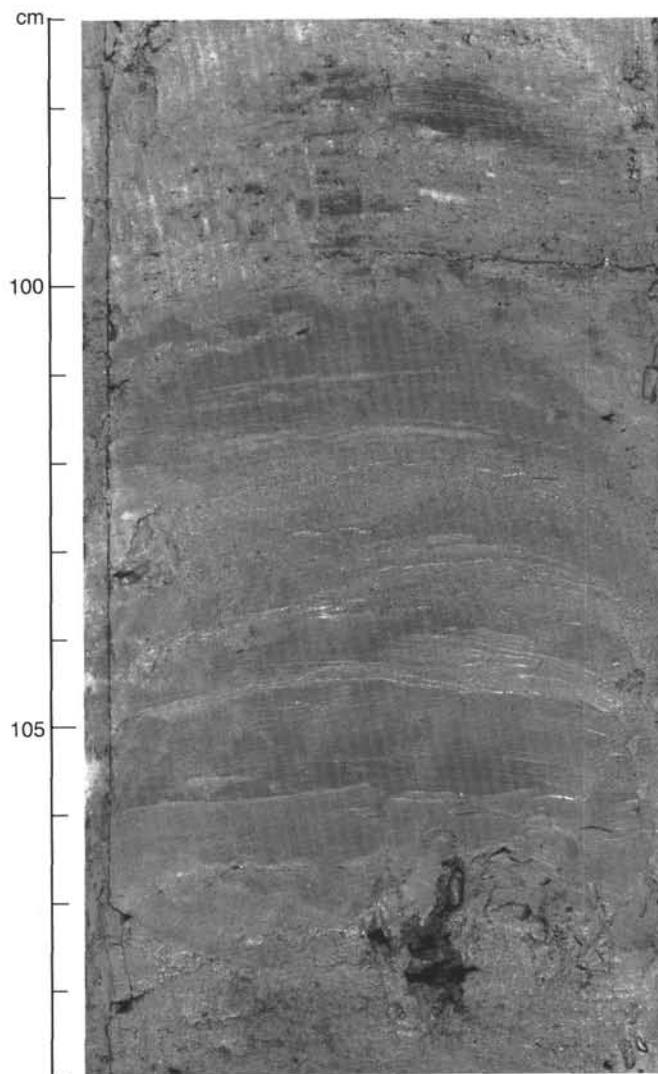


Figure 17. Thin, graded, thinly laminated, sharp-based layers within dark-gray silty clay, immediately beneath a detritic unit of sand- and gravel-bearing silty mud. Bases of laminated thin beds occur at 103.5, 104.5, and 105 cm. Interval shown is Sample 105-645F-3H-3, 97–109 cm.

claystones, and muddy sandstones, having a maximum grain size of very fine to fine-grained sand. One sharp-based, graded muddy sand bed occurs at the top of the subunit (Table 4). In the upper part of the subunit, all lithologies are extensively burrowed, whereas in the silty claystones of the lower part, a distinct lamination is evident. Subunit IIIC (916.8–1147.1 mbsf) is characterized by muddy sandstones having maximum grain size of fine- to rarely medium-grained sand, by pervasive bioturbation with prominent spreiten in muddy sandstones and silty mudstones, and by increasing amounts of glauconite toward the base of the section. Most contacts in Subunits IIIB and IIIC are gradational, as are the boundaries between subunits of Unit III. Unit III evidently was deposited under the influence of sedimentary processes that changed progressively through time; the environment at the base of Unit III, therefore, was probably significantly different from that existing during deposition of the upper part of the unit.

The main features that distinguish Subunit IIIA from the overlying sediments are (1) significantly fewer and smaller scattered pebbles, often only a few per core, generally smaller than 1

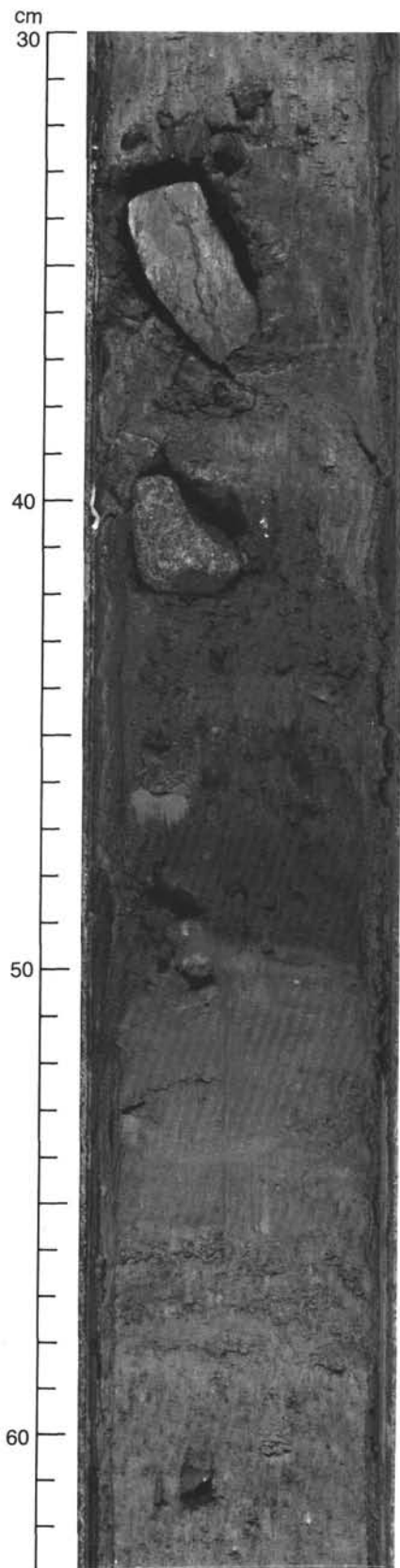


Figure 18. Reddish iron-stained zone at base of muddy sand (45–50 cm) overlying a greenish gray silty mud (50–56 cm). Interval shown is Sample 105-645F-3H-4, 30–63 cm.

Table 4. Location of graded beds, Subunits IIIA and IIIB, Site 645.

Unit	Hole	Core	Interval
IIIA	645D	10R	Section 3, 0–34 cm
		11R	Section 6, 30–40 cm
		19R	Section 5, 5–80 cm
		19R	Section 6, 5–30 cm
		20R	Section 3, 93–124 cm
	645E	6R	Section 3, 0–55 cm
		6R	Section 3, 72–120 cm
		6R	Section 4, 58–76 cm
		6R	Section 4, 76–140 cm
		6R	Section 5, 12–17 cm
		8R	Section 3, 75 cm to Section 2, 145 cm
		11R	Section 1, 69–112 cm
		11R	Section 4, 30–66 cm
		11R	Section 5, 93 cm to Section 4, 125 cm
		12R	Section 4, 120–140 cm
		12R	Section 5, 27–67 cm
		13R	Section 2, 102–150 cm
		14R	Section 3, 50–110 cm
		14R	Section 5, 70–118 cm
		20R	Section 3, 0–80 cm
20R	CC, 10 cm to Section 3, 143 cm		
29R	Section 7, 22–27 cm		
IIIB		37R	Section 6, 110 cm to Section 5, 100 cm

cm in maximum dimension (Fig. 13); (2) an overwhelming predominance in the pebble fraction of angular black shale clasts, accompanied by a few friable sandstone clasts (Fig. 19), and rare granitic and carbonate clasts; (3) a greater mean grain size (Fig. 56), having many muddy sand and silty mud units containing up to 20%–30% coarse sand grains and granules; (4) a presence of sharp-based, upward-fining beds from tens of centimeters to a meter thick (Fig. 20 and Table 4); (5) organic carbon contents of about 1.2%–1.5% (Fig. 56); and (6) an occurrence of layers and in some places elliptical zones, rich in carbonate minerals. The lowest pebble that is difficult to interpret without recourse to the ice-rafting explanation occurs in Core 105-645E-19R, at a depth of about 605 mbsf.

The major lithologic compositions of Subunit IIIA are sand-bearing silty mud (48% of recovered core) and muddy sand (25% of core) in shades of gray and greenish gray (Fig. 9). Minor lithologic compositions and their abundances are silty sand, 7%; clayey mud, 3%; clayey silt, 14%; and silty clay, 2%. The silty muds and many of the muddy sands are moderately bioturbated and have some traces tentatively identified as *Planolites* and *Chondrites*. The burrows are commonly distinct and dark gray to black. Sorting is generally very poor; scattered coarse and medium sand grains characterize many of the silty muds, and scattered coarse sand and granule grains characterize the muddy sands. In places, millimeter-thick, indistinct lenses and discontinuous layers of higher-than-normal sand content give a vague planar fabric to the sediment; this diffuse layering is too subtle to be called lamination or stratification. Most contacts between units of different grain size are gradational. Several muddy sand units, however, show features associated with deposition from density currents, such as relatively sharp bases, a lower division and scattered pebbles and granules, and evidence of initially slow but more rapid grading (i.e., delayed grading) from the base of the bed upward into silty mud and/or clayey silt (Fig. 20). Muddy sand units having these characteristics are apparently free from bioturbation, except near their top. The degree of primary layering in the silty mud, in particular, is difficult to assess because of ubiquitous drilling biscuits that obscure subtle primary features.

The muddy sands, silty muds, and minor clayey silts of Subunit IIIA are characterized by relatively low contents of detrital

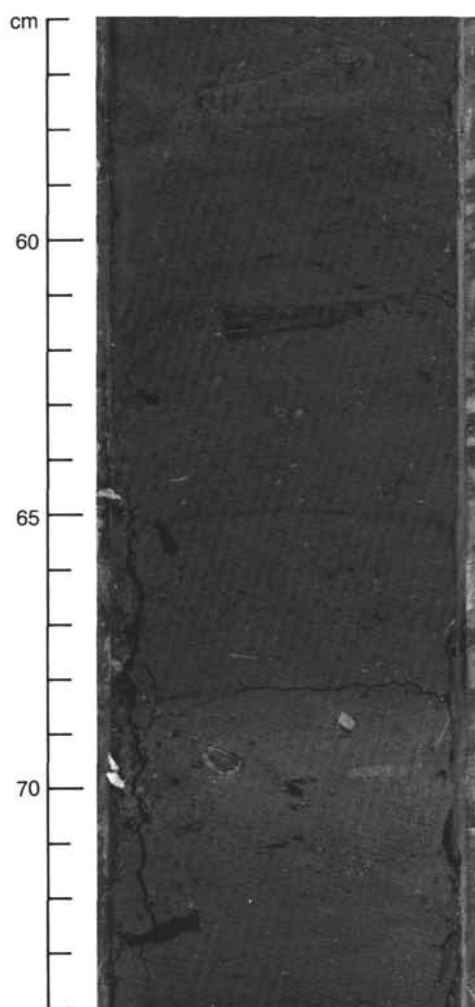


Figure 19. Carbonate-rich zone, relatively rich in scattered shale pebbles (68–71 cm). Note that this muddy sand contains a considerable quantity of coarse sand grains and granules as well as shale pebbles. Thin, dark laminae (e.g., at 65 cm) are probably related to drilling disturbance (i.e., biscuits). Interval shown is Sample 105-645D-14R-1, 56–74 cm.

carbonate, ranging from 5% to 25% and having a mean of about 10% (Fig. 56). In contrast, a few <25-cm units of light-gray, gray, and olive-gray clayey silt to clay have carbonate contents of 50%–70% (Fig. 21). Several of these carbonate-rich zones have a siliciclastic fraction that is texturally indistinguishable from the surrounding sediment and show a gradual decrease in carbonate content from the central part of the zone to its margins. The carbonate minerals in these zones include calcite, siderite, and rhodochrosite; in some places, these zones contain more scattered pebbles than do the surrounding sediment (Fig. 19).

Despite greater lithification, some fluctuation occurs in sediment induration throughout the interval. Below about 725 mbsf, lithification is sufficiently advanced to warrant use of “stone” in the sediment name. The carbonate-rich zones in muddy sands and silty muds are significantly more lithified than are the surrounding sediment.

In general, smear slides of dominant lithofacies contain authigenic pyrite, in several places about 10%. A significant minor lithofacies in Subunit IIIA, encountered at 105-645D-14R-5, 17 cm, is a pyritic (25% pyrite) ash layer about 1 mm thick.

The mineralogy of Subunit IIIB is much like that of Subunit IIIA, yet with small amounts of glauconite in some sandy/silty

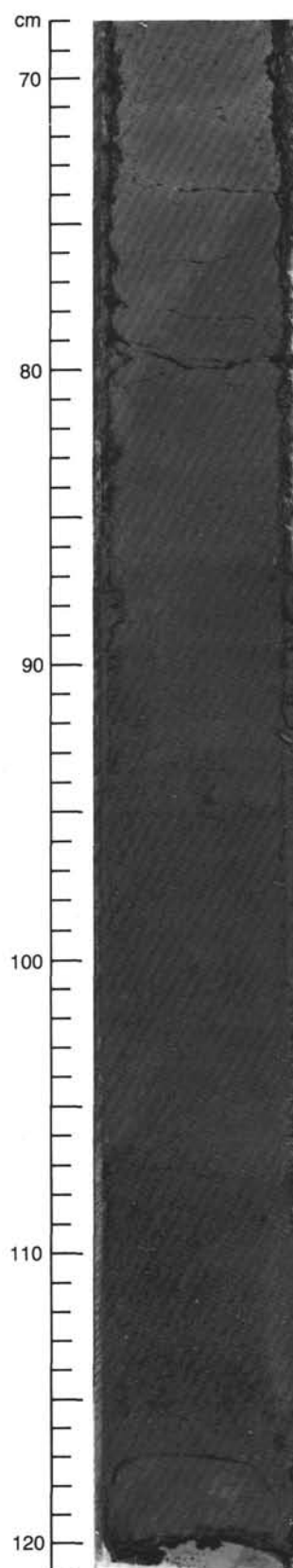
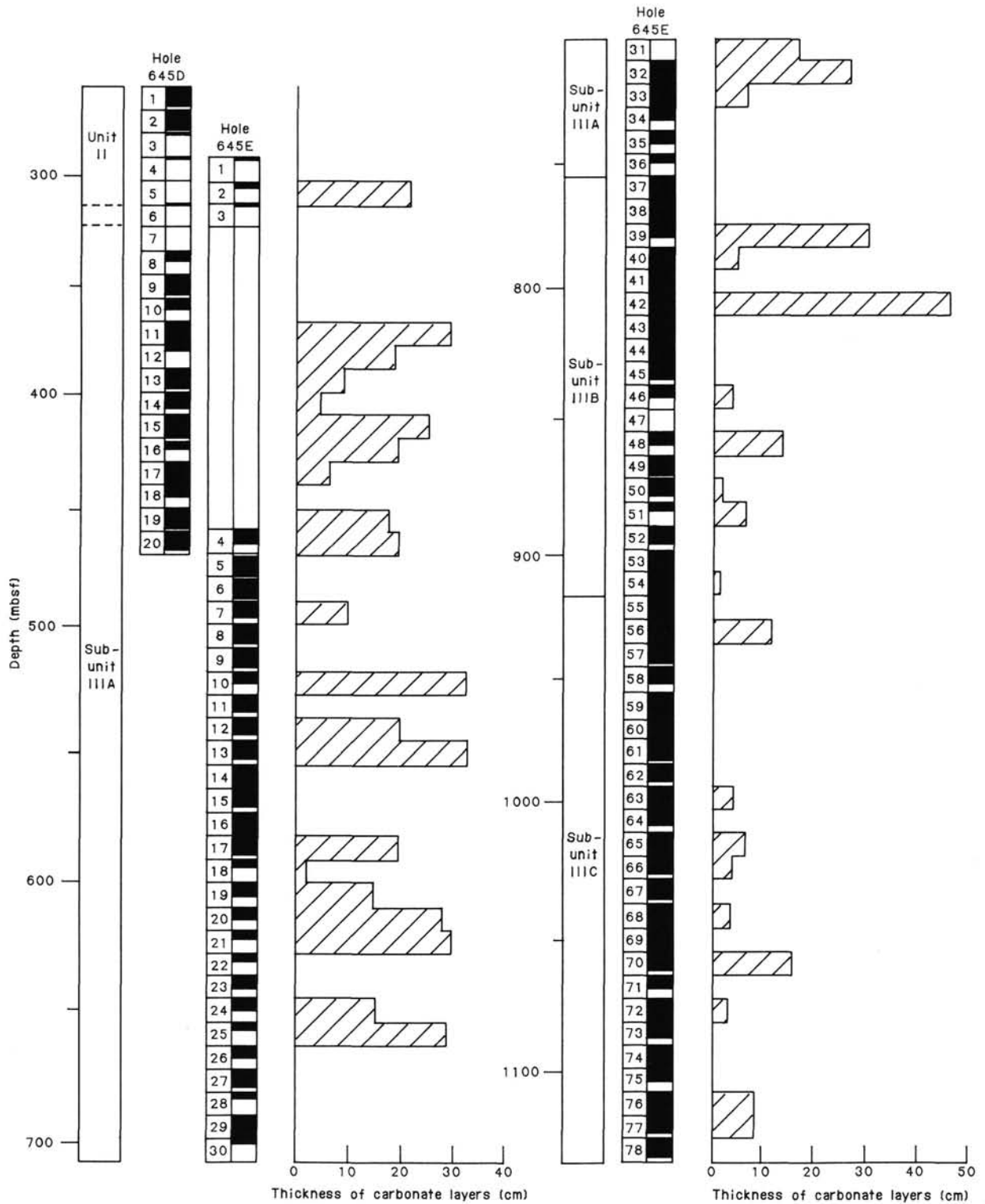


Figure 20. Sharp-based, graded, muddy sandstone bed. Base at 117 cm is overlain by granule-bearing muddy sand. The bed fines upward to about 80 cm, where grading apparently ceases. No internal structures are visible. Interval shown is Sample 105-645E-14R-5, 68–121 cm.



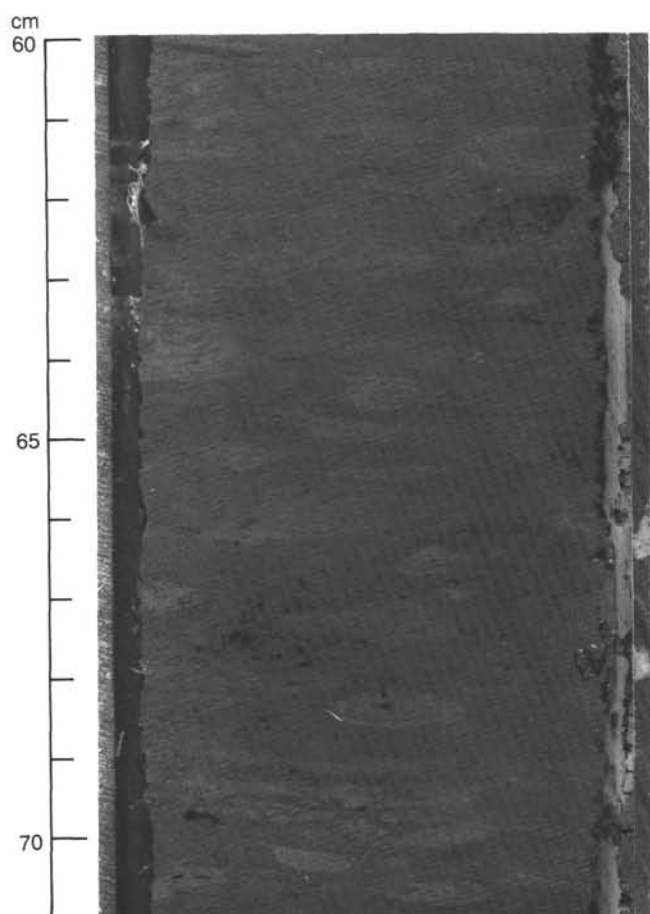


Figure 22. Moderately bioturbated, greenish gray, detritic silty claystone. The burrows have a relatively high content of carbonate minerals, are subhorizontal, and tend to give the sediment a subtle color banding. Interval shown is Sample 105-645E-39R-2, 60–71 cm.

terized by well-laminated units of carbonate-rich silty claystone to clayey mudstone, only slightly bioturbated, having a total organic carbon content of as much as 2.8% (Fig. 56). Some individual laminae are normally graded (Fig. 23). Terrestrial plant fragments, apparently unabraded gastropod shells, small nodules of authigenic pyrite, and carbonate-cemented bands and irregular pods in the coarser facies (Fig. 21), are scattered throughout this subunit.

Subunit IIIC is characterized by coarser grains than is Subunit IIIB (Fig. 9B). Maximum sand size increases toward the bottom of the subunit; many muddy sandstones have significant amounts of fine- to medium-grained sand. Burrows commonly show internal spreiten and resemble *Zoophycos* and *Scolicia* types of traces. The burrows are often light in color, subparallel to the original bedding planes, and contain more glauconitic grains than do the surrounding facies. The major lithofacies (Fig. 9B) are muddy sandstone (50.5%) and silty mudstone (45.0%). Minor lithologies are clayey mudstone (2.4%) and clayey siltstone (1.3%). Primary physical structures occur only in a few short intervals as strong lamination in muddy sandstones and in one place as part of a graded unit (Fig. 24). Grain-size variations between successive laminae are relatively sharp. The laminae are wavy near the base of the graded unit.

The mineralogy of Subunit IIIC is much like that of Subunits IIIA and IIIB, except for the occurrence of rare zeolite grains (e.g., in Core 105-645E-64R), which are probably clinoptilolite, and the dramatic increase toward the bottom of the cored sequence of glauconite grains, to a maximum of 10%

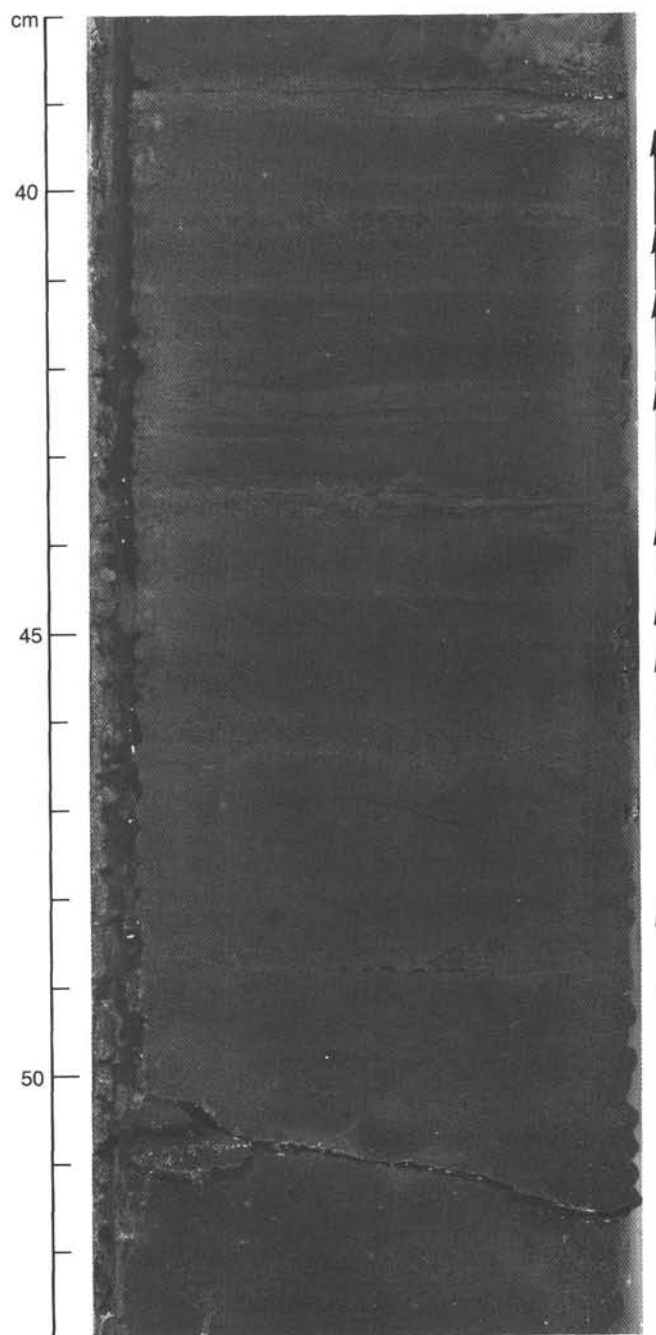


Figure 23. Olive clayey siltstone with 1–2-cm-thick, generally graded layers (e.g., at arrows). Unlike interbedded muddy sandstones and silty mudstones, this facies is essentially unbioturbated. Interval shown is Sample 105-645E-53R-2, 38–53 cm.

(Core 105-645E-76R). Carbonate is generally minor, except in concretions (Fig. 21).

Evidence of wet-sediment deformation exists in two cores. In Core 105-645E-66R, two recumbent slide folds disrupt the section (Fig. 25), and in Core 105-645E-71R, what are normally subhorizontal burrows are tipped as much as 20° from the horizontal.

Interpretation

The sedimentary sequence at Site 645 represents a completely terrigenous succession having a relatively high sediment-accumulation rate, ranging from about 40 m/m.y. in Unit III to

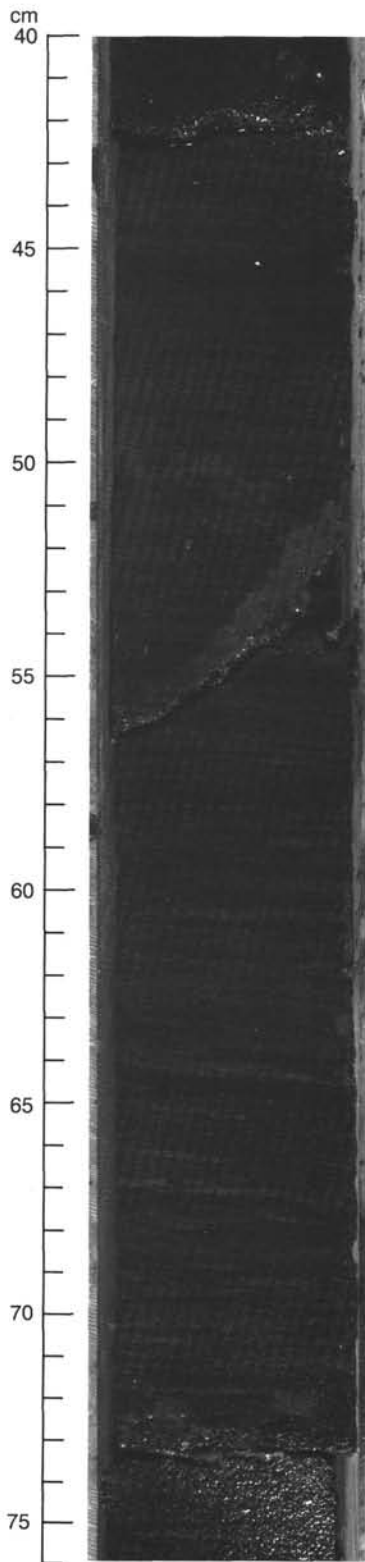


Figure 24. Upper part of a strongly laminated interval of muddy sandstone that extends from 43 cm, beyond the bottom of the photograph, to 95 cm. From 65–95 cm, the laminations of sand/silt are somewhat irregular and lens shaped; the interbedded silt/clay laminae look somewhat like flasers. From 43–65 cm, the laminae become progressively thinner and finer grained. Unlike surrounding facies, this interval is not bioturbated. The base of the unit is sharp. Interval shown is Sample 105-645E-68R-6, 40–76 cm.

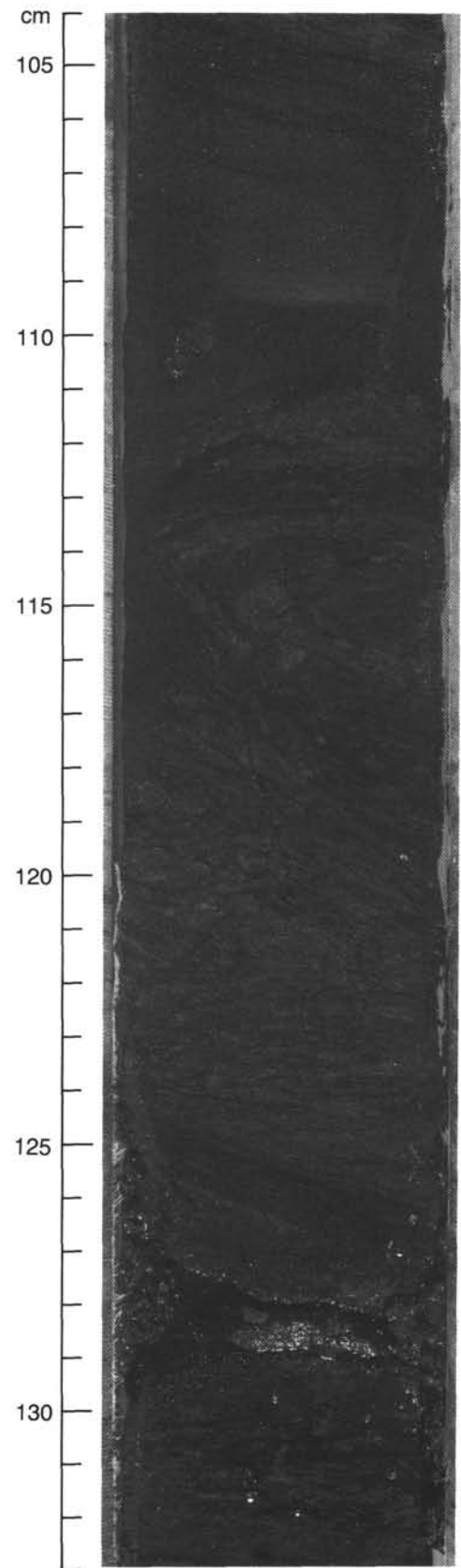


Figure 25. Slide fold in interbedded silty layers and silty mudstone. Fold is overturned; axis is at 114 cm. This cannot be attributed to coring disturbance. Interval shown is Sample 105-645E-66R-4, 104–133 cm.

about 130 m/m.y. in Units I and II (see "Sediment-Accumulation Rates" section, this chapter). Although the sands and silts of the lowermost unit (Unit III) may indicate some reworking and redeposition, generally all sediments are texturally and mineralogically immature. The overall poor sorting suggests rapid denudation of surrounding continental masses and little recycling. The occurrence of relatively fresh feldspar and associated ferromagnesian sand grains also indicates a rapid erosion rate, lacking deep weathering, and a swift sediment burial.

Two dominant sedimentary processes were inferred from the sedimentological data: ice rafting (Units I and II) and bottom-current transport (Subunit IIIC). These, however, were probably not the only important transport processes, both within the basin and as agents for transport of detritus from adjacent land masses. In all parts of the sequence, and particularly in Subunits IIIA and IIIB, other processes may have been low- and high-concentration turbidity currents, subaqueous debris flows, and eolian transport to the sea surface, followed by settling. Eolian transport is suggested by the high concentration of fine sand and silt in all units (Fig. 56, "Summary and Conclusions" section, this chapter). Katabatic winds (down-glacier gravitational flow of chilled air) are known to be an effective transport agent for silt-size material (Thorson and Bender, 1985) and may have been significant adjacent to large ice sheets, winnowing fines from the surface of proglacial outwash and blowing them out to sea.

Unit I

The pronounced textural variations in Subunit IA between (1) dark-colored, clay-rich muds and (2) light-colored, gravel-bearing detriticarbonate muddy sands and silty muds are interpreted as being a reflection of variations in the delivery of ice-rafted sediment to the basin. The lack of physical sedimentary structures in the gravel-bearing units and the observation that Unit I forms an essentially even drape over the seafloor in Baffin Bay (see "Background and Objectives" and "Seismic Stratigraphy" sections, this chapter), strongly suggest that ice rafting was the dominant transport process and that melting of sediment-laden icebergs was the dominant control on sedimentation. A similar interpretation of gravel-bearing muddy sands in the upper 10 m of sediment in Baffin Bay was made by Aksu and Piper (in press), using a piston-core analysis. Other processes may have included some resuspension and downslope transport, as a nepheloid layer, of the fine fraction from older glacial-marine sediments on the continental margin, forming hemipelagites. The absence of primary structures and generally poor sorting argue against the operation of significant bottom currents.

The direct cause of the cyclicity appears to have been rapid increases and gradual decreases in the supply rate of carbonate-rich clay- to gravel-size detritus, superimposed on persistent delivery of fine-grained clays, perhaps by bottom-current transport or dilute turbidity currents. Clay mineralogy from piston-core studies (Aksu and Piper, in press) is consistent with this proposal because the clay mineralogy of the detriticarbonate-rich and carbonate-poor intervals (Facies A and D of Aksu and Piper, in press) is indistinguishable.

One plausible interpretation of the observed cyclicity (Aksu and Piper, in press) is that the relatively fine-grained muds and clays represent the "glacial" part of each sequence. The coarsest debris carried by the ice would have been dropped on outwash plains or carried by icebergs well south of Baffin Bay because of cold surface-waters inhibiting iceberg melting in the bay. Only the finest size fractions would have been capable of reaching the deeper parts of the basin through coastal deltas as low-concentration turbidity currents (Aksu, 1984). Rising sea level during deglaciation could have promoted accelerated calv-

ing of icebergs, which may have dropped a greater part of their sedimentary load in Baffin Bay because of the introduction of relatively warmer waters from the North Atlantic (Aksu and Piper, in press).

We concur with Aksu and Piper (in press) that the dominant transport process for gravel-bearing muddy sands and gravel-bearing silty muds was probably ice rafting primarily because of the lack of primary structures that might suggest other processes. Conceivably, some gravel-bearing units, however, may have moved to the site as subaqueous debris flows because few criteria conclusively distinguish between poorly sorted, structureless pebbly debris flows and homogeneous ice-rafted units. Some debris-flow deposits were recognized from the northern slopes of Baffin Bay by Aksu (1984), although he did not interpret piston cores near Site 645 as containing identical facies. Nevertheless, apparent rapid lateral textural changes noted in attempts to correlate cores from Holes 645A, 645B, 645C, 645F, and 645G (Fig. 6) could be the result of intersection in some holes of areally restricted debris-flow tongues. High-resolution seismic profiles over the site indicate that lenticular slide or debris-flow tongues are present in the shallow subsurface. At the site, a chaotic slide unit occurs at 45–75 mbsf, in an interval of poor core recovery (Fig. 58, "Summary and Conclusions" section, this chapter).

The sedimentary cycles in Baffin Bay are different from those developed at other lower latitude marine locations, which are interpreted to represent glacial-interglacial cycles (Zimmerman, 1984; Ruddiman, Kidd, et al., in press), and are also different from those in the Norwegian Sea (Eldholm, Thiede, Taylor et al., in press), which, although at a high latitude, also record an open-marine sequence. At lower latitude locations and in the Norwegian Sea, interglacial light-colored biocarbonate ooze and biocarbonate clays having a minor detrital component alternate with darker colored sediments dominated by ice-rafted debris. This alternation of lithofacies characterizes North Atlantic sediments deposited in open-marine environments under glacial-interglacial climatic fluctuations.

Sedimentation rates of most open-marine, dominantly pelagic glacial sequences average about 20 m/m.y. (Zimmerman, 1984; Eldholm, Thiede, Taylor et al., in press). According to the preliminary magnetostratigraphy of Site 645, the average sedimentation rate of the Baffin Bay glacial sequence is about 130 m/m.y. (see "Sediment-Accumulation Rates" section, this chapter). If true, then each 1-m cycle would represent about 7,700 yr, a much higher frequency of cyclicity than found in open-ocean cores and five times more frequent than that inferred by Aksu (1983) from nearby piston cores. Aksu (1983) presented a possible correlation of oxygen-isotope curves from Baffin Bay and Davis Strait (his cores 040 and 017) with the oxygen-isotope record of global ice volume, extending back as far as Oxygen Isotope Stage 8. His correlation suggests a depositional rate at the Baffin Bay site (near Site 645) of about 1 m/40,000 yr. This is clearly an inconsistency. If the sedimentation rate inferred by Aksu (1983) is correct, then sediments at 95 mbsf should have an age of about 3.5 Ma, at variance with preliminary paleomagnetic results (see "Paleomagnetism" section, this chapter). Either the sedimentation rate increases sharply below piston-core depths to allow an age of 0.73 Ma at 95 mbsf (see "Paleomagnetism" section, this chapter) or Aksu's (1983) correlation of oxygen-isotope records is incorrect; the cycles that we see in the core each represent about 7,700 yr (i.e., high-frequency cycles). At present, we see no evidence of a dramatic change in depositional rate within Subunit IA.

We have no evidence from this site that the observed cyclicity is related to full glacial-interglacial events. The sheer number of observed "cycles" in Unit I makes it highly unlikely that each represents a discrete glacial-interglacial episode. The cycles, if

climatically controlled, may correspond to relatively short-term variations in (1) extent of iceberg calving, (2) surface-water temperatures in the bay (warmer waters would accelerate melting of icebergs and increase detrital supply), (3) melt-water runoff, and so forth.

Alternatively, the cycles may simply represent systematic changes in sediment sources or in the trajectories of icebergs from glaciers sampling distinctive source rocks. Paleozoic bedrock north of Baffin Bay (Ellesmere and Devon Islands) is the most likely source for the carbonate detritus that characterizes the gravel-bearing detritic muddy sands (Aksu and Piper, in press). In Subunit IA, an iron-stained coarse sand commonly marks the base of the gravel-bearing detritic units. This sand may be the product of oxidation resulting from periodic, climatically controlled overturn of the water column and concomitant oxygen renewal of bottom water in the basin, or the sand may represent tapping of a different source just at the onset of ice rafting. According to Aksu and Piper (in press), the light-red sandy units contain unusually rounded quartz grains and reworked Cretaceous palynomorphs, suggesting derivation from iron-rich Cretaceous sediments, not affecting bottom-water chemistry.

Distinct color and textural variations become more subtle downcore into Subunit IB. Pebble- and cobble-sized dropstone abundance, however, remains generally constant throughout the unit, suggesting that ice rafting, as in Subunit IA, was a major sediment-dispersal mechanism. The poorly defined cyclicity of the sediment record is thought to reflect variations in sediment supply that may be providing a record of climatic fluctuations. The distinctly finer grain size of Subunit IB, compared with Subunit IA, might suggest that (1) the contribution of ice-rafted material to an essentially hemipelagic record was smaller or (2) the texture of the ice-rafted material was more fine grained. In the former case, the smaller proportion of ice-rafted material could be the result of a low rate of iceberg calving and insignificant melting of icebergs over the site. As for Subunit IA, the source for the carbonate grains is probably lower Paleozoic rocks to the north of Baffin Bay. If ice rafting was the dominant transport process, it is difficult to explain why the sediment would be so uniformly fine grained. Other possible processes that could have contributed to the basinward transport of the detrital carbonate and siliciclastic components in Subunit IB are surface or mid-water plumes of suspended sediment from glacial streams, transport by bottom currents in a near-bottom nepheloid layer, suspension of fine sediment on adjacent shelves and cascading into deep water (lutite flows), and low-concentration turbidity currents. However, no sedimentary structures indicating deposition by turbidity currents or bottom currents were observed in split cores. Bioturbation may have degraded or destroyed evidence of physical processes, although clearly defined burrows were also not commonly visible.

The significance of the decrease in detrital carbonate content at the Unit I/II boundary remains obscure but may reflect a change from dominantly hemipelagic, bottom-current and turbidity-current transport in Unit II to dominantly ice rafting in Unit I. Alternatively, the compositional difference may simply reflect a change in source area. Probable climatically induced rhythms and an ice-rafting overprint continue into at least Unit II.

Unit II

Unit II can be interpreted as being the record of Pliocene to early Pleistocene glacial-interglacial cycles in Baffin Bay. The interpretation of the sedimentary facies, however, is not entirely clear. High sediment yields to Baffin Bay from surrounding land masses resulted in an exclusively terrigenous record, with few biogenic pelagic components. Nevertheless, typical characteristics

of turbidites or other mass-flow deposits are absent. The abundance and the dispersed nature of the gravel-sized clasts in all silty, clayey, and muddy sediments suggest important terrigenous supply by ice rafting. This sediment could subsequently have been reworked by bottom currents. However, the absence of characteristic structures of bottom-current deposits would suggest no more than weak modification by slow-moving bottom currents.

Sediments near the base of Unit II (Cores 105-645B-27X through 105-645B-30X) are rich in palynomorphs indicative of cool-humid conditions. This suggests a time, subsequent to the inferred onset of major glaciation near the base of Unit II (first common dropstones), when the land masses surrounding Baffin Bay were still well vegetated. Notably, most sediments above Core 105-645B-27X and below Core 105-645B-30X are relatively rich in clasts interpreted as being dropstones (Fig. 13) and poor in palynomorphs, most of which are reworked (see "Biostratigraphy" section, this chapter). These sediments may record times of substantial ice cover of land masses around Baffin Bay. Cores 105-645B-27X through 105-645B-30X, however, are relatively poor in gravel-size constituents, although they do contain some scattered inferred dropstones, but are rich in apparently contemporary pollen and dinocysts of subarctic type (see "Biostratigraphy" section, this chapter). This suggests a time of relatively reduced ice cover and establishment of cool-humid (boreal to tundra forest) conditions.

The high concentration of heavy minerals (as much as 10%) in the sand unit at the base of Unit II (Core 105-645B-30X) can be explained by current sorting. However, the presence of foraminifers and diatoms indicating neritic environments and the absence of gravel suggest that the sand was transported rapidly from a littoral or shelf environment into the basin. Density-current transport from the slope of Baffin Island, from Davis Strait, or westward from Greenland (see interpretation of seismic lines in "Background and Objectives" and "Seismic Stratigraphy" sections, this chapter) is the most probable process for emplacement of these sands. The high concentration of heavy minerals could then be inherited from coastal or shelf environments having relatively efficient hydraulic-sorting processes.

In summary, mechanisms of detrital supply during deposition of Unit II probably included a combination of ice rafting, weak bottom currents, and turbidity currents.

Unit III

The sedimentary sequence of Unit III records a period when Baffin Bay gradually changed from a basin dominated by bottom currents to one dominated by a mixture of processes, including waning bottom currents, high-density turbidity currents, and perhaps ice rafting and contributions from katabatic winds in the upper part of Subunit IIIA.

About 10% of the recovered section in Subunit IIIA consists of relatively sharp-based, graded, unbioturbated muddy sands that could be the deposits of immature, high-concentration turbidity currents. The limited range of maximum grain sizes in the sand fraction and poor overall sorting make the recognition of grain-size breaks difficult, and subtly amalgamated units with indistinct contacts may be undiscernible in the split cores.

Subunit IIIA consists mainly of partly bioturbated silty muds and muddy sands, which show no grading or only slow upward-coarsening or -fining trends over tens of centimeters or meters. Bioturbation, lack of current-formed structures, and the presence of common gradational contacts make these sediments strongly resemble contourites described by Gonthier et al. (1984) and Stow and Holbrook (1984). The major difference is in grain size. Sediments from clear contourite drifts generally have a maximum grain size of fine sand, the bulk of the sediment being in the silt fraction. The reason for this limit is that modern

contour currents rarely reach mean velocities $>30\text{--}50\text{ cm/s}$ (Richardson et al., 1981; Carter and Schafer, 1983; Bulfinch and Ledbetter, 1984; Hollister and McCave, 1984), and maximum shear velocities are about 1 cm/s (more commonly about 0.3 cm/s ; Grant et al., 1985). Such flows are capable of rolling grains with diameters of only less than about 0.2 mm and commonly much smaller, i.e., $<0.01\text{ mm}$ (Blatt et al., 1980, p. 103). In Subunit IIIA, grain sizes commonly range as large as coarse sand (0.5 mm), even in units classified as silty mud. If bottom currents deposited these sediments, then they would have been stronger than any known contour currents and would probably have winnowed fines from the muddy sands to produce tractional structures, e.g., ripples in fine sands and silts, similar to those originally proposed as characteristic of sandy contourites by Heezen et al. (1966) and Hollister and Heezen (1972). No such tractional structures were noted in Subunit IIIA, either visually or with X-radiography. In some places, it could be argued that all physical structures may have been destroyed by burrowers, but several muddy sand intervals that were examined with X-radiography showed no evidence of either primary lamination or burrowing.

A reasonable hypothesis is that much of the sediment in Subunit IIIA was subjected to bottom currents that perhaps were capable only of winnowing away the finer fractions. The transport of coarse sand grains to the deposition site apparently occurred through agents other than bottom currents. The occurrence of graded beds suggests that turbidity currents were partly responsible for introduction of sands into the basin. High-concentration turbidity currents could have carried the observed shale clasts in suspension. Bottom currents and burrowers may have subsequently reworked thinner turbidite units and produced some of the diffuse coarser grained lenses in the silty muds and some muddy sands. Some sediment may also have been delivered to the bottom by ice rafting. This would be consistent with the observed presence of scattered pebbles. Most shale clasts lie more-or-less parallel with bedding, which is the predicted orientation for platy ice-rafted pebbles settling onto a flat bottom. No conclusive evidence exists, however, for ice rafting during deposition of Subunit IIIA. Rare pebbles could also have been dropped from floating winter shore ice, a process that is known to carry large boulders across the modern Gulf of St. Lawrence annually (Dionne, 1972). The increasingly numerous outsized clasts (Fig. 13) toward the top of Subunit IIIA, however, suggest to some of the sedimentological party that ice rafting had begun during the deposition of Subunit IIIA.

Whatever the dominant depositional process or combination of processes may have been, the source must have been one capable of providing substantial quantities of sand, including coarse sand and granules, and one in which dark shales and, perhaps, friable micaceous sandstones formed much of the bedrock. Carbonate rocks and igneous and metamorphic basement lithofacies that formed important sources for Units I and II appear to be only a minor source for Unit III.

A potential nearby source for the detritus in Subunit IIIA is the poorly consolidated Mesozoic or Paleogene sandstones and shales on the nearby shelves of Baffin Island or Greenland (Henderson et al., 1981; West et al., 1981; Rolle, 1985) and these are required to account for the sandy texture, the general lack of pebbles of Precambrian basement rocks or carbonates, and the ubiquity of shale pebbles and granules.

The maximum size of sediments in Subunit IIIB is finer than that of Subunit IIIA sediments; in fact, Subunit IIIB rarely contains grains coarser than fine sand. Pervasive bioturbation in most silty mud and muddy sand units, gradational contacts over stratigraphic distances of tens of centimeters or more, and common suggestions of diffuse or wispy lamination are all consistent with deposition beneath bottom currents of strength similar

to those currents that sweep the modern continental rise of eastern North America. Well-laminated, carbonate-rich silty claystones are unusually free of severe bioturbation, perhaps resulting from higher rates of deposition. Some laminae appear graded (Fig. 23) and resemble very thinly bedded turbidites deposited from low-concentration flows ("lutite flows") similar to those described by Chough and Hesse (1980) in the Labrador Sea (levees of Northwest Atlantic Mid-Ocean Canyon, NAMOC). Bottom-current transport may have been periodically overwhelmed by downslope transport of mud turbidites from the shelf edge.

In Subunit IIIC, the sediments are coarser grained than those in Subunit IIIB; intervals having $<10\%$ sand are absent. Toward the base of the recovered section, fine- to medium-grained sand becomes more abundant, as do glauconite grains in the sediments. Although post-cruise studies suggest that glauconite may be less prevalent than shipboard analyses indicated (P. Giresse, pers. comm., 1985), the intensity of *Zoophycos*- and *Scolicia*-type burrows and the common occurrence of benthic foraminifers indicate a well-oxygenated bottom. Sedimentary and biogenic structures are much like those in Subunit IIIB, and we similarly interpret Subunit IIIC to have been deposited beneath geostrophic bottom currents but with somewhat greater velocity than the currents that existed during deposition of Subunit IIIB.

Like the deep-water glauconites at Sites 552 and 553 (Morton et al., 1984), the presence of glauconite in Subunit IIIC in Baffin Bay may be attributed to three possible origins: (1) reworking of previously deposited, significantly older glauconite, a possible source being Paleocene-Eocene strata of West Greenland (Rolle, 1985); (2) glauconite formation in relatively shallow water and subsequently transported to the present deposition site; and (3) authigenic formation of glauconite in deep water without significant reworking.

Glauconite of deep-water origin (third possibility) commonly requires periods of slow deposition or nondeposition, often related to strong bottom-water currents. Bottom currents are an integral part of our interpretation of Subunit IIIC, but we have no concrete information on deposition rate. The observed close association of the glauconite grains with burrows suggests *in-situ* formation, perhaps by replacement of fecal pellets. There is no evidence that the glauconite was transported from shallow water to the site, although redeposited shallow-water benthic foraminifers indicate that some of the sediment grains may have followed such a course.

Soft-sediment slide folds in Core 105-645E-66R suggest a sloping bottom, perhaps as much as a few degrees, although sliding of rapidly deposited muds is known to occur on slopes of <1 degree. These slide horizons indicate a sloping bottom at the site during deposition of Subunit IIIC.

The precise origin of the strongly laminated, unbioturbated, locally graded intervals (Cores 105-645E-63R and 105-645E-68R) is uncertain. One hypothesis is that they are turbidite units and that the parallel lamination indicates upper-flow-regime conditions during deposition. The textural contrast between adjacent laminae seems to be greater than that normally observed in upper-flow-regime plane beds, however, and the basal laminae in one of the units are irregular and somewhat wavy. These units clearly were deposited by waning flows, but a turbidity-current origin is not compelling. Perhaps these units were deposited on the slope during or immediately after large storms on the shelf, which sent plumes of suspended sediment across the shelf-slope break and into deeper water. Such a process would also be consistent with the observation that Subunit IIIC contains redeposited, shallow-water benthic foraminifers, brought into the basin from the adjacent shelf areas.

Incipient diagenesis in Unit III may be indicated by the carbonate-rich zones (calcite, siderite, and rhodocrosite) having gradational boundaries in some muddy sands and silty muds. These

zones may be interpreted as being diagenetic concretions. Pore-water geochemical data (see "Inorganic Geochemistry" section, this chapter) indicate high alkalinities and Ca^{2+} concentrations and reducing conditions favoring authigenic precipitation of such carbonate phases.

History of Ice Rafting

One important objective of studies at Site 645 was to determine, if possible, the sedimentary record of ice rafting in Baffin Bay. Biostratigraphic resolution is inadequate to provide accurate dates for stratigraphic intervals at the site, so our comments are restricted to relative stratigraphic positions in Holes 645D and 645E.

Units I and II contain abundant inferred dropstones, up to cobble size, of both carbonate and granitic/gneissic lithologies and clearly were deposited under a glacial regime. In some parts of Subunit IB and Unit II, however, dropstones are relatively rare (Fig. 13). These intervals have no features that suggest unusually high sedimentation rates, so a reasonable inference is that the frequency of iceberg calving and/or melting was relatively low. These intervals may correspond to times of reduced ice cover, sedimentation being temporarily dominated by other processes and perhaps including low-density turbidity currents and bottom currents.

Our general conclusion is that ice rafting provided the bulk of the sediment in Units I and II. If true, then the source for Unit II must have been of much wider extent than the source for Unit I. Unit II detritus is dominantly siliciclastic but also includes a gravel fraction rich in limestone and dolostone clasts, similar to those that characterize Unit I, as well as plutonic and metamorphic clasts. Apparently the carbonate source contribution was substantially diluted during deposition of Unit II, whereas it predominated during deposition of Unit I.

The cycles apparent in Unit I are essentially the result of fluctuations in the amount or character of ice-rafted detritus. These cycles are about 1 m or less. The only larger-scale cyclicity that we observe is shown by variations in Units I and II on a scale of about 50 m in the percentages of sandy lithofacies (Fig. 56, "Summary and Conclusions" section, this chapter, and preliminary shore-based data). Poorly constrained variations in total organic carbon (Fig. 56) are on a scale of tens of meters. It would be interesting to test whether these apparent longer-term variations in lithologic properties represent first-order fluctuations in climate or glacial processes.

Below the contact between Units II and III, large pebbles and cobbles are rare. The small pebbles that do occur (Figs. 13 and 19) are dominantly shale clasts and may have been carried into the basin by turbidity currents. Pebbles of this type occur as deep in the section as 760 mbsf (105-645E-37R-6). Scattered pebbles to about 3 cm diameter, however, occur in muddy lithofacies, and are difficult to interpret except as dropstones. The deepest such occurrence is at 605 mbsf (Core 105-645E-19R). These pebbles are so rare that care must be exercised in using their presence as compelling evidence of high-latitude iceberg calving and glaciation. Pebbles of this type may have been rafted over the deeper parts of the basin by floating fragments of winter shore ice. Compelling evidence of significant ice rafting is really present only in Units I and II, although we cannot exclude the possibility that icebergs were contributing some pebbles to the seafloor during deposition of Subunit IIIA.

Interestingly, ice rafting is evident right to the base of Unit II but cannot be unambiguously demonstrated in Unit III. In seismic sections through the site (see "Background and Objectives" and "Seismic Stratigraphy" sections, this chapter), Unit II (= seismic unit 1B) is contained within a major sedimentary body (seismic unit 1) that thickens toward Greenland and pinches out westward against the continental slope of Baffin Island. Reflec-

tors within this seismic unit progressively onlap an eastward-dipping unconformable surface that is thought to define the base of the unit (reflector R1), so that the base of seismic unit 1 is considerably older in the central part of the bay than it is at Site 645. In fact, seismic unit 1C, about 600 m thick, is almost completely missing at Site 645, and Lithologic Unit II rests directly on the unconformity. The seismic sections clearly indicate a major hiatus between Lithologic Units II and III, during which about 600 m of sediments accumulated in the central part of Baffin Bay. Limited biostratigraphic data suggest that the hiatus lasted for no more than 1 m.y. The onset of significant iceberg calving may have occurred in the time interval between deposition of Units II and III, leaving no record at Site 645.

BIOSTRATIGRAPHY

Core-catcher samples from the seven holes cored at Baffin Bay Site 645 were examined for planktonic and benthic foraminifers, calcareous nannofossils, diatoms, dinocysts, radiolarians, pollen, and spores. Biostratigraphic results of Site 645 studies are limited because (1) except dinocysts and benthic foraminifers, all microfossil groups occur only rarely or sporadically. Siliceous microfossils (radiolarians or diatoms) were observed in only about 15% of the samples examined. Planktonic foraminifers and calcareous nannofossils were observed in about 12% and 16% of the samples, respectively. Benthic foraminifers occur in about 50% and dinocysts in about 98% of the examined samples. (2) The microfossil assemblages that were observed are generally composed of species with long geologic ranges. Most diatom species observed characterize coastal or neritic environments. Stratigraphically useful species are generally rare. (3) Temperate and warm-temperate species were not commonly observed in post-Miocene samples. Thus, recognition of the microfossil zones developed for the lower latitudes was not possible. (4) Because age determinations are typically based on the rare occurrence of a species, the high abundance of observed reworked specimens (primarily Paleozoic-Paleogene pollen and spores having some reworked specimens of Mesozoic-Paleogene dinocysts and Eocene-Miocene diatoms) in the samples introduces uncertainty into the stratigraphic placement of several of the last-occurrence datums.

The interpretations expressed herein are, therefore, considered preliminary and will be revised following further on-shore studies.

Calcareous Nannofossils

We examined 158 samples from Holes 645B, 645C, 645D, 645E, 645F, and 645G for nannofossils. Only 26 were found to contain nannofossils. The assemblages were generally low in diversity (commonly only one or two species) and in abundances. Martini's (1971) standard zonation scheme was not applicable at this site because of the absence of many warm- or temperate-water species that serve as zonal boundary markers. However, two zones, defined in Müller's (1976) high-latitude zonation of the Norwegian Sea, were observed at this site. Müller's zones are combinations of Martini's zones and, therefore, lack Martini's stratigraphic resolution. These zones are discussed in the following "Results" section.

Results

Single specimens of *Gephyrocapsa* sp. were observed in Sections 105-645B-1X, CC, and 105-645B-8X, CC. The specimen in Section 105-645B-8X, CC, is possibly *Gephyrocapsa* cf. *oceanica*. The genus *Gephyrocapsa* ranges from the Pliocene to Holocene (Gartner, 1977); however, dating these samples from single specimens is risky. Sample 105-645B-29X-3, 84-85 cm, contains rare specimens of *Coccolithus pelagicus*, which is a long-ranging, cosmopolitan species having no age or environ-

mental implications. Sample 105-645B-22X-6, 58–60 cm, contains a single small *Reticulofenestra*, which also has no age implications.

No nannofossils were observed in samples from Holes 645C, 645D, and the upper part of Hole 645E. This barren interval extends down through Section 105-645E-34R, CC, except for a solitary occurrence of *Coccolithus pelagicus* in Section 105-645E-22R, CC.

Rare specimens of *Reticulofenestra pseudoumbilica* and *C. pelagicus* were observed in Section 105-645E-35R, CC. Sporadic occurrences of this assemblage, separated by barren intervals, continue down to, but do not include, Sample 105-645E-70R-5, 61–63 cm. In Sample 105-645E-70R-2, 42–44 cm, species diversity and abundance increase. In addition to the aforementioned two species, *Helicosphaera* spp., small *Reticulofenestras* and *Coccolithus* sp., *Braarudosphaera bigelowi*, *Discolithina multipora*, and *Coronocyclus* sp. also occur. In the Norwegian Sea, Müller (1976) observed an "interval with *Reticulofenestra pseudoumbilica*," consisting mainly of *R. pseudoumbilica* and *C. pelagicus*. The last-appearance datum (LAD) of *R. pseudoumbilica* marks the top of her interval and is also used by Martini (1971) as the NN15/NN16 boundary marker. The base of her interval is marked by the LAD of *Helicosphaera ampliaperta*, which also marks Martini's NN4/NN5 boundary. Thus, she equated this interval with Zones NN5 to NN15 of Martini's standard zonation. None of Martini's (1971) other low-latitude zonal markers are present at Site 645, and the few other species observed are not stratigraphically significant. Therefore, no subdivisions of the interval between Sections 105-645E-35R, CC, and 105-645E-70R-5, 61–63 cm, can be made. If the calcareous nannofossils in this interval are not reworked, they suggest a zonal range from Zones NN5 to NN15.

Samples 105-645E-70R-5, 61–63 cm, and 105-645E-70R, CC, have a similar assemblage to 105-645E-70R-2, 42–44 cm, but also contain few *Helicosphaera ampliaperta*. The abundance of *H. ampliaperta* decreases considerably below Core 105-645E-70R, and only single specimens were found in Samples 105-645E-71R-2, 40–42 cm, and 105-645E-71R-3, 39–41 cm. The overall species abundance and diversity also decrease in these two samples. An interval containing *H. ampliaperta* was observed by Müller (1976) in the Norwegian Sea and was equated roughly to Martini's (1971) Zones NN3 to NN4, on the basis of the total range of *H. ampliaperta*. According to Bramlette and Wilcoxon (1967), the first-appearance datum (FAD) of *H. ampliaperta* approximates the Oligocene/Miocene boundary in Trinidad, whereas Martini (1971) uses *H. ampliaperta*'s LAD as the marker for the NN4/NN5 boundary. Therefore, we think that the presence of *H. ampliaperta* suggests a zonal range from NN1 to NN4 for the interval from Sample 105-645E-70R-5, 61–63 cm, to 105-645E-71R-3, 39–41 cm.

Sample 105-645E-73R, CC, contains a diverse assemblage, including *C. pelagicus*, small *Coccolithus* sp., *R. pseudoumbilica*, *Discolithina* sp., *Reticulofenestra* sp., *Syracosphaera* sp., *Helicosphaera* sp., and *Braarudosphaera bigelowi*. No specimens of *H. ampliaperta* were observed; therefore, no definite age assignment can be made for this sample.

Smear slides were prepared from core-catcher samples from Holes 645F and 645G, as well as from Sample 105-645G-1H-3, 33 cm. Nanofossils were not observed in any of these samples.

Paleoenvironment

Absolute abundances of calcareous nannofossils are greater in warm to temperate regions than in colder regions. In colder water, high-latitude regions, genera such as *Coccolithus* and *Reticulofenestra* increase in relative abundance. The sparse nannofossil assemblage composed primarily of *Coccolithus* and *Reticulofenestra*, which occurs from the top of Hole 645 down to

Sample 105-645E-70R-2, 42–44 cm, indicates a cold-water environment. Helicosphaerids, braarudosphaerids, and discolithinas are more common in warm to temperate shelf environments than in cold, open-marine environments. Their presence in the interval from Samples 105-645E-70R-2, 42–44 cm, to 105-645E-73R, CC, suggests a shelf environment or a sediment influx from a shelf area, as well as warmer-than-arctic temperatures and perhaps cool-temperate conditions.

Preservation

The preservation of species is generally good. In samples having relatively high abundances (Cores 105-645E-70R and 105-645E-73R), preservation is variable, ranging from moderate to good. In samples with low nannofossil abundances (all other samples), preservation is good.

Foraminifers

Hole 645A

No core-catcher samples were studied from Hole 645A.

Hole 645B

Foraminifers from Hole 645B were examined from core-catcher samples of each core; the preliminary stratigraphy is presented in Figure 26. From foraminiferal stratigraphy, Hole 645B can be divided into three intervals.

Interval I (0–110 mbsf) displays common benthic and planktonic foraminiferal abundances and low benthic to planktonic foraminiferal ratios. The planktonic fauna consists generally of >90% sinistral *Neogloboquadrina pachyderma* and smaller percentages of dextral *N. pachyderma*, *Globigerina bulloides*, *Globigerina quinqueloba*, and *Globigerinita uvula*. These species range at least from the late Miocene to Holocene; therefore, a precise age assignment based on the ranges of these taxa cannot be made. The dextral to sinistral coiling change of *N. pachyderma* reported to occur in both the Arctic (Herman, 1974) and in the Labrador Sea (Berggren, 1972) was not observed. In the Labrador Sea, this datum lies in the upper part of Zone N21 of Blow (1969) (at about 2.7 Ma) and suggests a younger age for the section. Benthic foraminifers in Interval I are represented by *Cassidulina teretis*, *C. reniforme*, *Stetsonia horvathi*, *Melonis zandaamae*, *Epistominella takayanagii*, and some intervals containing a high abundance of miliolid species. This fauna displays arctic affinities and is similar to the glacial fauna of the north-east Atlantic Ocean (Murray, 1985) and the Norwegian–Greenland Sea (Berggren and Schnitker, 1983).

The ratio of benthic to planktonic (B/P) foraminifers has been used to determine the preservation state of calcareous biogenic debris on the seafloor (Thunell, 1976); increased B/P ratios indicate higher rates of dissolution. The B/P ratios in the core-catcher samples from Interval I range from 0.0 to 0.4. Very low B/P ratios and the presence of dissolution-susceptible species (i.e., *Globigerina bulloides*, *G. quinqueloba*, and *G. uvula*) suggest relatively good preservation of calcareous fauna. Studies of short piston cores from Baffin Bay demonstrated that biogenic carbonate cycles are largely controlled by dissolution, and periods of intense dissolution correlate with interglacial stages (Aksu, 1983).

Interval II (120–298.9 mbsf) contains a predominantly benthic foraminiferal fauna, which is similar to that of Interval I but with a lower abundance of *Stetsonia horvathi*. Only two core-catcher samples (105-645B-30X, 105-645B-31X) contain planktonic foraminifers, which consists of *Neogloboquadrina pachyderma* sinistral, *G. bulloides*, and rare *N. pachyderma paraobesa*. The B/P ratios in this interval are >10, suggesting poor preservation of biogenic carbonate. The sparse benthic and

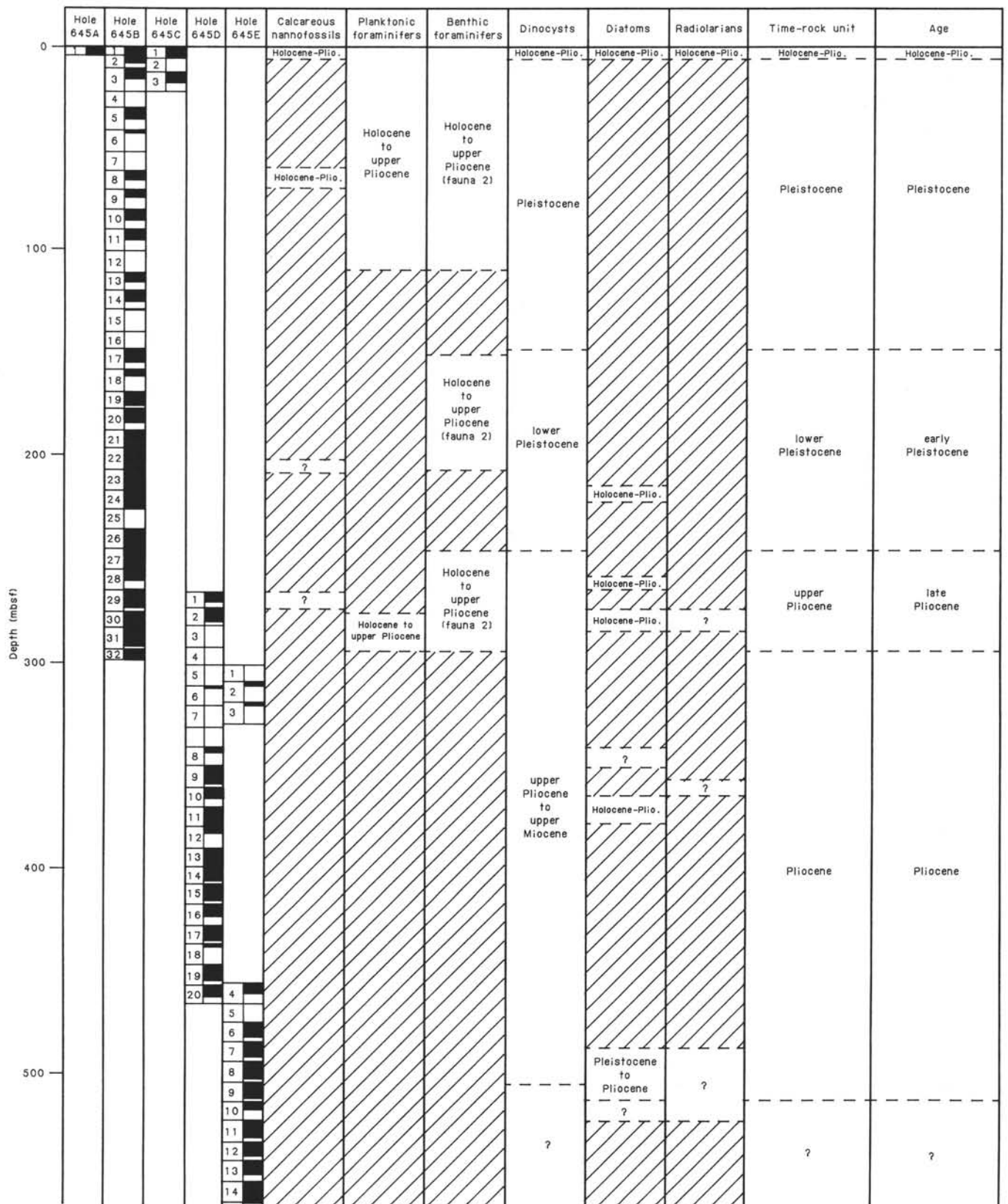


Figure 26. Biostratigraphic summary, Site 645, based on calcareous nanofossils, foraminifers, dinocysts, diatoms, and radiolarians. Cored interval is in meters; recovered interval is represented by shaded region. Diagonal lines indicate stratigraphic intervals in which no microfossils were observed.

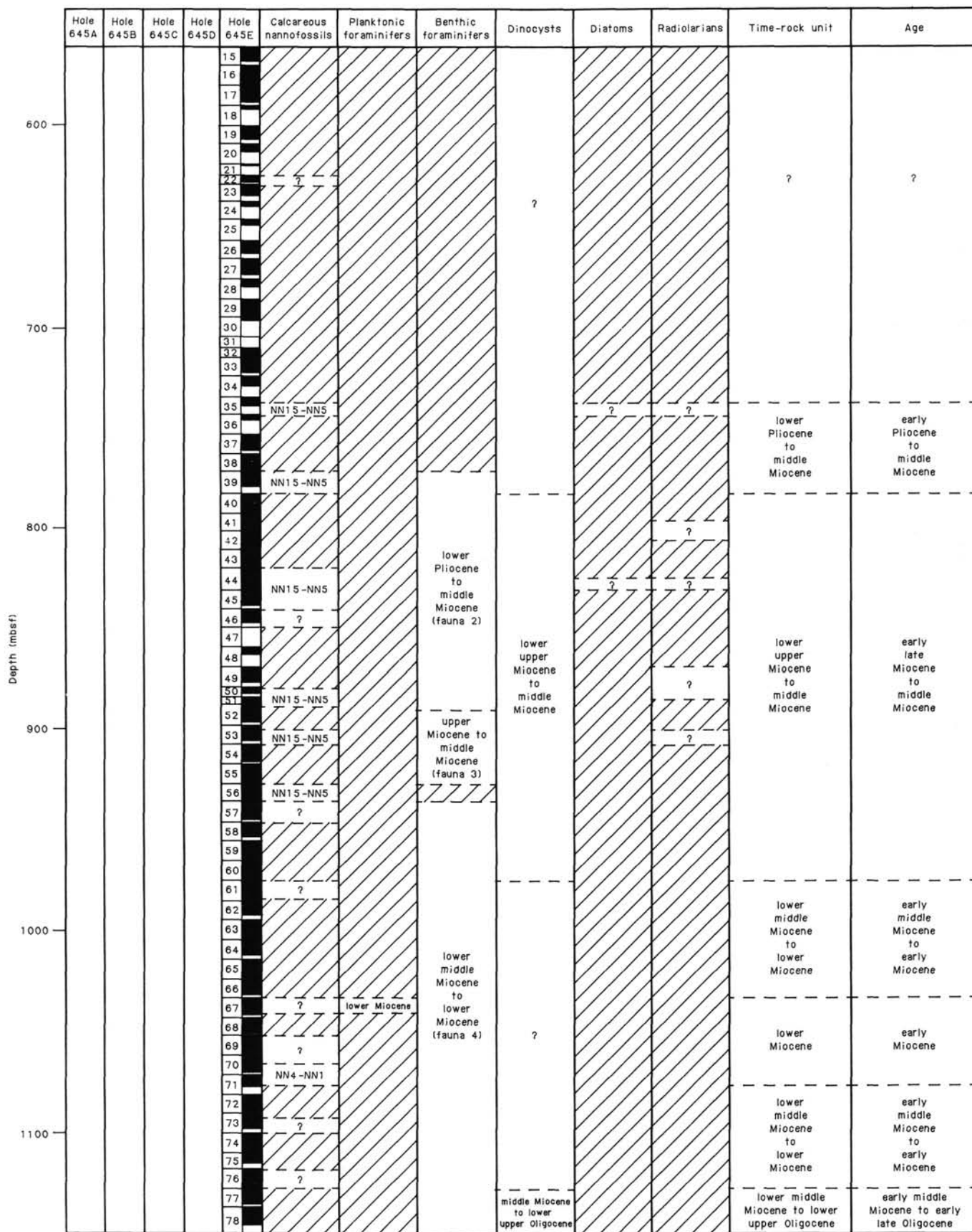


Figure 26 (continued).

planktonic fauna do not allow a detailed zonation to be established, but the occurrence of sinistral *N. pachyderma* in Sample 105-645B-30X, CC, may indicate an age younger than 2.7 Ma for Interval II.

Hole 645C

Only two core-catcher samples were analyzed from Hole 645C, both containing a glacial fauna similar to that described in Interval I.

Hole 645D

Except Sections 105-645D-6R, CC, and 105-645D-13, CC, core-catcher samples analyzed from this hole are barren of foraminifers. These samples (105-645D-6R, CC, and 105-645D-13R, CC) contain a calcareous benthic foraminiferal fauna similar to that described in Hole 645B.

Hole 645E

From 301.1 to 772.7 mbsf, all core-catcher samples are barren of foraminifers, but the section from 772.7 to 1147.1 m can be subdivided into three intervals on the basis of its content of benthic foraminifers.

Interval I (772.7–884.9 mbsf) contains a benthic foraminiferal fauna characterized by *Melonis zaandamae*. The presence of both this species and a planktonic microfossil of unknown affinity, *Bolboforma metzmacheri*, suggests a late middle Miocene to early Pliocene age for the section above 772.1 mbsf. *Bolboforma* seems to be concentrated in high-latitude contourite drift deposits of middle Miocene–early Pliocene age (Murray, 1985). This interval also contains diverse agglutinated foraminifers, including *Bathysiphon* sp., *Rhabdammina discreta*, *Hyperammia friabilis*, *Saccammina difflugiformis*, *Psammosphaera fusca*, and *Cyclammina cancellata*.

Interval II (884.9–926 mbsf) also contains *Melonis zaandamae* and *Bolboforma metzmacheri* in addition to a more diverse assemblage of agglutinated foraminifers, including *Cyclammina* cf. *C. arctica*, *Haplophragmoides carinata*, and *Martinotiella communis*. The latter species characterizes the middle to late Miocene in the Norwegian–Greenland Sea (Verdenius and van Hinte, 1983) and the Labrador Margin (F. Gradstein, pers. comm., 1986).

Interval III (945.9–1147.1 mbsf) is characterized by sparse agglutinated foraminifers and the absence of *M. zaandamae* and *B. metzmacheri*. Calcareous foraminifers were found in two samples (105-645E-67R-2, 84–86 cm, and 105-645E-70R, CC) and consist of *Cibicidoides* sp., *Uvigerina* sp., *Oridorsalis tener*, *Gyroidinoides* sp., *Pullenia bulloides*, *Melonis barleanus*, *Lagena* spp., and very rare specimens of the planktonic species *Globigerina praebulloides*. The benthic fauna is probably early middle Miocene in age or older, but the occurrence of *G. praebulloides* in Labrador Margin wells indicates an early Miocene age. Near the base of the hole, the agglutinated foraminiferal fauna again becomes more diverse, *Psammosphaera*, *Saccammina*, *Ammodiscus*, *Haplophragmoides*, and *Trochammina* being the most common genera.

Diatoms

Holes 645A and 645B

No samples were examined for diatoms in the 4.9-m core recovered from Hole 645A. Thirty-three samples, consisting primarily of core-catcher samples, were analyzed for diatoms from Hole 645B. Except in Sample 105-645B-24X-3, 66–67 cm, and Sections 105-645B-28X, CC, and 105-645B-30X, CC, diatoms were not observed in samples examined from Cores 105-645B-1X through 105-645B-32X. Samples 105-645B-24X-3, 66–67 cm, and 105-645B-28X, CC, contain rare, non-age-diagnostic species.

The few poorly preserved diatoms observed in Section 105-645B-30X, CC, include *Coscinodiscus marginatus*, *Melosira sol*, *Nitzschia cylindra*, *Nitzschia grunowii*, *Thalassionema nitzschioides*, and *Thalassiosira decipiens*. Although primary stratigraphic indicators were not observed in this sample, the diatom assemblage is characteristic of the Pliocene–Pleistocene. Koizumi (1973) reports *Fragilariopsis cylindrus* (currently referred to as *Nitzschia cylindra*) and *Porosira glacialis* in Pliocene–Pleistocene sediments from Japan and the North Pacific, which are equivalent to or younger than the *Denticulopsis seminae*-*D. kamtschatica* Zone. These species are also reported from Pliocene–Pleistocene sediments of the Bering Sea (Baldauf, 1981; Sancetta, 1982).

The occurrence of *Melosira sol*, *Nitzschia cylindra*, and *N. grunowii* in samples from Hole 645B suggests a shallow environment. The maximum abundance of *M. sol* in Quaternary sediments of the Bering Sea is reported by Sancetta (1982) to occur in shallow water (<50-m water depth). The abundance of this species in the Bering Sea also decreases with increased water depth (Sancetta, 1982). *Nitzschia cylindra* is a bipolar species commonly associated with pack ice as well as with plankton (Sancetta, 1982). Within the Bering Sea, *N. cylindra* and *N. grunowii* are most abundant in sediments deposited on the continental shelf (Baldauf, 1981; Sancetta, 1982).

Hole 645C

Four samples were examined from Hole 645C. Except in Sample 105-645C-1H-1, 3–5 cm, diatoms were not observed in these samples (105-645C-1H, CC, 105-645C-2H, CC, and 105-645C-3H, CC). No primary stratigraphic indicators occur in Sample 105-645C-1H-1, 3–5 cm, but the similarity of the diatom assemblage in this sample to that observed in samples from Hole 645B suggests a Pliocene–Pleistocene age.

Hole 645D

Diatoms were observed in core-catcher samples taken from Cores 105-645D-2R, 105-645D-8R, and 105-645D-10R as well as in Samples 105-645D-2R-3, 70–72 cm, 105-645D, 8R-3, 80–81 cm, and 105-645D-11R-3, 48–50 cm. The diatom abundance and preservation vary from sample to sample.

Samples 105-645D-2R-3, 70–72 cm, and 105-645D-2R, CC, contain few well-preserved diatoms. The assemblage is dominated by specimens of *Actinopterychus senarius*, *Coscinodiscus marginatus*, *Melosira sol*, *Nitzschia cylindra*, *N. grunowii*, and *Thalassionema nitzschioides*. One specimen of *Thalassiosira oestrupii* was observed in Sample 105-645D-2R, CC, and suggests a Pliocene or younger age for this sample. The remaining part of the observed assemblage is similar to that observed in Hole 645B and supports this age assignment.

One specimen of *Melosira sol* was observed in Sample 105-645D-8R-3, 80–81 cm. This species is not stratigraphically useful. Rare diatoms occur in Sample 105-645D-8R, CC, and few, moderately well-preserved diatoms occur in Sample 105-645D-10R, CC. The assemblage observed in these samples is similar to that in Hole 645B and suggests a Pliocene–Pleistocene age. Additional Pliocene–Pleistocene indicators observed included *Thalassiosira gravida* and *Porosira glacialis*. Rare, reworked specimens of *Mediaria splendida* (middle to lower-upper Miocene) also occur in Section 105-645D-10R, CC.

Sample 105-645D-11R-3, 48–50 cm, contains few well-preserved diatoms. In addition to the diatom aforementioned assemblage, specimens of *Thalassiosira* cf. *hyalina*, *Thalassiosira* cf. *trifulta*, and reworked specimens of *Coscinodiscus plicatus* (Miocene) were also observed.

Hole 645E

Diatoms were observed only in the following samples: core catchers of Cores 105-645E-7R, 105-645E-8R, 105-645E-9R, 105-

645E-10R, 105-645E-35R, 105-645E-41R, and Samples 105-645E-44R-2, 37-39 cm, and 105-645E-51R-1, 90-91 cm. The diatom abundance and preservation vary from sample to sample.

Core catchers of Cores 105-645E-7R, 105-645E-8R, 105-645E-9R, and 105-645E-10R contain few to abundant and poor to well-preserved specimens. The assemblage observed is similar to that discussed previously and includes specimens of *Nitzschia grunowii*, *N. cylindra*, *Porosira glacialis*, and *Melosira sol.* The assemblage differs from that described previously in that numerous specimens of *Actinocyclus senarius*, *A. splendens*, *A. vulgaris*, *Stephanopyxis turris*, and *Rhizosolenia hebetata* commonly occur in these samples. In addition, many neritic species such as *Biddulphia aurita*, *Melosira cf. islandica*, *Rhaphoneis amphiceros*, *Grammatophora* sp., *Diploneis* sp., and *Navicula* sp. 3 (Baldauf, 1981) were observed. This assemblage is typical of a near-shore (shelf-slope) environment. The occurrence of *Rhizosolenia barboi* in these samples indicates that they are younger than the late middle Miocene.

Specimens of *Coscinodiscus flexuosus* (Miocene) occur in Section 105-645E-7R, CC, and specimens of *Stephanogonia hanazawae* occur in Sections 105-645E-8R, CC, and 105-645E-9R, CC, which suggests a late middle Miocene to late Miocene age for this interval. However, the additional occurrence of *Nitzschia grunowii*, *N. cylindra*, and *Porosira glacialis* (Pliocene-Pleistocene) in these samples suggests that the specimens of *C. flexuosus* and *S. hanazawae* may have been reworked. Sample 105-645E-9R, CC, contains a few reworked specimens of *Goniothecium decoratum* (Eocene to early Miocene).

Rare specimens of *Coscinodiscus marginatus* and *Melosira* sp. were observed in Section 105-645E-35R, CC. This sample primarily contains fragments. Diatom fragments were also observed in Sections 105-645E-41R, CC, 105-645E-44R-2, 37-39 cm, and 105-645E-51R-1, 90-91 cm. No age-diagnostic species were observed within these samples. Some specimens of pyritized diatoms were recorded from Hole 645E between Core 105-645E-11R and the base of the hole.

Holes 645F and 645G

Diatoms were not observed in core-catcher samples from Holes 645F and 645G. Sample 105-645F-1H-1, 0-2 cm, contains a few well-preserved diatoms, including *Actinocyclus curvatus*, *Thalassiothrix longissima*, *Coscinodiscus oculus-iridis*, *Rhizosolenia hebetata*, and *Thalassiosira trifulta*. One specimen each of both *Nitzschia cylindra* and *N. grunowii* was also recorded in this sample. These species characterize the Pliocene-Pleistocene, but their rare occurrence disallows any accurate age determination.

Radiolarians

Except for a single surface sample, radiolarians were observed in only trace amounts (one, or at most eight, specimens per slide) in a few samples at Site 645 (see "Summary and Conclusions" section, this chapter), generally coinciding with the occurrence of monaxon sponge spicules and centric diatom fragments. Only fragments of radiolarians, which could not be confidently identified, were observed. However, the morphology of most of the fragments indicates that they were probably derived from prunoid, lithelid, and spongodiscid species. We also observed three partial specimens possibly assignable to *Stichocorys* sp. in Samples 105-645E-44R-2, 36-39 cm, and 105-645E-50R, CC; one specimen in Section 105-645B-28R, CC, possibly belonging to *Lychnocanium* (feet missing and assumed broken off); a single specimen of *Antarctissa* sp. in Section 105-645D-2R, CC; and one specimen, possibly *Lamprocyclus aegles* (?) in Section 105-645E-8R, CC.

The extreme rarity and poor preservation of radiolarians at Site 645 preclude any stratigraphic analysis. The specimens seen are typical of high-latitude environments, although too few specimens were observed to permit precise biogeographic classification. The virtual absence of radiolarians in these sediments may have paleoceanographic significance or may be due to diagenesis.

Common, well-preserved radiolarians were observed only in the surface sediments (Sample 105-645F-1H-1, 0-2 cm). Species observed include *Cycladophora davisiana*, *Lithomelissa* spp., *Pseudodictyophimus gracilipes*, *Spongotrochus glacialis*, *Cladocinium tricolpium*, *Amphimelissa setosa*, *Lithelius* spp., *Phormacantha hystrix*, and *Androcyclas gamphonycha*. This assemblage is similar to the "glacial" Pleistocene to Holocene assemblage observed in the Norwegian Sea and adjacent Norwegian fjords (Bjørklund, 1976) and is different from the more temperate assemblages observed in the North Atlantic basin (Goll and Bjørklund, 1971). Except *Spongotrochus glacialis*, all the aforementioned species are delicately silicified and easily dissolved, and their absence in older sediments may thus be a result of dissolution.

Palynology

Holes 645A, 645B, and 645C

Core-catcher samples were analyzed for dinocyst, pollen, and spore contents. Palynomorphs are few to abundant and relatively well preserved. However, reworked palynomorphs commonly dominate assemblages. The more commonly reworked palynomorphs are pre-Tertiary trilete spores and bisaccate pollen grains.

Dinoflagellate Cysts

Dinocyst diversity and concentration are generally low. The number of dinocysts per cubic centimeter rarely exceeds 100 individuals. The more frequently recorded taxa are *Brigantedinium simplex*, *Brigantedinium* spp., *Operculodinium centrocarpum*, and rare *Bitectedinium tepikiense*. An increase in concentration and diversity is apparent below about 245 mbsf.

Biostratigraphy

A few biostratigraphic interpretations can be made:

1. The presence of the arctic species *Multispinula minuta* suggests a Pleistocene age for the uppermost 177 m in Hole 645B. *M. minuta*, recorded in upper Pleistocene sediments from the North Atlantic (Mudie, in press), has a Pleistocene range in the Arctic Ocean (Aksu and Mudie, 1985).

2. *Filisphaera filifera* occurs between 148.8 and 298.9 mbsf in Hole 645B. *F. filifera* is reported from the Pliocene to the lower Pleistocene sediments of the North Atlantic (Mudie, in press) and from upper Miocene to lower Pleistocene sediments of the North Pacific (Bujak, 1984). The co-occurrence of *F. filifera* and *M. minuta* indicates an early Pleistocene age for the 148.8-177-m sub-bottom interval.

3. The occurrence of few to common cf. *Labyrinthidium* sp. below 245.2 mbsf at Hole 645B suggests a Pliocene or older age. This age assignment is mainly based on the comparison between the dinocyst stratigraphy of the Labrador Sea and that of Baffin Bay. Specimens of cf. *Labyrinthidium* are common to abundant at the Labrador Sea Sites 646 and 647, where it last appears at the Pliocene/Pleistocene boundary. This species is identical to a form described as *Labyrinthidium truncatum* by Mudie (in press; pers. comm., 1985) and is recorded in Miocene to upper Pliocene sediments from the North Atlantic. However, because the exact taxonomic affinity of this species is un-

certain, it is provisionally referred to here as cf. *Labyrinthodinium* sp.

4. The occurrence of *Brigantedinium* spp., *F. filifera*, *Operculodinium crassum*, and cf. *Labyrinthodinium* sp. collectively suggests that the lower part of Hole 645B (245.2–298.9 mbsf) has an age between late Miocene and late Pliocene (Harland, 1979; Bujak, 1984; Mudie, in press).

Paleoenvironments

The generally low dinocyst diversity and concentration (<100 specimens per cm³) in the upper part of Hole 645B (0–139.1 mbsf) indicate low primary productivity. The dinocyst assemblages are characterized by two main components:

1. The most common taxa recorded, *Brigantedinium simplex*, is associated with low-salinity conditions during summer (<30‰; Mudie and Short, 1985); *B. simplex* is frequently observed in Holocene fjord sediments (Dale, 1976; Mudie and Deonarine, 1983). The occurrence of *B. simplex* through Hole 645B sedimentary sequence suggests general low-salinity conditions, probably as a consequence of meltwater input into Baffin Bay. The presence of *M. minuta* also indicates arctic-type conditions and a low salinity of surficial water masses (31–33‰; Mudie and Short, 1985).

2. The few occurrences of *Operculodinium centrocarpum* and *Bitectadodinium tepikiense* reflect episodic incursions of North Atlantic waters into Baffin Bay. High-resolution studies on the uppermost 22 m of Site 645 sediments and on piston cores (Hudson 77-027-013, 76-029-033; de Vernal, 1986) confirm that significant penetration of North Atlantic water into Baffin Bay occurred only during rare and brief intervals. The present interglacial is one of these exceptional episodes.

In the lower part of Hole 645B (139.1–298.9 mbsf), dinocyst concentration varies between about 100 and 2000 specimens per cm³ and suggests relatively high, but still fluctuating, primary productivity. The few to common occurrences of *Operculodinium* species (*O. centrocarpum* and *O. crassum*), *Filisphaera filifera*, cf. *Labyrinthodinium* sp., and *Tectatodinium simplex* indicate some influence of North Atlantic surficial water masses and cool-temperate to subarctic conditions. However, the dinocyst diversity and concentrations are much lower than those in correlative sediments from the Labrador Sea Site 646, indicating that Baffin Bay was a relatively confined environment.

Pollen and Spores

In the uppermost part of Hole 645B (0–177.1 mbsf), pollen and spore concentrations are generally low (<100 specimens per cm³). The offshore location of Site 645 and the paucity of the vegetation on adjacent continents certainly partly caused the low pollen content of the deposits. The few pollen grains and spores counted do not allow precise interpretation of paleovegetation and atmospheric paleocirculation. The high amount of reworking also limits the interpretation of poor pollen assemblages. High-resolution studies on piston core Hudson 76-029-033 permit calculation of a correlation coefficient (R) of 0.78 between the pollen and reworked palynomorph concentrations, indicating that erosional and sedimentary processes may be largely responsible for the pollen content in the sediment (de Vernal, 1986).

In the lower part of Hole 645B (177.1–298.9 mbsf), a common to abundant terrestrial palynoflora is present. In this interval, pollen and spore concentrations vary between about 100 and 20,000 specimens per cm³. *Pinus*, *Picea*, *Betula*, *Alnus*, and *Sphagnum* constitute the main taxa. *Lycopodium*, *Selaginella*, Polypodiaceae, and Ericaceae are also present. Because of the small size of *Betula* pollen grains (<25 µm), this genus is proba-

bly represented by a shrub species (*B. nana* or *B. glandulosa*?). The assemblages, interpreted as representing a forest tundra vegetation in the main source area, indicate a cool, subarctic to semi-arctic, and very humid climate. Even though the source area is unknown, a more northern tree line (perhaps on Baffin Island or Greenland) than the present one may be inferred. The high pollen concentration as well as the presence of plant tissues in samples analyzed suggests strongly that a relatively dense vegetation developed on the continent adjacent to Baffin Bay. Fluctuations in pollen percentages and concentrations indicate that variations in the density and composition of the vegetation may have occurred.

The palynostratigraphy of Hole 645B suggests an important change at about 177 mbsf from subarctic to arctic conditions in the Baffin Bay area.

Hole 645D

Most samples analyzed are characterized by very abundant detrital organic matter and terrestrial palynomorphs. The main problem encountered in the analysis of Hole 645D samples is the distinction of reworked and in-place palynomorphs. Reworked palynomorphs are certainly present, notably Paleogene dinocysts such as *Apectodinium*, *Glaphyrocysta*, *Wetzeliella*, and the Cretaceous dinocyst *Chatangiella*. Furthermore, varying stages of preservation (or diagenesis) observed in the pollen grains and spores suggest that part of the assemblages may be reworked. However, reworked palynomorphs are not necessarily altered; the aforementioned dinocysts are generally well preserved. An unequivocal distinction between reworked and nonreworked palynomorphs is therefore difficult using routine microscopical examination. The use of fluorescence microscopy is required to resolve this problem.

Dinoflagellate Cysts

Low diversity and concentration characterize the dinocyst assemblages. *Brigantedinium* species and cf. *Labyrinthodinium* sp. are the most common dinocysts recorded. The presence of these dinocysts indicates an age of late Miocene to late Pliocene (Bujak, 1984; Mudie, in press). The occurrence of *Filisphaera filifera* also indicates a late Miocene or younger age (Bujak, 1984; Mudie, in press).

Protoperidiniaceae cysts such as *Brigantedinium* spp. and *Selenopemphix* spp. observed in Hole 645D typically characterize a neritic environment. The common occurrence of these dinocysts as well as the abundance of terrestrial organic matter may suggest nearshore-type conditions or sedimentation in an epicontinental-type basin. Nevertheless, the occurrence of *Filisphaera filifera*, cf. *Cannosphaeropsis* sp. I, and cf. *Labyrinthodinium* sp. indicates some exchange with oceanic, probably North Atlantic, surficial water masses.

Pollen and Spores

Pinus, *Picea*, *Sphagnum*, and Polypodiaceae were the more common pollen grains and spores observed. *Selaginella*, *Abies*, and *Tsuga* are also present. The assemblages reflect the existence of a dense tundra forest or coniferous boreal forest in the source area and indicate the existence of a cool-humid temperate to subarctic climate. The very abundant detrital organic matter and notably the ligneous fibers suggest a relatively dense vegetation in continental areas surrounding Baffin Bay.

Hole 645E

Most samples from Hole 645E were prepared and analyzed for their palynomorph contents. The samples examined are generally characterized by abundant detrital terrestrial organic matter. As in Hole 645D, making the distinction between the reworked and in-place palynomorphs is difficult.

Dinocysts

In the upper part of Hole 645E (465–782 mbsf), the abundance of dinocysts is generally low. However, relatively rich assemblages observed in some samples are characterized by *Achomosphaera ramulifera*, *Tectadodinium simplex*, or *Impagidinium* species, notably *I. patulum*. In the lower part of Hole 645E (782–1147.1 mbsf), dinocyst diversity increases.

Although most of the identified dinocysts have a long stratigraphic range, a few biostratigraphic interpretations can be made:

1. The presence of *Impagidinium patulum* between 310 and 628.4 mbsf suggests an age of middle Miocene to Holocene (Harland, 1978; Costa and Downie, 1979).

2. In Sections 105-645E-57, CC, and 105-645E-60R, CC, the presence of "*Nematosphaeropsis*" *aquaeducta* indicates a middle Miocene to early Pliocene age (Piasecki, 1980; Edwards, 1985; Mudie, in press).

3. *Paleocystodinium* species were observed in many samples from the lower part of Hole 645E (782–1147 mbsf). *Paleocystodinium* has an upper age of early late Miocene in the North Atlantic (Brown and Downie, 1985; Edwards, 1985). The occurrence of "*Nematosphaeropsis*" *aquaeducta* and *Paleocystodinium* in the 782–975-mbsf interval suggests an age of middle to early late Miocene. However, the *Paleocystodinium* specimens may have been reworked.

4. In the lowest part of Hole 645E (975–1147.1 mbsf), the presence of *Impletosphaeridium* sp. 1 of Manum (1976) suggests a middle Oligocene or younger age (Manum, 1976; Harland, 1978; Costa and Downie, 1979). The presence of *Distadodinium paradoxum* in Sections 105-645E-77R, CC, and 105-645E-78R, CC, indicates an age no younger than middle Miocene for the interval from 1137 to 1147.1 mbsf (Piasecki, 1980), and the presence of *Impletosphaeridium* sp. 1 of Manum (1976) in Sample 105-645E-78R, CC, constrains the bottom of the hole as being no older than early late Oligocene (Costa and Downie, 1979).

The environmental interpretation of the upper part of Hole 645E (465–782 mbsf) is difficult to make because of the sporadic occurrence of dinocysts. However, the general dominance of Gonyaulaceae cysts (*Impagidinium* spp., *Operculodinium* spp., and *Bitectadodinium tepikiense*) reflects more oceanic than neritic conditions. The occurrence of *Impagidinium* species in a few samples clearly indicates an open-ocean environment and suggests warm-temperate or subtropical surficial water masses (Harland, 1983).

In the lower part of Hole 645E (782–1147.1 mbsf), the presence of *Impagidinium* spp. and *Systematophora* sp. may indicate open-marine conditions. However, the Protoperidiniaceae cysts (*Selenopemphix* spp. and *Lejeunecysta* spp.) and *Lingulodinium machaerophorum* are relatively abundant in this interval, suggesting outer-neritic influences. All these taxa further reflect temperate surficial water masses. Similar assemblages, but having greater diversity, were described from Miocene sediments in the North Atlantic (Costa and Downie, 1979; Brown and Downie, 1985; Edwards, 1985).

Pollen and Spores

Pollen assemblages in the samples analyzed from Hole 645E are largely dominated by *Pinus* and *Picea*. Boreal indicators (*Selaginella*, *Sphagnum*, and *Alnus*) are present but scarce. The pollen and spore assemblages reflect coniferous boreal forest vegetation and a cool to temperate, humid climate. An increase in the abundance of *Tsuga* was observed downhole, indicating more temperate, but humid, conditions.

Summary

Biostratigraphy

Figure 26 summarizes the calcareous nannofossil, foraminifer, dinocyst, diatom, and radiolarian stratigraphies of Site 645. Because of the nature of the microfossil record (see previous discussion), recognition of zonal or stage/series boundaries is difficult. Samples were, therefore, assigned the most restricted age range possible based on the microfossil assemblages observed.

The composite stratigraphic section recovered at Site 645 is considered to be Oligocene or earliest Miocene to Holocene in age. As indicated by the occurrence of the dinocyst species *Multispinula minuta*, the upper 177 mbsf are of Pleistocene age. The occurrence of the dinocyst species *Filispheera filifera* and *M. minuta* suggests an early Pleistocene age for samples between 148.8 and 177 mbsf. The Pliocene/Pleistocene boundary may be tentatively placed at about 245 mbsf. This age assignment is based on the last occurrence of few to common cf. *Labrynthodinium* sp., which characterizes the Pliocene/Pleistocene boundary at Sites 646 and 647 in the Labrador Sea. Section 105-645B-31X, CC (292 mbsf), is probably younger than early Pliocene (3.4 Ma). This late Pliocene age assignment is based on the common occurrence of sinistral specimens of *Neogloboquadrina pachyderma* compared with only few dextral specimens in Sections 105-645B-30X, CC, and 105-645B-31X, CC. Currently, the left-coiling population in the North Atlantic is separated from the right-coiling population by the 7.2° April isotherm (Ericson, 1959). In the Labrador Sea and the high Arctic, Bé and Tolderlund (1971) found that 90% or more of *N. pachyderma* individuals are of the left-coiling variety. The high sinistral-to-dextral ratio observed in samples from Site 645 suggests that these samples are stratigraphically above the coiling change from dextral to sinistral *N. pachyderma* reported by Berggren (1972) to occur in upper Pliocene sediments from Labrador Sea. This placement, however, is tentative because the change in coiling direction may have been missed either because of the sampling interval or more probably because it occurred in an interval where calcareous microfossils are not preserved. This age is supported by the occurrence of *Cassidulina teretis*, which was not found to range below the late Pliocene in the Norwegian–Greenland Sea (Berggren and Schnitker, 1983) and the Rockall margin (Murray, 1985).

On the basis of occurrence of a Pliocene–Pleistocene diatom assemblage, Section 105-645E-9R, CC (515 mbsf), is Pliocene (5.3 Ma) or younger in age. The rare occurrence of the nannofossil species *Reticulofenestra pseudumbilica* in Section 105-645E-35R, CC (743.7 mbsf), suggests that this sample is early Pliocene or older. Although specimens of this species are rare and may be reworked, such an age is also suggested by species of benthic foraminifers observed in Section 105-645E-39R, CC, where the fauna is characterized by *Melonis zaandamae*. The occurrence of this species and a microfossil of unknown affinity, *Bolboforma metzmacheri*, suggests that the interval from Section 105-645E-39R, CC, to 105-645E-50R, CC (772.7–884.9 mbsf), is early Pliocene to middle Miocene in age. The occurrence of the dinocyst species *Paleocystodinium* spp. in the interval from 782 to 1147.1 mbsf also suggests an early late Miocene or older age for Section 105-645-45R, CC.

The occurrence of "*Nematosphaeropsis*" *aquaeducta* in the interval from Section 105-645E-56R, CC, to 105-645E-60R, CC, indicates that this interval is no older than middle Miocene. The occurrence of benthic foraminifers (Samples 105-645E-67R-2, 84–86 cm, and 105-645E-70R, CC) characteristic of the early middle Miocene or older and the occurrence of *Globigerina praebulloides*, which has a local extinction level in the early Mi-

ocene of Labrador Margin wells (F. Gradstein, pers. comm., 1986), suggest that this interval (974.9–1071.1 mbsf) is early Miocene in age.

Calcareous nannofossils, including *Helicosphaera amplipecta*, occur in Samples 105-645E-70R-5, 61–63 cm, to 105-645E-71R-3, 39–41 cm, and suggest a zonal age of NN1–NN4 for this interval. Because of the sample preservation, the rare occurrence of microfossils, and the lack of age diagnostic dinocysts, it was not possible to determine the age of the lowermost 60 m of the hole.

Paleoenvironment

The paleoenvironmental discussion is divided into four parts, which are based on four stratigraphic intervals, as defined by the microfossil assemblages observed:

1. Interval 1 (0–110 mbsf). This interval, represented by the occurrence of calcareous microfossils, corresponds to the upper part of Lithostratigraphic Unit I. Planktonic and benthic foraminifers are common in the uppermost 110 m examined from Site 645 (Sections 105-645B-1X, CC, through 105-645B-12X, CC). The presence of dissolution-susceptible planktonic foraminiferal species, such as *Globigerina bulloides*, *G. quinqueloba*, and *Globigerinoides uvula*, and the very low benthic to planktonic foraminiferal ratios suggest a relatively good preservation state of biogenic carbonate debris on the seafloor. Therefore, the common occurrence of foraminifers within the upper part of Site 645 most likely indicates higher zooplankton productivity in Baffin Bay during the middle and late Pleistocene. However, studies of shorter piston cores (upper 10 m) also indicate the presence of dissolution cycles correlating with light-oxygen-isotopic stages (Aksu, 1983).

The observed benthic foraminiferal assemblage at Site 645 resembles the Arctic upper-slope fauna, where common specimens of *Cassidulina teretis* and *Stetsonia horvathi* occur between a water depth of 350 and 900 m (Lagoe, 1979).

Dinoflagellate, pollen, and spore abundances are generally low throughout this interval. The presence in the uppermost 110 m of dinocysts such as *Brigantedinium simplex* and *Multispinula minuta* may indicate relatively low surface-water salinities; whereas the occurrence of *Operculodinium centrocarpum* and *Bitectadodinium tepikiense* suggests some episodic influence of Atlantic water in Baffin Bay. Detailed palynological studies of shorter piston cores (<10 m long) showed that dinocysts exhibit large fluctuations in abundance, suggesting cycles of higher and lower productivity in surface waters during the late Quaternary (de Vernal, 1986).

Diatoms and radiolarians were observed only in samples examined from the uppermost 5 cm within the upper 110 m of Site 645. However, studies on shorter piston cores show alternating diatom-rich and diatom-poor zones throughout the uppermost 10 m of sediment in Baffin Bay (A. Aksu, pers. comm., 1985). The absence of diatoms and radiolarians in core-catcher samples may be caused by low primary productivity in Baffin Bay during certain periods, silica dissolution in surface waters as well as in sediment, or dilution resulting from high sedimentation rates.

Calcareous nannofossils are present only in two core-catcher samples within the uppermost 110 m. Because calcareous nannofossils are not expected to occur in large abundances in arctic water masses, their rare occurrence in Baffin Bay sediments is not surprising. As with diatoms, sediment dilution may also be a factor, controlling the low abundance of calcareous nannofossils.

2. Interval 2 (110–265 mbsf). This interval corresponds to the lower part of Lithostratigraphic Unit I and the upper part of Unit II and is distinguished by the paucity of marine microfossils.

Benthic foraminifera are rare and, except in Section 105-645B-28X, CC, planktonic foraminifers are absent from this interval. The foraminiferal data suggest moderate syndepositional and postdepositional dissolution of calcareous debris. The occurrence of planktonic foraminifers indicates some surface-water productivity.

Dinocysts are not abundant in this interval (Sections 105-645B-13X, CC, through 105-645B-27X, CC), but their concentration is significantly higher (100–2000 cm³) than the uppermost 110 m (Interval 1). Samples contain neritic and true oceanic species. More pollen and spores were observed in this interval than in Interval 1. The interval from about 177–299 mbsf is particularly rich in pollen and spores. The assemblages indicate tundra forest vegetation and reflect a very humid and cool climate. In general the pollen data suggest a major transition to sparse vegetation above 177 mbsf (Hole 645B).

Diatoms occur only sporadically in Interval 2 (Sections 105-645B-24X, CC, 105-645B-29X, CC, and 105-645B-30X, CC). The assemblage observed is similar to that described from the Bering Sea continental shelf (Baldauf, 1981; Sancetta, 1982). The high number of neritic and brackish-fresh-water specimens suggests possible redeposition of sediment from the slope and shelf.

3. Interval 3 (265.7–465.8 mbsf). This interval corresponds to the lower part of Lithostratigraphic Unit II and the upper part of Unit III and is barren of foraminifers, radiolarians, and nannofossils. Diatoms are rare; some reworked Miocene species occur. Samples also contain dinoflagellates, including a substantial Paleogene reworked flora and very abundant detrital plant matter. The dinocyst assemblage indicates neritic conditions, and the diatom assemblage suggests coastal conditions (shelf-slope). Pollen and spore assemblages generally reflect a coniferous boreal forest to tundra forest in the source area. Pyritized organic material, worm tubes, diatoms, and the presence of inferred diagenetic carbonate concretions suggest a reducing depositional environment and extensive postdepositional carbonate dissolution.

4. Interval 4 (465.2–1147.1 mbsf). Foraminifers are absent in the upper part of this interval (465.2–772.0 mbsf; Sections 105-645E-4R, CC, through 105-645E-38R, CC), which corresponds to the lower part of Lithostratigraphic Unit III. A mixed, low-diversity agglutinated and calcareous benthic foraminiferal assemblage is observed from 772.0 to 884 mbsf (Sections 105-645E-39R, CC, through 105-645E-50R, CC). The first appearance of agglutinated foraminifers correlates closely with the increase of marine organic content in sediments (see “Organic Geochemistry” section, this chapter). The data may be interpreted as suggesting “restricted deep circulation,” according to the model of Gradstein and Berggren (1981). The interval from 884.0 to 926.0 mbsf (Sections 105-645E-52R, CC, through 105-645E-55R, CC) contains a calcareous benthic foraminiferal fauna similar to that observed from 772.0 to 884 mbsf, whereas the agglutinated assemblage appears to be more diverse, displays affinity to the Miocene agglutinated fauna from the Norwegian-Greenland Sea, and indicates an upper-slope setting. Calcareous benthic foraminifers found in two samples (105-645E-67R-2, 85–87 cm, and 105-645E-70R, CC) also indicate upper-slope depths. From 955.6 to 1147.1 mbsf (Sections 105-645E-58R, CC, through 105-645E-78R, CC), a diverse agglutinated fauna occurs that differs from that found above 955.6 mbsf, in that it contains forms probably redeposited from shallower depths.

Dinoflagellates, pollen, and spores are common throughout this interval. Samples in the upper part of this interval show low diversity and abundance and large amounts of woody fragments. The floral diversity and abundance increase slightly downhole (below 936 mbsf; Section 105-645E-56R, CC). The downhole increase in *Tsuga* may represent a warming trend.

Calcareous nanofossils occur sporadically throughout Interval 4. The occurrence of helicosphaerids, braarudosphaerids, and discolithinas (from Samples 105-645E-70R-2, 42-44 cm, to 105-645E-73R, CC (1064-1100 mbsf), which are most common in warm through temperate shelf environments, suggests slightly warmer conditions and possible sediment influx from a shelf area.

SEDIMENT-ACCUMULATION RATES

The results of biostratigraphic and magnetostratigraphic studies provide a working age-depth relationship for Site 645 sediments (Fig. 27). The data presented in the "Biostratigraphy" and "Paleomagnetism" sections (this chapter) are summarized in Table 5 and are discussed as follows in terms of the age constraints they place on the sediment-accumulation rates observed at this site.

Biostratigraphy

Because of the limited biostratigraphic data (see "Biostratigraphy" section, this chapter) from Site 645, few tie points are available for estimating the sediment-accumulation rates. In addition, the biostratigraphic constraints used are not datums but are age ranges based on the microfossil assemblage observed. Biostratigraphic constraints for Site 645 are as follows.

Event 5 (Fig. 27; 148-245 mbsf, 65-1.6 Ma)

The occurrence of the dinocyst species *Multispinula minuta* places the upper 177 mbsf in the Pleistocene. This species is reported from upper Pleistocene sediments in the North Atlantic (Mudie, in press) and from Pleistocene sediments in the Arctic

Ocean (Aksu and Mudie, 1985). The occurrence of both *Filiosphaera filifera* and *M. minuta* in samples between 148.8 and 177 mbsf suggests an early Pleistocene age for this interval. The Pliocene/Pleistocene boundary is tentatively placed at approximately 245 mbsf. This age assignment is based on the last common occurrence of cf. *Labyrinthodinium* sp., which characterizes the Pliocene-Pleistocene at Labrador Sea Sites 646 and 647.

Event 6 (Fig. 27; 245-294 mbsf, 1.6-3.4 Ma)

The occurrence of the benthic foraminifer *Cassidulina teretis* suggests that this interval is late Pliocene to Holocene in age. This species is recorded in sediments having an age younger than the early Pliocene in both the Rockall Plateau region of the North Atlantic (Murray, 1985) and the Norwegian-Greenland Sea (Berggren and Schnitker, 1983). This age constraint is also suggested by the dominance (>90%) of sinistral *N. pachyderma* and absence of *N. atlantica* in samples examined throughout this interval. A change in coiling direction of *N. pachyderma* was reported by Berggren (1972) to occur during the late Pliocene in the Labrador Sea. The dominance of sinistral over dextral forms in the samples examined from Site 645 tentatively suggests that the 245-294-mbsf interval is above the level where the coiling change should occur (see "Biostratigraphy" section, this chapter, for detailed discussion).

Event 8 (Fig. 27; 294-512 mbsf, 1.6-5.3 Ma)

This interval is considered to be Pliocene in age, as indicated by the dinocyst and benthic foraminifer assemblages. The diatom assemblage consists of species that have been reported from Pliocene-Pleistocene sediments in the North Pacific (Koizumi,

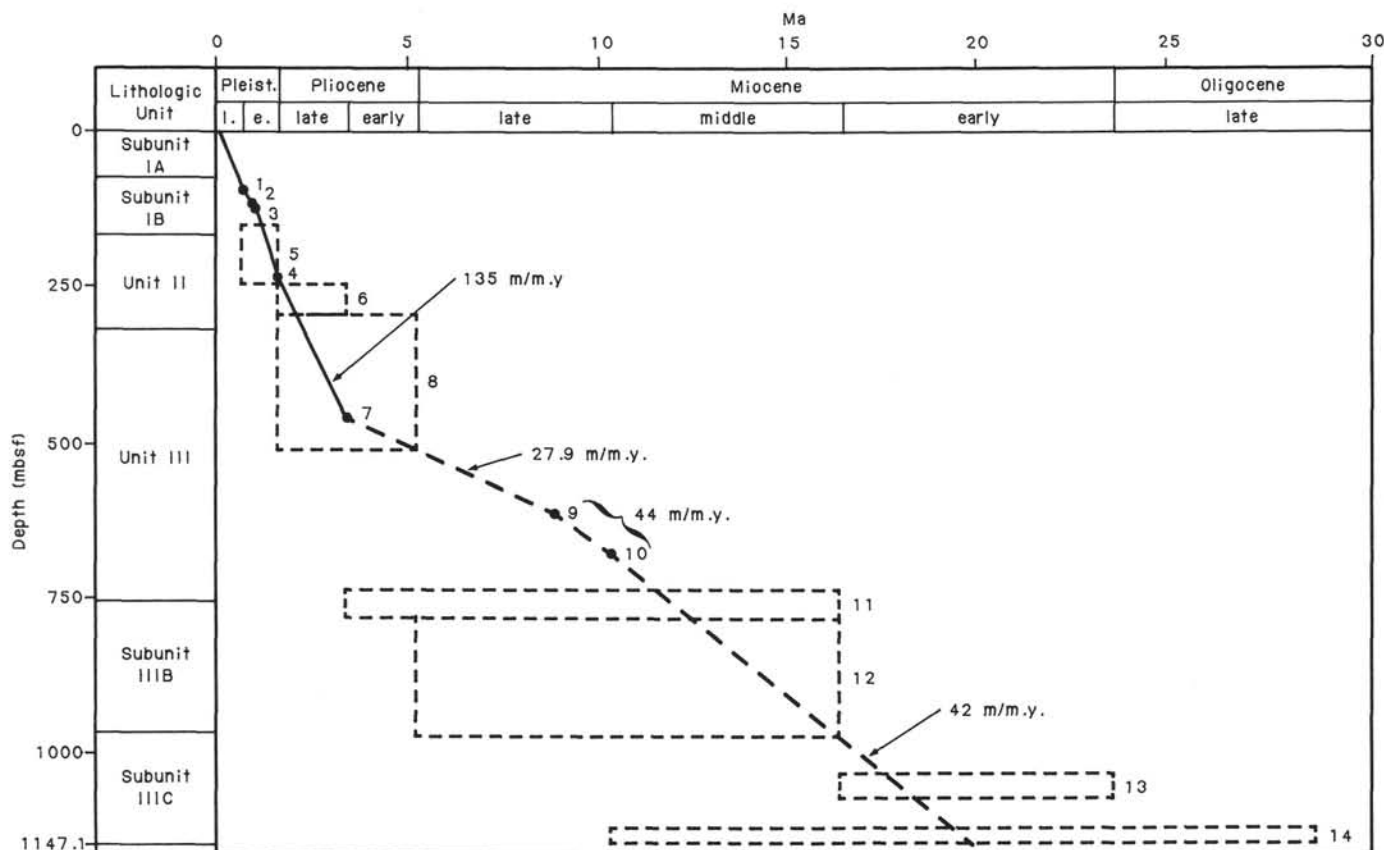


Figure 27. Sediment-accumulation-rate curves, Site 645, indicating the depths of biostratigraphic and magnetostratigraphic tie points. Data used to construct figure are summarized in Table 5.

Table 5. Sediment-accumulation-rate data, Site 645.

Event no.	Type	Datum	Age (Ma)	Depth (mbsf)
1	Magnetostratigraphy	Brunhes/Matuyama	0.73	95
2	Magnetostratigraphy	Top Jaramillo	0.91	115
3	Magnetostratigraphy	Base Jaramillo	0.98	126
4	Magnetostratigraphy	Top Olduvai	1.66	242
5	Dinocysts	Occurrence <i>Multispinula minuta</i> , <i>Filispheera filifera</i>	0.65–1.6	148–245
6	Dinocysts and planktonic foraminifers	Occurrence <i>Cassidulina teretis</i> , <i>Neogloboquadrina pachyderma</i>	1.6–3.4	245–294
7	Magnetostratigraphy	Base Gauss	3.4	459
8	Dinocysts and benthic foraminifers	Assemblage	1.6–5.3	294–512
9	Planktonic foraminifers and magnetostratigraphy	Top N1, top Chron C-11	8.92	613
10	Planktonic foraminifers and magnetostratigraphy	Base N1, base Chron C-11	10.42	679
11	Nannofossils	Occurrence <i>Reticulofenestra pseudoumbilica</i>	3.4–16.5	738–782
12	Dinocysts and benthic foraminifers	Occurrence <i>Melonis</i> sp., <i>Paleocystid.</i> sp.	5.3–16.5	782–935
13	Foraminifers	Occurrence <i>Globigerina praebulloides</i> , <i>Helicosphaera ampliaptera</i>	10.4–23.7	1035–1075
14	Dinocysts	LAD <i>Distatodinium paradoxum</i> , FAD <i>Impletosphaeridium</i> sp.	10.4–30.0	1074–1149

1973) and the Bering Sea (Baldauf, 1981; Sancetta, 1982). Except in Section 105-645E-22R, CC, microfossils were not observed in samples examined between 512 and 738 mbsf. The dinocyst assemblage in Section 105-645E-22R, CC, suggests a middle Miocene–early Pliocene age.

Event 11 (Fig. 27; 738–782 mbsf, 3.4–16.5 Ma)

The sporadic occurrence of *Reticulofenestra pseudoumbilica* suggests placement of this interval in Zones NN15–NN5 (early Pliocene to middle Miocene). A similar age is suggested by the benthic foraminifers in the lowermost part of this interval (772–782 mbsf). The benthic foraminiferal fauna consists dominantly of an agglutinated assemblage and rare calcareous forms. A similar assemblage was observed in middle Miocene through lower Pliocene sediments in the Norwegian–Greenland Sea (Berggren and Schnitker, 1983; Verdenius and van Hinte, 1983). The absence in this interval of the benthic foraminifer *Cassidulina teretis* also suggests an early Pliocene or older age.

Event 12 (Fig. 27; 782–935 mbsf, 5.3–16.5 Ma)

The last occurrence of *Paleocystodinium* species is recorded at 782 mbsf. *Paleocystodinium* has an upper range from early to late Miocene in the North Atlantic (Brown and Downie, 1985). The occurrence of the benthic foraminifer *Melonis zandaamae* suggests that this interval is no older than middle Miocene. *M. zandaamae* is recorded by Berggren and Schnitker (1983) in the Norwegian–Greenland Sea middle and upper Miocene sediments. *Bolboforma metzmacheri* also occurs in this interval. Murray (1985) recorded this microfossil from sediments in the Rockall Plateau region of the North Atlantic. The occurrence of this microfossil suggests an age between Zones NN6 and NN16.

Event 13 (Fig. 27; 1035–1075 mbsf, 10.4–23.7 Ma)

Age constraints for this interval are based on the occurrence of a benthic foraminifer fauna lacking *Melonis* sp., which suggests an age older than this species' first occurrence (Zone NN6), and the presence of *Globigerina praebulloides*, which is observed only in the lower Miocene of Labrador Margin wells. This interval is determined by the occurrence of the calcareous nannofossil *Helicosphaera ampliaptera* in samples between 1066 and 1074 mbsf and suggests placement between Zones NN4 and NN1.

Event 14 (Fig. 27; 1074–1149 mbsf, 10.4–30.0 Ma)

This interval is based on the last occurrence of *Distatodinium paradoxum* (middle Miocene) and the first occurrence of *Impletosphaeridium* sp. 1 Manum (1976) (lower upper Oligocene).

Magnetostratigraphy

The frequent changes observed in the magnetic polarity of sediments cored at Site 645 are interpreted as recording geomagnetic polarity reversals (see "Paleomagnetism" section, this chapter). Correlation of the observed polarity sequence to the geomagnetic-polarity time scale, however, is hampered by the lack of refined biostratigraphic control and the poor core recovery, particularly in the upper sections. Even within the existing biostratigraphic control, the sedimentological evidence (see "Sedimentology" section, this chapter), which suggests varied sediment-accumulation rates (on the 1–10-m scale) to be the result of bottom-current and/or turbidity-current action, makes any attempt at pattern recognition in the polarity sequence difficult.

Within these limitations, the upper and lower parts of the magnetostratigraphic data can be correlated with the time scale in a way that fits reasonably with the biostratigraphic results. Above 94 mbsf, no reversely magnetized sediments were observed in any of the recovered sediments. Therefore, the reversal observed at this depth is interpreted as being the base of the Brunhes Chronozone (0.73 Ma; Berggren et al., 1986). The short normal-polarity subchronozone extending from 115 to 126 mbsf is interpreted as being correlative with the Jaramillo Subchron (0.91–0.98 Ma). The long normal-polarity sequence observed from 613 to 679 mbsf possibly correlates with Chron 11 (8.92–10.42 Ma). Chron 11 is the only long normal-polarity chron within the middle Miocene; thus, this correlation is made assuming relatively constant sedimentation rates across this interval. The observed reversals immediately above and below this interval may be correlated to the time scale if this assumption is held. However, the geomagnetic-reversal frequency in this period makes these correlations tenuous.

Sediment-Accumulation Rates

The data presented in Figure 27 provide some constraints on the sediment-accumulation rates at this site. Biostratigraphic and magnetostratigraphic results place an average accumulation rate

of 135 m/m.y. on the upper 460 m of the section. The depths of the Brunhes and Jaramillo reversals are consistent with a rate of 130–146 m/m.y. at this interval. These rates are six to nine times higher than the accumulation rates of 15–20 m/m.y. calculated from piston-core data of the last 75,000 yr (Aksu, 1983).

Four biostratigraphic ranges (the aforementioned Events 11 through 14) observed for the interval from 679 mbsf to the bottom of Hole 645E yield a minimum sedimentation rate of 42 m/m.y. If the Chronozone 11 correlation is correct, it indicates a sedimentation rate of 44 m/m.y. from 613 to 679 mbsf.

Despite the uncertainty of the existing data, a dramatic change in the sediment-accumulation rate evidently occurred between the upper and lower parts of the section. The exact depth of this inflection in the sediment-accumulation-rate curve is difficult to detect. Biostratigraphic data indicate that the sediment at 512 mbsf is Pliocene or younger in age. The base of the Gauss Chronozone is tentatively placed at 459 m. Additional biostratigraphic age control is required to further refine the depth at which the change in the sediment-accumulation rate occurs.

Because of the limited age constraints for the interval between 750 mbsf and the bottom of Hole 645, it was not possible to constrain tightly the rate of sediment accumulation. Based on biostratigraphic data, a tentative estimate of 42 m/m.y. is suggested.

INORGANIC GEOCHEMISTRY

Forty interstitial-pore-water samples were taken at varying intervals of 20–60 m from 2.9 to 1147.1 mbsf at Site 645. Al-

kalinity, pH, chloride, calcium, and magnesium concentrations were determined by methods described by Gieskes (1974). Sulfate analyses were carried out by ion chromatography. Results of these analyses are presented in Table 6 and Figure 28.

Alkalinity values gradually increase with depth to about 190 mbsf, where the values show a sudden increase of about 6–8 meq/dm³ (Fig. 28). Below this depth, values appear to be much more erratic, increasing then decreasing several times. Sulfate concentrations (Fig. 28) show a more definite trend, decreasing by 20 mmol/dm³ over the first 40 m. The sulfate concentrations remain relatively depleted for most of the rest of the hole although the values increase by several mmol toward the base. Such excursions in sulfate values are common in rapidly deposited, organic-carbon-rich hemipelagic sediments (Manheim and Sayles, 1974). The depleted values combined with the higher alkalinity values and the presence of pyrite over this same interval indicate that significant sulfate reduction has occurred.

Within the upper 30 m at Site 645, both interstitial calcium (Ca) (Fig. 28) and magnesium (Mg) (Fig. 28) become rapidly depleted from inferred bottom-water concentrations. Below 200 mbsf depth, calcium values gradually increase as magnesium values decrease. Calcium concentrations reach a maximum value of 18 mmol at 800 mbsf, below which values fluctuate by 2–3 mmol. The overall increase in calcium-ion concentration and decrease in magnesium-ion concentration with depth is a characteristic trend of deep-sea-core interstitial-water profiles and is generally attributed to the upward migration of calcium-enriched and magnesium-depleted pore waters from layer 2 ba-

Table 6. Summary of analyses of interstitial-water chemistry, Site 645. Alkalinity and pH measurements were discontinued at 800 mbsf as a result of decreasing sample size.

Sample interval (cm)	Depth (mbsf)	pH	Alkalinity (meq/DM ³)	Salinity (‰)	Chlorinity (‰)	Ca ⁺⁺ (mmol)	Mg ⁺⁺ (mmol)	Sulfate ⁼ (mmol)
105-645B-1X-2, 140–150	2.90	7.81	3.99	34.0	19.467	10.08	49.54	21.91
105-645B-5X-2, 140–150	35.10	7.9	4.71	30.05	18.662	4.41	32.35	0.58
105-645B-9X-2, 140–150	74.5	7.83	4.36	30.0	18.788	5.65	33.06	3.060
105-645B-11X-2, 140–150	93.8	7.94	4.8	31.0	19.344	5.45	31.54	0.873
105-645B-14X-3, 140–150	124.3	8.05	4.51	30.8	19.002	5.29	32.56	1.286
105-645B-19X-3, 140–150	172.5	7.99	5.11	31.6	19.633	4.94	32.52	1.842
105-645B-21X-5, 140–150	194.8	7.93	5.99	31.0	17.505	4.71	34.31	2.191
105-645B-24X-5, 140–150	223.6	7.93	12.13	32.0	19.850	4.61	32.53	1.171
105-645B-27X-3, 140–150	249.6	7.96	9.26	30.1	18.459	6.31	32.95	9.250
105-645B-30X-6, 140–150	283.1	8.07	12.88	29.9	17.119	6.14	28.05	1.743
105-645D-1X-3, 140–150	269.84	8.00	12.38	32.5	19.090	7.06	33.71	5.962
105-645D-8R-2, 140–150	304.7	7.94	16.48	25.0	20.667	7.88	29.54	1.390
105-645D-11R-5, 140–150	376.8	8.05	13.5	30.5	18.085	7.48	26.90	2.344
105-645B-14R-3, 140–150	402.7	8.01	12.29	30.0	19.922	7.51	28.19	3.453
105-645D-17R-4, 140–150	433.1	8.16	12.52	32.1	19.704	7.59	27.57	2.836
105-645D-20R-3, 140–150	460.6	8.21	13.81	31.0	19.114	8.03	26.66	1.480
105-645E-4R-3, 140–150	459.6	8.01	11.108	32.5	19.326	7.73	26.91	3.18
105-645E-7R-4, 140–150	490.0	7.80	13.57	31.9	18.55	8.42	25.83	3.41
105-645E-10R-2, 140–150	515.9	7.85	13.66	31.9	19.649	9.13	24.03	2.49
105-645E-13R-5, 140–150	549.2	—	—	31.0	19.449	9.69	20.52	2.95
105-645E-18R-4, 140–150	576.7	7.91	8.02	31.5	19.120	10.27	24.68	4.11
105-645E-19R-4, 140–150	605.7	7.91	8.02	31.4	18.509	10.51	24.75	5.49
105-645E-23R-2, 140–150	631.3	8.13	6.62	31.0	19.282	10.73	22.28	6.68
105-645E-26R-2, 140–150	660.0	8.20	6.66	30.5	19.276	11.97	21.27	3.24
105-645E-29R-5, 140–150	693.4	7.92	7.66	30.5	18.689	12.95	18.97	3.70
105-645E-33R-3, 140–150	719.1	—	—	30.0	18.648	14.93	20.72	3.72
195-645E-38R-1, 140–150	745.1	7.96	12.66	31.5	18.689	13.86	18.29	2.74
105-645E-39R-4, 140–150	778.6	8.24	12.77	30.2	17.672	14.15	18.24	4.85
105-645E-43R-5, 140–150	818.6	—	—	30.5	18.374	18.06	15.65	7.62
105-645E-46R-3, 140–150	844.5	—	—	30.4	17.971	17.24	15.48	3.96
105-645E-49R-5, 140–150	876.0	—	—	32.1	19.467	15.24	15.83	3.97
105-645E-53R-5, 140–150	905.0	—	—	30.5	18.785	14.20	17.41	—
105-645E-56R-4, 140–150	932.6	—	—	30.7	18.924	15.80	16.04	5.06
105-645E-59R-5, 140–150	963.0	—	—	30.0	17.838	17.73	15.66	6.41
105-645E-62R-5, 140–150	991.6	—	—	33.0	21.370	18.14	16.34	—
105-645E-65R-5, 140–150	1021.0	—	—	29.0	19.677	16.38	13.60	—
105-645E-68R-5, 140–150	1050.0	—	—	29.0	17.601	16.89	15.73	6.37
105-645E-69R-5, 140–150	1059.6	—	—	28.0	17.048	17.43	14.02	6.86
105-645E-75R-3, 140–150	1113.7	—	—	29.0	16.658	15.66	14.24	3.86
105-645E-78R-4, 140–150	1143.7	—	—	27.9	16.966	14.93	13.03	3.86

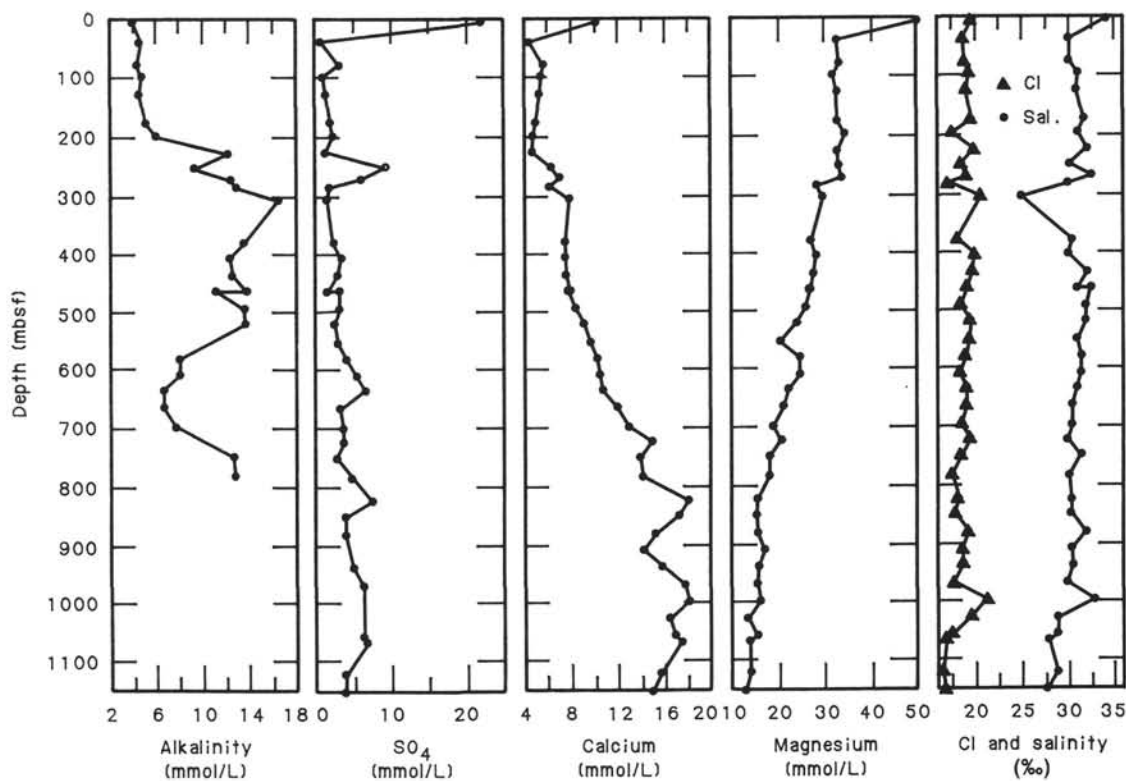


Figure 28. Summary of shipboard analyses of interstitial-water chemistry, Site 645. As a result of decreasing interstitial-water sample volume with depth, analyses for alkalinity were discontinued at 800 mbsf. Site 645 sulfate concentration–depth, calcium concentration–depth, magnesium concentration–depth, and chlorinity–salinity–depth profiles.

salts (Gieskes, 1983). However, the nonlinearity of change at this site indicates that sediment diagenetic reactions may have had a moderate influence on the observed calcium and magnesium-ion gradients as well. Over the upper 200 m, sulfate-reduction processes appear to cause the large depletions in both calcium and magnesium, primarily by production of excess bicarbonate ion and subsequent carbonate precipitation (Manheim and Sayles, 1974). In addition, authigenic clay formation may account for the excess depletion of magnesium ion.

Large downhole variations in salinity and chlorinity concentrations (Fig. 28) also occur at Site 645. Salinity concentrations range from 34.9 to 25.0 ‰, most of the values generally falling below 32.5 ‰, whereas chlorinity concentrations range from 19.5 to 17.0 ‰. Most of the decrease in salinity occurs in the upper 30–40 m of the sediment column. A fraction of the downhole decrease in salinity may result from the loss of sulfate through sulfate-reduction processes. However, changes in chlorinity concentrations, which should not be affected by sulfate reduction, generally correlate with the salinity variations. This suggests that the fluctuations in salinity with depth cannot be entirely attributed to postburial chemical processes. Glacial-to-interglacial-produced salinity changes in Baffin Bay deep-water masses may account for some of the variation. This variation, however, may be due to the presence of gas hydrates at various intervals that would dilute salinity concentrations upon melting when brought to the surface in cores (Harrison et al., 1982). Shore-based analyses of interstitial-water oxygen-isotope composition should help determine whether the observed salinity variations relate to glacial-interglacial episodes and/or to the occurrence of gas hydrates.

ORGANIC GEOCHEMISTRY

At Site 645, two to four samples per core were used for (1) measurement of hydrocarbon gases, (2) determination of organ-

ic and inorganic carbon, and/or (3) Rock-Eval analysis. Following the recommendation of Kvenvolden and McDonald (1985a), a 10-cm³ “carbon organic” (CO) sample was taken every third core just above or below the organic geochemistry (OG) sample. We routinely ran all three types of the aforementioned measurements on these CO samples. This provides an estimate of the amount and type of organic carbon in the adjacent OG sample.

Hydrocarbon Gases

For safety considerations, at least one gas sample per core was routinely analyzed for composition of light hydrocarbons. Gas was sampled by vacutainer from gas pockets in gassy cores (Fig. 29 and Table 7).

Because we did not detect ethane in the upper 250 m of Site 645, the C1/C2 ratio could not be calculated. The C1/C2 ratio ranges from about 2000 to 10,000 at the interval from 250 to 580 mbsf (Fig. 29). The interval between 580 and 750 m sub-bottom depth is characterized by high-amplitude variations of the C1/C2 ratio between 2000 and 12,800. The maximum of 12,800 is reached at about 640 mbsf depth. Below this depth, the trend of the C1/C2 values shows a continuous decrease. Below 750 mbsf down to the final level of 1147.1 mbsf, the C1/C2 ratios have values between 3000 and 600, fluctuating around a mean value of approximately 1500. Throughout the entire sediment sequence of Site 645, the C1/C2 ratio stayed above the risk limit of about 400 (Fig. 29).

The high amount of gas in the upper 300 m may have been caused by the occurrence of gas hydrates. Because of the depth and temperature conditions and the high organic carbon content at Site 645, the occurrence of gas hydrates is highly possible (Kvenvolden and Barnard, 1983; cf. “Inorganic Geochemistry” section, this chapter). However, we did not observe any gas hydrates in the cores.

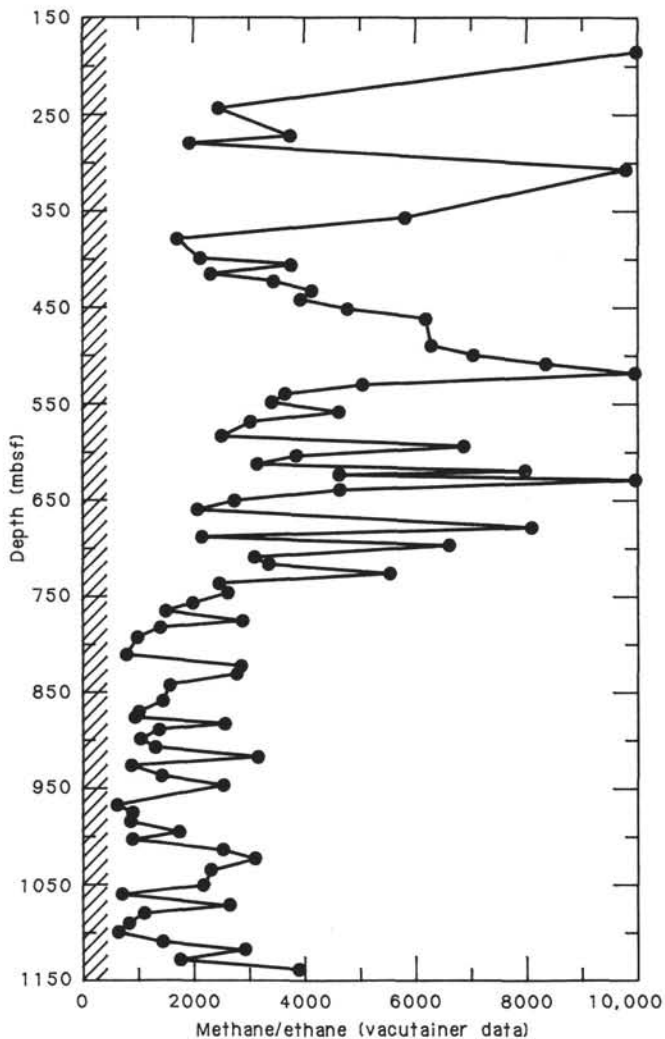


Figure 29. Methane/ethane ratio plotted versus sub-bottom depth, Holes 645B, 645D, and 645E. Hatch-marked areas are the risk zone as defined by methane/ethane ratios below 400.

Table 7 (continued).

Core	Vacutainer sample		
	C1	C2	C1/C2
Hole 645E (cont.)			
105-645D-18R	815759	210	3884
105-645D-19R	836042	176	4758
105-645D-20R	944071	153	6170
Hole 645E			
105-645E-1R	365484	37.3	9798
105-645E-6R	10545		
105-645E-7R	891893	142	6280
105-645E-8R	465083	66.8	7046
105-645E-9R	323924	38.8	8348
105-645E-10R	395584	22.8	17350
105-645E-11R	816819	162	5038
105-645E-12R	896199	245	3657
105-645E-13R	741605	218	3394
105-645E-14R	916380	196	4658
105-645E-15R	937086	309	3033
105-645E-16R	498744		
105-645E-17R	882925	353	2501
105-645E-18R	473824	69	6867
105-645E-19R	899229	235	3827
105-645E-20R	898357	287	3124
105-645E-21R	130942	16	7984
105-645E-22R	1009089	219	4607
105-645E-23R	385244	30.5	12841
105-645E-24R	922634	199	4636
105-645E-25R	551115	201	2742
105-645E-26R	1044595	507	2060
105-645E-27R	827522		
105-645E-28R	644740	13.6	8106
105-645E-29R	895484	409	2139
105-645E-30R	132144	20	6613
105-645E-32R	563550	183	3079
105-645E-33R	539499	160	3372
105-645E-34R	77844	14.8	5560
105-645E-35R	753951	306	2464
105-645E-36R	704154	271	2667
105-645E-37R	897680	442	2031
105-645E-38R	905742	612	1480
105-645E-39R	463429	158	2933
105-645E-40R	868927	623	1395
105-645E-41R	910237	900	1011
105-645E-43R	919333	1172	784
105-645E-44R	441733	153	2887
105-645E-45R	445047	159	2799
105-645E-46R	553438	348	1590
105-645E-48R	12253	8.4	1458
105-645E-49R	685534	667	1027
105-645E-50R	842898	910	924
105-645E-51R	408494	157	2607
105-645E-52R	522233	378	1381
105-645E-53R	594988	573	1038
105-645E-54R	507249	384	1322
105-645E-55R	139669	60	2328
105-645E-56R	707981	822	861
105-645E-57R	451800	312	1449
105-645E-58R	383047	148	2589
105-645E-59R	14712	—	—
105-645E-60R	940814	1481	635
105-645E-61R	586395	622	943
105-645E-62R	540472	607	890
105-645E-63R	375139	207	1812
105-645E-64R	677996	751	904
105-645E-65R	808967	315	2568
105-645E-66R	393767	124	3176
105-645E-67R	67500	29	2334
105-645E-68R	17242	—	—
105-645E-69R	343380	155	2215
105-645E-70R	612127	863	709
105-645E-71R	268610	99	2713
105-645E-72R	520697	463	1124
105-645E-73R	605441	709	854
105-645E-74R	634242	971	653
105-645E-75R	49320	34	1461
105-645E-76R	597640	199	3009
105-645E-77R	176150	99	1779
105-645E-78R	29310	7.5	3908

Table 7. Amount of light hydrocarbons in ppm and methane/ethane (C1/C2) ratios. Data from vacutainer analyses.

Core	Vacutainer sample		
	C1	C2	C1/C2
Hole 645B			
105-645B-1X	571		
105-645B-14X	57071		
105-645B-17X	40594		
105-645B-18X	31726		
105-645B-20X	111835	8	13979
105-645B-26X	9799	4	2390
105-645B-28X	2073		
Hole 645D			
105-645D-1R	686281	183.9	3731.8
105-645D-2R	160000	85	1882.3
105-645D-8R	71832		
105-645D-9R	799170	138	5791
105-645D-11R	833484	495	1683
105-645D-13R	965033	450	2149
105-645D-14R	830565	220	3775
105-645D-15R	954741	414	2306
105-645D-16R	863350	251	3439
105-645D-17R	942506	229	4115

Organic and Inorganic Carbon

In the upper 300 m of Site 645 (i.e., Holes 645A, 645B, and 645C), organic carbon was determined by the difference between the total organic carbon (TOC) (from the Perkin Elmer 240C Elemental Analyzer) and the inorganic carbon (from the Coulometrics Carbonate Carbon Apparatus and Coulometer). This method, being less time consuming compared with the direct measurement of TOC on acidified samples, avoids the loss of organic matter by hydrolysis during treatment with HCl, especially in young, diagenetically immature sediments (Peters and Simoneit, 1982). Comparison of TOC data obtained by our method and TOC data obtained by direct measurement on acidified samples shows similar results (cf. Kvenvolden and McDonald, 1985b). At Holes 645D and 645E (i.e., in sediments below 340 mbsf), we changed the procedure of TOC measurement because of difficulties encountered in the use of the coulometer for carbonate determination (inaccurate measurements of standards). TOC was determined from the carbonate-free residue (see "Explanatory Notes" chapter, this volume).

Inorganic carbon (IC) data were obtained by means of the carbonate bomb, the coulometer, and/or the difference between IC and TOC. The carbonate values of samples analyzed by all three methods agree well.

In general, the TOC values at Site 645 are relatively high. Only 6 of the 144 TOC values are between about 0.1% and 0.3%; all other values fall between 0.4% and 2.8% (Fig. 30 and Table 8). Lithologic Subunit IA (0–71.6 mbsf) is characterized by low C_{org} values that vary between 0.14% and 0.75% (mean value of 0.45%). In Subunit IB (71.6 m–168 mbsf), higher TOC values between 0.53% and 1.47% (mean value of 0.91%) occur. The maximum TOC value of 1.47% (Core 105-645B-13X) is recorded in a very dark gray to very dark olive sediment interval. In Unit II, the percentages of organic carbon vary between about 0.1% and 0.93% (mean value 0.56%), the higher values (0.40%–0.93%) occurring in the upper part of the unit (180–280 mbsf) and the lower values (0.06%–0.44%) occurring in the lower part of the unit (280–300 mbsf). The minimum TOC values are associated with more sandy intervals (see "Sedimentology" section, this chapter). Because of low core recovery, the interval between about 300 and 335 mbsf is not documented in the record. Unit III (335–1147.1 mbsf) is characterized by high TOC values ranging from 0.62% to 2.8% (mean value of 1.12%). The maximum TOC values of as much as 2.8% occur between 753.4 and 916.8 mbsf (Lithologic Subunit IIIB).

According to the carbonate content, the sediment sequence of Site 645 can be divided into three parts (Fig. 30). The upper 170 mbsf, corresponding to Lithologic Unit I, is characterized by high-amplitude variations of $CaCO_3$ between about 10% and 50%. Between 170 and 420 mbsf, the carbonate content decreases to values between 0% and 20%. Below 420 mbsf, the carbonate values of the dominant lithology are extremely low, ranging between 0% and 5%. In some places, 10- to 30-cm-thick intervals of more lithified, light-colored sediments occur in the lower two parts of Site 645 (see "Sedimentology" section, this chapter), which are characterized by higher $CaCO_3$ values of as much as 50%. Whereas in the dominant lithology (and between 0 and 170 mbsf) dolomite and calcite are the dominant carbonate minerals, rhodochrosite and siderite are most important in the light-colored minor lithology (carbonate minerals are determined by XRD; see "Sedimentology" section, this chapter).

Rock-Eval Pyrolysis

To characterize the type and maturity of organic matter, we used the Rock-Eval pyrolysis technique (Espitalie et al., 1977; Peters and Simoneit, 1982). The Rock-Eval on board *JOIDES Resolution* is a Rock-Eval II Plus TOC instrument, which also

measures the TOC content. The TOC values obtained from the Rock-Eval, however, did not agree with those derived from the elemental analyzer (Table 9). In general, the Rock-Eval values are distinctly lower than the elemental analyzer values. The hydrogen indices (HI) and oxygen indices (OI) also differ accordingly. In Figure 31, the HI and OI values (based on the TOC data from the elemental analyzer) are plotted in a van Krevelen diagram (Tissot and Welte, 1984). This diagram implies that most of the organic matter in the sediments of Holes 645B and 645D is of type III or is terrestrial in origin. Most of the organic matter is highly oxidized, as indicated by high OI values. One sample from Hole 645B (105-645B-30X-5, 109 cm) has a high HI of about 280, suggesting a type II/III mixture, i.e., a mixture of marine and terrigenous organic matter. At Hole 645E, below 460 mbsf, this mixed type of organic matter becomes dominant (Fig. 31 and Table 9). This may suggest that the amount of marine organic matter is higher in these older (middle to late Miocene) sediments than in the uppermost 460 mbsf (Pliocene to Pleistocene?). However, the terrigenous material in this older interval still remains the main component of the organic matter. The composition of palynomorph assemblages (see "Biostratigraphy" section, this chapter) and the common occurrence of woody material in the smear slides (see "Sedimentology" section, this chapter) confirm this interpretation of the van Krevelen diagram.

The temperature of maximum pyrolysis yield (T_{max}) indicates the immaturity of the organic matter found in the Site 645 sediments. The T_{max} values are $<435^\circ C$ throughout the entire sediment sequence, with two exceptions (Table 9). The higher T_{max} of two samples (105-645B-32X-5, 85 cm, and 105-645D-1R-1, 150 cm; $T_{max} = 456^\circ C$) may suggest an increased amount of reworked, more mature organic matter.

Discussion and Conclusions

The sediments at Site 645 are characterized by a high content of organic carbon throughout almost the entire section. The TOC values, ranging generally between 0.4% and 2.8%, are distinctly higher than those recorded in open-marine (i.e., oxic) deep-sea sediments, which are $<0.3\%$ (McIver, 1975). Uncommonly high amounts of C_{org} in deep-sea sediments may be caused by (1) high oceanic productivity, as seen in upwelling areas, (2) anoxic deep-water conditions caused by reduced deep-water circulation, (3) increased supply of terrestrial organic matter, and (4) rapid burial of C_{org} by high sedimentation rates (Arthur et al., 1984; Stein et al., in press; Zimmerman et al., in press). A distinctly increased primary productivity as observed in upwelling areas is less probable because of the lack of biogenic silica. Dominantly anoxic deep-water conditions are also less probable because of the moderate to intensive bioturbation recorded in most parts of the sediment sequence. Although dating of sediments at Site 645 is poor, we suggest a high sedimentation rate of at least 40 m/m.y. (see "Biostratigraphy" section, this chapter). This sedimentation rate is already high enough to explain the preservation of from 1% to 2% of marine organic matter without any need of restricted deep-water circulation (Mueller and Suess, 1979; Stein, in press). At Site 645, the organic carbon is dominantly terrigenous, however, showing a distinct increase in amount of marine organic matter below about 500 mbsf. Using the correlation between HI and amount of terrestrial and marine macerals shown for immature sediments from the Cenozoic and Mesozoic Atlantic Ocean (Stein et al., in press), the content of marine organic matter in the older (late/middle Miocene?) sediments at Site 645 can be roughly estimated to range between about 10% and 40%. The higher amount of marine organic matter in the lower part of the sediment sequence may have been caused by an increased supply of terrigenous matter, i.e., organic, inorganic, as well as nutrients. An increase

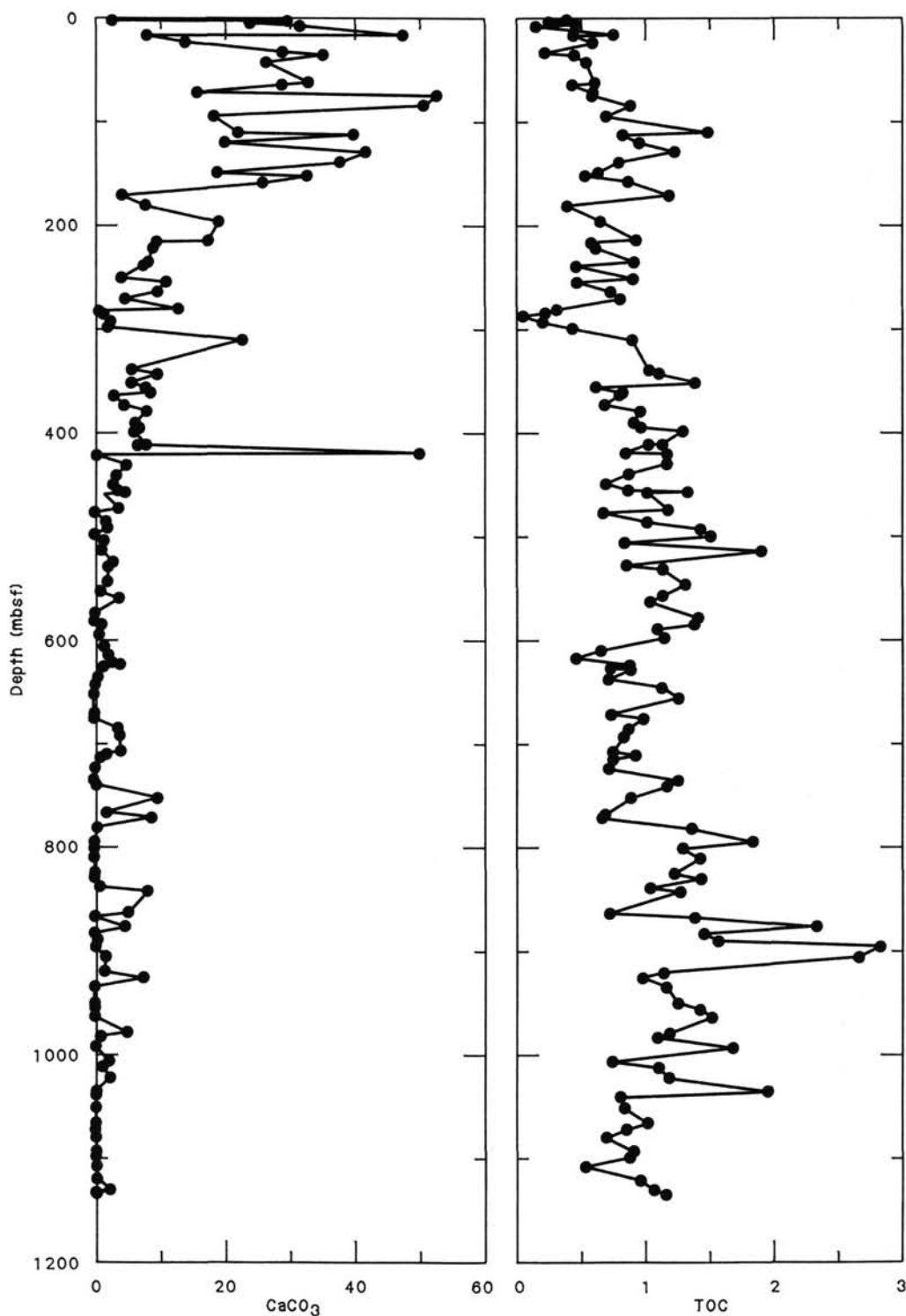


Figure 30. Organic carbon and carbonate (TOC) contents plotted versus sub-bottom depth.

in nutrient supply may have caused higher oceanic productivity during middle Miocene times (see "Sediment-Accumulation Rates," Fig. 27, this chapter).

PALEOMAGNETICS

Shipboard paleomagnetic studies of the sediments cored at Site 645 included both natural remanent magnetization (NRM) and rock magnetic measurements. The NRM measurements are

used to establish a magnetic-polarity stratigraphy that can then be correlated with the geomagnetic-polarity time scale (Berggren et al., 1986). Poor core recovery and the great uncertainty in the shipboard biostratigraphic results of this site study, however, render the correlation of the observed polarity record with the time scale tenuous. Considered in the context of the available data, however, the magnetostratigraphy does provide some constraints on the age of the sediments cored at this site. Shore-

Table 8. Organic carbon and carbonate contents in sediments of Site 645. Asterisk (*) marks CO samples.

Sample	Depth (m)	Carbonate (%)	TOC (%)
Hole 645A			
105-645A-01H-01, 75-77	0.75	39.6	
105-645A-01H-03, 96-98	3.96	34.1	0.42
Hole 645B			
105-645B-01X-01, 45-47	0.45	22.0	
105-645B-01X-01, 148-150	1.50	2.4	0.38
105-645B-01X-03, 45-47	3.45	29.4	0.25
105-645B-02X-01, 72-74	4.73	15.0	
105-645B-02X-01, 148-150	5.50	23.9	0.44
105-645B-02X-03, 85-87	7.85	31.4	0.14
105-645B-03X-01, 73-75	14.23	18.0	
105-645B-03X-02, 148-150	16.50	47.2	0.75
105-645B-03X-03, 53-55	17.03	7.6	0.42
105-645B-04X-01, 39-41	23.19	13.7	0.58
105-645B-05X-01, 75-77	32.95	28.8	0.22
105-645B-05X-01, 148-150	33.70	35.	
105-645B-05X-03, 66-68	35.86	34.9	0.44
105-645B-06X-01, 73-75	43.33	26.3	0.54
105-645B-08X-01, 75-77	62.75	32.8	0.59
105-645B-08X-02, 148-150	64.70	28.8	0.42
105-645B-08X-03, 51-53	65.51	31.	
105-645B-09X-01, 81-83	72.41	15.8	0.59
105-645B-09X-01, 148-150	73.10	26.	
105-645B-09X-03, 75-77	75.35	52.4	0.58
105-645B-09X-03, 112-114	75.72	46.	
105-645B-09X-03, 121-123	75.81	45.	
105-645B-10X-01, 75-77	82.05	46.	
105-645B-10X-02, 0-2	82.80	45.	
105-645B-10X-03, 5-7	84.35	50.6	0.88
105-645B-11X-01, 60-62	91.50	9.	
105-645B-11X-01, 140-142	92.30	40.	
105-645B-11X-03, 37-39	94.27	43.	
105-645B-11X-03, 80-82	94.70	18.3	0.68
105-645B-11X-03, 110-112	95.00	4.	
105-645B-13X-01, 65-67	110.95	22.1	1.47
105-645B-13X-02, 120-122*	113.00	39.6	0.81
105-645B-13X-03, 80-82	114.10	25.	
105-645B-14X-01, 75-77	120.65	19.9	0.94
105-645B-14X-02, 82-84	122.22	41.	
105-645B-14X-03, 90-92	123.80	10.	
105-645B-15X-01, 50-52	130.00	41.6	1.22
105-645B-16X-01, 0-2	139.10	23.	
105-645B-16X-01, 10-12	139.20	37.9	0.79
105-645B-17X-01, 75-77	149.55	19.0	0.64
105-645B-17X-02, 75-77	151.05	35.	
105-645B-17X-03, 69-71	152.49	39.	
105-645B-17X-03, 120-122*	153.00	32.7	0.53
105-645B-18X-01, 65-67	159.05	25.9	0.86
105-645B-19X-01, 75-77	168.85	11.	
105-645B-19X-03, 75-77	171.85	4.2	1.18
105-645B-19X-03, 140-142	172.50	2.	
105-645B-19X-05, 75-77	174.85	9.	
105-645B-20X-01, 75-77	178.45	4.	
105-645B-20X-02, 120-122*	181.90	7.8	0.40
105-645B-21X-01, 71-73	188.11	10.	
105-645B-21X-01, 148-150	188.90	13.	
105-645B-21X-03, 75-77	191.15	2.	
105-645B-21X-05, 83-85	194.23	11.	
105-645B-21X-07, 40-42	196.80	1.	
105-645B-22X-01, 69-71	197.43	19.2	0.65
105-645B-22X-01, 148-150	198.30	9.	
105-645B-22X-03, 69-71	200.49	6.	
105-645B-22X-05, 78-80	203.58	23.	
105-645B-22X-07, 45-47	206.25	15.	
105-645B-23X-01, 80-82	207.40	8.	
105-645B-23X-03, 25-27	209.85	17.	
105-645B-23X-05, 60-62	213.20	10.	
105-645B-23X-06, 120-122*	215.30	17.6	0.93
105-645B-23X-07, 5-7	215.65	0.	
105-645B-24X-01, 100-102	217.20	9.6	0.58
105-645B-24X-02, 148-150	219.20	0.	
105-645B-24X-03, 90-92	220.10	2.	
105-645B-24X-05, 69-71	222.89	9.0	0.62
105-645B-26X-01, 105-107	236.65	8.3	0.92
105-645B-26X-03, 75-77	239.35	0.	

Table 8 (continued).

Sample	Depth (m)	Carbonate (%)	TOC (%)
Hole 645B (cont.)			
105-645B-26X-03, 120-122*	239.80	7.5	0.47
105-645B-26X-05, 55-57	242.15	0.	
105-645B-26X-07, 17-19	244.77	4.	
105-645B-27X-01, 64-66	245.84	22.6	
105-645B-27X-03, 75-77	248.95	4.	
105-645B-27X-05, 73-75	251.93	4.0	0.91
105-645B-27X-07, 27-29	254.47	2.	
105-645B-28X-01, 87-89	255.77	11.1	0.47
105-645B-28X-03, 76-78	258.66	4.	
105-645B-29X-01, 75-77	265.35	9.7	0.73
105-645B-29X-03, 75-77	268.35	5.	
105-645B-29X-05, 74-76	271.34	1.	
105-645B-29X-05, 120-122*	271.80	4.7	0.81
105-645B-30X-01, 75-77	274.95	6.	
105-645B-30X-05, 109-111	281.29	13.0	0.32
105-645B-30X-07, 40-42	283.60	5.	
105-645B-31X-01, 75-77	284.55	0.6	0.23
105-645B-31X-03, 76-78	287.56	1.4	0.06
105-645B-31X-05, 67-69	290.47	16.	
105-645B-32X-01, 80-82	294.30	2.3	0.22
105-645B-32X-03, 120-122*	297.70	11.	
105-645B-32X-05, 85-87	300.35	2.0	0.44
105-645B-32X-07, 23-25	302.73	0.	
Hole 645C			
105-645C-01H-01, 90-92	0.90	32.	
105-645C-01H-03, 105-107	4.05	5.5	0.86
105-645C-03H-01, 80-82	14.80	41.	
105-645C-03H-02, 120-122*	16.70	35.7	0.37
105-645C-03H-03, 76-78	17.76	58.	
105-645C-03H-05, 90-92	20.90	24.	
Hole 645D			
105-645D-01R-01, 90-92	266.80	8.	
105-645D-01R-01, 148-150	267.40	18.5	0.57
105-645D-01R-03, 111-113	269.81	8.5	0.70
105-645D-02R-01, 55-57	273.45	9.	
105-645D-02R-05, 100-102	279.90	4.	
105-645D-08R-01, 80-82	341.20	5.7	1.03
105-645D-08R-03, 50-52	343.90	9.7	1.10
105-645D-09R-02, 80-82	352.00	5.6	1.39
105-645D-09R-04, 75-77	355.25	6.	
105-645D-09R-05, 120-122*	357.20	7.8	0.62
105-645D-09R-06, 75-77	358.25	4.	
105-645D-10R-02, 92-94	362.12	8.7	0.83
105-645D-10R-04, 37-39	364.57	2.8	0.81
105-645D-11R-02, 70-72	371.60	23.	
105-645D-11R-04, 55-57	374.45	4.6	0.69
105-645D-11R-06, 85-87	377.75	6.	
105-645D-12R-01, 88-90	379.88	8.0	0.96
105-645D-13R-02, 93-95	391.03	6.2	0.92
105-645D-13R-04, 65-67	393.75	9.	
105-645D-13R-05, 140-142	396.00	6.8	0.97
105-645D-13R-06, 93-95	397.03	5.	
105-645D-14R-01, 85-87	399.15	6.0	1.29
105-645D-14R-03, 90-92	402.20	9.	
105-645D-14R-05, 45-47	404.75	5.	
105-645D-15R-01, 75-77	408.65	3.	
105-645D-15R-03, 65-67	411.55	8.0	1.14
105-645D-15R-03, 120-122*	412.10	6.6	1.03
105-645D-15R-05, 100-102	414.90	0.	
105-645D-16R-01, 74-76	418.34	6.	
105-645D-16R-03, 0-2	420.60	50.1	0.85
105-645D-16R-03, 78-80	421.38	0.3	1.17
105-645D-17R-03, 71-73	430.91	4.8	1.17
105-645D-17R-05, 60-62	433.80	0.	
105-645D-18R-01, 77-79	437.67	0.	
105-645D-18R-02, 120-122*	439.60	3.3	0.88
105-645D-18R-03, 75-77	440.65	0.	
105-645D-19R-01, 90-92	447.40	0.	
105-645D-19R-03, 90-92	450.40	2.9	0.70
105-645D-19R-05, 82-84	453.32	6.	
105-645D-20R-01, 97-99	457.17	4.	
105-645D-20R-03, 100-102	460.20	1.5	1.02
105-645D-20R-05, 99-101	463.19	0.	

Table 8 (continued).

Sample	Depth (m)	Carbonate (%)	TOC (%)
Hole 645E			
105-645E-02R-01, 55-57	311.35	23.	0.90
105-645E-04R-01, 99-101	456.19	3.6	0.87
105-645E-04R-03, 25-27	458.95	4.7	1.33
105-645E-06R-01, 87-89	475.37	3.7	1.18
105-645E-06R-03, 76-78	478.26	0.	
105-645E-06R-03, 120-122*	478.70	0.	0.68
105-645E-06R-05, 120-122	481.25	0.	
105-645E-07R-01, 67-69	484.77	0.	
105-645E-07R-03, 76-78	487.86	1.6	1.02
105-645E-07R-05, 75-77	490.85	0.	
105-645E-08R-01, 75-77	494.45	2.1	1.43
105-645E-08R-03, 75-77	497.45	0.	
105-645E-08R-05, 75-77	500.42	0.	
105-645E-08R-05, 120-122*	500.90	0.	1.51
105-645E-09R-01, 75-77	504.15	0.	
105-645E-09R-03, 78-80	507.18	1.4	0.86
105-645E-09R-05, 75-77	510.15	0.	
105-645E-10R-01, 75-77	513.75	2.	
105-645E-10R-03, 75-77	516.75	1.3	1.91
105-645E-11R-03, 60-62	526.20	1.	
105-645E-11R-05, 75-77	529.35	0.	
105-645E-11R-05, 120-122*	529.80	2.9	0.86
105-645E-12R-01, 75-77	532.95	0.	
105-645E-12R-03, 75-77	533.95	2.1	1.14
105-645E-12R-05, 75-77	538.95	1.	
105-645E-13R-01, 75-77	542.55	5.	
105-645E-13R-03, 75-77	545.55	1.	
105-645E-13R-05, 75-77	548.55	2.	1.32
105-645E-14R-03, 60-62	555.10	0.	
105-645E-14R-05, 74-76	558.24	0.	
105-645E-14R-05, 120-122*	558.70	0.9	1.15
105-645E-14R-07, 35-37	560.85	1.	
105-645E-15R-01, 118-120	562.28	0.	
105-645E-15R-03, 75-77	564.85	3.8	1.04
105-645E-15R-05, 75-77	567.85	0.	
105-645E-16R-02, 75-77	573.05	0.	
105-645E-16R-06, 110-112	579.40	0.	1.42
105-645E-17R-01, 75-77	581.25	0.	
105-645E-17R-03, 75-77	584.25	0.	
105-645E-17R-05, 75-77	587.25	0.	
105-645E-17R-05, 120-122*	587.70	0.	1.39
105-645E-18R-01, 72-74	590.82	1.2	1.10
105-645E-19R-01, 75-77	600.55	0.8	1.15
105-645E-19R-04, 70-77	605.00	1.	
105-645E-20R-02, 120-122*	612.00	1.6	0.67
105-645E-20R-03, 85-87	613.15	11.	
105-645E-21R-01, 100-102	619.90	2.2	0.47
105-645E-22R-02, 70-72	626.60	2.8	0.89
105-645E-22R-CC	628.40	4.1	0.74
105-645E-23R-02, 75-77	630.65	1.4	0.90
105-645E-24R-02, 75-77	640.25	0.	
105-645E-24R-02, 120-122*	640.70	0.5	0.74
105-645E-25R-01, 75-77	648.45	0.	1.14
105-645E-26R-01, 77-79	657.87	0.	1.27
105-645E-27R-02, 80-82	669.00	0.	
105-645E-27R-04, 50-52	673.20	0.	
105-645E-27R-05, 120-122*	673.90	0.	0.75
105-645E-28R-02, 86-88	678.76	0.	1.00
105-645E-29R-02, 76-78	688.26	3.5	0.88
105-645E-29R-05, 75-77	683.15	0.	
105-645E-30R-01, 75-77	696.35	4.0	0.85
105-645E-32R-01, 75-77	710.45	4.2	0.76
105-645E-32R-03, 120-122*	713.90	1.9	0.94
105-645E-32R-04, 120-122	716.90	0.	
105-645E-33R-02, 40-42	716.60	1.0	0.76
105-645E-33R-05, 72-74	721.42	0.	
105-645E-34R-02, 74-76	726.64	0.	0.74
105-645E-34R-04, 70-72	731.10	0.	
105-645E-35R-02, 70-72	736.20	0.	
105-645E-35R-03, 120-122*	738.20	0.	1.27
105-645E-35R-04, 44-46	740.44	0.	
105-645E-36R-01, 50-52	744.20	0.5	1.18
105-645E-37R-02, 74-76	755.64	9.9	0.90
105-645E-37R-05, 78-80	760.18	0.	
105-645E-38R-02, 95-97	766.45	0.	
105-645E-38R-05, 59-61	769.59	0.	
105-645E-38R-06, 0-2	770.50	1.9	0.70
105-645E-39R-02, 55-57	774.35	9.0	0.68
105-645E-39R-05, 63-65	779.33	0.	

Table 8 (continued).

Sample	Depth (m)	Carbonate (%)	TOC (%)
Hole 645E (cont.)			
105-645E-40R-02, 92-94	784.22	0.5	1.37
105-645E-40R-05, 95-97	789.25	9.	
105-645E-41R-02, 70-72	794.20	0.	
105-645E-41R-05, 0-2	798.00	0.	1.84
105-645E-41R-05, 71-73	798.71	9.	
105-645E-42R-02, 76-78	803.86	0.	1.30
105-645E-42R-05, 68-70	808.28	6.	
105-645E-43R-02, 83-85	813.53	0.	1.43
105-645E-43R-05, 83-85	818.05	0.	
105-645E-44R-02, 100-102	823.30	0.	
105-645E-44R-05, 90-92	827.70	0.	
105-645E-44R-05, 120-122*	828.00	0.1	1.23
105-645E-45R-02, 70-72	832.70	0.	1.44
105-645E-45R-05, 70-72	837.20	0.	
105-645E-46R-02, 71-73	842.31	0.9	1.05
105-645E-46R-04, 91-93	845.51	8.3	1.29
105-645E-48R-01, 126-128	860.66	7.	
105-645E-48R-03, 120-122*	865.10	5.3	0.73
105-645E-48R-04, 42-44	864.32	4.	
105-645E-49R-02, 60-62	870.70	0.	1.40
105-645E-49R-05, 95-97	875.55	7.	
105-645E-50R-02, 79-81	880.39	4.7	2.35
105-645E-50R-05, 56-58	884.76	7.	
105-645E-51R-02, 79-81	887.19	0.	1.48
105-645E-52R-02, 62-64	890.02	21.	
105-645E-52R-04, 120-122*	893.60	0.4	1.58
105-645E-52R-05, 53-55	894.43	0.	
105-645E-53R-02, 78-80	899.88	0.	2.84
105-645E-53R-05, 61-63	904.21	6.	
105-645E-54R-02, 76-78	909.46	1.8	2.67
105-645E-54R-05, 77-79	913.97	0.	
105-645E-55R-02, 75-77	919.05	2.	
105-645E-55R-05, 74-76	923.54	3.	
105-645E-55R-05, 120-122*	924.00	1.6	1.16
105-645E-56R-02, 88-90	928.98	7.6	0.99
105-645E-56R-05, 75-77	933.35	0.	
105-645E-57R-02, 57-59	938.27	0.	1.18
105-645E-57R-05, 54-56	942.74	0.	
105-645E-58R-02, 66-68	948.06	4.	
105-645E-58R-05, 72-74	952.62	0.	
105-645E-58R-05, 120-122*	953.10	0.	1.26
105-645E-59R-03, 73-75	959.33	0.	1.44
105-645E-59R-06, 79-81	963.89	2.	
105-645E-60R-02, 73-75	967.53	0.	1.53
105-645E-60R-05, 74-76	972.04	3.	
105-645E-61R-02, 48-50	976.88	6.	
105-645E-61R-05, 66-68	981.56	0.	
105-645E-61R-05, 120-122*	982.10	5.1	1.21
105-645E-62R-02, 71-73	986.21	0.9	1.11
105-645E-62R-05, 83-85	991.33	12.	
105-645E-63R-02, 75-77	996.45	0.	1.70
105-645E-63R-05, 89-91	1001.09	0.	
105-645E-64R-02, 69-71	1006.09	0.	
105-645E-64R-04, 120-122*	1009.60	2.2	0.76
105-645E-64R-05, 67-69	1010.57	0.	
105-645E-65R-02, 78-80	1015.88	1.1	1.12
105-645E-66R-02, 89-91	1025.69	2.3	1.20
105-645E-66R-05, 50-52	1029.80	1.	
105-645E-67R-02, 79-81	1035.19	0.	
105-645E-67R-04, 148-150*	1038.90	0.	1.97
105-645E-67R-05, 75-77	1039.65	0.	
105-645E-68R-01, 69-71	1043.29	0.	0.82
105-645E-68R-05, 66-68	1049.26	0.	
105-645E-69R-02, 94-96	1054.64	0.	0.86
105-645E-69R-04, 43-45	1057.13	0.	
105-645E-70R-02, 66-68	1064.06	0.	
105-645E-70R-05, 78-80	1068.68	0.	
105-645E-70R-05, 120-122*	1069.10	0.	1.03
105-645E-71R-02, 69-71	1075.30	0.	0.87
105-645E-71R-04, 46-48	1076.06	0.	
105-645E-72R-02, 81-83	1083.01	0.	0.72
105-645E-72R-05, 74-76	1087.44	0.	
105-645E-73R-04, 120-122*	1096.10	0.	0.92
105-645E-74R-02, 75-77	1102.05	0.	0.89
105-645E-75R-02, 75-77	1111.55	0.	0.55
105-645E-76R-04, 120-122*	1124.50	0.	0.98
105-645E-77R-04, 128-130	1133.90	2.0	1.08
105-645E-78R-01, 31-33	1138.01	0.	1.16

Table 9. Rock-Eval results. Asterisk (*) marks CO samples. The HI-2 and OI-2 data are shown in Figure 31.

Sample	T _{max}	S1	S2	S3	P1	S2/S3	PC	TOC-1	TOC-2	HI-1 ^a	HI-2 ^b	OI-1 ^a	OI-2 ^b
Hole 645B													
105-645-03X-03, 148-150	433	0.04	0.38	0.90	0.10	0.42	0.03	0.54	0.00	70	51	166	120
105-645-05X-03, 66-68	290	0.01	0.02	0.50	0.50	0.04	0.00	0.22	0.44	9	5	229	114
105-645-08X-02, 120-122	364	0.02	0.09	0.73	0.20	0.12	0.00	0.29	0.42	31	21	251	174
105-645-09X-03, 75-77	447	0.04	0.16	0.88	0.20	0.18	0.01		0.58	28		152	
105-645-13X-01, 65-67	382	0.03	0.15	0.94	0.17	0.15	0.01	0.25	1.47	60	10	376	64
105-645-13X-02, 120-122	421	0.01	0.03	0.91	0.25	0.03	0.00	0.18	0.81	16	4	505	112
105-645-14X-01, 75-77	366	0.02	0.02	0.64	0.50	0.03	0.00	0.23	0.94	8	2	278	68
105-645-15X-01, 50-52	430	0.08	0.38	1.32	0.17	0.28	0.03	0.56	1.22	67	31	235	108
105-645-16X-01, 10-12	441	0.02	0.21	0.75	0.09	0.28	0.01	0.61	0.79	34	27	122	95
105-645-17X-03, 120-122	434	0.02	0.33	1.10	0.06	0.30	0.02	0.35	0.53	94	62	314	208
105-645-18X-01, 65-67	405	0.00	0.04	0.46	0.00	0.08	0.00	0.27	0.86	14	5	170	53
105-645-19X-03, 75-77	418	0.05	0.50	0.92	0.09	0.54	0.04	0.59	1.18	84	42	155	78
105-645-20X-03, 120-122	407	0.03	0.24	0.58	0.12	0.41	0.02	0.26	0.40	92	60	223	145
105-645-23X-06, 120-122	426	0.08	0.74	1.32	0.10	0.56	0.06	0.80	0.93	92	80	165	142
105-645-26X-01, 105-107	387	0.20	0.54	0.00	0.27	—	0.06	0.51	0.92	105	59	0	0
105-645-26X-03, 120-122*	415	0.07	0.39	1.02	0.15	0.38	0.03	0.34	0.47	114	83	300	217
105-645-29X-01, 75-77	408	0.08	0.58	0.86	0.12	0.67	0.05	0.68	0.73	85	79	126	118
105-645-29X-05, 120-122*	395	0.18	0.60	0.59	0.23	1.01	0.06	0.54	0.81	111	74	109	73
105-645-30X-05, 109-111	406	0.28	0.91	0.35	0.24	2.60	0.09	0.54	0.32	168	284	64	109
105-645-32X-05, 85-87	456	0.04	0.46	1.37	0.08	0.33	0.04	0.33	0.44	139	104	415	311
Hole 645C													
105-645C-03H-02, 120-122	438	0.00	0.32	1.26	0.00	0.25	0.02	0.43	0.37	74	86	293	341
Hole 645D													
105-645D-01R-01, 148-150	456	0.05	0.40	3.53	0.11	0.11	0.03	0.61	0.57	65	70	578	619
105-645D-02R-01, 55-57	409	0.05	0.51	1.40	0.09	0.36	0.04	0.38	—	134	—	369	—
105-645D-08R-03, 50-52	402	0.31	1.06	1.23	0.23	0.86	0.11	0.70	1.10	135	96	157	112
105-645D-09R-05, 120-122*	383	0.01	0.22	3.53	0.05	0.06	0.01	0.36	0.62	61	35	980	569
105-645D-10R-02, 92-94	396	0.23	0.78	0.95	0.23	0.82	0.08	0.64	0.83	121	94	148	114
105-645D-13R-05, 140-142	408	0.19	0.95	1.35	0.17	0.70	0.09	0.55	0.97	172	98	245	159
105-645D-15R-03, 120-122*	410	0.17	0.93	2.34	0.15	0.39	0.09	0.59	1.03	157	90	396	227
105-645D-16R-03, 0-2	421	0.09	0.67	14.11	0.12	0.04	0.06	0.59	0.85	113	81	2391	1666
105-645D-16R-03, 78-80	421	0.06	0.79	1.52	0.07	0.51	0.07	0.56	1.17	141	68	271	130
105-645D-17R-03, 71-73	418	0.06	0.73	1.82	0.08	0.40	0.06	0.61	1.17	119	62	298	156
105-645D-18R-03, 120-122*	411	0.06	0.51	1.07	0.11	0.47	0.04	0.42	0.88	121	58	254	122
105-645D-19R-03, 90-92	405	0.09	0.60	1.65	0.13	0.36	0.05	0.40	0.70	150	86	412	236
105-645D-20R-03, 100-102	418	0.16	1.04	1.34	0.13	0.77	0.10	0.58	1.02	179	102	231	131
Hole 645E													
105-645E-06R-03, 120-122*	398	0.12	0.57	0.84	0.18	0.67	0.05	—	0.68	—	83	—	103
105-645E-08R-05, 120-122*	418	0.54	2.40	1.16	0.18	2.06	0.24	—	1.51	—	158	—	76
105-645E-11R-05, 120-122*	409	0.11	0.52	1.45	0.18	0.35	0.05	—	0.86	—	60	—	169
105-645E-14R-05, 120-122*	420	0.24	1.31	1.19	0.16	1.10	0.12	—	1.15	—	114	—	103
105-645E-17R-05, 120-122*	429	0.32	2.35	1.07	0.12	2.19	0.22	—	1.39	—	169	—	77
105-645E-20R-02, 120-122*	413	0.14	0.62	1.39	0.18	0.44	0.06	—	0.67	—	93	—	207
105-645E-22R-CC	418	0.18	1.07	4.41	0.15	0.24	0.10	—	0.74	—	145	—	596
105-645E-24R-02, 120-122*	416	0.22	1.20	0.66	0.15	1.81	0.11	—	0.74	—	162	—	89
105-645E-27R-05, 120-122*	414	0.15	0.92	0.50	0.14	1.84	0.08	—	0.75	—	123	—	67
105-645E-32R-03, 120-122*	286	0.00	0.00	2.66	—	0.00	0.00	—	0.94	—	—	—	283
105-645E-35R-03, 120-122*	419	0.34	1.93	0.83	0.15	2.32	0.18	—	1.27	—	152	—	65
105-645E-38R-06, 000-2*	424	0.17	1.49	2.05	0.10	0.72	0.13	—	0.70	—	213	—	293
105-645E-38R-06, 000-2*	426	0.14	1.40	2.06	0.09	0.67	0.12	—	0.70	—	200	—	294
105-645E-41R-05, 000-2*	427	0.43	3.78	1.34	0.10	2.82	0.35	—	1.84	—	205	—	72
105-645E-44R-05, 120-122*	428	0.11	1.54	1.20	0.07	1.29	0.13	—	1.23	—	125	—	98
105-645E-48R-03, 120-122*	429	0.02	0.87	2.68	0.02	0.32	0.07	—	0.73	—	119	—	367
105-645E-52R-04, 120-122*	431	0.14	2.80	1.91	0.05	1.46	0.24	—	1.58	—	177	—	121
105-645E-55R-05, 120-122*	431	0.15	1.80	1.78	0.08	1.01	0.16	—	1.16	—	155	—	153
105-645E-58R-05, 120-122*	429	0.14	1.88	1.41	0.07	1.33	0.16	—	1.26	—	149	—	112
105-645E-61R-01, 120-122*	429	0.13	1.62	1.63	0.07	0.99	0.14	—	1.21	—	134	—	135
105-645E-64R-04, 120-122*	423	0.04	0.89	0.87	0.04	1.02	0.07	—	0.76	—	117	—	114
105-645E-67R-04, 148-150*	426	0.17	2.69	1.42	0.06	1.89	0.23	—	1.97	—	137	—	72
105-645E-70R-05, 120-122*	429	0.07	1.34	1.09	0.05	1.22	0.11	—	1.03	—	130	—	106

^a Hydrogen index (HI) -1 and oxygen index (OI) -1 were calculated using the TOC-1 values from Rock-Eval measurements.^b HI-2 and OI-2 were calculated using the TOC-2 values from the elemental analyzer.

based studies of both the magnetostratigraphy and biostratigraphy will attempt to refine these correlations.

Downcore changes in the magnetic properties of these sediments provide a record of the variations in the source and nature of the magnetic mineralogy with depth. Measurements of these changes, therefore, provide a rapid method of quantifying lithologic variations. These changes may be used to assist in

correlating the overlapping sections that were cored in Holes 645A, 645C, 645F, and 645G.

Magnetostratigraphy

We measured the direction and magnitude of the NRM of sediments cored at Site 645, using both the spinner magnetometer to measure discrete samples and the pass-through cryogenic

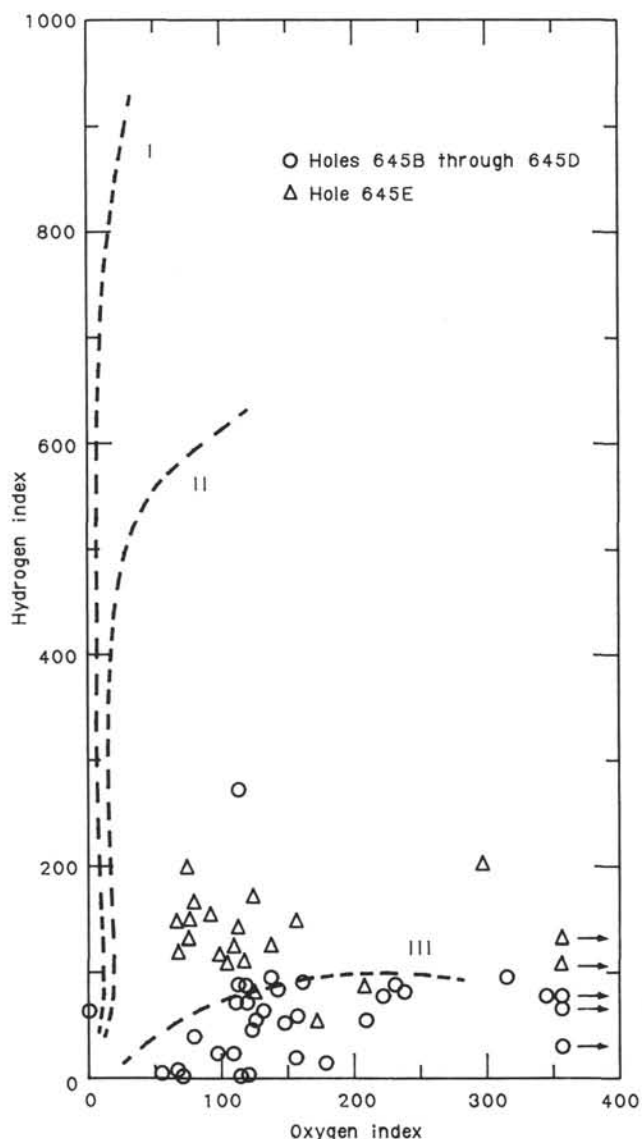


Figure 31. Hydrogen index ($\text{mg HC/g C}_{\text{org}}$) versus oxygen index ($\text{mg CO}_2/\text{g C}_{\text{org}}$) of organic matter at Site 645.

magnetometer to measure the archive halves of the split core sections. Discrete 5–12-cm³ samples were taken at nominal intervals of 1.5 m when possible. Pilot samples, chosen on the basis of lithology, were subjected to progressive alternating-field demagnetization studies. Results of these studies indicate that the sediments are stably magnetized and that treatment at 5–10 milliTesla (mT) is sufficient to isolate a component that decays in a linear manner under treatment at progressively higher fields in samples from the upper intervals. On the basis of these results, we treated the remaining samples at 5–10 mT.

In general, both positive and negative inclination values observed, after part demagnetization, agree well with the predicted axial dipole field directions (79°) for this site location. The steep inclinations observed here allow determination of polarity on the basis of the inclination record alone.

Sporadic recovery in Hole 645B prevented a continuous record from being obtained, but only normal-polarity inclinations are observed from the top of the hole to 95 mbsf. This reversal, therefore, is interpreted as being the base of the Brunhes Chronozone; otherwise, at least two successive reversals would have to have been missed in the unrecovered sections. Assuming this reversal to be the base of the Brunhes Chronozone, the short

normal-polarity zone from 115 to 126 mbsf is interpreted as being the Jaramillo Subchronozone. Interpreting the polarity record further downcore is difficult because of the noise in the record resulting primarily from drilling disturbance and limited recovery. The normal-polarity zone observed in Cores 105-645B-26X and 105-645B-27X may possibly be correlative with the Olduvai Chron.

The inclination records obtained using the pass-through cryogenic from Holes 645E and 645D agree well with the discrete sample records. Below 800 mbsf, the pass-through intensities dropped to values near the noise level of the instrument, producing steep downward magnetizations. Comparison with the discrete samples below 800 mbsf revealed significant discrepancies between the two sets of results. These discrepancies originate from remagnetization of the cores in a vertically downward direction, interpreted as resulting from the drilling process. The observation of normal-polarity "rind" samples and reverse-polarity samples from the center of the core supports this interpretation. Below 900 mbsf, the discrete samples also appear to be remagnetized, as evidenced by the dominance of steep downward directions and a drop in the median destructive field to approximately 5 mT. Thus, the remagnetization process apparently progressed with depth from the rind to the center of the core. Until further shore-based studies can be conducted, the polarities are not interpreted below 850 mbsf.

Correlation of the polarity record obtained at Sites 645E and 645D with the geomagnetic-polarity time scale is difficult given the poor core recovery and the paucity of biostratigraphic tie points. The lack of continuous recovery results in gaps in the record, making recognition of distinctive reversal patterns difficult. The likelihood of greatly varying sedimentation rates (see "Sediment-Accumulation Rates" section, this chapter) in this terrigenous section also hinders the correlation.

If the long normal-polarity zone, which extends from 613 to 679 mbsf in Hole 645E, is correlated with Chron 11, a relatively good fit to the available biostratigraphic data is obtained. The correlations may be cautiously extended to the reversal sequences observed above and below this long normal-polarity zone. This extrapolation would place the base of the Gauss Chronozone at 459 mbsf. Although this correlation produces reasonable fits with the depth of the base of the Brunhes Chronozone as observed in Hole 645B and the biostratigraphic data, it is based on only three correlations: the base of the Brunhes Chronozone in Hole 645B, the boundaries of the Jaramillo Subchronozone in Hole 645B, and the correlation of the long normal-polarity sequence in Hole 645E with Chron 11. The remaining correlations are based on interpolations between these picks and extrapolations below the base of Chronozone 11. These interpolations and extrapolations assume relatively constant sedimentation rates between the tie points. This assumption is weak at best, given the lithologic character of the sections cored at Site 645.

Rock Magnetism

The magnetic susceptibility of half-core sections of the entire lengths of Holes 645C, 645F, and 645G, and down to 100 m (the base of the Brunhes Chronozone) of Hole 645B was measured at 5-cm intervals. By using this sampling interval, we were attempting to use variations in downcore magnetic susceptibility to characterize small-scale lithologic variations.

The frequency dependence of magnetic susceptibility on Cores 105-645B-1X, 105-645B-2X, 105-645C-1H, and 105-645C-2H was examined by measuring sections at both frequency ranges of the susceptibility meter (Fig. 32). The results did not show any variation between the two sets of measurements; therefore, dual frequency measurements were not continued.

The high-frequency (HF)/low-frequency (LF) ratio does not change much from 1 and, in fact, is at times > 1. The mechan-

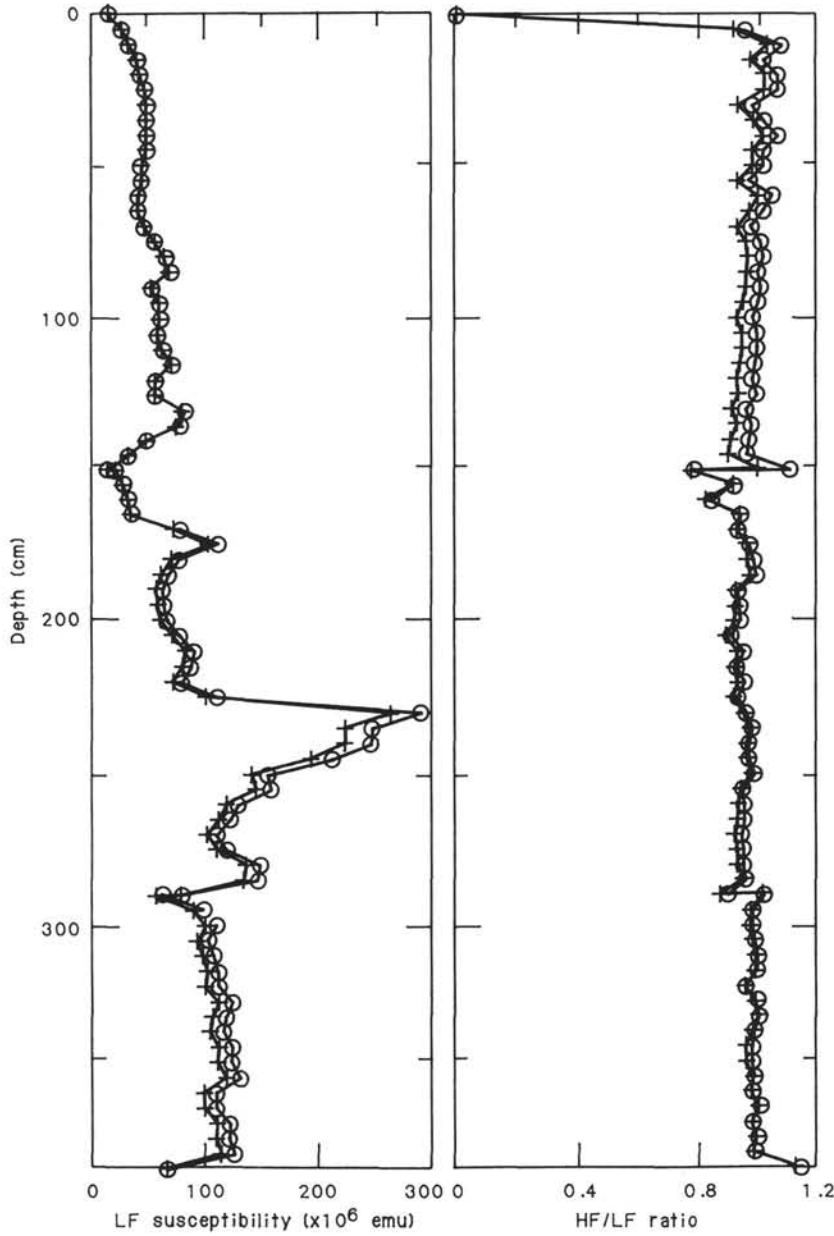


Figure 32. Downcore magnetic-susceptibility measurements of Core 105-645B-1X. Uncorrected (+) and corrected (o) data taken at 5-cm intervals in the core show the same pattern. Two points plotted on the same level indicate a section break. The peak at 2.5 m indicates a graded bed that begins at about 2.9 mbsf. This peak appears in Holes 645C, 645G, and 645F and can be used for hole to hole correlations. The high-frequency/low-frequency (HF/LF) ratio indicates relative size variations in magnetic mineral grains. For it to be an accurate measurement, the ratio must be <1. Because these values stay near 1 and at times are >1, this measurement is considered to be unreliable.

ics of this measurement dictate that HF must be <LF. Because this is not true, this ratio is unreliable and was not measured beyond Core 105-645C-3H.

Discrete-sample measurements were performed on 412 samples from Holes 645B, 645D, and 645E, using the 1-kHz frequency setting. Most of these samples were also used for paleomagnetic analyses. Therefore, they were generally taken where core disturbance was minimum. Twenty samples were taken for rock-magnetic studies only and are included in the 412 total. However, as explained in the "Explanatory Notes" section (this volume), these values have not been corrected for volume or mass.

Results

The susceptibility results of the following graphs are all in units of $10^{-5} (\times 4\pi \text{ SI})$. Because of the density of data points in the downcore susceptibility measurements, depths are given in centimeters.

Figure 33 is a plot of susceptibility versus depth for the first section of Core 105-645B-1X. Uncorrected and corrected data for a standard and machine drift are presented. Both sets of data have the same trends downcore.

As discussed in the "Explanatory Notes" chapter, during sample measurement, the susceptibility of the standard changed from

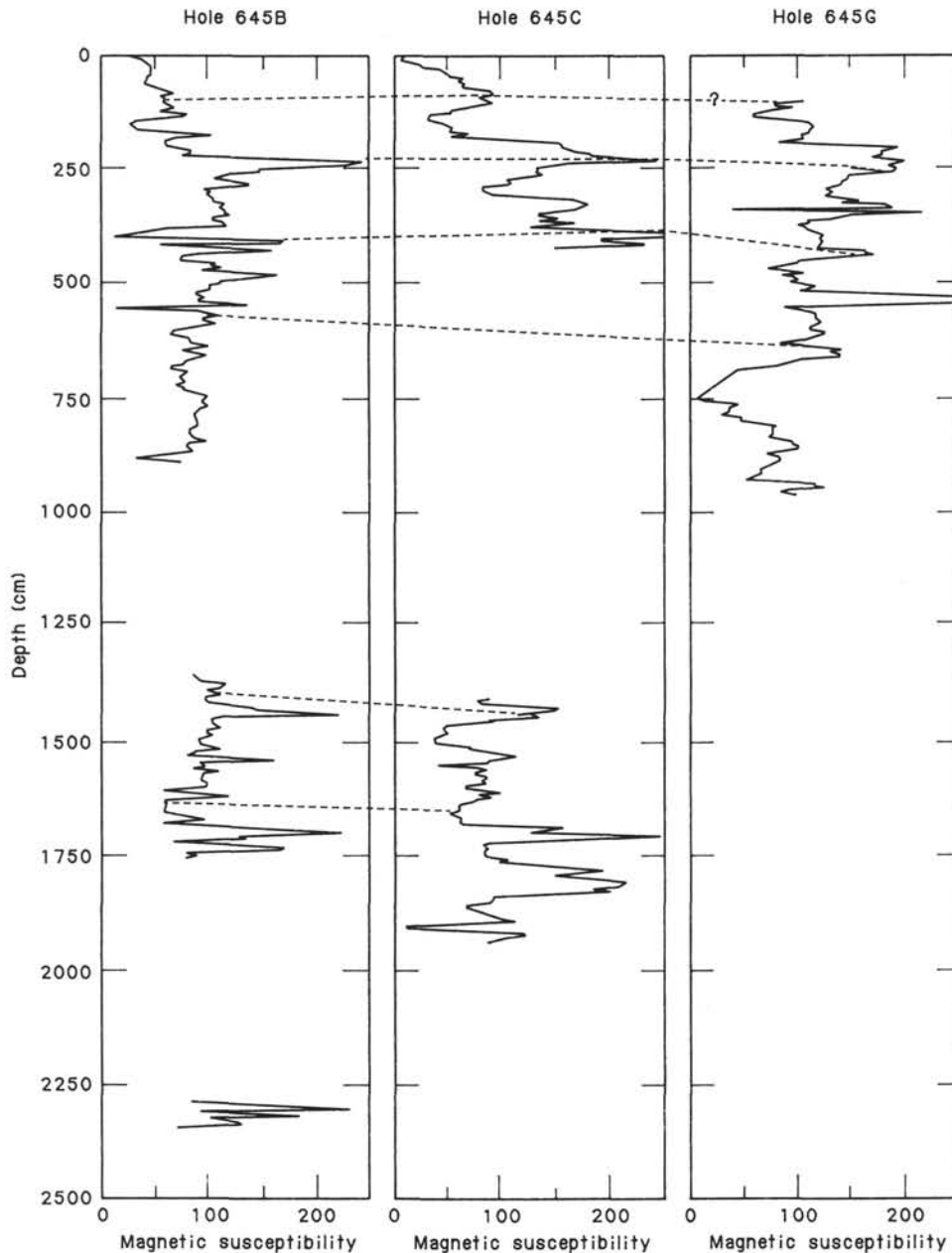


Figure 33. Downcore magnetic-susceptibility variations for the top 25 m of Hole 645B, 645C, and 645G. This pattern is used to correlate the three holes. The similarity in patterns suggests similar lithologic units. Connected areas consistently occur in each core that covers the upper meters of sediment. The gradual rise to a peak at 2.5 m indicates the graded sequence seen in Figure 32.

an initial 320×10^{-5} ($\times 4\pi$ SI) to 450×10^{-5} ($\times 4\pi$ SI). The standard was prepared before the cruise by pouring dry Mn_2O_3 powder into a 25-cm-long core liner. During the cruise, this powder visibly compacted, altering its density and therefore its susceptibility. Because of this, only uncorrected data are presented here.

Figure 33 shows the downcore comparison of Holes 645B, 645C, and 645G. Lines are drawn connecting trends in the graphs that appear to represent similar lithologic variations.

Downcore variations in magnetic susceptibility result from changes in texture of the sediment; higher concentrations occur in the finer grained units. This is shown for Core 105-645C-3H in Figure 34.

For each of the five graded units, higher susceptibilities occur near the top of the section.

Figure 35 represents the data from Hole 645B, collected to the base of the Brunhes Chronozone, thereby giving the downcore variations to approximately glacial stage 19.

Figure 36 represents discrete-sample susceptibility observed at Site 645. This pattern suggests a general decrease in susceptibility from the top of the hole to approximately 175 mbsf (the Layer I/II boundary). Below this depth, the susceptibility stabilizes with intermittent peaks of higher intensity. A correlation between the susceptibility values and physical parameters of the sediment, i.e., particle size and bulk density, is not apparent. The pattern appears to follow changes in silt/clay concentrations in Lithologic Units I and II and may be influenced by the formation of authigenic pyrite in Unit III.

The formation of pyrite would result in decreased susceptibility because magnetic minerals are being chemically altered to

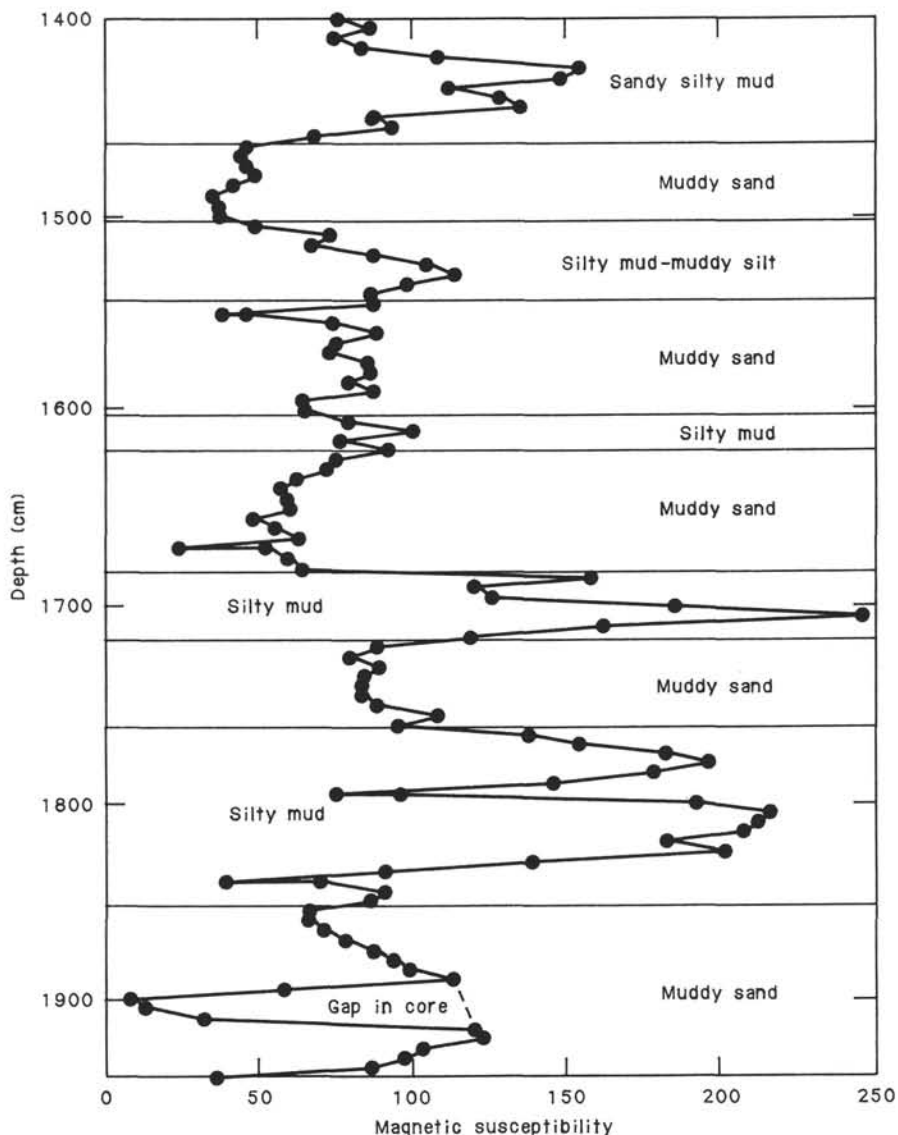


Figure 34. Downcore magnetic susceptibility ($10^{-6} \times 4\pi\text{SI}$) of Core 105-645C-3H, with lithologic boundaries. Magnetic mineral concentrations appear highest in the finer lithologic units (silty muds/muddy silts), just below the top of the sequence. This testifies to the fine-grained nature of the magnetic minerals and particles settling, as described by Stokes' Law. Magnetic minerals are commonly denser than matrix minerals and settle at a faster rate at the same grain diameter. As in Figure 32, depths with two points are at section breaks.

a nonmagnetic mineral. Even though pyrite was seen throughout most of Unit III, its concentration has not been determined quantitatively, so a direct correlation is difficult.

PHYSICAL PROPERTIES

Index Properties

Results of index-property measurements from all holes at Site 645 are shown in vertical profile in Figure 37 and listed in Table 10. Grain density is nearly constant in the sediments; consequently, a well-developed inverse relationship exists between bulk density and water content and porosity in the vertical profiles. GRAPE bulk-density estimates were compared with gravimetric-density determinations and found to agree well for sections in which sediment completely filled the core liner. The profiles show that the bulk density is high near the surface, approximately 2.00 g/cm^3 , and decreases irregularly with depth to 1.64

g/cm^3 at 362 mbsf. From 600 mbsf to the bottom of Hole 645E at 1147 mbsf, a more or less continuous increase in density occurs from 2.00 to 2.20 g/cm^3 . The corresponding values of porosity and water content are approximately 50% and 35% (dry weight), respectively, near the surface, 60% and 60% at 360 mbsf, and 30% and 17% at the bottom of Hole 645E.

GRAPE profiles of cores that recovered the sediment-water interface (Fig. 38) show that a thin, low-density layer, which is approximately 30 cm thick, is present at the surface. At about 0.25 mbsf, wet-bulk density increases sharply from approximately 1.5 to 2.0 g/cm^3 . Variation in bulk density that accompanies the near-surface cyclic lithologic changes is also evident in these records (Fig. 38).

Superimposed on the overall pattern of first decreasing and then increasing bulk density with depth is a small-scale fluctuation of meters to tens of meters. This variation greatly reflects textural changes. Higher density intervals correspond to coarser

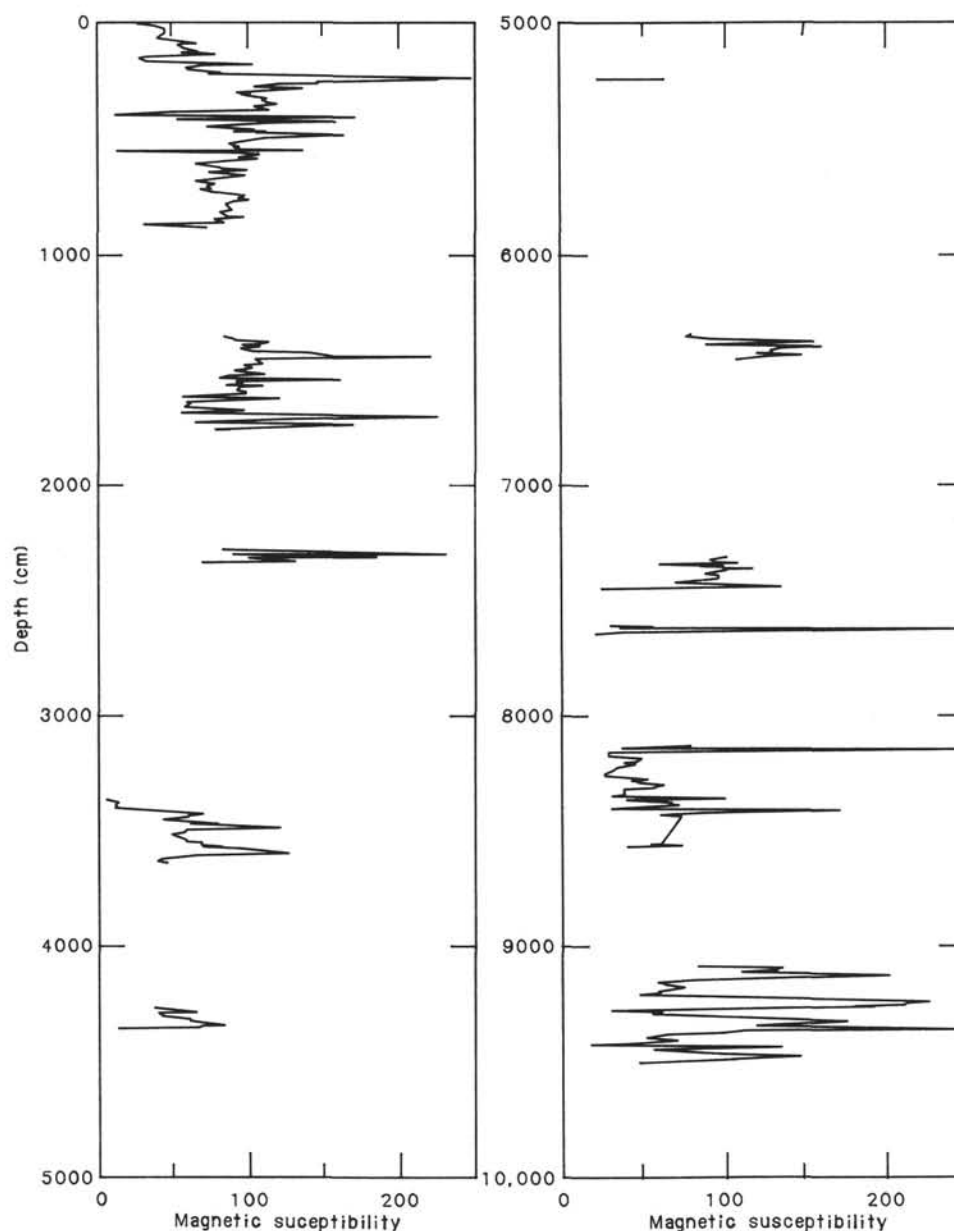


Figure 35. Downcore magnetic susceptibility ($10^{-6} \times 4\pi\text{SI}$) variations of the top 100 m of Hole 645B. This analysis was taken down to the Brunhes/Chronozone boundary. Unfortunately, poor core recovery leaves numerous gaps in the record, and no other core is available with which to compare results. For lithologic comparisons, this analysis may be useful for correlation with future cores taken in Baffin Bay.

grained sediment, and lower density intervals reflect finer grained material. The small-scale variability lessens below 900 mbsf as the amount of clay-size material decreases.

The boundaries between lithologic units roughly correlate with changes in index properties. The boundary between Lithologic Subunits IA and IB is near the base of a high-density interval (Fig. 56, "Summary and Conclusions" section, this chapter). The transition from Subunits IIIA to IIIB is near the base of a low-density layer, and the transition from Subunits IIIB to IIIC is at the diminished small-scale fluctuation that occurs at approximately 900 mbsf. Boundaries between Lithologic Subunit IB and Unit II and between Units II and III do not display distinct changes in index properties.

The primary seismic reflectors correspond to changes in the vertical profiles. Reflector R1 is at a sharp increase in density (Fig. 37), and Reflector R2 is at the change to reduced small-

scale density variation that marks the Subunit IIIB/IIIC boundary.

The high bulk density displayed at Site 645 is typical of terrigenous deep-sea sediments. Near-surface values at the site are slightly higher than the maximum density of terrigenous surficial sediments, 1.93 g/cm^3 , reported by Keller and Bennett (1970). Coarse grain size and poor sorting are most likely responsible for the high density. The decrease in density with depth in the upper 370 m is unusual, but the absence of compaction in the first several hundred meters below the seafloor has been observed at Deep Sea Drilling Project sites (Mayer, 1982). The laboratory-measured bulk density is less than the *in-situ* density, as a result of the release of stress as the sediment is brought to the surface. However, mechanical rebound cannot produce a bulk density less than the initial surficial density. Expansion of the sediment can result from the presence of gas, and this expansion

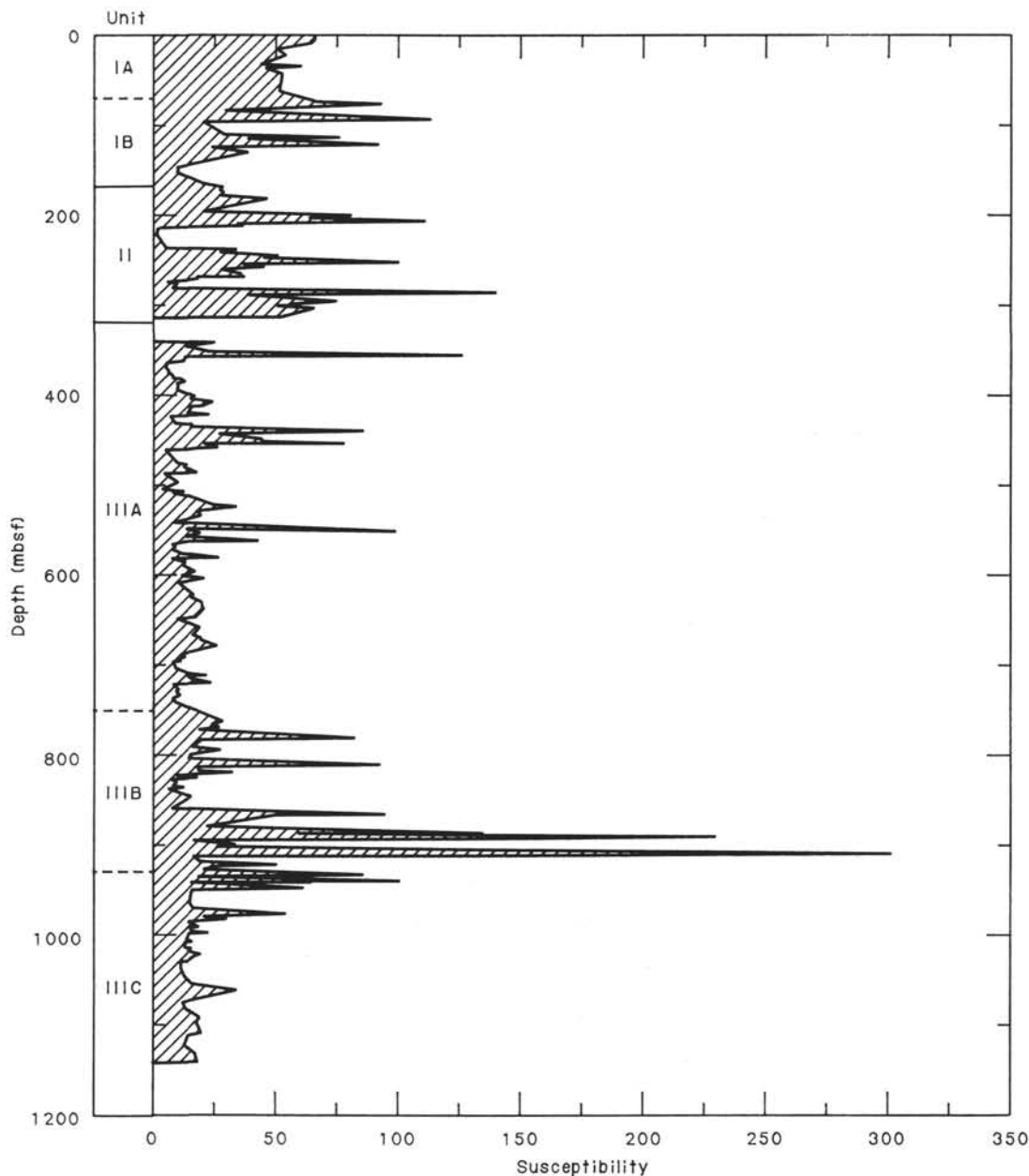


Figure 36. Discrete-sample magnetic susceptibility, Site 645. The discrete-sample susceptibility is combined with data from Holes 645B, 645D, and 645E. This pattern results from pyritization and particle size variations downcore. The peaks develop in areas of low to nil sand content.

was observed in some cores. Because the Quantachrome Penta-Pycnometer directly measures the volumes of solid particles and interstitial fluid, gas expansion is not reflected in the bulk-density determination if the sample is not outgassing at the time of measurement. The decrease in bulk density in the upper 370 mbsf most likely results from lithology-controlled variation. Below 600 mbsf, the vertical profiles reflect the increase in density that accompanies sediment compaction (Moore and Shumway, 1959).

Shear Strength

Shear-strength values at Site 645 display a great degree of variability with depth (see Fig. 37), ranging from a minimum of 2.70 to 177 kPa (Moore, 1964). Anomalous low values are attributed to drilling disturbance and the presence of methane gas in the sediments. In general, the first section of each core is the

most disturbed and thus exhibits fairly low strength, particularly below approximately 100 mbsf. However, some cores (e.g., Cores 105-645B-23X, 207-216 mbsf, and 105-645B-27X, 245-255 mbsf) seem to be disturbed throughout. In addition, many of the low values below approximately 300 mbsf result from the failure of the sediment as the vane was inserted. As we reached material that was more lithified and more coarse grained, this phenomenon became a greater problem. Measurements were discontinued below 475 mbsf as shear-strength values decreased and became unrealistically low.

A clear change in shear strengths is present near the Lithologic Units I/II contact. Values in the upper, carbonate-rich Unit I tend to be considerably lower (< 53 kPa) and more uniform than those in either Lithologic Units II or III. Unit II shear strengths are the highest and most variable, averaging 71.5 kPa. Those in Unit III average 58.0 kPa and appear to decrease with

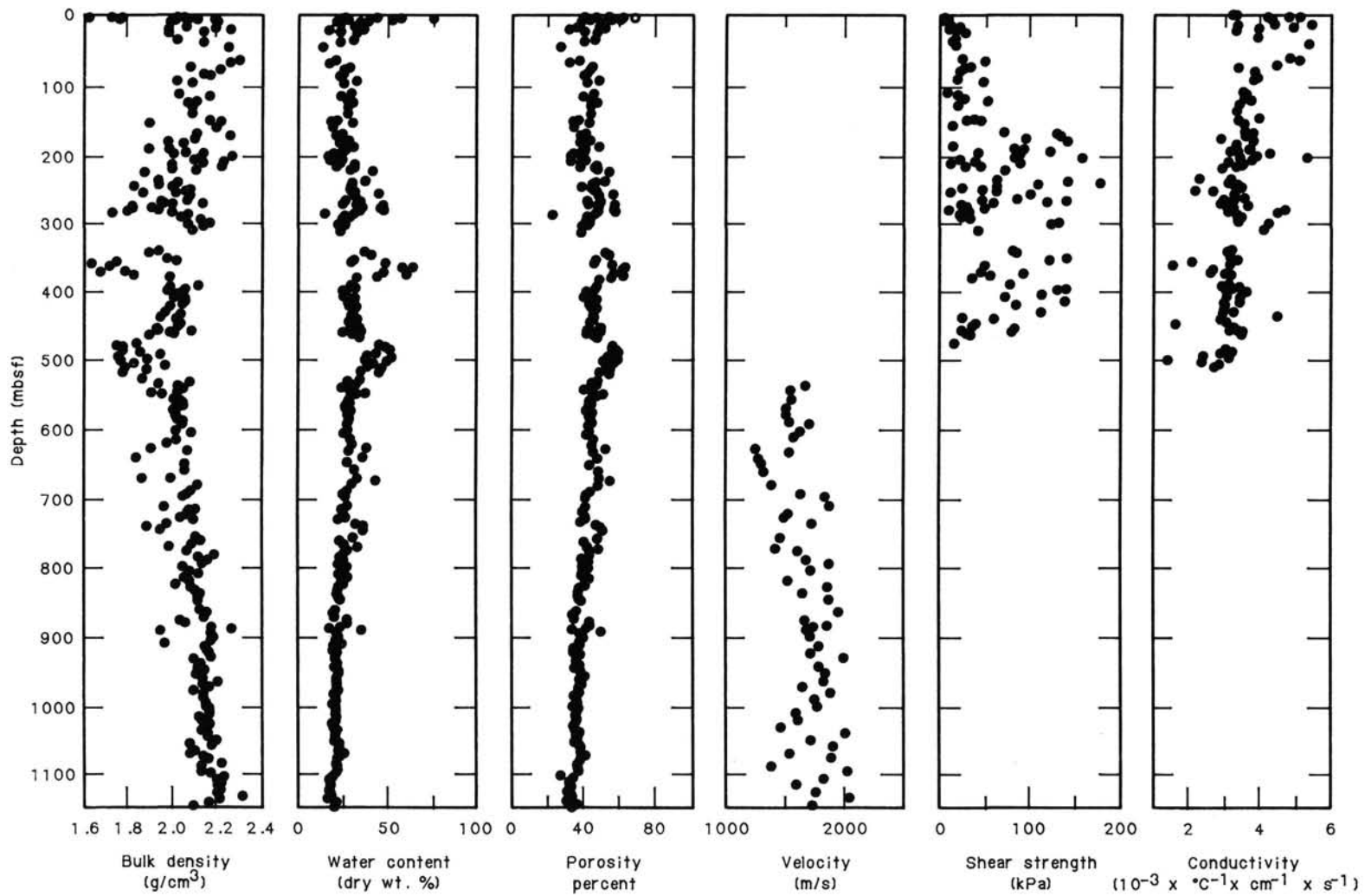


Figure 37. Profiles of the physical-properties variation with depth.

Table 10. Physical-properties measurements, Site 645.

Section	Depth (m)	Bulk density (g/cm ³)	Water content (dry wt. %)	Porosity (%)	Shear strength (kPa)	Thermal conductivity (10 ⁻³ cal × °C ⁻¹ × cm ⁻¹ × s ⁻¹)	Velocity m/s
Hole 645A							
105-645A-1H-1	0.75	2.05	25	39.7			
105-645A-1H-3	3.96	2.07	27	42.6	3.95		
Hole 645B							
105-645B-1X-1	0.75	1.72	57	61.1	3.12	3.24	
105-645B-1X-3	3.45	2.19	22	37.7	5.95	5.10	
105-645B-2X-1	4.70					4.19	
105-645B-2X-1	4.72	2.01	38	54.1	8.29		
105-645B-2X-3	7.75					4.31	
105-645B-2X-3	7.85	1.99	34	49.8	2.70		
105-645B-3X-1	14.23	2.06	31	47.3	9.99		
105-645B-3X-1	14.30					4.39	
105-645B-3X-3	17.03	1.98	36	51.1	8.95		
105-645B-3X-3	17.25					3.38	
105-645B-4X-1	23.10					3.33	
105-645B-4X-1	23.19	1.98	32	46.4	27.26		
105-645B-5X-1	32.95	2.02	30	45.3	14.98	3.95	
105-645B-5X-3	35.86	2.14	23	39.2	12.69		
105-645B-5X-3	35.95					4.53	
105-645B-6X-1	43.33	2.25	13	26.1	16.02		
105-645B-6X-1	43.35					5.35	
105-645B-8X-1	62.75	2.30	20	36.8	23.53	4.81	
105-645B-8X-3	65.50					5.10	
105-645B-8X-3	65.51	2.26	17	31.5	47.98		
105-645B-9X-1	72.35					4.45	
105-645B-9X-1	72.41	2.08	28	44.1	31.83		
105-645B-9X-3	75.35	2.21	25	43.1	26.30	3.39	
105-645B-10X-1	82.05	2.14	25	41.3	20.76	3.84	
105-645B-10X-3	84.35	2.17	23	40.0			
105-645B-11X-1	91.50	2.02	32	47.9	18.45		
105-645B-11X-1	91.65					3.94	
105-645B-11X-3	94.70	2.09	25	41.2	45.72	3.85	
105-645B-13X-1	110.95	2.03	29	45.0	7.31		
105-645B-13X-1	111.05					3.55	
105-645B-13X-3	114.10	2.17	23	39.0	18.68	3.64	
105-645B-14X-1	120.65	2.11	27	43.7	25.55	3.58	
105-645B-14X-3	123.80	2.07	30	47.0	52.25		
105-645B-14X-3	123.90					3.76	
105-645B-15X-1	129.80					3.45	
105-645B-15X-1	130.00	2.09	27	43.1	19.04		
105-645B-16X-1	139.20	2.09	27	43.6		3.35	
105-645B-17X-1	149.55	2.17	21	36.6	36.61	3.99	
105-645B-17X-2	151.05	2.22	18	33.6	29.12		
105-645B-17X-3	152.49	1.90	30	42.3	44.24		
105-645B-17X-3	152.55					3.42	
105-645B-18X-1	159.05	2.20	19	33.9	12.59		
105-645B-18X-1	159.09					3.58	
105-645B-19X-1	168.85	2.11	24	40.3	69.03	3.61	
105-645B-19X-3	171.83	2.26	21	37.8	129.29		
105-645B-19X-3	171.85					3.83	
105-645B-19X-5	174.85	2.10	23	38.4	132.25	3.64	
105-645B-20X-1	178.45	1.98	28	42.9	94.12	2.92	
105-645B-20X-3	181.43	2.05	23	37.4	139.40		
105-645B-20X-3	181.45					3.84	
105-645B-21X-1	188.11	1.90	31	48.1	13.11		
105-645B-21X-1	188.15					3.36	
105-645B-21X-3	191.15	1.99	26	40.3	91.74	3.36	
105-645B-21X-5	194.20					3.73	
105-645B-21X-5	194.23	2.06	24	39.6	79.83		
105-645B-21X-7	196.80	2.01	24	37.4	122.72	3.22	
105-645B-22X-1	197.49	2.14	19	33.6	40.51		
105-645B-22X-1	197.51					3.38	
105-645B-22X-3	200.49	2.27	17	32.4	84.59		
105-645B-22X-3	200.55					4.31	
105-645B-22X-5	203.55					3.97	
105-645B-22X-5	203.58	2.12	23	38.1	81.02		
105-645B-22X-7	206.20					3.47	
105-645B-22X-7	206.25	2.10	24	40.3	156.08		
105-645B-23X-1	207.40	2.23	17	32.3	20.99	5.31	
105-645B-23X-3	209.85	2.14	23	38.4	37.32	3.82	
105-645B-23X-5	213.20	2.00	31	46.7	11.08		
105-645B-23X-5	213.25					3.20	
105-645B-23X-7	215.65	2.22	21	37.6	86.88		

Table 10 (continued).

Section	Depth (m)	Bulk density (g/cm ³)	Water content (dry wt. %)	Porosity (%)	Shear strength (kPa)	Thermal conductivity (10 ⁻³ cal × °C ⁻¹ × cm ⁻¹ × s ⁻¹)	Velocity m/s
Hole 645B (cont.)							
105-645B-23X-7	215.75					3.55	
105-645B-24X-1	217.20	2.00	31	46.0	45.48	3.52	
105-645B-24X-3	220.00					3.35	
105-645B-24X-3	220.10	2.11	29	46.6	27.40		
105-645B-24X-5	222.89	1.88	41	53.5	71.14		
105-645B-24X-5	222.95					3.01	
105-645B-26X-1	236.65	1.94	37	51.0	61.81		
105-645B-26X-1	236.75					2.32	
105-645B-26X-3	239.35					3.23	
105-645B-26X-3	239.35	2.02	30	45.7	139.94		
105-645B-26X-5	242.15	1.94	30	44.5	177.25	3.15	
105-645B-26X-7	244.77	1.83	28	38.8	107.28		
105-645B-26X-7	244.85					3.40	
105-645B-27X-1	245.84	2.00	29	43.9	61.81		
105-645B-27X-1	245.95					3.29	
105-645B-27X-3	248.95	2.08	28	44.9	23.32	3.52	
105-645B-27X-5	251.93	2.06	30	46.6	44.31		
105-645B-27X-5	251.98					3.39	
105-645B-27X-7	254.47	2.02	31	46.5	60.64		
105-645B-27X-7	254.52					2.20	
105-645B-28X-1	255.65					2.72	
105-645B-28X-1	255.77	1.87	44	56.1	10.50		
105-645B-28X-3	258.65					3.30	
105-645B-28X-3	258.66	2.08	31	47.8	99.12		
105-645B-29X-1	265.35	2.07	26	41.4	85.13	3.57	
105-645B-29X-3	268.35	1.96	34	49.0	138.77	3.01	
105-645B-29X-5	271.34	2.00	32	47.8	117.78		
105-645B-29X-5	271.35					3.08	
105-645B-30X-1	274.95	1.91	35	48.1		3.72	
105-645B-30X-5	280.60					3.16	
105-645B-30X-5	281.29	1.80	48	57.0	8.77		
105-645B-30X-7	283.60	2.00	31	46.6	30.91	4.71	
105-645B-31X-1	284.55	2.21	15	28.7			
105-645B-31X-1	284.80					3.16	
105-645B-31X-3	287.55					4.53	
105-645B-31X-3	287.56	2.07	25	40.9	20.99		
105-645B-31X-5	290.47	2.04	28	43.2	22.16		
105-645B-31X-5	290.55					3.38	
105-645B-32X-1	294.30	2.13	24	40.6	32.07	3.53	
105-645B-32X-3	297.70	2.17	25	42.8	58.31	3.44	
105-645B-32X-5	300.25					3.43	
105-645B-32X-5	300.35	2.07	26	42.0	130.61		
105-645B-32X-7	302.73	2.14	22	38.3	122.44		
105-645B-32X-7	302.75					4.25	
Hole 645C							
105-645C-1H-1	0.90	2.02	30	45.8	3.36	3.35	
105-645C-1H-3	3.75					4.78	
105-645C-1H-3	4.05	1.76	53	59.6	6.14		
105-645C-3H-1	14.75					5.43	
105-645C-3H-1	14.80	2.19	20	35.1	20.39		
105-645C-3H-3	17.75					4.90	
105-645C-3H-3	17.76	2.26	16	30.9	12.47		
105-645C-3H-5	20.75					3.97	
105-645C-3H-5	20.90	2.14	23	39.4	15.69		
105-645C-3X-3	17.25					3.38	
Hole 645D							
105-645D-1R-1	266.60	1.95	34	48.4	44.90	3.30	
105-645D-1R-3	269.55					3.28	
105-645D-1R-3	269.81	2.14	25	42.1	57.14		
105-645D-2R-1	273.45	1.82	47	56.3	23.32	2.91	
105-645D-2R-3	276.65	1.82	46	55.7	27.99	3.11	
105-645D-2R-5	279.85					3.28	
105-645D-2R-5	279.90	1.94	34	48.0	47.81		
105-645D-8R-1	341.17					3.24	
105-645D-8R-1	341.20	1.94	37	51.4	79.14		
105-645D-8R-3	343.90	1.90	40	53.2	82.80	3.10	
105-645D-9R-2	352.30	1.98	31	46.1	138.77	3.20	
105-645D-9R-4	355.25	2.02	30	45.5	120.11	3.39	
105-645D-9R-6	358.25	1.75	48	55.3		2.10	
105-645D-10R-2	361.95					3.18	
105-645D-10R-2	362.12	1.64	63	62.4	47.81		

Table 10 (continued).

Section	Depth (m)	Bulk density (g/cm ³)	Water content (dry wt. %)	Porosity (%)	Shear strength (kPa)	Thermal conductivity (10 ⁻³ cal × °C ⁻¹ × cm ⁻¹ × s ⁻¹)	Velocity m/s
Hole 645D (cont.)							
105-645D-10R-4	364.57	1.72	58	61.5			
105-645D-10R-4	364.95					1.57	
105-645D-11R-2	371.60	1.79	47	56.2	43.73		
105-645D-11R-2	371.65					2.68	
105-645D-11R-4	374.45	1.68	60	61.3	91.54		
105-645D-11R-4	374.65					2.64	
105-645D-11R-6	377.65					3.03	
105-645D-11R-6	377.75	1.83	44	54.8	53.64		
105-645D-12R-1	379.75					3.23	
105-645D-12R-1	379.88	1.99	33	48.4	34.98		
105-645D-13R-2	391.03	2.12	29	46.6	75.22		
105-645D-13R-2	391.03					3.17	
105-645D-13R-4	393.10					3.44	
105-645D-13R-4	393.75	1.99	31	46.0			
105-645D-13R-4	393.85					2.96	
105-645D-13R-6	397.00					3.27	
105-645D-13R-6	397.03	2.06	25	40.7	137.02		
105-645D-14R-1	399.10					3.07	
105-645D-14R-1	399.15	1.98	29	43.2	129.44		
105-645D-14R-3	402.20	2.04	26	40.8		3.65	
105-645D-14R-5	404.30					3.54	
105-645D-14R-5	404.75	2.02	25	39.6	111.40		
105-645D-14R-5	404.80					3.55	
105-645D-15R-1	408.60					3.09	
105-645D-15R-1	408.65	2.01	31	46.6	70.00		
105-645D-15R-3	411.55	2.06	27	43.2		3.49	
105-645D-15R-5	414.57					3.03	
105-645D-15R-5	414.90	2.06	27	42.2	137.00		
105-645D-16R-1	418.34	2.05	28	43.7	82.80		
105-645D-16R-1	418.35					3.46	
105-645D-16R-3	421.36					3.04	
105-645D-16R-3	421.38	1.99	32	47.0			
105-645D-17R-1	427.94					3.01	
105-645D-17R-3	430.91	1.97	30	44.6	110.80		
105-645D-17R-3	430.94					3.30	
105-645D-17R-5	433.74					2.96	
105-645D-17R-5	433.80	2.04	29	45.0			
105-645D-18R-1	437.67	1.95	31	45.0	23.32		
105-645D-18R-1	438.10					4.52	
105-645D-18R-3	440.65	2.02	28	43.0	58.31		
105-645D-18R-3	440.95					2.91	
105-645D-19R-1	447.40	2.04	29	45.1	38.48		
105-645D-19R-1	447.50					3.10	
105-645D-19R-3	450.40	2.03	33	49.6	34.98		
105-645D-19R-3	450.50					1.66	
105-645D-19R-5	453.32	1.93	28	41.2	80.46		
105-645D-19R-5	453.50					3.32	
105-645D-20R-1	457.17	2.09	25	40.9	23.32		
105-645D-20R-3	460.20	2.01	30	45.6	29.15		
105-645D-20R-3	460.26					3.52	
105-645D-20R-5	463.17					3.53	
105-645D-20R-5	463.19	1.90	34	47.3	32.65		
Hole 645E							
105-645E-2R-1	311.35	2.09	23	38.0	40.23		
105-645E-2R-1	311.45					4.11	
105-645E-4R-1	455.95					3.41	
105-645E-4R-1	456.19	1.94	35	49.3	22.16		
105-645E-4R-3	458.95	1.99	32	46.9	78.13		
105-645E-6R-1	475.25					3.17	
105-645E-6R-1	475.37	1.84	45	55.4	13.99		
105-645E-6R-3	478.25					3.16	
105-645E-6R-3	478.26	1.75	48	55.5		3.37	
105-645E-6R-5	481.20					3.17	
105-645E-6R-5	481.25	1.78	50	57.8			
105-645E-7R-1	484.77	1.78	51	58.8			
105-645E-7R-1	484.85					3.03	
105-645E-7R-3	487.85					3.24	
105-645E-7R-3	487.86	1.86	43	54.4			
105-645E-7R-5	490.85	1.95	38	52.8		2.92	
105-645E-8R-1	494.45	1.76	52	59.1		2.42	
105-645E-8R-3	497.45	1.89	37	49.6		3.17	
105-645E-8R-5	500.45	1.77	49	56.6		1.44	
105-645E-9R-1	504.15	1.83	41	52.0		2.38	

Table 10 (continued).

Section	Depth (m)	Bulk density (g/cm ³)	Water content (dry wt. %)	Porosity (%)	Shear strength (kPa)	Thermal conductivity (10 ⁻³ cal × °C ⁻¹ × cm ⁻¹ × s ⁻¹)	Velocity m/s
Hole 645E (cont.)							
105-645E-9R-3	507.15					2.88	
105-645E-9R-3	507.18	1.97	39	53.8			
105-645E-9R-5	510.15	1.79	46	54.9		2.79	
105-645E-10R-1	513.75	1.89	35	48.1			
105-645E-10R-3	516.75	1.78	45	54.3			
105-645E-11R-3	526.20	1.87	34	46.9			
105-645E-11R-5	529.35	2.08	27	43.3			
105-645E-12R-1	532.95	1.94	32	46.4			
105-645E-12R-3	535.95	2.03	28	43.7			1670
105-645E-12R-5	538.95	2.05	24	39.2			
105-645E-13R-1	542.55	2.03	29	44.7			1540
105-645E-13R-3	545.55	1.91	37	50.6			
105-645E-13R-5	548.55	1.96	32	46.8			
105-645E-14R-3	555.10	2.01	28	42.8			1550
105-645E-14R-5	558.24	2.04	27	42.1			
105-645E-14R-7	560.85	2.05	28	43.9			
105-645E-15R-1	562.28	2.03	27	42.5			
105-645E-15R-3	564.85	2.05	26	41.5			
105-645E-15R-5	567.85	2.03	26	40.8			1500
105-645E-16R-2	571.93	2.01	29	43.9			
105-645E-16R-6	578.28	2.02	27	42.1			1510
105-645E-17R-1	581.25	2.02	28	43.5			
105-645E-17R-3	584.25	2.03	27	42.7			
105-645E-17R-5	587.25	2.05	28	44.3			1530
105-645E-18R-1	590.82	2.05	27	42.2			1700
105-645E-19R-1	600.75	2.02	27	42.1			1620
105-645E-19R-4	604.30	2.09	25	41.2			
105-645E-20R-1	610.42						1570
105-645E-20R-3	613.15	2.02	29	44.8			
105-645E-21R-1	619.90	1.98	30	44.3			
105-645E-22R-2	625.60	1.91	38	51.2			
105-645E-22R-2	626.79						1240
105-645E-23R-2	630.65	2.07	28	44.1			1530
105-645E-24R-2	640.25	1.84	36	47.5			
105-645E-24R-2	640.51						1270
105-645E-25R-1	648.45	2.06	27	43.0			1300
105-645E-26R-1	657.87	2.06	31	48.0			
105-645E-26R-2	659.43						1320
105-645E-27R-2	669.00	2.00	33	48.6			
105-645E-27R-4	671.70	1.87	43	54.5			
105-645E-28R-2	678.76	2.12	30	47.6			1380
105-645E-29R-2	688.26	2.09	27	42.9			
105-645E-29R-5	692.75	2.07	25	40.9			1630
105-645E-30R-1	696.35	2.05	26	40.8			1830
105-645E-32R-1	710.45	1.97	27	40.7			1870
105-645E-32R-4	715.40	2.11	24	39.9			
105-645E-33R-2	716.60	2.08	24	38.6			
105-645E-33R-5	721.42	2.07	25	40.0			1520
105-645E-34R-2	726.64	2.04	26	40.6			1490
105-645E-34R-4	729.60	2.10	22	37.7			
105-645E-35R-2	736.20	1.98	32	46.7			1720
105-645E-35R-4	738.94	1.89	36	48.9			
105-645E-36R-1	744.20	1.95	36	50.1			
105-645E-37R-2	755.64	2.11	30	47.1			1450
105-645E-37R-5	760.18	2.13	23	39.3			
105-645E-38R-2	765.45	2.09	25	41.2			
105-645E-38R-5	769.59	1.99	33	47.8			
105-645E-38R-6	771.52						1410
105-645E-39R-2	774.75	2.07	27	43.0			
105-645E-39R-2	774.92						1600
105-645E-39R-5	779.33	2.20	25	42.8			
105-645E-40R-2	784.72	2.12	23	38.4			
105-645E-40R-5	789.09						1670
105-645E-40R-5	789.25	2.16	25	41.9			
105-645E-41R-2	794.20	2.14	22	38.1			1850
105-645E-41R-5	798.71	2.05	27	41.9			
105-645E-42R-2	803.86	2.08	24	38.7			1710
105-645E-42R-5	808.28	2.12	22	38.0			
105-645E-43R-2	813.53	2.06	27	42.4			
105-645E-43R-5	818.05	2.08	24	39.9			
105-645E-43R-5	818.16						1520
105-645E-44R-2	823.30	2.02	25	40.0			
105-645E-44R-5	827.70	2.09	22	36.6			1850
105-645E-45R-2	832.70	2.11	21	36.0			
105-645E-45R-5	837.20	2.13	21	36.1			1640

Table 10 (continued).

Section	Depth (m)	Bulk density (g/cm ³)	Water content (dry wt. %)	Porosity (%)	Shear strength (kPa)	Thermal conductivity (10 ⁻³ cal × °C ⁻¹ × cm ⁻¹ × s ⁻¹)	Velocity m/s
Hole 645E (cont.)							
105-645E-46R-2	842.31	2.12	22	36.9			
105-645E-46R-4	845.51	2.12	23	38.3			1860
105-645E-48R-1	860.66	2.13	20	35.0			
105-645E-48R-4	864.27	2.16	19	33.4			1940
105-645E-49R-4	870.70	2.15	20	34.4			
105-645E-49R-2	875.55	2.04	27	42.5			1650
105-645E-50R-2	880.39	2.06	27	42.5			
105-645E-50R-5	884.76	2.18	23	40.3			1840
105-645E-51R-1	885.44						1730
105-645E-51R-2	887.19	2.27	17	32.6			
105-645E-52R-2	890.02	1.95	35	49.0			1670
105-645E-52R-5	894.43	2.18	21	37.1			
105-645E-53R-2	899.88	2.19	22	38.8			1700
105-645E-54R-2	909.46	1.97	24	37.0			
105-645E-54R-5	913.97	2.15	19	33.5			1770
105-645E-55R-2	919.05	2.16	19	33.4			
105-645E-55R-5	923.54	2.17	21	37.2			1700
105-645E-56R-2	928.98	2.18	20	35.1			
105-645E-56R-5	930.75	2.10	20	34.7			1970
105-645E-57R-2	938.44	2.13	21	36.8			
105-645E-57R-5	942.74	2.12	20	34.4			1770
105-645E-58R-2	948.06	2.15	22	37.6			
105-645E-58R-5	952.62	2.11	22	39.9			1820
105-645E-59R-3	959.33	2.14	21	36.9			
105-645E-59R-6	963.89	2.21	21	38.2			1810
105-645E-60R-2	967.53	2.14	21	36.8			
105-645E-60R-5	972.04	2.17	21	36.5			1630
105-645E-61R-2	976.88	2.10	22	36.9			
105-645E-61R-5	981.56	2.14	19	33.4			1870
105-645E-62R-2	986.71	2.14	20	35.2			
105-645E-62R-5	991.33	2.15	20	35.3			1730
105-645E-63R-2	996.45	2.15	18	32.6			
105-645E-63R-5	1001.09	2.16	20	35.9			1760
105-645E-64R-2	1006.09	2.17	20	35.6			
105-645E-64R-5	1010.57	2.17	20	34.6			1570
105-645E-65R-2	1015.88	2.12	21	35.3			
105-645E-65R-5	1020.30	2.13	20	34.3			1600
105-645E-66R-2	1025.69	2.17	18	32.8			
105-645E-66R-5	1029.80	2.16	19	34.0			1440
105-645E-67R-2	1035.19	2.13	21	36.5			
105-645E-67R-5	1039.65	2.16	20	34.7			1990
105-645E-68R-1	1043.29	2.16	20	35.5			
105-645E-68R-5	1049.26	2.20	19	33.9			1700
105-645E-69R-2	1054.64	2.08	22	36.7			
105-645E-69R-4	1057.13	2.18	22	37.6			
105-645E-69R-5	1058.85						1880
105-645E-70R-2	1064.06	2.10	22	37.3			
105-645E-70R-5	1068.68	2.08	25	40.1			1520
105-645E-71R-2	1073.29	2.14	22	37.4			
105-645E-71R-4	1076.06	2.16	21	36.6			1870
105-645E-72R-2	1083.01	2.22	20	35.2			
105-645E-72R-5	1087.44	2.13	21	35.6			1360
105-645E-73R-2	1092.63	2.13	21	36.3			
105-645E-73R-4	1095.53						2000
105-645E-73R-5	1096.96	2.17	20	25.8			
105-645E-74R-2	1102.05	2.23	18	32.4			
105-645E-74R-5	1106.70	2.20	16	30.4			1800
105-645E-75R-2	1111.55	2.22	17	31.2			
105-645E-75R-4	1114.70	2.20	17	32.0			1570
105-645E-76R-2	1121.09	2.21	16	29.5			
105-645E-76R-5	1125.60	2.20	17	31.6			1740
105-645E-77R-2	1130.45	2.31	17	32.3			
105-645E-77R-4	1133.98	2.21	15	28.9			2010
105-645E-78R-2	1139.88	2.16	20	34.8			
105-645E-78R-5	1144.45	2.09	19	32.0			1700
Hole 645F							
105-645F-1H-1	0.25	1.77	44	53.1			
105-645F-1H-2	2.10	1.62	75	67.6	4.89		
105-645F-1H-3	3.60	2.11	23	38.9			
Hole 645G							
105-645G-1H-4	6.29	2.20	21	37.8	7.07		

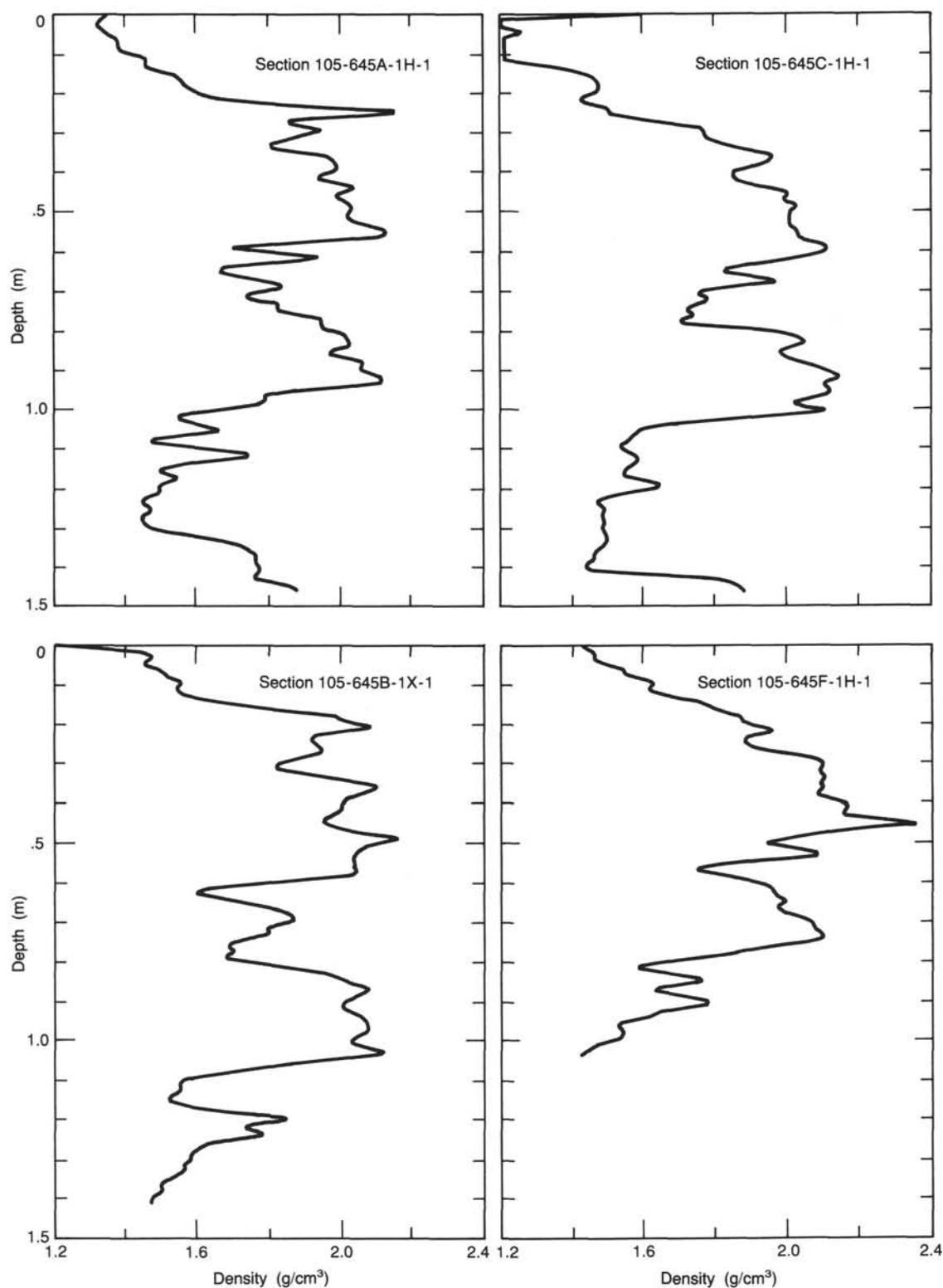


Figure 38. GRAPE bulk-density profiles of core tops for first cores of Holes 645A, 645B, 645C, and 645F.

depth. This trend is thought to be anomalous, however, because of suspect values deeper in the section. No correlations of the shear strength with the measured index properties, particularly water content, are evident, although an inverse relationship has been suggested by many investigators (Bryant and Trabant, 1972; Silva, 1974).

Thermal Conductivity

The variation in thermal conductivity mimics the variation in bulk density (Fig. 37). The overall trend is of decreasing conductivity from the near surface to approximately 500 mbsf. Values range from $5.43 \times 10^{-3} \text{ cal} \times \text{°C}^{-1} \times \text{cm}^{-1} \times \text{s}^{-1}$ at

14.53 mbsf in Hole 645C to $1.40 \times 10^{-3} \text{ cal} \times ^\circ\text{C}^{-1} \times \text{cm}^{-1} \times \text{s}^{-1}$ at 500.45 mbsf in Hole 645E. The latter value is low, probably as a result of poor contact between the probe and sediment. Most sediment conductivities are in the range of from 3 to $3.5 \times 10^{-3} \text{ cal} \times ^\circ\text{C}^{-1} \times \text{cm}^{-1} \times \text{s}^{-1}$; values $>4.0 \times 10^{-3} \text{ cal} \times ^\circ\text{C}^{-1} \times \text{cm}^{-1} \times \text{s}^{-1}$ coincide with density maxima (Fig. 37).

Compressional-Wave Velocity

Compressional-wave velocities were measured from depths of from 535 to 1144 mbsf in Hole 645E. Numerous problems were encountered in obtaining measurements in samples from depths <535 mbsf. Sediment in this interval (<535 mbsf) was soft and deformed when placed in the velocimeter and thus produced anomalously low values. The vertical profile (Fig. 37) displays an irregular increase with depth, reflecting the increasing density between 535 and 1144 mbsf. Values range from approximately 1300 to 2000 m/s. Irregularity in the profile is the product of differences in sediment type and the difficulty in obtaining velocity measurements. The velocities that were determined are generally lower than the seismic interval velocities, probably as a result of inherent changes in the state of stress and expansion that the sample underwent from *in-situ* to laboratory conditions. The velocity variation does not appear to correspond to lithologic boundaries or to predicted location of major seismic reflectors.

Summary

Sediments at Site 645 are characterized by high bulk densities and low water contents, consistent with the coarse-grained texture, poor sorting, and terrigenous origin of the materials. The variation in physical properties with depth reflects lithologic changes: intervals of high density correspond to coarse sediments, and lower density intervals correspond to finer sediments. The site is somewhat unusual in that density decreases with depth in the first 370 mbsf. This trend is not completely understood but may reflect changes in lithology and differences in bulk density at the time of deposition. Most of the sediments display the expected interrelationships among physical properties. A well-developed inverse relationship between bulk density and water content and porosity exists, as well as a positive correlation between bulk density and both thermal conductivity and compressional wave velocity. Shear strength varies irregularly with depth and cannot be correlated with changes in the other physical properties. Sediment behavior changes near the Lithologic Unit I/II boundary. Below this level shear strengths are markedly higher and more variable.

DOWNHOLE LOGGING

Downhole logging at Site 645 had two primary purposes: (1) determination of continuous records of lithologic and mineralogic variations and (2) tying core depths to seismic reflectors through a synthetic seismogram based on sonic and density logs. The first purpose involved comparison of sedimentological and log data and was intended to be most useful in intervals of poor core recovery. The second purpose involved comparison of physical-properties and log data.

To achieve these goals, two or three logging runs were planned. The first run was with the LSS combination: sonic (LSS), gamma ray (GR), resistivity (SFL, ILM, and ILD), and caliper (MCD). The second run was to be with a new GST combination: gamma spectrometry (GST), neutron porosity (CNTG), and NGT. The GST, usually run alone, was to be substituted for the density log (LDT), normally run with the CNTG and NGT, because (1) the LDT is unreliable when hole conditions are poor and (2) the use of barite mud makes the LDT measurement of the photoelectric effect unreliable as a lithology indicator. The

third log run was to be a possible pass with the multichannel sonic (MCS) tool. Factors influencing a decision on its use were (1) the quality of the LSS, (2) the presence of bridges that could stop the light-weight MCS tool, and (3) quality of the GST and need for additional GST passes. All logs were to be run in open hole rather than through pipe. Thirty-six hours were allotted for logging.

Operations

Logging-related operations at Site 645 began at 1200 hr local time on 25 September 1985 with the first attempt to drop the bit and concluded 55.5 hr later at 1930 hr on 27 September 1985. Dropping the bit was much slower than anticipated. The bit stuck in a partly released position, necessitating pulling the drill string and reentering the hole; this procedure took 23.5 hr. The proximity of an iceberg caused two temporary suspensions of logging activities, consuming an additional 8.5 hr. Thus, despite the extension of "logging time" from 36 to 55.5 hr, only 23.5 hr were actually available for logging. During this time, four logging runs were made with the LSS-combination tool. Each logging run was stopped by a clay bridge, necessitating removal of the tool from the pipe and subsequent lowering of the drill string past the bridge. Logging with the GST combination and the MCS was cancelled because the former is a radioactive tool, for which risks of loss in a sticky hole should not be taken, and the latter is a light tool having little ability to penetrate bridges.

Measurements were made at 6-in. (0.152-m) intervals while logging down at about 1000 m/hr and logging up at about 700 m/hr for Runs 2 through 4. Run 1 logged down only. Including repeat runs and excluding down-going runs (except for Run 1), the following intervals were logged: 2197.5–2251.9, 2282.8–2365.4, 2311.6–2467.8, 2318.3–2369.2, 2368.0–2465.4, and 2347.0–2401.2 m below drill floor. Schlumberger software required recording data in feet below drill floor; conversion to meters was undertaken for subsequent display and analysis. A total of 239.4 m of section was logged. Excluding intervals for which the tool was either in or affected by the pipe, 217.5 m of usable open-hole logs were obtained, covering the intervals of 200.1–242.9 and 280.5–455.2 mbsf.

Interpretation of Lithology and Porosity

Lithologic interpretation is limited for Site 645 because of the cancellation of the GST-combination run. Because of the relatively high abundance of potassium feldspar at Site 645, observed variations in the gamma-ray log may have been caused by variations in quantity of either clay minerals or potassium feldspar. The overall correlation of gamma-ray logs with both resistivity and sonic logs is poor; this observation may suggest that either potassium feldspars are affecting the gamma-ray log significantly or that clay mineralogy changes with depth. However, two observations indicate that the dominant influence on the gamma-ray log is short-term variation in clay percentage. First, gamma-ray character does correlate with resistivity over short intervals. Second, almost all the intervals with highest gamma-ray values show caliper kicks to smaller diameter (Fig. 39). This strongly suggests that swelling of clays had occurred, even when the hole diameter had been enlarged <1.5 hr previously by drill-pipe passage. These constricted intervals form the bridges that often stopped the logging tool.

If one assumes that the gamma-ray log is responding primarily to clay content, then the gamma-ray log is consistent with core data in indicating that the logged intervals are predominantly composed of a mixture of quartz and clay minerals. Approximately even percentages of quartz and clay are most common; intervals of both 80%–100% clay minerals and 0%–20% clay minerals are much rarer.

Assuming that the intervals rich in clay minerals are finer grained than the intervals rich in quartz, the gamma-ray log can

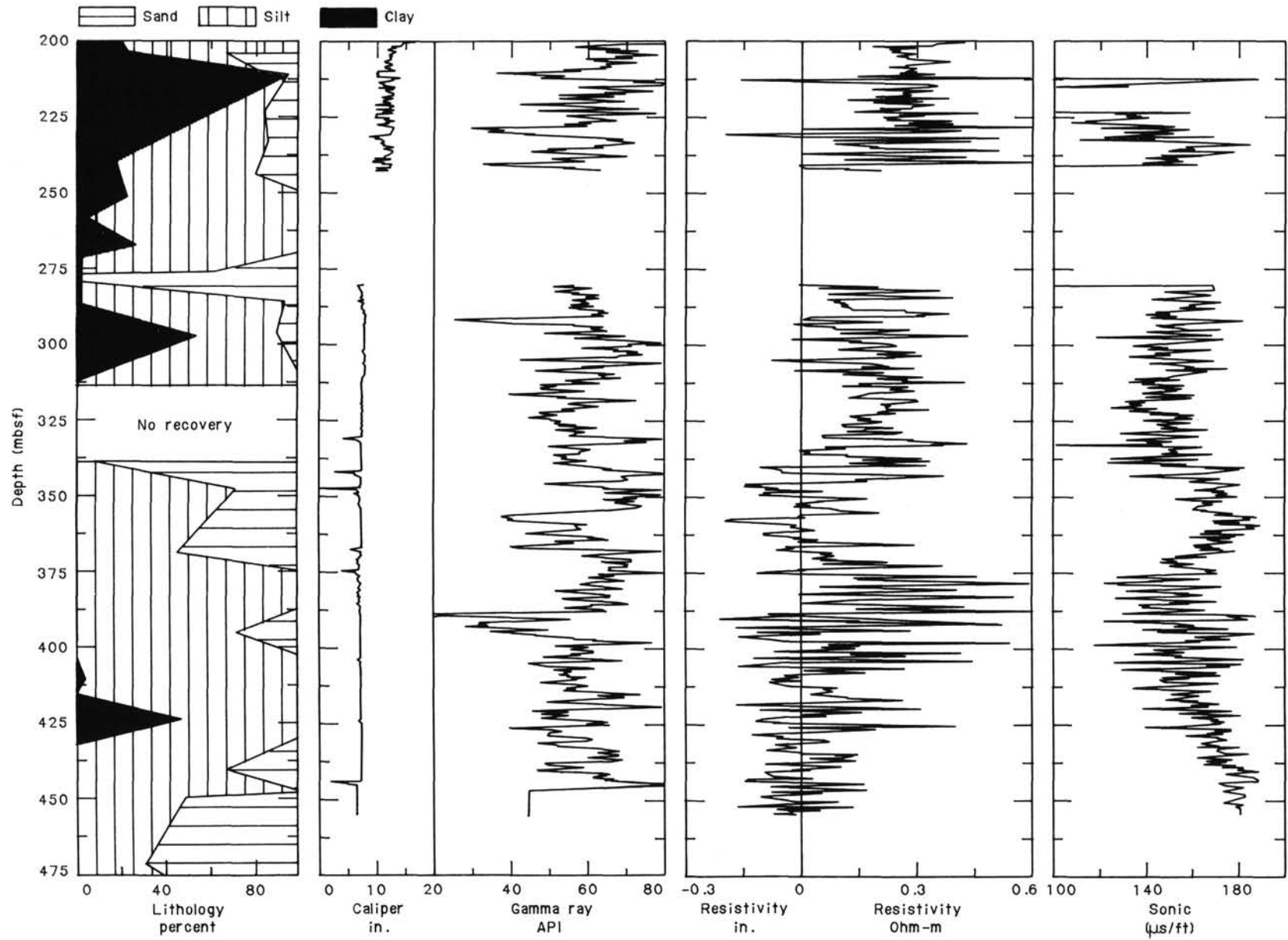


Figure 39. Plot of final logs as a function of depth below seafloor. For clarity, only one of the three resistivity logs is shown (SFL).

be interpreted in terms of sequences that fine upward or coarsen upward. For example, turbidites generally produce a distinctive saw-tooth gamma-ray log, which has a sharp gamma-ray decrease at the base of a bed and a gradual up-log increase in gamma-ray count as clay minerals become more common. Because the gamma ray responds to mineralogy rather than directly to grain size, quartz sands and silts can have a similar log response; the log responds primarily to the upward increase in clay minerals within either a turbidite bed or an overall upward-fining sequence. An upward-decreasing grain size should be apparent on resistivity logs, because quartz sands or silts are more porous than clay-rich parts of the interval logged. The vertical resolution of both gamma-ray and resistivity logs is about 0.5 m, precluding the detection of upward-fining or upward-coarsening sequences shorter than about 2 m. The technique works best for detection of multiple sequences thicker than 2 m.

No convincing evidence of repeated short upward-fining or upward-coarsening sequences is apparent in the gamma-ray or resistivity logs at Site 645. The possibility of thick turbidites in this interval cannot be excluded on the basis of either log alone. However, the combination of the two logs makes it unlikely that turbidite deposition is a major factor affecting porosity and clay mineral distribution in the logged interval. In the interval from 320 to 410 mbsf, the resistivity log may be indicating gradual changes in porosity with a wavelength of about 50–60 m. No simple correlation of these changes with the gamma ray is apparent, except that two thick “sands” (low gamma-ray response) are also high in porosity.

Virtually no core recovery was achieved for the interval from 300 to 340 mbsf. Log interpretation of this interval is particularly important because this interval brackets a lithologic change from Subunit IIIA to Unit II, associated with the onset of common ice-rafted dropstones.

The explanation for poor core recovery from 300 to 340 mbsf is not apparent from the sonic, resistivity, or gamma-ray logs. For 300–340 mbsf, all three log types yield generally similar responses to those in the higher-recovery interval of 280–300 mbsf. Unfortunately, the caliper log became saturated at 9-in. diameter below 280 mbsf, so it was unable to detect possible washouts associated with poorly consolidated sediments. However, the sonic, resistivity, and gamma-ray logs indicate that the interval from 300 to 340 mbsf exhibits no systematic difference in cementation, porosity, or clay content when compared with adjacent intervals. Thus, the poor core recovery probably cannot be attributed to the presence of thick unconsolidated sand or gravel beds. The possibility of a higher-than-average quantity of dropstones cannot be excluded.

The largest change observable in the logged interval occurs at 332–336 mbsf (Figs. 39 and 40). This change is most obvious as a substantial change in resistivity, from 1.0–1.5 ohm below 336 mbsf to 1.6–2.0 ohm above 336 mbsf. Velocities also decrease markedly below 332 mbsf, though some higher velocities are found deeper. A gamma-ray change to subtly higher clay mineral concentration above 336 mbsf is possible but not clearly delineated.

If the Unit II/Subunit IIIA boundary is a major lithologic change occurring somewhere between 300 and 340 mbsf, then the combination of log response changes at 332–336 mbsf, coupled with the lack of consistent changes at other depths, suggests that this boundary occurs at 332–336 mbsf. From resistivity log responses, this boundary may be either a sharp change at about 332–336 mbsf or a transitional zone from 332 to 346 mbsf. The resistivity and sonic log responses strongly suggest that the upper part of Subunit IIIA is significantly higher in porosity than the lower part of Unit II. However, physical-properties measurements of core porosities show a somewhat different pattern, with only a limited zone of substantially lower porosities and lit-

tle or no overall shift of the porosity base line. Significantly higher grain densities above the boundary are indicated by the physical-properties measurements (see “Physical Properties” section, this chapter).

One hypothesis that accounts for both physical properties and log measurements is that a substantial change in clay mineralogy occurs at the boundary. If clays beneath the boundary are higher in bound water than those above, then substantially lower resistivity, slightly lower velocity, and substantially lower grain density are expected even if porosity is unchanged. This hypothesis is readily testable through X-ray diffraction.

An alternative hypothesis focuses more on the anomalous porosity profile of the entire cored section. Physical-properties measurements indicate a normal compaction profile of decreasing porosity with greater depth below the Unit II/Subunit IIIA boundary. Above the boundary, however, porosity actually increases with greater depth. Porosity of the uppermost sediments is much lower than normal surface sediments. This behavior may be linked to ice rafting. Before major ice rafting, a normal compaction profile is expected. Onset of major dropstones at the Unit II/Subunit IIIA boundary may be accompanied by a significant decrease in the grain-size sorting of the sediments, glacial flour partly filling interstices of larger nonglacial grains. This decrease in sorting could account for the significant increases in resistivity, velocity, and density above the boundary. However, it does not explain why the change in core porosities is less than that implied by resistivities. Above the boundary, an increase in glacial component with time would cause a gradual decrease in porosities, because sorting becomes poorer.

Sediment Velocities

The unedited sonic log is highly variable in quality. Most intervals exhibit reasonable agreement between short- and long-spaced sonic logs (DT and DTL) and good correlation with resistivity. These intervals are probably reliable, and fluctuations in velocity are primarily attributable to changes in porosity. Other intervals show wildly fluctuating values, some having velocities slower than water and rarely even having negative velocities (Fig. 41). Such intervals are clearly plagued by noise and cycle skipping. Because transit times from shot to receiver are based on first breaks of the waveform above a threshold, attenuation or noise can cause different parts of the wavetrain to exceed the threshold on different shots or receivers. Examination of the waveform plots (Fig. 42) confirms this. At the slow velocities encountered, shear arrivals are not distinguished; instead, the low-amplitude *P* arrival is followed by the large-amplitude normal mode of *P*. Some entire *P* arrivals are below the threshold, and tripping is on the normal mode.

The sonic log can be substantially improved by taking advantage of the redundancy of measurements inherent in the Schlumberger LSS log. At any depth, four measurements of transit time are available: one 8-ft, two 10-ft, and one 12-ft spacing (Fig. 43A). Using two sets of these four measurements and proper depth justification, four measurements of transit time over a 2-ft interval centered on the depth of interest can be determined, each on the basis of the difference in transit time between a pair of transducers or receivers (Fig. 43B).

A crossplot of the 10-ft-spaced pairs illustrates the problem (Fig. 44). Most values fall on a line sloping 45°, and both transit times are > 1400 μ s, indicating potentially good measurements and tripping on the same peaks. A few points fall far to the left or far below the main grouping, which indicates that one of the two shots is unreliably tripping on noise prematurely. The lower of these two measurements should be excluded from transit-time calculation.

A second exclusion criterion attempts to avoid cycle skipping between the two shots used to determine transit time over a 2-ft

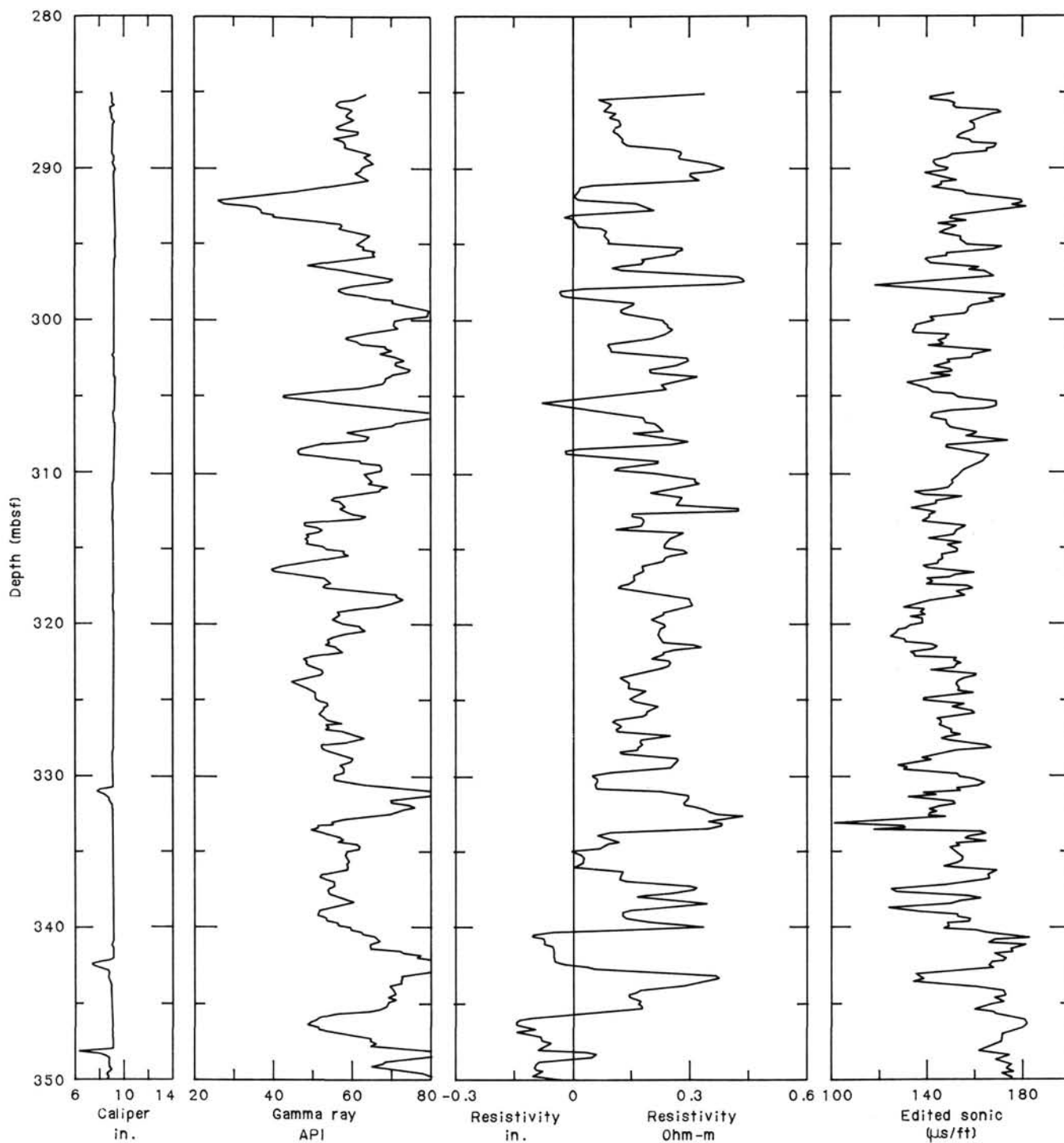


Figure 40. Plot of logs bracketing the interval in which the Unit II/Subunit IIIA boundary is thought to occur.

interval. Slowness (inverse of velocity) of $< 50 \mu\text{s}$ per ft of $> 190 \mu\text{s}$ per ft is physically impossible (except for gas sands) and is therefore excluded. This criterion probably excludes most but not all data having cycle skips.

A short computer program was written to recalculate the sonic log from raw Schlumberger transit times, using the aforementioned two exclusion criteria to reduce the number of redundant measurements applied at some depths. Comparison of the resulting sonic log (DLTE) with the original logs (DT and DTL) shows that the algorithm was highly successful (Fig. 41).

In two intervals, none of the four measurements passed the exclusion criterion, so a value of zero is displayed (Fig. 41). In addition, the constant-velocity interval shown at the bottom of the logging run is an artifact, caused by the sonic log being near the top of the logging tool and, therefore, beginning to record at a shallower depth than the resistivity logs. For these intervals, the sonic log was edited, using the resistivity logs as a guideline. The empirical basis of such editing is the observation that the sonic log is strongly correlated with the logarithm of resistivity. This correlation is evident either on a log/depth plot (Figs. 39

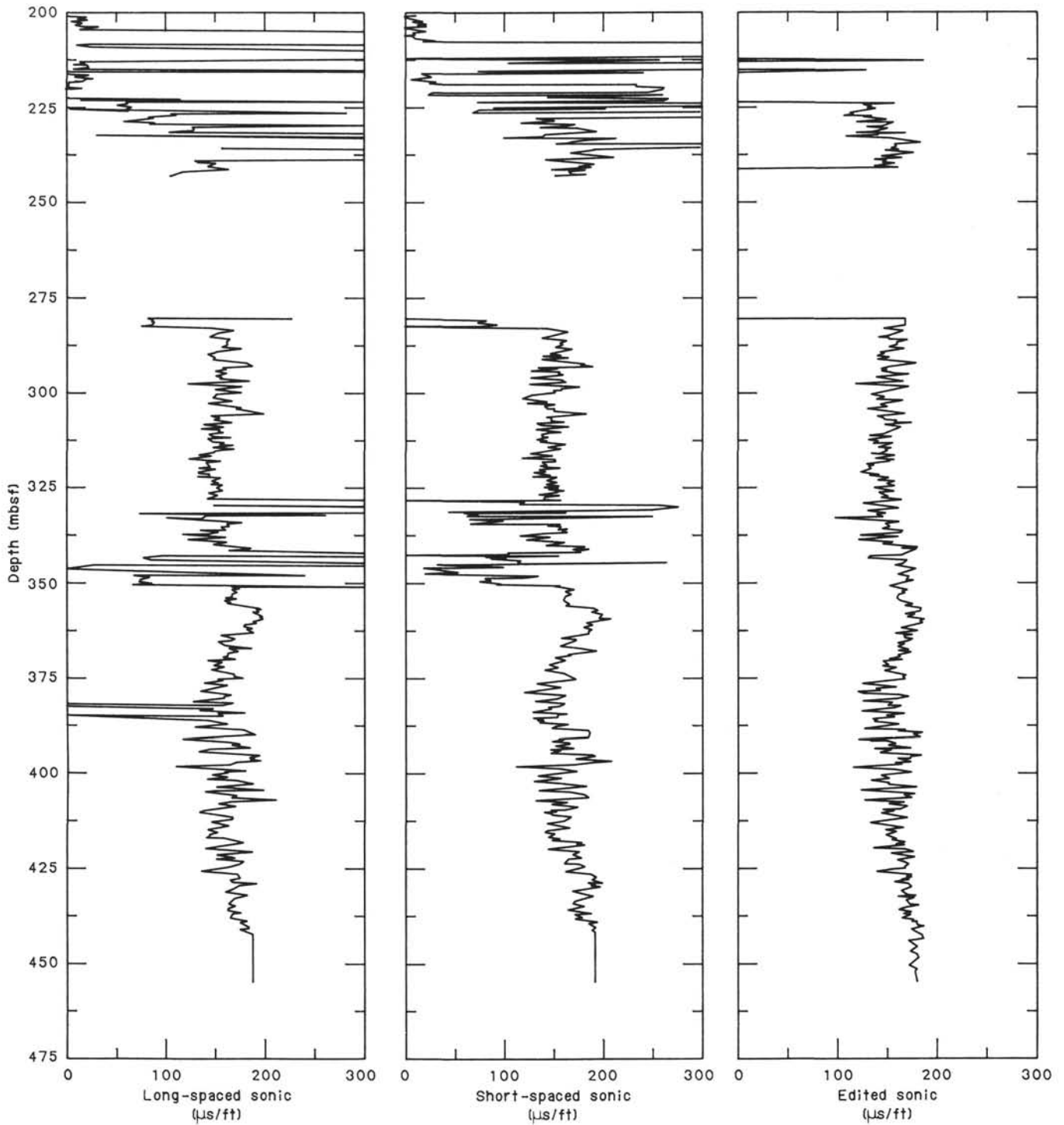


Figure 41. Comparison of Schlumberger short (DT) and long (DTL) spaced sonic logs with the final edited sonic log (DLTE).

and 40) or on a crossplot (Fig. 45). The physical basis of such editing is that sonic slowness (dt) is related to resistivity (R_t) through the effect of porosity on both logs. Combining the Wyllie time-average equation and the Archie water-saturation equation and assuming that water saturation is 1 (i.e., no hydrocarbons) and that the Archie cementation factor m is 2, we find that

$$dt = dt_{ma} + (dt_f - dt_{ma}) \times \text{sqrt}[(a \times R_w)/R_t],$$

where dt_{ma} is matrix slowness, dt_f is water slowness, a is an Archie coefficient (≈ 0.81), and R_w is the resistivity of the formation water (which is unknown at Site 645). All four of these variables are probably approximately constant at Site 645; thus

$$dt = K1 + K2 \times \text{sqrt}(1/R_t),$$

where $K1$ and $K2$ are empirically determined constants for the interval analyzed.

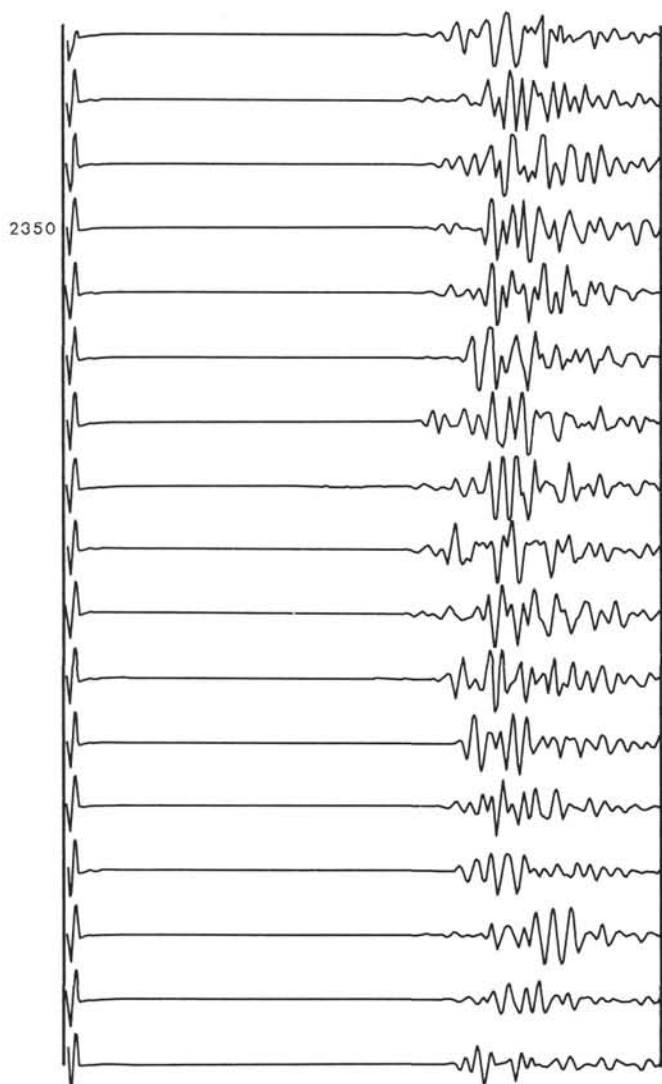


Figure 42. Example of sonic waveforms recorded at adjacent depths. Note the substantial amplitude changes occurring in the earliest (left-most) arrivals; these frustrate attempts to determine *P*-wave transit time from a threshold criterion. The large changes in arrival time of the first trough on different traces probably do not reflect real velocity changes.

The edited sonic log is displayed in units of km/s in Figure 46. Velocities are generally about 1.8–2.2 km/s and average 2.0 km/s over the entire interval. This velocity is broadly consistent with stacking velocities of about 1.8–2.1 km/s from a Petro-Canada seismic line (BE74-51) across the site (see “Background and Objectives” and “Seismic Stratigraphy” sections, this chapter). However, comparison to stacking velocities is hazardous because stacking velocities are averaged over a much longer depth interval, which includes shallower sediments.

No physical-properties measurements of velocity are available from the logged interval because of inadequate consolidation of the sediments and problems with the velocimeter. Core-velocity measurements start about 50 m below the logged interval, in a part of Subunit IIIA that has a generally similar porosity, density, and lithology to the lower part of the logged interval (see “Physical Properties” section, this chapter). These measured velocities of 1.5–1.7 km/s are significantly lower than expected velocities based on the sonic log, measured densities, and stacking velocities. In view of the moderate porosities and compaction exhibited by the sediments, the 1.5–1.7 km/s veloc-

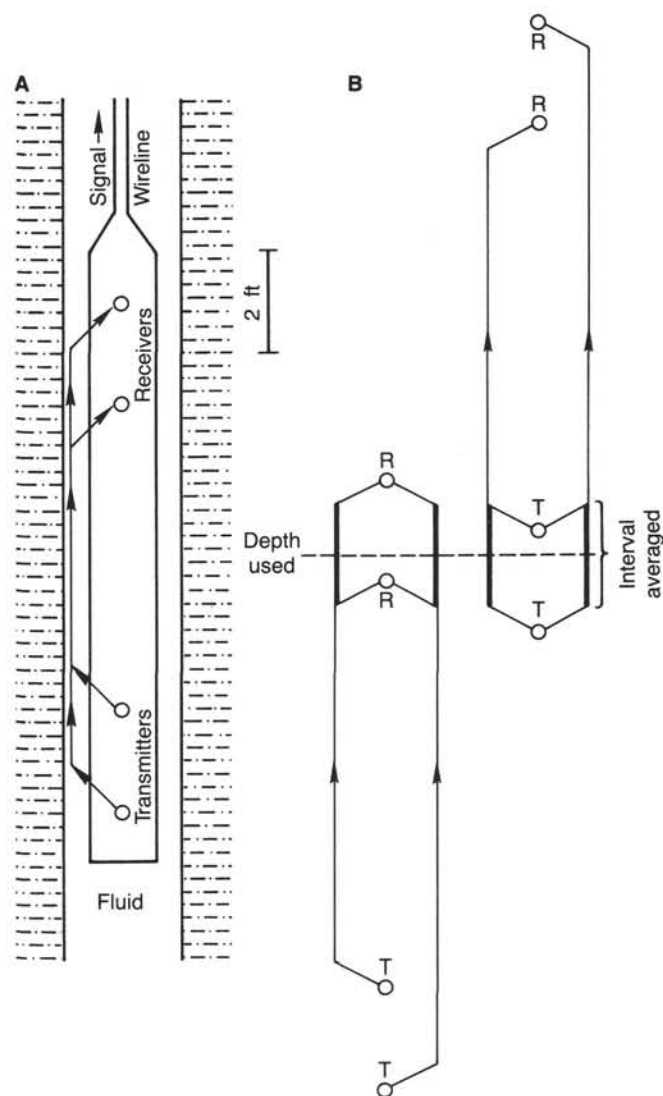


Figure 43. Illustration of the source-receiver geometry of a Schlumberger LSS sonic tool, showing the four paths measured (A) and the 2-ft-interval transit times available at each depth (B).

ities of core samples must be unreliable. A likely explanation is that the cores swelled slightly during the short time between arrival on deck and velocity measurement. Such swelling is expected because of pressure release. Even a small amount of swelling in the presence of air sucks air into the pores. Industry research on the effects of gas (or air) on sediment velocities indicates that only 2% pore filling by air is sufficient to cause a major decrease in velocity. This is both the cause of seismic bright spots as direct hydrocarbon indicators and the greatest weakness of the bright spot technique (because 2% gas is not an economic resource).

Synthetic Seismogram

The edited sonic log for the interval 280.5–457.7 mbsf was used to construct a synthetic seismogram for Site 645. The upper logged interval of 200–243 mbsf was not used in this initial synthetic seismogram for two reasons. First, only the part of this upper interval between 222 and 240 mbsf yielded a reliable sonic log. Thus velocities for half of the upper interval would have needed to have been based on a pseudosonic log. Second, no logs of any kind were obtained between 243 and 280.5 mbsf.

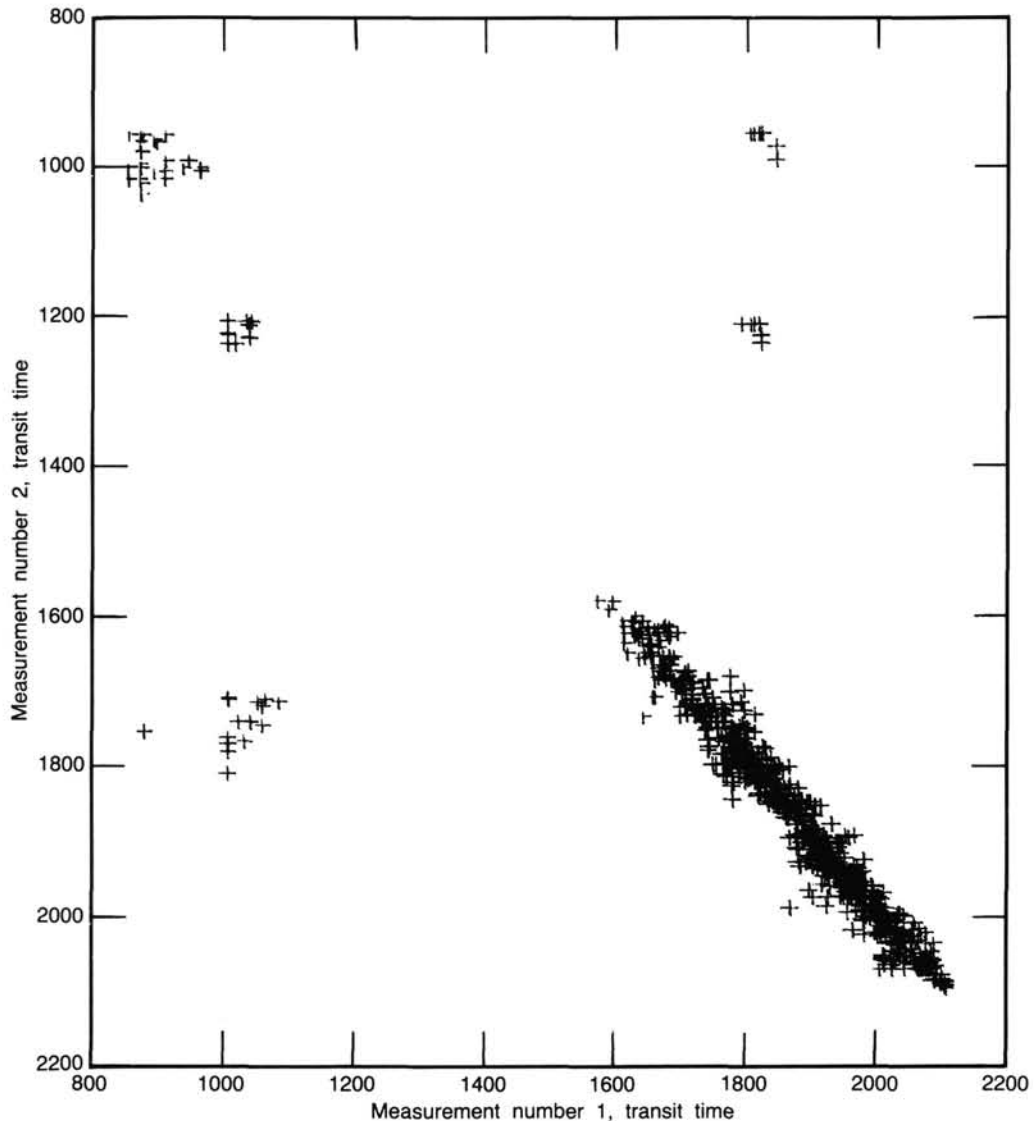


Figure 44. Crossplot of the two measurements of 10-ft transit time available at each depth. The heavy clustering of about 800 points at the upper right may be reliable. All other points are unreliable in one or both of the 10-ft transit times.

No density log was available. A pseudodensity log was constructed from the resistivity log by simply taking the logarithm of resistivity and rescaling the log to a range of about 1.8–2.2 (Fig. 46). The selected density range of 1.8–2.2 was based on measured densities of core samples. The physical basis of pseudodensity logs is similar to that for the velocity/resistivity relation of the previous section. Experience has shown that inclusion of a density log rarely affects a synthetic seismogram significantly because (1) owing to their larger percentage change, velocity changes usually affect impedance more than density changes and (2) density and velocity are usually strongly correlated. The latter is particularly true for Site 645 pseudodensity because velocity is well correlated with resistivity at this site (Fig. 44).

The algorithm used for calculating the synthetic seismogram is a simple one-dimensional (1-D) convolution. Log data were used rather than a multilayer model. Internal multiples were included, but seafloor multiples were not included. The water-path seafloor multiple (5.5 s) is much deeper than the relevant seismic interval of about 3.0–3.5 s. To include internal seafloor

multiples would be desirable, but lack of logs between the seafloor and 243 mbsf precludes this. Experience has shown that a 1-D convolutional synthetic seismogram including internal multiples is nearly always virtually indistinguishable from a 1-D synthetic seismogram based on a more complete wave equation.

The wavelet used for the synthetic seismogram is a 25-Hz zero-phase Ricker wavelet. Examination of the multichannel seismic section (Fig. 47) indicates that wavelet control used by Petro-Canada in their deconvolution must have been very good. The seafloor seismic signature is well approximated by a zero-phase 25-Hz Ricker wavelet, and deeper reflectors lack consistent signatures such as double peaks indicative of a more complex residual wavelet.

Comparison of the synthetic seismogram to the seismic signature is hampered by two uncertainties: shotpoint location of the well and traveltime from the seafloor to 280 mbsf. The observed water depth is greater than the water depth at the nominal shotpoint location of Site 645 along the multichannel line; thus, the actual appropriate shotpoint for comparison is probably east of the nominal location. The round-trip traveltime from

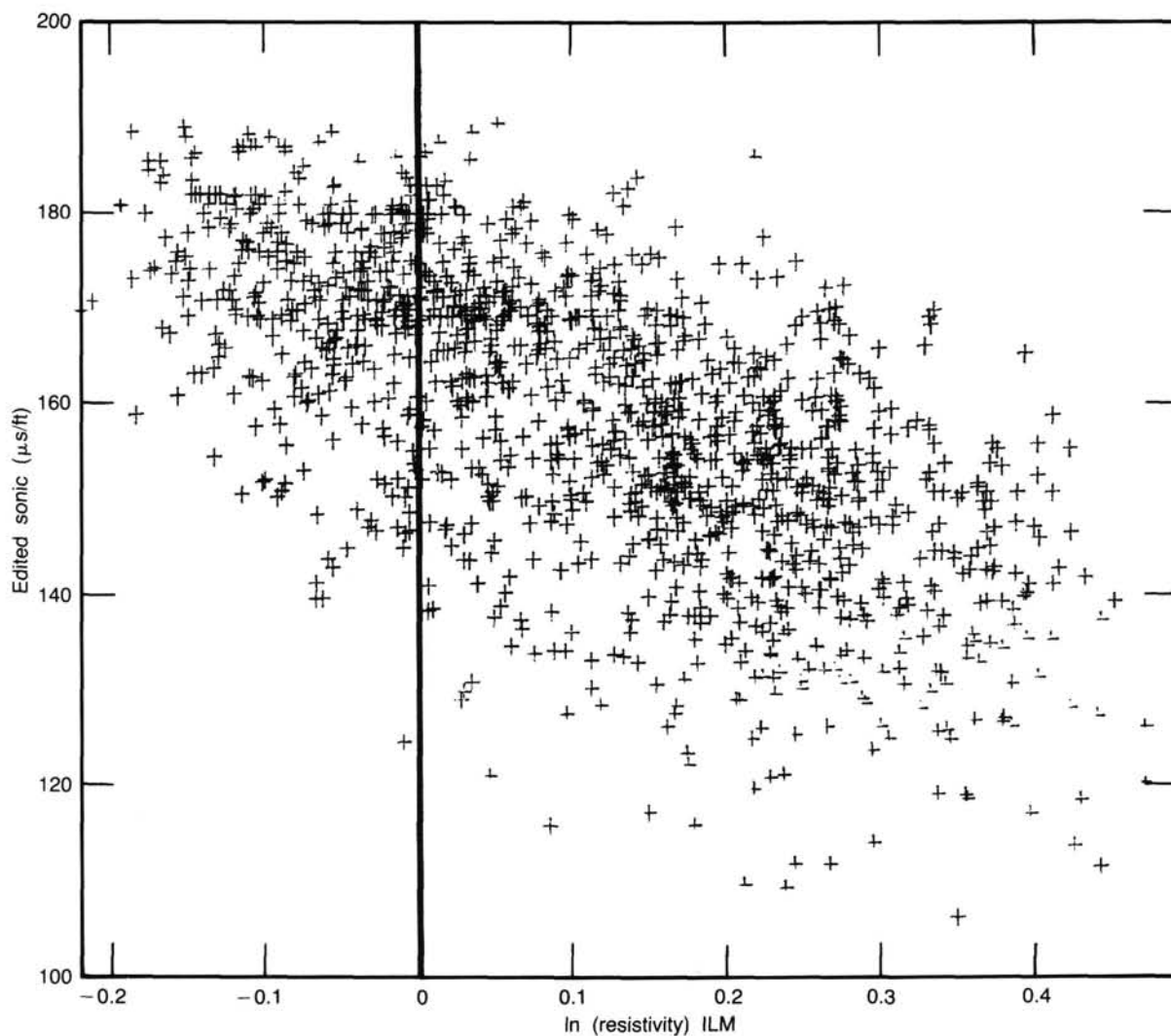


Figure 45. Crossplot of the logarithm of resistivity (ILM) versus edited sonic log (DLTE). The linear relationship between the two logs on this plot indicates that (1) sonic variations are largely caused by porosity variations, and (2) resistivity can be used to estimate velocity in intervals having a poor sonic log.

the seafloor to 280 mbsf is probably about 0.3 ± 0.1 s, according to stacking velocities. Thus the starting time for the synthetic seismogram should be about 3.05 ± 0.10 s.

Comparison of the synthetic seismogram to the seismic signature (Fig. 47) yields a good character match. The largest positive peak on the synthetic seismogram, at 370 mbsf, is clearly reflector R1. Plausible correlation of the lesser peaks is also possible; the best match occurs for the interval 3.13–3.33 s. Detailed correlation of the smaller peaks is hazardous because all reflectors undergo significant character changes over lateral distances smaller than the uncertainty in site location. Even the R1 reflector changes markedly to the east of the nominal site location, taking on a large peak/large trough/small peak character similar to that of the synthetic seismogram.

The R1 reflector was identified as a major sequence boundary (see "Seismic Stratigraphy" section, this chapter). Even with the good match of synthetic seismogram to seismic signature at Site 645, two factors complicate the identification of this sequence boundary in cores and logs. First, the resolution of seismic data makes it difficult to distinguish whether the sequence boundary is the major peak (corresponding to 370-mbsf depth) or the overlying trough (corresponding to 340-mbsf depth). The

370-mbsf pick suggests that the unconformity is at the base of a sandy, porous unit that is evident on both logs (Fig. 39) and on plots of physical properties at 355–370 mbsf. In contrast, the 340-mbsf pick suggests that the unconformity is the Unit II/Subunit IIIA boundary, which was identified on logs as either a sharp change at 332–336 mbsf or a more gradual change from 332 to 346 mbsf. Secondly, both the peak and trough are composite reflectors, resulting from impedance changes over broad intervals. For example, the peak is a composite effect of the upward decrease in impedance from 380 to 360 mbsf and the side lobes of the upward increases in impedance at 400–380 and 360–332 mbsf.

SEISMIC STRATIGRAPHY

Site 645 is on multichannel line 74-51 at shotpoint 511 (Fig. 2, "Background and Objectives" section, this chapter; Fig. 53, "Seismic Unit 4," this section). Examination of this and several other lines that lie in this region shows the presence of many prominent and widespread seismic reflectors. The reflector sequence is divided into four seismic units on the basis of their uniformity and seismic characteristics. Here we discuss the im-

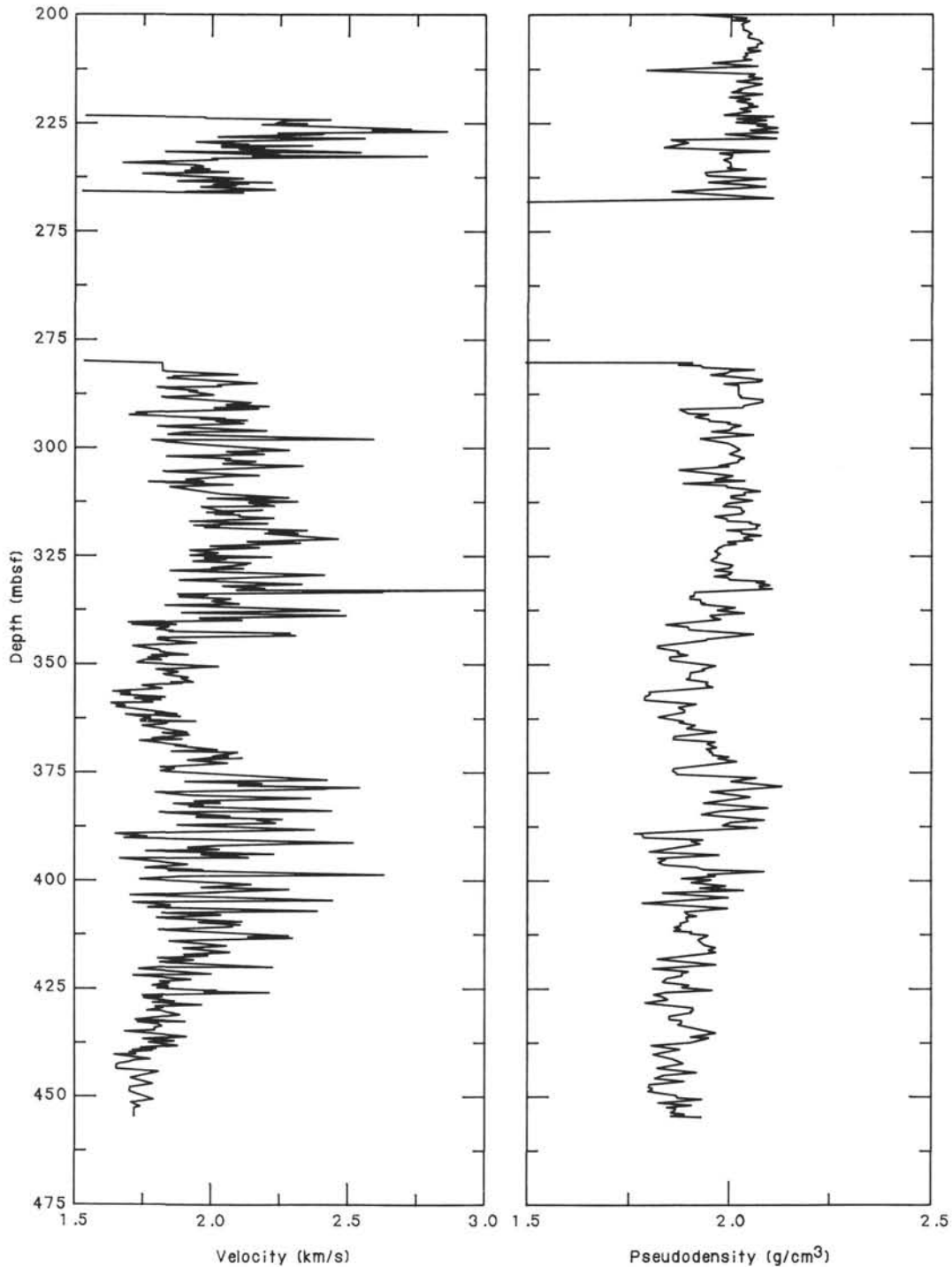


Figure 46. Velocity log (transformed sonic) and pseudodensity log (based on resistivity). The interval deeper than 278 mbsf was used for calculation of the synthetic seismogram of Figure 47.

plications of drilling at Site 645 for seismic stratigraphy near the site and for the southern Baffin Bay region as a whole. We identified major and some minor reflectors and gave them numerical designations (Figs. 48 and 49 and Table 11). We measured the depth in seconds below the seafloor to each reflector at the site location and calculated a sub-bottom depth for each one using interval velocities from the stacked and depth-migrated version of the multichannel line 74-51 that crosses the site (Table 11). The correlation of reflector depths with changes in lithology and physical properties (density, porosity, and water con-

tent) is surprisingly good (Fig. 56, "Summary and Conclusions" section, this chapter). This suggests that the interval velocities used to calculate the depths are reasonable approximations. Such a conclusion is important because the measured velocities on board ship are apparently at least 20% too low (see "Physical Properties" section, this chapter) and the attempt to obtain a downhole sonic log was largely unsuccessful. However, within the interval where logging was successful, a reasonable correlation exists between the interval velocities and those obtained from sonic logging (see "Downhole Logging" section, this chapter).

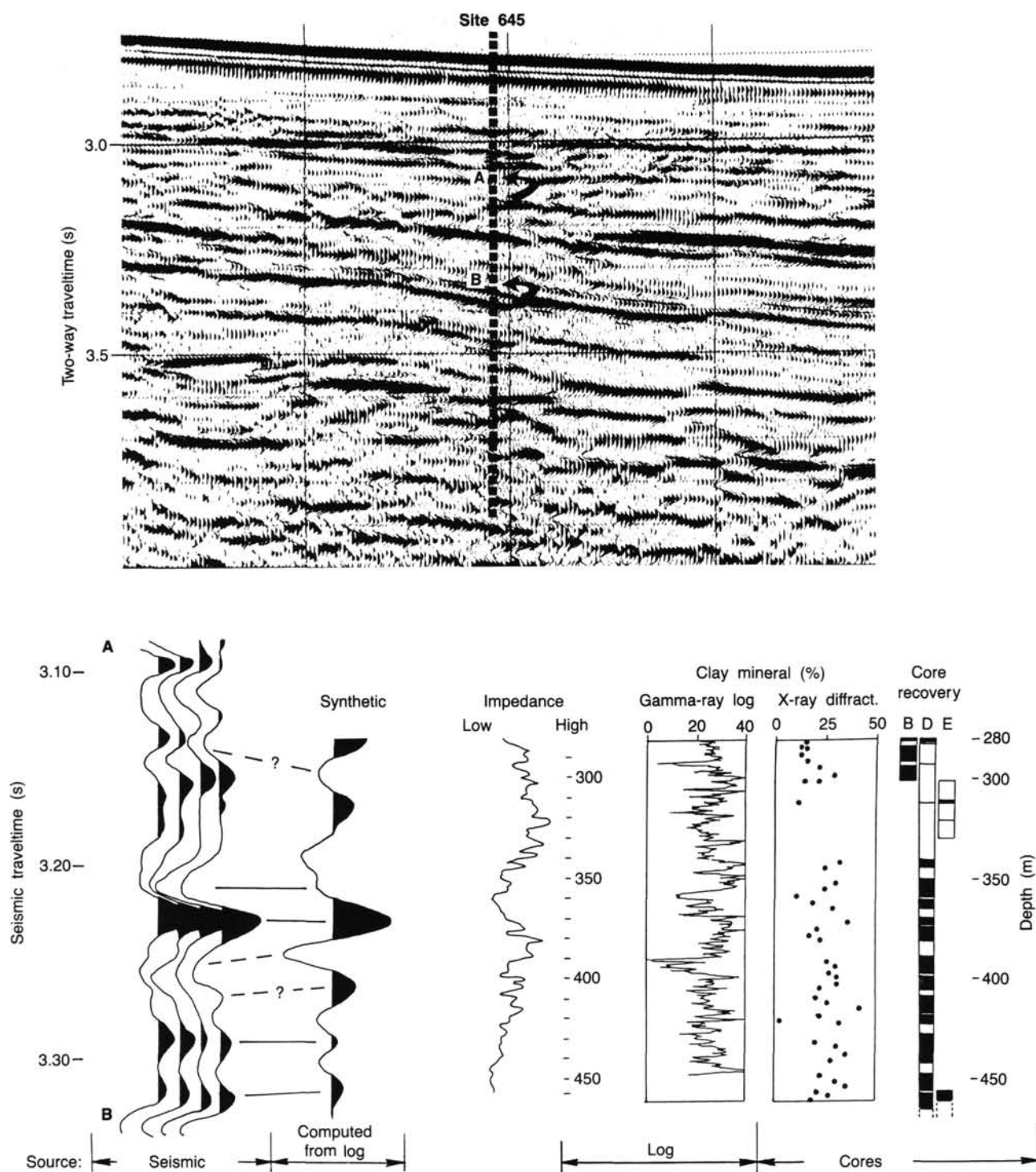


Figure 47. Top: part of Petro-Canada stacked multichannel seismic line crossing Site 645. The interval of A–B, shown in expanded scale at lower left, is best matched with the synthetic seismogram. Bottom: seismic traces correlate well with a synthetic seismogram based on the impedance log for the interval of 280–460 mbsf. The major peak correlated with the R1 seismic reflector at 3.22 s results primarily from the impedance increase from 360 to 380 m. This impedance change is evident on the gamma-ray log as a transition from low to high clay mineral percentage. Note the greater resolution of clay mineral variations in the gamma-ray log than in X-ray diffraction measurement.

Seismic Unit 1

Seismic unit 1 comprises three subunits, only two of which are represented at Site 645 (Fig. 53). The entire unit is 0.4 s thick near Site 645 from the seafloor to the top of what has been defined as reflector R1. The base of seismic unit 1 at Site 645 occurs at 388 mbsf (calculated using an interval velocity of 1850

m/s, Fig. 48). On the other hand, calculation of synthetic seismographs using sonic and resistivity logs suggests that such a discontinuity lies near 370 mbsf (Fig. 47). The latter figure is probably closer to being correct. Seismic unit 1 corresponds to Lithologic Units I and II except that the lower boundary of Lithologic Unit II occurs about 50 m above the depth calculated to the reflector R1 (Fig. 49).

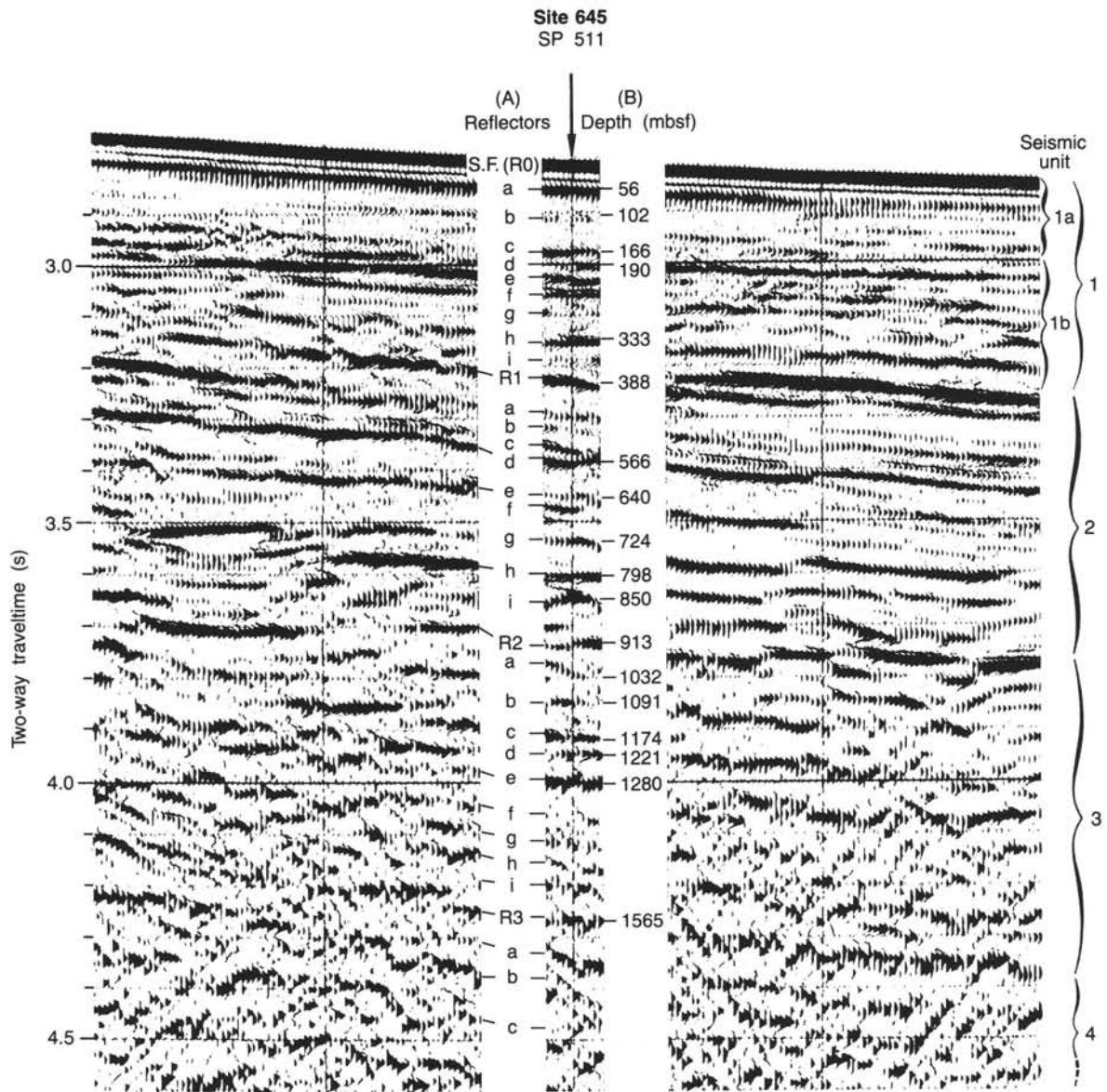


Figure 48. Enlargement of part of multichannel line 74-51 showing reflector terminology used in this report and depths to each reflector calculated using the interval velocities from the stacked and depth-migrated multichannel data. Shown also are the seismic units.

We subdivided seismic unit 1 into three subunits on the basis of internal reflection characteristics. Seismic unit 1A extends from the seafloor to a depth of 0.18 s at Site 645 (0-166 mbsf) and is seismically transparent to slightly reflective in the multichannel profile but exhibits numerous horizontal reflections in the single channel lines. These characteristics are maintained over much of the region, and there is little variation in thickness of seismic unit 1A. Seismic unit 1A corresponds to Lithologic Unit I, which consists of rhythmically interbedded calcareous muddy sand and silty mud in the uppermost 72 mbsf (Lithologic Subunit IA) and interbedded calcareous silty clay and silty mud from 72 to 168 mbsf (Subunit IB). Dropstones and other sedimentary characteristics indicate a primarily ice-rafted origin for the unit. The transparent nature of seismic unit 1A and its rather uniform drape over topography in the region agrees with the evidence from the cores that these sediments were deposited mainly by ice rafting. On the eastern side of the basin, seismic unit 1A thickens to >0.4 s, where multiple, fairly high-ampli-

tude reflectors occur and appear to interfinger with or fade into the transparent unit toward the west (Fig. 52, "Seismic Unit 2," this section). We think that these reflectors represent deposits of multiple episodes of sediment redeposition from the edge of the West Greenland Shelf. The age of Lithologic Unit I is early Pleistocene to Holocene.

Seismic unit 1B occurs at Site 645 from 0.18 to 0.42 s sub-bottom (Figs. 48 and 53, "Seismic Unit 4," this section). We calculate a top of 167 mbsf and a base of about 388 mbsf at the site. The internal reflection characteristics are chaotic, having predominant multiple diffractions. Seismic unit 1B pinches out to the west on the flanks of the pronounced basement high and terminates against or passes into an interval of more pronounced horizontal reflectors to the east of the site (Fig. 53). Seismic unit 1B, reaching about 0.4 s (360 m) thick, is thickest toward the deepest point in the basin. In our cores from Site 645, seismic unit 1B corresponds closely to Lithologic Unit II, which extends from 168.1 to 335 mbsf. These sediments are pri-

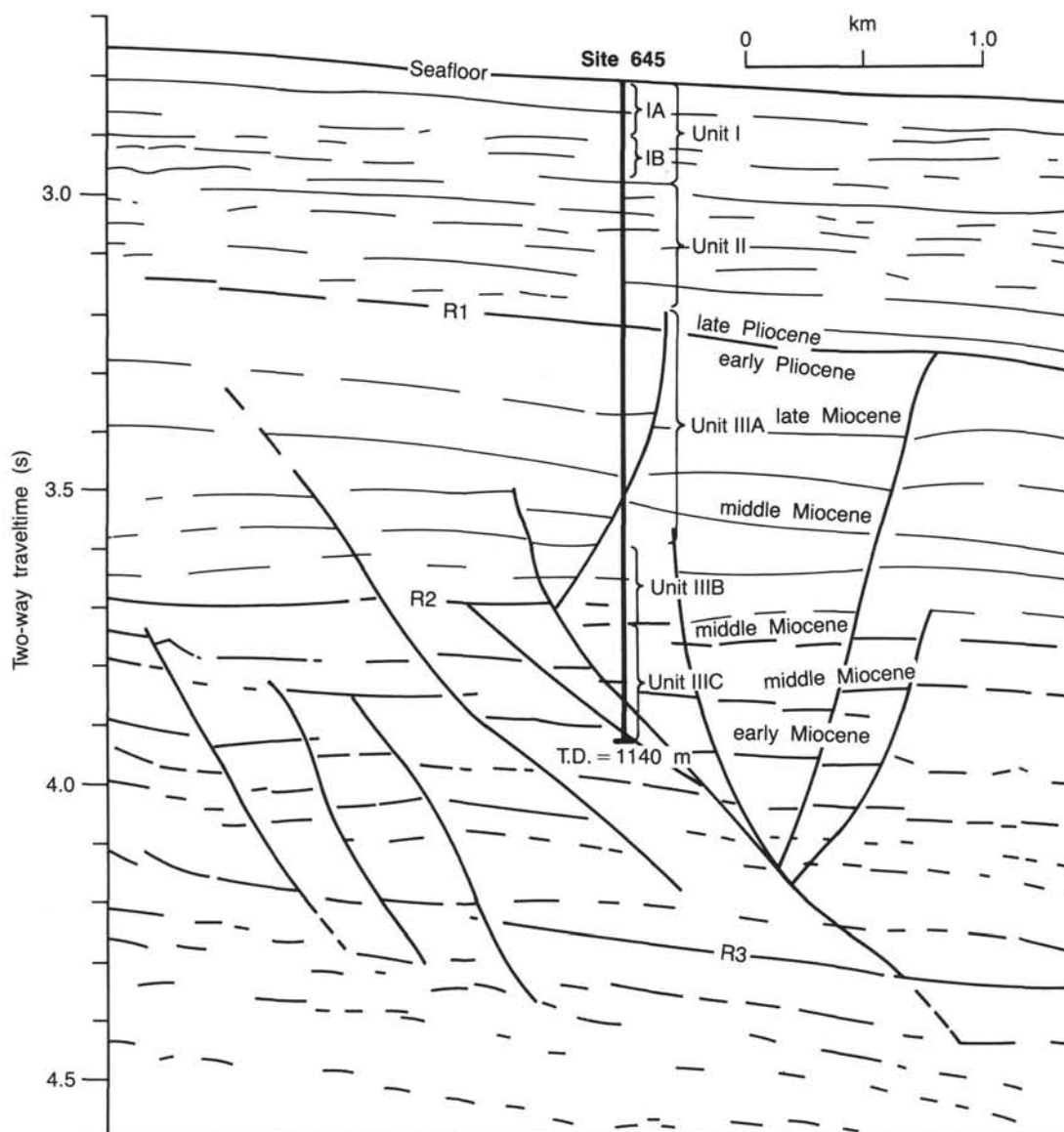


Figure 49. Interpretation of the seismic line shown in Figure 48 indicating the major reflectors, lithologic unit correlations to seismic packages, and ages based on preliminary magnetobiostratigraphic results from Site 645.

marily interbedded, noncalcareous silty mud, clayey silt, and silty clay; dropstones are distributed throughout. The chaotic nature of the internal reflections within subunit 1B is perhaps caused by one or more layers of very coarse ice-rafted debris. A 5-m-thick, fine-grained sand occurs at about 275 mbsf (Fig. 56, "Summary and Conclusions" section, this chapter), closely corresponding to reflector R0g (Fig. 48). The base of Lithologic Unit II probably corresponds to reflector R0h, for which we calculated a depth of 333 mbsf. This reflector may represent the top or bottom of a thick sequence of gravelly mud that we failed to recover in three separate attempts to core the interval.

Geophysical logs give no indication that an interval of unconsolidated sand exists at 333 mbsf. In fact, the interval is characterized by higher density similar to that of ice-rafted gravelly mud intervals higher in the hole. Lithologic Unit II is primarily composed of ice-rafted material and perhaps some finer-grained material derived from the east by dilute-suspension turbidity currents. Relatively strong, deep currents were present during deposition of seismic unit 1, as illustrated by the depositional features upslope from Site 645 in about 900–1000 m of

water (Fig. 50). These upslope, migrating large dunelike features are typical of current-deposited depositional ridges associated with deep contour currents.

Seismic unit 1C is not represented at Site 645 in the seismic records. If it is present, it is only as a thin horizon above R1, and it is essentially absent from the region west of the site. This subunit thickens substantially toward the West Greenland Margin, where it is as much as 1 s thick (perhaps 900 m). A number of weak to strong parallel reflectors characterize the subunit. Most of these reflectors terminate against R1 progressively westward. Perhaps a bit of unit 1C sediment was recovered in Site 645 at the top of what has been defined as Lithologic Subunit IIIA. As much as 50 m of muddy sand and silt occurs in the interval between 330 and 388 mbsf in Site 645 (Fig. 56), primarily above what we have picked as the R1 reflector. These interbedded muddy sands and silts may represent the progradation of sediment derived from West Greenland over the R1 surface.

The age of seismic unit 1 is late Pliocene through Pleistocene. The parallel reflectors of seismic unit 2 appear to extend across the basin, and if the upper surface (R1) can be inter-

Table 11. Depth to seismic reflectors and pick of various reflectors.

(A) Depth to seismic reflectors				
R1	-----	0.42 s bsf		
	-----	387.5 mbsf		
		velocity = 1850 m/s		
R2	-----	0.92 s bsf		
	-----	0.50-s interval		
	-----	912.5 mbsf		
		interval = 525 m		
		velocity = 2100 m/s		
R3	-----	1.47 s bsf		
	-----	0.55-s interval		
	-----	1562.5 mbsf		
		interval = 650 m		
		velocity = 2370 m/s		
		Average velocity = 1562.5/0.735		
		= 2130 m/s		
(B) Pick of various reflectors, as shown in Fig. 48				
No.	Depth (s)	Depth (s bsf)	Depth (m)	Depth (mbsf)
Unit 1				
R0 (Seafloor)	From R0		From R0	
a	0.06	0.06	55.5	55.5
b	0.11	0.11	101.8	101.8
c	0.18	0.18	166.5	166.5
d	0.205	0.205	190	190
e	0.24	0.24	222	222
f	0.26	0.26	240	240
g	0.30	0.30	278	278
h	0.36	0.36	333	333
i	0.40	0.40	370	370
R1	0.42	0.42	388	388
Unit 2				
	From R1		From R1	
a	0.08	0.5	84	472
b	0.105	0.525	110	498
c	0.150	0.57	158	546
d	0.170	0.59	178	566
e	0.240	0.66	252	640
f	0.26	0.68	273	661
g	0.32	0.74	336	724
h	0.39	0.81	410	798
i	0.44	0.86	462	850
R2	0.50	0.92	525	913
Unit 3				
	From R2		From R2	
a	0.10	1.02	119	1032
b	0.15	1.07	178	1091
c	0.22	1.14	261	1174
d	0.26	1.18	308	1221
e	0.31	1.23	367	1280
f	0.38	1.30	450	1363
g	0.43	1.35	510	1423
h	0.475	1.395	563	1476
i	0.515	1.435	610	1523
R3	0.550	1.47	652	1565

preted as a time-synchronous reflector, the disconformable lower part of unit 1 must be time transgressive. Such an interpretation suggests a significant increase in time represented by a hiatus toward the top of seismic unit 2 and the base of seismic unit 1 toward the west.

Near the center of the basin, some erosion of the upper part of seismic unit 2 appears to have occurred under the lenticular zones of subunit 1C (Fig. 51). These lenticular reflector packages can be interpreted as either channel deposits or small, bottom-current-induced depositional features. Relatively strong currents may have caused erosion of the seafloor during the early

time of deposition of seismic unit 1C (early to late Pliocene) before sediment supply increased as a result of the large sediment wedge propagating from the West Greenland Margin. Physical-properties data (Fig. 37) show a pronounced change in character at the point that we have chosen for the R1 reflector, where density becomes much less variable, steadily but not steeply increasing, and porosity and water content correspondingly decrease. In addition to recording a lithologic change, the physical-properties data may suggest some removal of original overburden by erosion.

Seismic Unit 2

Seismic unit 2 comprises many flat-lying reflectors below R1 that onlap reflector R2 at the top of the underlying seismic unit 3. Examination of multichannel line 74-51 and other seismic lines across Baffin Bay shows that seismic unit 2 is relatively constant in thickness except in places where the top of the unit eroded and where underlying reflectors crop out at the R-1 surface (Figs. 51 and 52). At Site 645 and to the west of the basement high, which lies landward of the site, seismic unit 2 thickens to perhaps 0.6 s (>600 m). The unit at the site is about 0.5 s (525 m) thick (388–913 mbsf) but has a maximum thickness of about 0.65 s (790 m) to the east. The base of this unit is a prominent unconformity, which is marked by the strong reflector (R2) at the top of seismic unit 3 at 913 mbsf at Site 645. Seismic unit 2 corresponds to Lithostratigraphic Subunits IIIA and IIIB. Our pick for the depth of reflector R2 corresponds closely to the lower boundary of Lithostratigraphic Subunit IIIB.

The strata of Subunits IIIA and IIIB are predominantly muddy sandstones and siltstones with interbedded silty and sandy mudstone. Subunit IIIA contains some graded sandstone beds, but most of both lithostratigraphic units are bioturbated to homogeneous or somewhat laminated. Variations in the proportions of sandstone and siltstone beds occur downcore, apparently giving rise to impedance contrasts that cause several strong to weak, continuous to discontinuous reflectors within seismic unit 2. The depth of the major reflectors given in Table 11 corresponds fairly well to important changes in lithology as shown in Figure 56.

In contrast to seismic unit 1, seismic unit 2 does not seem to thicken toward the east (West Greenland), suggesting that the strong progradation and high sediment supply that characterized unit 1 deposition were not present as seismic unit 2 was deposited during the middle Miocene through early Pliocene. The uniformity in thickness of this unit, its onlap onto reflector R2 to the west, and the sedimentary textures and structures in Lithologic Subunits IIIA and IIIB suggest that deposition of this unit was largely controlled by bottom currents. In the western part of the basin, deposition was profoundly affected by bottom currents, as indicated by the presence of large migrating depositional ridges (Fig. 50). However, some evidence of sediment re-deposition by turbidity currents exists at Site 645 in Lithologic Subunits IIIA and IIIB, although the source is unknown at present. In addition, some of the coarse-sand-size to granular particles and isolated pebbles may indicate an ice-rafted source, but currently we have no firm indication of this possibility.

Seismic Unit 3

Seismic unit 3, comprising continuous to discontinuous parallel reflectors, is bounded at the top by a pronounced reflector (R2), which is probably an unconformable surface, and is bounded at the base either by basement highs or by the R3 reflector, which defines the top of seismic unit 4. Although the top of seismic unit 3 is an unconformity, the base is more or less conformable with the underlying unit in the deep part of the basin. The base of seismic unit 3, however, appears to be a surface of onlap west of the site. The biostratigraphic control at Site 645 is

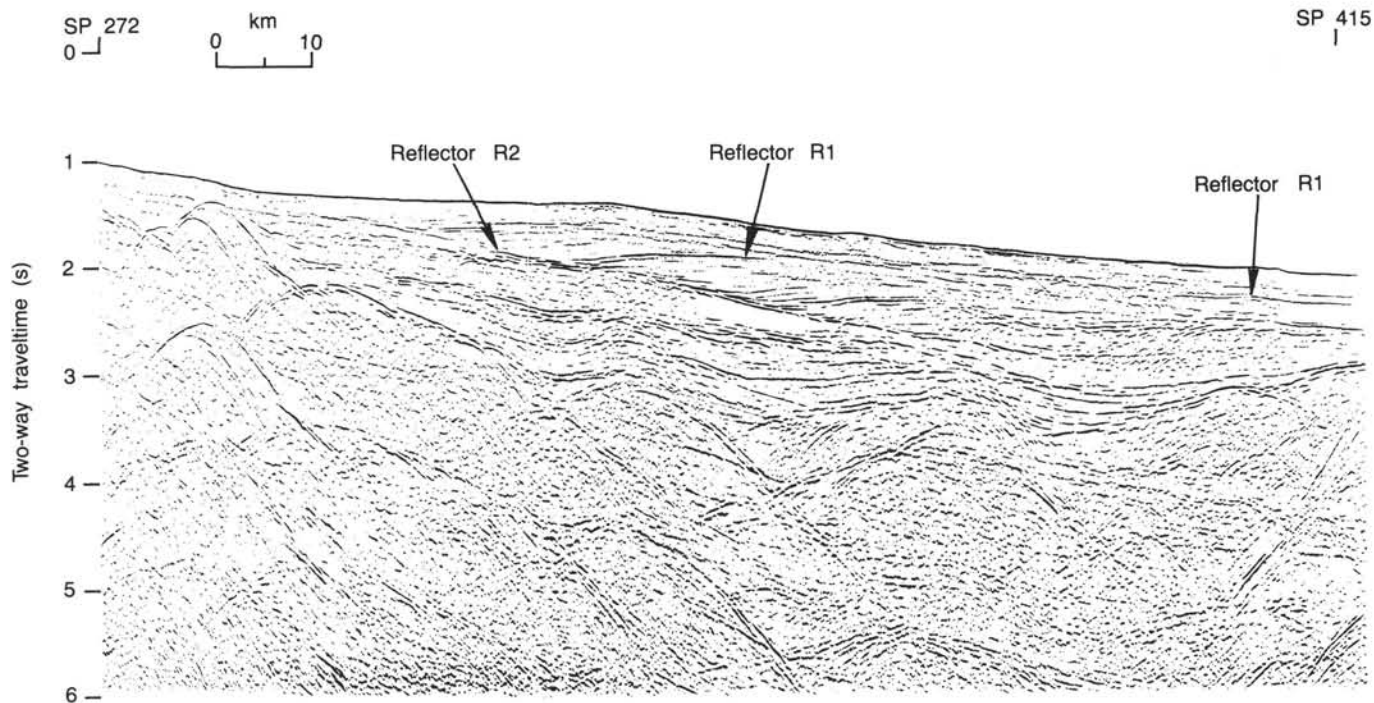


Figure 50. Shelfward section of multichannel line 74-51 between shotpoint 272 and shotpoint 415, showing character of reflector sequence above R2 that suggests erosional unconformity at R2 overlain by current-deposited sediment drifts.

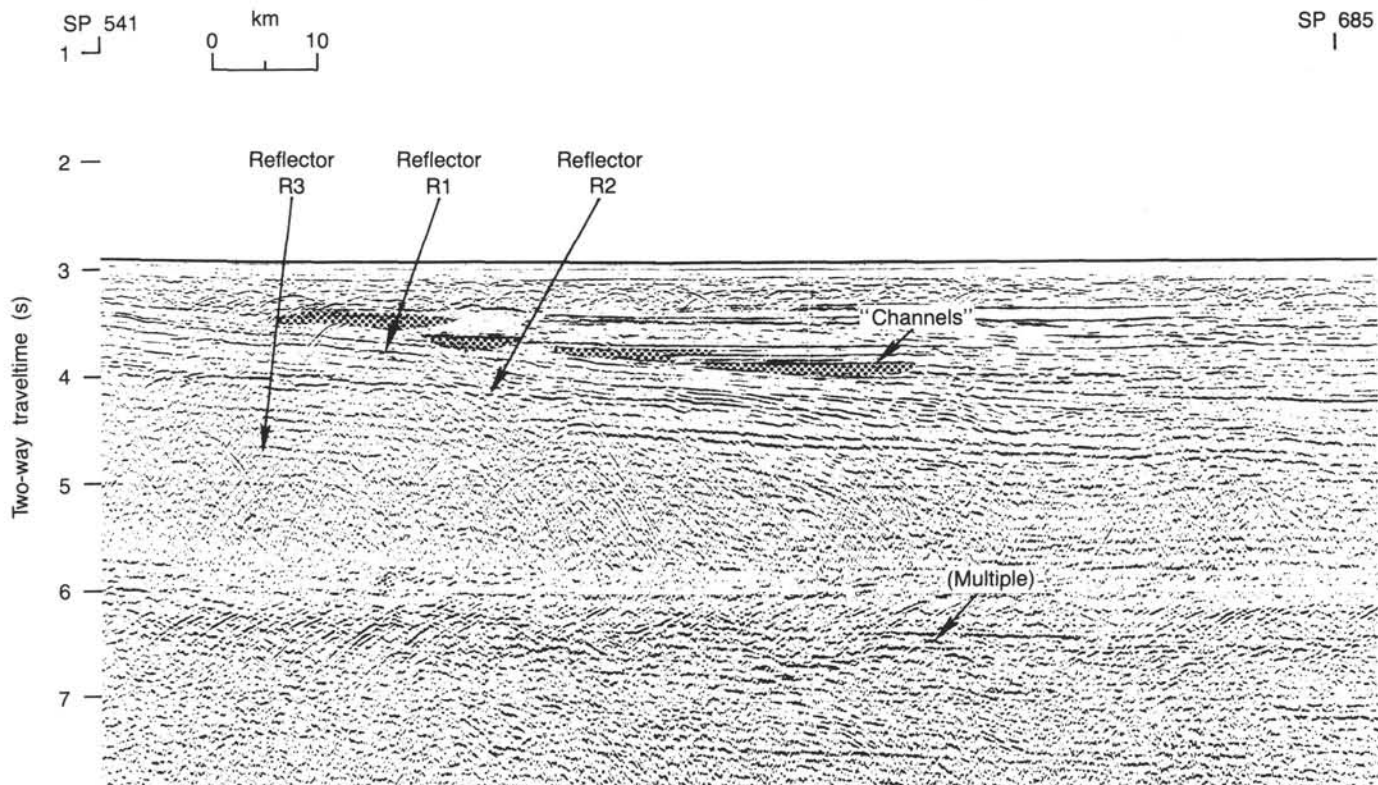


Figure 51. Part of multichannel line 74-51 between shotpoint 541 and shotpoint 685 east of Site 645. Note that basement is deeper than 6 s and largely obscured by seafloor multiple. This part of the line extends across the extinct "rift" zone near the basin center.

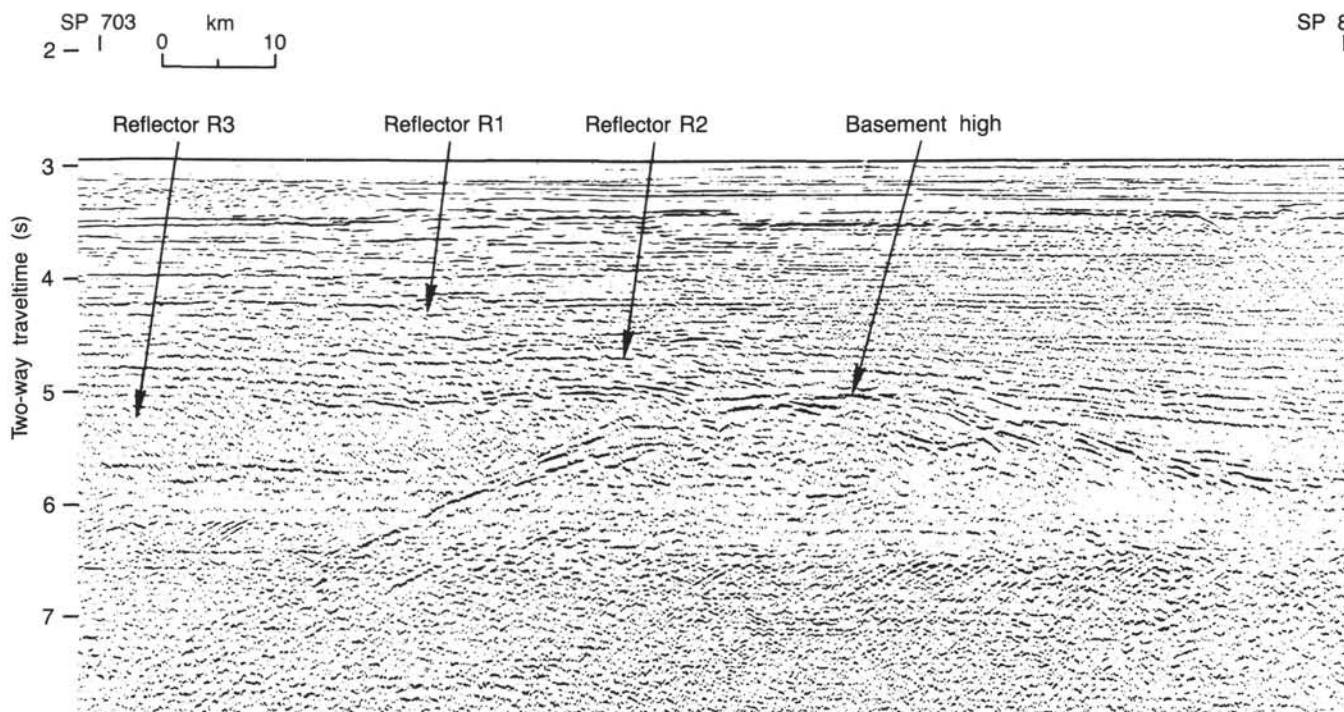


Figure 52. Part of multichannel line 74-51 between shotpoint 703 and shotpoint 841 toward West Greenland margin. Note thick seismic unit 1 (above reflector R1) relative to that shown in Figures 3 and 53. Note also prominent basement high that bounds extinct "rift" zone on eastern (Greenland) side.

not sufficient to constrain the duration of this unconformity, which is not as pronounced in the seismic sections near the site as it is to the west. The thickness of the unit varies; it is fairly uniform in the deep part of the basin (0.7 s, or 800 m) but thins considerably (to 0.1 s, or 165 m) on the continental slope as a result of termination of some of the reflectors in the lower part of the unit against basement highs. Beneath the upper part of the slope and shelf, seismic unit 3 varies in thickness because its upper surface is cut by the R2 unconformity. The reflectors in this region are no longer conformable with the reflectors in the underlying unit.

The reflectors within seismic unit 3 are much more pronounced than those in the overlying and underlying units, making it the most prominent unit in the entire basin. The top of unit 3 is nearly conformable to the overlying unit 2 in the central part of the basin, except that unit 2 appears to gently onlap the R2 reflector (top of unit 3) toward the west. Reflector R2 obviously cuts into older deposits on the shelf and upper slope, indicating the erosive nature of processes that formed the unconformity. The duration of the hiatus is probably longer upslope than in the basin center. The variability in the thickness of unit 3 on the shelf and slope and its eastward progradation suggest that the deposition of this unit was at least partly contemporaneous with the subsidence of the basin to the east.

Drilling at Site 645 penetrated only the upper 234 m of seismic unit 3, which is equivalent to Lithologic Subunit IIIC (916.8–1147.1 mbsf). Lithologic Subunit IIIC consists of fine- to medium-grained muddy sandstone and interbedded muddy siltstone. The textures and sedimentary structures suggest possible influence of bottom currents during deposition, but downslope movement of sediment to the site in the form of thin slump units also occurred. Pronounced reflectors in the upper part of seismic unit 3 appear to coincide with major changes in proportion of muddy sand beds (Fig. 56).

Seismic Unit 4

Seismic unit 4 is the lowermost seismic unit in the deep part of the basin that was not reached by the drill and is bounded at the top by seismic unit 3 and at the bottom by the basement reflector. In line 74-51, seismic unit 4 wedges out against a basement high under the slope (SP 481) (Figs. 3 and 53), and its continuation further upslope west of the basement high (Fig. 50) is difficult to see. We tentatively recognized only a thin section of this unit, which is interpreted to lie in this region beneath unit 3 and over another unit consisting of a set of pronounced reflectors that cap the basement rocks.

Reflectors within unit 4, though not distinct, are conformable with those in unit 3. The thickness of unit 4 varies from place to place, depending on the basement topography, and is probably greatest at the center of the basin where the basement lies at depths >5.0 s below the sea-surface. At Site 645, unit 4 is about 0.7 s thick. The interval velocity of unit 4 varies considerably across the basin (2.1–2.8 km/s), but near the site its average velocity is similar to that of unit 3 (2.1 km/s), which suggests that the base of this unit lies at about 2235 mbsf (735 m thick). The normal faults that cut reflectors in units 2 and 3 cannot be definitely traced through or below R3. However, the broken nature of the reflectors beneath R3 may indicate some faulting; diffractions from within unit 4 can be seen in parts of the record.

In comparison to unit 3, unit 4 is largely devoid of internal reflectors, though a few can be seen west of the site. Beneath the slope west of the basement high, a group of pronounced reflectors appears below the upper, less-reflective part of unit 4 (Fig. 50). These form seismic unit 4B, which probably represents basaltic flows interbedded with sediments and thus produce such pronounced reflections. Like unit 3, unit 4 progrades downslope and was probably deposited early during major subsidence of

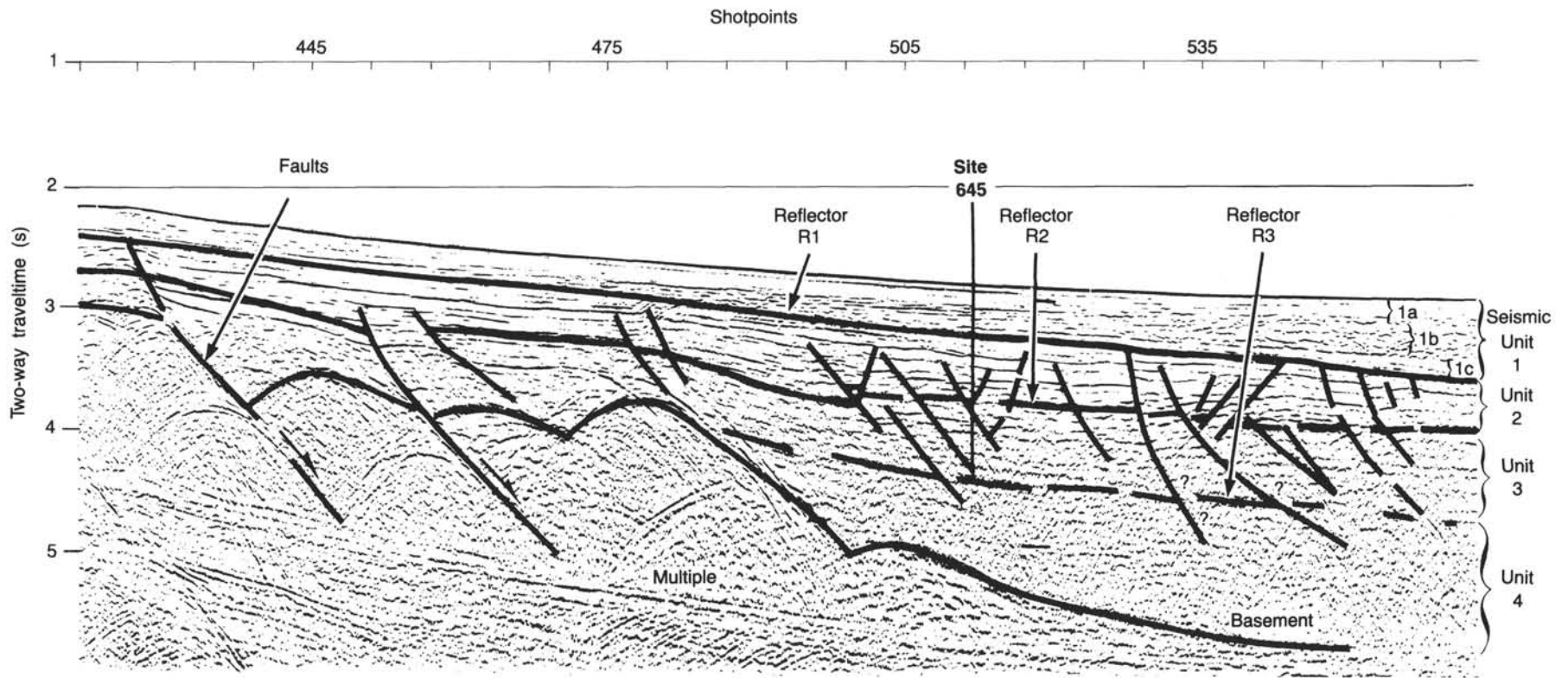


Figure 53. Section of multichannel seismic-reflection record 74-51 crossing Site 645, showing major reflectors, faults, and seismic units.

the basin. East of Site 645, the top of unit 4 barely caps a basement high at SP 775 (Fig. 52). If this basement high forms a part of the ridge complex associated with opening of the Baffin Bay basin (Srivastava et al., 1981), then it provides an age constraint of early Oligocene to late Eocene to the top of seismic unit 4.

This interpretation is supported by multichannel lines from the West Greenland Shelf that show similar features (Henderson et al., 1981). The reflector sequence composing unit 4b, interpreted as being basalt flows, may be late Paleocene–early Eocene in age, as are those on the West Greenland side (Henderson et al., 1981; Rolle, 1985).

Acoustic Basement

The lowermost seismic unit characterized by very sharp hyperbolic reflectors in line 74-51 is designated as acoustic basement. Under the shelf and slope, it is readily indicated by its undulating nature, giving rise to numerous hyperbolic reflections (Figs. 3 and 52). In the deep part of the basin and near the bottom of the slope, the basement cannot be seen because of its excessive depth and also because of interference from the multiple reflections of the seafloor (Fig. 51).

Under the slope to the west of Site 645, the basement is faulted, forming small graben structures filled with sediments and probably with interbedded basaltic flows, giving rise to pronounced reflections (Fig. 50). The fault planes are relatively steep and resemble listric faults. The east-facing basement slopes (probably fault scarps) are steeper than the west-facing tops of the tilted blocks. Reflectors within the small grabens tend to fan upward from bottom to top of each sequence as though sedimentation took place during faulting and subsidence of the blocks. Site 645 lies on the eastern flank of the last major faulted block. If we assume that the basin east of Site 645 was formed by seafloor spreading, then the faulting of the basement and stretching of crust as seen here were caused during the initial stages of separation of Greenland from Baffin Island (Early to Late Cretaceous, Srivastava et al., 1981). Figure 4 shows depth to basement from sea level, as interpreted from the multichannel network by Petro-Canada.

Faulting

Many of the seismic lines exhibit moderate- to high-angle normal faults (Figs. 53 through 55). Most of the faults cut the sediments of Lithologic Unit III but cut none of the younger strata, demonstrating that the faulting occurred during the early Miocene through early Pliocene. Whether the faults cut deeper strata is difficult to discern in any of the seismic lines, but offsets of reflector R3 do not appear to be major. We interpret the faulting to be related to differential compaction in rapidly sedimented strata of primarily early Miocene through early Pliocene age. The episode of faulting predates the formation of the R1 reflector, which might indicate that the major period of loading and compaction occurred before deposition of Lithologic Units I and II. Visible signs of faulting or fracturing were not noted in cores from Site 645, even though one or more faults are interpreted to disrupt strata at the site.

SUMMARY AND CONCLUSIONS

Background

Baffin Bay is an intracontinental basin that is thought to have been formed by an episode of extension that began in the Late Cretaceous and culminated in active seafloor spreading that occurred between the early Eocene and the Oligocene (Keen et al., 1974; Srivastava et al., 1981). However, the exact timing and style of the tectonic events that led to the separation of Greenland from northern North America, forming Baffin Bay, and

the nature of the crust underlying central Baffin Bay are still a subject of debate (Grant, 1982). Knowledge of the timing of formation and subsidence of Baffin Bay is crucial to models of paleoclimate and paleocirculation because Baffin Bay is likely to have been an important conduit between the Arctic and the North Atlantic oceans since at least Paleocene time (Gradstein and Srivastava, 1980). Site 645, Holes 645A through 645G, was occupied from 3 September to 28 September 1985 in Baffin Bay at a position of 70°27.49'N, 64°39.42'W, and a water depth of 2005 m. The total depth of penetration was 1147.1 mbsf, and average recovery for all holes was 66%.

Major objectives of drilling at Site 645 were as follows:

1. To penetrate and date reflector R3, which is the top of the oldest sedimentary unit overlying faulted and subsided basement on the margins and presumed oceanic crust in central Baffin Bay. The reflector is probably of Eocene–Oligocene age, but firm knowledge of its age would allow a better understanding of the tectonic and sedimentologic evolution of Baffin Bay.
2. To recover the sedimentologic and paleontologic record spanning the R3 reflector (Paleogene to Miocene sequence) to examine possible evidence of warm, equable humid climates at high latitudes during the Paleogene and possible indications of northward transport of warm, North Atlantic water through Baffin Bay to the Arctic basin.
3. To investigate the rate and degree of climate deterioration occurring from the late Eocene through the Miocene before the onset of major northern hemisphere glaciation.
4. To establish the timing of the major buildup of continental ice sheets in the circum-Baffin Bay region, an event that may have occurred earlier in this region than elsewhere because of its high continentality and the proximity of moisture sources for ice-sheet growth.
5. To determine the high-resolution record of glacial advances and retreats during the glacial epoch. The data derived from drilling are expected to help elucidate the rates of ice-sheet growth and decline and test prevailing models of the Milankovitch orbital forcing of glacial advances and retreats.

The deepest objective at the site, penetration of the R3 reflector of probable Eocene–Oligocene age at about 1540 mbsf, was not reached because of time limitations and delays resulting from a series of equipment difficulties early in the drilling of the site. Nonetheless, the recovery of a thick sequence of Miocene to Holocene terrigenous sediments and sedimentary rocks from southwest Baffin Bay provides a unique opportunity to unravel the complexities of climatic change, paleoenvironment, and sedimentation in this oceanic corridor between the Arctic and the North Atlantic.

General Features and Lithostratigraphic Framework

We recovered three major lithologic units, which are defined and subdivided into several subunits (Fig. 56) as follows:

Unit I. (Cores 105-645B-1X to 105-645B-18X, 105-645C-1H to 105-645C-3H, 105-645F-1H to 105-645F-3H, and 105-645G-1H to 105-645G-2H) 0–168.1 mbsf. Age: Pleistocene–Holocene. Description: subdivided into two units as follows:

Subunit IA. (Cores 105-645B-1X to 105-645B-8X, 105-645C-1H to 105-645C-3H, 105-645F-1H to 105-645F-3H, and 105-645G-1H to 105-645G-2H) 0–71.6 mbsf. Age: Pleistocene–Holocene. Description: alternating beds of light tan to gray, commonly gravel-bearing detritic carbonate muddy sand and typically dark-gray silty mud, scattered dropstones grading to cobble size (at least 6-cm diameter); average sand content, about 50%. Carbonate content (detrital), 10%–40%, with a mean of 20%. Dolomite/calcite ratio, 2:1. Cyclicity of lithofacies, on a scale of

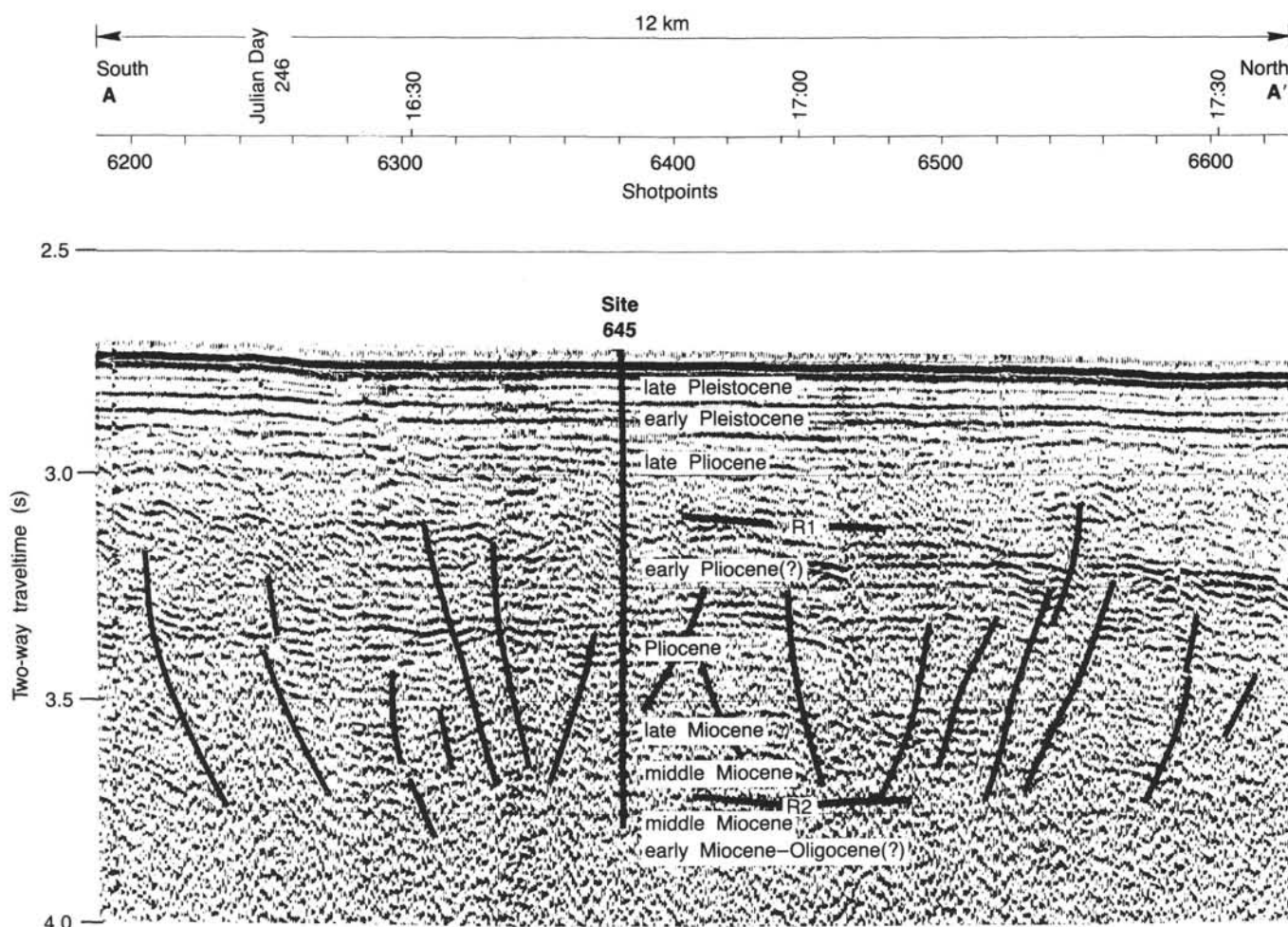


Figure 54. Processed digital single-channel seismic-reflection profile shot by *JOIDES Resolution*, running approximately north-south across Site 645 and showing nature and age of reflectors based on drilling results. Times shown are UTC. See Figure 2 for trackline.

tens of cms to 1–2 m; bioturbation, slight. Contacts between individual beds, typically sharp.

Subunit IB. (Cores 105-645B-9X to 105-645B-18X) 71.6–168.1 mbsf. Age: Pleistocene. Description: alternating beds of gray detrital silty clay to dark olive-gray silty mud, with dropstones to cobble size. Average sand content, <10%. Carbonate content (detrital), 30%–40%, but with dolomite/calcite ratio of 2:1; distinct to subtle cyclicity of lithofacies and slight bioturbation.

Unit II. (Cores 105-645B-19X to 105-645B-32X, 105-645D-1R to 105-645D-7R, and 105-645E-1R to 105-645E-3R) 168.1–335 mbsf. Age: Pliocene–early Pleistocene. Description: non-carbonate silty mud, clayey silt, and silty clay with dropstones to cobble size. Percentage of clasts decreases downsection, but abundance increases at base of unit. Silty mud predominates, with subordinate dark-gray silty clay and clayey silt. Carbonate content is 5%–10% and is predominantly dolomite. Cyclicity of lithofacies occurs but is more subtle than in Unit I. Beds are bioturbated to faintly laminated in places. A 5-m-thick homogeneous fine sand layer occurs near the base of Unit II (within the interval of 274–284 mbsf). The basal 30-m interval of low recovery may contain some sand and gravel, but interpretation of geophysical logs suggests that silty mud predominates (we attempted to core this interval at three different holes and had little success). Precise definition of the lower boundary of Unit II

was therefore difficult, but the character of geophysical logs constrains the boundary to 332–336 mbsf.

Unit III. (Cores 105-645D-8R to 105-645D-20R and 105-645E-4R to 105-645E-78R) 335–1147.1 mbsf. Age: early Miocene–Pliocene. Description: subdivided into three units as follows:

Subunit IIIA: (Cores 105-645D-8R to 105-645D-20R and 105-645E-4R to 105-645E-36R) 335–753.4 mbsf. Age: late Miocene–Pliocene. Description: poorly sorted olive-gray muddy sandstone predominating with interbedded sand-bearing silty mudstone. These strata contain a mean of about 25% coarse sand and granules. Scattered pebbles, predominantly black shale clasts with some granitic, carbonate, and friable sandstone clasts, occur in coarser beds. Maximum quartz grain size extends up to granules. The lowest occurrence of pebbles is at 605 mbsf. Sediment textures are homogeneous to slightly bioturbated, having few primary structures. Variations in grain size occur on the scale of meters and have gradational boundaries, but some beds are graded and have sharp bases, ranging in thickness from 20 to 100 cm.

Subunit IIIB. (Cores 105-645E-37R to 105-645E-54R) 753.4–916.8 mbsf. Age: middle to late Miocene. Description: olive-gray muddy sandstone and dark-gray silty mudstone, interbedded with well-laminated medium-gray calcareous silty claystones having organic carbon contents to 3% (abundant wood fragments) and moderate to strong bioturbation. The unit is charac-

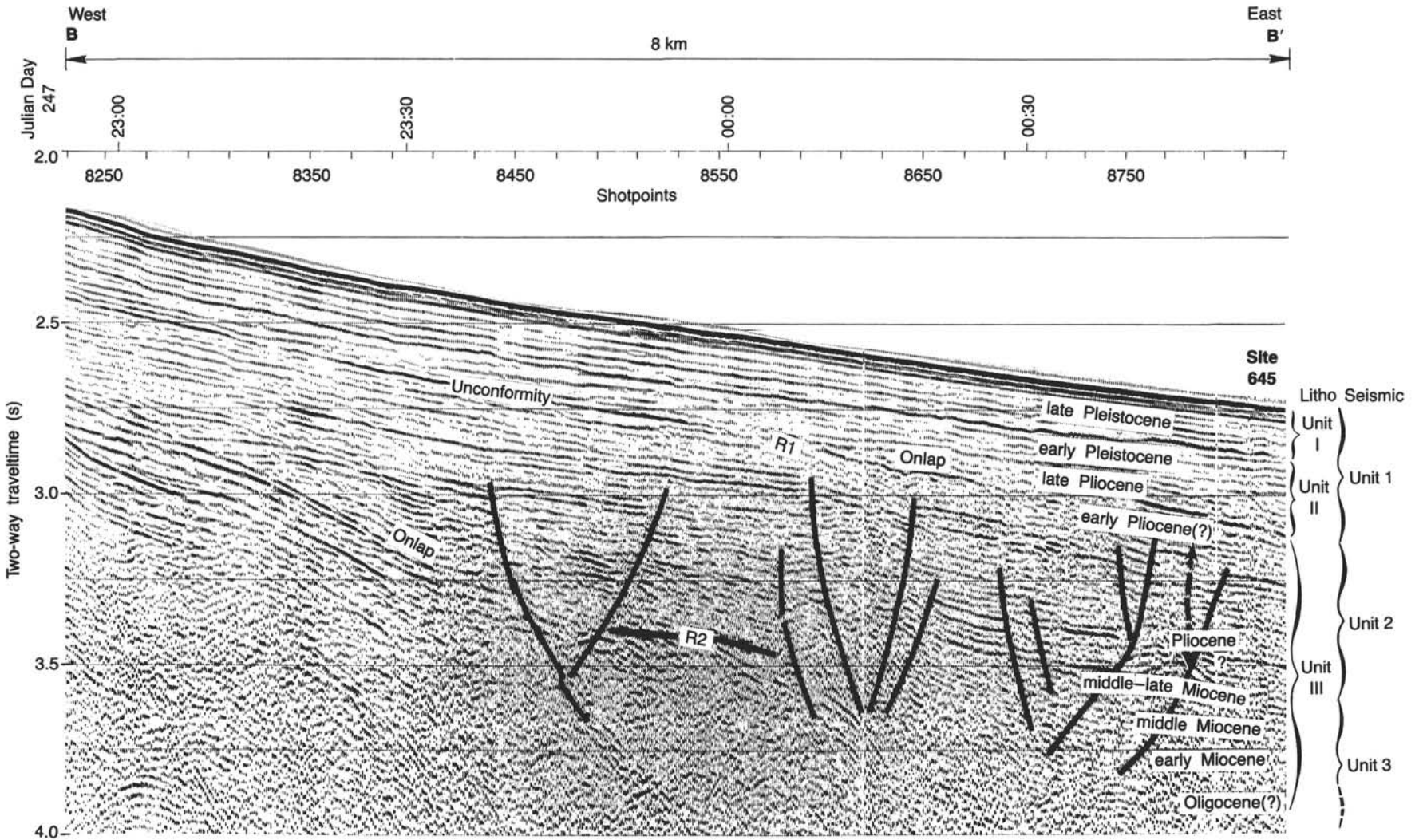


Figure 55. Processed digital single-channel seismic-reflection profile shot by *JOIDES Resolution*, running approximately east-west across Site 645 and showing age of seismic units based on drilling results. Times shown are UTC. See Figure 2 for trackline.

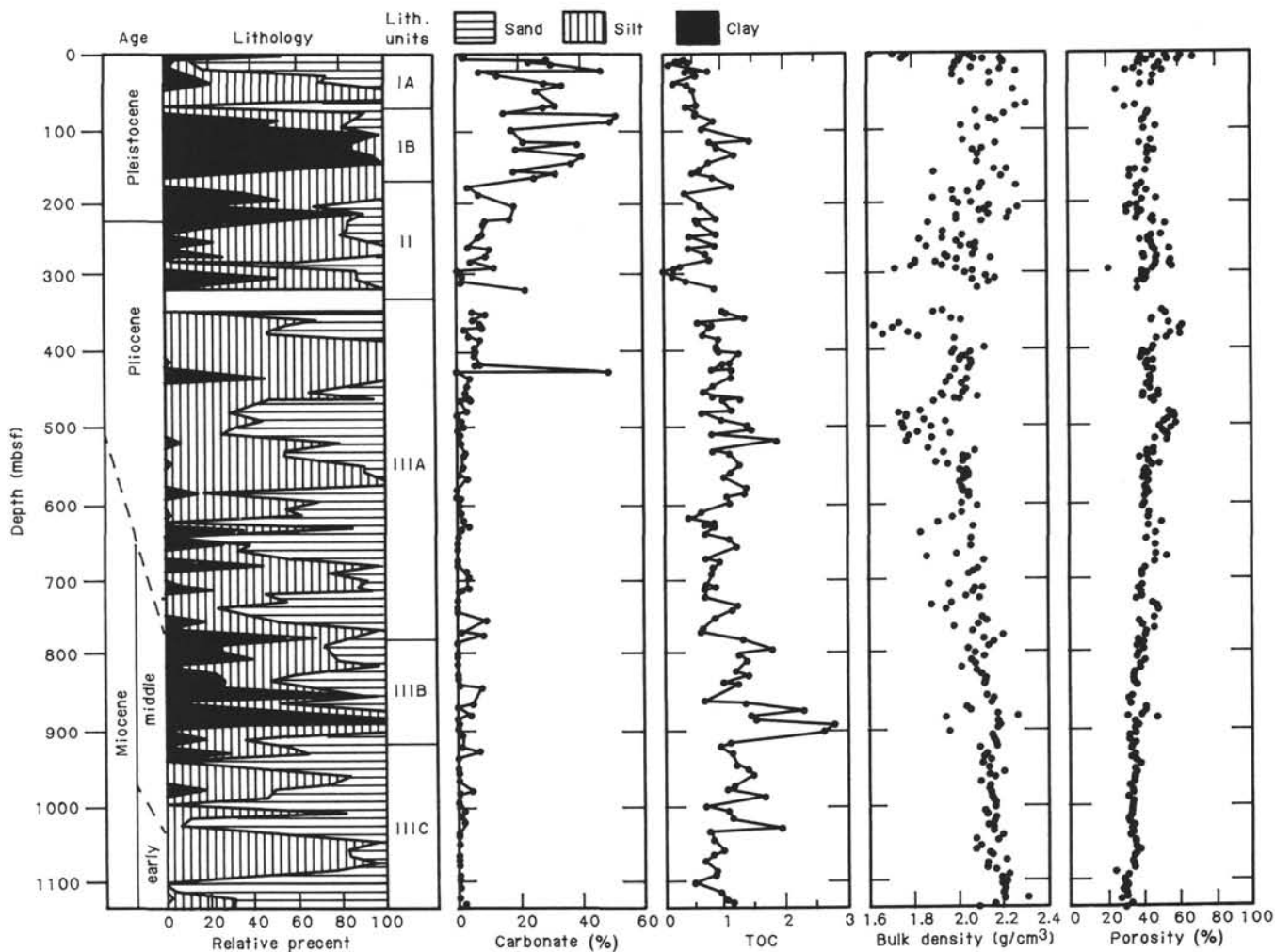


Figure 56. Lithologic units, relative proportion of sand, silt or clay beds, organic carbon, carbonate contents, and ages of units at Site 645, Baffin Bay.

terized by a smaller mean grain size and more abundant claystone beds.

Subunit IIIC. (Cores 105-645E-55R to 105-645E-78R) 916.8–1147.1 mbsf. Age: early to middle Miocene. Description: predominantly olive-gray green to gray fine- to medium-grained muddy sandstone and silty mudstone. The sandstone may contain as much as 10% glauconite in certain intervals. Subunit IIIB is coarser grained on the whole than is Subunit IIIA. The coarser facies show moderate to strong bioturbation, but some interbedded fine-grained intervals are well stratified. A few horizons show features of soft-sediment deformation (mainly in Core 105-645E-66R).

The sequence recovered at Site 645 has a pronounced terrigenous character with surprisingly sparse remains of planktonic biota. Muddy sand (sandstone) and silt (siltstone) dominate most of the sequence, except the intervals between 75 and 225 mbsf and 770 to 900 mbsf, in which silty clays (claystones) and clayey silts (siltstones) are more abundant. The sand and silt units are primarily mineralogically and texturally immature. Quartz predominates over feldspar (average ratio about 2.5:1), and K-feldspar and plagioclase occur in roughly subequal proportions, according to both smear slide and X-ray mineralogical analyses. The composition of outsized clasts in the upper 330 m of the sequence is highly variable; granitic, gneissic, and shallow-water

limestone or micritic carbonate clasts are most common, but friable sandstone, shale, and basalt pebbles also are present. Siliceous microfossils, particularly radiolarians, are rare to absent over the entire interval, and calcareous microfossils are also rare, except in the uppermost and lowermost parts of the sequence. Only organic-walled microfossils occur throughout most of the sequence. The section below about 160 m is characterized by average total carbonate content of < 10% and usually < 5%. Little biogenic carbonate is present, and authigenic dolomite, siderite, and rhodochrosite predominate. Above 160 mbsf, carbonate mineral contents average about 20%, but the particles are almost entirely detrital, dolomite being about twice as abundant as calcite, on the basis of shipboard X-ray mineralogical studies. Contrary to our expectations, no biogenic silica-rich intervals were encountered in the sequence. Organic carbon contents range from 0.1% to 2.8% and average about 0.8% for the entire section, but distinct relatively organic-carbon-depleted and -enriched zones occur (Fig. 56). The organic matter is predominantly terrigenous above 460 mbsf and is terrestrial mixed with some marine material below 460 mbsf.

Stratigraphy and Sedimentation Rates

The sparse siliceous and calcareous planktonic assemblages and evidence of reworking make precise age assignments diffi-

cult. We primarily depend upon dinocyst and benthic foraminifer age picks and a few tie points from calcareous nannofossils and diatoms. Unfortunately, most of the dinocysts and benthic foraminifers are rather long-ranging species and do not provide precise age control. The major age constraints provided by shipboard paleontological studies (Fig. 27) are (1) 0–245 mbsf, Pleistocene and younger (< 1.6 Ma); (2) 245–680 mbsf, Pliocene to late Miocene (3.4–10.5 Ma); (3) 680–975 mbsf, middle Miocene (10.5–16.5 Ma); and (4) 975–1147 mbsf, early Miocene (16.5–22.7 Ma).

Additional constraints on the age of parts of the section are imposed by the paleomagnetic results from the site. The three most important and easily recognized datums, considering the lack of continuous recovery, that have been tentatively identified in the reversal records are the top of the reversed zone at the Brunhes/Matuyama Chronozone boundary (0.73 Ma), at 95 mbsf; the Jaramillo Subchronozone (0.91–0.98 Ma), recognized between 115 and 126 mbsf; and Chron 11 (8.92–10.42 Ma), the long normal-polarity interval of the middle Miocene, between 613 and 679 mbsf. The age–depth relationships provided by the paleontological and paleomagnetic data are shown in Figure 27. The two sets of constraints agree reasonably well.

If we assume that the paleomagnetic stratigraphy gives us a higher resolution picture of the age–depth relationships for the upper 900 m of the sequence and we use the biostratigraphic constraints below that level, we can calculate interval sedimentation rates (Fig. 27) as follows: (1) 0–460 mbsf (late Pliocene to Holocene), 135 m/m.y. (13.5 cm/1000 yr); (2) 460–613 mbsf (early Pliocene to late Miocene), 28 m/m.y. (2.8 cm/1000 yr); and (3) 615–1147 mbsf (early Miocene to early-late Miocene), 42 m/m.y. (4.2 cm/1000 yr).

Magnetostratigraphy from the shipboard pass-through cryogenic magnetometer and from discrete samples is helpful down to 900 mbsf, below which the section is badly remagnetized, probably as a result of drilling disturbances. Further shore-based studies of fairly abundant dinocysts will undoubtedly provide better stratigraphic control, and it is likely as well that more detailed examination of samples other than the core-catcher material will turn up age-diagnostic species of other groups. The following conclusions concerning timing of events and rates of deposition are based on our preliminary stratigraphy and should be considered highly tentative.

Paleoenvironmental Evolution of Baffin Bay

Nature of the Glacial Climate and Sedimentation

Recovery in Unit I with the HPC and XCB was poor, probably because of the unusual firmness of the sediment and the abundance of dropstones. Piecing together recovery from Holes 645A, 645B, 645C, 645F, and 645G for the upper 25 m of HPC/XCB cored material, using careful correlations of distinctive lithologic units between holes, indicates that we obtained a nearly complete sequence of the upper part of the Pleistocene interval. This will allow high-resolution studies of glacial–interglacial paleoenvironment changes in Baffin Bay. Rhythmic sedimentation is highly evident throughout Units I and II (Pliocene–Pleistocene), but unfortunately, recovery in the top 170 m is not sufficient for tests of orbital forcing over long time series in Baffin Bay. However, geophysical logs from some intervals show significant cyclicity and may be useful for time-series studies. In Unit I the most characteristic rhythm is that of interbedded dark-gray to olive-gray silty clay and light brownish to grayish brown detrital carbonate muddy sand, silty clay, or mud. Contacts between each lithofacies are sharp, and bioturbation is minor. The light-colored intervals contain a greater proportion of coarser detritus, including detrital carbonate. Pebbles and cobbles, apparently randomly distributed in both lithofacies, are interpreted

as being ice-rafted detritus. The smallest scale cycles that are noticeable average about 1 m in thickness. These were interpreted by Aksu (1983) as representing glacial–interglacial cycles, on the basis of his studies of oxygen-isotope stratigraphy in shallow piston cores from this area. His correlation of the oxygen-isotope data to the standard oxygen-isotope stages suggests that a record exists of glacial–interglacial fluctuations in climate at least back to the bottom of Stage 9 (347 k.y.) in the top 10 m of the deeper Baffin Bay sequence. With this interpretation, therefore, each approximately 1-m cycle represents about 40 k.y.

We also interpret the cycles as representing relative changes in ice cover over the bay and in amount of ice rafting of coarse-grained detritus. The darker silty clay part of each cycle apparently represents either a period of predominant ice cover or low rates of melting of icebergs in surface waters. Planktonic foraminifers in such layers have heavy (i.e. “glacial”) oxygen-isotope values in the cores studied by Aksu (1983). The light-colored layers, rich in detrital carbonate and coarser grained on the whole, probably represent times of increased iceberg calving and melting; the oxygen-isotope work of Aksu (1983) shows that surface waters had anomalously light values, indicating lower-than-normal salinity.

However, the stratigraphy at Site 645 indicates that either a major change in sedimentation rate occurs between 10 and 95 mbsf or that Aksu’s oxygen-isotope correlations are incorrect. Because the average depositional rate for the upper 470 m at Site 645 is probably about 135 m/m.y. (13.5 cm/k.y.), the average 1-m cycle represents about 8 k.y. Such a period is much shorter than the 41-k.y. period predicted to dominate the climatic spectra at this latitude (Berger, 1978; Ruddiman and McIntyre, 1981a, b). We cannot prove that the observed cycle is periodic, but our results strongly suggest that melting of sea ice and advance and retreat of glacial ice on the margins of Baffin Bay region occurred on a much shorter time scale than expected. If the pronounced fluctuations in the oxygen-isotopic and faunal- and floral-abundance data of Aksu (1983) and Mudie and Aksu (1984) are interpreted as being phenomena of a shorter period, then the data support short-term melting of sea ice and periodic establishment of low-salinity surface layers formed by meltwater outflow concurrent with or followed by incursions of somewhat warmer North Atlantic water characterized by a subarctic fauna and flora. The sharp contacts between individual beds suggest rapid changes from one regime to the other, but detailed faunal and floral studies across the cycles will provide more constraints on models.

Data from one such cycle (Section 105-645C-3H-3, Fig. 57) illustrate the difficulty of interpreting the lithologic changes. The effects of dilution and probable environmental restriction are apparent in the decreasing abundance of both planktonic foraminifers and dinocysts. The increasing abundance of reworked palynomorphs in the muddy sands is interpreted as representing intervals of warming and increased melting and ice rafting of sediment. Pollen and spore contents increase in the same interval, suggesting increased vegetation on surrounding land areas or advection from regions to the south, but at the same time the proportion of dextral *Neogloboquadrina pachyderma*, an indicator of subarctic water masses, declines. The higher proportions of *N. pachyderma* in the silty clays, which apparently represent intervals of less ice rafting, are puzzling in that they indicate the presence of subarctic water masses in the region during intervals of “glacial” climate, when almost complete ice cover might have existed. Dissolution during warm “interglacial” periods could have modified the planktonic foraminiferal-abundance patterns, as suggested by Aksu (1983), yet no evidence of changes in degree of dissolution appears in this particular cycle. The main conclusion that can be drawn from this example is that a relatively restricted environment existed in Baf-

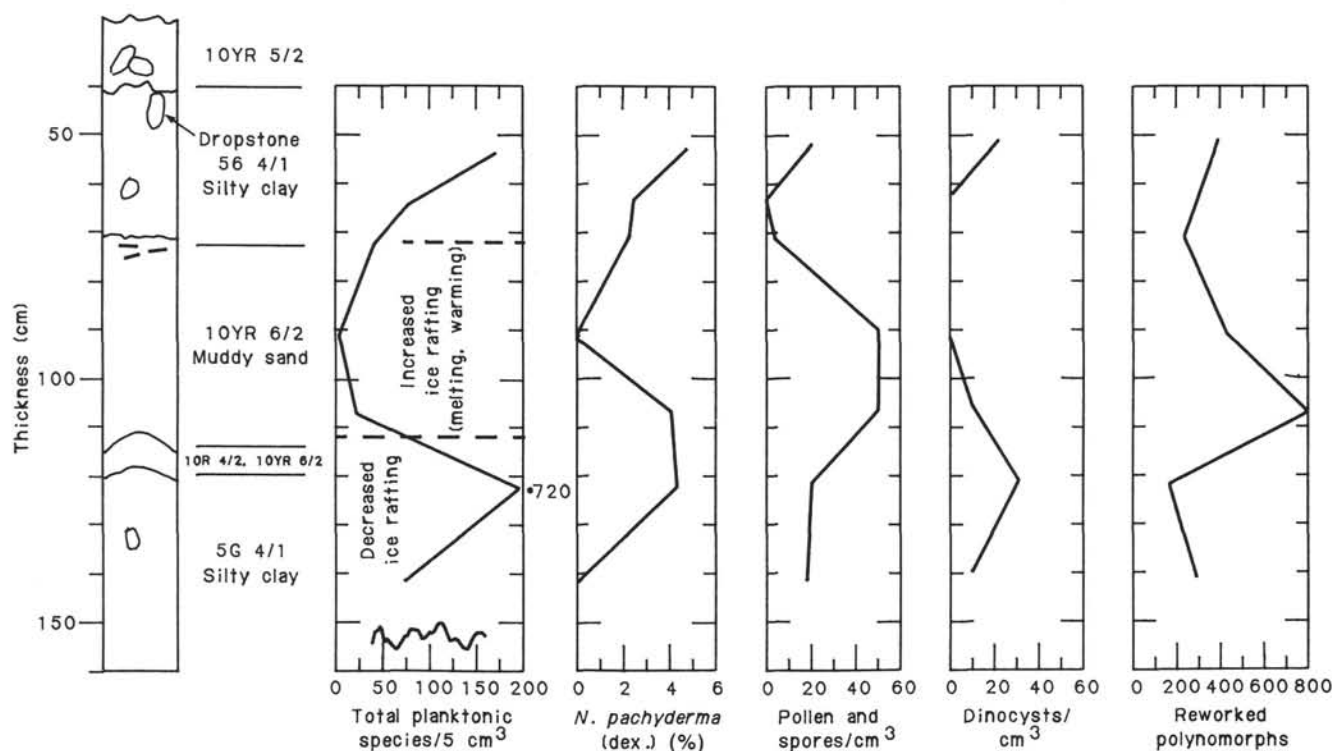


Figure 57. Results of detailed micropaleontological study of one typical cycle in upper Pleistocene sequence at Site 645 (Section 105-645C-3H-3).

fin Bay during the entire cycle and that no permanent ice cover appears to have prevailed during deposition of the cycle. Rates of iceberg calving and melting over the site merely changed.

Similar cycles having about the same average thickness persist through Lithologic Unit II although the cyclicity is more subtle. One possibility for the short-term (about 10-k.y.) cycles is that they represent events that are typically below the resolution of most pelagic sequences from which the standard oxygen-isotope curves and stages have been constructed, as well as being of lower amplitude than the overall glacial-interglacial signal. For example, oxygen-isotope curves published by Ruddiman and McIntyre (1981b) exhibit short-term but significant fluctuations of as great as 0.5 per mil on a 10–15-k.y. scale within each isotope stage. The stage 5 fluctuations demonstrate this.

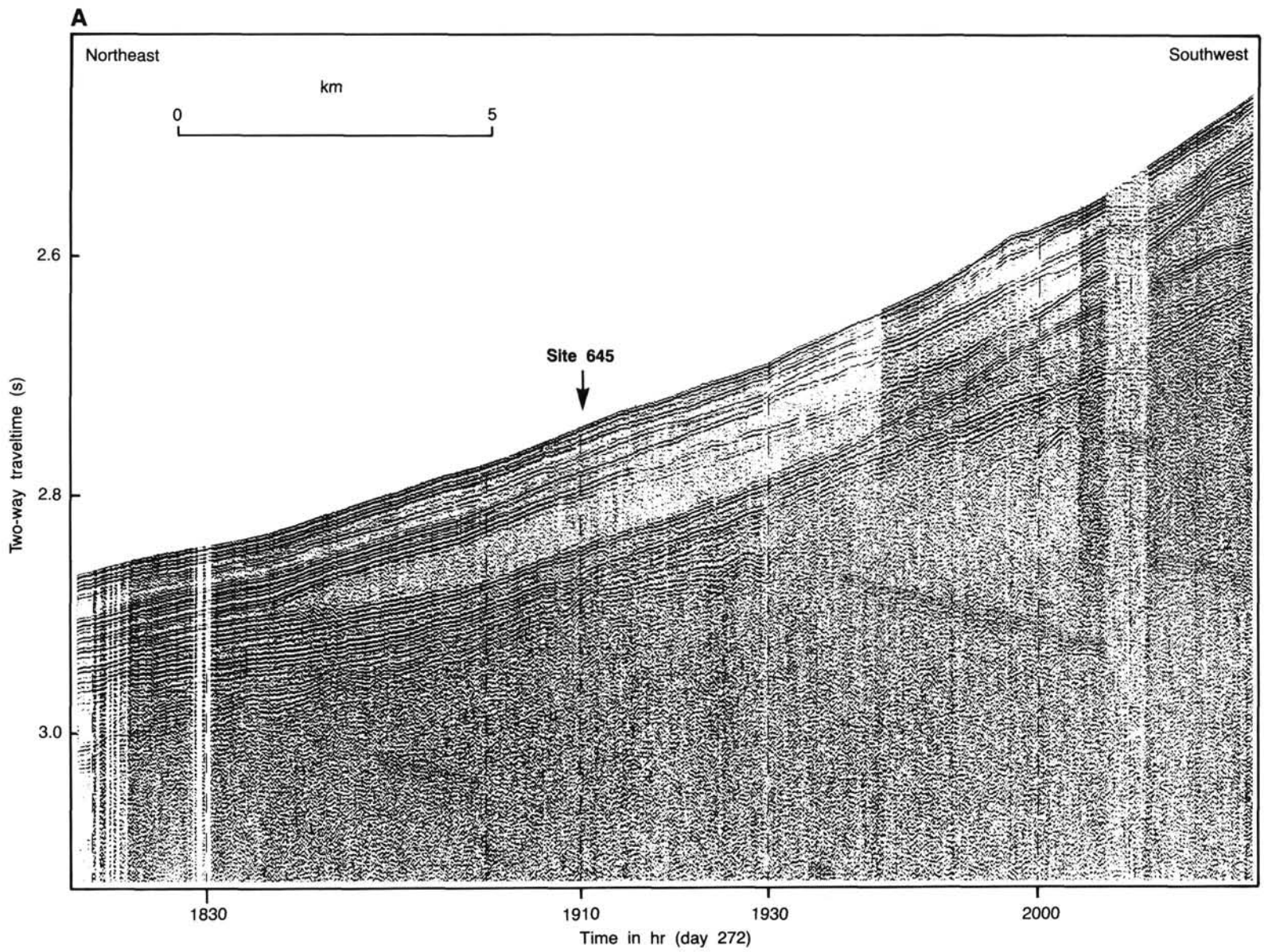
We interpret the strata of Lithologic Unit I as having been deposited mainly by melting ice and as having had some contribution by downslope redeposition of various sorts. Bottom currents played a minor role in deposition or winnowing of the sediment. The seismic character of Unit I (defined as seismic unit 1A; see “Seismic Stratigraphy” section, this chapter) supports this interpretation in that the deposits are of uniform thickness over much of the region, including the Baffin Island lower slope, and the interval is somewhat uniform and seismically transparent (Fig. 58B). However, a high-resolution single-channel seismic record across Site 645 (Fig. 58A) illustrates that downslope redeposition was important near the site. At least one thick (40–70 mbsf), chaotic mass interpreted as being a slump deposit reached the site during Unit I deposition. Other such slump intervals are also visible. Sparse, low-diversity dinocyst assemblages in the upper 135 m suggest cold, low-salinity surface waters during much of the deposition of Lithologic Unit I. Planktonic foraminifers are present in the interval above 100 mbsf, but are absent below that level. Dissolution and low productivity probably caused their disappearance (see “Biostratigraphy” section, this chapter). Diatoms and radiolarians occur only at the surface, again suggesting relatively low productivity and dissolution of opaline

silica. Organic carbon contents average 0.5%, and accumulation rates are low. Most of the organic matter is terrigenous and reworked.

Onset of Glaciation

The onset of major glacial ice rafting in Baffin Bay, recorded by the first abundant dropstones and other coarse sediment, was at least as early as 2.5 Ma (base of Unit II at 335 mbsf) or perhaps as early as about 3.5 Ma (465 mbsf). The beginning of major glacial activity in this region, therefore, could have preceded ice rafting in the northern North Atlantic by about 1 m.y., on the basis of a 2.3–2.4-Ma date obtained as the result of drilling on DSDP Legs 81 (Roberts, Schnitker, et al., 1984) and 94 (Ruddiman, Kidd, et al., 1985). However, isolated pebbles and granules in strata as old as late Miocene (605 mbsf) at Site 645 could indicate the presence of at least seasonal sea ice in Baffin Bay as early as 8.5 Ma. Pebbles are common in strata above 460 mbsf, but strata consist predominantly of sedimentary clasts, especially black shale, below 320 mbsf. Clark (1982) argues for a beginning of glaciation in the Arctic region at 5–6 Ma, and Eldholm, Thiede, Taylor, et al. (in press) suggest a 4.3-Ma timing for beginning of glacial regime in the Norwegian–Greenland Sea. The latter timing is based primarily on an increase in the terrigenous component in sediments at Site 642. An earlier timing for continental glaciation in the Baffin Bay region is not unreasonable considering its high continentality and the lack of influence by advection of warm-water masses in contrast to those associated with the Gulf Stream in the North Atlantic–Norwegian–Greenland Sea area.

A major unconformity (reflector R1), observed in a regional multichannel seismic net, probably represents a change in depositional style in the late Pliocene, coincident with the beginning of major continental glaciation, and is overlain by a thick wedge of upper Pliocene–Pleistocene “glacial” sediment that prograded westward from the West Greenland margin. The upper 160 m of Pleistocene sediment is mainly ice rafted, but sediments from



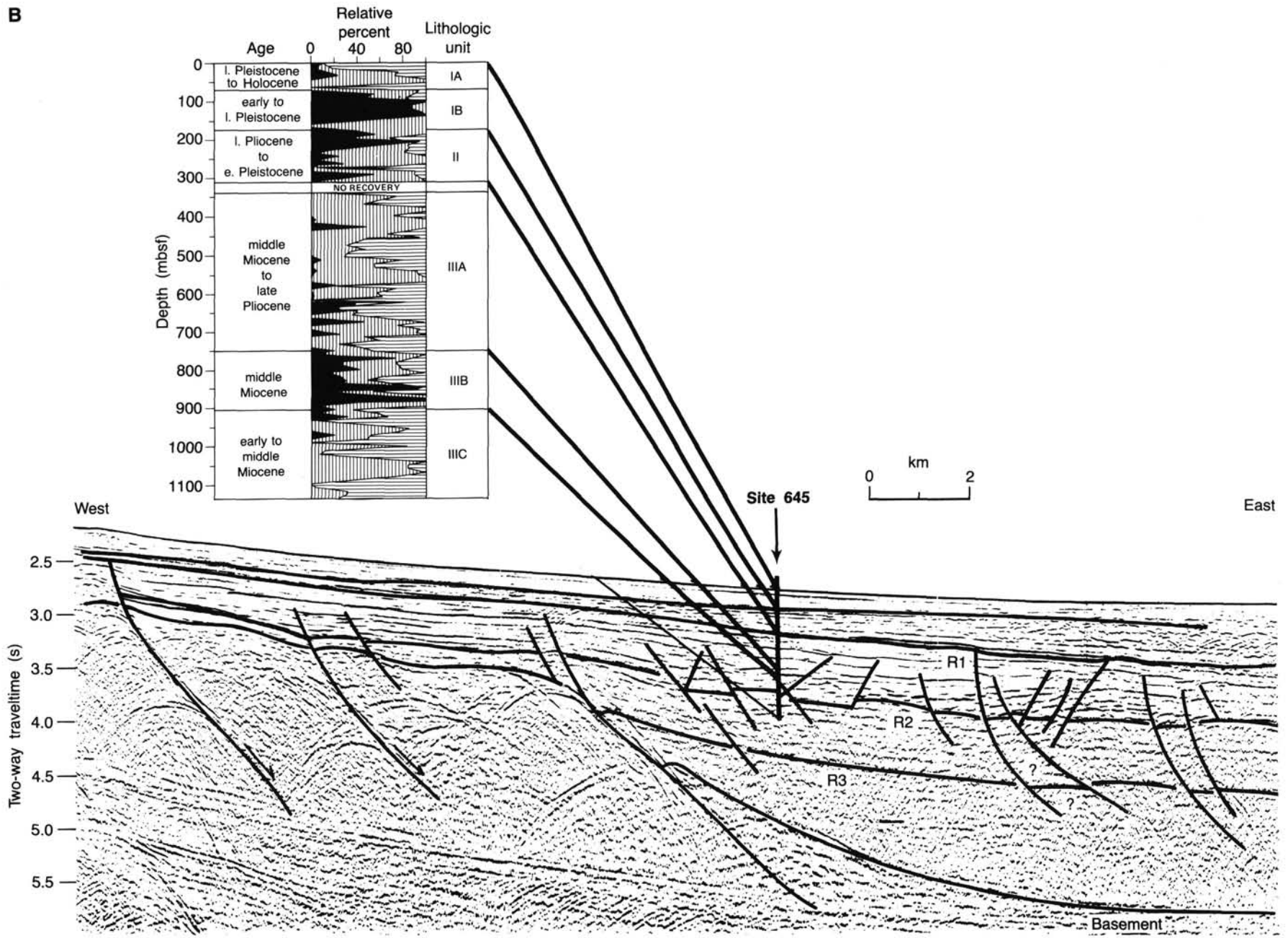
B

Figure 58. A. Single-channel, high-resolution seismic line acquired by *CSS Hudson* (85) across Site 645. B. Part of multichannel seismic line 74-51, showing location of Site 645 and correlation of major reflectors and seismic units to lithology at Site 645.

Lithologic Unit II may have been deposited by ice rafting, turbidity currents, and perhaps winnowed by weak bottom currents. No definitive evidence of either major turbidite or bottom-current deposition was found at Site 645 in Lithologic Units I and II. However, important features on seismic lines along the Baffin Island margin at water depths between 1200 and 800 m strongly resemble bottom-current-deposited sediment drifts (Fig. 51), which we interpret as the product of strong southward-flowing contour currents. Correlation of the major seismic reflectors with strata recovered at Site 645 indicates that the main current-influenced sedimentary bodies are probably middle Miocene through early Pleistocene in age. The currents at lower slope depths do not appear to have been as active during much of the late Pleistocene because Lithologic Unit I drapes the drift structures.

Even with the apparent beginning of major glaciation on the adjoining land masses, evidence of nearby open coniferous boreal or tundra forests exists in the pollen record, particularly in Lithologic Unit II between 340 and 265 mbsf (unless the spores and pollen were transported north by surface currents or southerly winds). Above 265 mbsf, sparse spores and pollen suggest impoverished vegetation on nearby land masses. From 465 to 265 mbsf, the sequence is barren of radiolarians, foraminifers, and calcareous nannofossils; only rare dinocysts and diatoms were observed. The diatoms suggest a neritic environment, and dinocysts probably indicate relatively low-salinity surface waters. The faunal and floral evidence taken with high sedimentation rates and the increasing frequency of clasts, which may be dropstones, may signal the beginning of a true glacial regime in the late Pliocene or earlier (at about 465 mbsf).

Neogene Climate, Circulation, and Productivity

Sedimentary textures and structures at Site 645 suggest an unexpectedly pronounced but variable influence of deep currents during deposition of Lithologic Unit III (early Miocene to late Pliocene) in western Baffin Bay. These features, and the rare occurrence of planktonic biota (above about 720 mbsf) indicating the incursion of warmer North Atlantic waters into the basin, suggest possible primarily southward-directed flow of Arctic water masses to the Labrador Sea beginning during the middle Miocene. Some dinocysts with subarctic or North Atlantic affinities occur in sediment of middle to late Miocene age (Lithologic Unit IIIB) and indicate that cool-temperate conditions existed in part of the bay at that time and probably reflect periodic incursions of North Atlantic waters. Calcareous microfossils and dinocysts having North Atlantic warm-temperate affinities occur in some intervals of the lower Miocene at Site 645, possibly indicating the waning influence of relatively warmer northward flow from the North Atlantic to Baffin Bay at that time. Evidence of development of the cold Labrador Current running over the Labrador Shelf is found in sediments as old as the Miocene and certainly the early Pliocene (Gradstein and Srivastava, 1980). Such evidence indicates that cooling at high latitudes led to the increasing influence of Arctic water masses that penetrated into the North Atlantic as surface currents and possibly as deep-water masses. Overflow from Baffin Bay across the Davis Strait during the middle Miocene to Pliocene possibly contributed to the volume and rapid advection of North Atlantic deep water formed at that time, although we currently have no direct evidence of this. We also do not know the extent of inflow of North Atlantic surface waters to Baffin Bay during the middle Miocene to Pliocene.

Reflector R2 is an erosional unconformity over at least part of the region, particularly on the Baffin Island shelf and slope, where it cuts deeply into strata of probable Paleocene to early Miocene age. Middle Miocene, partly bottom-current-deposited strata of Lithologic Subunit IIIB overlie R2, suggesting that this reflector and unconformity marks the onset of vigorous south-

ward-directed circulation in the basin. The onset of this circulation was coincident with evidence of cooling and/or more restricted environmental conditions from faunal and floral assemblages after about 14 Ma. Redeposition and reworking of benthic foraminiferal faunas from shallower depths and strata from Paleogene to Miocene age in parts of Lithologic Unit III are consistent with erosion and transport of detritus to the site by both bottom and some turbidity currents.

A middle Miocene climatic amelioration observed elsewhere in the circum-North Atlantic region is not immediately obvious in strata at Site 645, but evidence of a possible middle Miocene productivity event can be seen in the increasing abundance of agglutinated benthic foraminifers and in the slightly higher content and accumulation rates of marine organic matter (approximately 40% of the TOC).

Nonetheless, the paucity of siliceous and calcareous biota, the neritic aspect suggested by those diatoms and dinocysts that are present, and the dominance of organic matter of terrestrial derivation (even though organic carbon contents in some intervals were as high as 3% and accumulation rates were high in some intervals of the Pliocene-Pleistocene; Fig. 56) indicate predominance of cool, nutrient-poor surface waters. These waters generally exhibited lower-than-normal salinity and low primary productivity for most of the Miocene to Holocene. Dissolution and/or diagenesis cannot be ruled out, at least as a partial explanation of the poor preservation or absence of calcareous and siliceous faunal/floral remains. Overall, however, the carbonate-accumulation rate is very low (Fig. 59a), whereas the accumulation rate of the terrigenous fraction is high. We calculated an average paleoproductivity for the sequence, using Müller and Suess's (1979) method, which accounts for the organic carbon preservation factor related to sedimentation rate. Using a value of 40% as the average proportion of marine organic matter in TOC (Fig. 59b), we obtained typical oligotrophic values of $<100 \text{ gCm}^{-2}\text{yr}^{-1}$ for most of the sequence.

Tectonics and Subsidence of Baffin Bay

Although we did not reach our deep objective of reflector R3 (this reflector terminology bears no relationship to that informally used for one in the northeastern North Atlantic) at about 1565 mbsf, extrapolation of sedimentation rates give it an Eocene/Oligocene age. The drilling results and the constraints they impose on age models for the entire sequence observed in seismic lines are important because they also help to constrain tectonic models of the formation of Baffin Bay. For example, if Baffin Bay were formed by seafloor spreading or crustal stretching during the Tertiary, then its margin must show subsidence similar to that observed elsewhere along passive margins. The drilling results from Site 645, together with other subsurface information can then be used to study the subsidence history of the western Baffin Bay margin.

Many approaches have been used to study the subsidence history of passive margins (for details see Watts and Steckler, 1979), and they all show that the subsidence of passive margins with time is caused by two main factors: the loading effect of the overlying sediments (and water), and the thermal contraction of the lithosphere with time and/or the extent of crustal thinning. If the loading effect from the overlying sediments can be removed, then we can isolate that part of the subsidence not caused by the weight of the sediments. For this exercise, we need detailed biostratigraphic and lithologic information. However, from the somewhat limited information available on the deeper part of the section and from Site 645 data, we made the following assumptions:

1. The age of the R3 reflector, which lies at an approximate depth of 1565 mbsf, is Eocene/Oligocene (36 Ma). Extrapolation of the sedimentation rate of Subunit IIIC (about 42 m/

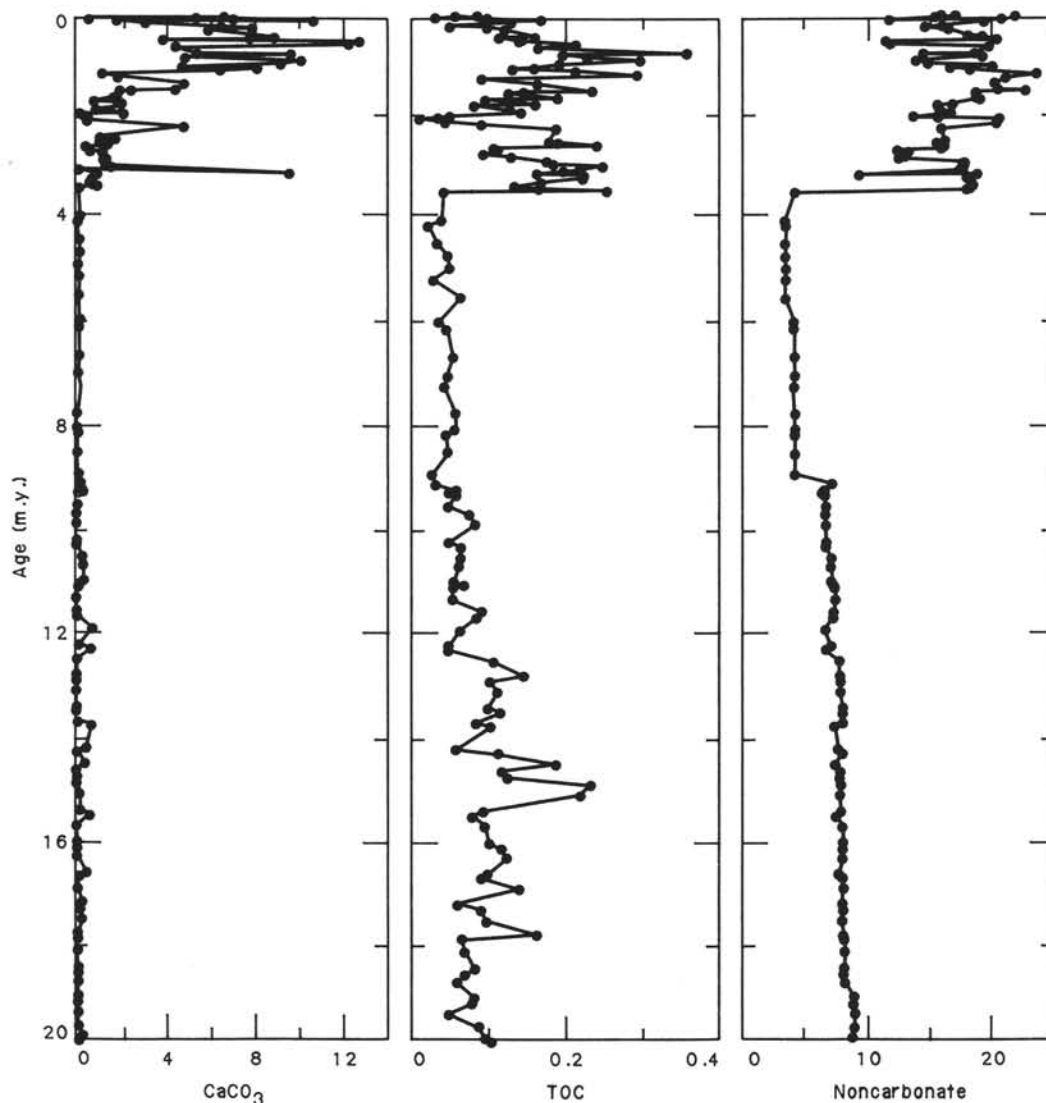


Figure 59. Accumulation rates of (A) total carbonate minerals (expressed as CaCO_3), (B) organic carbon (showing estimated proportions of marine versus terrigenous organic matter), and (C) detrital siliciclastic material. All are expressed in $\text{g/cm}^2/\text{k.y.}$

m.y.) to this reflector results in an age of 33 Ma for this reflector, which is not excessively different from 36 Ma, considering the long range of species used in deriving the average rate of sedimentation.

2. If we assume a reasonable sedimentation rate, similar to or higher than that observed in the overlying sequence (i.e., $>42 \text{ m/m.y.}$), then the underlying basement surface at Site 645 is no older than Late Cretaceous (72 Ma). This is the same age as the initiation of seafloor spreading in the Labrador Sea and the extension in Baffin Bay. This same argument indicates that minimum age of the basement is early Eocene. This younger (55 Ma) age for the basement surface is also favored by the presence of probable basalt flows noted in seismic lines over the slope and shelf west of Site 645, which we believe to be middle Paleocene in age, on the basis of dating of a similar sequence on West Greenland.

At Site 645, we followed the backstripping method that Watts and Steckler (1979) used to calculate the loading effect caused by the overlying sediments and water column; the results are shown in Figure 60. The resulting subsidence plot shows that

since the early Oligocene (36 Ma), the rate of "tectonic" (unloaded) subsidence of the crust underlying Site 645 has been exponential, as expected from a thermal-contraction hypothesis. Furthermore, the rate of subsidence before 36 Ma is not definite; three possibilities are presented on the basis of an assigned age of the basement surface of (1) 72 Ma, (2) 63 Ma, (3) 55 Ma. The 55-Ma age lies more or less in line with the "best-fit" exponential trend for age versus depth.

The resulting rate of basement subsidence under Site 645 shows that it is largely caused by stretching and thinning or thermal contraction of the lithosphere, as expected in regions of transitional crust formed by rifting and seafloor spreading. Crustal extension across the Baffin Island margin probably caused thinning and subsidence of this crustal block, but seafloor spreading better explains the anomalously thin crust (5 km versus 9 km thick for normal oceanic crust) in the central part of Baffin Bay (Keen and Peirce, 1982). The results of our preliminary backstripping model, combined with other geophysical constraints, therefore, indicate that a combination of crustal thinning and subsidence as well as limited seafloor spreading most satisfactorily account for the formation of Baffin Bay, and that

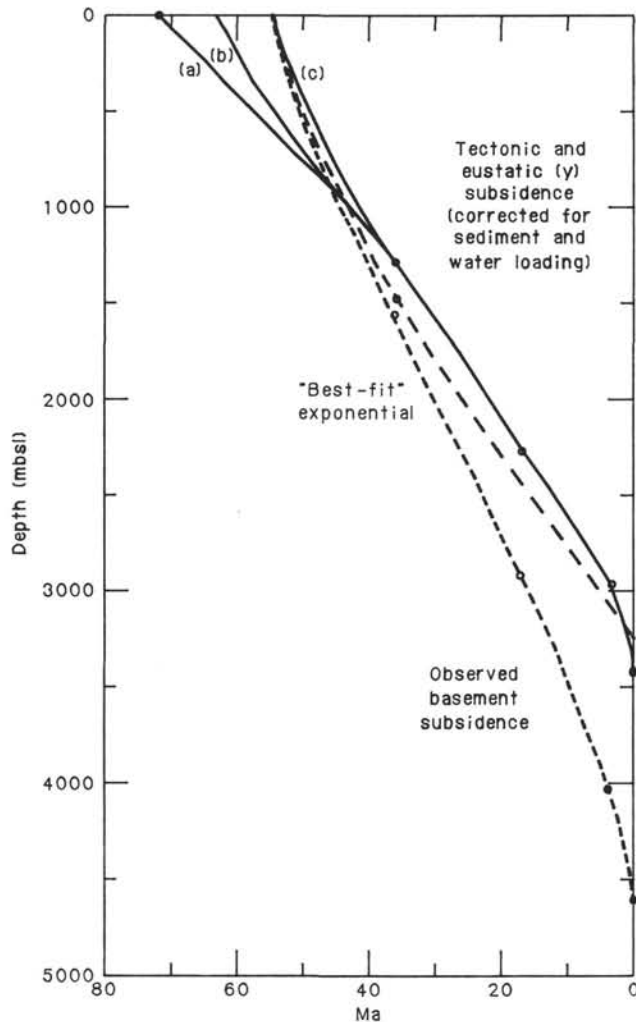


Figure 60. Plot of observed basement subsidence and subsidence calculated by correcting for sediment-induced and water-loading-induced subsidences (isostatic adjustment). Estimates of average paleowater depths are as follows: 0 Ma, 2020 m; 3.4 Ma, 1600 (± 200) m; 16.5 Ma, 750 (± 150) m; 36 Ma, 450 (± 150) m; 55 Ma, 0 m. See text for details.

the period from 55 Ma to 36 Ma was probably the main interval of spreading, as suggested by Srivastava et al. (1981).

The main period of faulting, tilting, basaltic volcanism, and rapid subsidence of basement blocks on the Baffin margin apparently occurred between the Late Cretaceous and early Eocene. Subsidence and sedimentation have continued to the Holocene, whereas seafloor spreading probably ceased by the end of the Eocene (Srivastava et al., 1981). This is supported by the fact that the reflector R3, which we gave an extrapolated age of 36–33 Ma, extends across Baffin Bay, even crossing the pronounced central graben. Extensional faults can be observed in seismic lines (Fig. 58); these faults affect only upper Pliocene and older strata but do not appear to profoundly affect strata below R3. We interpret the faulting as being related to differential compaction and not to an episode of later tectonism.

Correlation of drilling results, measurements of physical properties, and evaluation of seismic data at the site will allow further correlation of events across much of the basin. Geophysical logs were obtained for only slightly more than 200 m of the sequence because of hole problems. A detailed set of organic and inorganic geochemical analyses is providing a good understanding of the diagenesis of this terrigenous sequence.

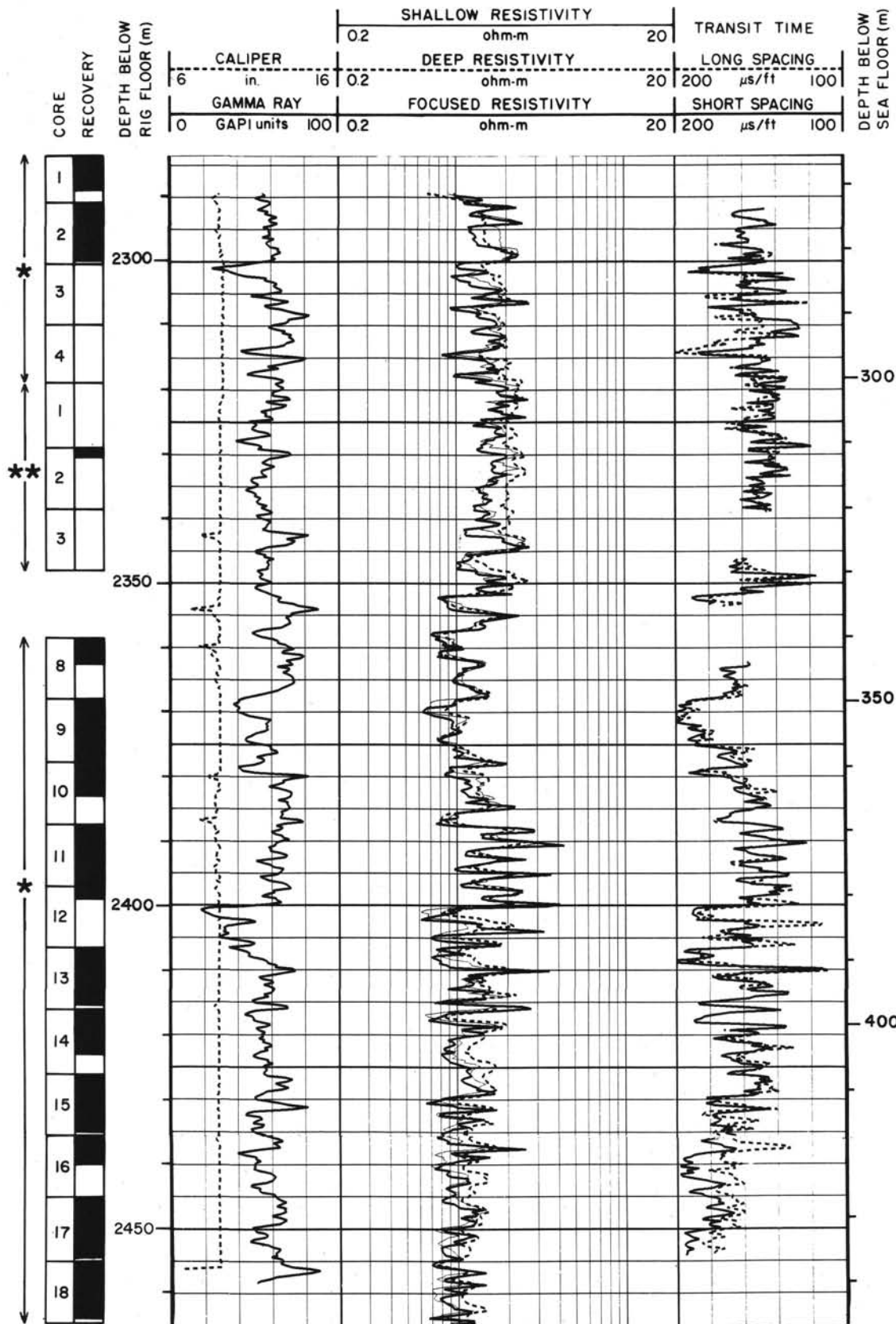
REFERENCES

- Aksu, A. E., 1981. Late Quaternary stratigraphy, paleoenvironmentology and sedimentation history of Baffin Bay and Davis Strait [Ph.D. thesis]. Dalhousie University, Halifax, Nova Scotia.
- _____, A. E., 1983. Holocene and Pleistocene dissolution cycles in deep-sea cores of Baffin Bay and Davis Strait: palaeoceanographic implications. *Mar. Geol.*, 53:331–348.
- _____, A. E., 1984. Subaqueous debris flow deposits in Baffin Bay. *Geomar. Lett.*, 4:83–90.
- Aksu, A. E., and Mudie, P. J., 1985. Magnetostratigraphy and palynology demonstrate at least 4 million years of Arctic Ocean sedimentation. *Nature*, 318:280–283.
- Aksu, A. E., and Piper, D.J.W., in press. Late Quaternary sedimentation in Baffin Bay. *Can. J. Earth Sci.*
- Andrews, J. T., Shilts, W. W., and Miller, G. H., 1983. Multiple deglaciations of the Hudson Bay lowlands, Canada, since deposition of the Missinaibi (last-interglacial?) formation. *Quat. Res.*, 19:18–37.
- Arthur, M. A., Dean, W. E., and Stow, D.A.V., 1984. Models for the deposition of Mesozoic-Cenozoic fine-grained organic-carbon-rich sediments in the deep sea. In Stow, D.A.V., and Piper, D.J.W. (Eds.), *Fine-Grained Sediments: Deep-Water Processes and Facies*, Geol. Soc. London, Spec. Publ.: 15: 527–560.
- Baldauf, J. G., 1981. Identification of the Holocene/Pleistocene boundary in the Bering Sea by diatoms. *Boreas*, 11:113–118.
- Banerjee, S. K., King, J., and Marvin, J., 1981. A rapid method for magnetic granulometry with applications to environmental studies. *Geophys. Res. Lett.*, 8:333–336.
- Bé, A.W.H., and Tolderlund, D. S., 1971. Distribution and ecology of living planktonic foraminifera in surface waters of the Atlantic and Indian oceans. In Funnell, B. M., and Riedel, W. R. (Eds.), *The Micropaleontology of Oceans*: Cambridge (Cambridge University Press), 105–149.
- Berger, A. L., 1978. Long-term variations of caloric insulation resulting from the earth's orbital elements. *Quat. Res.*, 9:139–167.
- Berggren, W. A., 1972. Cenozoic biostratigraphy and paleobiogeography of the North Atlantic. In Laughton, A. S., Berggren, W. A., et al., *Init. Repts. DSDP*, 12: Washington (U.S. Govt. Printing Office), 965–1002.
- Berggren, W. A., Kent, D. V., and van Couvering, J. A., 1986. Neogene geochronology and chronostratigraphy. In Snelling, N. J., (Ed.) *Geochronology and the Geologic Time Scale*: Geol. Soc. London, Mem., 10:211–250.
- Berggren, W. A., and Schnitker, D., 1983. Cenozoic marine environments in the North Atlantic and Norwegian-Greenland Sea. In Bott, M.H.P., Saxov, S., Talwani, M., Thiede, J. (Eds.), *Structure and Development of the Greenland-Scotland Ridge—New Methods and Concepts*. NATO Conference Series IV, 8:495–548.
- Björklund, K. R., 1976. Radiolarians from the Norwegian Sea, Leg 38 of the Deep Sea Drilling Project. In Talwani, M., Udintsev, G., et al., *Init. Repts. DSDP*, 38: Washington (U.S. Govt. Printing Office), 1101–1168.
- Blatt, H., Middleton, G., and Murray, R., 1980. *Origin of Sedimentary Rocks* (2nd ed.): Englewood Cliffs, NJ (Prentice-Hall).
- Blow, W. H., 1969. Late middle Eocene to Recent planktonic foraminiferal biostratigraphy. In Bronnimann, P., and Renz, H. H. (Eds.), *Proc., First Int. Conf. Planktonic Microfossils*, Geneva, Vol. 1: Leiden (E. J. Brill), 199–422.
- Bramlette, M. N., and Wilcoxon, J. A., 1967. Middle Tertiary calcareous nannoplankton of the Cipero Section, Trinidad, W. I. *Tulane Studies in Geology and Paleontology*, 5:93–131.
- Brown, S., and Downie, C., 1985. Dinoflagellate cyst stratigraphy of Paleogene to Miocene sediments from the Goban Spur (Sites 548–550, Leg 80). In de Graciansky, P. C., Poag, C. W., et al., *Init. Repts. DSDP*, 80: Washington (U.S. Govt. Printing Office), 643–651.
- Bryant, W. R., and Trabant, P. K., 1972. Statistical relationships between geotechnical properties of Gulf of Mexico sediments: *Proc., Fourth Ann. Offshore Tech. Conf.*, Houston, 363–368.
- Bujak, J. P., 1984. Cenozoic dinoflagellate cysts and acritarchs from the Bering Sea and northern North Pacific, DSDP Leg 19. *Micropaleontology*, 30:180–212.
- Bulfinch, D. L., and Ledbetter, M. T., 1984. Deep western boundary undercurrent delineated by sediment texture at base of North American continental rise. *Geomar. Lett.*, 3:31–36.

- Carter, L., and Schafer, C. T., 1983. Interaction of the western boundary undercurrent with the continental margin off Newfoundland. *Sedimentology*, 30:751-768.
- Chough, S. K., and Hesse, R., 1980. The northwest Atlantic mid-ocean channel of the Labrador Sea: III. head spill vs. body spill deposits from turbidity currents on natural levees. *J. Sed. Pet.*, 59:227-234.
- Clark, D. B., and Pedersen, A. K., 1976. Tertiary volcanic province of West Greenland. In Escher, A., Watt, W. S. (Eds.), *Geology of Greenland*; Copenhagen (Geological Survey of Greenland), 365-385.
- Clark, D. L., 1982. Origin, nature and world climate effect of Arctic Ocean ice-cover. *Nature*, 300:321-325.
- Collinson, D. W., 1983. *Methods in Rock Magnetism and Paleomagnetism: Techniques and Instrumentation*: London (Chapman and Hall).
- Costa, L. I., and Downie, C., 1979. Cenozoic dinocyst stratigraphy of Sites 403 and 406 (Rockall Plateau), Leg 48. In Montadert, L., Roberts, D. G., et al., *Init. Repts. DSDP*, 48: Washington (U.S. Govt. Printing Office), 513-529.
- Dale, B., 1976. Cyst formation, sedimentation and preservation: factors affecting Dinoflagellate assemblages in recent sediments from Trondheimsfjord, Norway. *Rev. Paleobot. Palyn.*, 22:36-60.
- de Vernal, A., 1986. Analyses palynologiques et isotopiques de sédiments de la baie de Baffin et de la mer du Labrador: Éléments d'une climatostratigraphie de Pléistocène supérieur dans l'est du Canada [Ph.D. dissert.]. Université de Montréal, Canada.
- Dionne, J.-C., 1972. Caractéristiques des blocs erratiques des rives de l'Estuaire du Saint-Laurent. *Rev. Géograph. Montréal*, 26:125-152.
- Edwards, L. E., 1985. Miocene dinocysts from Deep Sea Drilling Project Leg 81, Rockall Plateau, eastern North Atlantic Ocean. In Roberts, D. G., Schnitker, D., et al., *Init. Repts. DSDP*, 81: Washington (U.S. Govt. Printing Office), 581-594.
- Eldholm, O., Thiede, J., Taylor, E., et al., in press. *Proc. Init. Repts., ODP*, 104.
- Ericson, D. B., 1959. Coiling direction of *Globigerina pachyderma* as a climatic index. *Science*, 130:210-220.
- Espitalie, J., Madec, M., and Tissot, B. P., 1977. Source rock characterization method for petroleum exploration. *Proc., Ninth Ann. Offshore Tech. Conf.*, Houston, 439-448.
- Gartner, S., 1977. Calcareous nannofossil biostratigraphy and revised zonation of the Pleistocene. *Mar. Micropaleontol.*, 2:1-25.
- Gieskes, J. M., 1974. Interstitial water studies, Leg 25. In Simpson, E.S.W., Schlich, R., et al., *Init. Repts. DSDP*, 25: Washington (U.S. Govt. Printing Office), 361-394.
- Gieskes, J. M., 1983. The chemistry of interstitial waters of deep sea sediments: interpretation of Deep Sea Drilling data. In Riley, J. P., and Chester, R. (Eds.), *Chemical Oceanography* (Vol. 8): New York (Academic Press), 221-269.
- Goll, R. M., and Björklund, K. R., 1971. Radiolaria in surface sediments of the South Atlantic. *Micropaleontology*, 20:38-75.
- Gonthier, E. G., Faugères, J.-C., and Stow, D.A.V., 1984. Contourite facies of the Faro Drift, Gulf of Cadiz. In Stow, D.A.V., and Piper, D.J.W. (Eds.), *Fine-Grained Sediments: Deep-Water Processes and Facies*. Geol. Soc. Am. Spec. Publ., 15:275-292.
- Gradstein, E., and Berggren, W. A., 1981. Flysch-type agglutinated foraminifera and the Maestrichtian to Paleogene history of the Labrador and North Seas. *Mar. Micropaleontol.*, 6:211-268.
- Gradstein, F. M., and Srivastava, S. P., 1980. Aspects of Cenozoic stratigraphy and paleoceanography of the Labrador Sea and Baffin Bay. *Palaeogeogr., Palaeoclimatol., Palaeoecol.*, 30:261-295.
- Grant, A. C., 1980. Problems with plate tectonics: the Labrador Sea. *Bull. Can. Pet. Geol.*, 28:252-278.
- _____, 1982. Problems with plate tectonic models for Baffin Bay-Nares Strait: evidence from the Labrador Sea. In *Meddelelser om Gronland, Geoscience*, 8:313-326.
- Grant, W. D., Williams, A. J., III, and Gross, T. F., 1985. A description of the bottom boundary layer at the HEBBLE site: low frequency forcing, bottom stress and temperature structure. *Mar. Geol.*, 66: 219-241.
- Hamilton, E. L., 1976. Variations of density and porosity with depth in deep-sea sediments. *J. Sed. Pet.*, 46:280-300.
- Harland, R., 1978. Quaternary and Neogene dinoflagellate cysts. In Thustu, B. (Ed.), *Distribution of Diagnostic Dinoflagellate Cysts and Miospores From the Northwest European Continental Shelf and Adjacent Areas*; Norway (Continental Shelf Institute), 100:7-17.
- _____, 1979. Dinoflagellate biostratigraphy of Neogene and Quaternary sediments at Holes 400/400A in the Bay of Biscay (DSDP Leg 48). In Montadert, L., Roberts, D. G., et al., *Init. Repts. DSDP*, 48: Washington (U.S. Govt. Printing Office), 531-545.
- _____, 1983. Distribution maps of recent dinoflagellate cysts in bottom sediments from the North Atlantic Ocean and adjacent seas. *Palaeontology*, 26:321-387.
- Harrison, W. E., Hesse, R., and Gieskes, J. M., 1982. Relationship between sedimentary facies and interstitial water chemistry of slope, trench, and Cocos Plate sites from the Middle America Trench transect, active margin off Guatemala, Deep Sea Drilling Project Leg 67. In Aubouin, J., von Huene, R., et al., *Init. Repts. DSDP*, 67: Washington (U.S. Govt. Printing Office), 603-616.
- Heezen, B. C., Hollister, C. D., and Ruddiman, W. F., 1966. Shaping of the continental rise by deep geostrophic contour currents. *Science*, 152:502-508.
- Henderson, G., Schiener, E. J., Risum, J. B., Croxton, C. A., and Andersen, B. B., 1981. The West Greenland Basin. In Kerr, J. W., Fergusson, A. J., and Machan, L. C. (Eds.), *Geology of North Atlantic Borderlands*: Calgary (Can. Soc. of Pet. Geol.) CSPG Mem. 7:399-428.
- Herman, Y., 1974. Arctic Ocean sediments, microfauna, and the climatic record in late Cenozoic time. In Herman, Y. (Ed.), *Marine Geology and Oceanography of the Arctic Seas*: Berlin (Springer Verlag), 283-348.
- Hollister, C. D., and Heezen, B. C., 1972. Geologic effects of ocean bottom currents: western North Atlantic. In Gordon, A. L. (Ed.), *Studies in Physical Oceanography 2*: New York (Gordon and Breach), 37-66.
- Hollister, C. D., and McCave, I. N., 1984. Sedimentation under deep-sea storms. *Nature*, 309:220-225.
- Keen, C. E., and Barrett, D. L., 1972. Seismic refraction studies in Baffin Bay: an example of a developing ocean basin. *Geophys. J. R. Astron. Soc.*, 30:253-271.
- Keen, C. E., Keen, M. J., Ross, D. I., and Lack, M., 1974. Baffin Bay: small ocean basin formed by sea-floor spreading. *AAPG Bull.*, 58: 1089-1108.
- Keen, C. E., and Peirce, J. W., 1982. The geophysical implications on minimal Tertiary motion along Nares Strait. In *Meddelelser om Gronland, Geoscience*, 8:327-337.
- Keller, G. H., and Bennett, R. H., 1970. Variations in the mass physical properties of selected submarine sediments. *Mar. Geol.*, 9:215-223.
- Kerr, J. W., 1967. A submerged continental remnant beneath the Labrador Sea. *Earth Planet. Sci. Lett.*, 2:283-289.
- King, J., Banerjee, S. K., Marvin, J., and Ozdemir, Ö. 1982. A comparison of different magnetic methods for determining the relative grain size of magnetite in natural materials: some results from lake sediments. *Earth Planet. Sci. Lett.*, 59:404-419.
- Klose, G. W., Malterre, E., McMillan, N. J., and Zinkan, C. G., 1982. Petroleum exploration offshore southern Baffin Island, Northern Labrador Sea, Canada. In Embry, A. F., and Balkwill, H. R. (Eds.), *Arctic Geology and Geophysics*: Calgary (Can. Soc. Pet. Geol.) CSPG Mem. 8:245-265.
- Koizumi, I., 1973. The late Cenozoic diatoms of Sites 183-193, Leg 19, Deep Sea Drilling Project. In Creager, J. S., Scholl, D. W., et al., *Init. Repts. DSDP*, 19: Washington (U.S. Govt. Printing Office), 805-856.
- Kvenvolden, K. A., and Barnard, L. A., 1983. Gas hydrates of the Blake Outer Ridge, Site 533, Deep Sea Drilling Project Leg 76. In Sheridan, R. E., Gradstein, F. M., et al., *Init. Repts. DSDP*, 76: Washington (U.S. Govt. Printing Office), 353-366.
- Kvenvolden, K. A., and McDonald, T. J., 1985a. Organic Geochemistry on the JOIDES Resolution—an assay. In Eldholm, O., Thiede, J., Taylor, E., et al., *Proc. Init. Repts. (Pt. A); ODP*, 104.
- _____, 1985b. Organic geochemistry report Site 643. In Eldholm, O., Thiede, J., Taylor, E., et al., in press. *Proc., Init. Repts. (Pt. A), ODP*, 104.
- Lagoe, M. B., 1979. Recent benthonic foraminiferal biofacies in the Arctic Ocean. *Micropaleontology*, 25:214-224.
- Manheim, F. T., and Sayles, F. L., 1974. Composition and origin of interstitial waters of marine sediments, based on deep sea drill cores. In Goldberg, E. D. (Eds.), *The Sea* (Vol.5): New York (Wiley-Interscience), 527.

- Manum, S., 1976. Dinocysts in Tertiary Norwegian-Greenland Sea sediments (Deep Sea Drilling Project Leg 38) with observations on palynomorphs and palynodebris in relation to environment. In Talwani, M., Udintsev, G., et al., *Init. Repts. DSDP*, 38: Washington (U.S. Govt. Printing Office), 897-919.
- Martini, E., 1971. Standard Tertiary and Quaternary calcareous nannoplankton zonation. *Proc., Second Planktonic Conf., Rome, 1970*, 2: 739-785.
- Matthews, D. J., 1939. Table of Velocity of Sound in Pore Water and in Seawater: London (Admiralty, Hydrographic Dept.).
- Mayer, L. A., 1982. Physical properties of sediment recovered on Deep Sea Drilling Project Leg 68 with the hydraulic piston corer. In Prell, W. L., Gardner, J. V., et al., *Init. Repts. DSDP*, 68: Washington (U.S. Govt. Printing Office), 365-382.
- McIver, R., 1975. Hydrocarbon occurrence from JOIDES Deep Sea Drilling Project. *Proc., Ninth Pet. Congr.*, 269-280.
- Moore, D. G., 1964. Shear strength and related properties of sediments from experimental Mohole (Guadalupe site). *J. Geophys. Res.*, 69: 4271-4291.
- Moore, D. G., and Shumway, G., 1959. Sediment thickness and physical properties: Pigeon Point Shelf, California. *J. Geophys. Res.*, 64: 367-374.
- Morton, A. C., Merriman, R. J., and Mitchell, J. G., 1984. Genesis and significance of glauconitic sediments of the southwest Rockall Plateau. In Roberts, D. G., Schnitker, D., et al., *Init. Repts. DSDP*, 81: Washington (U.S. Govt. Printing Office), 645-651.
- Mudie, P. J., in press. Palynology and dinoflagellate biostratigraphy of DSDP Leg 94, Sites 607 and 611, North Atlantic Ocean. In Ruddiman, W. F., Kidd, R., et al., *Init. Repts. DSDP*, 94: Washington (U.S. Govt. Printing Office).
- Mudie, P. J., and Aksu, A. E., 1984. Palaeoclimate of Baffin Bay from 300,000-year record of foraminifera, dinoflagellates and pollen. *Nature*, 312:630-634.
- Mudie, P. J., and Deonarine, B., 1983. Dinoflagellates and pollen from plankton tows and surface sediments, Baffin Island Fjords. In Syvitski, J.P.M., and Blakeney, C. P. (Eds.), *Sedimentology of Arctic Fjords*: Can. Rept. Hydrogra. Ocean Sci., 12:20-1-20-7.
- Mudie, P. J., and Short, S. K., 1985. Marine palynology of Baffin Bay. In Andrews, J. T. (Ed.), *Quaternary History of Baffin Island, Baffin Bay and Greenland*: London (Allen and Unwin), 263-308.
- Müller, C., 1976. Tertiary and Quaternary calcareous nannoplankton in the Norwegian-Greenland Sea, DSDP Leg 38. In Talwani, M., Udintsev, G., et al., *Init. Repts. DSDP*, 38: Washington (U.S. Govt. Printing Office), 823-841.
- Müller, P. J., and Suess, E., 1979. Productivity, sedimentation rate, and sedimentary organic carbon content in the oceans. 1. organic carbon preservation. *Deep-Sea Res.*, 26A:1347-1362.
- Murray, J. W., 1985. Paleogene and Neogene benthic foraminifers from Rockall Plateau. In Roberts, D. G., Schnitker, D., et al., *Init. Repts. DSDP*, 81: Washington (U.S. Govt. Printing Office), 503-534.
- Peters, K. E., and Simoneit, B.R.T., 1982. Rock-Eval pyrolysis of Quaternary sediments from Leg 64, Sites 497 and 480, Gulf of California. In Curray, J. R., Moore, D. G., et al., *Init. Repts. DSDP*, 64: Washington (U.S. Govt. Printing Office), 925-931.
- Piasecki, S., 1980. Dinoflagellate cyst stratigraphy of the Miocene Huddle and Gram Formations. *Bull. Geol. Soc. Den.*, 19:53-76.
- Richardson, M. J., Wimbush, M., and Mayer, L., 1981. Exceptionally strong near-bottom flows on the continental rise of Nova Scotia. *Science*, 213:887-888.
- Roberts, D. G., Schnitker, D., et al., 1984. *Init. Repts. DSDP*, 81: Washington (U.S. Govt. Printing Office).
- Rolle, F., 1985. Late Cretaceous-Tertiary sediments offshore central West Greenland: lithostratigraphy, sedimentary evolution, and petroleum potential. *Can. J. Earth Sci.*, 22:1001-1019.
- Ruddiman, W. F., Kidd, R., et al., in press. *Init. Repts. DSDP*, 94: Washington (U.S. Govt. Printing Office).
- Ruddiman, W. F., and McIntyre, A., 1981a. Oceanic mechanisms for amplification of the 23,000-year ice-volume cycle. *Science*, 212:617-627.
- _____, 1981b. The North Atlantic Ocean during the last deglaciation. *Palaeogeogr., Palaeoclim., Palaeoecol.*, 35:145-214.
- Sancetta, C., 1982. Distribution of diatom species in surface sediments of the Bering and Okhotsk seas. *Micropaleontology*, 28:221-257.
- Silva, A. J., 1974. Marine geomechanics: overview and projections. In Inderbitzen, A. (Ed.), *Deep Sea Sediments: Physical and Mechanical Properties*: New York (Plenum Press), 45-76.
- Srivastava, S. P., Falconer, R.K.H., and MacLean, B., 1981. Labrador Sea, Davis Strait, Baffin Bay: geology and geophysics—a review. In Kerr, J. W., Fergusson, A. J., and Machan, L. C. (Eds.), *Geology of the North Atlantic Borderlands*: Calgary (Can. Soc. Pet. Geol.) CSPG Mem. 7:333-398.
- Srivastava, S. P., and Tapscoff, C. R., 1986. Plate kinematics of the North Atlantic. In Vogt, P. R. and Tucholke, B. E., (Eds.), *The Geology of North Atlantic: The Western Atlantic Region*: Geological Society of America, DNAG Series, Vol. M:379-404.
- Stein, R., in press. Organic carbon and sedimentation rate—further evidence for stagnation episodes in the Cenomanian/Turonian Atlantic Ocean. *Mar. Geol.*, 72.
- Stein, R., Rullkötter, J., and Welte, D. H., in press. Accumulation of organic-carbon-rich sediments in the Late Jurassic and Cretaceous Atlantic Ocean—a synthesis. *Chem. Geol.*, 56.
- Stow, D.A.V., and Holbrook, J. A., 1984. North Atlantic contourites: an overview. In Stow, D.A.V., and Piper, D.J.W. (Eds.), *Fine-Grained Sediments: Deep-Water Processes and Facies*. Geol. Soc. Am. Spec. Publ., 15:245-256.
- Thorson, R. M., and Bender, G., 1985. Eolian deflation by ancient katabatic winds: a late Quaternary example from the North Alaska Range. *Geol. Soc. Am. Bull.*, 96:702-709.
- Thunell, R. C., 1976. Calcium carbonate dissolution in late Quaternary deep-sea sediments, western Gulf of Mexico. *Quat. Res.*, 6:281-297.
- Tissot, B. P., and Welte, D. H., 1984. *Petroleum Formation and Occurrence*: Heidelberg (Springer-Verlag).
- Verdenius, J. G., and van Hinte, J. E., 1983. Central Norwegian-Greenland Sea; Tertiary arenaceous foraminifera, biostratigraphy and environment. In Verdenius, J. G., van Hinte, J. E., and Fortuin, A. R. (Eds.), *Proc., First Workshop Arenaceous Foraminifera*: Norway (Continental Shelf Institute), 108:173-224.
- Watts, A. B., and Steckler, M. S., 1979. Subsidence and eustasy at the continental margin of eastern North America. In Talwani, M., Hay, W. W., and Ryan, W.B.F. (Eds.), *Deep Drilling Results in the Atlantic Ocean: Continental Margins and Paleoenvironment*: Washington (Am. Geophys. Union), Maurice Ewing Series, 3:218-234.
- West, R. M., Dawson, M. R., Hickey, L. J., and Miall, A. D., 1981. Upper Cretaceous and Paleogene sedimentary rocks, eastern Canadian Arctic and related North Atlantic areas. In Kerr, J. W., Fergusson, A. J., and Machan, L. C., *Geology of the North Atlantic Borderlands*: Can. Soc. Pet. Geol., Mem. 7:279-298.
- Zimmerman, H. B., 1984. Lithostratigraphy and clay mineralogy of the western margin of the Rockall Plateau and the Hatton sediment drift. In Roberts, D. G., Schnitker, D., et al. *Init. Repts. DSDP*, 81: Washington (U.S. Govt. Printing Office), 683-693.
- Zimmerman, H. B., Boersma, A., and McCoy, F. W., in press. Carbonaceous sediments and paleoenvironment of the Cretaceous South Atlantic Ocean. In Brooks, J., and Fleet, A. J. (Eds.), *Marine Petroleum Source Rocks*: Geol. Soc. London, Spec. Publ.

Summary log for Hole 645E

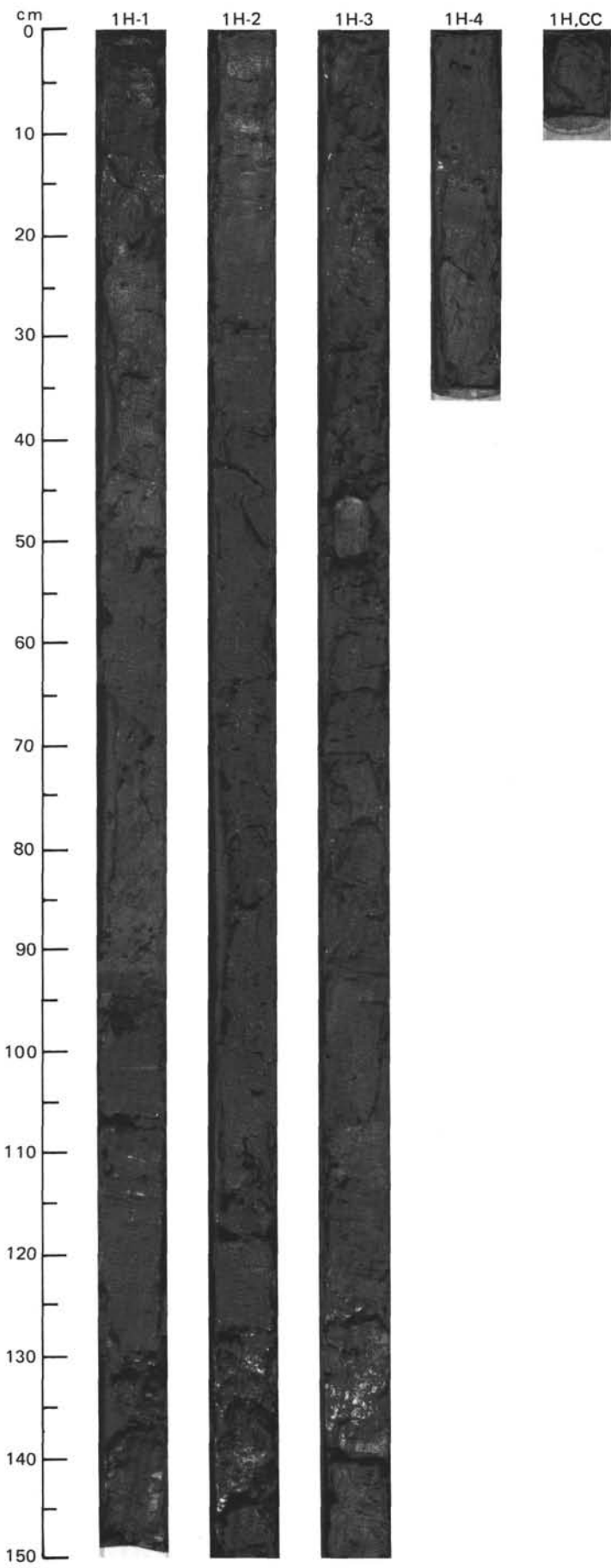


* cores from Hole 645D ** cores from Hole 645E

SITE 645 HOLE A CORE 1H CORED INTERVAL 2007.1-2012.04 mbsl; 0-4.94 mbsf

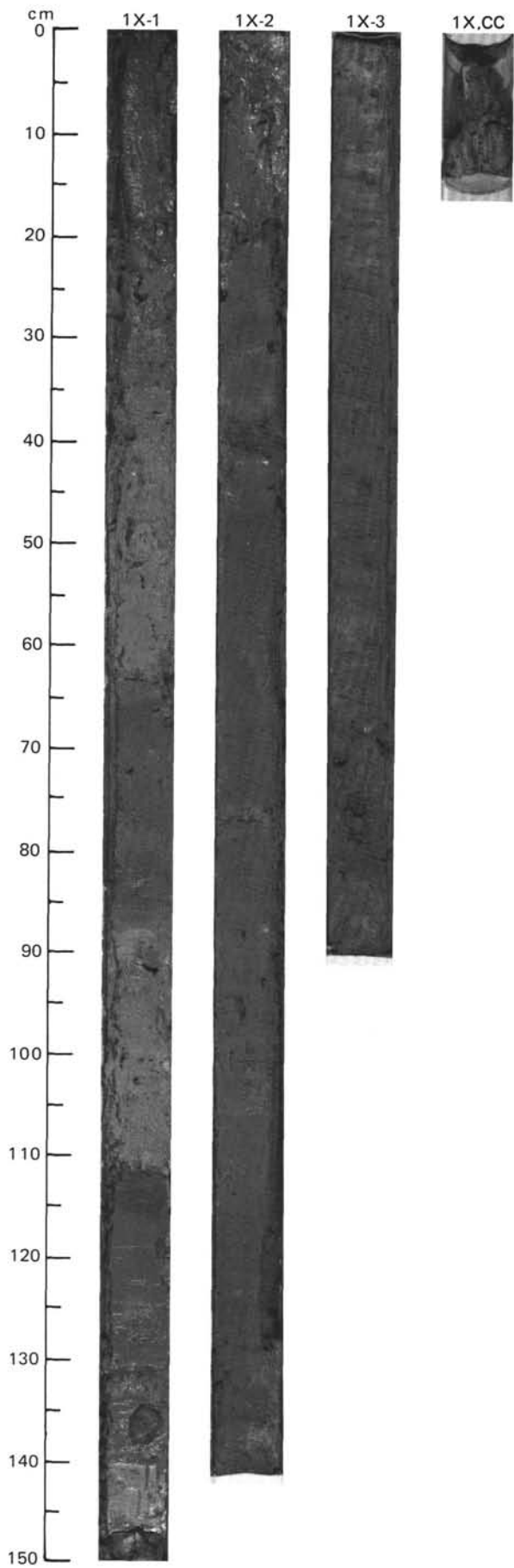
TIME-ROCK UNIT	BIOSTRAT. ZONE/ FOSSIL CHARACTER				PALEOMAGNETICS	PHYS. PROPERTIES	CHEMISTRY	SECTION	METERS	GRAPHIC LITHOLOGY	DRILLING DISTURB.	SED. STRUCTURES	SAMPLES	LITHOLOGIC DESCRIPTION																																																							
	FORAMINIFERS	MANNOFOSSILS	RADIOLARIANS	DIATOMS																																																																	
														<p>GRAVEL-BEARING MUDDY SAND TO SILTY MUD</p> <p>Gravel-bearing detrital carbonate muddy sand to locally silty mud, gray (5Y 6/1) with vague color mottling. This core shows no primary structures and contains a range of gravel sizes from granule to cobble (max. 6 cm), granules and fine pebbles being most abundant.</p> <p>Minor lithologies: a. Section 1, 0-12 cm: brown (7.5YR 4/4) silty mud with very little sand or coarser detritus. b. Section 1, 92-115 cm: alternations of dark silty mud and about 1-cm-thick medium- to coarse-grained muddy sand layers with gradational boundaries. c. Section 1, 115-130 cm: very fine-grained, faintly mottled, light olive gray (5Y 6/2) silty clay with no sand or coarser detritus.</p> <p>SMEAR SLIDE SUMMARY (%):</p> <table border="1"> <tr> <td></td> <td>1, 7</td> <td>1, 88</td> <td>1, 121</td> <td>3, 98</td> </tr> <tr> <td></td> <td>M</td> <td>D</td> <td>M</td> <td>D</td> </tr> </table> <p>TEXTURE:</p> <table border="1"> <tr> <td>Sand</td> <td>30</td> <td>10</td> <td>—</td> <td>10</td> </tr> <tr> <td>Silt</td> <td>50</td> <td>70</td> <td>30</td> <td>70</td> </tr> <tr> <td>Clay</td> <td>20</td> <td>20</td> <td>70</td> <td>20</td> </tr> </table> <p>COMPOSITION:</p> <table border="1"> <tr> <td>Quartz</td> <td>10</td> <td>30</td> <td>10</td> <td>30</td> </tr> <tr> <td>Feldspar</td> <td>20</td> <td>10</td> <td>—</td> <td>10</td> </tr> <tr> <td>Rock fragments</td> <td>5</td> <td>5</td> <td>—</td> <td>5</td> </tr> <tr> <td>Clay</td> <td>20</td> <td>20</td> <td>70</td> <td>20</td> </tr> <tr> <td>Calcite/dolomite</td> <td>40</td> <td>30</td> <td>15</td> <td>30</td> </tr> <tr> <td>Accessory minerals</td> <td>5</td> <td>5</td> <td>5</td> <td>5</td> </tr> </table>		1, 7	1, 88	1, 121	3, 98		M	D	M	D	Sand	30	10	—	10	Silt	50	70	30	70	Clay	20	20	70	20	Quartz	10	30	10	30	Feldspar	20	10	—	10	Rock fragments	5	5	—	5	Clay	20	20	70	20	Calcite/dolomite	40	30	15	30	Accessory minerals	5	5	5	5
	1, 7	1, 88	1, 121	3, 98																																																																	
	M	D	M	D																																																																	
Sand	30	10	—	10																																																																	
Silt	50	70	30	70																																																																	
Clay	20	20	70	20																																																																	
Quartz	10	30	10	30																																																																	
Feldspar	20	10	—	10																																																																	
Rock fragments	5	5	—	5																																																																	
Clay	20	20	70	20																																																																	
Calcite/dolomite	40	30	15	30																																																																	
Accessory minerals	5	5	5	5																																																																	

Information on Core Description Forms, for ALL sites, represents field notes taken aboard ship. Some of this information has been refined in accord with post-cruise findings, but production schedules prohibit definitive correlation of these forms with subsequent findings. Thus the reader should be alerted to the occasional ambiguity or discrepancy.

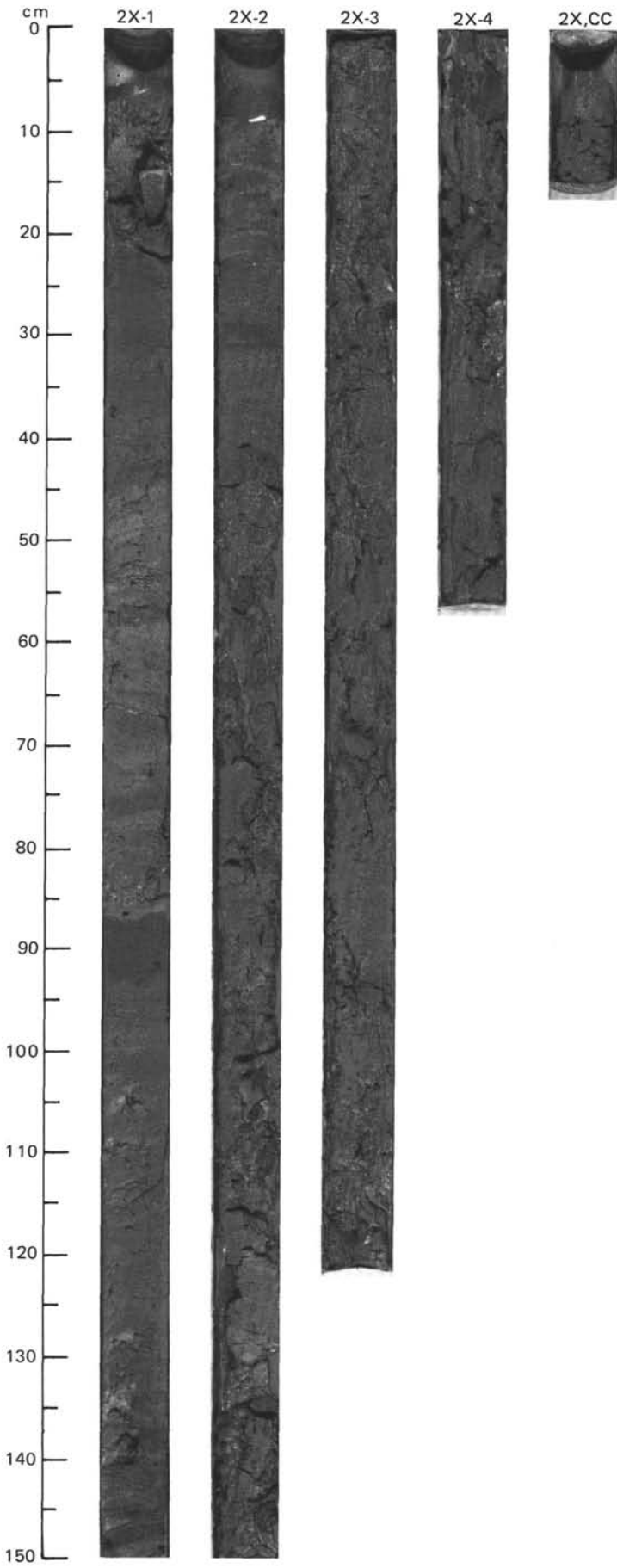


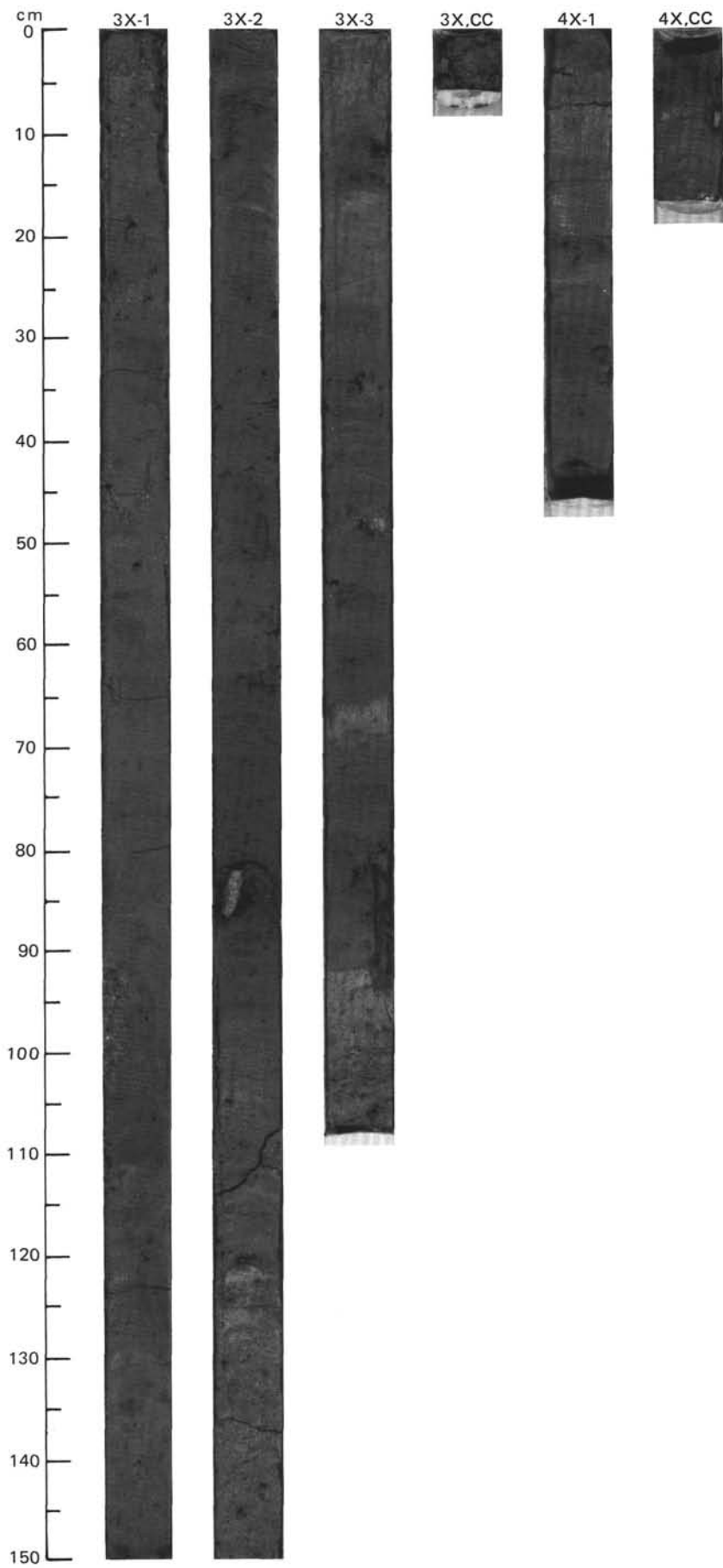
SITE 645 HOLE B CORE 1 X CORED INTERVAL 2008.2-2012.2 mbsl; 0.0-4.0 mbsf

TIME-ROCK UNIT	BIOSTRAT. ZONE/ FOSSIL CHARACTER					PALEOMAGNETICS	PHYS. PROPERTIES	CHEMISTRY	SECTION	METERS	GRAPHIC LITHOLOGY	DRILLING DISTURB.	SED. STRUCTURES	SAMPLES	LITHOLOGIC DESCRIPTION																																																																																																									
	FORAMINIFERS	NANNOFOSSILS	RADIOLARIANS	DIATOMS	DINOCYSTS																																																																																																																			
PLEISTOCENE-RECENT															<p>DETRICARBONATE MUDDY SAND</p> <p>Detriticarbonate muddy sand, light brown (10YR 3/4); grading downward to gravel-bearing detriticarbonate clayey and silty mud and silty clays, olive gray (5Y 4/2) to dark gray (5Y 4/1), in cyclically interbedded units, about 25-70 cm in thickness.</p> <p>Muddy sand, weak red (10Y 4/3), about 3-5 cm thick, cap dark gray clayey mud sequences.</p> <p>Sediments are relatively undeformed, with coarse sand and pebbles throughout.</p> <p>SMEAR SLIDE SUMMARY (%):</p> <table border="1"> <thead> <tr> <th></th> <th>1, 80 D</th> <th>1, 100 D</th> <th>2, 50 D</th> <th>3, 25 D</th> <th>3, 80 D</th> <th>5, 5 D</th> </tr> </thead> <tbody> <tr> <td>TEXTURE:</td> <td></td> <td></td> <td></td> <td></td> <td></td> <td></td> </tr> <tr> <td>Sand</td> <td>5</td> <td>40</td> <td>—</td> <td>20</td> <td>50</td> <td>10</td> </tr> <tr> <td>Silt</td> <td>45</td> <td>30</td> <td>40</td> <td>30</td> <td>30</td> <td>40</td> </tr> <tr> <td>Clay</td> <td>60</td> <td>30</td> <td>60</td> <td>50</td> <td>20</td> <td>50</td> </tr> </tbody> </table> <p>COMPOSITION:</p> <table border="1"> <thead> <tr> <th></th> <th>1, 80 D</th> <th>1, 100 D</th> <th>2, 50 D</th> <th>3, 25 D</th> <th>3, 80 D</th> <th>5, 5 D</th> </tr> </thead> <tbody> <tr> <td>Quartz</td> <td>25</td> <td>30</td> <td>25</td> <td>40</td> <td>50</td> <td>25</td> </tr> <tr> <td>Feldspar</td> <td>Tr</td> <td>Tr</td> <td>—</td> <td>10</td> <td>—</td> <td>Tr</td> </tr> <tr> <td>Rock frag., calcite</td> <td>5</td> <td>20</td> <td>—</td> <td>—</td> <td>—</td> <td>5</td> </tr> <tr> <td>Clay</td> <td>40</td> <td>20</td> <td>35</td> <td>20</td> <td>10</td> <td>30</td> </tr> <tr> <td>Volcanic glass</td> <td>Tr</td> <td>—</td> <td>—</td> <td>—</td> <td>—</td> <td>—</td> </tr> <tr> <td>Calcite/dolomite</td> <td>30</td> <td>30</td> <td>35</td> <td>30</td> <td>40</td> <td>40</td> </tr> <tr> <td>Accessory minerals</td> <td>Tr</td> <td>Tr</td> <td>—</td> <td>—</td> <td>—</td> <td>Tr</td> </tr> <tr> <td>Fe-Oxides</td> <td>—</td> <td>—</td> <td>5</td> <td>—</td> <td>—</td> <td>—</td> </tr> <tr> <td>Sponge spicules</td> <td>Tr</td> <td>—</td> <td>—</td> <td>—</td> <td>—</td> <td>—</td> </tr> </tbody> </table>		1, 80 D	1, 100 D	2, 50 D	3, 25 D	3, 80 D	5, 5 D	TEXTURE:							Sand	5	40	—	20	50	10	Silt	45	30	40	30	30	40	Clay	60	30	60	50	20	50		1, 80 D	1, 100 D	2, 50 D	3, 25 D	3, 80 D	5, 5 D	Quartz	25	30	25	40	50	25	Feldspar	Tr	Tr	—	10	—	Tr	Rock frag., calcite	5	20	—	—	—	5	Clay	40	20	35	20	10	30	Volcanic glass	Tr	—	—	—	—	—	Calcite/dolomite	30	30	35	30	40	40	Accessory minerals	Tr	Tr	—	—	—	Tr	Fe-Oxides	—	—	5	—	—	—	Sponge spicules	Tr	—	—	—	—	—
	1, 80 D	1, 100 D	2, 50 D	3, 25 D	3, 80 D	5, 5 D																																																																																																																		
TEXTURE:																																																																																																																								
Sand	5	40	—	20	50	10																																																																																																																		
Silt	45	30	40	30	30	40																																																																																																																		
Clay	60	30	60	50	20	50																																																																																																																		
	1, 80 D	1, 100 D	2, 50 D	3, 25 D	3, 80 D	5, 5 D																																																																																																																		
Quartz	25	30	25	40	50	25																																																																																																																		
Feldspar	Tr	Tr	—	10	—	Tr																																																																																																																		
Rock frag., calcite	5	20	—	—	—	5																																																																																																																		
Clay	40	20	35	20	10	30																																																																																																																		
Volcanic glass	Tr	—	—	—	—	—																																																																																																																		
Calcite/dolomite	30	30	35	30	40	40																																																																																																																		
Accessory minerals	Tr	Tr	—	—	—	Tr																																																																																																																		
Fe-Oxides	—	—	5	—	—	—																																																																																																																		
Sponge spicules	Tr	—	—	—	—	—																																																																																																																		
F/G	N22-23																																																																																																																							
R/G																																																																																																																								
B																																																																																																																								
B																																																																																																																								
F/G																																																																																																																								
		Brunhes Chronozone																																																																																																																						
							W=56 ● Y=1.72 δ=37.7 ● θ=61.1																																																																																																																	
							TOC=0.38 ● CaCO ₃ =2.5 ●																																																																																																																	
							γ=2.19 ● δ=37.7 ●																																																																																																																	
							TOC=0.25 ● CaCO ₃ =2.8 ●																																																																																																																	
							CC																																																																																																																	



TIME-ROCK UNIT		BIOSTRAT. ZONE/ FOSSIL CHARACTER	PALEOMAGNETICS	PHYS. PROPERTIES	CHEMISTRY	SECTION	METERS	GRAPHIC LITHOLOGY	DRILLING DISTURB.	SED. STRUCTURES	SAMPLES	LITHOLOGIC DESCRIPTION																														
FORAMINIFERS	NANNOFOSSILS																																									
PLEISTOCENE TO RECENT																																										
FG	N22-23				W=30 Y=2.01 φ=54.1 C&CO ₃ =24 C&CO ₃ =15		0.5 1.0					<p>DETRICARBONATE MUDDY SAND AND GRAVEL-BEARING DETRICARBONATE MUDDY SAND</p> <p>Detritic carbonate muddy sand and gravel-bearing detritic carbonate muddy sand, gray (10YR 5/1) with dropstones to about 5 cm (quartz arenite and dark gneiss).</p> <p>Minor lithologies: a. Section 1, 37-86 cm; Section 2, 7-44 cm: gray, crudely stratified, detritic carbonate muddy sand, silty sand, and silty mud with scattered coarse sand grains and granules. b. Section 1, 21-37, 86-96 cm: mottled silty clay with minor burrows.</p> <p>SMEAR SLIDE SUMMARY (%):</p> <table border="1"> <tr> <td></td> <td>1, 92</td> <td>2, 22</td> </tr> <tr> <td></td> <td>M</td> <td>D</td> </tr> </table> <p>TEXTURE:</p> <table border="1"> <tr> <td>Sand</td> <td>10</td> <td>40</td> </tr> <tr> <td>Silt</td> <td>40</td> <td>30</td> </tr> <tr> <td>Clay</td> <td>50</td> <td>30</td> </tr> </table> <p>COMPOSITION:</p> <table border="1"> <tr> <td>Quartz</td> <td>30</td> <td>20</td> </tr> <tr> <td>Feldspar</td> <td>15</td> <td>20</td> </tr> <tr> <td>Clay</td> <td>40</td> <td>20</td> </tr> <tr> <td>Calcite/dolomite</td> <td>10</td> <td>35</td> </tr> <tr> <td>Accessory minerals</td> <td>5</td> <td>5</td> </tr> </table>		1, 92	2, 22		M	D	Sand	10	40	Silt	40	30	Clay	50	30	Quartz	30	20	Feldspar	15	20	Clay	40	20	Calcite/dolomite	10	35	Accessory minerals	5	5
	1, 92	2, 22																																								
	M	D																																								
Sand	10	40																																								
Silt	40	30																																								
Clay	50	30																																								
Quartz	30	20																																								
Feldspar	15	20																																								
Clay	40	20																																								
Calcite/dolomite	10	35																																								
Accessory minerals	5	5																																								
B					W=49.9 Y=34 φ=31 C&CO ₃ =31	2																																				
B																																										
B																																										
F/G	<i>M. minuta</i>					3																																				
						4																																				



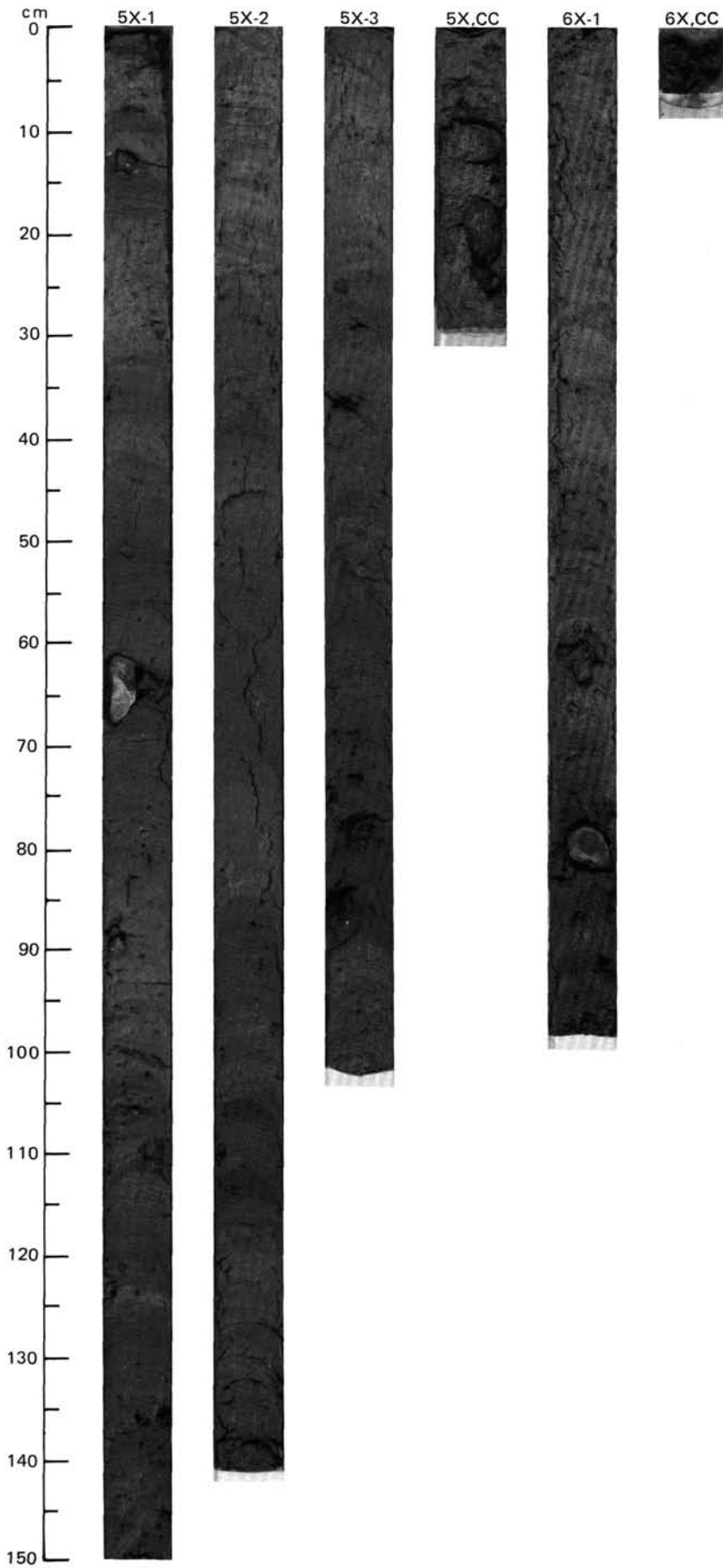


SITE 645 HOLE B CORE 5X CORED INTERVAL 2040.4-2050.8 mbsl; 32.2-42.6 mbsf

TIME-ROCK UNIT	BIOSTRAT. ZONE/ FOSSIL CHARACTER				PALEOMAGNETICS	PHYS. PROPERTIES	CHEMISTRY	SECTION	METERS	GRAPHIC LITHOLOGY	DRILLING DISTURB.	SED. STRUCTURES	SAMPLES	LITHOLOGIC DESCRIPTION																																																																		
	FORAMINIFERS	NANNOFOSSILS	RADIOLARIANS	DIATOMS																																																																												
PLEISTOCENE-RECENT	C/G													<p>DETRICARBONATE SILTY MUD</p> <p>Detriticarbonate silty mud, greenish gray (5GY 5/1), dark gray (5Y 4/1), gray (5Y 5/1) and black mottled, weakly stratified with up to 10% gravel.</p> <p>Minor lithologies:</p> <p>a. Section 1, 9-20, 33-56, 106-134 cm; Section 2, 105-112 cm; Section 3, 56-76 cm: greenish gray (5GY 5/1) clayey mud with only a few pebbles.</p> <p>b. Section 1, 56-106 cm; Section 3, 25-56 cm: gray to dark gray (5Y 5/1 to 5Y 4/1) gravel-bearing detriticarbonate muddy sand (10% gravel).</p> <p>c. Section 1, 1-9 cm; Section 2, 112-120 cm: cyclic weak red (10R 4/2), greenish gray (5G 5/1), and gray (5Y 6/1) silty sand.</p> <p>d. Section 3, 91-103 cm: light gray detriticarbonate silty sand with 5% gravel.</p> <p>SMEAR SLIDE SUMMARY (%):</p> <table border="1"> <tr> <td></td> <td>1, 75</td> <td>1, 116</td> <td>1, 140</td> <td>2, 114</td> <td>3, 97</td> </tr> <tr> <td></td> <td>D</td> <td>D</td> <td>D</td> <td>M</td> <td>D</td> </tr> </table> <p>TEXTURE:</p> <table border="1"> <tr> <td>Sand</td> <td>60</td> <td>10</td> <td>30</td> <td>40</td> <td>30</td> </tr> <tr> <td>Silt</td> <td>15</td> <td>30</td> <td>40</td> <td>40</td> <td>50</td> </tr> <tr> <td>Clay</td> <td>25</td> <td>60</td> <td>30</td> <td>20</td> <td>20</td> </tr> </table> <p>COMPOSITION:</p> <table border="1"> <tr> <td>Quartz</td> <td>30</td> <td>40</td> <td>50</td> <td>40</td> <td>30</td> </tr> <tr> <td>Feldspar</td> <td>10</td> <td>10</td> <td>15</td> <td>20</td> <td>10</td> </tr> <tr> <td>Clay</td> <td>25</td> <td>10</td> <td>10</td> <td>10</td> <td>10</td> </tr> <tr> <td>Calcite/dolomite</td> <td>30</td> <td>40</td> <td>25</td> <td>30</td> <td>50</td> </tr> <tr> <td>Accessory minerals</td> <td>5</td> <td>Tr</td> <td>Tr</td> <td>Tr</td> <td>Tr</td> </tr> <tr> <td>Foraminifers</td> <td>—</td> <td>—</td> <td>Tr</td> <td>—</td> <td>—</td> </tr> </table>		1, 75	1, 116	1, 140	2, 114	3, 97		D	D	D	M	D	Sand	60	10	30	40	30	Silt	15	30	40	40	50	Clay	25	60	30	20	20	Quartz	30	40	50	40	30	Feldspar	10	10	15	20	10	Clay	25	10	10	10	10	Calcite/dolomite	30	40	25	30	50	Accessory minerals	5	Tr	Tr	Tr	Tr	Foraminifers	—	—	Tr	—	—
	1, 75	1, 116	1, 140	2, 114	3, 97																																																																											
	D	D	D	M	D																																																																											
Sand	60	10	30	40	30																																																																											
Silt	15	30	40	40	50																																																																											
Clay	25	60	30	20	20																																																																											
Quartz	30	40	50	40	30																																																																											
Feldspar	10	10	15	20	10																																																																											
Clay	25	10	10	10	10																																																																											
Calcite/dolomite	30	40	25	30	50																																																																											
Accessory minerals	5	Tr	Tr	Tr	Tr																																																																											
Foraminifers	—	—	Tr	—	—																																																																											
	N22-23																																																																															

SITE 645 HOLE B CORE 6 X CORED INTERVAL 2050.8-2060.5 mbsl; 42.6-52.3 mbsf

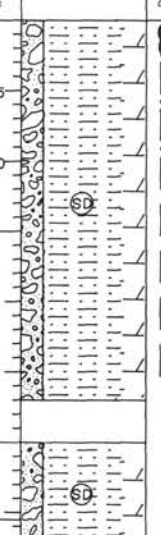
TIME-ROCK UNIT	BIOSTRAT. ZONE/ FOSSIL CHARACTER				PALEOMAGNETICS	PHYS. PROPERTIES	CHEMISTRY	SECTION	METERS	GRAPHIC LITHOLOGY	DRILLING DISTURB.	SED. STRUCTURES	SAMPLES	LITHOLOGIC DESCRIPTION																														
	FORAMINIFERS	NANNOFOSSILS	RADIOLARIANS	DIATOMS																																								
PLEISTOCENE-RECENT	C/G													<p>DETRICARBONATE SILTY MUD</p> <p>Detriticarbonate silty mud, pale brown (10YR 6/3) to dark greenish gray (5BG 4/1) at base; with banding (about 1-2 cm in thickness). Scattered dropstones to 5 cm (dolomite).</p> <p>SMEAR SLIDE SUMMARY (%):</p> <table border="1"> <tr> <td></td> <td>1, 8</td> <td>1, 88</td> </tr> <tr> <td></td> <td>D</td> <td>D</td> </tr> </table> <p>TEXTURE:</p> <table border="1"> <tr> <td>Sand</td> <td>10</td> <td>30</td> </tr> <tr> <td>Silt</td> <td>50</td> <td>50</td> </tr> <tr> <td>Clay</td> <td>40</td> <td>20</td> </tr> </table> <p>COMPOSITION:</p> <table border="1"> <tr> <td>Quartz</td> <td>35</td> <td>40</td> </tr> <tr> <td>Feldspar</td> <td>10</td> <td>10</td> </tr> <tr> <td>Clay</td> <td>10</td> <td>5</td> </tr> <tr> <td>Calcite/dolomite</td> <td>45</td> <td>40</td> </tr> <tr> <td>Accessory minerals</td> <td>Tr</td> <td>5</td> </tr> </table>		1, 8	1, 88		D	D	Sand	10	30	Silt	50	50	Clay	40	20	Quartz	35	40	Feldspar	10	10	Clay	10	5	Calcite/dolomite	45	40	Accessory minerals	Tr	5
	1, 8	1, 88																																										
	D	D																																										
Sand	10	30																																										
Silt	50	50																																										
Clay	40	20																																										
Quartz	35	40																																										
Feldspar	10	10																																										
Clay	10	5																																										
Calcite/dolomite	45	40																																										
Accessory minerals	Tr	5																																										
	N22-23																																											

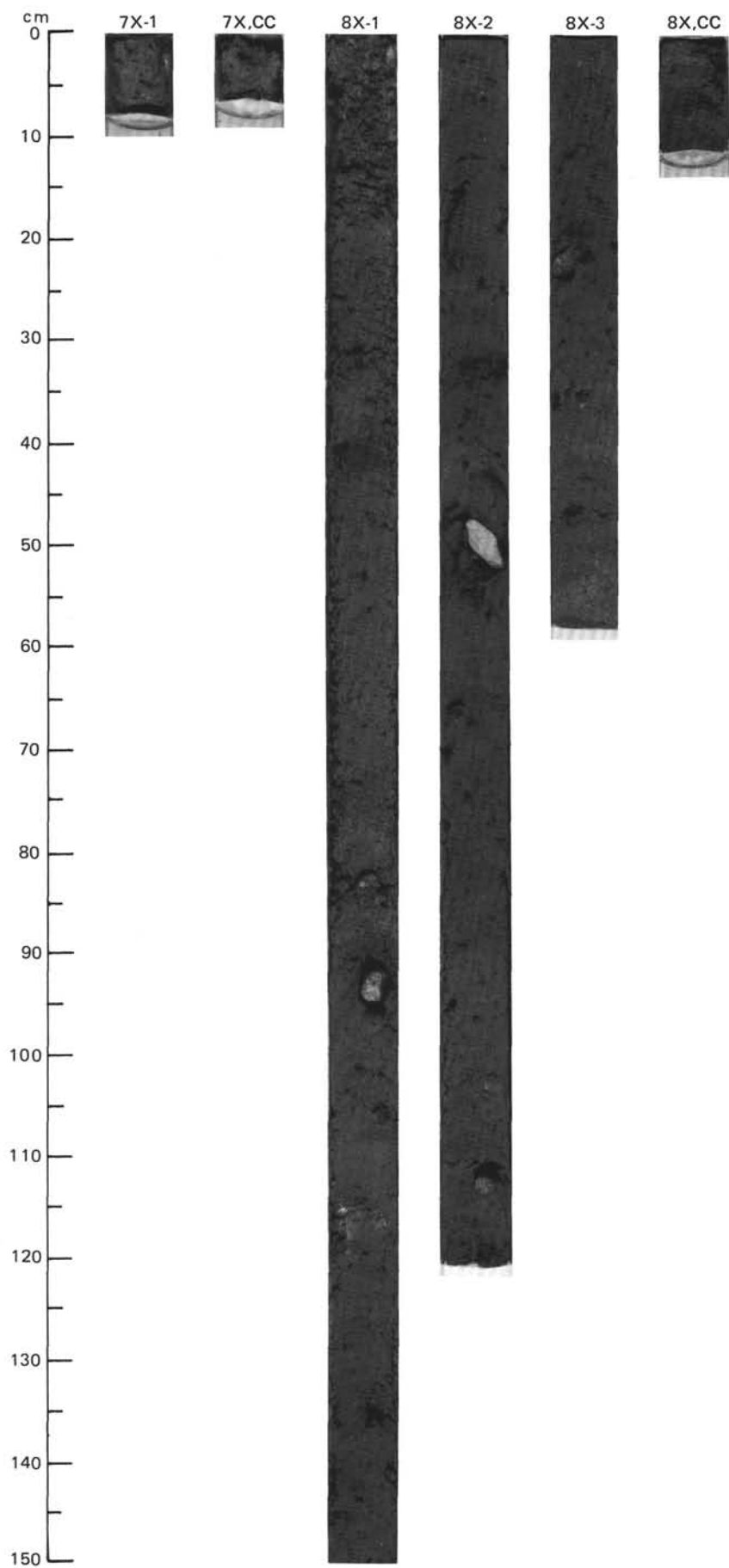


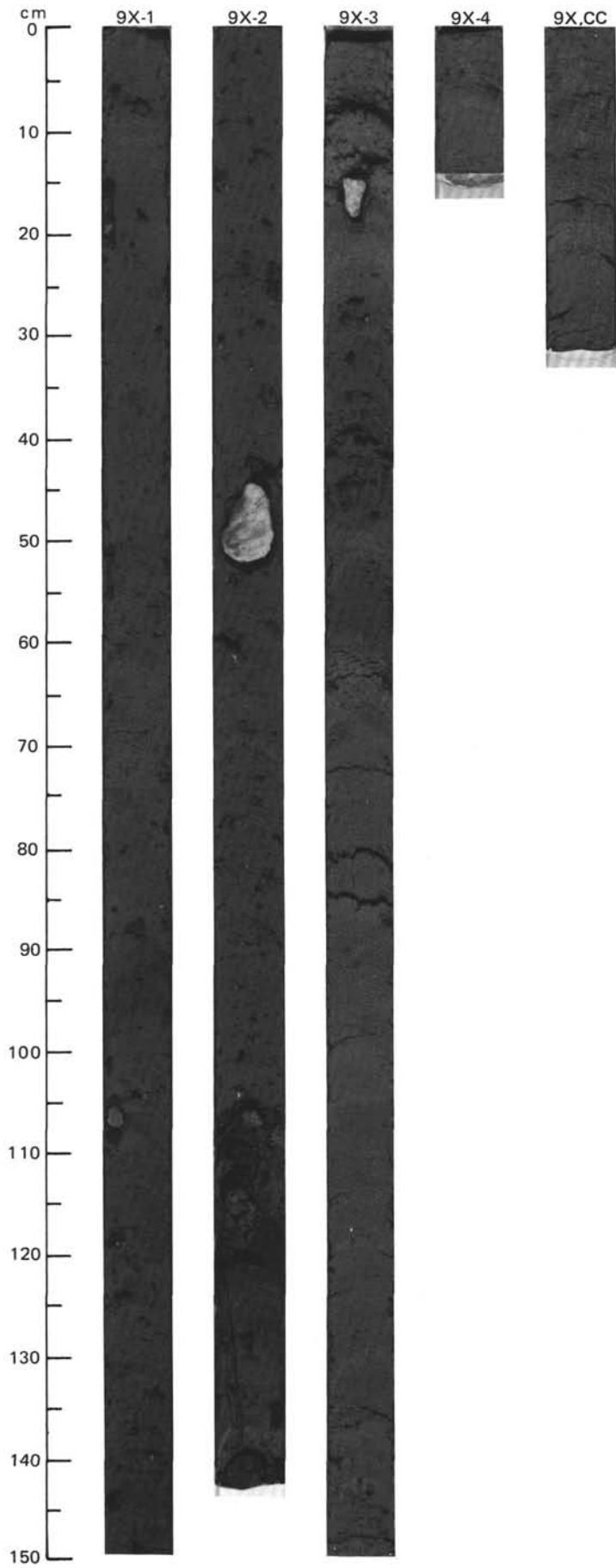
SITE 645 HOLE B CORE 7 X CORED INTERVAL 2060.5-2070.2 mbsl; 52.3-62.0 mbsf

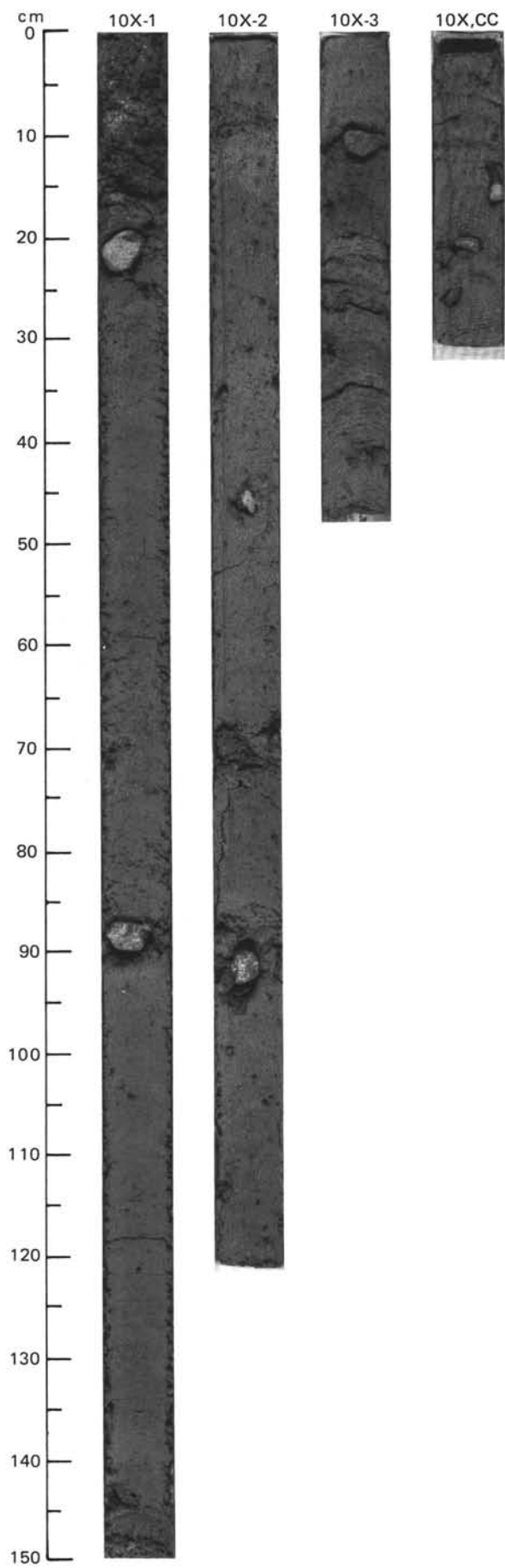
TIME-ROCK UNIT	BIOSTRAT. ZONE/ FOSSIL CHARACTER					PALEOMAGNETICS	PHYS. PROPERTIES	CHEMISTRY	SECTION	METERS	GRAPHIC LITHOLOGY	DRILLING DISTURB.	SED. STRUCTURES	SAMPLES	LITHOLOGIC DESCRIPTION
	FORAMINIFERS	NANNOFOSSILS	RADIOLARIANS	DIATOMS	DINOCTYSTS										
PLEISTOCENE-RECENT	C/G	B	B	B	F/M				CC						SILTY MUD Silty mud, greenish gray (5G 5/1) and gray (5Y 6/1).

SITE 645 HOLE B CORE 8 X CORED INTERVAL 2070.2-2079.8 mbsl; 62.0-71.6 mbsf

TIME-ROCK UNIT	BIOSTRAT. ZONE/ FOSSIL CHARACTER					PALEOMAGNETICS	PHYS. PROPERTIES	CHEMISTRY	SECTION	METERS	GRAPHIC LITHOLOGY	DRILLING DISTURB.	SED. STRUCTURES	SAMPLES	LITHOLOGIC DESCRIPTION																																								
	FORAMINIFERS	NANNOFOSSILS	RADIOLARIANS	DIATOMS	DINOCTYSTS																																																		
PLEISTOCENE-RECENT	F/G	R/G	B	B	F/G	Brunhes Chronozone	$\gamma = 2.30$ $\delta = 36.8$ $TOC = 0.59$ $CaCO_3 = 32.8$	$TOC = 0.42$ $CaCO_3 = 29$	CC	0.5 1.0 2 3				*	<p>DETRICARBONATE MUDDY SAND</p> <p>Detriticarbonate muddy sand, gray (5Y 5/1), with 5-10% gravel. Sediment is structureless.</p> <p>Minor lithology:</p> <p>a. Section 1, 40-43: dark greenish gray (5Y 4/1) silty sand lens.</p> <p>SMEAR SLIDE SUMMARY (%):</p> <table border="1"> <tr> <td></td> <td>1, 42</td> <td>1, 115</td> <td>2, 71</td> </tr> <tr> <td></td> <td>M</td> <td>M</td> <td>D</td> </tr> </table> <p>TEXTURE:</p> <table border="1"> <tr> <td>Sand</td> <td>70</td> <td>—</td> <td>50</td> </tr> <tr> <td>Silt</td> <td>20</td> <td>25</td> <td>30</td> </tr> <tr> <td>Clay</td> <td>10</td> <td>75</td> <td>20</td> </tr> </table> <p>COMPOSITION:</p> <table border="1"> <tr> <td>Quartz</td> <td>60</td> <td>10</td> <td>50</td> </tr> <tr> <td>Feldspar</td> <td>10</td> <td>—</td> <td>10</td> </tr> <tr> <td>Clay</td> <td>10</td> <td>—</td> <td>10</td> </tr> <tr> <td>Calcite/dolomite</td> <td>20</td> <td>90</td> <td>30</td> </tr> <tr> <td>Accessory minerals</td> <td>Tr</td> <td>—</td> <td>Tr</td> </tr> </table>		1, 42	1, 115	2, 71		M	M	D	Sand	70	—	50	Silt	20	25	30	Clay	10	75	20	Quartz	60	10	50	Feldspar	10	—	10	Clay	10	—	10	Calcite/dolomite	20	90	30	Accessory minerals	Tr	—	Tr
	1, 42	1, 115	2, 71																																																				
	M	M	D																																																				
Sand	70	—	50																																																				
Silt	20	25	30																																																				
Clay	10	75	20																																																				
Quartz	60	10	50																																																				
Feldspar	10	—	10																																																				
Clay	10	—	10																																																				
Calcite/dolomite	20	90	30																																																				
Accessory minerals	Tr	—	Tr																																																				





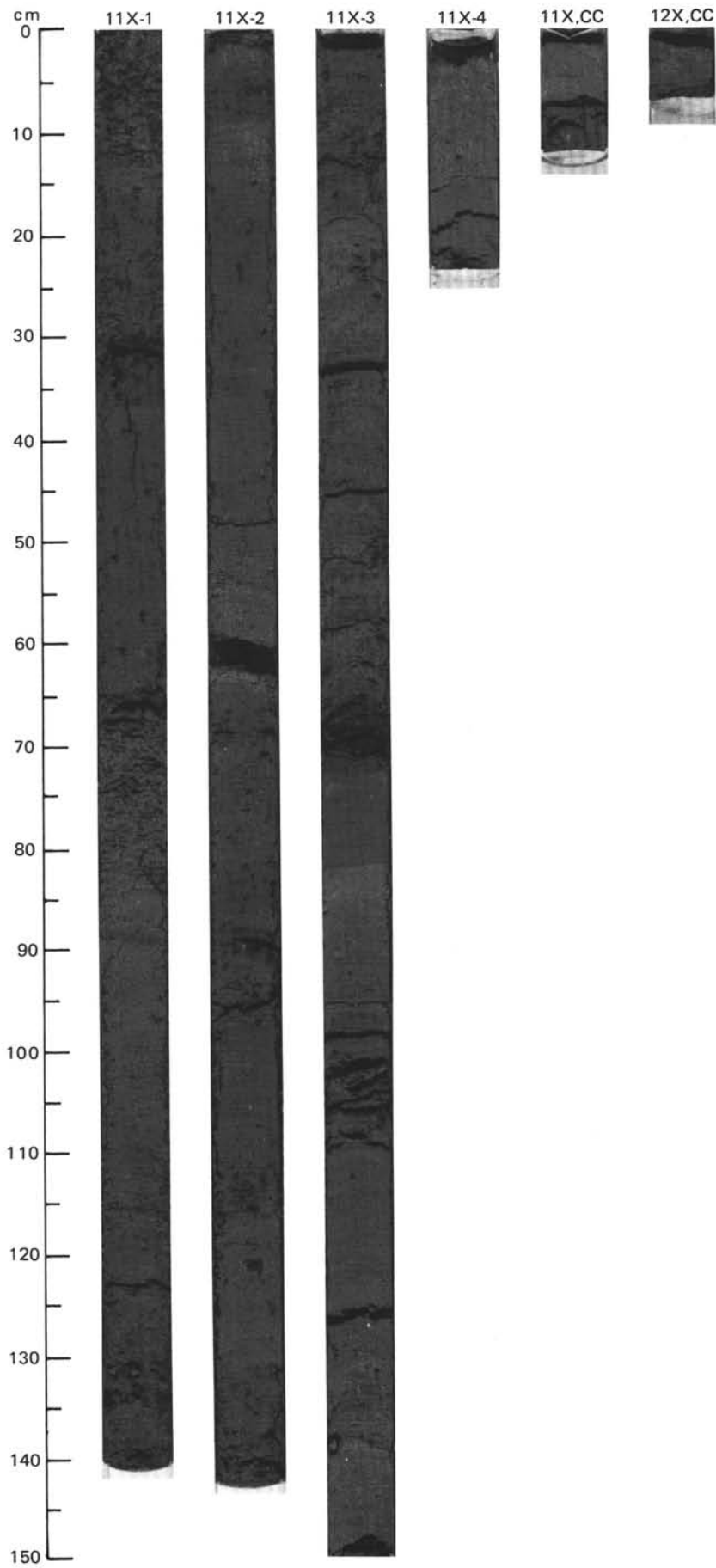


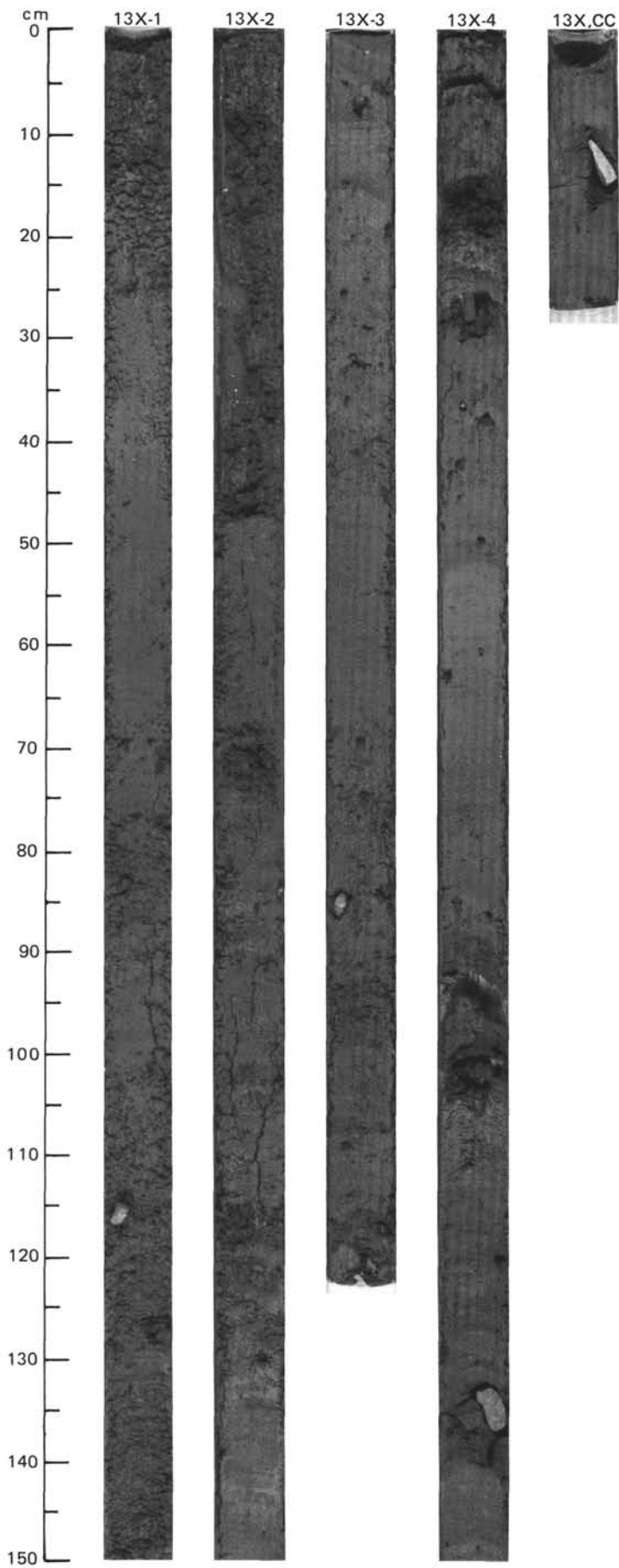
SITE 645 HOLE B CORE 11 X CORED INTERVAL 2099.1-2108.8 mbsl; 90.9-100.6 mbsf

TIME-ROCK UNIT	BIOSTRAT. ZONE/ FOSSIL CHARACTER					PALEOMAGNETICS	PHYS. PROPERTIES	CHEMISTRY	SECTION	METERS	GRAPHIC LITHOLOGY	DRILLING DISTURB.	SED. STRUCTURES	SAMPLES	LITHOLOGIC DESCRIPTION																																																				
	FORAMINIFERS	NANNOFOSSILS	RADIOLARIANS	DIATOMS	DINOCYSTS																																																														
	N22-23																																																																		
	R/G																																																																		
PLEISTOCENE-RECENT	N22-23					Brunhes Chronozone	W=32 F=2.01 D=4.7.8	CaCO ₃ =9	1	0.5 1.0			* IW	DETRICARBONATE CLAYEY MUD AND DETRICARBONATE SILTY MUD Detrital carbonate clayey mud, dark olive gray (5Y 3, 5/1) to dark gray (5Y 4/1); interbedded with detrital carbonate silty mud, olive gray (5Y 3, 5/2) and dark grayish brown (2.5Y 4/2). Dropstones are scattered throughout. Minor lithologies: a. Section 1, 0-3 cm and 66-87 cm; Section 2, 131-140 cm; Section 3, 0-19 cm: detrital carbonate sandy mud, dark grayish brown (5Y 4/2) and olive gray (5Y 4/2). b. Section 2, 88-90 cm: silty clay, dark gray (5Y 4/1) and dark brown (7, 5Y 3/2). c. Section 2, 0-2 cm: black (5Y 2.5/1) silt. d. Section 2, 54-64 cm: interbedded finely laminated detrital carbonate silt (light), and detrital carbonate clay (dark) layers.																																																					
	F/M														Matuyama Chronozone	T0C=0.68 CaCO ₃ =1.8	CaCO ₃ =40	2				* IW	SMEAR SLIDE SUMMARY (%): <table border="1"> <tr> <td></td> <td>1, 114</td> <td>2, 62</td> <td>3, 37</td> <td>3, 66</td> <td>3, 110</td> </tr> <tr> <td>D</td> <td></td> <td>M</td> <td>D</td> <td>M</td> <td>D</td> </tr> </table>		1, 114	2, 62	3, 37	3, 66	3, 110	D		M	D	M	D																																
		1, 114	2, 62	3, 37	3, 66																			3, 110																																											
	D		M	D	M										D																																																				
R/G					Matuyama Chronozone	T0C=0.68 CaCO ₃ =1.8	CaCO ₃ =43	3				* IW	TEXTURE: <table border="1"> <tr> <td>Sand</td> <td>10</td> <td>35</td> <td>10</td> <td>5</td> <td>5</td> </tr> <tr> <td>Silt</td> <td>50</td> <td>60</td> <td>50</td> <td>35</td> <td>25</td> </tr> <tr> <td>Clay</td> <td>40</td> <td>5</td> <td>40</td> <td>60</td> <td>70</td> </tr> </table>	Sand	10	35	10	5	5	Silt	50	60	50	35	25	Clay	40	5	40	60	70																																				
Sand	10	35	10	5										5																																																					
Silt	50	60	50	35	25																																																														
Clay	40	5	40	60	70																																																														
R/G					Matuyama Chronozone	T0C=0.68 CaCO ₃ =1.8	CaCO ₃ =18	4				* IW	COMPOSITION: <table border="1"> <tr> <td>Quartz</td> <td>20</td> <td>25</td> <td>25</td> <td>30</td> <td>15</td> </tr> <tr> <td>Feldspar</td> <td>—</td> <td>10</td> <td>5</td> <td>5</td> <td>10</td> </tr> <tr> <td>Rock frag., calcite</td> <td>—</td> <td>60</td> <td>—</td> <td>—</td> <td>10</td> </tr> <tr> <td>Clay</td> <td>20</td> <td>—</td> <td>20</td> <td>20</td> <td>50</td> </tr> <tr> <td>Volcanic glass</td> <td>—</td> <td>Tr</td> <td>—</td> <td>—</td> <td>—</td> </tr> <tr> <td>Calcite/dolomite</td> <td>60</td> <td>—</td> <td>50</td> <td>45</td> <td>10</td> </tr> <tr> <td>Accessory minerals</td> <td>Tr</td> <td>5</td> <td>Tr</td> <td>—</td> <td>5</td> </tr> <tr> <td>Fe-Oxides</td> <td>Tr</td> <td>—</td> <td>—</td> <td>Tr</td> <td>—</td> </tr> <tr> <td>Pyrite</td> <td>—</td> <td>—</td> <td>—</td> <td>Tr</td> <td>—</td> </tr> </table>	Quartz	20	25	25	30	15	Feldspar	—	10	5	5	10	Rock frag., calcite	—	60	—	—	10	Clay	20	—	20	20	50	Volcanic glass	—	Tr	—	—	—	Calcite/dolomite	60	—	50	45	10	Accessory minerals	Tr	5	Tr	—	5	Fe-Oxides	Tr	—	—	Tr	—	Pyrite	—	—	—	Tr	—
Quartz	20	25	25	30										15																																																					
Feldspar	—	10	5	5	10																																																														
Rock frag., calcite	—	60	—	—	10																																																														
Clay	20	—	20	20	50																																																														
Volcanic glass	—	Tr	—	—	—																																																														
Calcite/dolomite	60	—	50	45	10																																																														
Accessory minerals	Tr	5	Tr	—	5																																																														
Fe-Oxides	Tr	—	—	Tr	—																																																														
Pyrite	—	—	—	Tr	—																																																														

SITE 645 HOLE B CORE 12 X CORED INTERVAL 2108.8-2118.5 mbsl; 100.6-110.3 mbsf

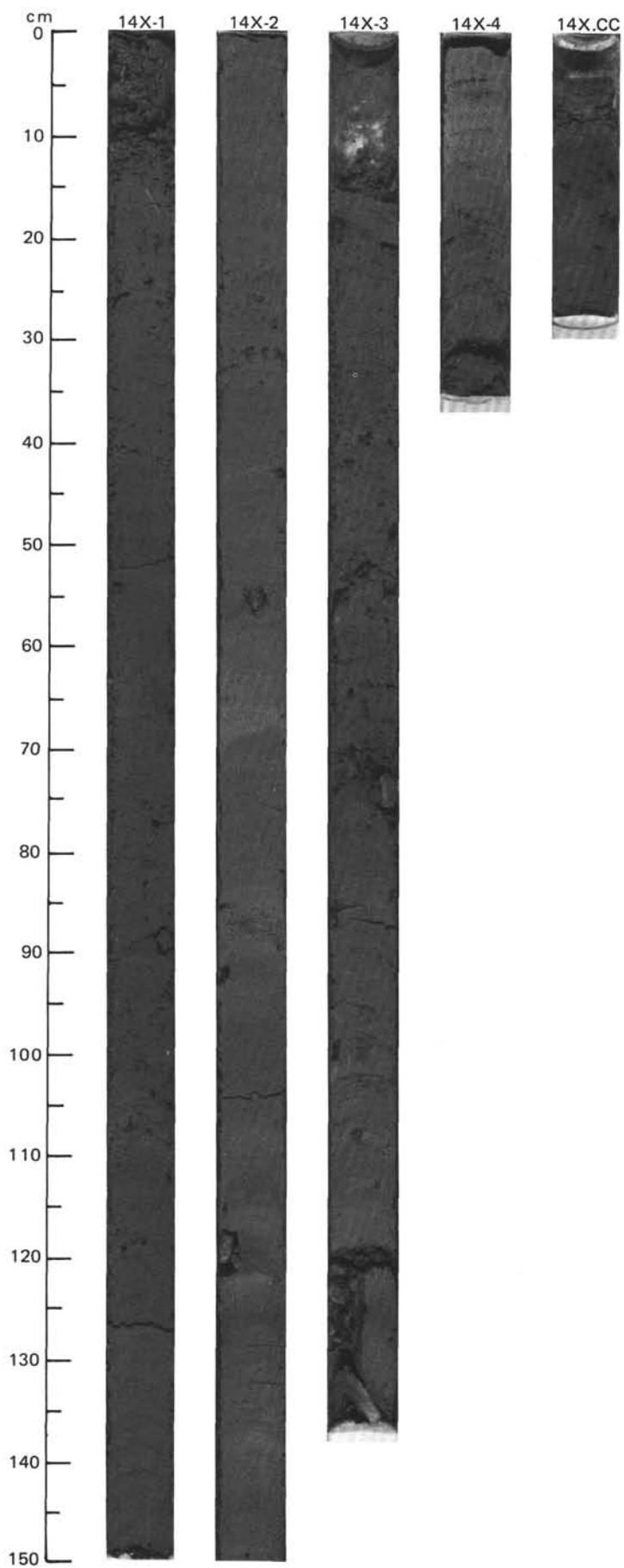
TIME-ROCK UNIT	BIOSTRAT. ZONE/ FOSSIL CHARACTER					PALEOMAGNETICS	PHYS. PROPERTIES	CHEMISTRY	SECTION	METERS	GRAPHIC LITHOLOGY	DRILLING DISTURB.	SED. STRUCTURES	SAMPLES	LITHOLOGIC DESCRIPTION				
	FORAMINIFERS	NANNOFOSSILS	RADIOLARIANS	DIATOMS	DINOCYSTS														
	N22-23																		
	C/G																		
PLEISTOCENE-RECENT	N22-23							CC					*	DETRICARBONATE SILTY CLAY Detrital carbonate silty clay, dark grayish brown (2.5Y 4/2). SMEAR SLIDE SUMMARY (%): <table border="1"> <tr> <td></td> <td>CC, 2</td> </tr> <tr> <td>D</td> <td></td> </tr> </table>		CC, 2	D		
		CC, 2																	
	D																		
	R/G																		
Sand	5																		
Silt	45																		
Clay	50																		
C/G												*	COMPOSITION: <table border="1"> <tr> <td>Quartz</td> <td>25</td> </tr> <tr> <td>Clay</td> <td>25</td> </tr> <tr> <td>Calcite/dolomite</td> <td>50</td> </tr> </table>	Quartz	25	Clay	25	Calcite/dolomite	50
Quartz	25																		
Clay	25																		
Calcite/dolomite	50																		
N22-23												*							





SITE 645 HOLE B CORE 14 X CORED INTERVAL 2128.1-2137.7 mbsl; 119.9-129.5 mbsf

TIME-ROCK UNIT	BIOSTRAT. ZONE/ FOSSIL CHARACTER				PALEOMAGNETICS	PHYS. PROPERTIES	CHEMISTRY	SECTION	METERS	GRAPHIC LITHOLOGY	DRILLING DISTURB.	SED. STRUCTURES	SAMPLES	LITHOLOGIC DESCRIPTION																																																																																																		
	FORAMINIFERS	NANNOFOSSILS	RADIOLARIANS	DIATOMS																																																																																																												
PLEISTOCENE -RECENT	B								0.5				*	<p>DETRICARBONATE SILTY CLAY AND DETRICARBONATE CLAYEY MUD</p> <p>Detriticarbonate silty clay, dark gray (5Y 4/1) and gray (5Y 5/1); locally color banded; interbedded with detriticarbonate clayey mud, dark gray (5Y 4/1) to very dark gray (5Y 3/1). Several dropstones scattered throughout.</p> <p>Minor lithology: Section 2, 32-69 cm: dark grayish brown (2.5Y 4/2) detriticarbonate silty mud.</p> <p>SMEAR SLIDE SUMMARY (%):</p> <table border="1"> <tr> <td></td> <td>1, 53</td> <td>2, 66</td> <td>2, 82</td> <td>3, 74</td> <td>2, 86</td> <td>3, 72</td> </tr> <tr> <td></td> <td>D</td> <td>D</td> <td>D</td> <td>D</td> <td>M</td> <td>M</td> </tr> </table> <p>TEXTURE:</p> <table border="1"> <tr> <td>Sand</td> <td>10</td> <td>5</td> <td>—</td> <td>15</td> <td>20</td> <td>60</td> </tr> <tr> <td>Silt</td> <td>40</td> <td>45</td> <td>40</td> <td>35</td> <td>50</td> <td>30</td> </tr> <tr> <td>Clay</td> <td>50</td> <td>50</td> <td>60</td> <td>50</td> <td>30</td> <td>10</td> </tr> </table> <p>COMPOSITION:</p> <table border="1"> <tr> <td>Quartz</td> <td>30</td> <td>20</td> <td>20</td> <td>35</td> <td>25</td> <td>50</td> </tr> <tr> <td>Feldspar</td> <td>10</td> <td>10</td> <td>—</td> <td>10</td> <td>10</td> <td>—</td> </tr> <tr> <td>Rock frag., calcite</td> <td>10</td> <td>25</td> <td>—</td> <td>5</td> <td>—</td> <td>—</td> </tr> <tr> <td>Clay</td> <td>30</td> <td>20</td> <td>10</td> <td>40</td> <td>10</td> <td>—</td> </tr> <tr> <td>Volcanic glass</td> <td>Tr</td> <td>—</td> <td>—</td> <td>Tr</td> <td>—</td> <td>—</td> </tr> <tr> <td>Calcite/dolomite</td> <td>20</td> <td>25</td> <td>70</td> <td>10</td> <td>40</td> <td>20</td> </tr> <tr> <td>Accessory minerals</td> <td>Tr</td> <td>Tr</td> <td>—</td> <td>Tr</td> <td>Tr</td> <td>—</td> </tr> <tr> <td>Pyrite</td> <td>—</td> <td>—</td> <td>—</td> <td>—</td> <td>—</td> <td>30</td> </tr> <tr> <td>Foraminifers</td> <td>—</td> <td>—</td> <td>—</td> <td>Tr</td> <td>—</td> <td>—</td> </tr> </table>		1, 53	2, 66	2, 82	3, 74	2, 86	3, 72		D	D	D	D	M	M	Sand	10	5	—	15	20	60	Silt	40	45	40	35	50	30	Clay	50	50	60	50	30	10	Quartz	30	20	20	35	25	50	Feldspar	10	10	—	10	10	—	Rock frag., calcite	10	25	—	5	—	—	Clay	30	20	10	40	10	—	Volcanic glass	Tr	—	—	Tr	—	—	Calcite/dolomite	20	25	70	10	40	20	Accessory minerals	Tr	Tr	—	Tr	Tr	—	Pyrite	—	—	—	—	—	30	Foraminifers	—	—	—	Tr	—	—
		1, 53	2, 66	2, 82	3, 74	2, 86	3, 72																																																																																																									
		D	D	D	D	M	M																																																																																																									
	Sand	10	5	—	15	20	60																																																																																																									
	Silt	40	45	40	35	50	30																																																																																																									
Clay	50	50	60	50	30	10																																																																																																										
Quartz	30	20	20	35	25	50																																																																																																										
Feldspar	10	10	—	10	10	—																																																																																																										
Rock frag., calcite	10	25	—	5	—	—																																																																																																										
Clay	30	20	10	40	10	—																																																																																																										
Volcanic glass	Tr	—	—	Tr	—	—																																																																																																										
Calcite/dolomite	20	25	70	10	40	20																																																																																																										
Accessory minerals	Tr	Tr	—	Tr	Tr	—																																																																																																										
Pyrite	—	—	—	—	—	30																																																																																																										
Foraminifers	—	—	—	Tr	—	—																																																																																																										
	B							1.0					◇																																																																																																			
	B							2					◇																																																																																																			
	B							3		VOID			◇																																																																																																			
	F/G							4					◇																																																																																																			
	Matuyama Chronozone							CC					IW																																																																																																			

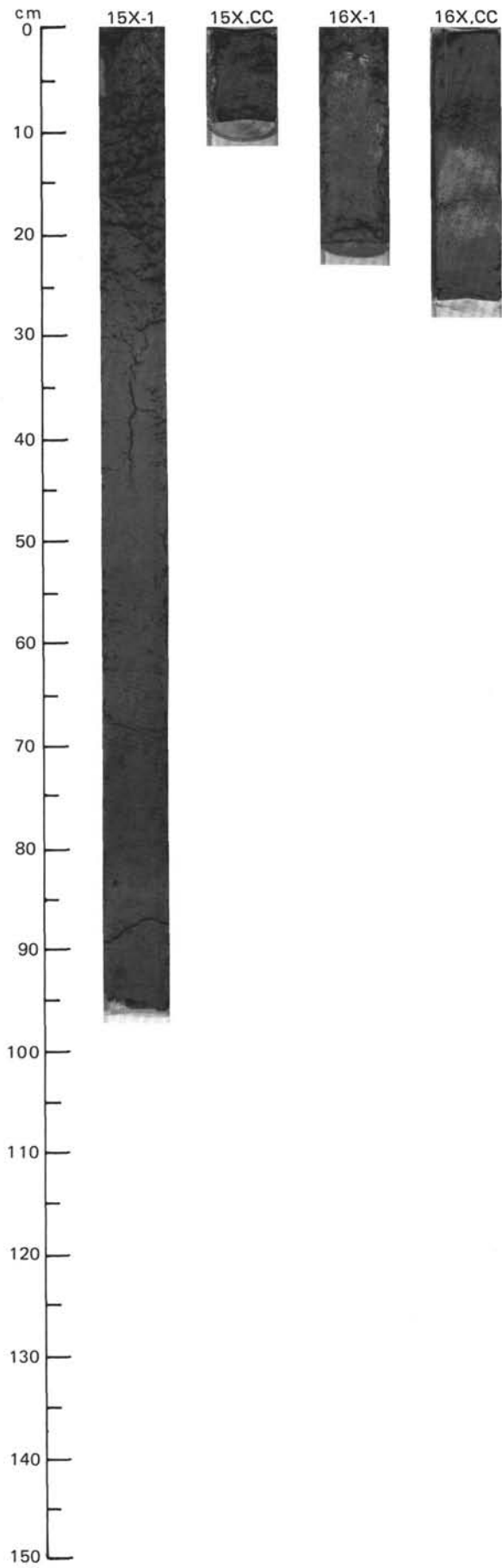


SITE 645 HOLE B CORE 15 X CORED INTERVAL 2137.7-2147.3 mbsl; 129.5-139.1 mbsf

TIME-ROCK UNIT	BIOSTRAT. ZONE/ FOSSIL CHARACTER				PALEOMAGNETICS	PHYS. PROPERTIES	CHEMISTRY	SECTION	METERS	GRAPHIC LITHOLOGY	DRILLING DISTURB.	SED. STRUCTURES	SAMPLES	LITHOLOGIC DESCRIPTION																																				
	FORAMINIFERS	NANNOFOSSILS	RADIOLARIANS	DIATOMS																																														
PLEISTOCENE	B				Matuyama Chronozone	Y-2, 09 0-4, 3 ● W=27	TOC=1.22 C/C0=0.42	1	0.5				* * *	<p>DETRICARBONATE CLAY AND DETRICARBONATE SILTY CLAY</p> <p>Detriticarbonate clay, dark grayish brown (2.5Y 4/2); homogeneous, interbedded with detriticarbonate silty clay, dark gray (5Y 4/1) to very dark gray (5Y 3/1), mottled. Dropstones are scattered throughout.</p> <p>Minor lithology: Section 1, 84-95 cm: detriticarbonate clayey silt, very dark gray (5Y 3/1).</p> <p>SMEAR SLIDE SUMMARY (%):</p> <table border="1"> <tr> <td></td> <td>1, 19</td> <td>1, 38</td> <td>1, 69</td> </tr> <tr> <td></td> <td>D</td> <td>D</td> <td>D</td> </tr> </table> <p>TEXTURE:</p> <table border="1"> <tr> <td>Sand</td> <td>—</td> <td>—</td> <td>5</td> </tr> <tr> <td>Silt</td> <td>60</td> <td>15</td> <td>40</td> </tr> <tr> <td>Clay</td> <td>40</td> <td>85</td> <td>55</td> </tr> </table> <p>COMPOSITION:</p> <table border="1"> <tr> <td>Quartz</td> <td>40</td> <td>5</td> <td>30</td> </tr> <tr> <td>Mica</td> <td>—</td> <td>—</td> <td>Tr</td> </tr> <tr> <td>Clay</td> <td>20</td> <td>10</td> <td>20</td> </tr> <tr> <td>Calcite/dolomite</td> <td>40</td> <td>85</td> <td>50</td> </tr> </table>		1, 19	1, 38	1, 69		D	D	D	Sand	—	—	5	Silt	60	15	40	Clay	40	85	55	Quartz	40	5	30	Mica	—	—	Tr	Clay	20	10	20	Calcite/dolomite	40	85	50
		1, 19	1, 38	1, 69																																														
	D	D	D																																															
Sand	—	—	5																																															
Silt	60	15	40																																															
Clay	40	85	55																																															
Quartz	40	5	30																																															
Mica	—	—	Tr																																															
Clay	20	10	20																																															
Calcite/dolomite	40	85	50																																															
	F/G																																																	

SITE 645 HOLE B CORE 16 X CORED INTERVAL 2147.3-2157.0 mbsl; 139.1-148.8 mbsf

TIME-ROCK UNIT	BIOSTRAT. ZONE/ FOSSIL CHARACTER				PALEOMAGNETICS	PHYS. PROPERTIES	CHEMISTRY	SECTION	METERS	GRAPHIC LITHOLOGY	DRILLING DISTURB.	SED. STRUCTURES	SAMPLES	LITHOLOGIC DESCRIPTION																																	
	FORAMINIFERS	NANNOFOSSILS	RADIOLARIANS	DIATOMS																																											
LOWER PLEISTOCENE	B				Matuyama Chronozone	Y-2, 09 0-4, 3 ●	TOC=0.79 C/C0=0.38	1					* *	<p>DETRICARBONATE SILTY CLAY</p> <p>Detriticarbonate silty clay, gray (5Y 5/1), dark gray (5Y 4/1), and olive gray (5Y 4/2).</p> <p>Minor lithology: CC, 6-8 cm, 23-25 cm: detriticarbonate clayey silt, dark gray (5Y 4/1) color banded.</p> <p>SMEAR SLIDE SUMMARY (%):</p> <table border="1"> <tr> <td></td> <td>1, 10</td> <td>CC, 14</td> </tr> <tr> <td></td> <td>D</td> <td>D</td> </tr> </table> <p>TEXTURE:</p> <table border="1"> <tr> <td>Silt</td> <td>30</td> <td>45</td> </tr> <tr> <td>Clay</td> <td>70</td> <td>55</td> </tr> </table> <p>COMPOSITION:</p> <table border="1"> <tr> <td>Quartz</td> <td>10</td> <td>25</td> </tr> <tr> <td>Feldspar</td> <td>10</td> <td>—</td> </tr> <tr> <td>Rock frag., calcite</td> <td>10</td> <td>—</td> </tr> <tr> <td>Clay</td> <td>40</td> <td>—</td> </tr> <tr> <td>Volcanic glass</td> <td>Tr</td> <td>—</td> </tr> <tr> <td>Calcite/dolomite</td> <td>30</td> <td>75</td> </tr> <tr> <td>Accessory minerals</td> <td>Tr</td> <td>—</td> </tr> </table>		1, 10	CC, 14		D	D	Silt	30	45	Clay	70	55	Quartz	10	25	Feldspar	10	—	Rock frag., calcite	10	—	Clay	40	—	Volcanic glass	Tr	—	Calcite/dolomite	30	75	Accessory minerals	Tr	—
		1, 10	CC, 14																																												
	D	D																																													
Silt	30	45																																													
Clay	70	55																																													
Quartz	10	25																																													
Feldspar	10	—																																													
Rock frag., calcite	10	—																																													
Clay	40	—																																													
Volcanic glass	Tr	—																																													
Calcite/dolomite	30	75																																													
Accessory minerals	Tr	—																																													
	C/G																																														

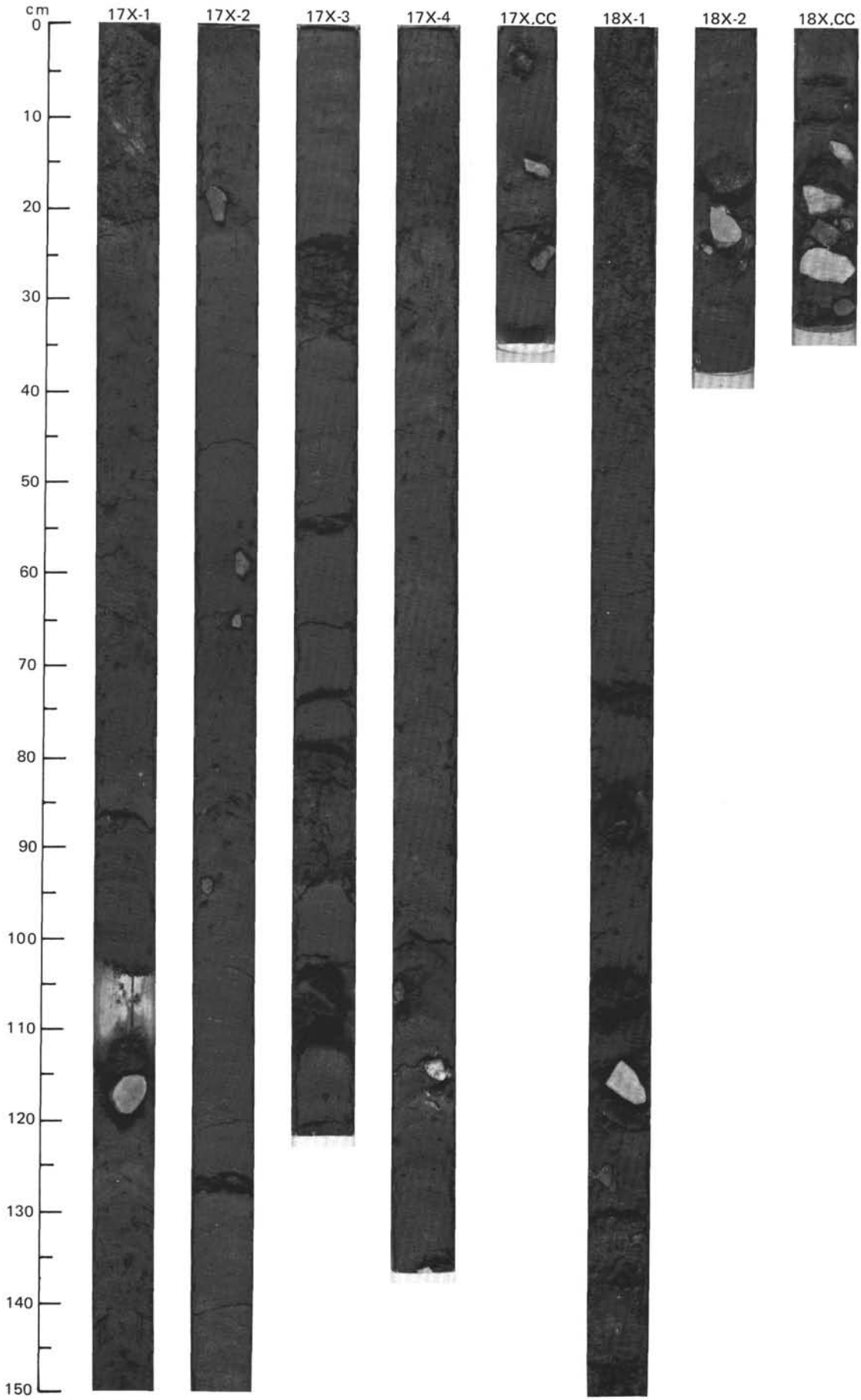


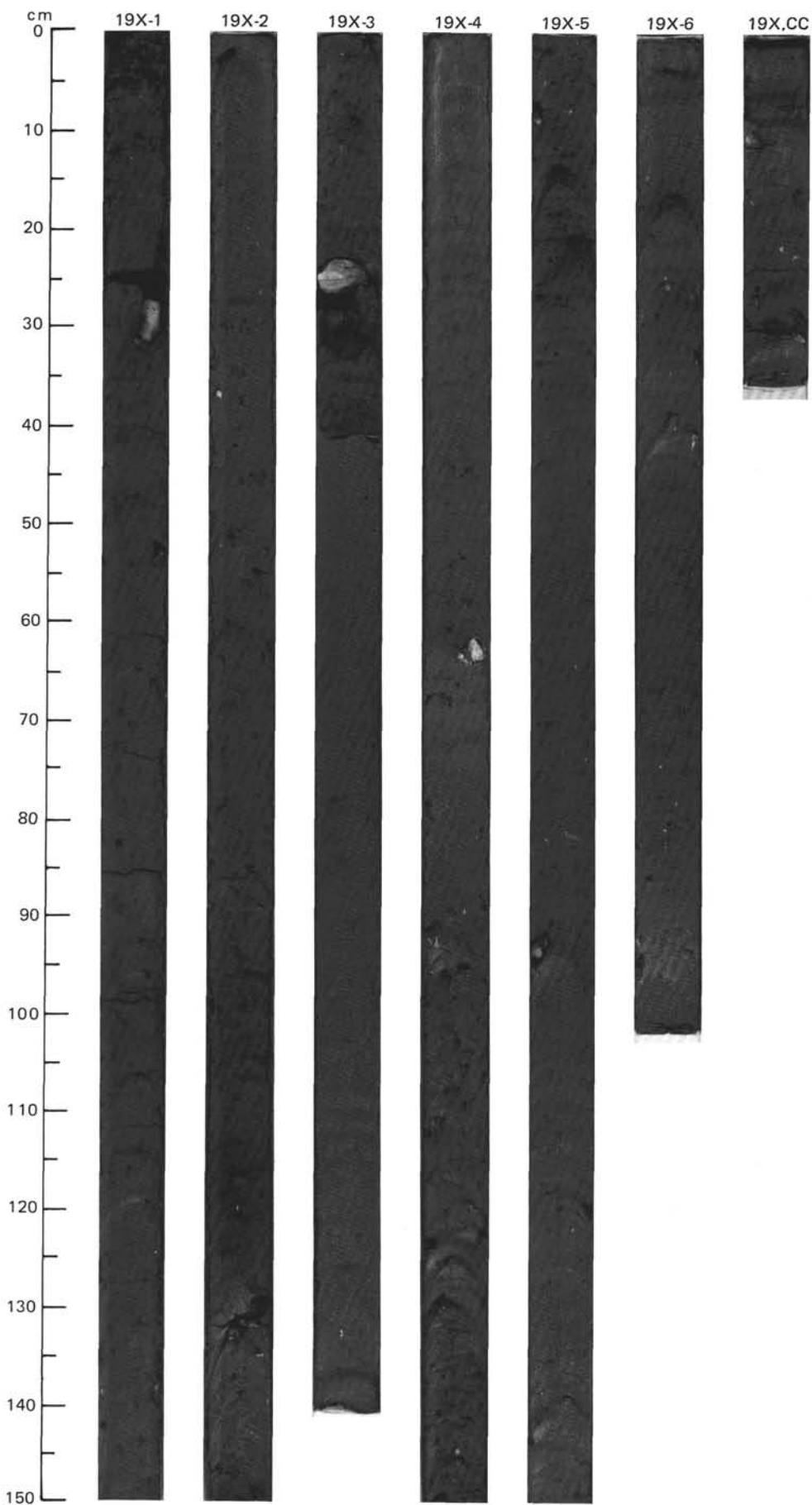
SITE 645 HOLE B CORE 17 X CORED INTERVAL 2157.0-2166.6 mbsl; 148.8-158.4 mbsf

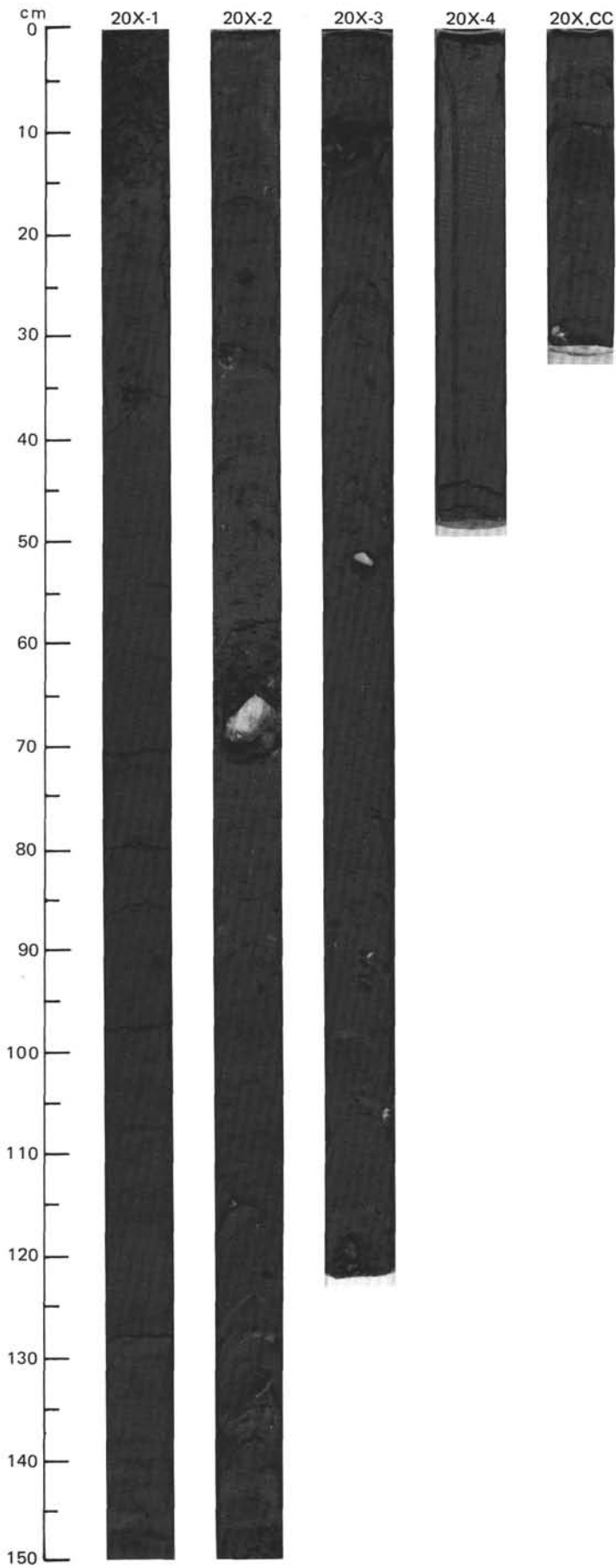
TIME-ROCK UNIT	BIOSTRAT. ZONE/ FOSSIL CHARACTER					PALEOMAGNETICS	PHYS. PROPERTIES	CHEMISTRY	SECTION	METERS	GRAPHIC LITHOLOGY	DRILLING DISTURB.	SED. STRUCTURES	SAMPLES	LITHOLOGIC DESCRIPTION																																																																
	FORAMINIFERS	NANNOFOSSILS	RADIOLARIANS	DIATOMS	DINOCYSTS																																																																										
LOWER PLEISTOCENE	R/M	B	B	B	R/M	Matuyama Chronozone	$\gamma=1.90$ $W=18$ $\phi=33.6$	$\gamma=2.09$ $W=21$ $\phi=36.6$ TOC=0.64 CaCO ₃ =19	1	0.5 1.0	VOID		*	<p>DETRICARBONATE SILTY MUD AND DETRICARBONATE SILTY CLAY</p> <p>Detriticarbonate silty mud, gray to dark gray (5Y 4/1 - 5Y 5/1), interbedded with detriticarbonate silty clay, dark gray (5Y 4/1); bearing numerous discontinuous silt laminae. Dropstones occur in silty mud layers; almost absent in silty clay.</p> <p>Minor lithology: Section 1, 82-102 cm; Section 4, 222-134 cm; interbedded silty clay and clayey silt with color banding.</p> <p>SMEAR SLIDE SUMMARY (%):</p> <table border="1"> <tr> <td></td> <td>1, 57</td> <td>2, 47</td> <td>2, 140</td> <td>4, 115</td> </tr> <tr> <td>D</td> <td></td> <td>D</td> <td>M</td> <td>D</td> </tr> </table> <p>TEXTURE:</p> <table border="1"> <tr> <td>Sand</td> <td>10</td> <td>—</td> <td>—</td> <td>5</td> </tr> <tr> <td>Silt</td> <td>50</td> <td>25</td> <td>70</td> <td>25</td> </tr> <tr> <td>Clay</td> <td>40</td> <td>75</td> <td>30</td> <td>70</td> </tr> </table> <p>COMPOSITION:</p> <table border="1"> <tr> <td>Quartz</td> <td>25</td> <td>10</td> <td>30</td> <td>20</td> </tr> <tr> <td>Feldspar</td> <td>5</td> <td>—</td> <td>5</td> <td>—</td> </tr> <tr> <td>Rock frag., calcite</td> <td>25</td> <td>—</td> <td>35</td> <td>—</td> </tr> <tr> <td>Clay</td> <td>20</td> <td>10</td> <td>20</td> <td>20</td> </tr> <tr> <td>Volcanic glass</td> <td>—</td> <td>—</td> <td>Tr</td> <td>—</td> </tr> <tr> <td>Calcite/dolomite</td> <td>—</td> <td>80</td> <td>10</td> <td>60</td> </tr> <tr> <td>Accessory minerals</td> <td>5</td> <td>—</td> <td>Tr</td> <td>—</td> </tr> <tr> <td>Pyrite</td> <td>Tr</td> <td>—</td> <td>—</td> <td>—</td> </tr> </table>		1, 57	2, 47	2, 140	4, 115	D		D	M	D	Sand	10	—	—	5	Silt	50	25	70	25	Clay	40	75	30	70	Quartz	25	10	30	20	Feldspar	5	—	5	—	Rock frag., calcite	25	—	35	—	Clay	20	10	20	20	Volcanic glass	—	—	Tr	—	Calcite/dolomite	—	80	10	60	Accessory minerals	5	—	Tr	—	Pyrite	Tr	—	—	—
	1, 57	2, 47	2, 140	4, 115																																																																											
D		D	M	D																																																																											
Sand	10	—	—	5																																																																											
Silt	50	25	70	25																																																																											
Clay	40	75	30	70																																																																											
Quartz	25	10	30	20																																																																											
Feldspar	5	—	5	—																																																																											
Rock frag., calcite	25	—	35	—																																																																											
Clay	20	10	20	20																																																																											
Volcanic glass	—	—	Tr	—																																																																											
Calcite/dolomite	—	80	10	60																																																																											
Accessory minerals	5	—	Tr	—																																																																											
Pyrite	Tr	—	—	—																																																																											
	B						$\gamma=1.90$ $W=30$ $\phi=42.3$	$\phi=33.6$ CaCO ₃ =35	2				*																																																																		
	B						$\gamma=1.90$ $W=18$ $\phi=33.6$	$\phi=33.6$ CaCO ₃ =35	3		VOID		*																																																																		
	R/M						TOC=0.53 CaCO ₃ =32.6		4		VOID		*																																																																		
									CC																																																																						

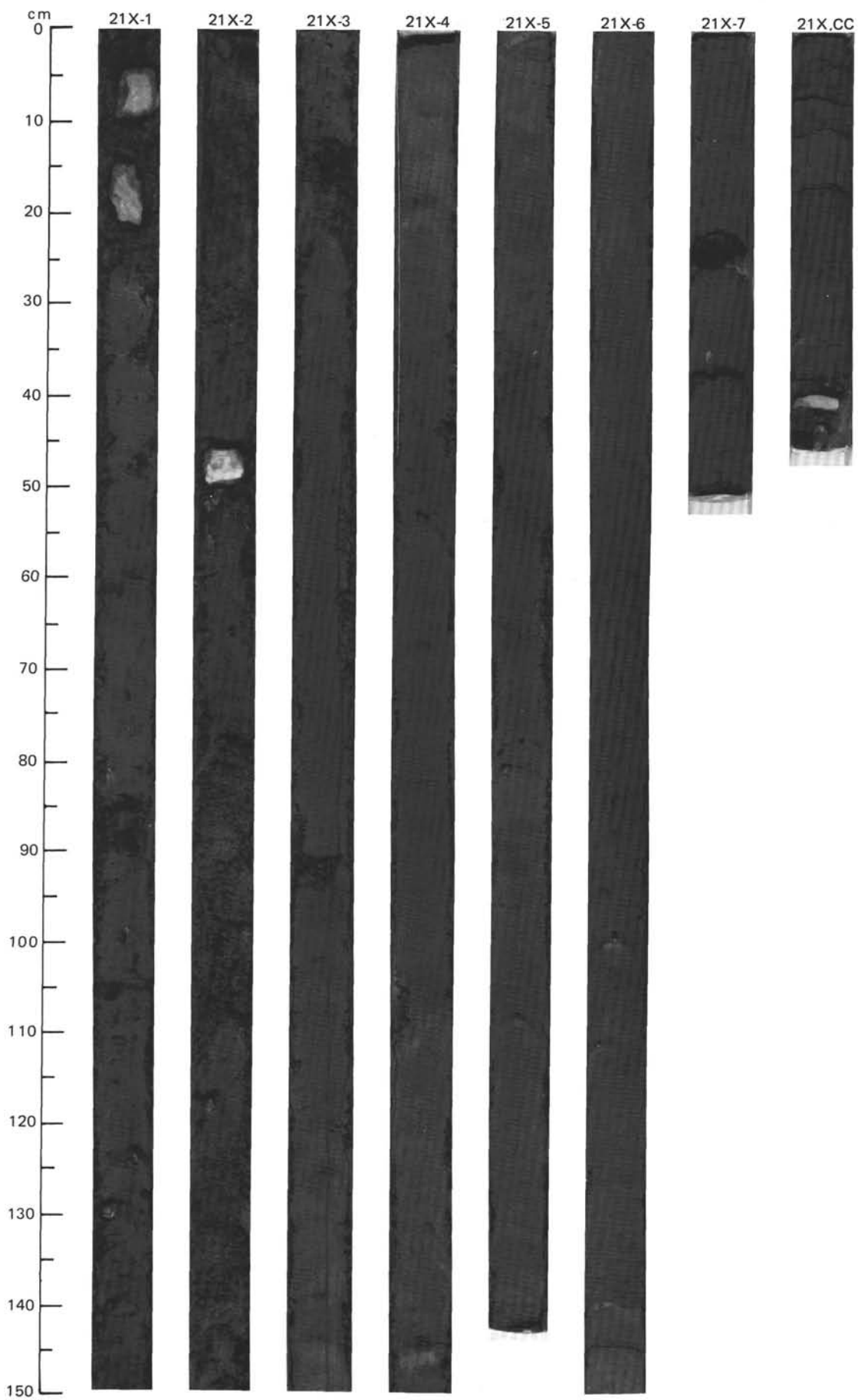
SITE 645 HOLE B CORE 18 X CORED INTERVAL 2166.6-2176.3 mbsl; 158.4-168.1 mbsf

TIME-ROCK UNIT	BIOSTRAT. ZONE/ FOSSIL CHARACTER					PALEOMAGNETICS	PHYS. PROPERTIES	CHEMISTRY	SECTION	METERS	GRAPHIC LITHOLOGY	DRILLING DISTURB.	SED. STRUCTURES	SAMPLES	LITHOLOGIC DESCRIPTION																			
	FORAMINIFERS	NANNOFOSSILS	RADIOLARIANS	DIATOMS	DINOCYSTS																													
LOWER PLEISTOCENE	F/M	B	B	B <i>Brigantedinium simplex</i>	F/G	Matuyama Chronozone?	$\gamma=2.20$ $W=19$ $\phi=53.9$	$\phi=53.9$ TOC=0.88 CaCO ₃ =26	1	0.5 1.0				<p>DETRICARBONATE SILTY MUD</p> <p>Detriticarbonate silty mud with 5% scattered gravel, dark greenish gray (5GY 4/1), dark gray (5Y 4/1).</p> <p>SMEAR SLIDE SUMMARY (%):</p> <table border="1"> <tr> <td>D</td> <td>1, 60</td> </tr> </table> <p>TEXTURE:</p> <table border="1"> <tr> <td>Sand</td> <td>30</td> </tr> <tr> <td>Silt</td> <td>50</td> </tr> <tr> <td>Clay</td> <td>20</td> </tr> </table> <p>COMPOSITION:</p> <table border="1"> <tr> <td>Quartz</td> <td>40</td> </tr> <tr> <td>Feldspar</td> <td>10</td> </tr> <tr> <td>Clay</td> <td>15</td> </tr> <tr> <td>Volcanic glass</td> <td>Tr</td> </tr> <tr> <td>Calcite/dolomite</td> <td>35</td> </tr> <tr> <td>Accessory minerals</td> <td>Tr</td> </tr> </table>	D	1, 60	Sand	30	Silt	50	Clay	20	Quartz	40	Feldspar	10	Clay	15	Volcanic glass	Tr	Calcite/dolomite	35	Accessory minerals	Tr
D	1, 60																																	
Sand	30																																	
Silt	50																																	
Clay	20																																	
Quartz	40																																	
Feldspar	10																																	
Clay	15																																	
Volcanic glass	Tr																																	
Calcite/dolomite	35																																	
Accessory minerals	Tr																																	
									CC																									

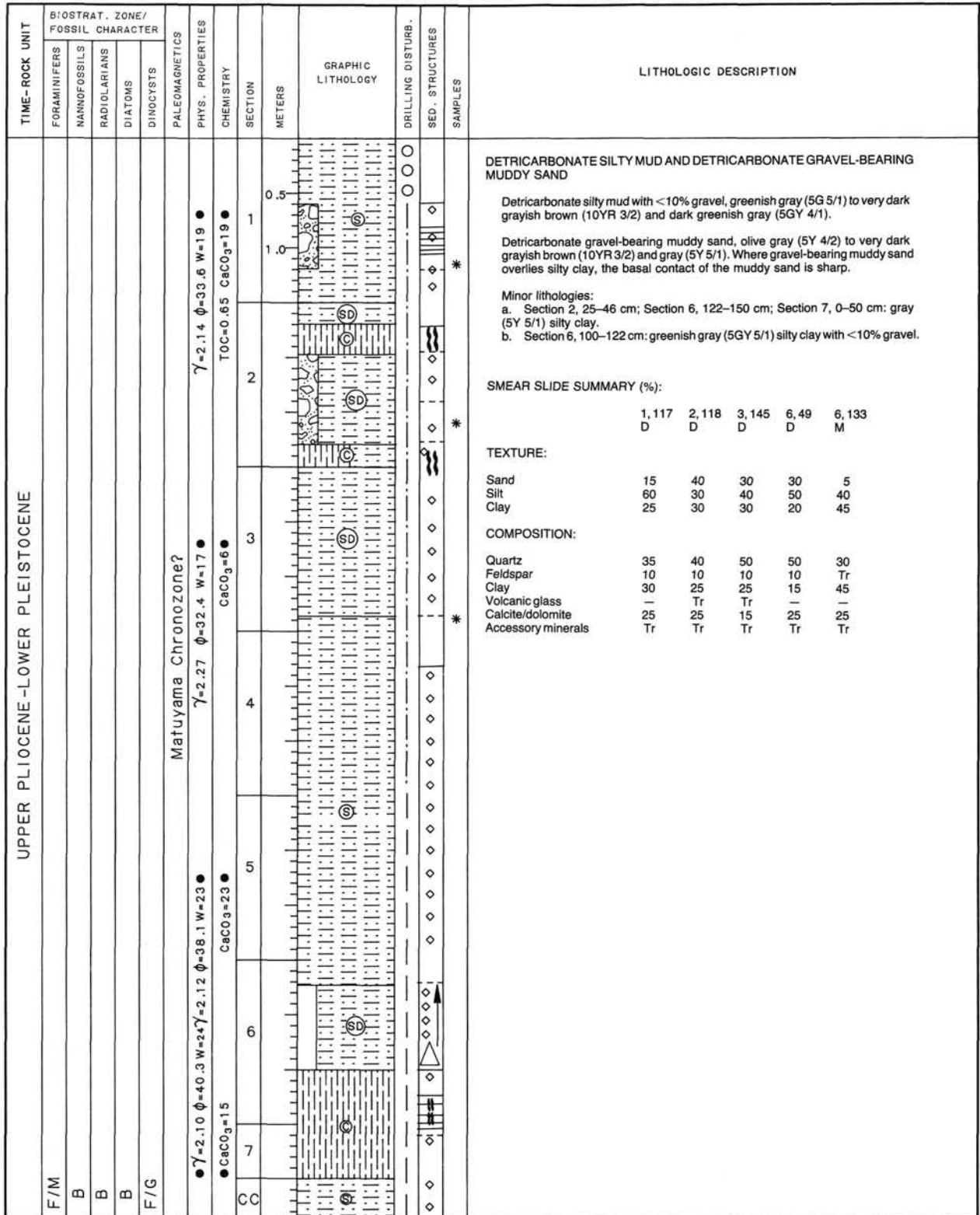


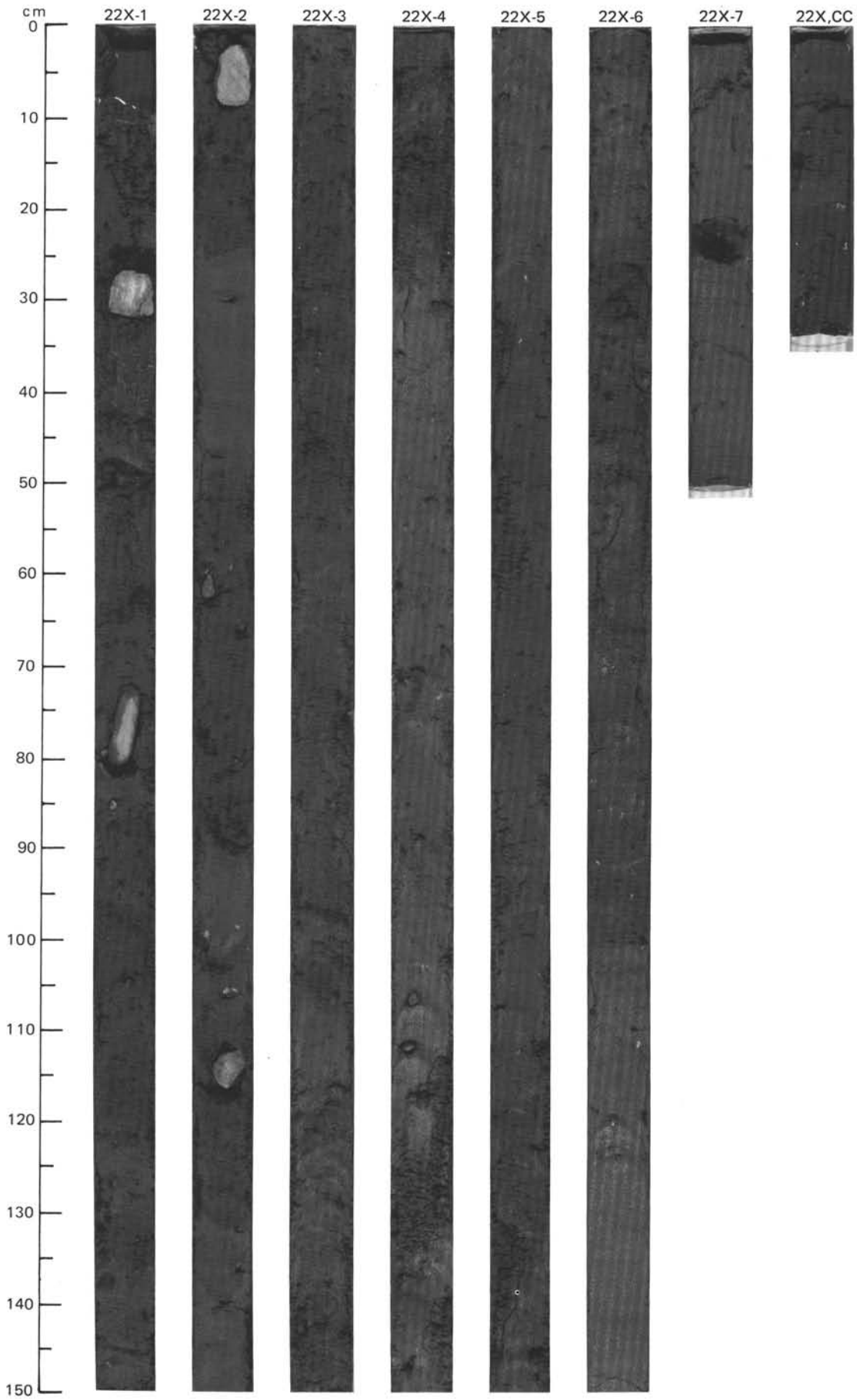


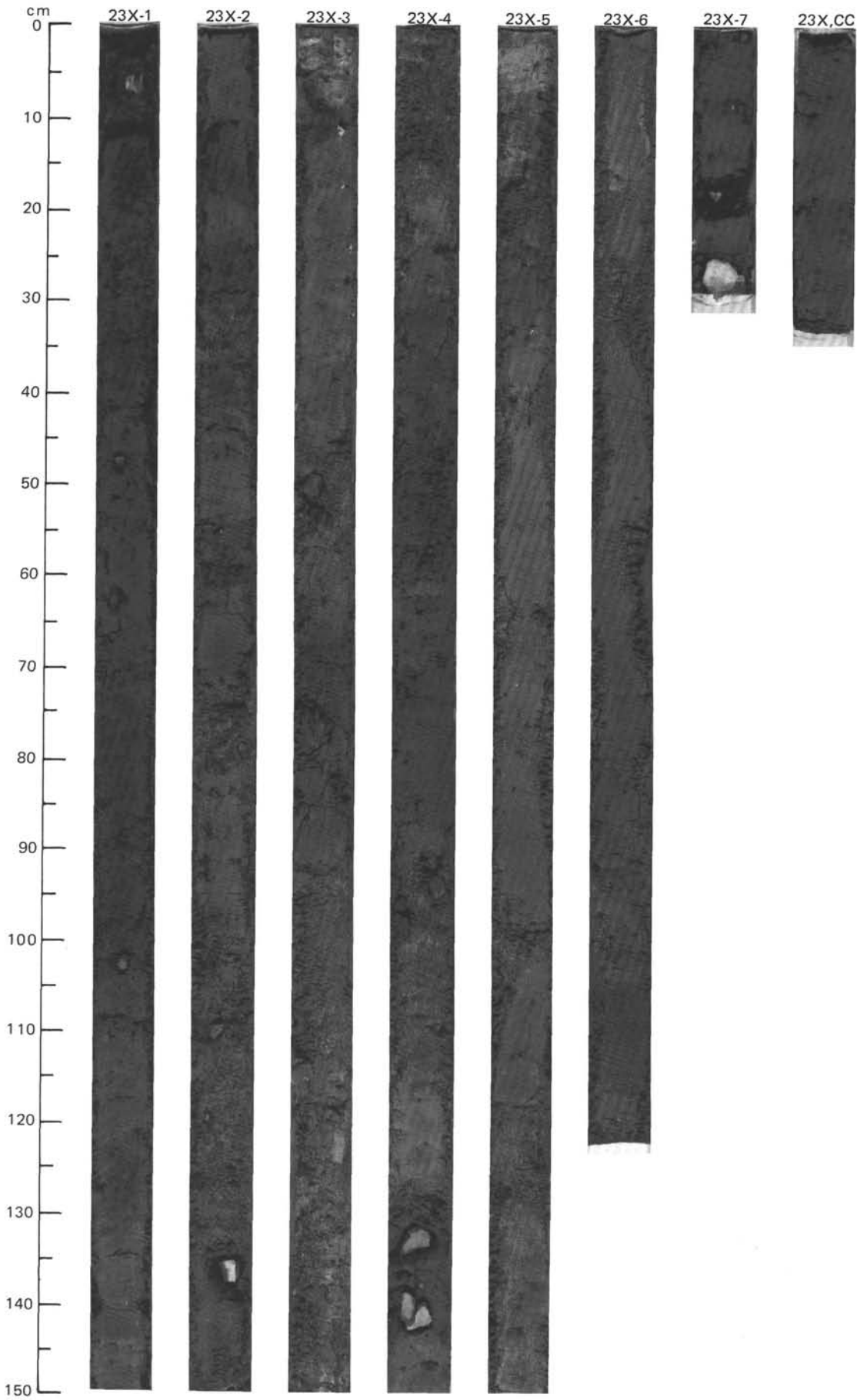




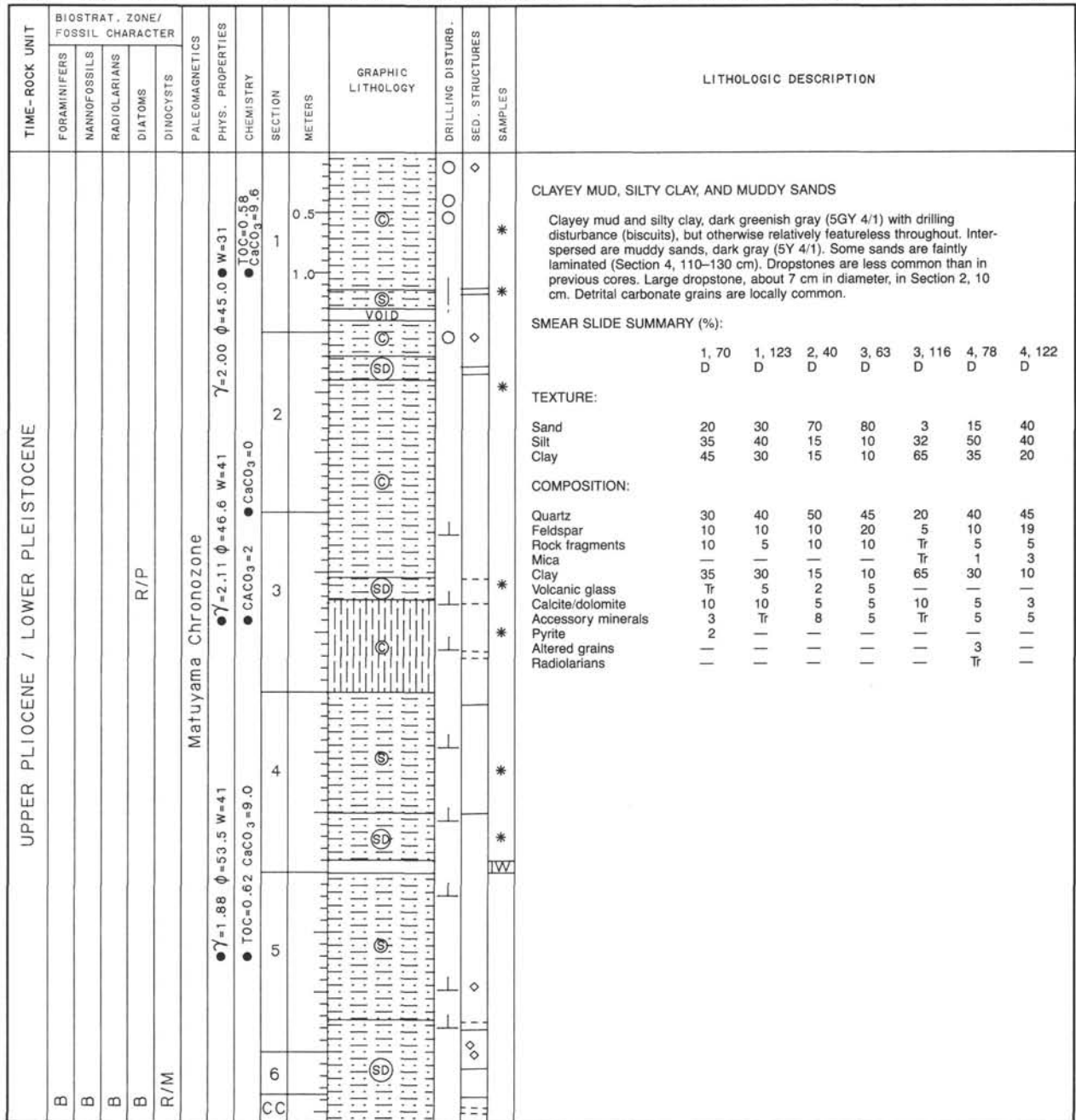
SITE 645 HOLE B CORE 22 X CORED INTERVAL 2205.0-2214.8 mbsl; 196.8-206.6 mbsf



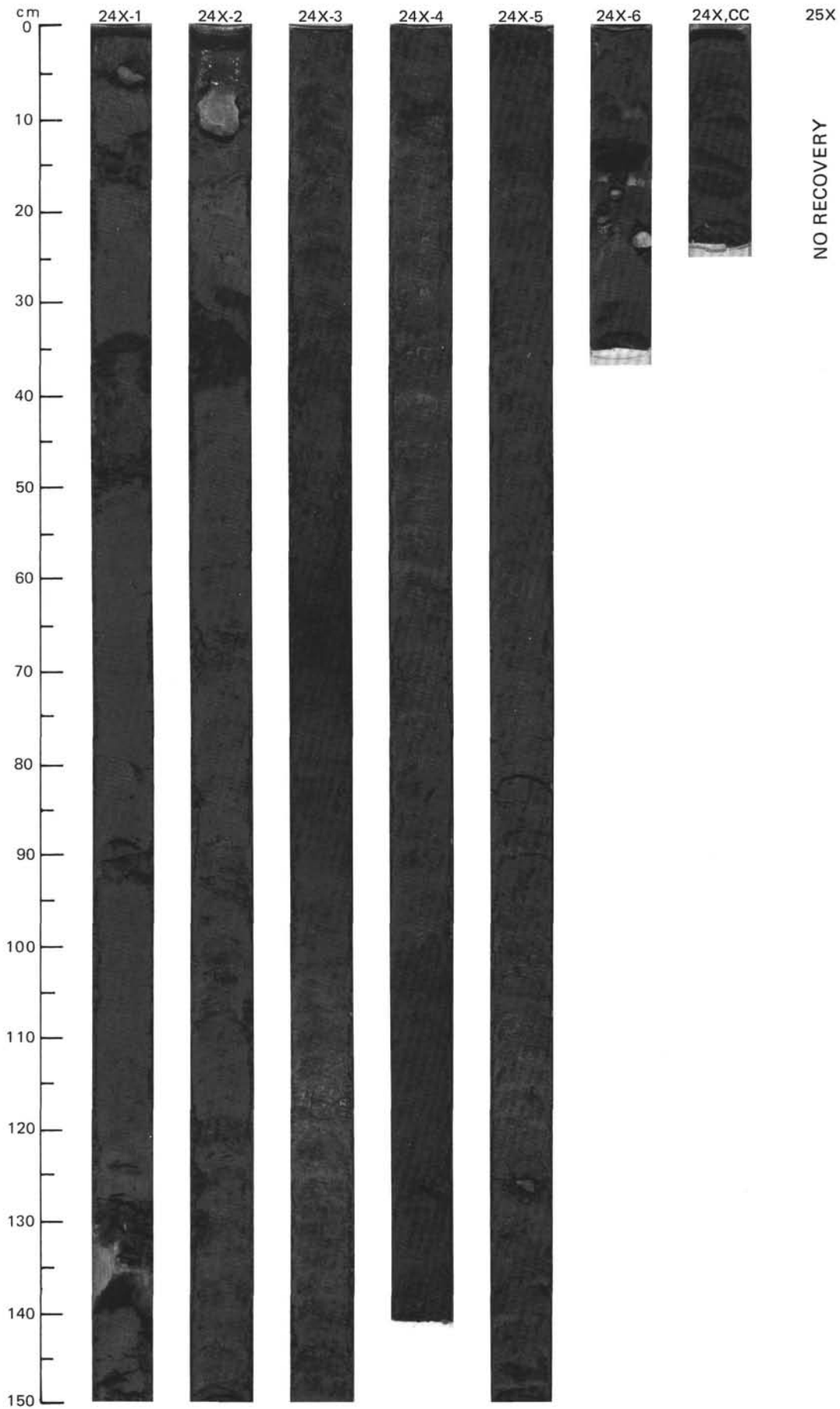


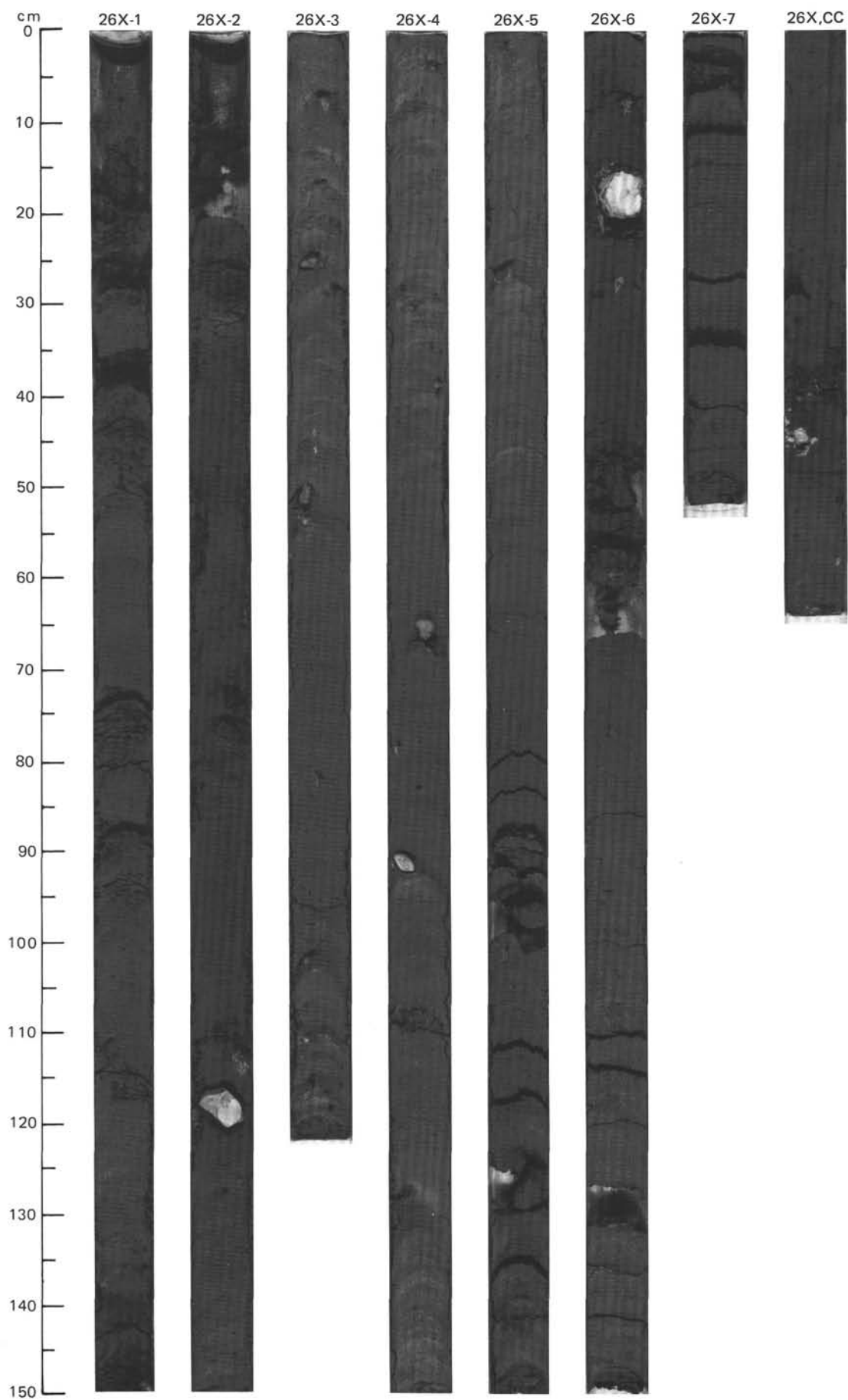


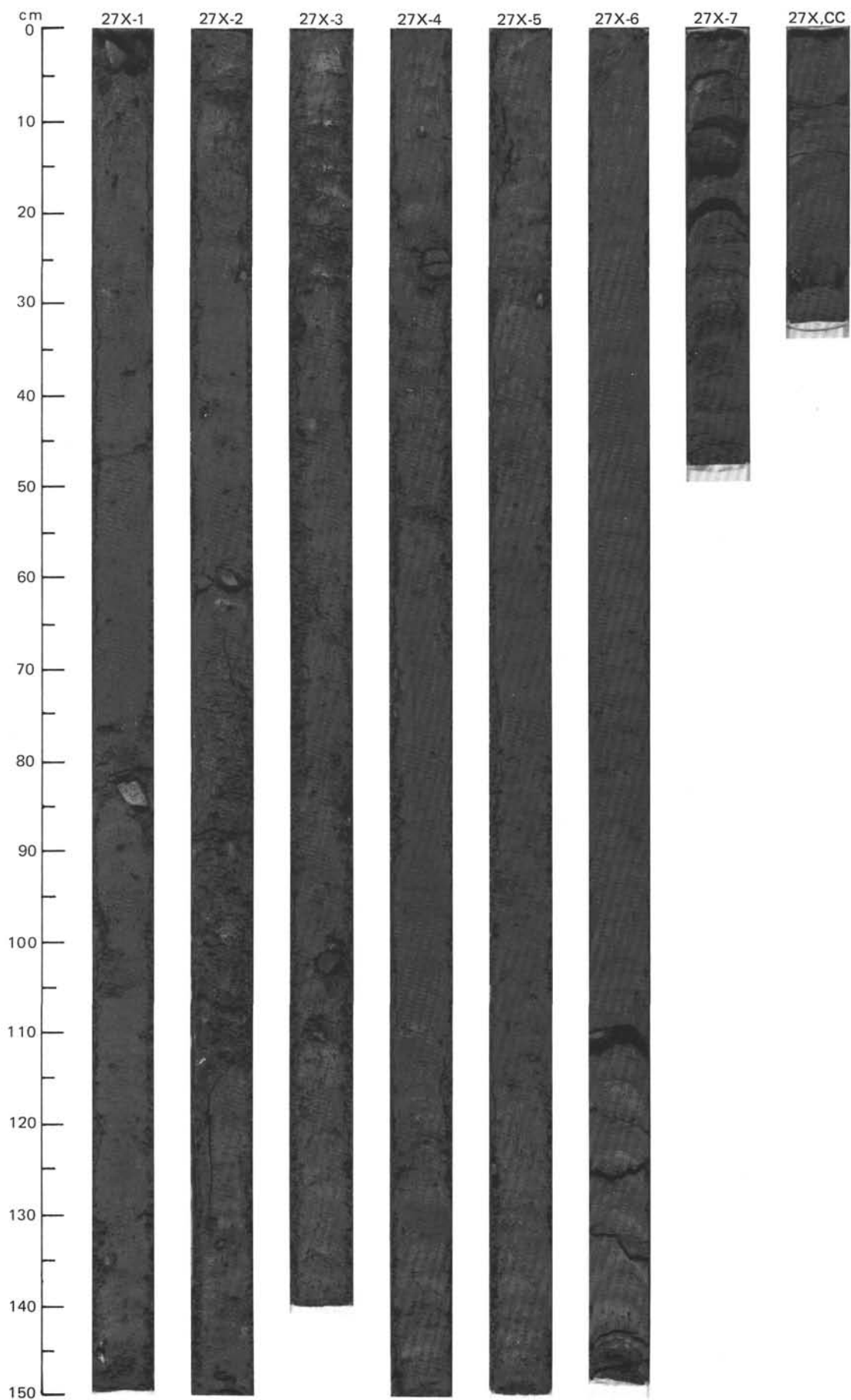
SITE 645 HOLE B CORE 24 X CORED INTERVAL 2224.4-2234.1 mbsl; 216.2-225.9 mbsf

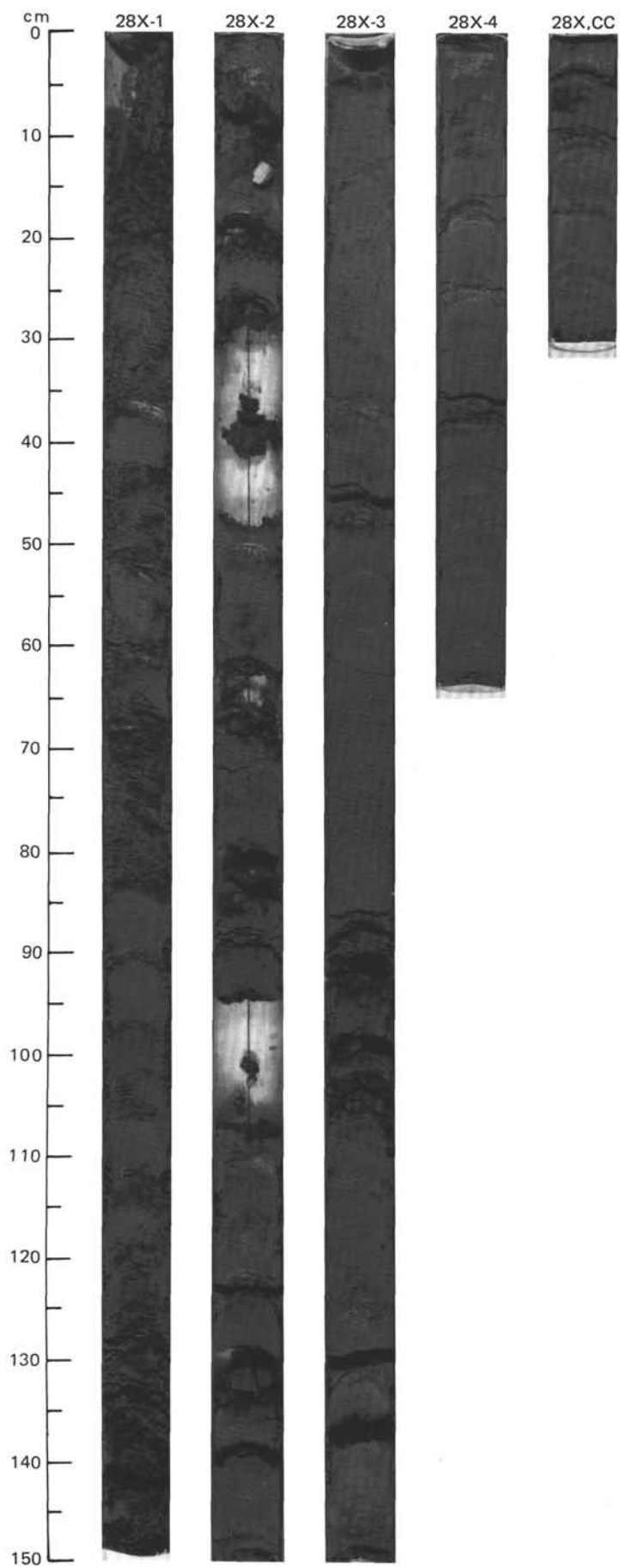


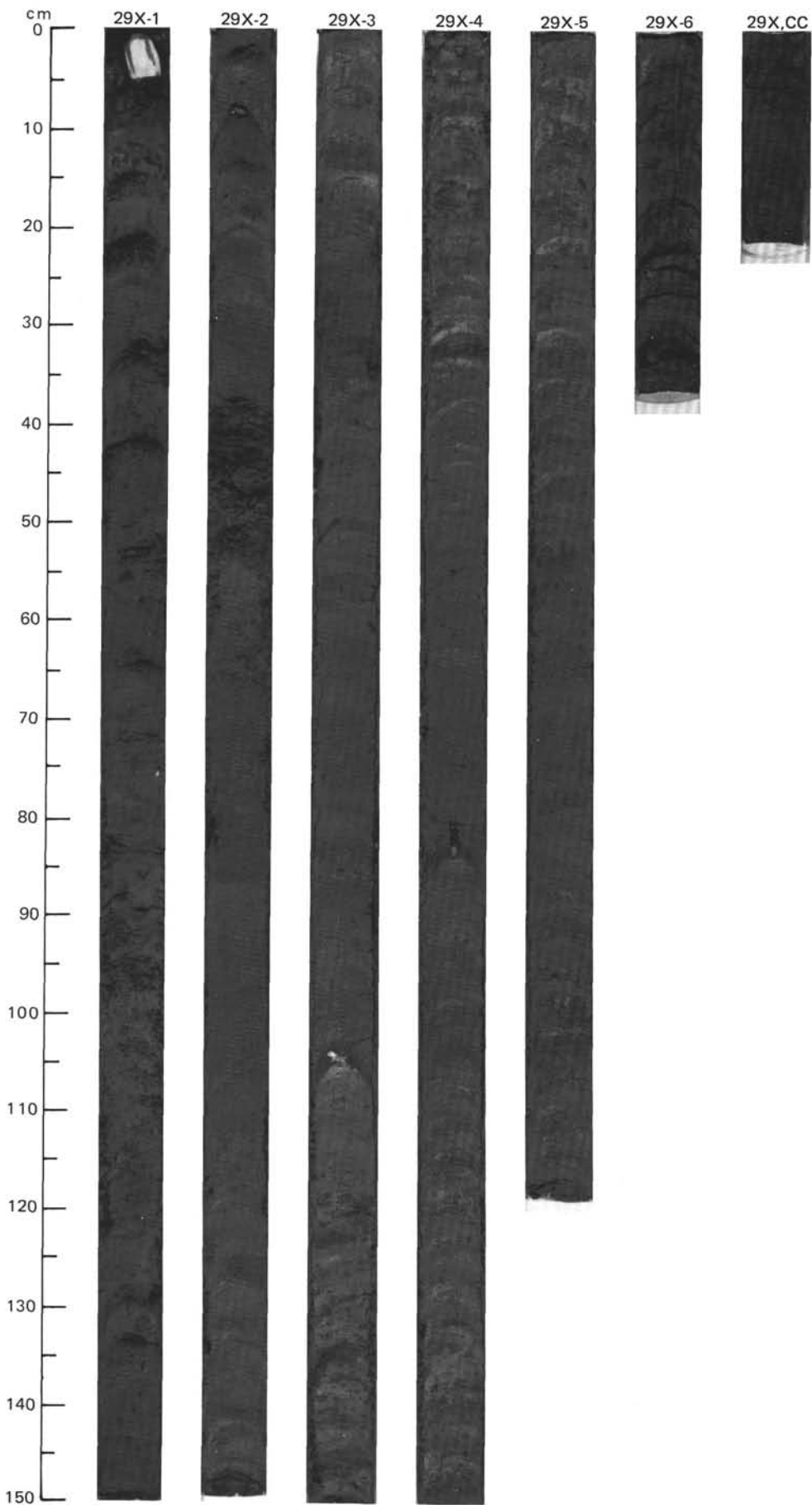
CORE 25 NO RECOVERY





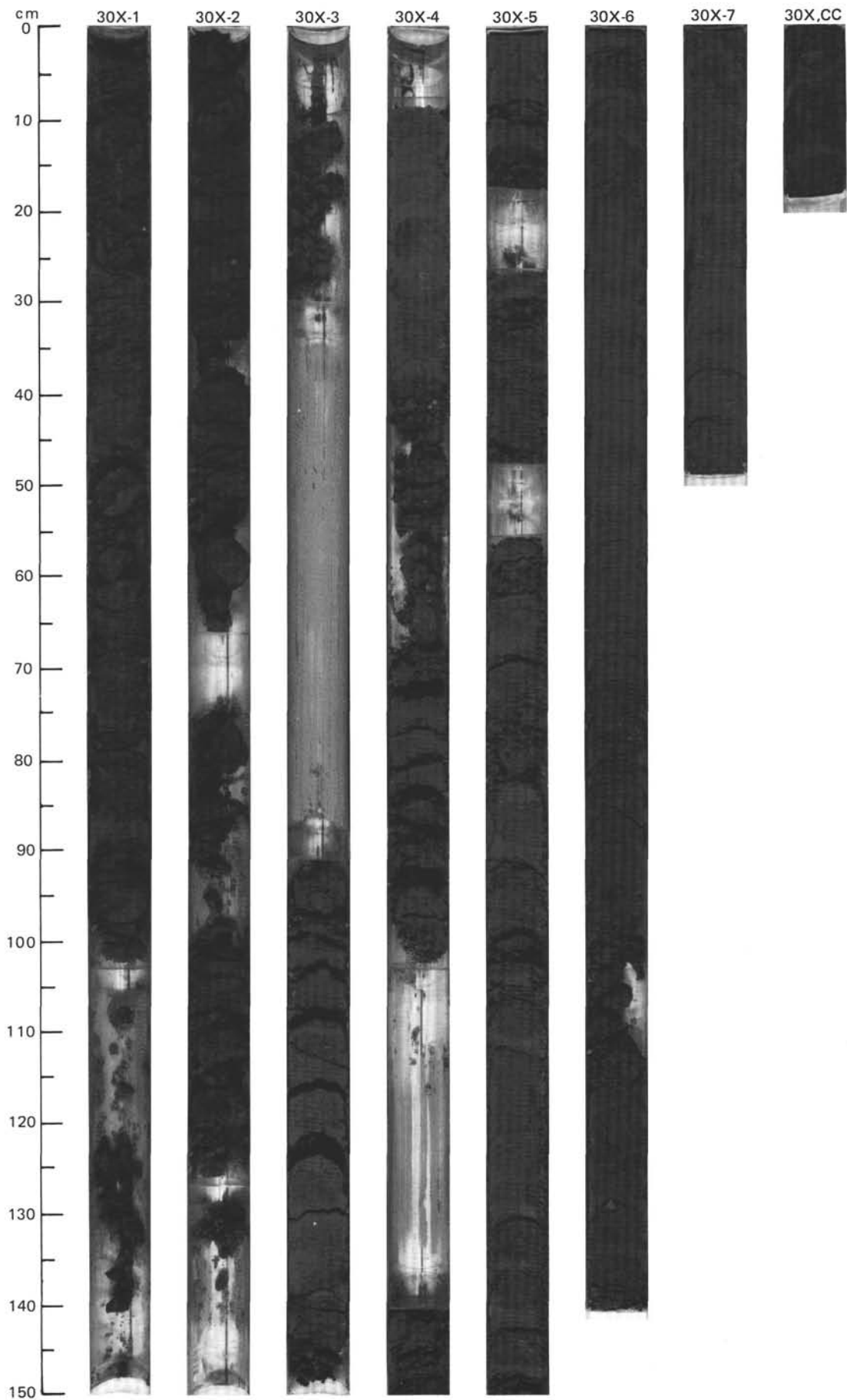


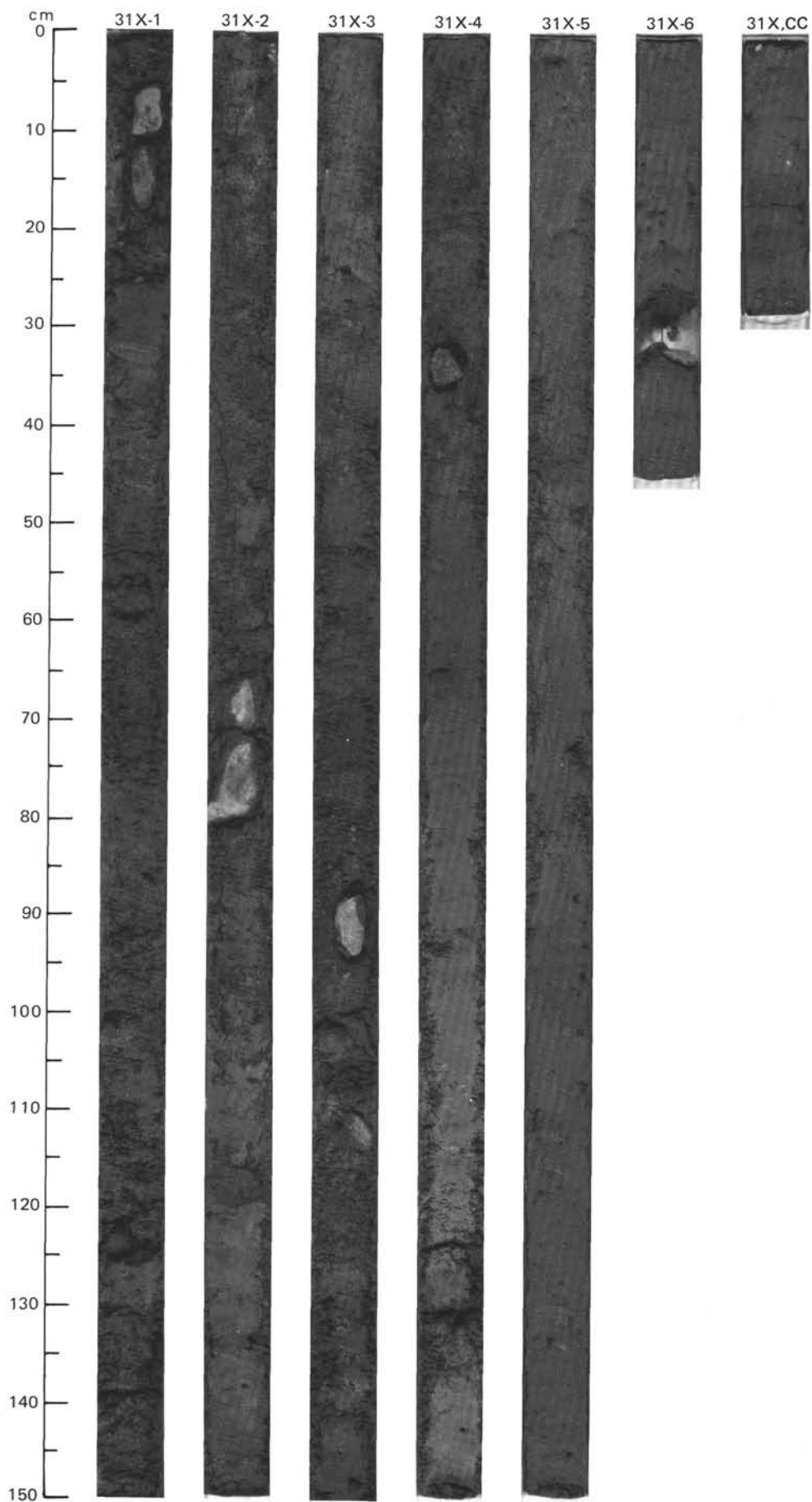


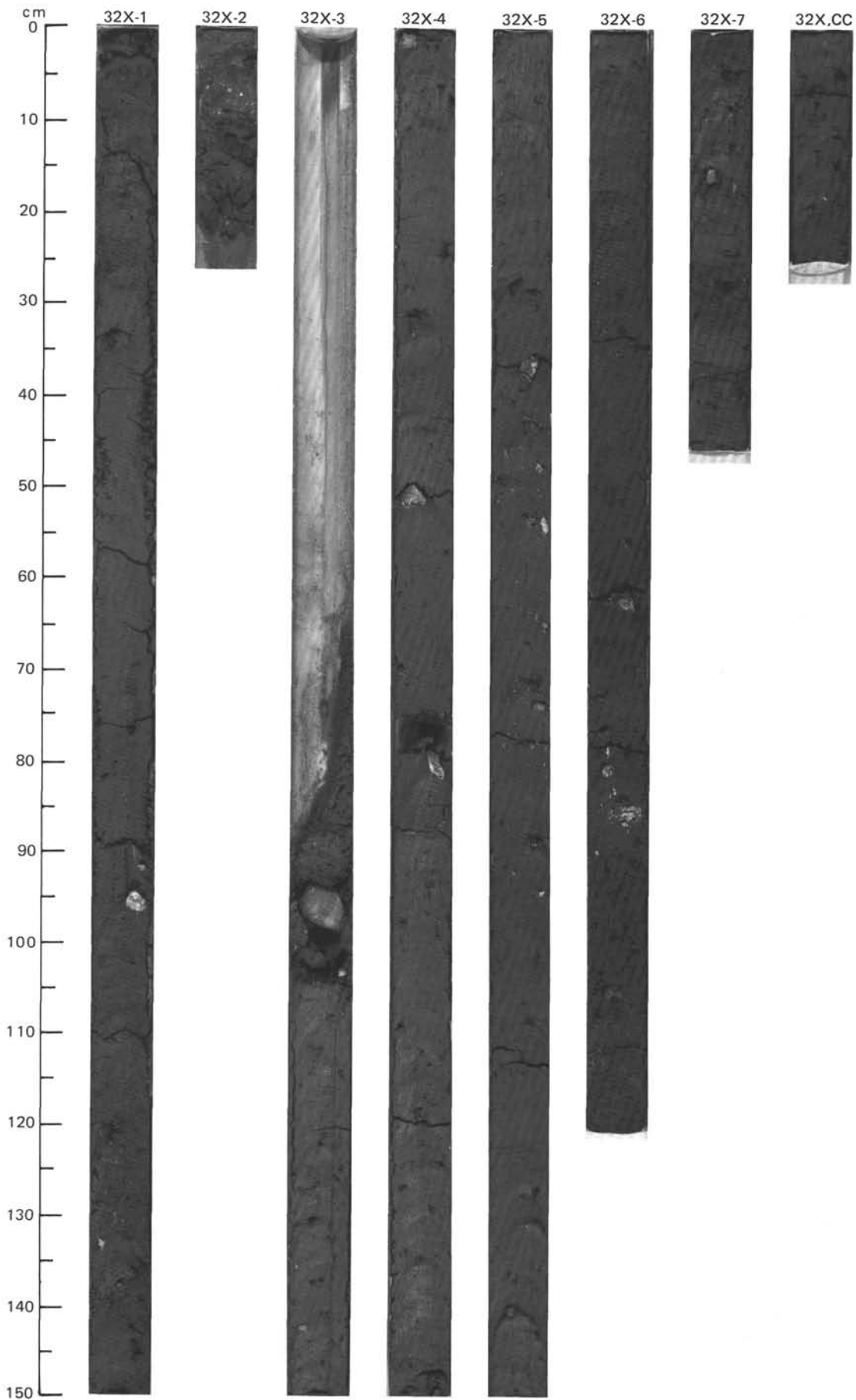


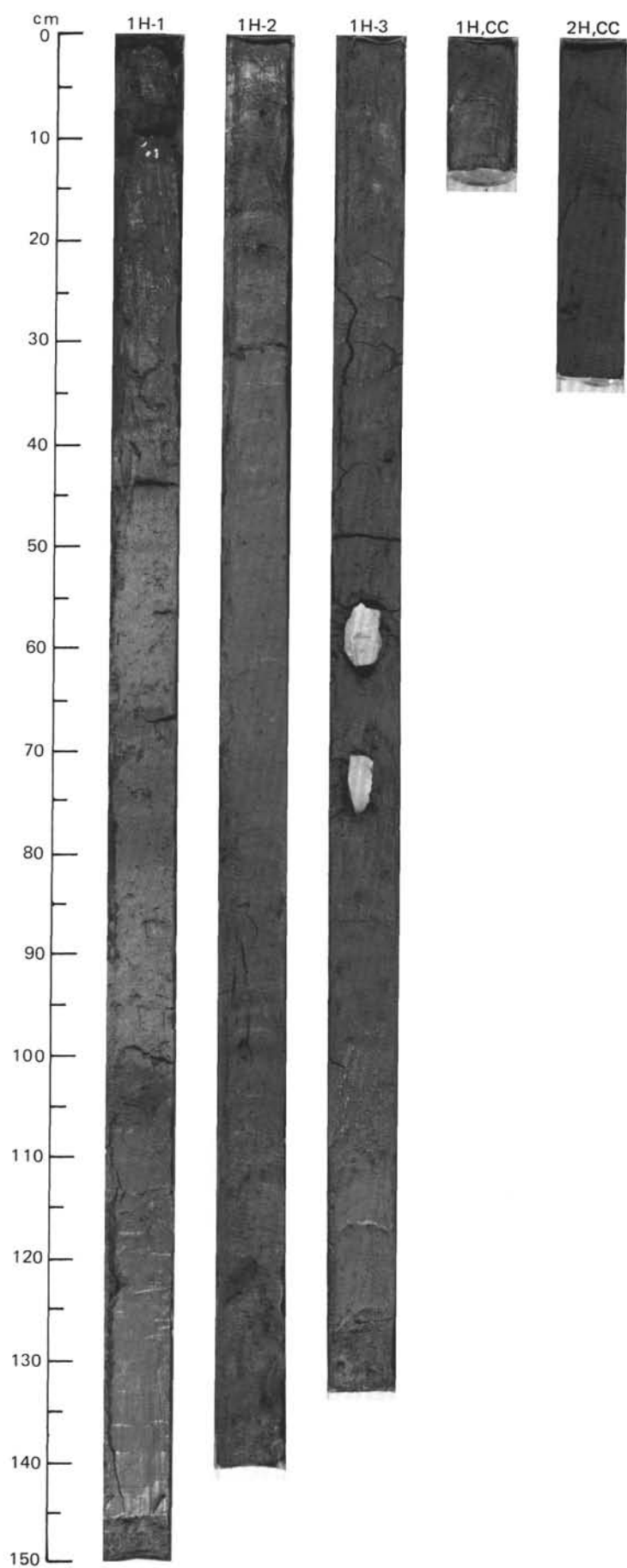
SITE 645 HOLE B CORE 30 X CORED INTERVAL 2282.4-2292.0 mbsl; 274.2 283.8 mbsf

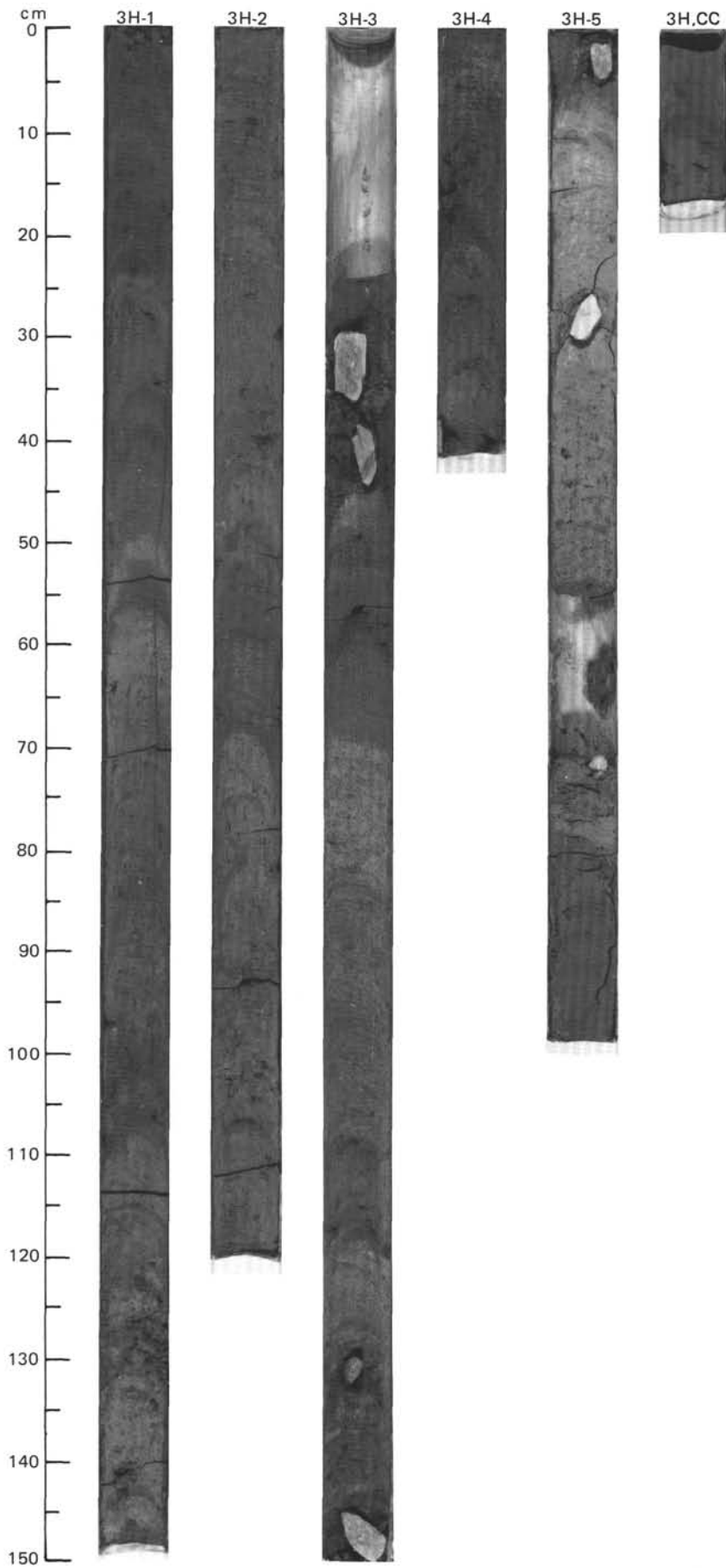
TIME-ROCK UNIT		BIOSTRAT. ZONE/ FOSSIL CHARACTER				PALEOMAGNETICS	PHYS. PROPERTIES	CHEMISTRY	SECTION	METERS	GRAPHIC LITHOLOGY	DRILLING DISTURB.	SED. STRUCTURES	SAMPLES	LITHOLOGIC DESCRIPTION																																																											
UPPER PLIOCENE	(<i>N. pachyderma</i>)	FORAMINIFERS	NANNOFOSSILS	RADIOLARIANS	DIATOMS											DINOCYSTS																																																										
F/M	B								0.5					<p>SAND AND SILTY SAND</p> <p>Sand, dark gray (5Y 4/1); micaceous, fine grained; grading downward into silty sand, dark greenish gray (5GY 4/1) and greenish gray (5GY 5/1); 10% heavy minerals and detrital carbonate grains; apparently structureless.</p> <p>SMEAR SLIDE SUMMARY (%):</p> <table border="1"> <tr> <td></td> <td>1, 90</td> <td>4, 31</td> <td>6, 102</td> </tr> <tr> <td></td> <td>D</td> <td>M</td> <td>D</td> </tr> </table> <p>TEXTURE:</p> <table border="1"> <tr> <td>Sand</td> <td>85</td> <td>10</td> <td>85</td> </tr> <tr> <td>Silt</td> <td>10</td> <td>80</td> <td>10</td> </tr> <tr> <td>Clay</td> <td>5</td> <td>10</td> <td>5</td> </tr> </table> <p>COMPOSITION:</p> <table border="1"> <tr> <td>Quartz</td> <td>54</td> <td>55</td> <td>54</td> </tr> <tr> <td>Feldspar</td> <td>20</td> <td>15</td> <td>20</td> </tr> <tr> <td>Mica</td> <td>5</td> <td>5</td> <td>5</td> </tr> <tr> <td>Clay</td> <td>—</td> <td>10</td> <td>—</td> </tr> <tr> <td>Volcanic glass</td> <td>Tr</td> <td>—</td> <td>—</td> </tr> <tr> <td>Calcite/dolomite</td> <td>10</td> <td>5</td> <td>10</td> </tr> <tr> <td>Accessory minerals</td> <td>10</td> <td>10</td> <td>10</td> </tr> <tr> <td>Diatoms</td> <td>Tr</td> <td>—</td> <td>Tr</td> </tr> <tr> <td>Radiolarians</td> <td>Tr</td> <td>—</td> <td>Tr</td> </tr> <tr> <td>Sponge spicules</td> <td>1</td> <td>Tr</td> <td>1</td> </tr> </table>		1, 90	4, 31	6, 102		D	M	D	Sand	85	10	85	Silt	10	80	10	Clay	5	10	5	Quartz	54	55	54	Feldspar	20	15	20	Mica	5	5	5	Clay	—	10	—	Volcanic glass	Tr	—	—	Calcite/dolomite	10	5	10	Accessory minerals	10	10	10	Diatoms	Tr	—	Tr	Radiolarians	Tr	—	Tr	Sponge spicules	1	Tr	1
	1, 90	4, 31	6, 102																																																																							
	D	M	D																																																																							
Sand	85	10	85																																																																							
Silt	10	80	10																																																																							
Clay	5	10	5																																																																							
Quartz	54	55	54																																																																							
Feldspar	20	15	20																																																																							
Mica	5	5	5																																																																							
Clay	—	10	—																																																																							
Volcanic glass	Tr	—	—																																																																							
Calcite/dolomite	10	5	10																																																																							
Accessory minerals	10	10	10																																																																							
Diatoms	Tr	—	Tr																																																																							
Radiolarians	Tr	—	Tr																																																																							
Sponge spicules	1	Tr	1																																																																							
									1.0	VOID			*																																																													
									2.0	VOID																																																																
									3.0	VOID																																																																
									4.0	VOID																																																																
									5.0	VOID																																																																
									6.0	VOID																																																																
									7.0	VOID																																																																
									8.0	VOID																																																																





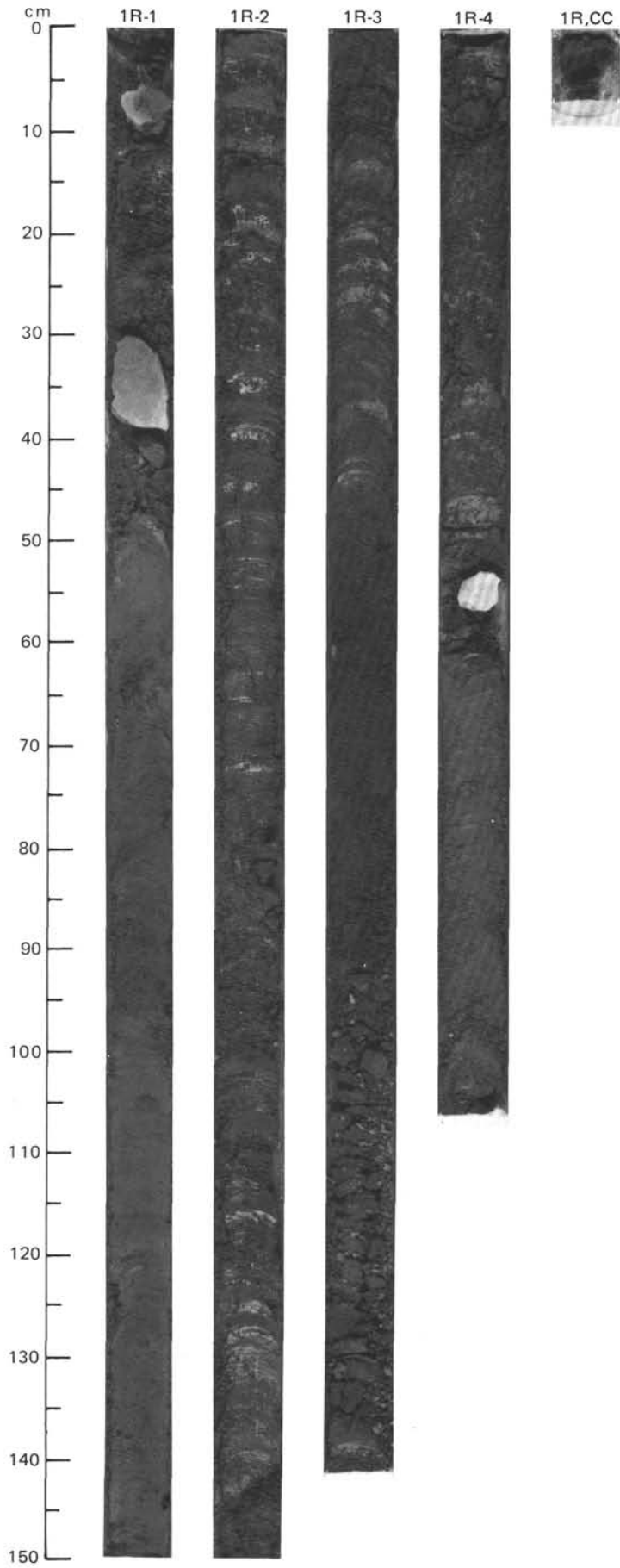


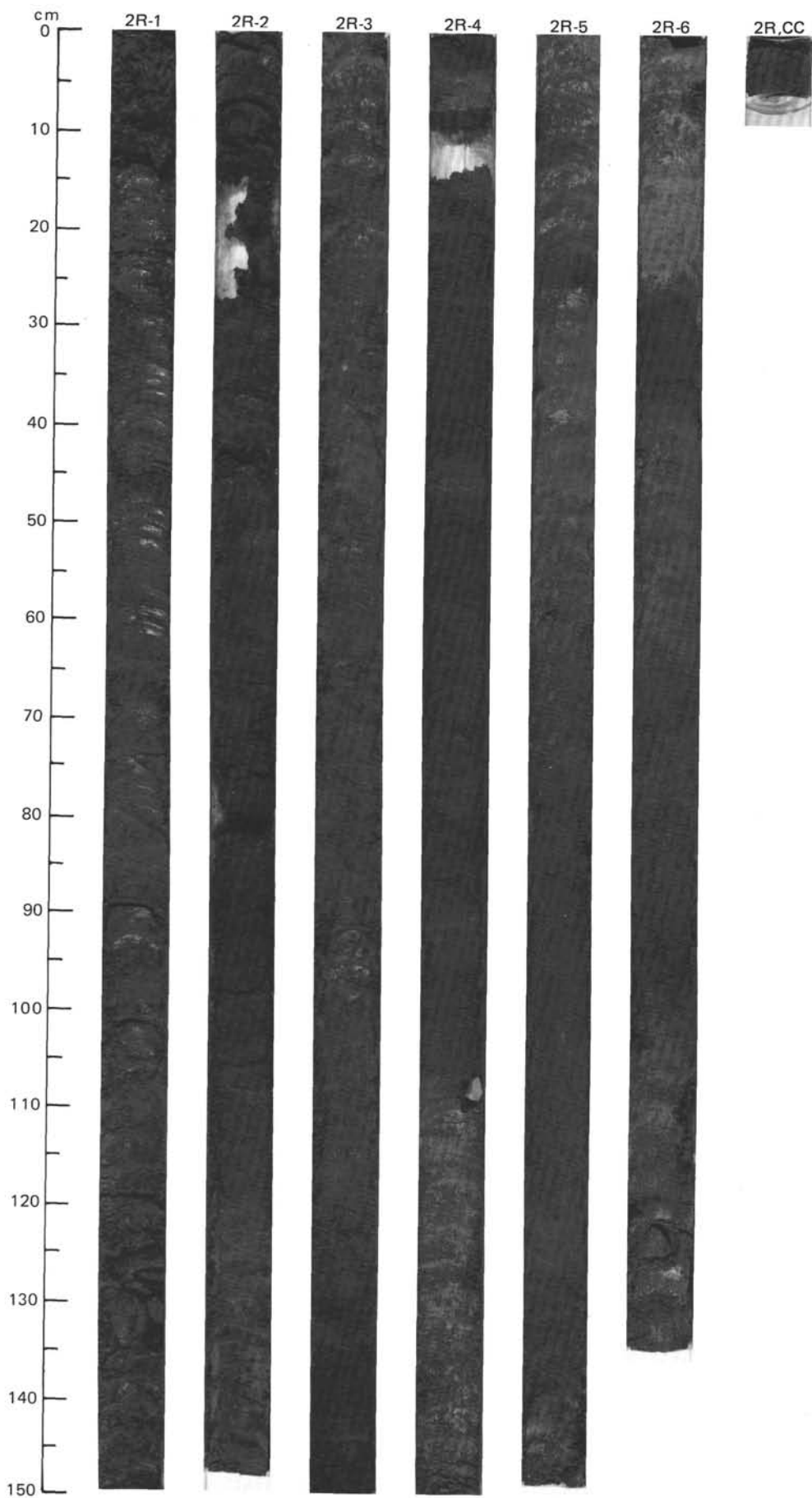




SITE 645 HOLE D CORE 1 R CORED INTERVAL 2273.2-2280.4 mbsl; 265.7-272.9 mbsf

TIME-ROCK UNIT	BIOSTRAT. ZONE/ FOSSIL CHARACTER				PALEOMAGNETICS	PHYS. PROPERTIES	CHEMISTRY	SECTION	METERS	GRAPHIC LITHOLOGY	DRILLING DISTURB.	SED. STRUCTURES	SAMPLES	LITHOLOGIC DESCRIPTION																																																																																																
	FORAMINIFERS	NANNOFOSSILS	RADIOLARIANS	DIATOMS																																																																																																										
	B													<p>SILTY MUD</p> <p>Silty mud, dark greenish gray (56Y 4/1), with local occurrences of detrital carbonate grains.</p> <p>A upward-fining sequence occurs from muddy sand, Section 3, 90 cm, to silty clay, Section 1, 100 cm. Granules and pebbles are sparse or absent in Sections 2 and 3.</p> <p>Minor lithologies: a. Section 3, 47-52 cm: homogeneous muddy sand, dark olive gray (5Y 4/2). b. Section 1, 50-68 cm, 100-121 cm: silty clay, dark greenish gray (56Y 4/1).</p> <p>SMEAR SLIDE SUMMARY (%):</p> <table border="1"> <tr> <td></td> <td>1, 86</td> <td>1, 115</td> <td>2, 53</td> <td>3, 56</td> <td>3, 133</td> </tr> <tr> <td>D</td> <td>D</td> <td>D</td> <td>D</td> <td>D</td> <td>D</td> </tr> </table> <p>TEXTURE:</p> <table border="1"> <tr> <td>Sand</td> <td>40</td> <td>5</td> <td>40</td> <td>70</td> <td>20</td> </tr> <tr> <td>Silt</td> <td>50</td> <td>30</td> <td>30</td> <td>20</td> <td>50</td> </tr> <tr> <td>Clay</td> <td>10</td> <td>65</td> <td>30</td> <td>10</td> <td>30</td> </tr> </table> <p>COMPOSITION:</p> <table border="1"> <tr> <td>Quartz</td> <td>40</td> <td>10</td> <td>55</td> <td>40</td> <td>45</td> </tr> <tr> <td>Feldspar</td> <td>20</td> <td>5</td> <td>10</td> <td>5</td> <td>10</td> </tr> <tr> <td>Rock fragments</td> <td>10</td> <td>—</td> <td>—</td> <td>30</td> <td>—</td> </tr> <tr> <td>Mica</td> <td>Tr</td> <td>Tr</td> <td>2</td> <td>2</td> <td>2</td> </tr> <tr> <td>Clay</td> <td>10</td> <td>60</td> <td>20</td> <td>10</td> <td>30</td> </tr> <tr> <td>Volcanic glass</td> <td>5</td> <td>Tr</td> <td>—</td> <td>Tr</td> <td>—</td> </tr> <tr> <td>Calcite/dolomite</td> <td>10</td> <td>20</td> <td>10</td> <td>Tr</td> <td>10</td> </tr> <tr> <td>Accessory minerals</td> <td>5</td> <td>5</td> <td>3</td> <td>5</td> <td>3</td> </tr> <tr> <td>Opaque grains</td> <td>—</td> <td>—</td> <td>—</td> <td>3</td> <td>—</td> </tr> <tr> <td>Diatoms</td> <td>—</td> <td>—</td> <td>—</td> <td>Tr</td> <td>—</td> </tr> <tr> <td>Sponge spicules</td> <td>—</td> <td>—</td> <td>—</td> <td>5</td> <td>—</td> </tr> </table>		1, 86	1, 115	2, 53	3, 56	3, 133	D	D	D	D	D	D	Sand	40	5	40	70	20	Silt	50	30	30	20	50	Clay	10	65	30	10	30	Quartz	40	10	55	40	45	Feldspar	20	5	10	5	10	Rock fragments	10	—	—	30	—	Mica	Tr	Tr	2	2	2	Clay	10	60	20	10	30	Volcanic glass	5	Tr	—	Tr	—	Calcite/dolomite	10	20	10	Tr	10	Accessory minerals	5	5	3	5	3	Opaque grains	—	—	—	3	—	Diatoms	—	—	—	Tr	—	Sponge spicules	—	—	—	5	—
	1, 86	1, 115	2, 53	3, 56	3, 133																																																																																																									
D	D	D	D	D	D																																																																																																									
Sand	40	5	40	70	20																																																																																																									
Silt	50	30	30	20	50																																																																																																									
Clay	10	65	30	10	30																																																																																																									
Quartz	40	10	55	40	45																																																																																																									
Feldspar	20	5	10	5	10																																																																																																									
Rock fragments	10	—	—	30	—																																																																																																									
Mica	Tr	Tr	2	2	2																																																																																																									
Clay	10	60	20	10	30																																																																																																									
Volcanic glass	5	Tr	—	Tr	—																																																																																																									
Calcite/dolomite	10	20	10	Tr	10																																																																																																									
Accessory minerals	5	5	3	5	3																																																																																																									
Opaque grains	—	—	—	3	—																																																																																																									
Diatoms	—	—	—	Tr	—																																																																																																									
Sponge spicules	—	—	—	5	—																																																																																																									
					W=3.4 M=1.95 D=48.4	CaCO ₃ =8%																																																																																																								
					W=2.14 M=2.5 D=42.1	TOC=0.37 CaCO ₃ =18.5																																																																																																								
					W=2.14 M=2.5 D=42.1	TOC=0.70 CaCO ₃ =8.5																																																																																																								





SITE 645 HOLE D CORE 3 R CORED INTERVAL 2290.0-2299.7 mbsl; 282.5-292.2 mbsf

TIME-ROCK UNIT	BIOSTRAT. ZONE/ FOSSIL CHARACTER					PALEOMAGNETICS	PHYS. PROPERTIES	CHEMISTRY	SECTION	METERS	GRAPHIC LITHOLOGY	DRILLING DISTURB.	SED. STRUCTURES	SAMPLES	LITHOLOGIC DESCRIPTION
	FORAMINIFERS	NANNOFOSSILS	RADIOLARIANS	DIATOMS	DINOCYSTS										
									CC	1 0.5					Single pebble: dark quartzite.

SITE 645 HOLE D CORE 4 R CORED INTERVAL 2299.7-2309.3 mbsl; 292.2-301.8 mbsf

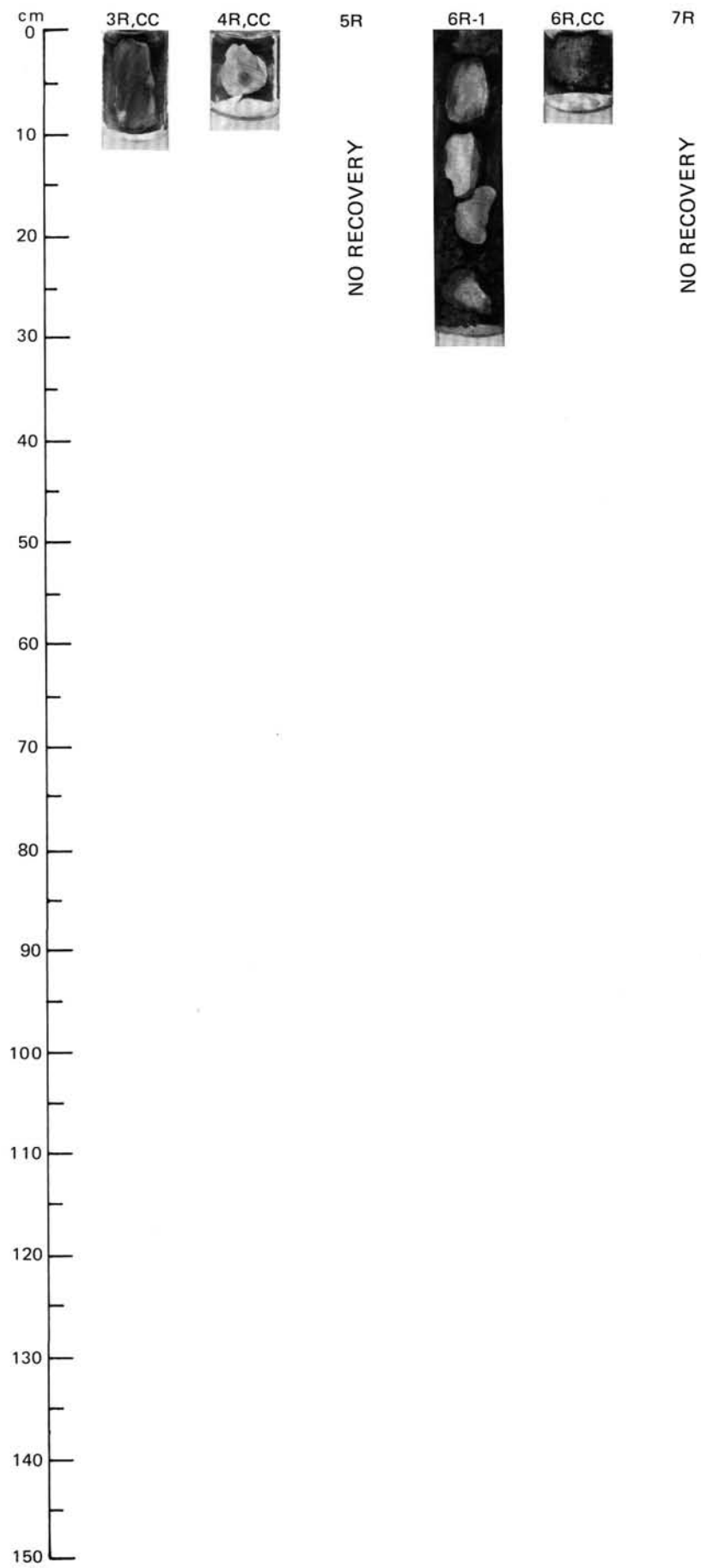
TIME-ROCK UNIT	BIOSTRAT. ZONE/ FOSSIL CHARACTER					PALEOMAGNETICS	PHYS. PROPERTIES	CHEMISTRY	SECTION	METERS	GRAPHIC LITHOLOGY	DRILLING DISTURB.	SED. STRUCTURES	SAMPLES	LITHOLOGIC DESCRIPTION
	FORAMINIFERS	NANNOFOSSILS	RADIOLARIANS	DIATOMS	DINOCYSTS										
									CC	1 0.5					Single pebble: dark gray micritic limestone.

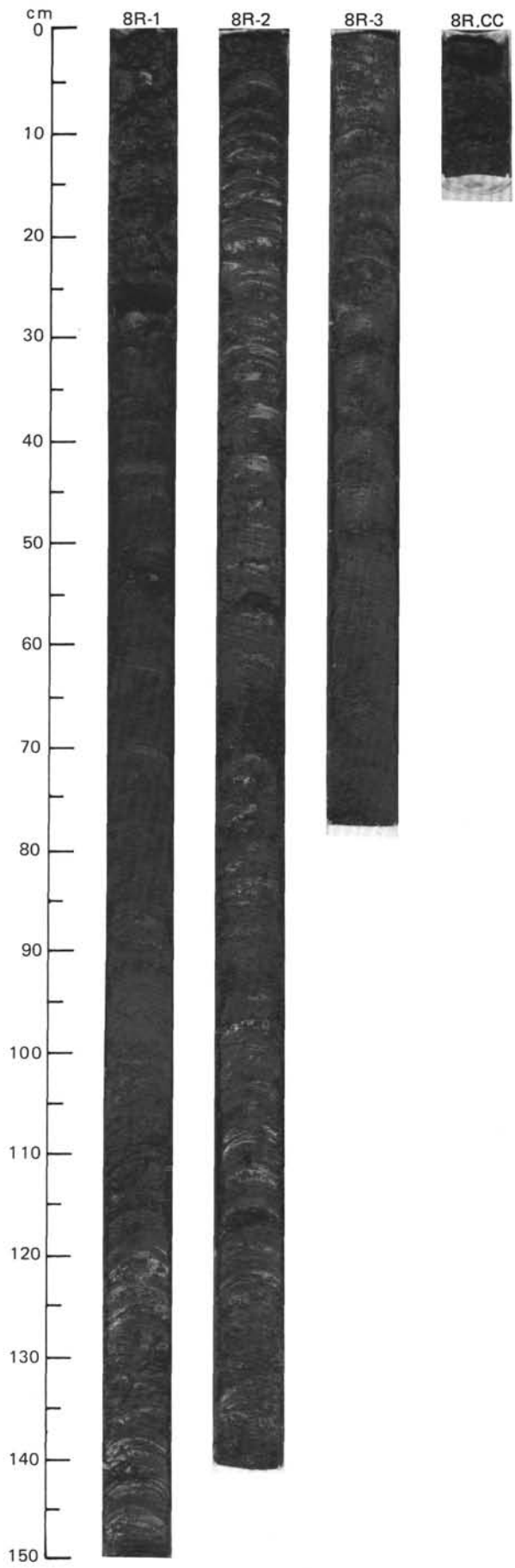
CORE 5 NO RECOVERY

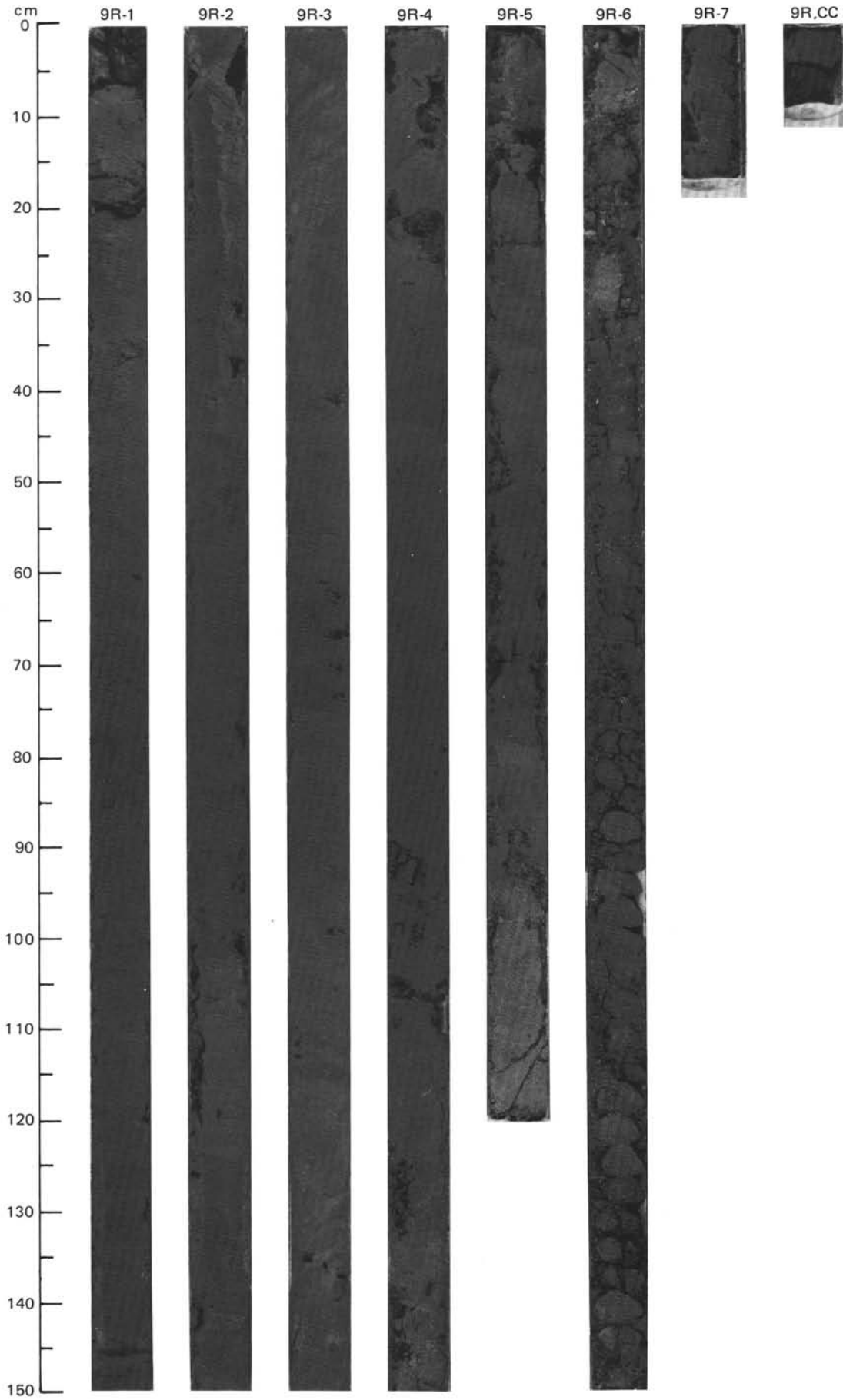
SITE 645 HOLE D CORE 6 R CORED INTERVAL 2318.9-2328.6 mbsl; 311.4-321.1 mbsf

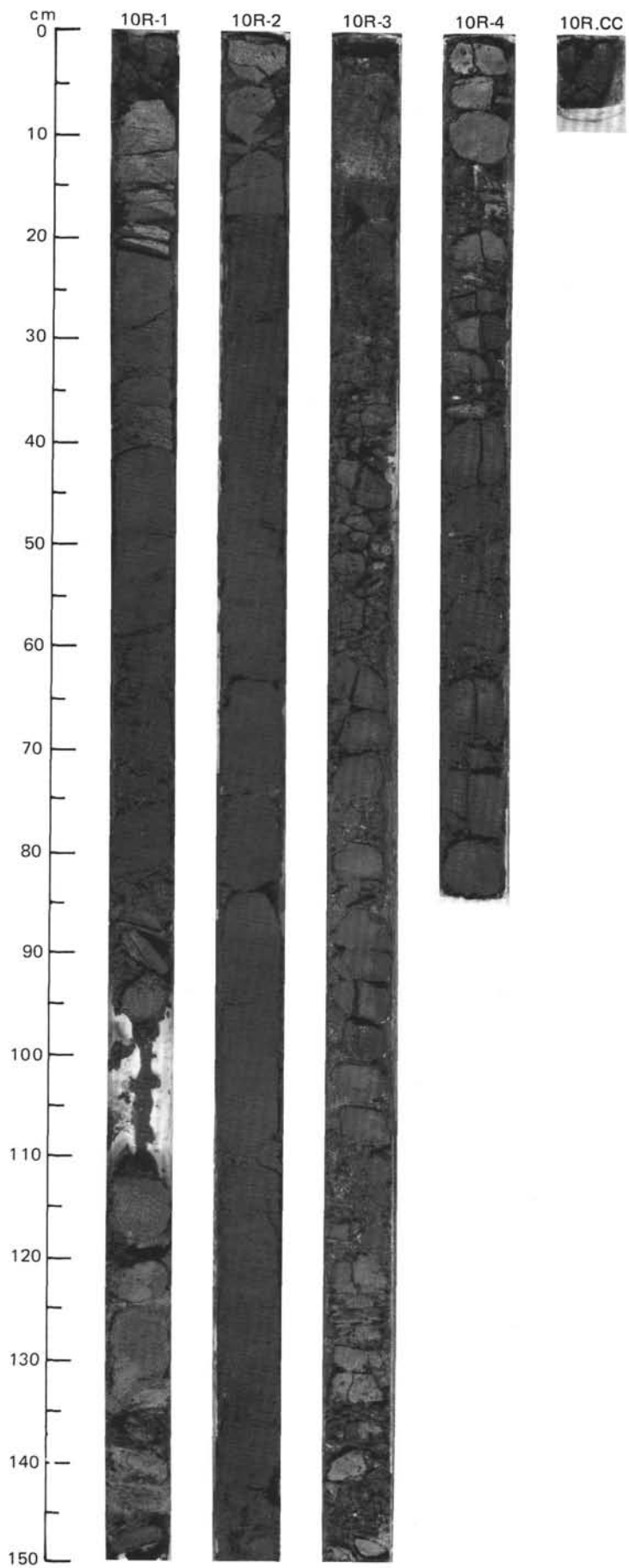
TIME-ROCK UNIT	BIOSTRAT. ZONE/ FOSSIL CHARACTER					PALEOMAGNETICS	PHYS. PROPERTIES	CHEMISTRY	SECTION	METERS	GRAPHIC LITHOLOGY	DRILLING DISTURB.	SED. STRUCTURES	SAMPLES	LITHOLOGIC DESCRIPTION																																		
	FORAMINIFERS	NANNOFOSSILS	RADIOLARIANS	DIATOMS	DINOCYSTS																																												
		B		B	B				CC	1				**	GRAVEL-BEARING DETRITICARBONATE SILTY MUD Gravel-bearing detriticarbonate silty mud, dark gray (5Y 4/1), with large dropstones (Section 1). SMEAR SLIDE SUMMARY (%): <table style="margin-left: 40px;"> <tr> <td>1, 23</td> <td>CC, 2</td> </tr> <tr> <td>D</td> <td>D</td> </tr> </table> TEXTURE: <table style="margin-left: 40px;"> <tr> <td>Sand</td> <td>20</td> <td>1</td> </tr> <tr> <td>Silt</td> <td>50</td> <td>45</td> </tr> <tr> <td>Clay</td> <td>30</td> <td>40</td> </tr> </table> COMPOSITION: <table style="margin-left: 40px;"> <tr> <td>Quartz</td> <td>50</td> <td>40</td> </tr> <tr> <td>Feldspar</td> <td>10</td> <td>10</td> </tr> <tr> <td>Mica</td> <td>Tr</td> <td>—</td> </tr> <tr> <td>Clay</td> <td>19</td> <td>30</td> </tr> <tr> <td>Volcanic glass</td> <td>Tr</td> <td>—</td> </tr> <tr> <td>Calcite/dolomite</td> <td>20</td> <td>20</td> </tr> <tr> <td>Accessory minerals</td> <td>1</td> <td>Tr</td> </tr> </table>	1, 23	CC, 2	D	D	Sand	20	1	Silt	50	45	Clay	30	40	Quartz	50	40	Feldspar	10	10	Mica	Tr	—	Clay	19	30	Volcanic glass	Tr	—	Calcite/dolomite	20	20	Accessory minerals	1	Tr
1, 23	CC, 2																																																
D	D																																																
Sand	20	1																																															
Silt	50	45																																															
Clay	30	40																																															
Quartz	50	40																																															
Feldspar	10	10																																															
Mica	Tr	—																																															
Clay	19	30																																															
Volcanic glass	Tr	—																																															
Calcite/dolomite	20	20																																															
Accessory minerals	1	Tr																																															

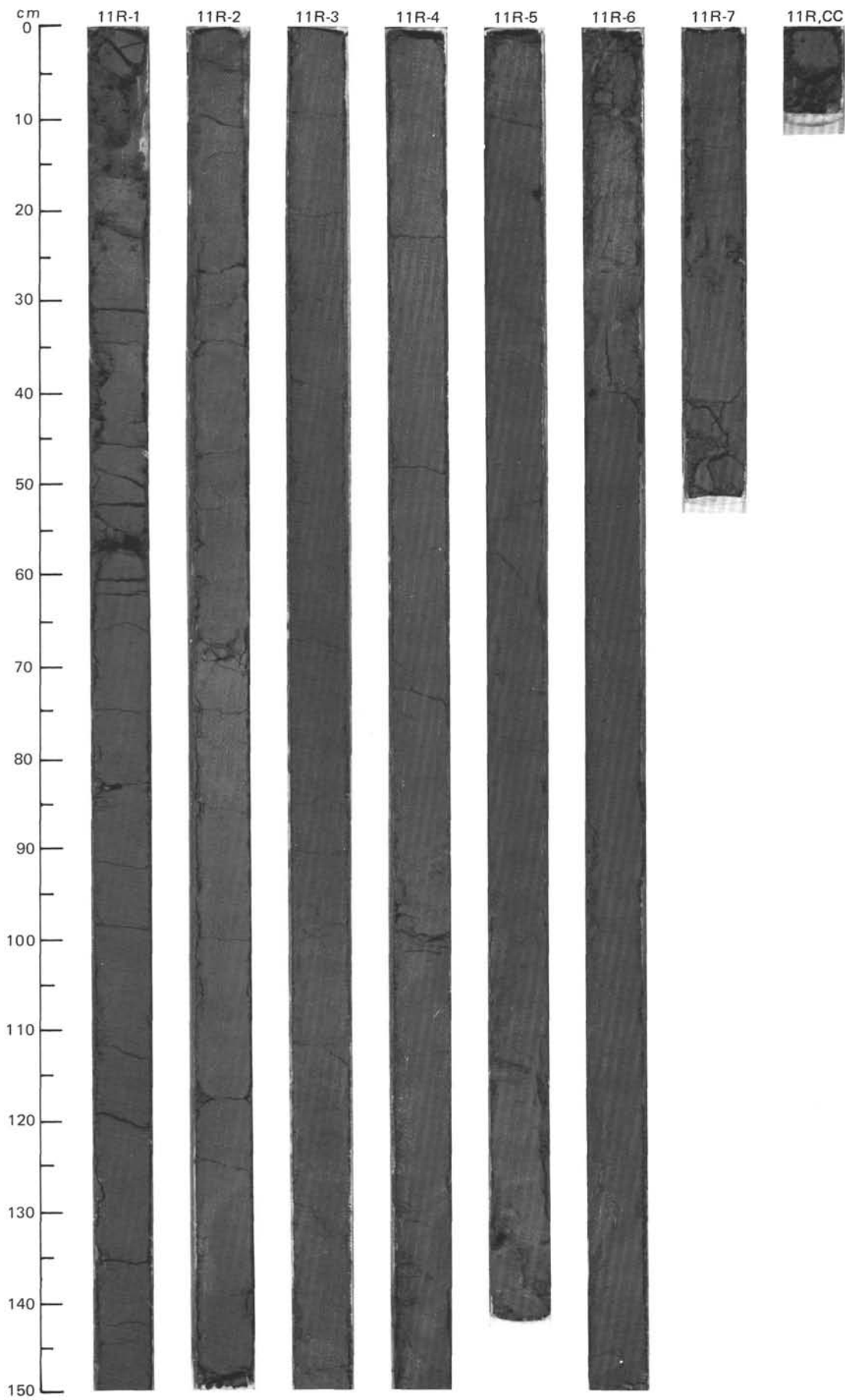
CORE 7 NO RECOVERY





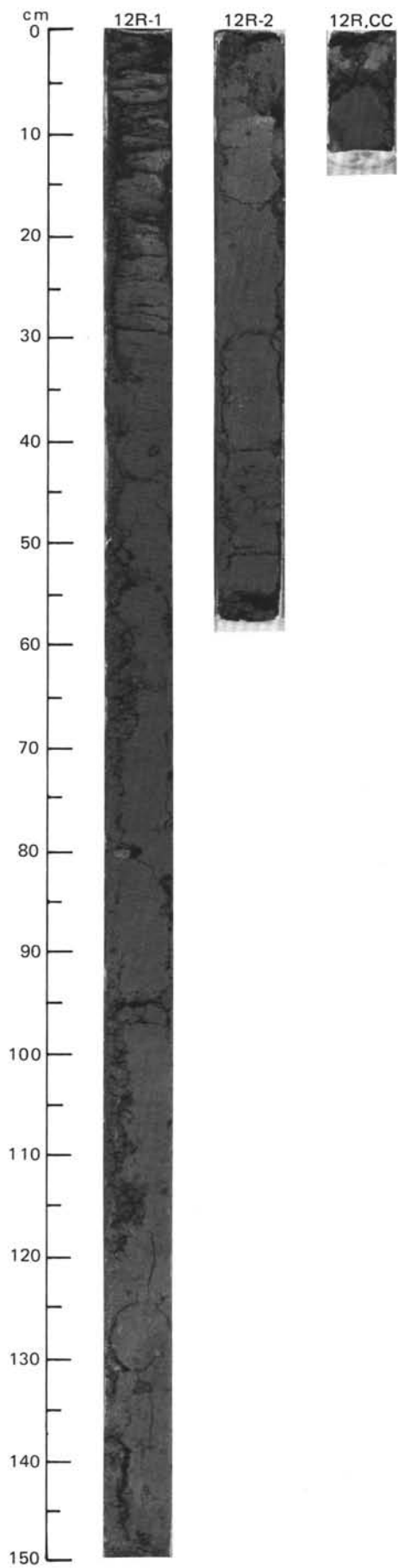


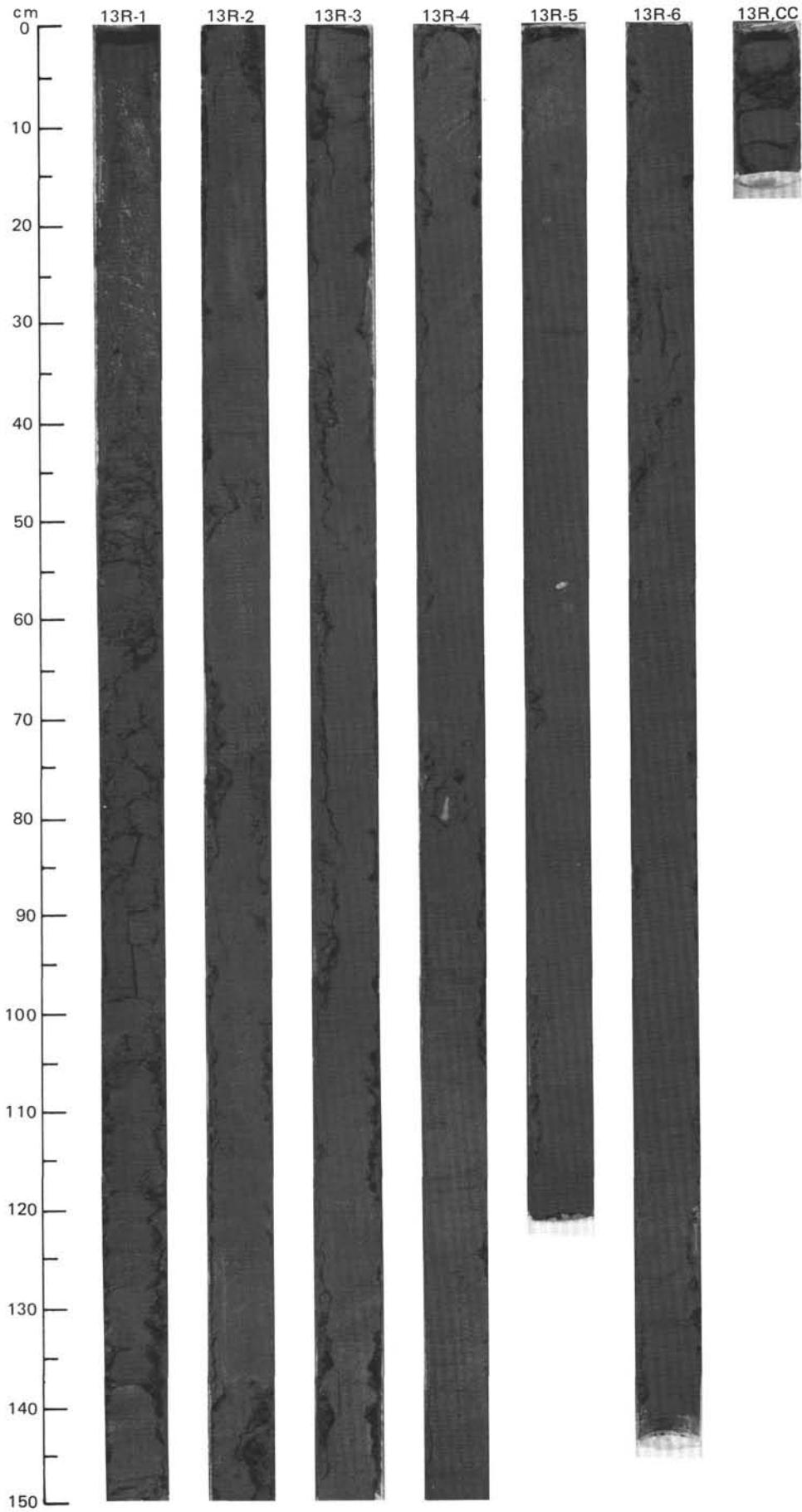


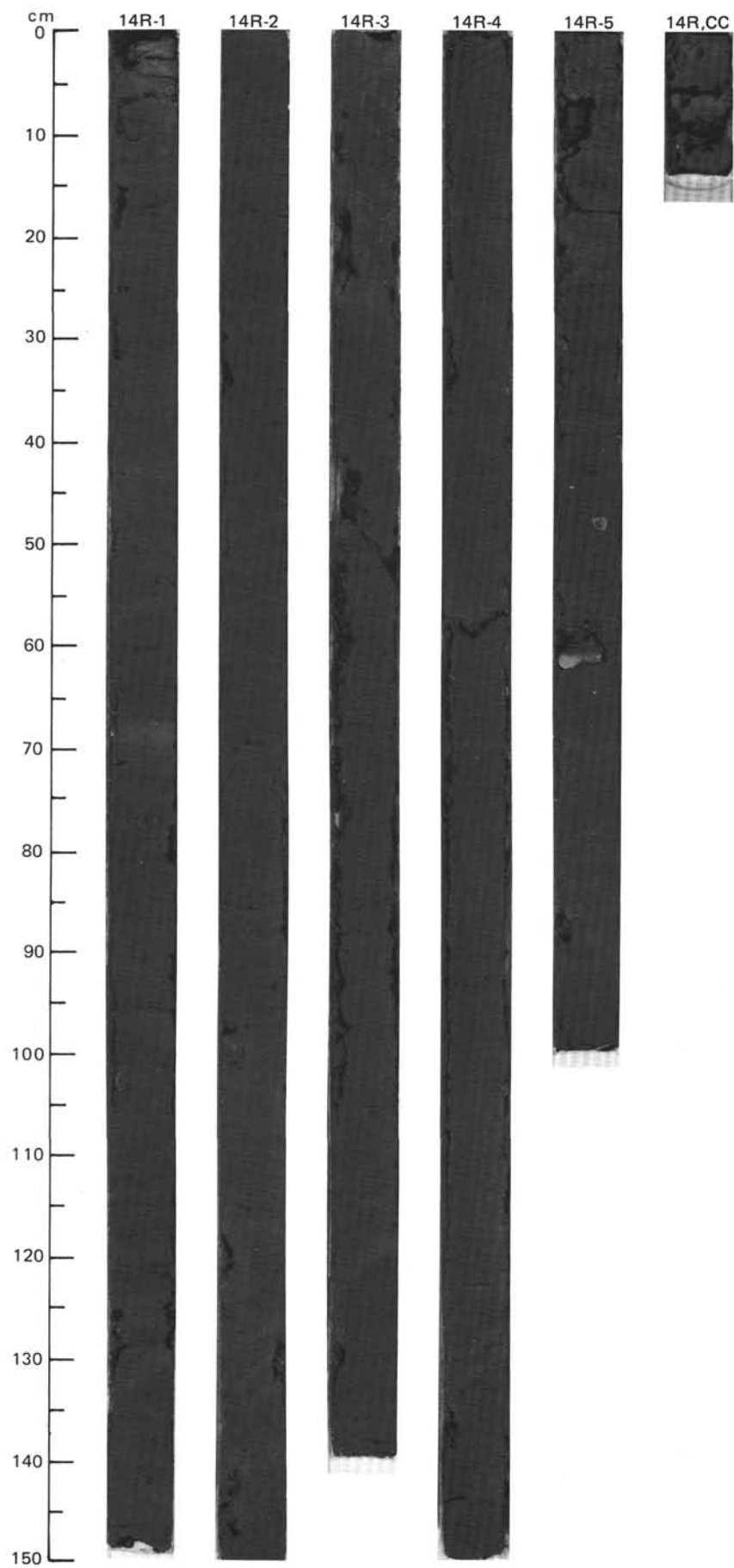


SITE 645 HOLE D CORE 12 R CORED INTERVAL 2386.5-2396.1 mbsl; 379.0-388.6 mbsf

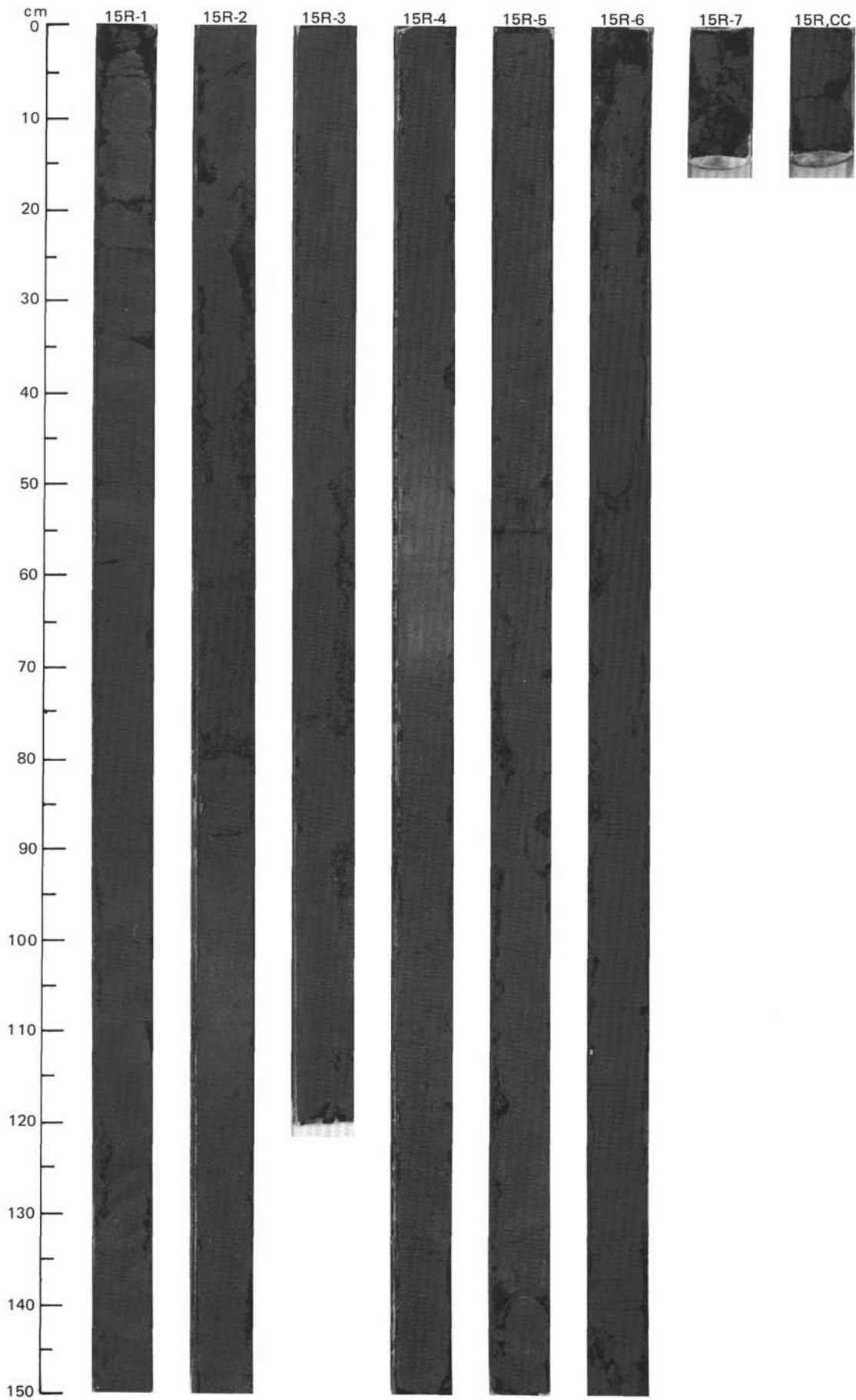
TIME-ROCK UNIT	BIOSTRAT. ZONE/ FOSSIL CHARACTER				PALEOMAGNETICS	PHYS. PROPERTIES	CHEMISTRY	SECTION	METERS	GRAPHIC LITHOLOGY	DRILLING DISTURB.	SED. STRUCTURES	SAMPLES	LITHOLOGIC DESCRIPTION																																																								
	FORAMINIFERS	NANNOFOSSILS	RADIOLARIANS	DIATOMS											DINOCTYSTS																																																							
	B	B	B	B	R/M	N.C.	W-33 ● $\gamma = 1.999/cm^3$ ● $\rho = 4.84$ ● TOC=0.96 ● CaCO ₃ =8.0	1	0.5 1.0			◇ * ◇ * ◇ *	* * *	<p>SILTY MUD</p> <p>Silty mud, dark greenish gray (5GY 4/1). Section 1 is disturbed by drilling biscuits. The sediment is vaguely mottled and bioturbated, otherwise structureless. Black granules of shale and occasional "dropstones" (about 1 cm) occur throughout.</p> <p>Minor lithology: a. Section 2, 7-26 cm: indistinct layer of carbonate silty mud, gray (5Y 5/1). b. Section 1, 0-30 cm: clayey silt, dark greenish gray (5GY 4/1).</p> <p>SMEAR SLIDE SUMMARY (%):</p> <table border="1"> <tr> <td></td> <td>1, 78</td> <td>2, 20</td> <td>1, 15</td> </tr> <tr> <td></td> <td>D</td> <td>D</td> <td>M</td> </tr> </table> <p>TEXTURE:</p> <table border="1"> <tr> <td>Sand</td> <td>10</td> <td>10</td> <td>5</td> </tr> <tr> <td>Silt</td> <td>40</td> <td>30</td> <td>55</td> </tr> <tr> <td>Clay</td> <td>50</td> <td>60</td> <td>40</td> </tr> </table> <p>COMPOSITION:</p> <table border="1"> <tr> <td>Quartz</td> <td>30</td> <td>20</td> <td>20</td> </tr> <tr> <td>Feldspar</td> <td>5</td> <td>2</td> <td>10</td> </tr> <tr> <td>Rock fragments</td> <td>5</td> <td>2</td> <td>10</td> </tr> <tr> <td>Mica</td> <td>3</td> <td>1</td> <td>Tr</td> </tr> <tr> <td>Clay</td> <td>45</td> <td>40</td> <td>40</td> </tr> <tr> <td>Volcanic glass</td> <td>—</td> <td>—</td> <td>Tr</td> </tr> <tr> <td>Calcite/dolomite</td> <td>10</td> <td>25</td> <td>5</td> </tr> <tr> <td>Accessory minerals</td> <td>—</td> <td>5</td> <td>2</td> </tr> <tr> <td>Pyrite</td> <td>2</td> <td>5</td> <td>3</td> </tr> </table>		1, 78	2, 20	1, 15		D	D	M	Sand	10	10	5	Silt	40	30	55	Clay	50	60	40	Quartz	30	20	20	Feldspar	5	2	10	Rock fragments	5	2	10	Mica	3	1	Tr	Clay	45	40	40	Volcanic glass	—	—	Tr	Calcite/dolomite	10	25	5	Accessory minerals	—	5	2	Pyrite	2	5	3
	1, 78	2, 20	1, 15																																																																			
	D	D	M																																																																			
Sand	10	10	5																																																																			
Silt	40	30	55																																																																			
Clay	50	60	40																																																																			
Quartz	30	20	20																																																																			
Feldspar	5	2	10																																																																			
Rock fragments	5	2	10																																																																			
Mica	3	1	Tr																																																																			
Clay	45	40	40																																																																			
Volcanic glass	—	—	Tr																																																																			
Calcite/dolomite	10	25	5																																																																			
Accessory minerals	—	5	2																																																																			
Pyrite	2	5	3																																																																			
								2				◇ * ◇ *	*																																																									
								CC				◇ *	*																																																									



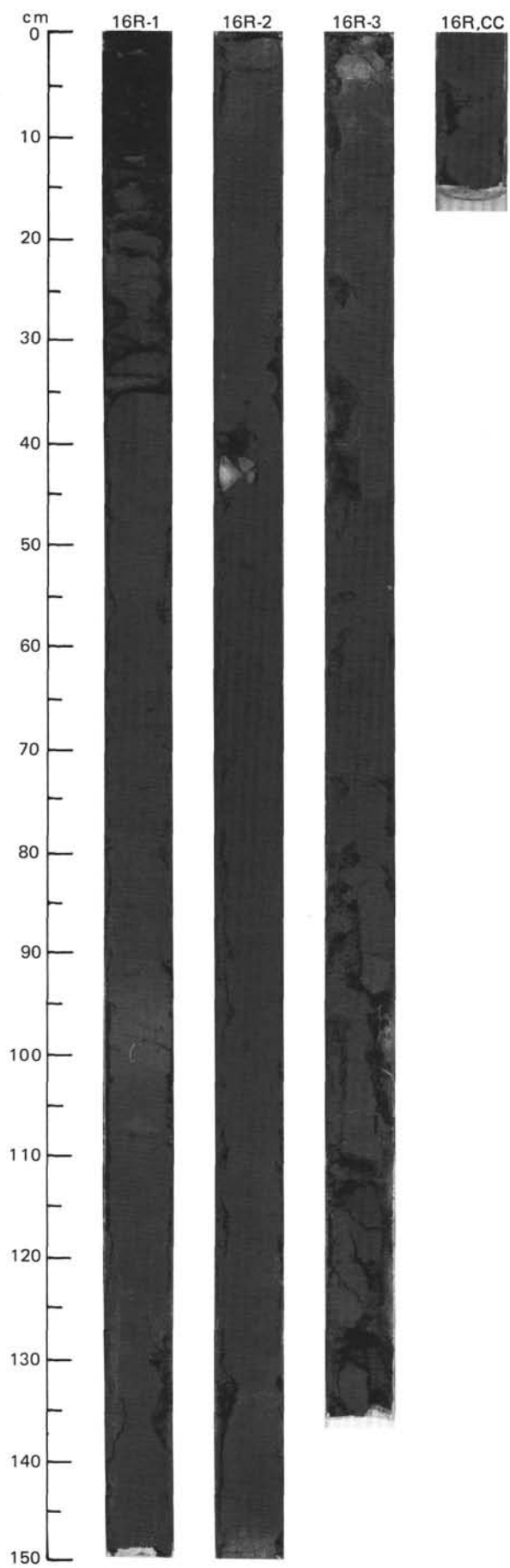


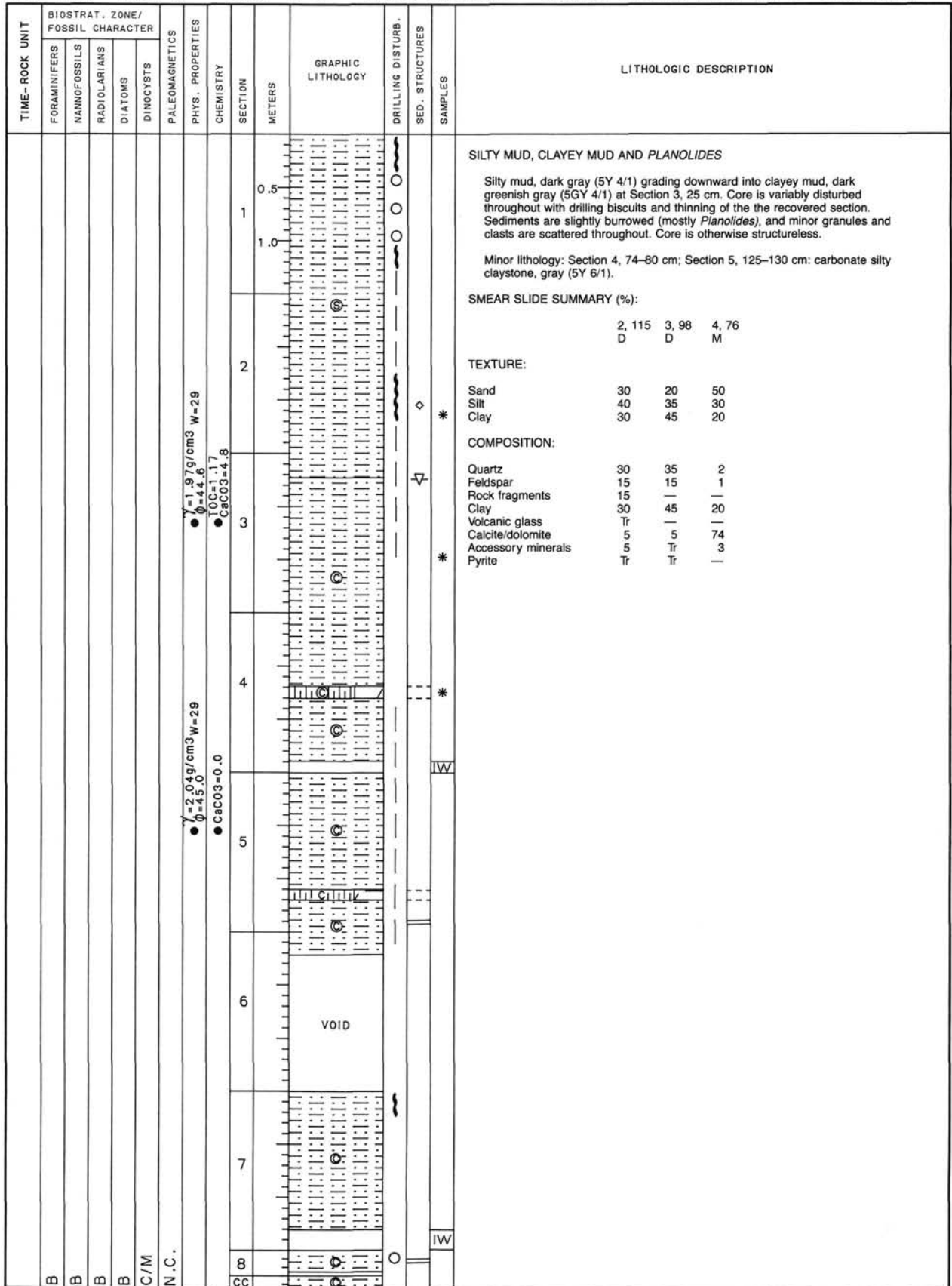


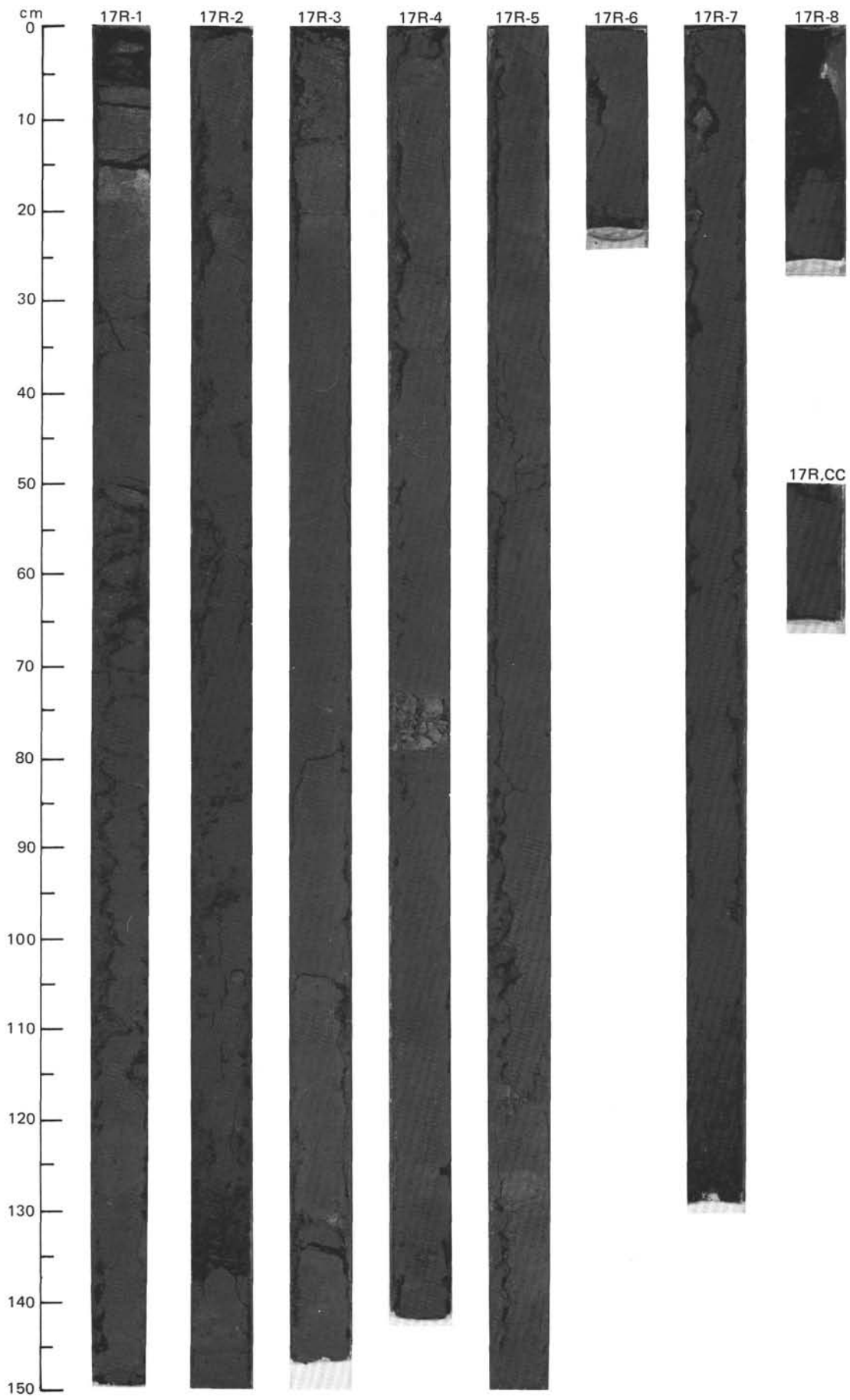
TIME-ROCK UNIT	BIOSTRAT. ZONE/ FOSSIL CHARACTER				PALEOMAGNETICS	PHYS. PROPERTIES	CHEMISTRY	SECTION	METERS	GRAPHIC LITHOLOGY	DRILLING DISTURB.	SED. STRUCTURES	SAMPLES	LITHOLOGIC DESCRIPTION																																																																						
	FORAMINIFERS	NANNOFOSSILS	RADIOLARIANS	DIATOMS											DINOCTYSTS																																																																					
B						W=31 γ=2.01 φ=46.6	CaCO3=3.0	1	0.5 1.0					<p>SILTY MUD</p> <p>Silty mud, greenish gray (5GY 4/1); moderately to strongly bioturbated. A silty matrix supports sand-sized grains, which may occur in distinct, but discontinuous, layers or lenses (coarsest grain size is in Section 4, 75-133 cm). Isolated pebbles are rare. The transitions between the different lithologies are gradational.</p> <p>Minor lithologies: a. Section 1, 100-113 cm: carbonate silty mud, gray (5Y 5/1). b. Section 4, 45-68 cm: carbonate claystone, gray (5Y 6/1).</p> <p>SMEAR SLIDE SUMMARY (%):</p> <table border="1"> <tr> <td></td> <td>1, 100</td> <td>4, 65</td> <td>4, 93</td> <td>6, 108</td> </tr> <tr> <td></td> <td>D</td> <td>M</td> <td>D</td> <td>D</td> </tr> </table> <p>TEXTURE:</p> <table border="1"> <tr> <td>Sand</td> <td>15</td> <td>—</td> <td>35</td> <td>20</td> </tr> <tr> <td>Silt</td> <td>50</td> <td>10</td> <td>45</td> <td>50</td> </tr> <tr> <td>Clay</td> <td>35</td> <td>90</td> <td>20</td> <td>30</td> </tr> </table> <p>COMPOSITION:</p> <table border="1"> <tr> <td>Quartz</td> <td>50</td> <td>10</td> <td>55</td> <td>40</td> </tr> <tr> <td>Feldspar</td> <td>5</td> <td>—</td> <td>10</td> <td>2</td> </tr> <tr> <td>Rock fragments</td> <td>5</td> <td>—</td> <td>—</td> <td>20</td> </tr> <tr> <td>Clay</td> <td>30</td> <td>30</td> <td>20</td> <td>30</td> </tr> <tr> <td>Volcanic glass</td> <td>—</td> <td>—</td> <td>—</td> <td>Tr</td> </tr> <tr> <td>Calcite/dolomite</td> <td>10</td> <td>60</td> <td>10</td> <td>5</td> </tr> <tr> <td>Accessory minerals</td> <td>—</td> <td>—</td> <td>5</td> <td>3</td> </tr> <tr> <td>Sponge spicules</td> <td>—</td> <td>—</td> <td>Tr</td> <td>—</td> </tr> <tr> <td>Plant debris</td> <td>Tr</td> <td>—</td> <td>—</td> <td>—</td> </tr> </table>		1, 100	4, 65	4, 93	6, 108		D	M	D	D	Sand	15	—	35	20	Silt	50	10	45	50	Clay	35	90	20	30	Quartz	50	10	55	40	Feldspar	5	—	10	2	Rock fragments	5	—	—	20	Clay	30	30	20	30	Volcanic glass	—	—	—	Tr	Calcite/dolomite	10	60	10	5	Accessory minerals	—	—	5	3	Sponge spicules	—	—	Tr	—	Plant debris	Tr	—	—	—
	1, 100	4, 65	4, 93	6, 108																																																																																
	D	M	D	D																																																																																
Sand	15	—	35	20																																																																																
Silt	50	10	45	50																																																																																
Clay	35	90	20	30																																																																																
Quartz	50	10	55	40																																																																																
Feldspar	5	—	10	2																																																																																
Rock fragments	5	—	—	20																																																																																
Clay	30	30	20	30																																																																																
Volcanic glass	—	—	—	Tr																																																																																
Calcite/dolomite	10	60	10	5																																																																																
Accessory minerals	—	—	5	3																																																																																
Sponge spicules	—	—	Tr	—																																																																																
Plant debris	Tr	—	—	—																																																																																
B						W=27 γ=2.06 φ=3.9	CaCO3=8.0	2																																																																												
B						W=27 γ=2.06 φ=3.9	CaCO3=8.0	3																																																																												
B						W=27 γ=2.06 φ=3.9	CaCO3=8.0	4																																																																												
F/M						W=27 γ=2.06 φ=3.9	CaCO3=8.0	5																																																																												
						W=27 γ=2.06 φ=3.9	CaCO3=8.0	6																																																																												
						W=27 γ=2.06 φ=3.9	CaCO3=8.0	7																																																																												



TIME-ROCK UNIT	BIOSTRAT. ZONE/ FOSSIL CHARACTER					PALEOMAGNETICS	PHYS. PROPERTIES	CHEMISTRY	SECTION	METERS	GRAPHIC LITHOLOGY	DRILLING DISTURB.	SED. STRUCTURES	SAMPLES	LITHOLOGIC DESCRIPTION																																																															
	FORAMINIFERS	NANNOFOSSILS	RADIOLARIANS	DIATOMS	DINOCTYSTS																																																																									
	B	B	B	B	R/M	N.C.	$\gamma = 2.05 \text{ g/cm}^3$ $W = 28$ $\phi = 43.7$ $\bullet \text{CaCO}_3 = 6.0$	$\gamma = 1.99 \text{ g/cm}^3$ $W = 32$ $\phi = 47.0$ $\bullet \text{TOC} = 1.17$ $\bullet \text{TOC} = 0.85$ $\bullet \text{CaCO}_3 = 0.3$ $\bullet \text{CaCO}_3 = 50.1$	1	0.5			*	<p>SILTY MUD AND SILTY CLAY</p> <p>Silty mud, dark gray (5Y 4/1) in Sections 1 and 2; and silty clay, dark gray (5Y 4/1) in Section 3. Black granules, scattered clasts and burrows occur throughout. A vague upward-fining sequence may be present in Section 3, 20-70 cm; core is otherwise structureless.</p> <p>Minor lithology: Section 1, 90-104 cm; Section 2, 146 cm, to Section 3, 4 cm: carbonate clayey silt, olive gray (5Y 5/2) to gray (5Y 5/1).</p> <p>SMEAR SLIDE SUMMARY (%):</p> <table border="1"> <tr> <td></td> <td>1, 60</td> <td>3, 3</td> <td>3, 61</td> </tr> <tr> <td>D</td> <td></td> <td>M</td> <td>M</td> </tr> </table> <p>TEXTURE:</p> <table border="1"> <tr> <td>Sand</td> <td>10</td> <td>1</td> <td>5</td> </tr> <tr> <td>Silt</td> <td>50</td> <td>70</td> <td>30</td> </tr> <tr> <td>Clay</td> <td>40</td> <td>29</td> <td>65</td> </tr> </table> <p>COMPOSITION:</p> <table border="1"> <tr> <td>Quartz</td> <td>30</td> <td>1</td> <td>30</td> </tr> <tr> <td>Feldspar</td> <td>5</td> <td>10</td> <td>18</td> </tr> <tr> <td>Rock fragments</td> <td>5</td> <td>—</td> <td>3</td> </tr> <tr> <td>Mica</td> <td>40</td> <td>—</td> <td>Tr</td> </tr> <tr> <td>Clay</td> <td>—</td> <td>—</td> <td>40</td> </tr> <tr> <td>Volcanic glass</td> <td>—</td> <td>Tr</td> <td>Tr</td> </tr> <tr> <td>Calcite/dolomite</td> <td>10</td> <td>88</td> <td>15</td> </tr> <tr> <td>Accessory minerals</td> <td>5</td> <td>1</td> <td>2</td> </tr> <tr> <td>Pyrite</td> <td>5</td> <td>—</td> <td>2</td> </tr> <tr> <td>Diatoms</td> <td>Tr</td> <td>—</td> <td>—</td> </tr> <tr> <td>Sponge spicules</td> <td>Tr</td> <td>—</td> <td>—</td> </tr> </table>		1, 60	3, 3	3, 61	D		M	M	Sand	10	1	5	Silt	50	70	30	Clay	40	29	65	Quartz	30	1	30	Feldspar	5	10	18	Rock fragments	5	—	3	Mica	40	—	Tr	Clay	—	—	40	Volcanic glass	—	Tr	Tr	Calcite/dolomite	10	88	15	Accessory minerals	5	1	2	Pyrite	5	—	2	Diatoms	Tr	—	—	Sponge spicules	Tr	—	—
	1, 60	3, 3	3, 61																																																																											
D		M	M																																																																											
Sand	10	1	5																																																																											
Silt	50	70	30																																																																											
Clay	40	29	65																																																																											
Quartz	30	1	30																																																																											
Feldspar	5	10	18																																																																											
Rock fragments	5	—	3																																																																											
Mica	40	—	Tr																																																																											
Clay	—	—	40																																																																											
Volcanic glass	—	Tr	Tr																																																																											
Calcite/dolomite	10	88	15																																																																											
Accessory minerals	5	1	2																																																																											
Pyrite	5	—	2																																																																											
Diatoms	Tr	—	—																																																																											
Sponge spicules	Tr	—	—																																																																											
								2	1.0																																																																					
								3																																																																						
								CC																																																																						

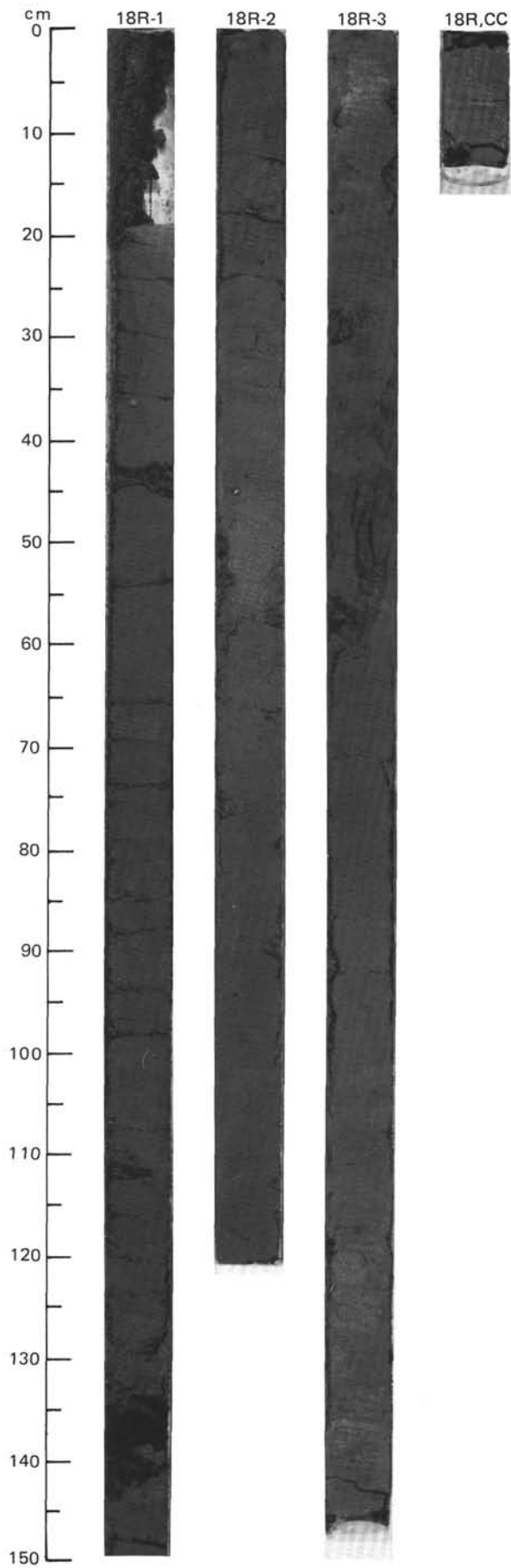




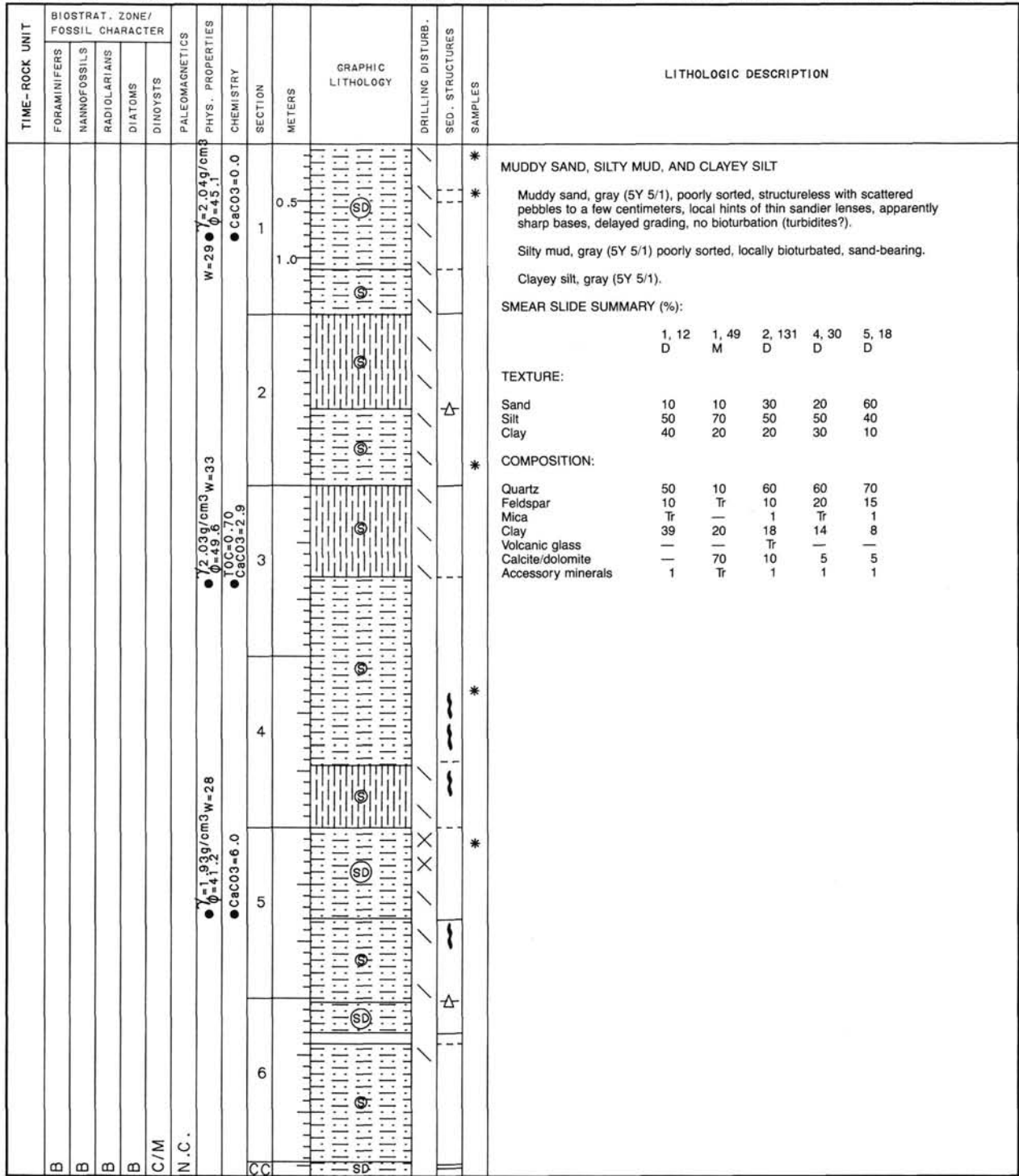


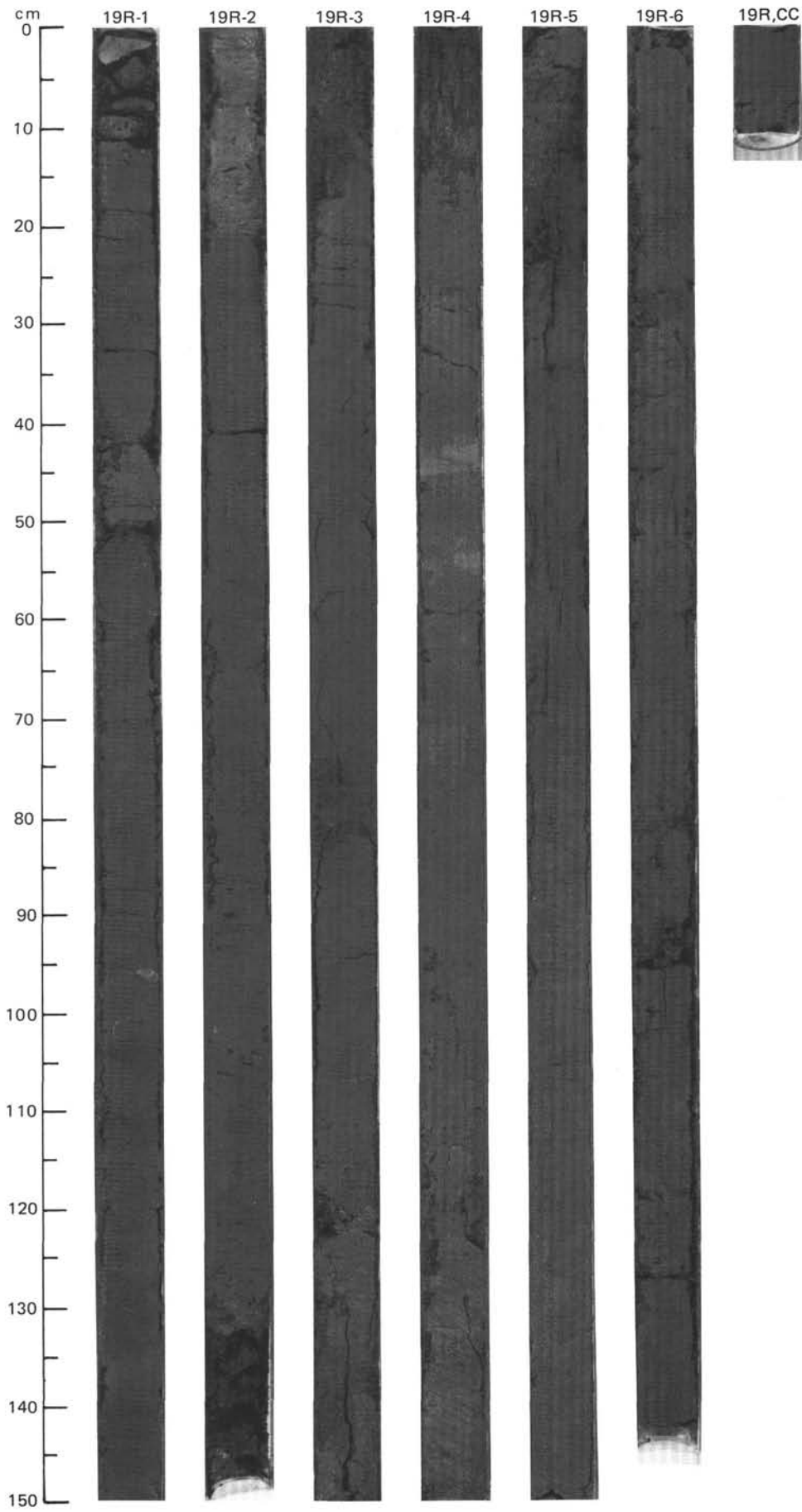
SITE 645 HOLE D CORE 18 R CORED INTERVAL 2444.5-2554.0 mbsl; 436.9-446.5 mbsf

TIME-ROCK UNIT	BIOSTRAT. ZONE/ FOSSIL CHARACTER				PALEOMAGNETICS	PHYS. PROPERTIES	CHEMISTRY	SECTION	METERS	GRAPHIC LITHOLOGY	DRILLING DISTURB.	SED. STRUCTURES	SAMPLES	LITHOLOGIC DESCRIPTION																																																
	FORAMINIFERS	NANNOFOSSILS	RADIOLARIANS	DIATOMS																																																										
B						$\gamma = 1.95 \text{ g/cm}^3$ $\rho = 45.0$ ● W=1.31	● CaCO ₃ =0.0	1	0.5 1.0					<p>SILTY MUD</p> <p>Silty mud, dark greenish gray (5GY 4/1), with slight bioturbation and inter-bedded clayey silt, greenish gray (5G 6/1) with blebs of pyrite. Thin lenses of coarser sand occur at Section 3, 60 cm to CC.</p> <p>SMEAR SLIDE SUMMARY (%):</p> <table border="1"> <tr> <td></td> <td>1, 142</td> <td>2, 52</td> <td>3, 122</td> </tr> <tr> <td></td> <td>D</td> <td>M</td> <td>D</td> </tr> </table> <p>TEXTURE:</p> <table border="1"> <tr> <td>Sand</td> <td>35</td> <td>5</td> <td>10</td> </tr> <tr> <td>Silt</td> <td>50</td> <td>50</td> <td>50</td> </tr> <tr> <td>Clay</td> <td>15</td> <td>45</td> <td>40</td> </tr> </table> <p>COMPOSITION:</p> <table border="1"> <tr> <td>Quartz</td> <td>70</td> <td>40</td> <td>50</td> </tr> <tr> <td>Feldspar</td> <td>10</td> <td>15</td> <td>10</td> </tr> <tr> <td>Mica</td> <td>Tr</td> <td>Tr</td> <td>Tr</td> </tr> <tr> <td>Clay</td> <td>14</td> <td>30</td> <td>35</td> </tr> <tr> <td>Volcanic glass</td> <td>Tr</td> <td>—</td> <td>Tr</td> </tr> <tr> <td>Calcite/dolomite</td> <td>5</td> <td>15</td> <td>5</td> </tr> <tr> <td>Accessory minerals</td> <td>1</td> <td>Tr</td> <td>Tr</td> </tr> </table>		1, 142	2, 52	3, 122		D	M	D	Sand	35	5	10	Silt	50	50	50	Clay	15	45	40	Quartz	70	40	50	Feldspar	10	15	10	Mica	Tr	Tr	Tr	Clay	14	30	35	Volcanic glass	Tr	—	Tr	Calcite/dolomite	5	15	5	Accessory minerals	1	Tr	Tr
	1, 142	2, 52	3, 122																																																											
	D	M	D																																																											
Sand	35	5	10																																																											
Silt	50	50	50																																																											
Clay	15	45	40																																																											
Quartz	70	40	50																																																											
Feldspar	10	15	10																																																											
Mica	Tr	Tr	Tr																																																											
Clay	14	30	35																																																											
Volcanic glass	Tr	—	Tr																																																											
Calcite/dolomite	5	15	5																																																											
Accessory minerals	1	Tr	Tr																																																											
F/M					$\gamma = 2.02 \text{ g/cm}^3$ $\rho = 43.0$ ●	● CaCO ₃ =0.0	2																																																							
N.C.					● TOC=0.88 ● CaCO ₃ =3.3	● CaCO ₃ =3.3	3																																																							
CC																																																														



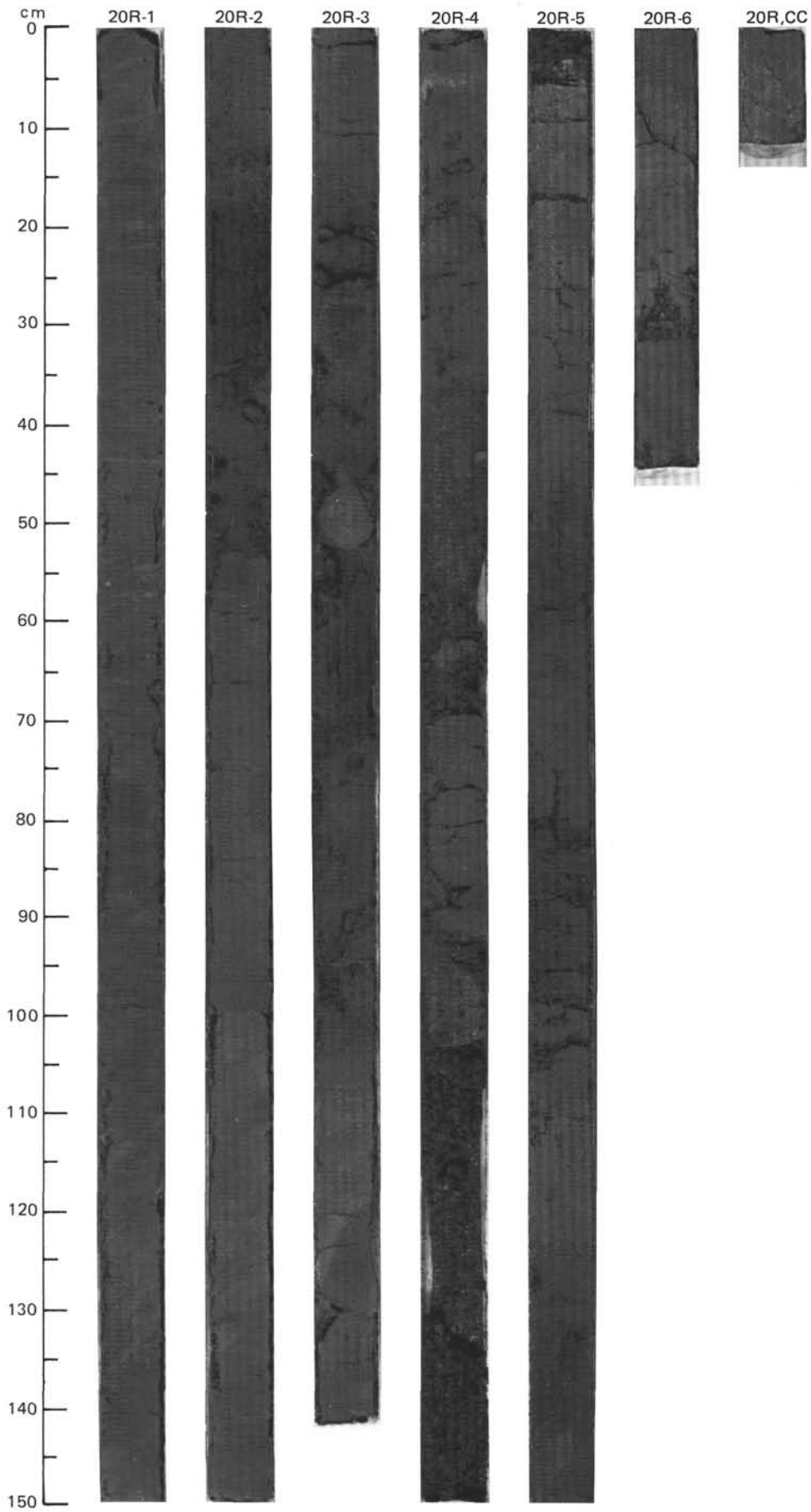
SITE 645 HOLE D CORE 19 R CORED INTERVAL 2454.0-2463.7 mbsl; 446.5-456.2 mbsf

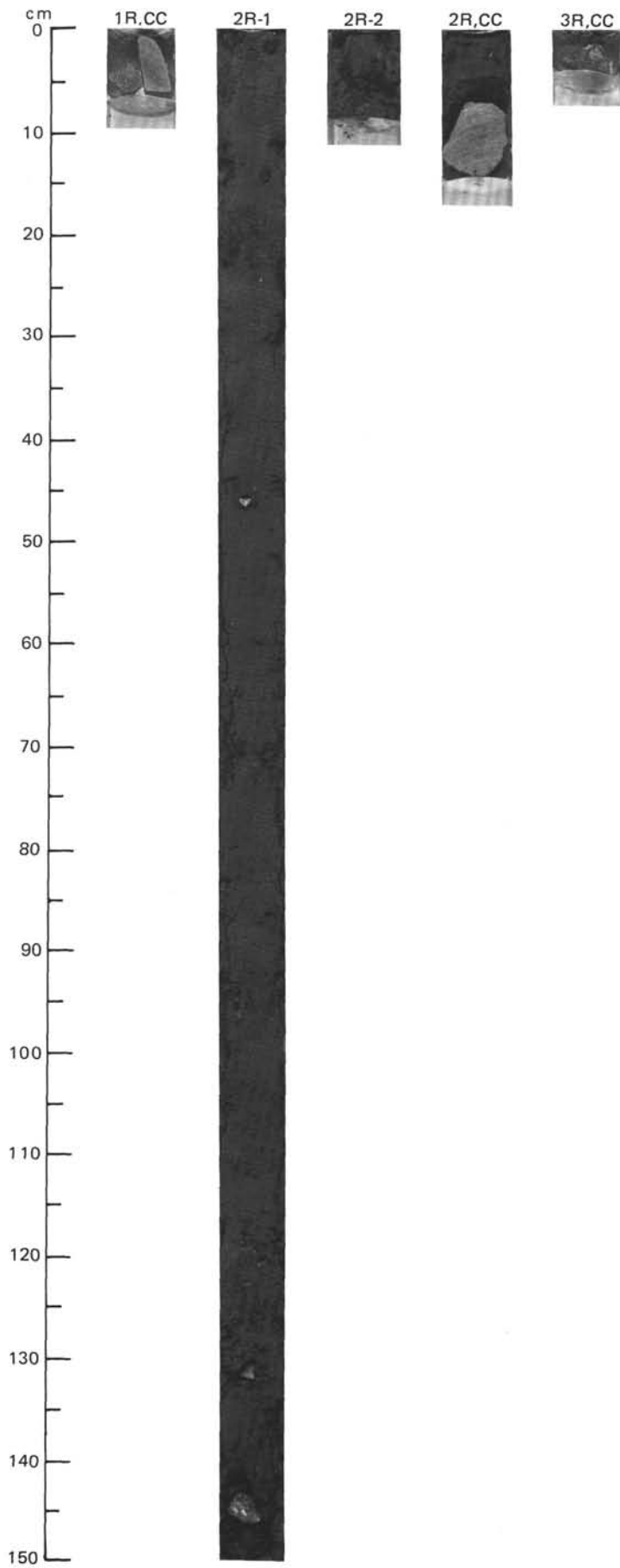




SITE 645 HOLE D CORE 20 R CORED INTERVAL 2463.7-2473.3 mbsl; 456.2-465.8 mbsf

TIME-ROCK UNIT	BIOSTRAT. ZONE/ FOSSIL CHARACTER				PALEOMAGNETICS	PHYS. PROPERTIES	CHEMISTRY	SECTION	METERS	GRAPHIC LITHOLOGY	DRILLING DISTURB.	SED. STRUCTURES	SAMPLES	LITHOLOGIC DESCRIPTION																																																																							
	FORAMINIFERS	NANNOFOSSILS	RADIOLARIANS	DIATOMS											DINOCTYSTS																																																																						
B						$\gamma = 2.09 \text{ g/cm}^3$ $\rho = 40.9$ $\bullet \text{ CaCO}_3 = 4.0$		1	0.5 1.0			*	<p>SILTY MUD, MUDDY SAND, AND SILTY SAND</p> <p>Silty mud, dark gray (5Y 4/1); with 5%–10% coarser scattered sand and less gravel.</p> <p>Muddy sand and silty sand, dark greenish gray (5GY 4/1) or dark gray (5Y 4/1); with 5%–10% coarser scattered sand and less shale clasts and gravel.</p> <p>SMEAR SLIDE SUMMARY (%):</p> <table border="1"> <tr> <td></td> <td>1, 12</td> <td>1, 57</td> <td>2, 100</td> <td>4, 110</td> <td>5, 82</td> </tr> <tr> <td></td> <td>D</td> <td>M</td> <td>D</td> <td>D</td> <td>D</td> </tr> </table> <p>TEXTURE:</p> <table border="1"> <tr> <td>Sand</td> <td>20</td> <td>5</td> <td>15</td> <td>75</td> <td>60</td> </tr> <tr> <td>Silt</td> <td>50</td> <td>70</td> <td>50</td> <td>20</td> <td>35</td> </tr> <tr> <td>Clay</td> <td>30</td> <td>25</td> <td>35</td> <td>5</td> <td>5</td> </tr> </table> <p>COMPOSITION:</p> <table border="1"> <tr> <td>Quartz</td> <td>70</td> <td>5</td> <td>60</td> <td>80</td> <td>65</td> </tr> <tr> <td>Feldspar</td> <td>5</td> <td>Tr</td> <td>10</td> <td>10</td> <td>20</td> </tr> <tr> <td>Mica</td> <td>Tr</td> <td>Tr</td> <td>1</td> <td>1</td> <td>1</td> </tr> <tr> <td>Clay</td> <td>25</td> <td>20</td> <td>23</td> <td>4</td> <td>12</td> </tr> <tr> <td>Volcanic glass</td> <td>Tr</td> <td>—</td> <td>Tr</td> <td>Tr</td> <td>—</td> </tr> <tr> <td>Calcite/dolomite</td> <td>—</td> <td>75</td> <td>5</td> <td>Tr</td> <td>—</td> </tr> <tr> <td>Accessory minerals</td> <td>Tr</td> <td>Tr</td> <td>1</td> <td>5</td> <td>2</td> </tr> </table>		1, 12	1, 57	2, 100	4, 110	5, 82		D	M	D	D	D	Sand	20	5	15	75	60	Silt	50	70	50	20	35	Clay	30	25	35	5	5	Quartz	70	5	60	80	65	Feldspar	5	Tr	10	10	20	Mica	Tr	Tr	1	1	1	Clay	25	20	23	4	12	Volcanic glass	Tr	—	Tr	Tr	—	Calcite/dolomite	—	75	5	Tr	—	Accessory minerals	Tr	Tr	1	5	2
	1, 12	1, 57	2, 100	4, 110	5, 82																																																																																
	D	M	D	D	D																																																																																
Sand	20	5	15	75	60																																																																																
Silt	50	70	50	20	35																																																																																
Clay	30	25	35	5	5																																																																																
Quartz	70	5	60	80	65																																																																																
Feldspar	5	Tr	10	10	20																																																																																
Mica	Tr	Tr	1	1	1																																																																																
Clay	25	20	23	4	12																																																																																
Volcanic glass	Tr	—	Tr	Tr	—																																																																																
Calcite/dolomite	—	75	5	Tr	—																																																																																
Accessory minerals	Tr	Tr	1	5	2																																																																																
B						$\gamma = 2.01 \text{ g/cm}^3$ W=30 $\rho = 45.6$ $\bullet \text{ CaCO}_3 = 1.5$		2				*																																																																									
B						$\gamma = 1.90 \text{ g/cm}^3$ $\rho = 47.3$ $\bullet \text{ CaCO}_3 = 0.0$		3					*																																																																								
B								4					*																																																																								
F/M								5					*																																																																								
N.C.								6					*																																																																								
CC													*																																																																								

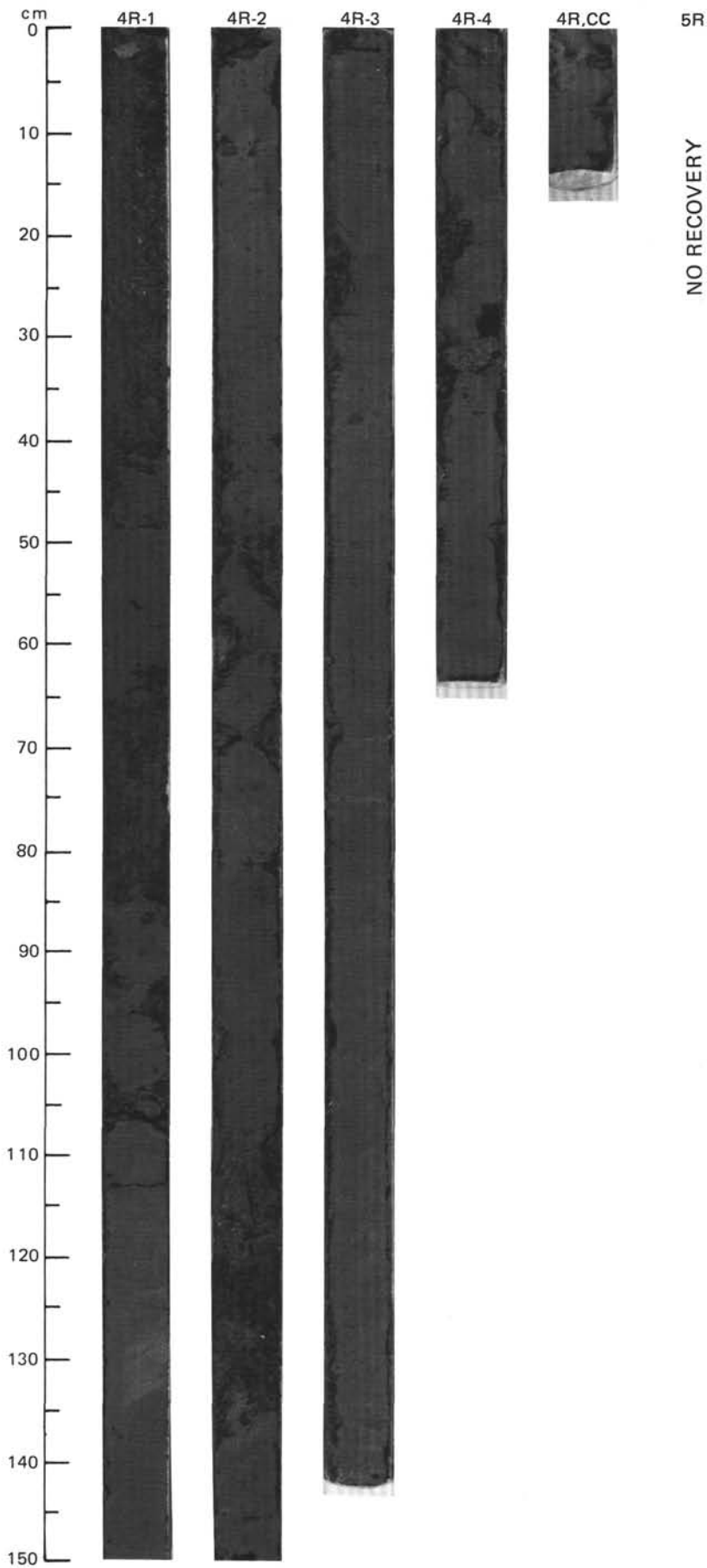


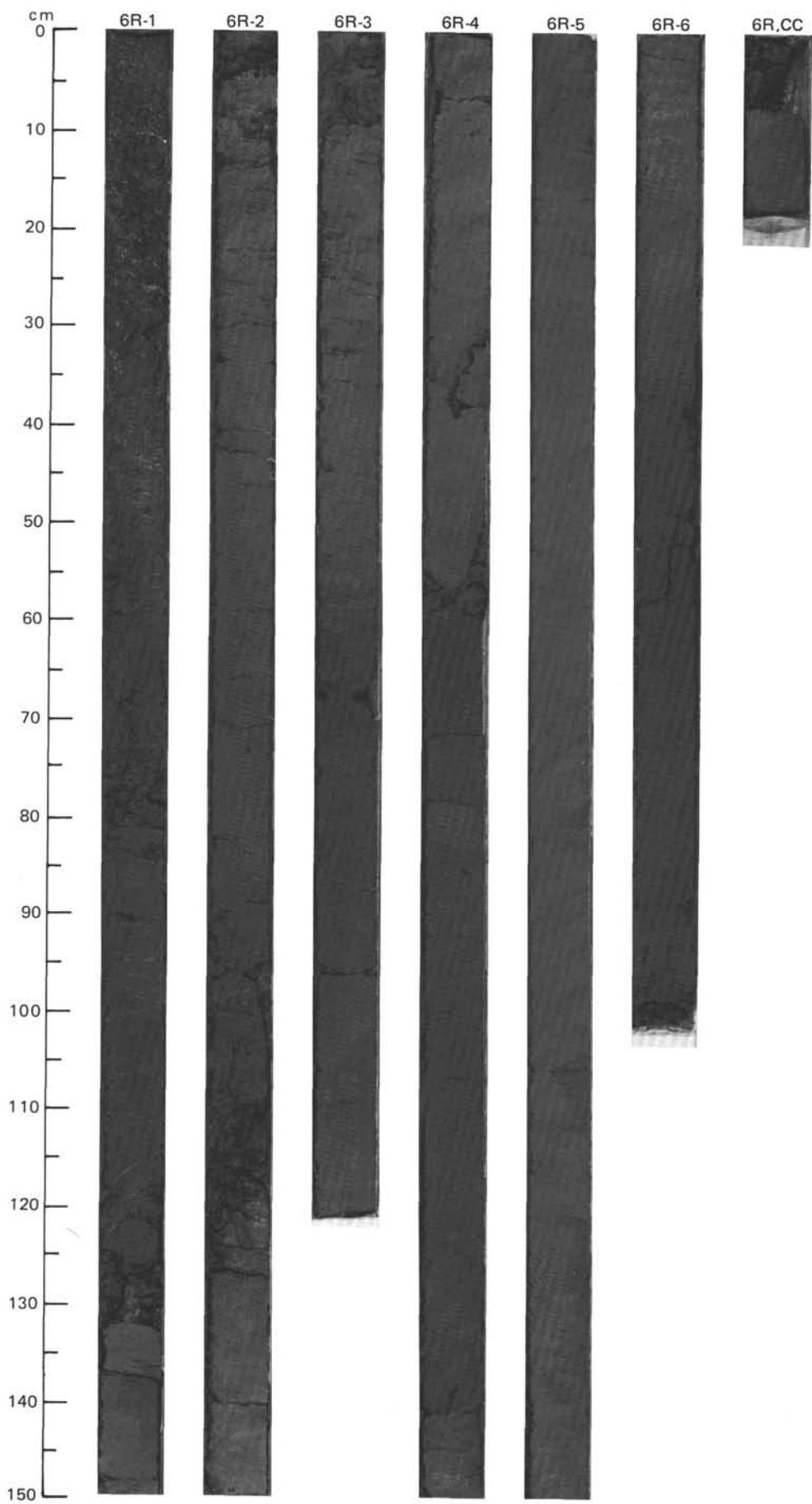


SITE 645 HOLE E CORE 4 R CORED INTERVAL 2462.7-2472.4 mbsl, 455.2-464.9 mbsf

TIME-ROCK UNIT	BIOSTRAT. ZONE/ FOSSIL CHARACTER				PALEOMAGNETICS	PHYS. PROPERTIES	CHEMISTRY	SECTION	METERS	GRAPHIC LITHOLOGY	DRILLING DISTURB.	SED. STRUCTURES	SAMPLES	LITHOLOGIC DESCRIPTION																																																																								
	FORAMINIFERS	NANNOFOSSILS	RADIOLARIANS	DIATOMS											DINOCYSTS																																																																							
B									0.5					<p>SILTY MUD</p> <p>Silty mud, dark gray (5G 4/1); variably bioturbated, with few shale clasts and "dropstones."</p> <p>SMEAR SLIDE SUMMARY (%):</p> <table border="1"> <tr> <td></td> <td>1, 80</td> <td>2, 60</td> <td>3, 27</td> <td>3, 76</td> <td>4, 50</td> </tr> <tr> <td></td> <td>D</td> <td>D</td> <td>D</td> <td>M</td> <td>D</td> </tr> </table> <p>TEXTURE:</p> <table border="1"> <tr> <td>Sand</td> <td>20</td> <td>20</td> <td>30</td> <td>5</td> <td>15</td> </tr> <tr> <td>Silt</td> <td>50</td> <td>60</td> <td>40</td> <td>20</td> <td>50</td> </tr> <tr> <td>Clay</td> <td>30</td> <td>20</td> <td>30</td> <td>75</td> <td>35</td> </tr> </table> <p>COMPOSITION:</p> <table border="1"> <tr> <td>Quartz</td> <td>70</td> <td>65</td> <td>65</td> <td>5</td> <td>70</td> </tr> <tr> <td>Feldspar</td> <td>10</td> <td>5</td> <td>15</td> <td>—</td> <td>10</td> </tr> <tr> <td>Mica</td> <td>1</td> <td>1</td> <td>Tr</td> <td>—</td> <td>Tr</td> </tr> <tr> <td>Clay</td> <td>13</td> <td>18</td> <td>14</td> <td>15</td> <td>14</td> </tr> <tr> <td>Volcanic glass</td> <td>Tr</td> <td>Tr</td> <td>Tr</td> <td>—</td> <td>—</td> </tr> <tr> <td>Calcite/dolomite</td> <td>5</td> <td>10</td> <td>5</td> <td>80</td> <td>5</td> </tr> <tr> <td>Accessory minerals</td> <td>1</td> <td>1</td> <td>1</td> <td>Tr</td> <td>1</td> </tr> </table>		1, 80	2, 60	3, 27	3, 76	4, 50		D	D	D	M	D	Sand	20	20	30	5	15	Silt	50	60	40	20	50	Clay	30	20	30	75	35	Quartz	70	65	65	5	70	Feldspar	10	5	15	—	10	Mica	1	1	Tr	—	Tr	Clay	13	18	14	15	14	Volcanic glass	Tr	Tr	Tr	—	—	Calcite/dolomite	5	10	5	80	5	Accessory minerals	1	1	1	Tr	1
	1, 80	2, 60	3, 27	3, 76	4, 50																																																																																	
	D	D	D	M	D																																																																																	
Sand	20	20	30	5	15																																																																																	
Silt	50	60	40	20	50																																																																																	
Clay	30	20	30	75	35																																																																																	
Quartz	70	65	65	5	70																																																																																	
Feldspar	10	5	15	—	10																																																																																	
Mica	1	1	Tr	—	Tr																																																																																	
Clay	13	18	14	15	14																																																																																	
Volcanic glass	Tr	Tr	Tr	—	—																																																																																	
Calcite/dolomite	5	10	5	80	5																																																																																	
Accessory minerals	1	1	1	Tr	1																																																																																	
B								1.0																																																																														
B								2																																																																														
B								3																																																																														
B								4																																																																														
N.C.								CC																																																																														

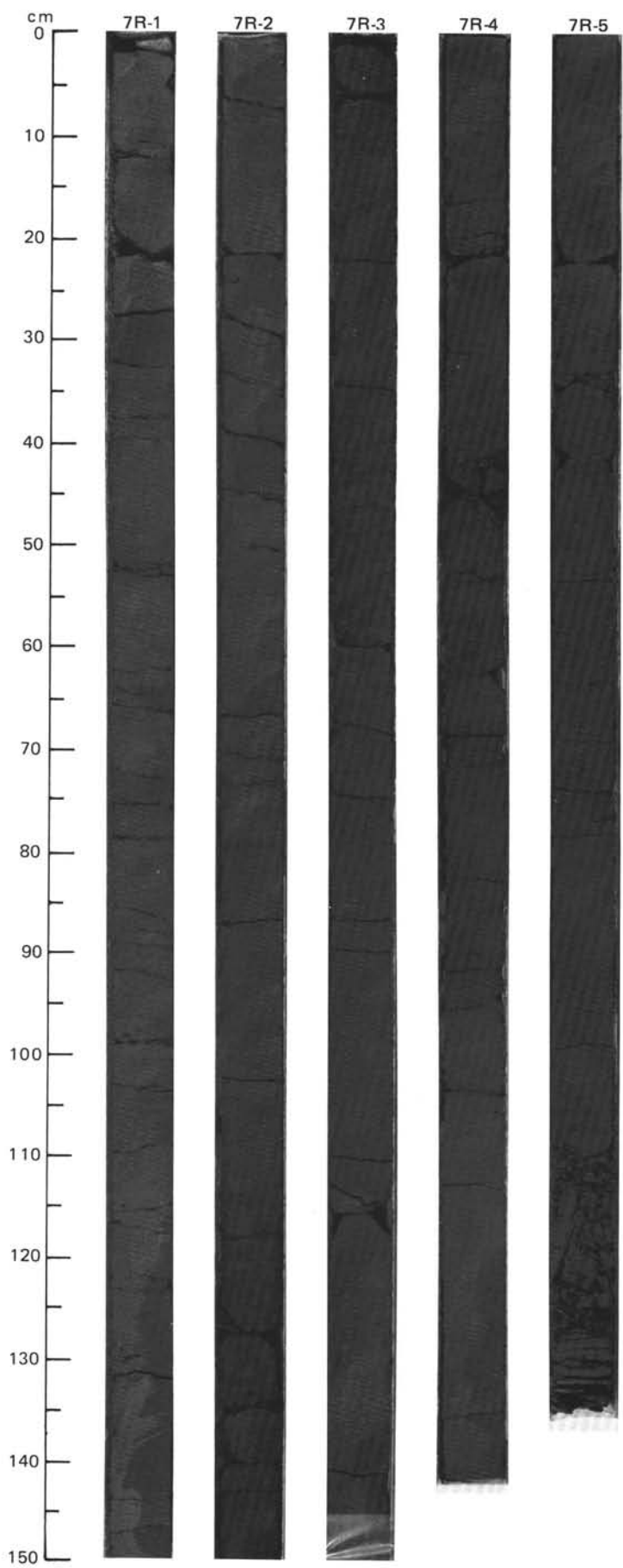
CORE 5 NO RECOVERY

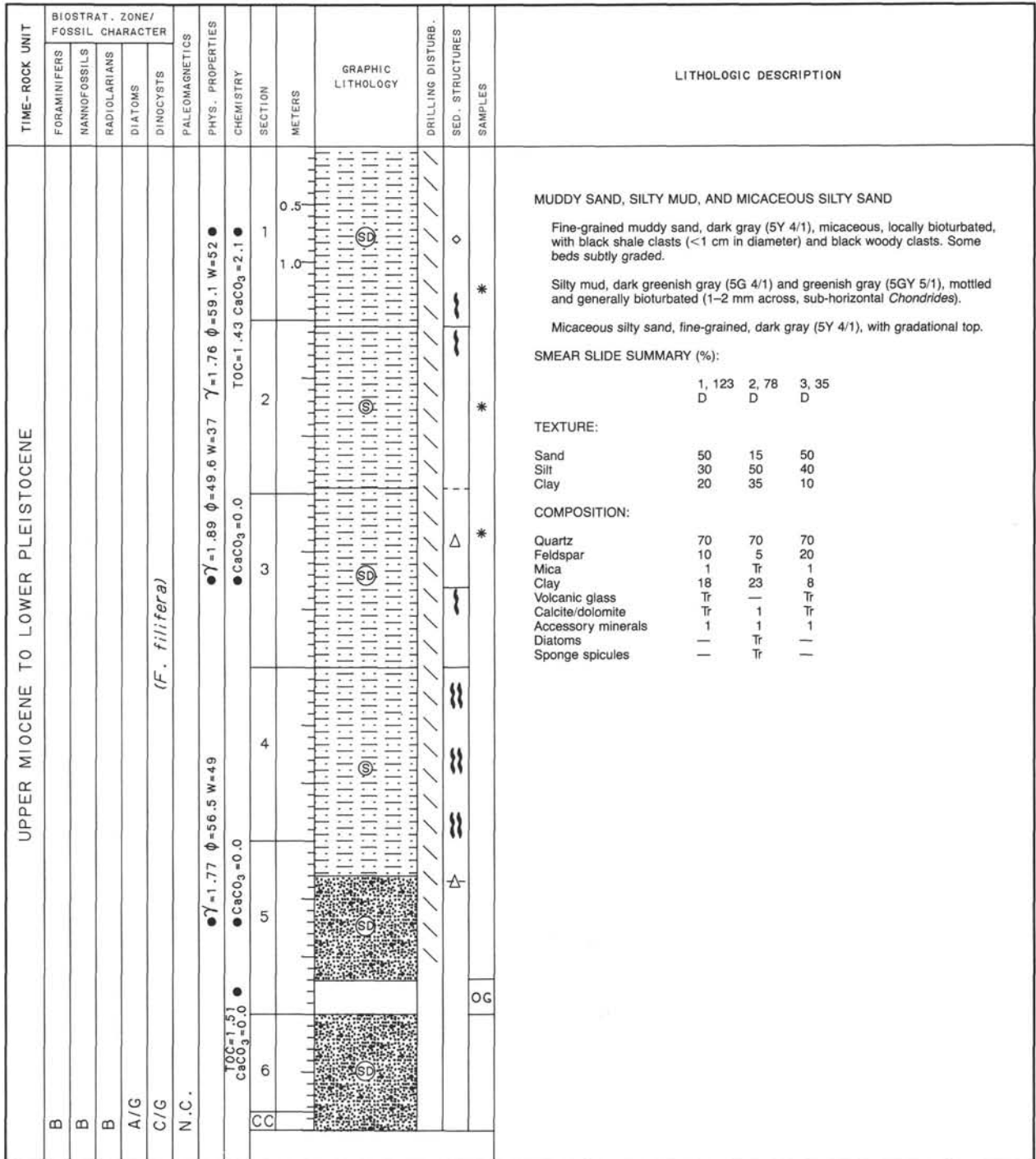


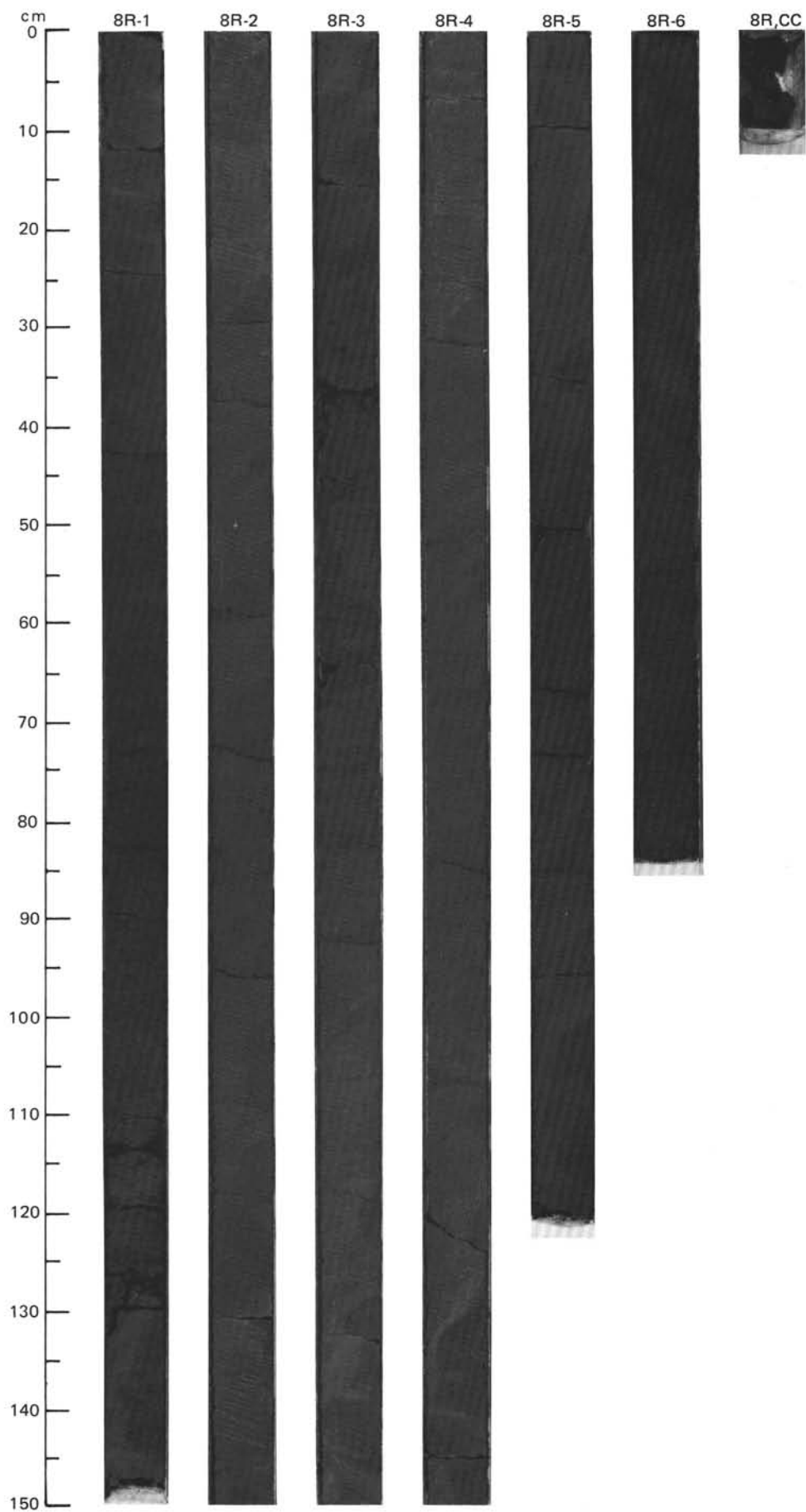


SITE 645 HOLE E CORE 7 R CORED INTERVAL 2491.6-2501.2 mbsl; 484.1-493.7 mbsf

TIME-ROCK UNIT	BIOSTRAT. ZONE/ FOSSIL CHARACTER					PALEOMAGNETICS	PHYS. PROPERTIES	CHEMISTRY	SECTION	METERS	GRAPHIC LITHOLOGY	DRILLING DISTURB.	SEC. STRUCTURES	SAMPLES	LITHOLOGIC DESCRIPTION																																																																										
	FORAMINIFERS	NANOFOSSELS	RADIOLARIANS	DIATOMS	DINOCYSTS																																																																																				
UPPER MIOCENE TO RECENT	B	B	B	P/G	N.C.		$\gamma = 1.86$ $\phi = 54.4$ $W = 43$ $\gamma = 1.78$ $\phi = 58.8$ $W = 51$ \bullet $\text{CaCO}_3 = 0.0$ \bullet $\text{TOC} = 1.02$ $\text{CaCO}_3 = 1.6$							<p>SILTY MUD AND SILTY SAND</p> <p>Silty mud, greenish gray (5G 5/1) with pyrite and very rare gravel, bioturbated.</p> <p>Silty sand, dark gray (5Y 4/1), micaceous, homogeneous, no pyrite with very rare gravel.</p> <p>Minor lithology: Section 1, 0-10 cm: silty mud, greenish gray (5GY 5/1), mottled, bioturbated.</p> <p>SMEAR SLIDE SUMMARY (%):</p> <table border="1"> <tr> <td></td> <td>1, 25</td> <td>1, 71</td> <td>2, 131</td> <td>4, 67</td> </tr> <tr> <td></td> <td>D</td> <td>M</td> <td>D</td> <td>D</td> </tr> </table> <p>TEXTURE:</p> <table border="1"> <tr> <td>Sand</td> <td>20</td> <td>5</td> <td>50</td> <td>50</td> </tr> <tr> <td>Silt</td> <td>50</td> <td>70</td> <td>40</td> <td>40</td> </tr> <tr> <td>Clay</td> <td>30</td> <td>25</td> <td>10</td> <td>10</td> </tr> </table> <p>COMPOSITION:</p> <table border="1"> <tr> <td>Quartz</td> <td>60</td> <td>40</td> <td>70</td> <td>70</td> </tr> <tr> <td>Feldspar</td> <td>10</td> <td>—</td> <td>20</td> <td>20</td> </tr> <tr> <td>Mica</td> <td>Tr</td> <td>Tr</td> <td>Tr</td> <td>1</td> </tr> <tr> <td>Clay</td> <td>20</td> <td>20</td> <td>9</td> <td>7</td> </tr> <tr> <td>Volcanic glass</td> <td>—</td> <td>—</td> <td>Tr</td> <td>—</td> </tr> <tr> <td>Calcite/dolomite</td> <td>5</td> <td>Tr</td> <td>Tr</td> <td>Tr</td> </tr> <tr> <td>Accessory minerals</td> <td>5</td> <td>—</td> <td>1</td> <td>1</td> </tr> <tr> <td>Pyrite</td> <td>—</td> <td>40</td> <td>—</td> <td>—</td> </tr> <tr> <td>Diatoms</td> <td>—</td> <td>—</td> <td>Tr</td> <td>Tr</td> </tr> <tr> <td>Sponge spicules</td> <td>—</td> <td>—</td> <td>Tr</td> <td>1</td> </tr> </table>		1, 25	1, 71	2, 131	4, 67		D	M	D	D	Sand	20	5	50	50	Silt	50	70	40	40	Clay	30	25	10	10	Quartz	60	40	70	70	Feldspar	10	—	20	20	Mica	Tr	Tr	Tr	1	Clay	20	20	9	7	Volcanic glass	—	—	Tr	—	Calcite/dolomite	5	Tr	Tr	Tr	Accessory minerals	5	—	1	1	Pyrite	—	40	—	—	Diatoms	—	—	Tr	Tr	Sponge spicules	—	—	Tr	1
	1, 25	1, 71	2, 131	4, 67																																																																																					
	D	M	D	D																																																																																					
Sand	20	5	50	50																																																																																					
Silt	50	70	40	40																																																																																					
Clay	30	25	10	10																																																																																					
Quartz	60	40	70	70																																																																																					
Feldspar	10	—	20	20																																																																																					
Mica	Tr	Tr	Tr	1																																																																																					
Clay	20	20	9	7																																																																																					
Volcanic glass	—	—	Tr	—																																																																																					
Calcite/dolomite	5	Tr	Tr	Tr																																																																																					
Accessory minerals	5	—	1	1																																																																																					
Pyrite	—	40	—	—																																																																																					
Diatoms	—	—	Tr	Tr																																																																																					
Sponge spicules	—	—	Tr	1																																																																																					

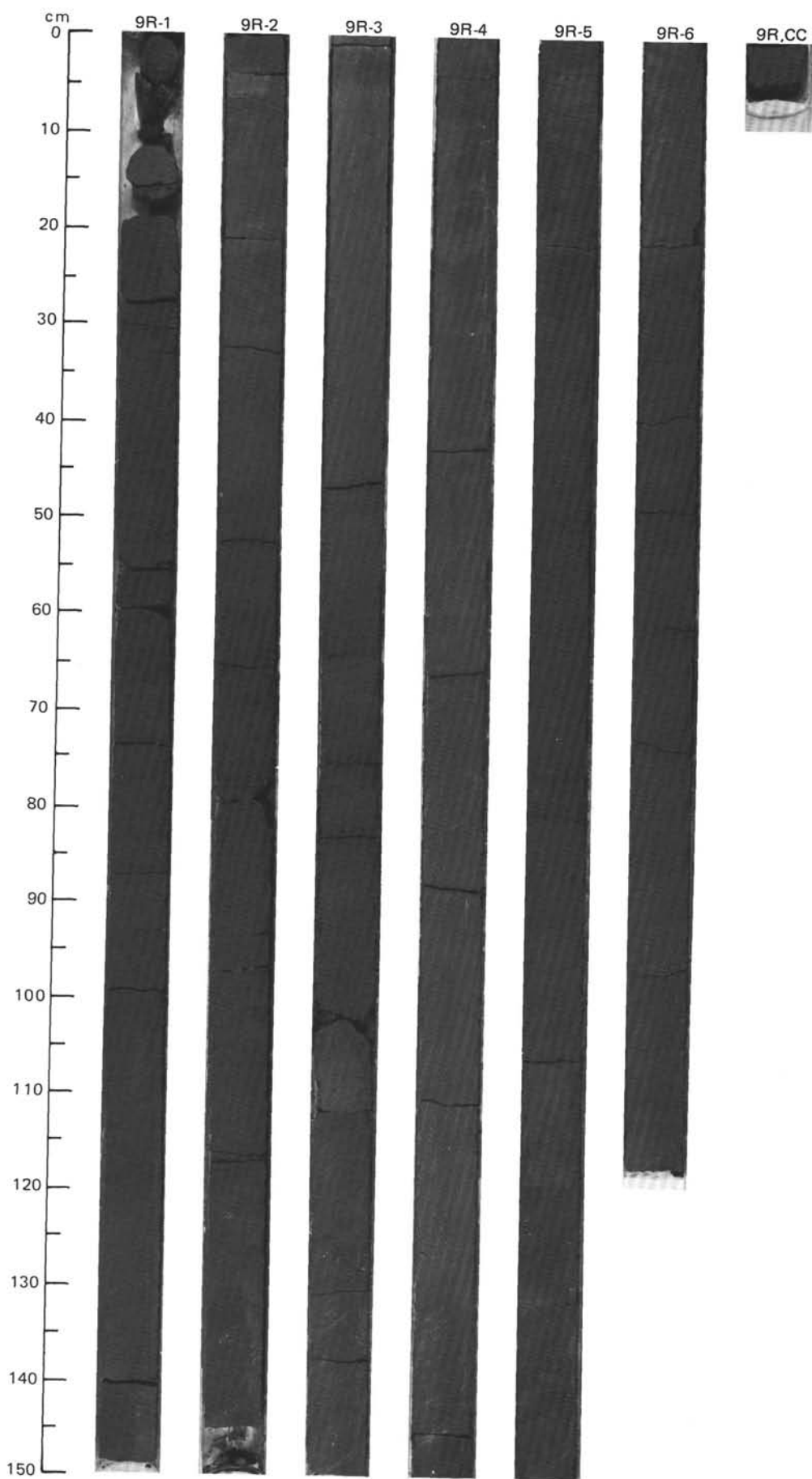






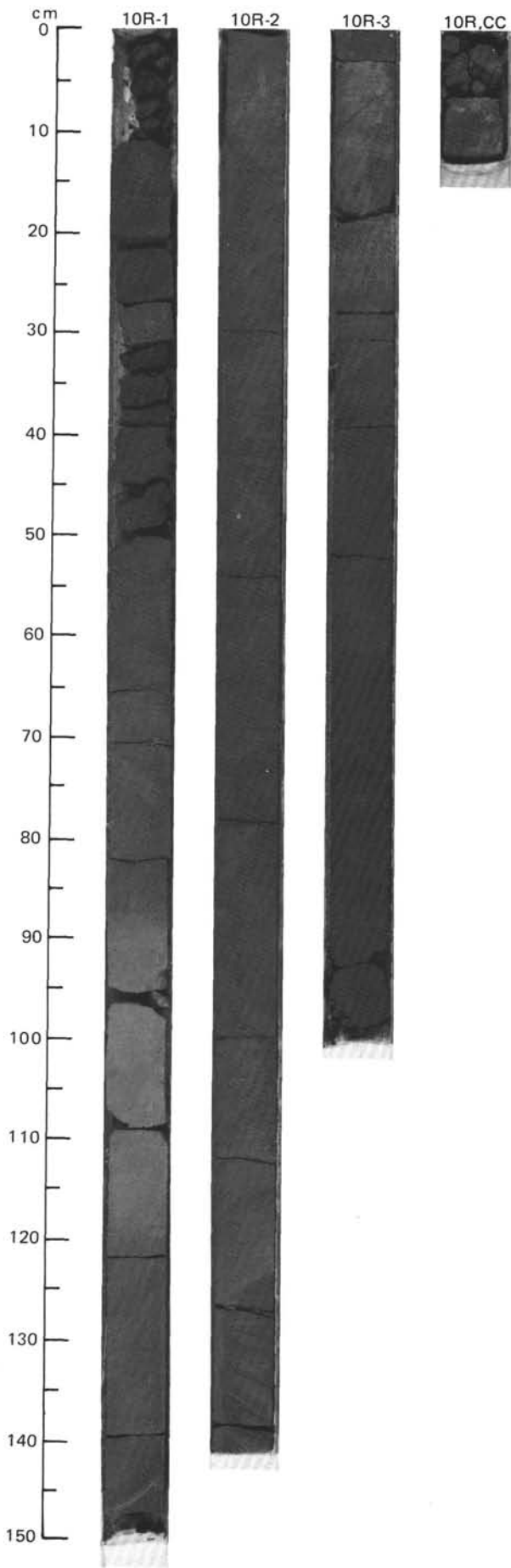
SITE 645 HOLE E CORE 9 R CORED INTERVAL 2510.9-2520.5 mbsf; 503.4-513.0 mbsf

TIME-ROCK UNIT	BIOSTRAT. ZONE/ FOSSIL CHARACTER				PALEOMAGNETICS	PHYS. PROPERTIES	CHEMISTRY	SECTION	METERS	GRAPHIC LITHOLOGY	DRILLING DISTURB.	SED. STRUCTURES	SAMPLES	LITHOLOGIC DESCRIPTION																																																																																
	FORAMINIFERS	NANNOFOSSILS	RADIOLARIANS	DIATOMS																																																																																										
UPPER MIOCENE TO LOWER PLEISTOCENE	B													<p>MUDDY SAND and CLAYEY SILT</p> <p>Muddy sand, dark gray (5Y 4/1), micaceous, generally fine grained, with gradational bases and tops. Local terrestrial plant debris. Clayey silt, greenish gray (5GY 5/1); bioturbated (1-2 mm diameter <i>Chondrites</i>).</p> <p>Minor lithology: Section 2, 20-67 cm; Section 6, 0-20 cm; silty mud, generally bioturbated (1-2 mm <i>Chondrites</i>).</p> <p>SMEAR SLIDE SUMMARY (%):</p> <table border="1"> <tr> <td></td> <td>1, 53</td> <td>2, 118</td> <td>3, 98</td> <td>4, 78</td> </tr> <tr> <td></td> <td>D</td> <td>M</td> <td>D</td> <td>D</td> </tr> </table> <p>TEXTURE:</p> <table border="1"> <tr> <td>Sand</td> <td>50</td> <td>—</td> <td>60</td> <td>—</td> </tr> <tr> <td>Silt</td> <td>30</td> <td>—</td> <td>20</td> <td>40</td> </tr> <tr> <td>Clay</td> <td>20</td> <td>—</td> <td>20</td> <td>60</td> </tr> </table> <p>COMPOSITION:</p> <table border="1"> <tr> <td>Quartz</td> <td>70</td> <td>—</td> <td>60</td> <td>10</td> </tr> <tr> <td>Feldspar</td> <td>20</td> <td>—</td> <td>20</td> <td>—</td> </tr> <tr> <td>Mica</td> <td>1</td> <td>—</td> <td>1</td> <td>—</td> </tr> <tr> <td>Clay</td> <td>6</td> <td>—</td> <td>12</td> <td>62</td> </tr> <tr> <td>Volcanic glass</td> <td>Tr</td> <td>—</td> <td>Tr</td> <td>—</td> </tr> <tr> <td>Calcite/dolomite</td> <td>—</td> <td>—</td> <td>—</td> <td>5</td> </tr> <tr> <td>Accessory minerals</td> <td>1</td> <td>—</td> <td>5</td> <td>3</td> </tr> <tr> <td>Pellets</td> <td>—</td> <td>—</td> <td>—</td> <td>10</td> </tr> <tr> <td>Diatoms</td> <td>1</td> <td>—</td> <td>1</td> <td>8</td> </tr> <tr> <td>Sponge spicules</td> <td>1</td> <td>—</td> <td>1</td> <td>1</td> </tr> <tr> <td>Plant debris</td> <td>—</td> <td>100</td> <td>—</td> <td>1</td> </tr> </table>		1, 53	2, 118	3, 98	4, 78		D	M	D	D	Sand	50	—	60	—	Silt	30	—	20	40	Clay	20	—	20	60	Quartz	70	—	60	10	Feldspar	20	—	20	—	Mica	1	—	1	—	Clay	6	—	12	62	Volcanic glass	Tr	—	Tr	—	Calcite/dolomite	—	—	—	5	Accessory minerals	1	—	5	3	Pellets	—	—	—	10	Diatoms	1	—	1	8	Sponge spicules	1	—	1	1	Plant debris	—	100	—	1
		1, 53	2, 118	3, 98	4, 78																																																																																									
		D	M	D	D																																																																																									
	Sand	50	—	60	—																																																																																									
	Silt	30	—	20	40																																																																																									
	Clay	20	—	20	60																																																																																									
Quartz	70	—	60	10																																																																																										
Feldspar	20	—	20	—																																																																																										
Mica	1	—	1	—																																																																																										
Clay	6	—	12	62																																																																																										
Volcanic glass	Tr	—	Tr	—																																																																																										
Calcite/dolomite	—	—	—	5																																																																																										
Accessory minerals	1	—	5	3																																																																																										
Pellets	—	—	—	10																																																																																										
Diatoms	1	—	1	8																																																																																										
Sponge spicules	1	—	1	1																																																																																										
Plant debris	—	100	—	1																																																																																										
									0.5		X																																																																																			
									1.0	Uphole Debris		*																																																																																		
									2																																																																																					
									3																																																																																					
									4																																																																																					
									5																																																																																					
									6																																																																																					



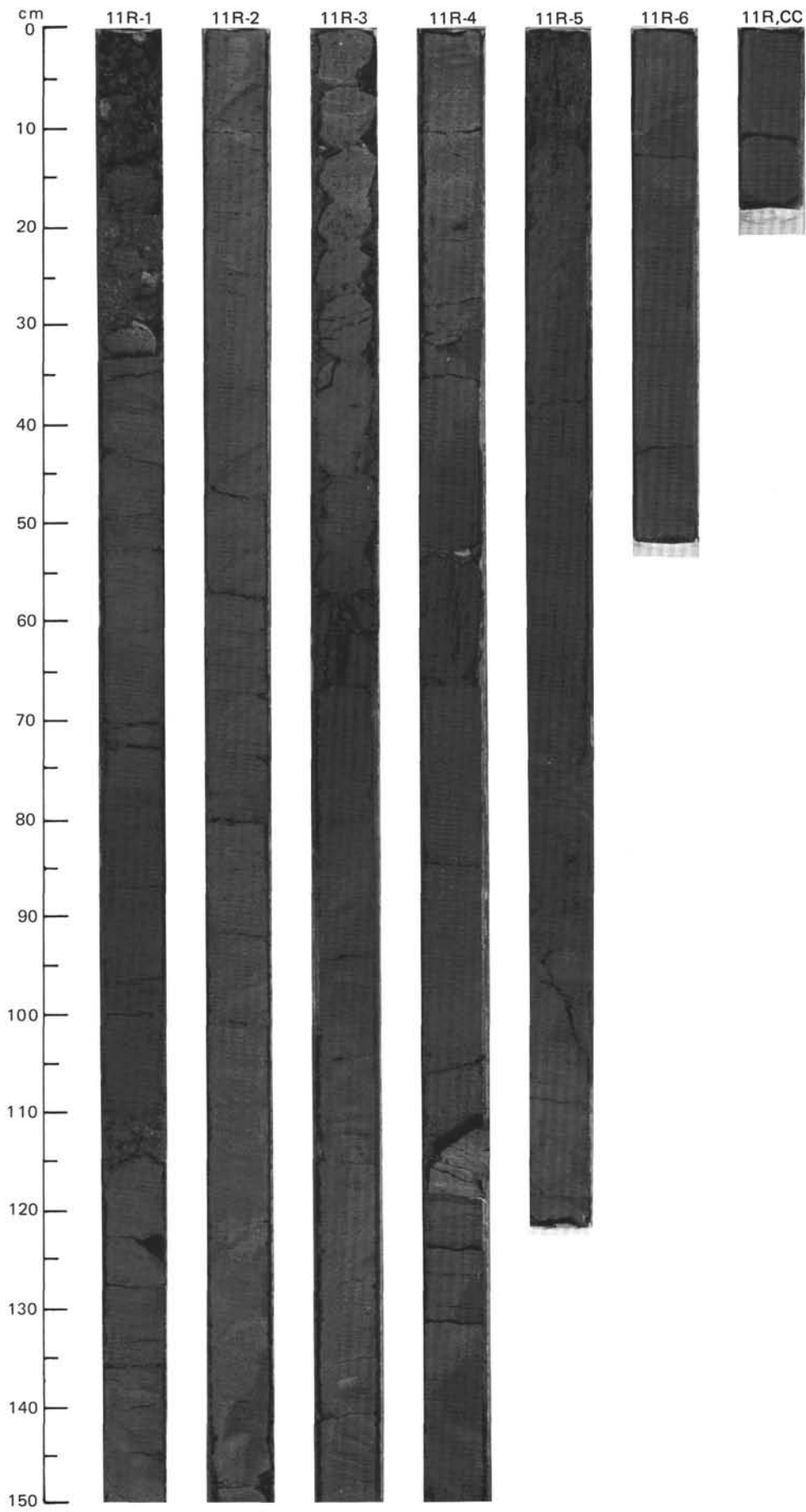
SITE 645 HOLE E CORE 10 R CORED INTERVAL 2520.5-2530.1 mbsl; 513.0-522.6 mbsf

TIME-ROCK UNIT	BIOSTRAT. ZONE/ FOSSIL CHARACTER					PALEOMAGNETICS	PHYS. PROPERTIES	CHEMISTRY	SECTION	METERS	GRAPHIC LITHOLOGY	DRILLING DISTURB.	SED. STRUCTURES	SAMPLES	LITHOLOGIC DESCRIPTION																																																				
	FORAMINIFERS	NANNOFOSSILS	RADIOLARIANS	DIATOMS	DINOCYSTS																																																														
	B	B	B	R/P	R/M	N.C.	$\gamma = 1.78$ $\phi = 54.3$ $W = 45$ $\gamma = 1.89$ $\phi = 48.1$ $W = 34$ $\text{CaCO}_3 = 2.0$ $\text{TOC} = 1.91$ $\text{CaCO}_3 = 1.3$		1	0.5 1.0					<p>CLAYEY SILT and MUDDY SAND</p> <p>Clayey silt, greenish gray (5G 5/1), bioturbated.</p> <p>Muddy sand, dark gray (5Y 4/1).</p> <p>Minor lithologies: a. Section 1, 0-51 cm: silty mud, dark gray (5Y 4/1). b. Section 1, 87-120 cm: carbonate silty clay, light greenish gray (5GY 7/1), bioturbated.</p> <p>SMEAR SLIDE SUMMARY (%):</p> <table border="1"> <tr> <td></td> <td>1, 26</td> <td>1, 113</td> <td>3, 94</td> </tr> <tr> <td></td> <td>D</td> <td>M</td> <td>D</td> </tr> </table> <p>TEXTURE:</p> <table border="1"> <tr> <td>Sand</td> <td>20</td> <td>5</td> <td>50</td> </tr> <tr> <td>Silt</td> <td>45</td> <td>20</td> <td>35</td> </tr> <tr> <td>Clay</td> <td>35</td> <td>75</td> <td>15</td> </tr> </table> <p>COMPOSITION:</p> <table border="1"> <tr> <td>Quartz</td> <td>50</td> <td>5</td> <td>70</td> </tr> <tr> <td>Feldspar</td> <td>20</td> <td>—</td> <td>15</td> </tr> <tr> <td>Mica</td> <td>1</td> <td>—</td> <td>1</td> </tr> <tr> <td>Clay</td> <td>26</td> <td>—</td> <td>10</td> </tr> <tr> <td>Calcite/dolomite</td> <td>Tr</td> <td>95</td> <td>Tr</td> </tr> <tr> <td>Accessory minerals</td> <td>1</td> <td>Tr</td> <td>2</td> </tr> <tr> <td>Diatoms</td> <td>1</td> <td>—</td> <td>1</td> </tr> <tr> <td>Sponge spicules</td> <td>1</td> <td>—</td> <td>1</td> </tr> </table>		1, 26	1, 113	3, 94		D	M	D	Sand	20	5	50	Silt	45	20	35	Clay	35	75	15	Quartz	50	5	70	Feldspar	20	—	15	Mica	1	—	1	Clay	26	—	10	Calcite/dolomite	Tr	95	Tr	Accessory minerals	1	Tr	2	Diatoms	1	—	1	Sponge spicules	1	—	1
	1, 26	1, 113	3, 94																																																																
	D	M	D																																																																
Sand	20	5	50																																																																
Silt	45	20	35																																																																
Clay	35	75	15																																																																
Quartz	50	5	70																																																																
Feldspar	20	—	15																																																																
Mica	1	—	1																																																																
Clay	26	—	10																																																																
Calcite/dolomite	Tr	95	Tr																																																																
Accessory minerals	1	Tr	2																																																																
Diatoms	1	—	1																																																																
Sponge spicules	1	—	1																																																																

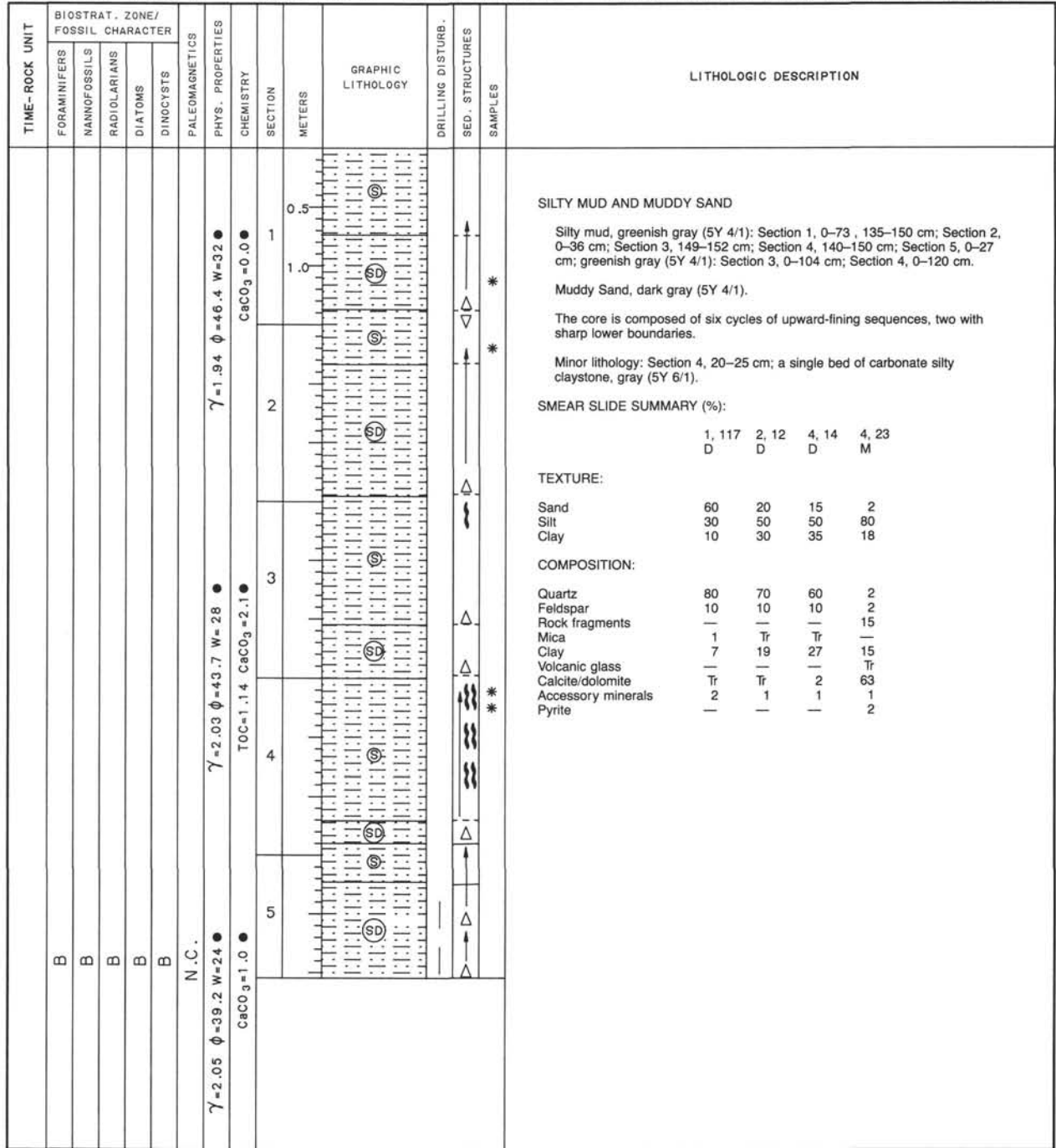


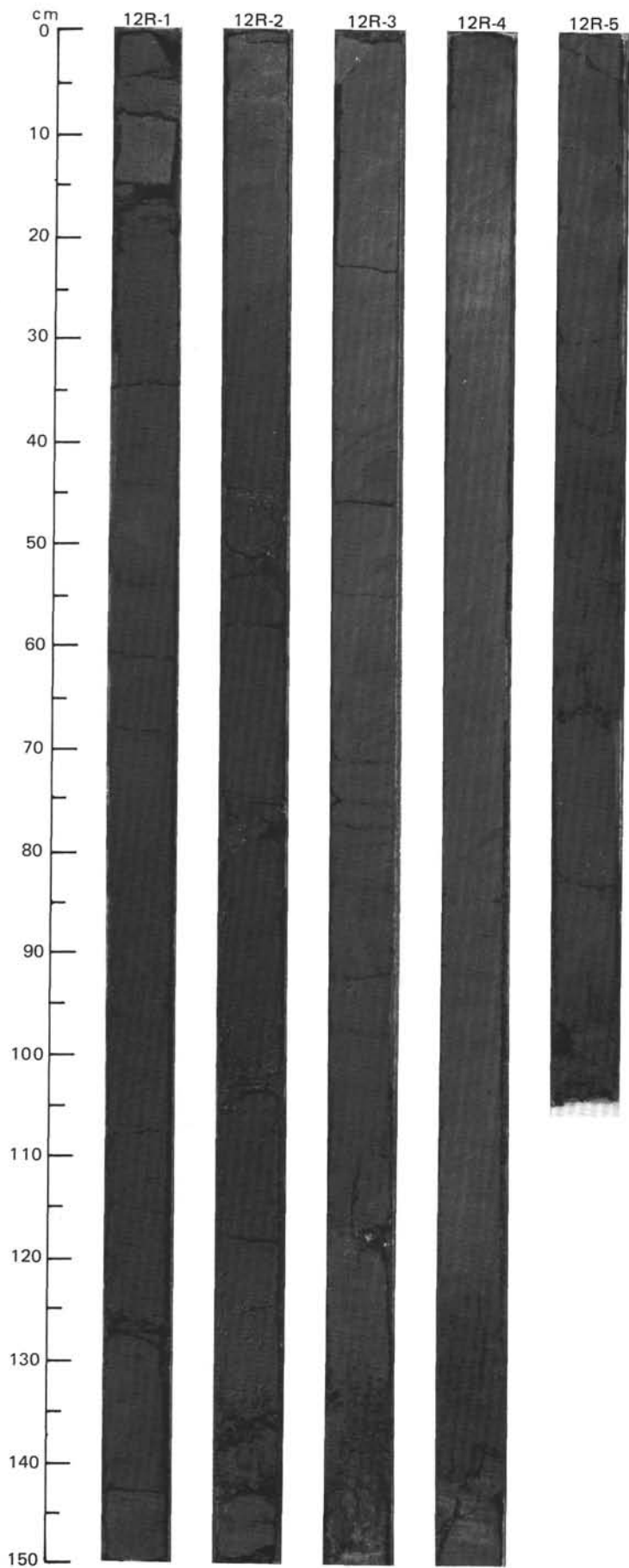
SITE 645 HOLE E CORE 11 R CORED INTERVAL 2530.1-2539.7 mbsl; 522.6-532.2 mbsf

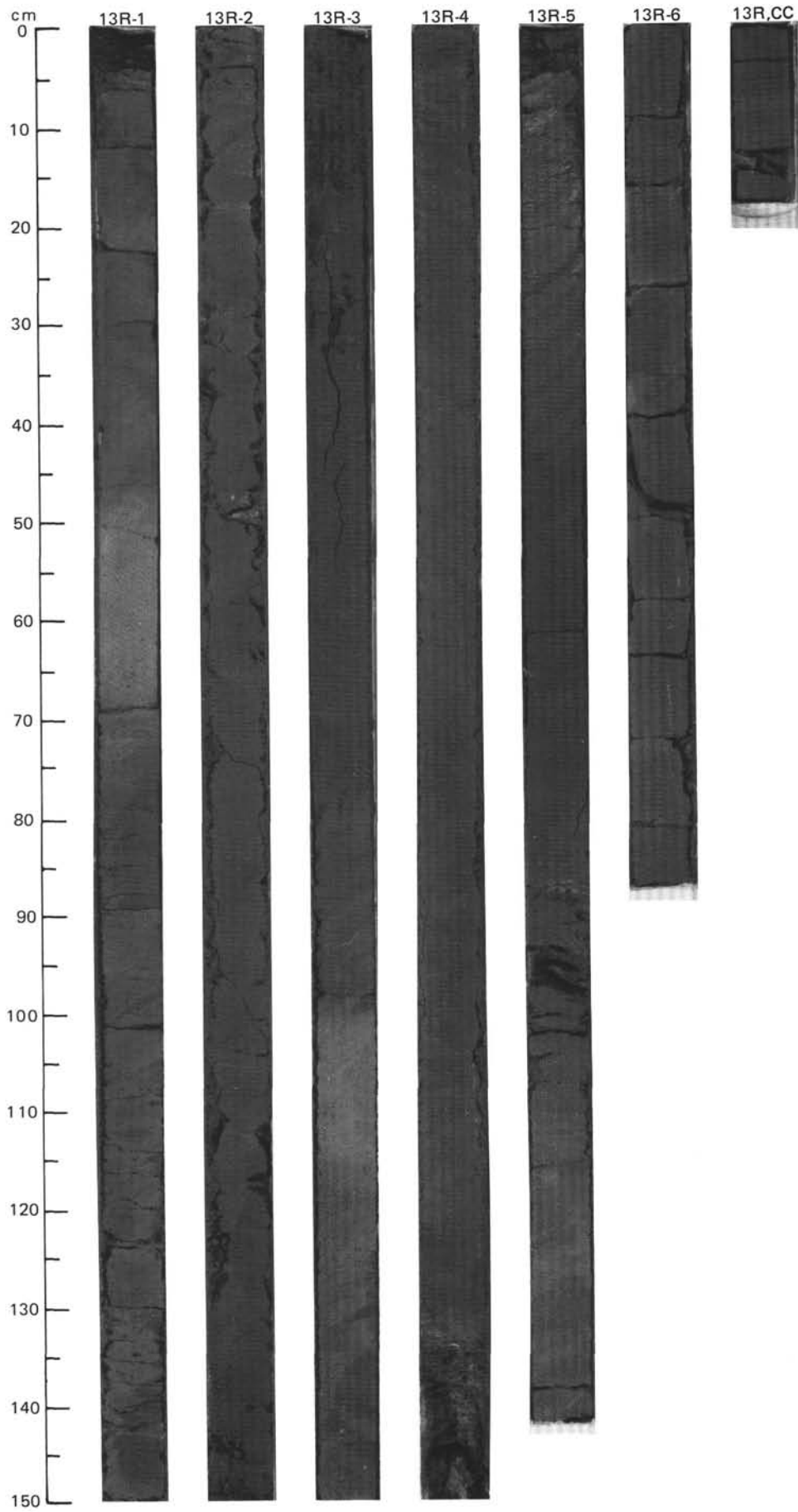
TIME - ROCK UNIT	BIOSTRAT. ZONE/ FOSSIL CHARACTER				PALEOMAGNETICS	PHYS. PROPERTIES	CHEMISTRY	SECTION	METERS	GRAPHIC LITHOLOGY	DRILLING DISTURB.	SED. STRUCTURES	SAMPLES	LITHOLOGIC DESCRIPTION																																																												
	FORAMINIFERS	NANNOFOSSILS	RADIOLARIANS	DIATOMS											DINOCYSTS																																																											
	B	B	B	B					0.5 1.0		X			<p>MICACEOUS MUDDY SAND AND SILTY MUD</p> <p>Micaceous muddy sand, greenish gray (5Gy 5/1), homogeneous, (clay-poor in places), commonly in graded beds with sharp bases.</p> <p>Silty mud, greenish gray (5Gy 5/1), locally bioturbated, locally pyrite bearing.</p> <p>Minor lithology: Section 1, 0-69 cm: greenish gray (5Gy 5/1) clayey siltstone, deformed at top of core.</p> <p>SMEAR SLIDE SUMMARY (%):</p> <table border="1"> <tr> <td></td> <td>1, 80</td> <td>2, 84</td> <td>3, 21</td> <td>5, 80</td> </tr> <tr> <td></td> <td>D</td> <td>D</td> <td>D</td> <td>D</td> </tr> </table> <p>TEXTURE:</p> <table border="1"> <tr> <td>Sand</td> <td>50</td> <td>10</td> <td>10</td> <td>70</td> </tr> <tr> <td>Silt</td> <td>35</td> <td>50</td> <td>50</td> <td>20</td> </tr> <tr> <td>Clay</td> <td>15</td> <td>40</td> <td>40</td> <td>10</td> </tr> </table> <p>COMPOSITION:</p> <table border="1"> <tr> <td>Quartz</td> <td>65</td> <td>55</td> <td>60</td> <td>80</td> </tr> <tr> <td>Feldspar</td> <td>10</td> <td>5</td> <td>Tr</td> <td>10</td> </tr> <tr> <td>Mica</td> <td>1</td> <td>Tr</td> <td>Tr</td> <td>1</td> </tr> <tr> <td>Clay</td> <td>9</td> <td>29</td> <td>29</td> <td>8</td> </tr> <tr> <td>Volcanic glass</td> <td>Tr</td> <td>Tr</td> <td>—</td> <td>Tr</td> </tr> <tr> <td>Calcite/dolomite</td> <td>5</td> <td>10</td> <td>10</td> <td>Tr</td> </tr> <tr> <td>Accessory minerals</td> <td>10</td> <td>1</td> <td>1</td> <td>1</td> </tr> </table>		1, 80	2, 84	3, 21	5, 80		D	D	D	D	Sand	50	10	10	70	Silt	35	50	50	20	Clay	15	40	40	10	Quartz	65	55	60	80	Feldspar	10	5	Tr	10	Mica	1	Tr	Tr	1	Clay	9	29	29	8	Volcanic glass	Tr	Tr	—	Tr	Calcite/dolomite	5	10	10	Tr	Accessory minerals	10	1	1	1
	1, 80	2, 84	3, 21	5, 80																																																																						
	D	D	D	D																																																																						
Sand	50	10	10	70																																																																						
Silt	35	50	50	20																																																																						
Clay	15	40	40	10																																																																						
Quartz	65	55	60	80																																																																						
Feldspar	10	5	Tr	10																																																																						
Mica	1	Tr	Tr	1																																																																						
Clay	9	29	29	8																																																																						
Volcanic glass	Tr	Tr	—	Tr																																																																						
Calcite/dolomite	5	10	10	Tr																																																																						
Accessory minerals	10	1	1	1																																																																						
								2				*																																																														
								3				*																																																														
								4				*																																																														
								5				*																																																														
								6				OG																																																														

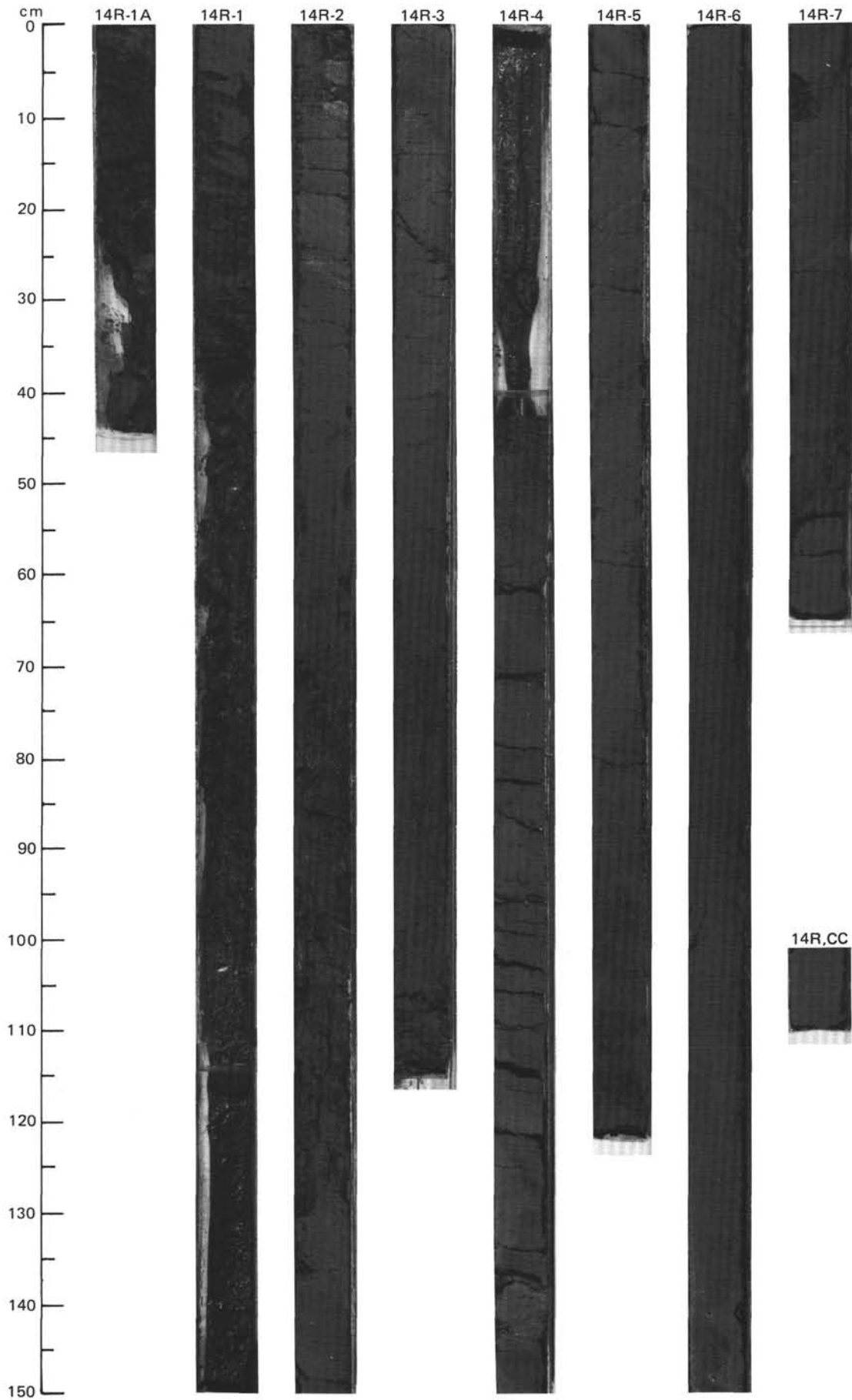


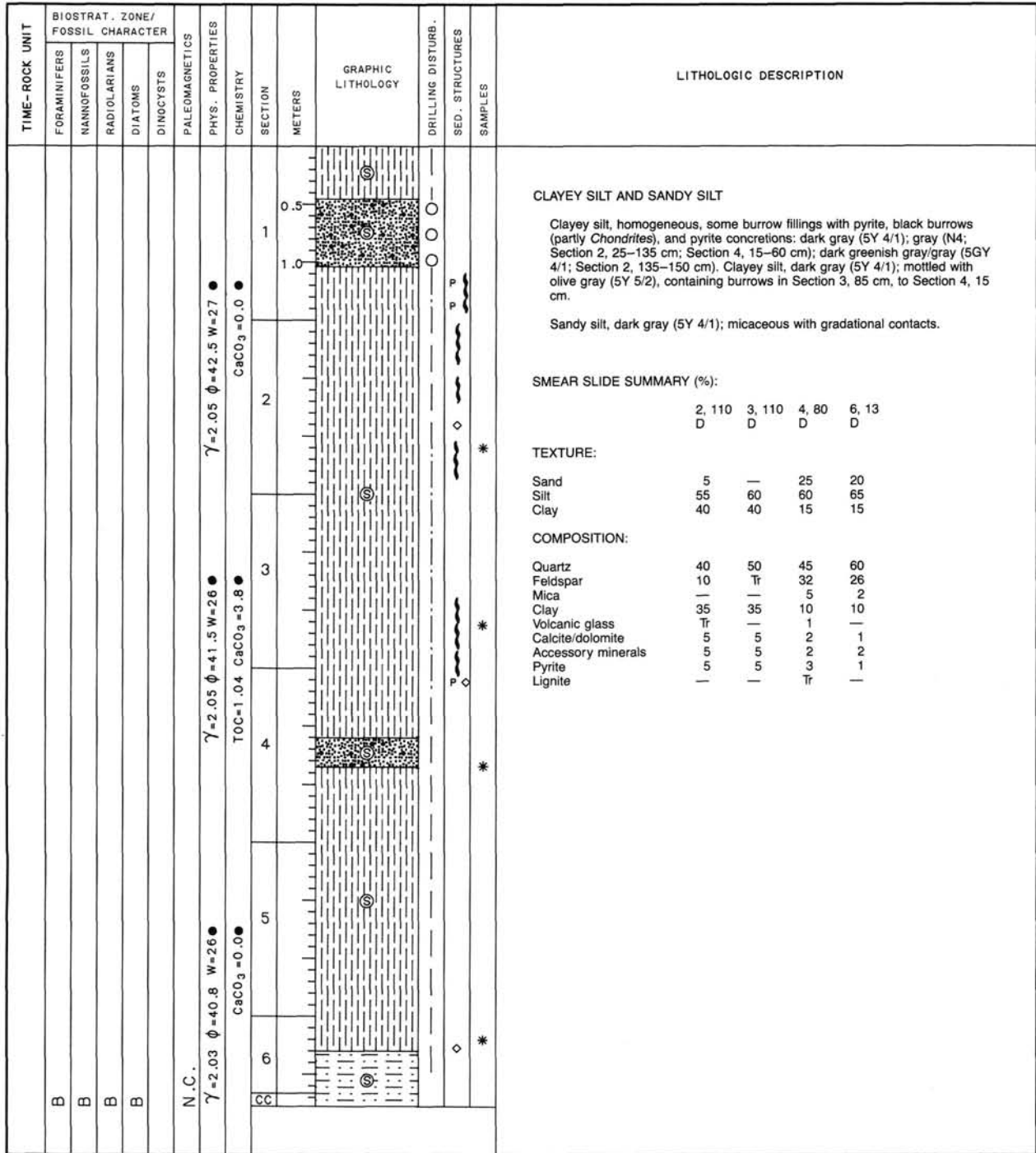
SITE 645 HOLE E CORE 12 R CORED INTERVAL 2539.7-2549.3 mbsf; 532.2-541.8 mbsf

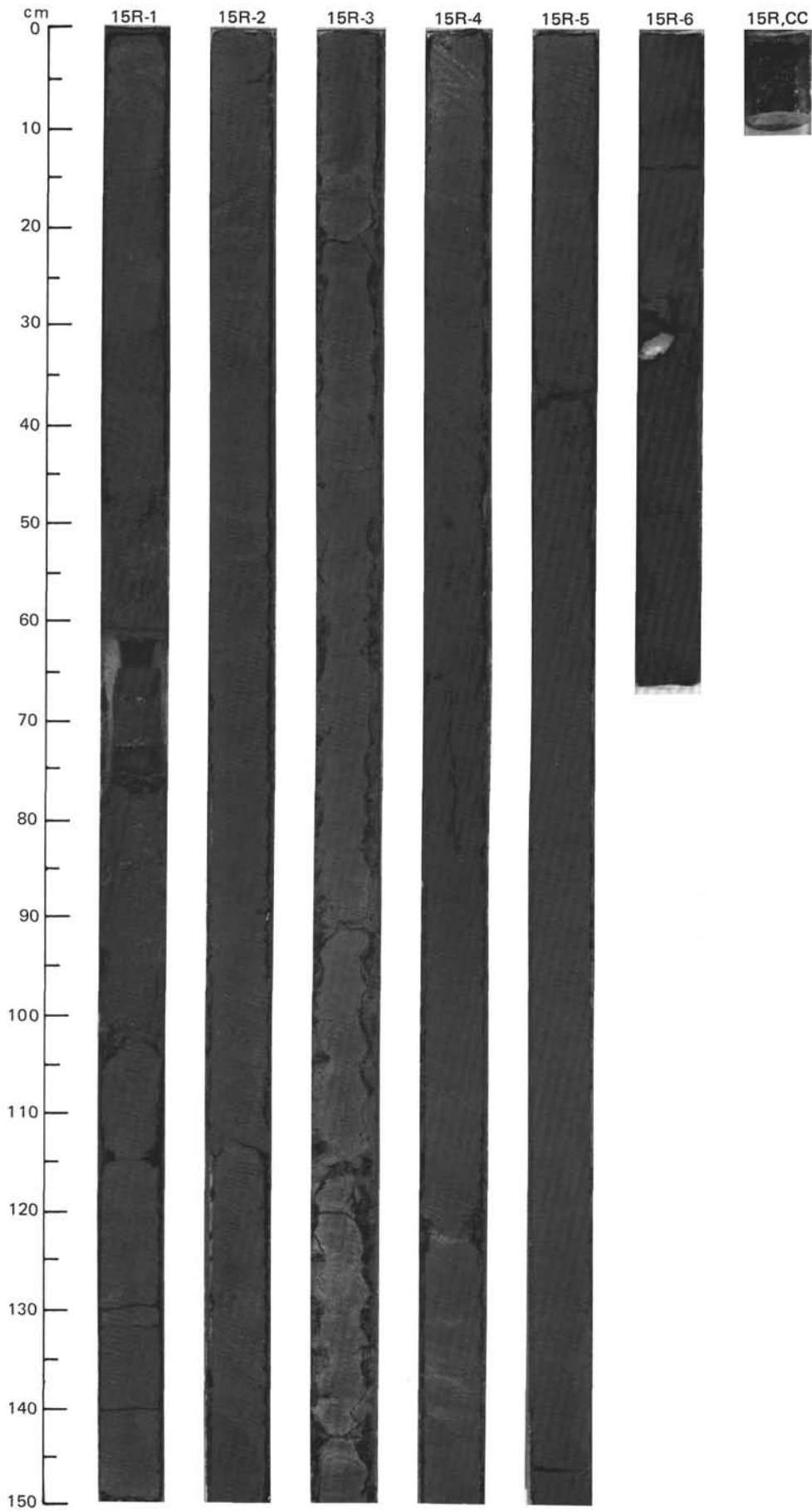




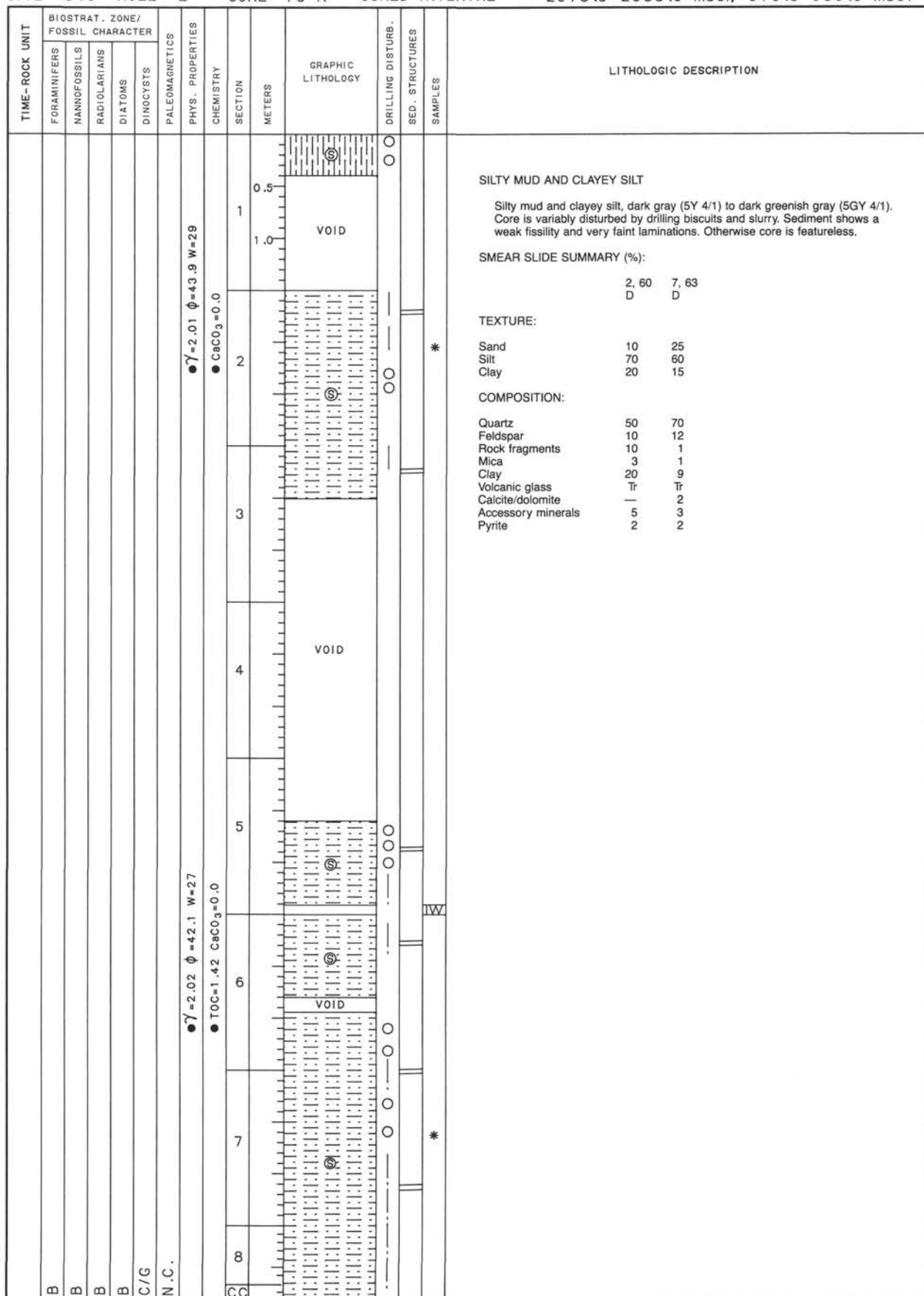


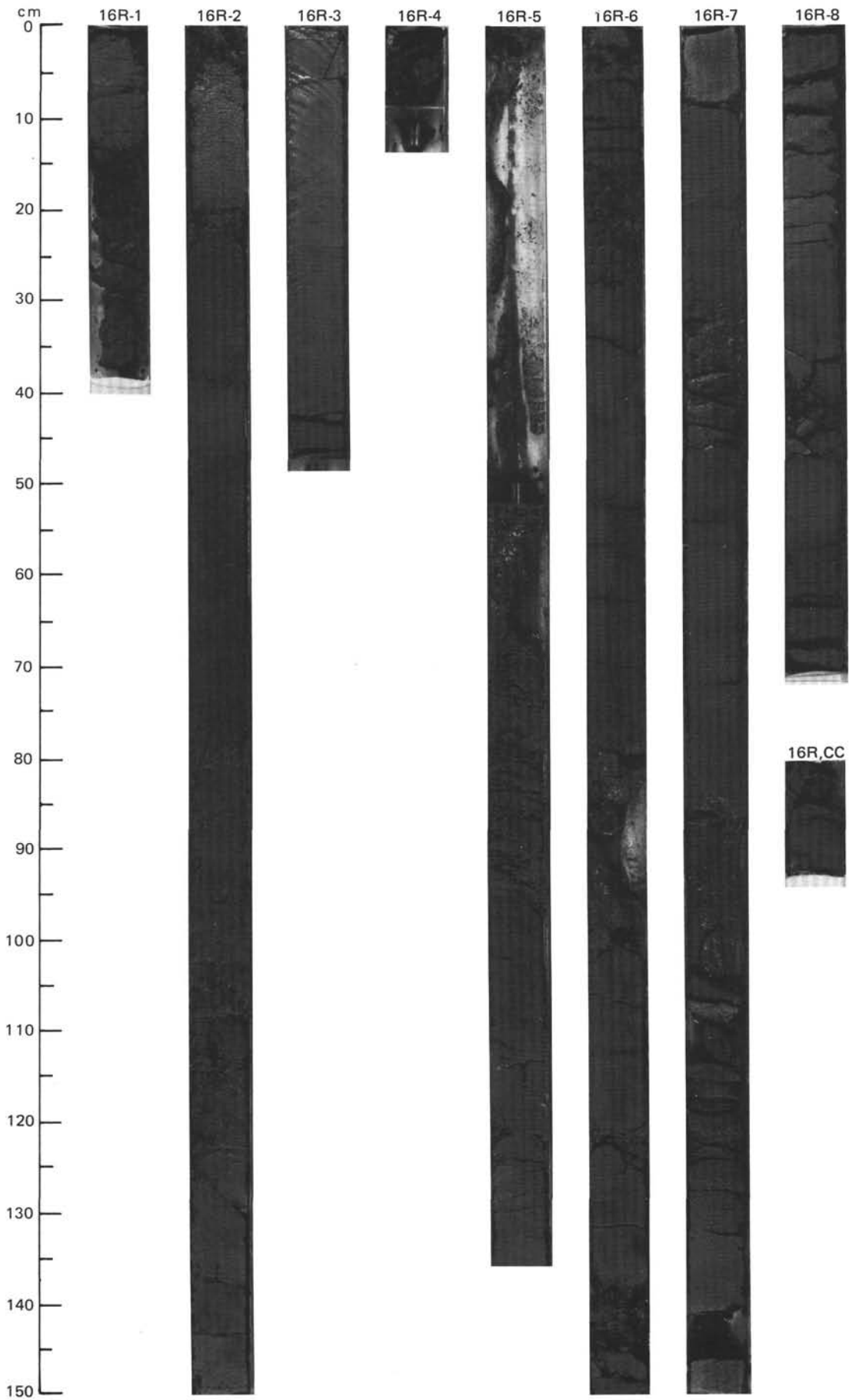


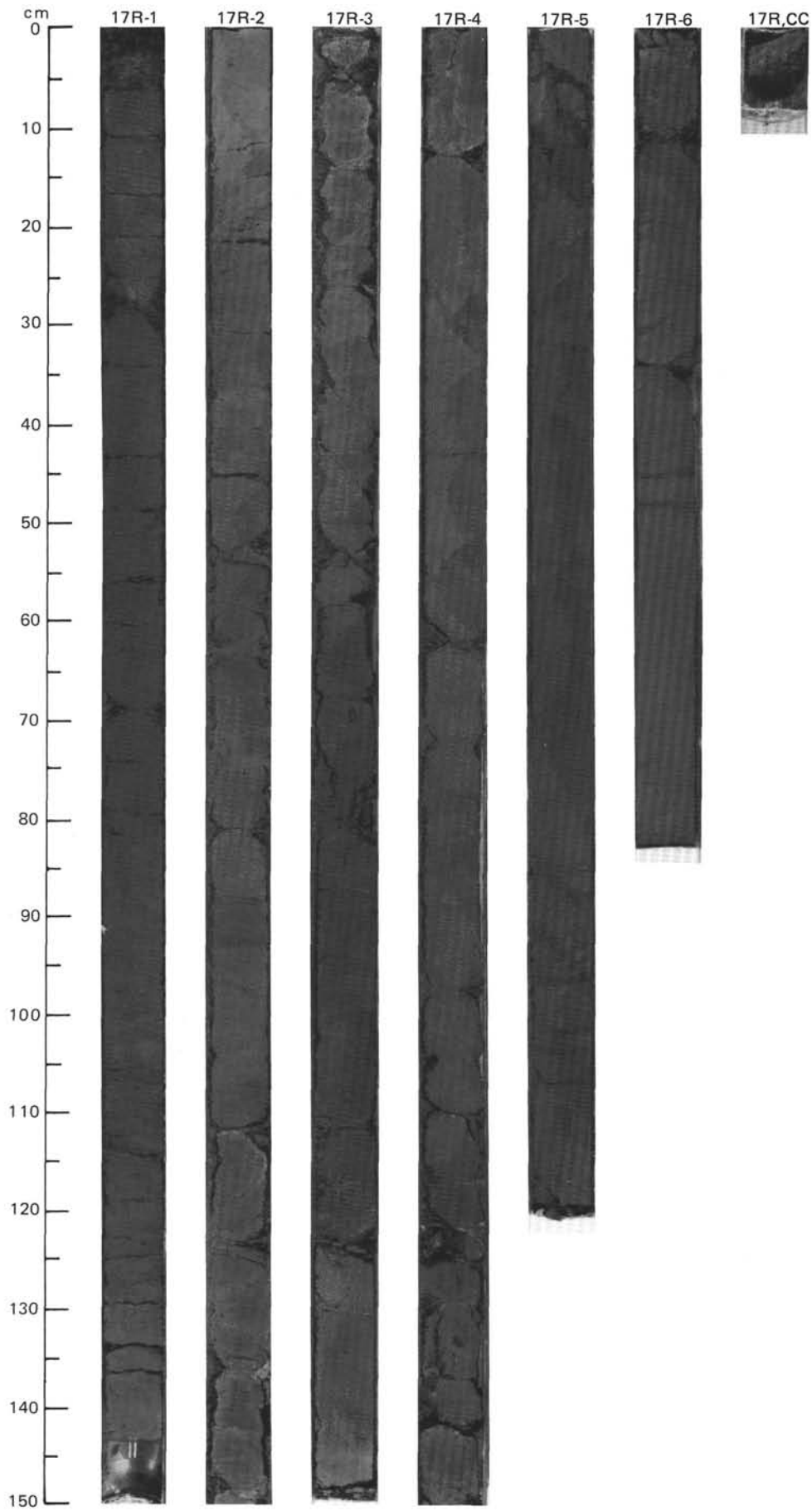




SITE 645 HOLE E CORE 16 R CORED INTERVAL 2578.3-2588.0 mbsl; 570.8-580.5 mbsf

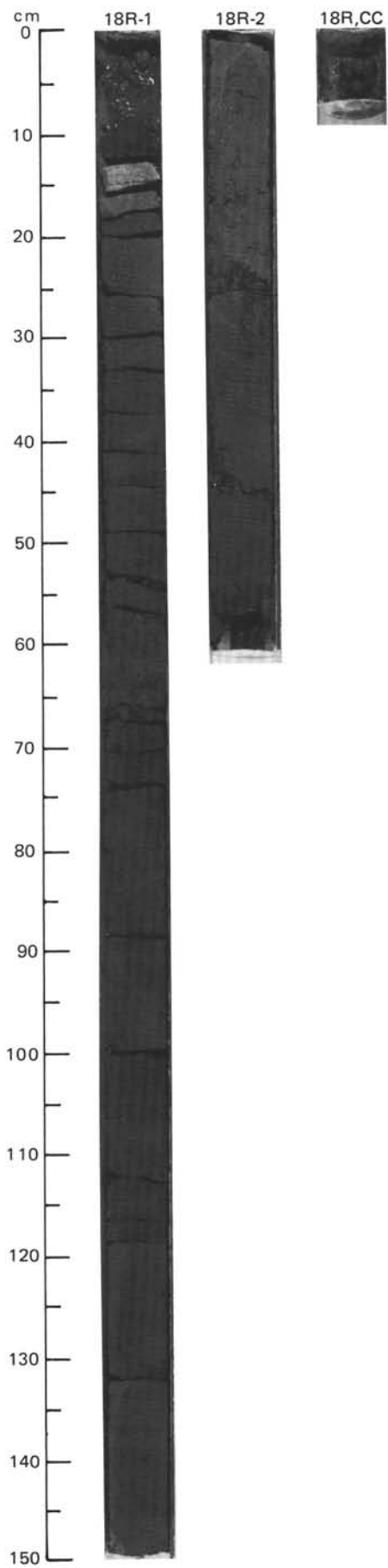


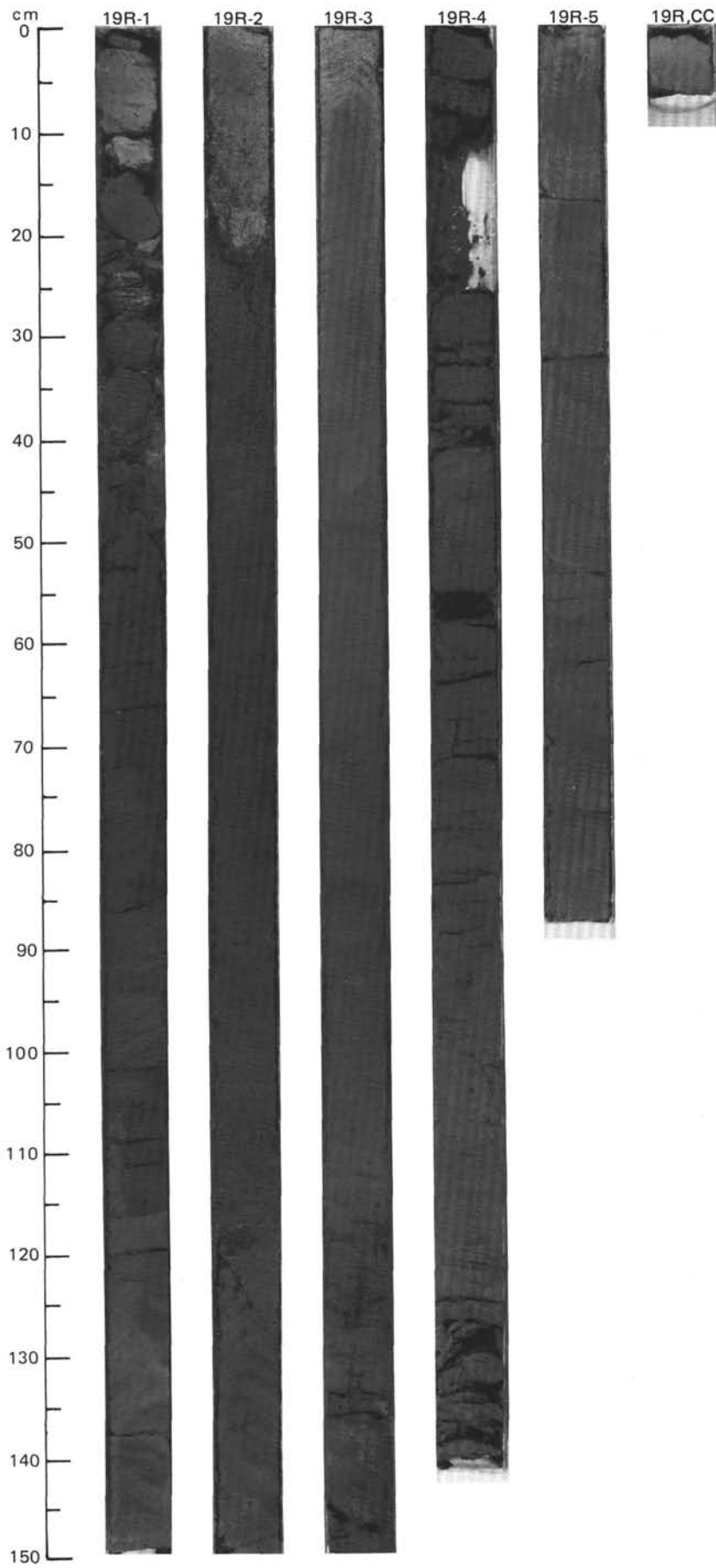




SITE 645 HOLE E CORE 18 R CORED INTERVAL 2597.6-2607.3 mbsl; 590.1-599.8 mbsf

TIME-ROCK UNIT	BIOSTRAT. ZONE/ FOSSIL CHARACTER				PALEOMAGNETICS	PHYS. PROPERTIES	CHEMISTRY	SECTION	METERS	GRAPHIC LITHOLOGY	DRILLING DISTURB.	SED. STRUCTURES	SAMPLES	LITHOLOGIC DESCRIPTION																																	
	FORAMINIFERS	NANNOFOSSILS	RADIOLARIANS	DIATOMS																																											
	B	B	B	B	N.C.	$\gamma = 2.05$ $\phi = 42.4$ $W = 27$ ●	TOC=1.10 CaCO ₃ =1.17 ●	1	0.5 1.0					<p>MUDDY SAND AND SILTY MUD</p> <p>Muddy sand grading upward into a silty mud, dark greenish gray (5GY 4/1). Generally homogeneous, and fissility well expressed in upper part.</p> <p>SMEAR SLIDE SUMMARY (%):</p> <table border="0"> <tr> <td></td> <td>1, 90</td> <td>2, 35</td> </tr> <tr> <td></td> <td>D</td> <td>D</td> </tr> </table> <p>TEXTURE:</p> <table border="0"> <tr> <td>Sand</td> <td>30</td> <td>40</td> </tr> <tr> <td>Silt</td> <td>50</td> <td>25</td> </tr> <tr> <td>Clay</td> <td>20</td> <td>35</td> </tr> </table> <p>COMPOSITION:</p> <table border="0"> <tr> <td>Quartz</td> <td>60</td> <td>45</td> </tr> <tr> <td>Feldspar</td> <td>10</td> <td>10</td> </tr> <tr> <td>Clay</td> <td>20</td> <td>30</td> </tr> <tr> <td>Calcite/dolomite</td> <td>5</td> <td>5</td> </tr> <tr> <td>Accessory minerals</td> <td>5</td> <td>5</td> </tr> <tr> <td>Pyrite</td> <td>—</td> <td>5</td> </tr> </table>		1, 90	2, 35		D	D	Sand	30	40	Silt	50	25	Clay	20	35	Quartz	60	45	Feldspar	10	10	Clay	20	30	Calcite/dolomite	5	5	Accessory minerals	5	5	Pyrite	—	5
	1, 90	2, 35																																													
	D	D																																													
Sand	30	40																																													
Silt	50	25																																													
Clay	20	35																																													
Quartz	60	45																																													
Feldspar	10	10																																													
Clay	20	30																																													
Calcite/dolomite	5	5																																													
Accessory minerals	5	5																																													
Pyrite	—	5																																													
								2																																							
								CC																																							



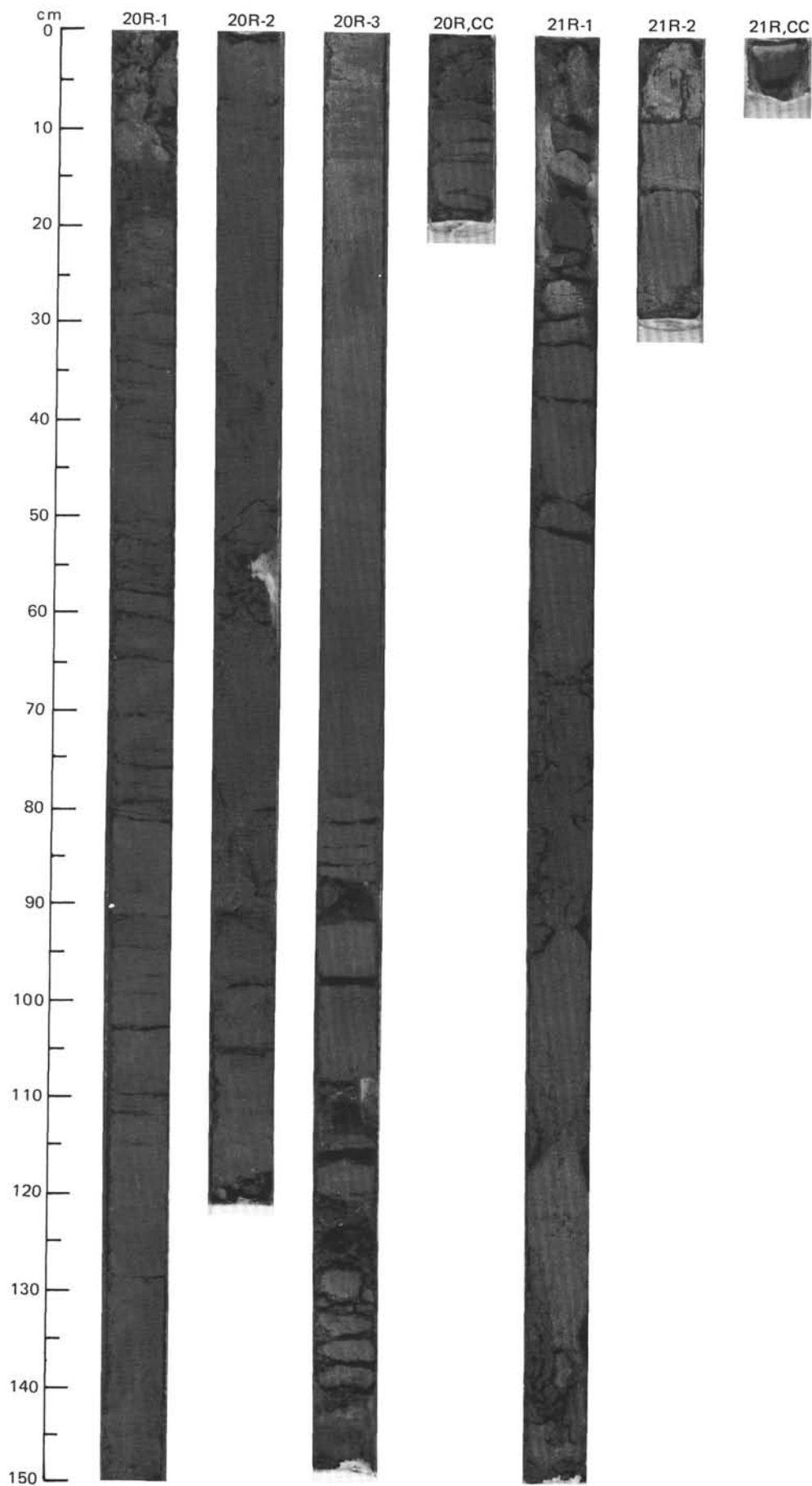


SITE 645 HOLE E CORE 20 R CORED INTERVAL 2616.8-2626.4 mbsl; 609.3-618.9 mbsf

TIME-ROCK UNIT	BIOSTRAT. ZONE/ FOSSIL CHARACTER				PALEOMAGNETICS	PHYS. PROPERTIES	CHEMISTRY	SECTION	METERS	GRAPHIC LITHOLOGY	DRILLING DISTURB.	SED. STRUCTURES	SAMPLES	LITHOLOGIC DESCRIPTION																																												
	FORAMINIFERS	NANNOFOSSILS	RADIOLARIANS	DIATOMS																																																						
B	B	B	B	B	N.C.	$\gamma = 2.02$ $\phi = 44.8$ W=29	● TOC=0.67 CaCO ₃ = 1.6	1	0.5 1.0		Δ	*		<p>SILTY MUD AND MUDDY SAND</p> <p>Silty mud, greenish gray (5GY 5/1), bioturbated with scattered authigenic pyrite, interbedded with muddy sand, dark greenish gray (5GY 4/1), micaceous. In upward-fining cycles, two with sharp bases and three gradational contacts.</p> <p>Minor lithologies: a. Section 3, 79-97 cm: carbonate silt, greenish gray (5GY 6/1), bioturbated. b. Section 1, 0-10 cm: carbonate silty clay, light greenish gray (5GY 7/1), bioturbated.</p> <p>SMEAR SLIDE SUMMARY (%):</p> <table border="1"> <tr> <td></td> <td>1, 12</td> <td>2, 96</td> <td>3, 84</td> </tr> <tr> <td></td> <td>M</td> <td>D</td> <td>M</td> </tr> </table> <p>TEXTURE:</p> <table border="1"> <tr> <td>Sand</td> <td>5</td> <td>50</td> <td>5</td> </tr> <tr> <td>Silt</td> <td>40</td> <td>35</td> <td>85</td> </tr> <tr> <td>Clay</td> <td>55</td> <td>15</td> <td>10</td> </tr> </table> <p>COMPOSITION:</p> <table border="1"> <tr> <td>Quartz</td> <td>45</td> <td>60</td> <td>10</td> </tr> <tr> <td>Feldspar</td> <td>5</td> <td>25</td> <td>Tr</td> </tr> <tr> <td>Mica</td> <td>Tr</td> <td>1</td> <td>Tr</td> </tr> <tr> <td>Clay</td> <td>44</td> <td>10</td> <td>9</td> </tr> <tr> <td>Calcite/dolomite</td> <td>5</td> <td>2</td> <td>80</td> </tr> <tr> <td>Accessory minerals</td> <td>2</td> <td>1</td> <td>—</td> </tr> </table>		1, 12	2, 96	3, 84		M	D	M	Sand	5	50	5	Silt	40	35	85	Clay	55	15	10	Quartz	45	60	10	Feldspar	5	25	Tr	Mica	Tr	1	Tr	Clay	44	10	9	Calcite/dolomite	5	2	80	Accessory minerals	2	1	—
	1, 12	2, 96	3, 84																																																							
	M	D	M																																																							
Sand	5	50	5																																																							
Silt	40	35	85																																																							
Clay	55	15	10																																																							
Quartz	45	60	10																																																							
Feldspar	5	25	Tr																																																							
Mica	Tr	1	Tr																																																							
Clay	44	10	9																																																							
Calcite/dolomite	5	2	80																																																							
Accessory minerals	2	1	—																																																							
B	B	B	B	N.C.	$\gamma = 1.98$ $\phi = 44.3$ W=30	● TOC=0.47 CaCO ₃ 2.2	2	0.5 1.0		Δ	*																																															
B	B	B	B	N.C.	$\gamma = 1.98$ $\phi = 44.3$ W=30	● TOC=0.47 CaCO ₃ 2.2	CC			Δ	*																																															

SITE 645 HOLE E CORE 21 R CORED INTERVAL 2626.4-2631.9 mbsl; 618.9-624.4 mbsf

TIME-ROCK UNIT	BIOSTRAT. ZONE/ FOSSIL CHARACTER				PALEOMAGNETICS	PHYS. PROPERTIES	CHEMISTRY	SECTION	METERS	GRAPHIC LITHOLOGY	DRILLING DISTURB.	SED. STRUCTURES	SAMPLES	LITHOLOGIC DESCRIPTION																																				
	FORAMINIFERS	NANNOFOSSILS	RADIOLARIANS	DIATOMS																																														
B	B	B	B	B	N.C.	$\gamma = 1.98$ $\phi = 44.3$ W=30	● TOC=0.47 CaCO ₃ 2.2	1	0.5 1.0		Δ	*		<p>MICACEOUS MUDDY SAND</p> <p>Micaceous muddy sand, dark greenish gray (5GY 4/1); fine grained, with local dark sulfide smears. Vague, sandier laminae (2-3 mm thick) in Section 2 may be ripple laminated. Cobbles at core top are probable uphole debris.</p> <p>SMEAR SLIDE SUMMARY (%):</p> <table border="1"> <tr> <td></td> <td>1, 8</td> <td>1, 122</td> </tr> <tr> <td></td> <td>M</td> <td>D</td> </tr> </table> <p>TEXTURE:</p> <table border="1"> <tr> <td>Sand</td> <td>2</td> <td>50</td> </tr> <tr> <td>Silt</td> <td>83</td> <td>30</td> </tr> <tr> <td>Clay</td> <td>15</td> <td>20</td> </tr> </table> <p>COMPOSITION:</p> <table border="1"> <tr> <td>Quartz</td> <td>2</td> <td>65</td> </tr> <tr> <td>Feldspar</td> <td>—</td> <td>15</td> </tr> <tr> <td>Mica</td> <td>—</td> <td>Tr</td> </tr> <tr> <td>Clay</td> <td>10</td> <td>14</td> </tr> <tr> <td>Volcanic glass</td> <td>—</td> <td>Tr</td> </tr> <tr> <td>Calcite/dolomite</td> <td>88</td> <td>5</td> </tr> <tr> <td>Accessory minerals</td> <td>Tr</td> <td>1</td> </tr> </table>		1, 8	1, 122		M	D	Sand	2	50	Silt	83	30	Clay	15	20	Quartz	2	65	Feldspar	—	15	Mica	—	Tr	Clay	10	14	Volcanic glass	—	Tr	Calcite/dolomite	88	5	Accessory minerals	Tr	1
	1, 8	1, 122																																																
	M	D																																																
Sand	2	50																																																
Silt	83	30																																																
Clay	15	20																																																
Quartz	2	65																																																
Feldspar	—	15																																																
Mica	—	Tr																																																
Clay	10	14																																																
Volcanic glass	—	Tr																																																
Calcite/dolomite	88	5																																																
Accessory minerals	Tr	1																																																
B	B	B	B	N.C.	$\gamma = 1.98$ $\phi = 44.3$ W=30	● TOC=0.47 CaCO ₃ 2.2	2	0.5 1.0		Δ	*																																							
B	B	B	B	N.C.	$\gamma = 1.98$ $\phi = 44.3$ W=30	● TOC=0.47 CaCO ₃ 2.2	CC			Δ	*																																							

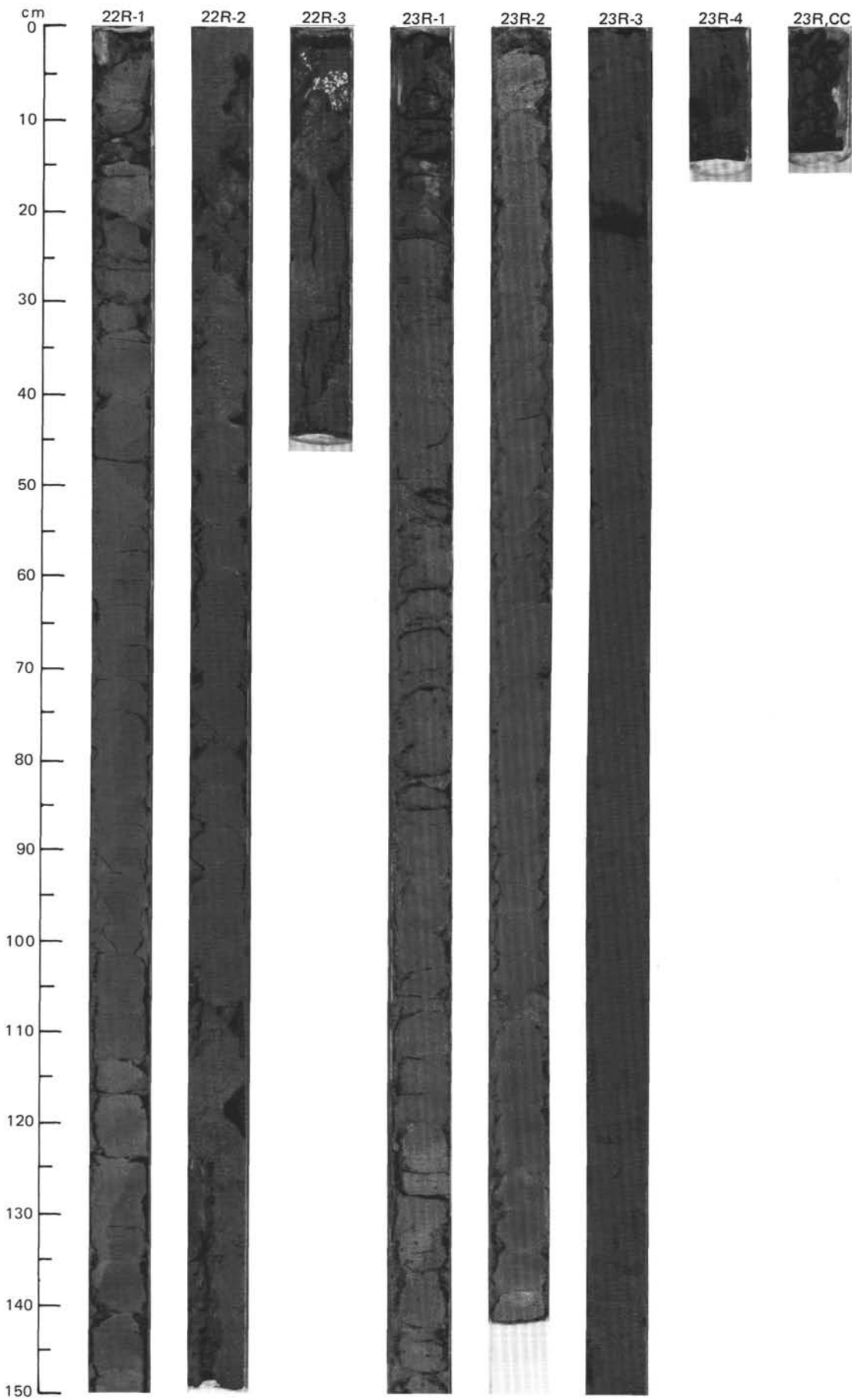


SITE 645 HOLE E CORE 22 R CORED INTERVAL 2631.9-2635.9 mbsl; 624.4-628.4 mbsf

TIME-ROCK UNIT	BIOSTRAT. ZONE/ FOSSIL CHARACTER					PALEOMAGNETICS	PHYS. PROPERTIES	CHEMISTRY	SECTION	METERS	GRAPHIC LITHOLOGY	DRILLING DISTURB.	SED. STRUCTURES	SAMPLES	LITHOLOGIC DESCRIPTION																																
	FORAMINIFERS	NAANNOFOSSILS	RADIODIOLARIANS	DIATOMS	DINOCYSTS																																										
MIDDLE MIOCENE TO LOWER PLIOCENE?	B	R/G	B	B	C/M	N.C.	<p>● $\gamma = 1.91$ $\phi = 51.2$ W=38</p> <p>● TOC=0.14 CaCO₃=4.1</p>	<p>● TOC=0.89 CaCO₃=2.8</p>	1	0.5 1.0				<p>CLAYEY SILT AND SILTY MUD</p> <p>Clayey silt, greenish gray (5GY 6/1) to gray (5Y 5/1); highly burrowed, grading downward into silty mud, dark greenish gray (5GY 4/1), with a few small black smears of iron sulfide.</p> <p>SMEAR SLIDE SUMMARY (%):</p> <table border="0"> <tr> <td></td> <td>1, 67</td> <td>2, 102</td> </tr> <tr> <td>D</td> <td>D</td> <td>D</td> </tr> </table> <p>TEXTURE:</p> <table border="0"> <tr> <td>Sand</td> <td>2</td> <td>30</td> </tr> <tr> <td>Silt</td> <td>55</td> <td>55</td> </tr> <tr> <td>Clay</td> <td>43</td> <td>15</td> </tr> </table> <p>COMPOSITION:</p> <table border="0"> <tr> <td>Quartz</td> <td>42</td> <td>45</td> </tr> <tr> <td>Feldspar</td> <td>5</td> <td>20</td> </tr> <tr> <td>Mica</td> <td>—</td> <td>10</td> </tr> <tr> <td>Clay</td> <td>43</td> <td>15</td> </tr> <tr> <td>Calcite/dolomite</td> <td>7</td> <td>5</td> </tr> <tr> <td>Accessory minerals</td> <td>3</td> <td>5</td> </tr> </table>		1, 67	2, 102	D	D	D	Sand	2	30	Silt	55	55	Clay	43	15	Quartz	42	45	Feldspar	5	20	Mica	—	10	Clay	43	15	Calcite/dolomite	7	5	Accessory minerals	3	5
	1, 67	2, 102																																													
D	D	D																																													
Sand	2	30																																													
Silt	55	55																																													
Clay	43	15																																													
Quartz	42	45																																													
Feldspar	5	20																																													
Mica	—	10																																													
Clay	43	15																																													
Calcite/dolomite	7	5																																													
Accessory minerals	3	5																																													

SITE 645 HOLE E CORE 23 R CORED INTERVAL 2635.9-2645.5 mbsl; 628.4-638.0 mbsf

TIME-ROCK UNIT	BIOSTRAT. ZONE/ FOSSIL CHARACTER					PALEOMAGNETICS	PHYS. PROPERTIES	CHEMISTRY	SECTION	METERS	GRAPHIC LITHOLOGY	DRILLING DISTURB.	SED. STRUCTURES	SAMPLES	LITHOLOGIC DESCRIPTION																																		
	FORAMINIFERS	NAANNOFOSSILS	RADIODIOLARIANS	DIATOMS	DINOCYSTS																																												
	B	B	B	B	N.C.	<p>● $\gamma = 2.07$ $\phi = 44.1$ W=28</p> <p>● TOC=0.90 CaCO₃=1.4</p>		1	0.5 1.0				<p>SILTY CLAY AND MUDDY SAND</p> <p>Silty clay, greenish gray (5GY 5/1), moderately to strongly bioturbated. Burrows are (a) 1-2 mm, black, <i>Chondrites</i>, or (b) about 1 cm, pale olive (5Y 6/4). Scattered authigenic pyrite.</p> <p>Muddy sand, dark gray (5Y 4/1) sand is homogeneous, micaceous, and fine grained with rare coarse sand grains and granules.</p> <p>SMEAR SLIDE SUMMARY (%):</p> <table border="0"> <tr> <td></td> <td>1, 43</td> <td>3, 65</td> </tr> <tr> <td>M</td> <td>D</td> <td>D</td> </tr> </table> <p>TEXTURE:</p> <table border="0"> <tr> <td>Sand</td> <td>15</td> <td>50</td> </tr> <tr> <td>Silt</td> <td>35</td> <td>30</td> </tr> <tr> <td>Clay</td> <td>50</td> <td>20</td> </tr> </table> <p>COMPOSITION:</p> <table border="0"> <tr> <td>Quartz</td> <td>40</td> <td>65</td> </tr> <tr> <td>Feldspar</td> <td>10</td> <td>15</td> </tr> <tr> <td>Mica</td> <td>1</td> <td>1</td> </tr> <tr> <td>Clay</td> <td>17</td> <td>13</td> </tr> <tr> <td>Volcanic glass</td> <td>—</td> <td>Tr</td> </tr> <tr> <td>Calcite/dolomite</td> <td>30</td> <td>1</td> </tr> <tr> <td>Accessory minerals</td> <td>2</td> <td>5</td> </tr> </table>		1, 43	3, 65	M	D	D	Sand	15	50	Silt	35	30	Clay	50	20	Quartz	40	65	Feldspar	10	15	Mica	1	1	Clay	17	13	Volcanic glass	—	Tr	Calcite/dolomite	30	1	Accessory minerals	2	5
	1, 43	3, 65																																															
M	D	D																																															
Sand	15	50																																															
Silt	35	30																																															
Clay	50	20																																															
Quartz	40	65																																															
Feldspar	10	15																																															
Mica	1	1																																															
Clay	17	13																																															
Volcanic glass	—	Tr																																															
Calcite/dolomite	30	1																																															
Accessory minerals	2	5																																															

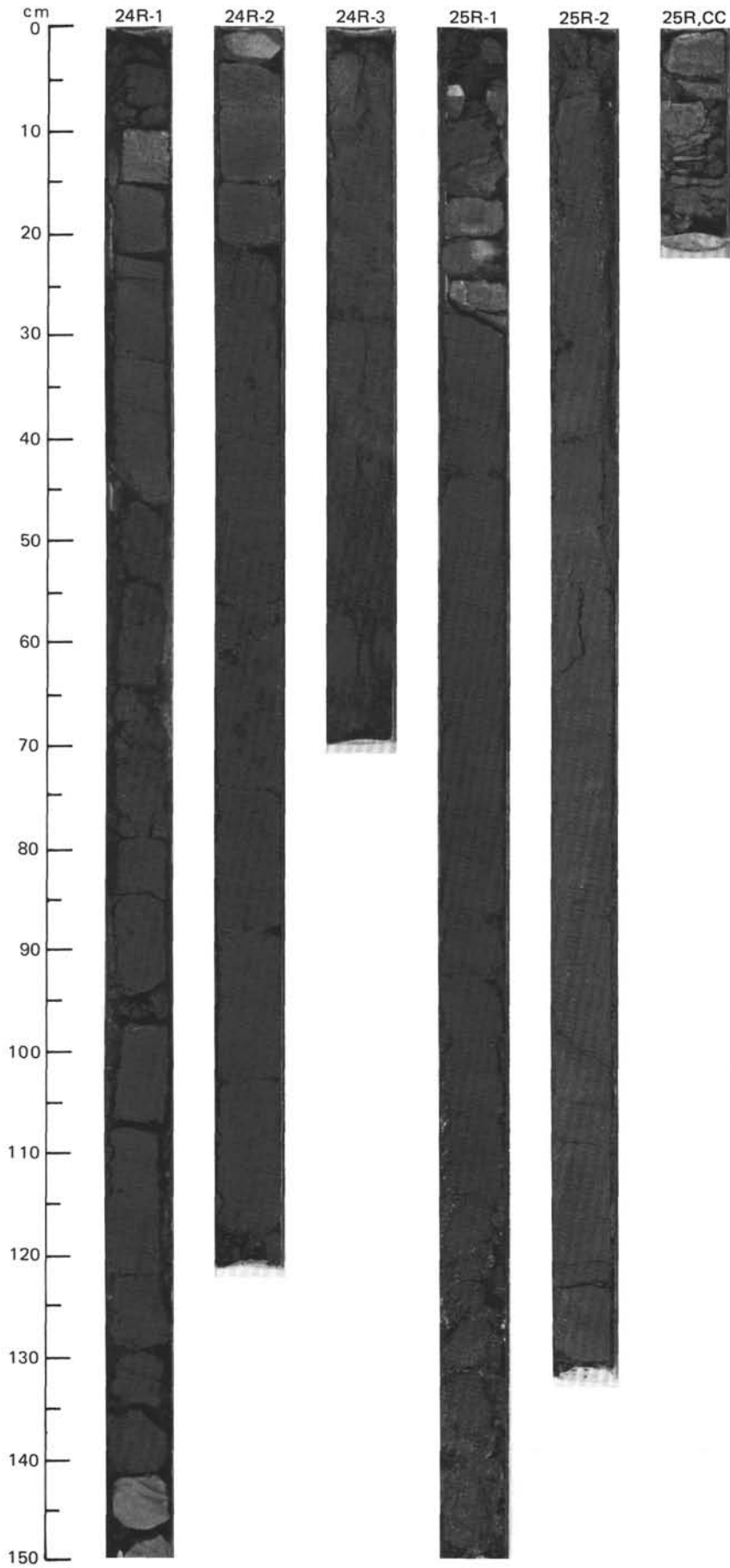


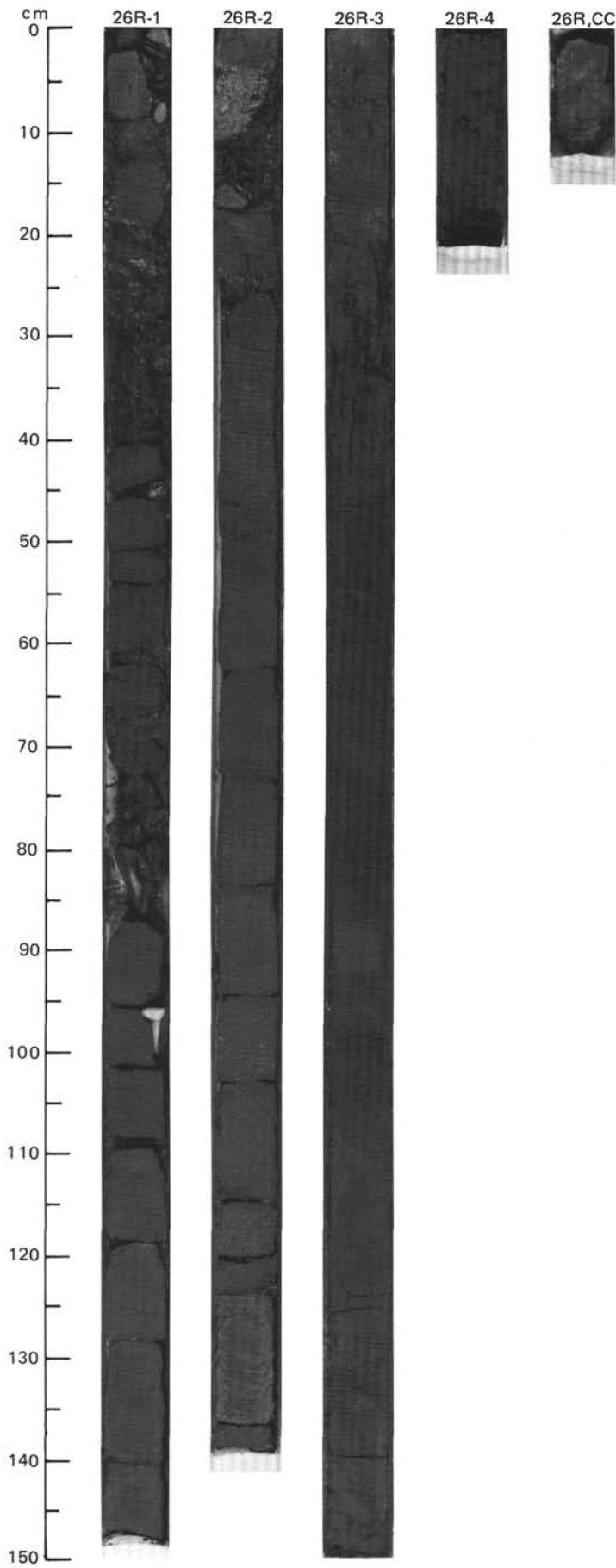
SITE 645 HOLE E CORE 24 R CORED INTERVAL 2645.5-2655.2 mbsl; 638.0-647.7 mbsf

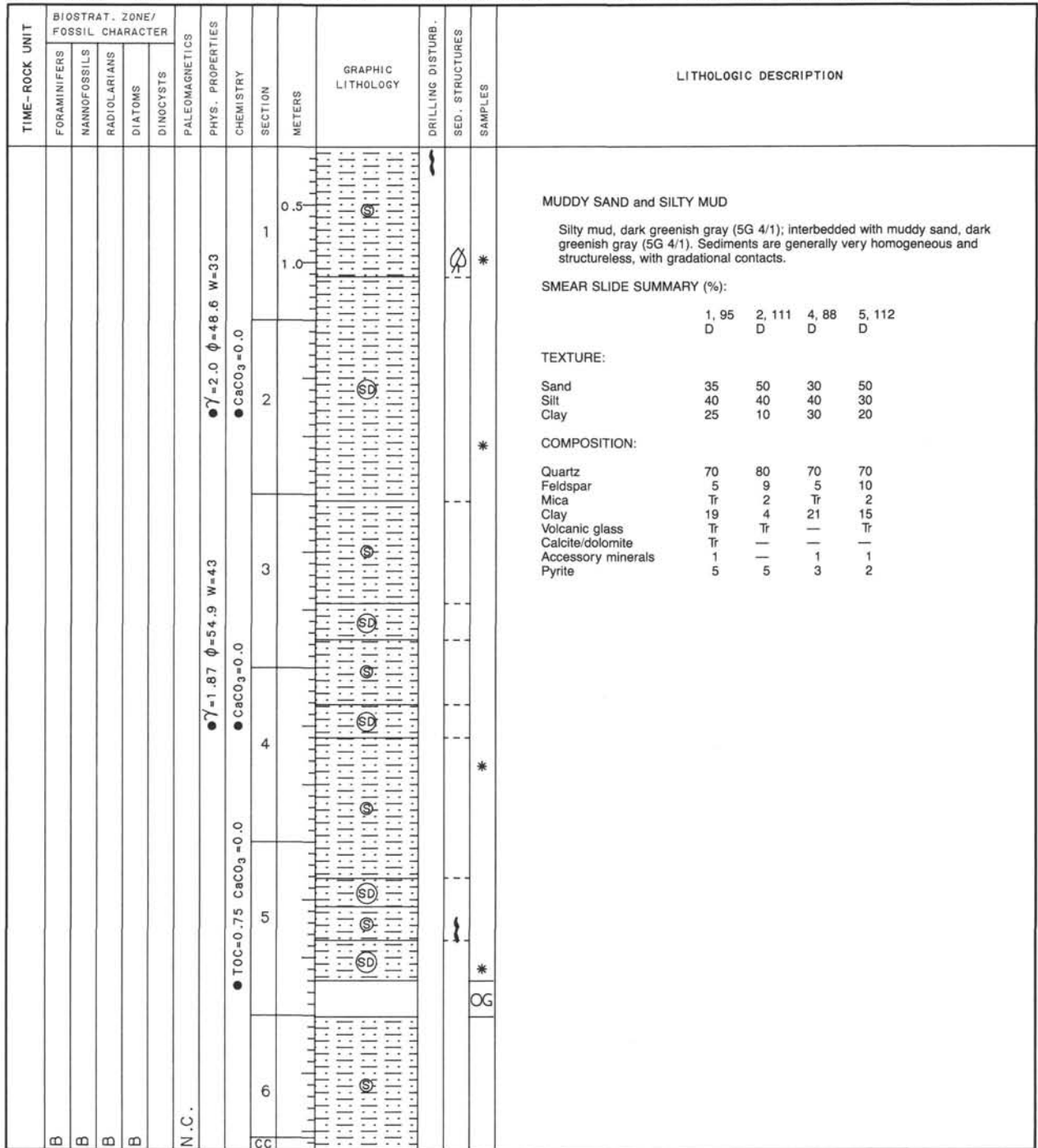
TIME-ROCK UNIT	BIOSTRAT. ZONE/ FOSSIL CHARACTER					PALEOMAGNETICS	PHYS. PROPERTIES	CHEMISTRY	SECTION	METERS	GRAPHIC LITHOLOGY	DRILLING DISTURB.	SED. STRUCTURES	SAMPLES	LITHOLOGIC DESCRIPTION																																	
	FORAMINIFERS	NANNOFOSSILS	RADIOLARIANS	DIATOMS	DINOCYSTS																																											
B	B	B	B	B	N.C.		$\gamma = 1.84 \phi = 47.5 W = 36$	TOC=0.74 CaCO ₃ =0.5	1	0.5 1.0					<p>MUDDY SAND and SILTY SAND</p> <p>Muddy sand, dark greenish gray (5GY 4/1), with interbedded silty sand, dark greenish gray (5GY 4/1).</p> <p>Minor lithology: Section 1, 140-150 cm; Section 2, 0-5 cm: two pebbles of calcite-cemented silty sandstone. These are lithologically like the surrounding sediment, except for carbonate content, and may be diagenetic concretions.</p> <p>SMEAR SLIDE SUMMARY (%):</p> <table border="1"> <tr> <td></td> <td>1, 131</td> <td>2, 31</td> </tr> <tr> <td>D</td> <td>D</td> <td>D</td> </tr> </table> <p>TEXTURE:</p> <table border="1"> <tr> <td>Sand</td> <td>50</td> <td>50</td> </tr> <tr> <td>Silt</td> <td>30</td> <td>42</td> </tr> <tr> <td>Clay</td> <td>20</td> <td>8</td> </tr> </table> <p>COMPOSITION:</p> <table border="1"> <tr> <td>Quartz</td> <td>65</td> <td>65</td> </tr> <tr> <td>Feldspar</td> <td>15</td> <td>18</td> </tr> <tr> <td>Mica</td> <td>1</td> <td>2</td> </tr> <tr> <td>Clay</td> <td>14</td> <td>10</td> </tr> <tr> <td>Calcite/dolomite</td> <td>Tr</td> <td>Tr</td> </tr> <tr> <td>Accessory minerals</td> <td>5</td> <td>5</td> </tr> </table>		1, 131	2, 31	D	D	D	Sand	50	50	Silt	30	42	Clay	20	8	Quartz	65	65	Feldspar	15	18	Mica	1	2	Clay	14	10	Calcite/dolomite	Tr	Tr	Accessory minerals	5	5
	1, 131	2, 31																																														
D	D	D																																														
Sand	50	50																																														
Silt	30	42																																														
Clay	20	8																																														
Quartz	65	65																																														
Feldspar	15	18																																														
Mica	1	2																																														
Clay	14	10																																														
Calcite/dolomite	Tr	Tr																																														
Accessory minerals	5	5																																														
B	B	B	B	B	N.C.				2																																							
B	B	B	B	B	N.C.				3																																							

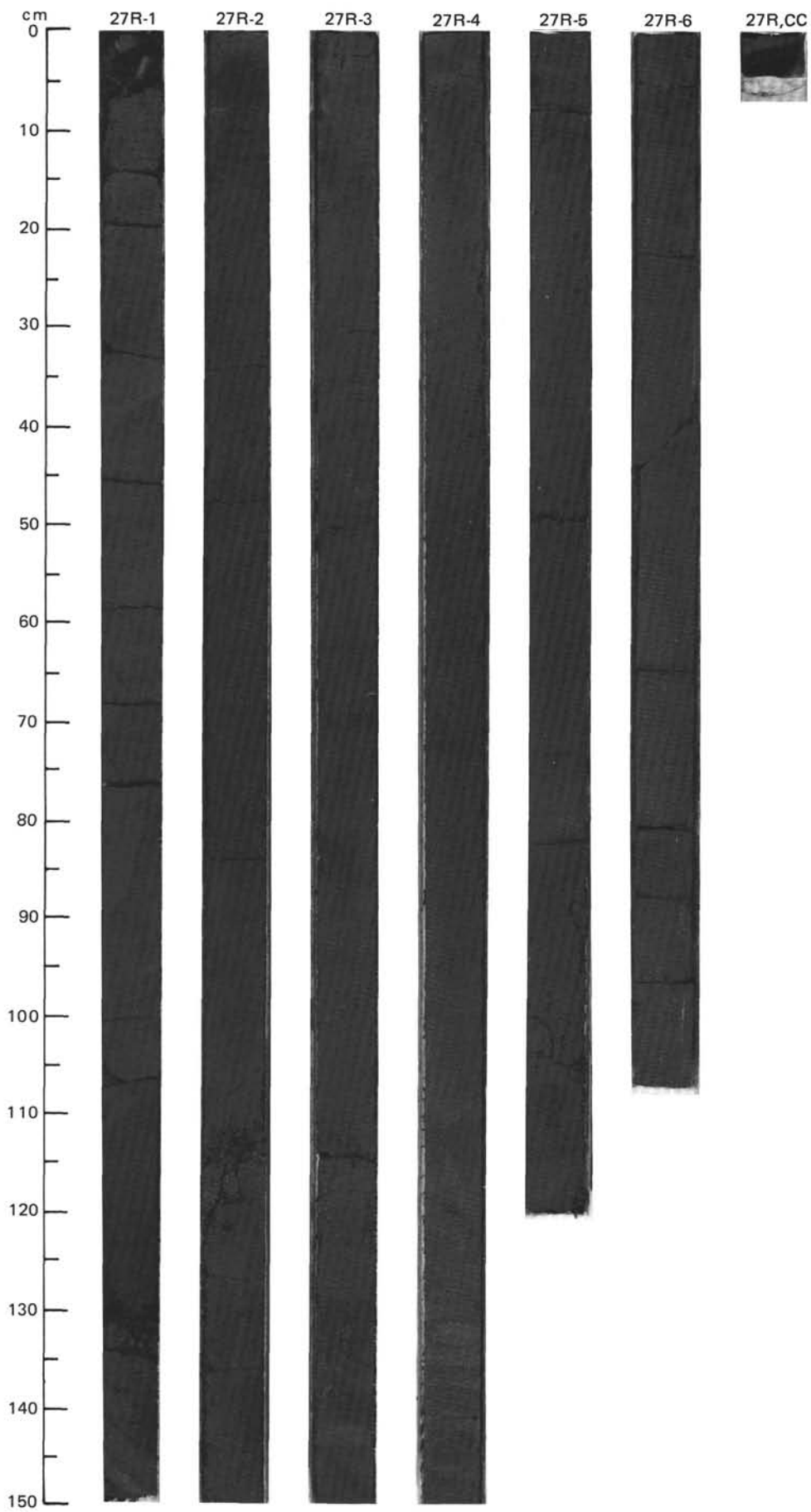
SITE 645 HOLE E CORE 25 R CORED INTERVAL 2655.2-2664.6 mbsl; 647.7-657.1 mbsf

TIME-ROCK UNIT	BIOSTRAT. ZONE/ FOSSIL CHARACTER					PALEOMAGNETICS	PHYS. PROPERTIES	CHEMISTRY	SECTION	METERS	GRAPHIC LITHOLOGY	DRILLING DISTURB.	SED. STRUCTURES	SAMPLES	LITHOLOGIC DESCRIPTION																																																
	FORAMINIFERS	NANNOFOSSILS	RADIOLARIANS	DIATOMS	DINOCYSTS																																																										
B	B	B	B	B	N.C.		$\gamma = 2.06 \phi = 43 W = 27$	TOC=1.14 CaCO ₃ =0.0	1	0.5 1.0					<p>MUDDY SAND AND CLAYEY MUD</p> <p>Muddy sand, dark greenish gray (5GY 4/1), with concretions of carbonate-cemented sediment (Section 1, 0-13 cm).</p> <p>Clayey mud, greenish gray (5G 4/1), with grains of pyrite filling burrows.</p> <p>Minor lithologies:</p> <ol style="list-style-type: none"> Section 1, 13-25 cm: carbonate silty clay, olive (5Y 5/3). Section 2, 30-45 cm: silty mud, greenish gray (5G 5/1). Section 2, 45-62 cm: carbonate silt, olive (5Y 4/3). <p>SMEAR SLIDE SUMMARY (%):</p> <table border="1"> <tr> <td></td> <td>1, 136</td> <td>2, 50</td> <td>2, 72</td> </tr> <tr> <td>D</td> <td>M</td> <td>D</td> <td>D</td> </tr> </table> <p>TEXTURE:</p> <table border="1"> <tr> <td>Sand</td> <td>60</td> <td>8</td> <td>20</td> </tr> <tr> <td>Silt</td> <td>30</td> <td>87</td> <td>30</td> </tr> <tr> <td>Clay</td> <td>10</td> <td>5</td> <td>50</td> </tr> </table> <p>COMPOSITION:</p> <table border="1"> <tr> <td>Quartz</td> <td>85</td> <td>10</td> <td>55</td> </tr> <tr> <td>Feldspar</td> <td>5</td> <td>Tr</td> <td>5</td> </tr> <tr> <td>Mica</td> <td>1</td> <td>Tr</td> <td>Tr</td> </tr> <tr> <td>Clay</td> <td>7</td> <td>5</td> <td>39</td> </tr> <tr> <td>Volcanic glass</td> <td>Tr</td> <td>Tr</td> <td>Tr</td> </tr> <tr> <td>Calcite/dolomite</td> <td>—</td> <td>84</td> <td>—</td> </tr> <tr> <td>Accessory minerals</td> <td>2</td> <td>1</td> <td>1</td> </tr> </table>		1, 136	2, 50	2, 72	D	M	D	D	Sand	60	8	20	Silt	30	87	30	Clay	10	5	50	Quartz	85	10	55	Feldspar	5	Tr	5	Mica	1	Tr	Tr	Clay	7	5	39	Volcanic glass	Tr	Tr	Tr	Calcite/dolomite	—	84	—	Accessory minerals	2	1	1
	1, 136	2, 50	2, 72																																																												
D	M	D	D																																																												
Sand	60	8	20																																																												
Silt	30	87	30																																																												
Clay	10	5	50																																																												
Quartz	85	10	55																																																												
Feldspar	5	Tr	5																																																												
Mica	1	Tr	Tr																																																												
Clay	7	5	39																																																												
Volcanic glass	Tr	Tr	Tr																																																												
Calcite/dolomite	—	84	—																																																												
Accessory minerals	2	1	1																																																												
B	B	B	B	B	N.C.				2																																																						
B	B	B	B	B	N.C.				CC																																																						



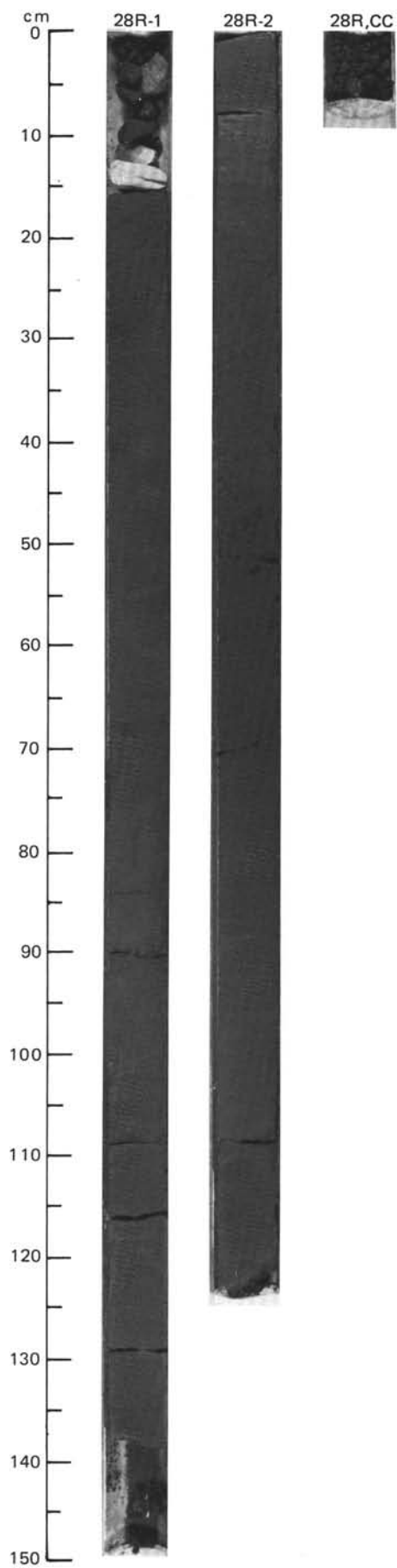


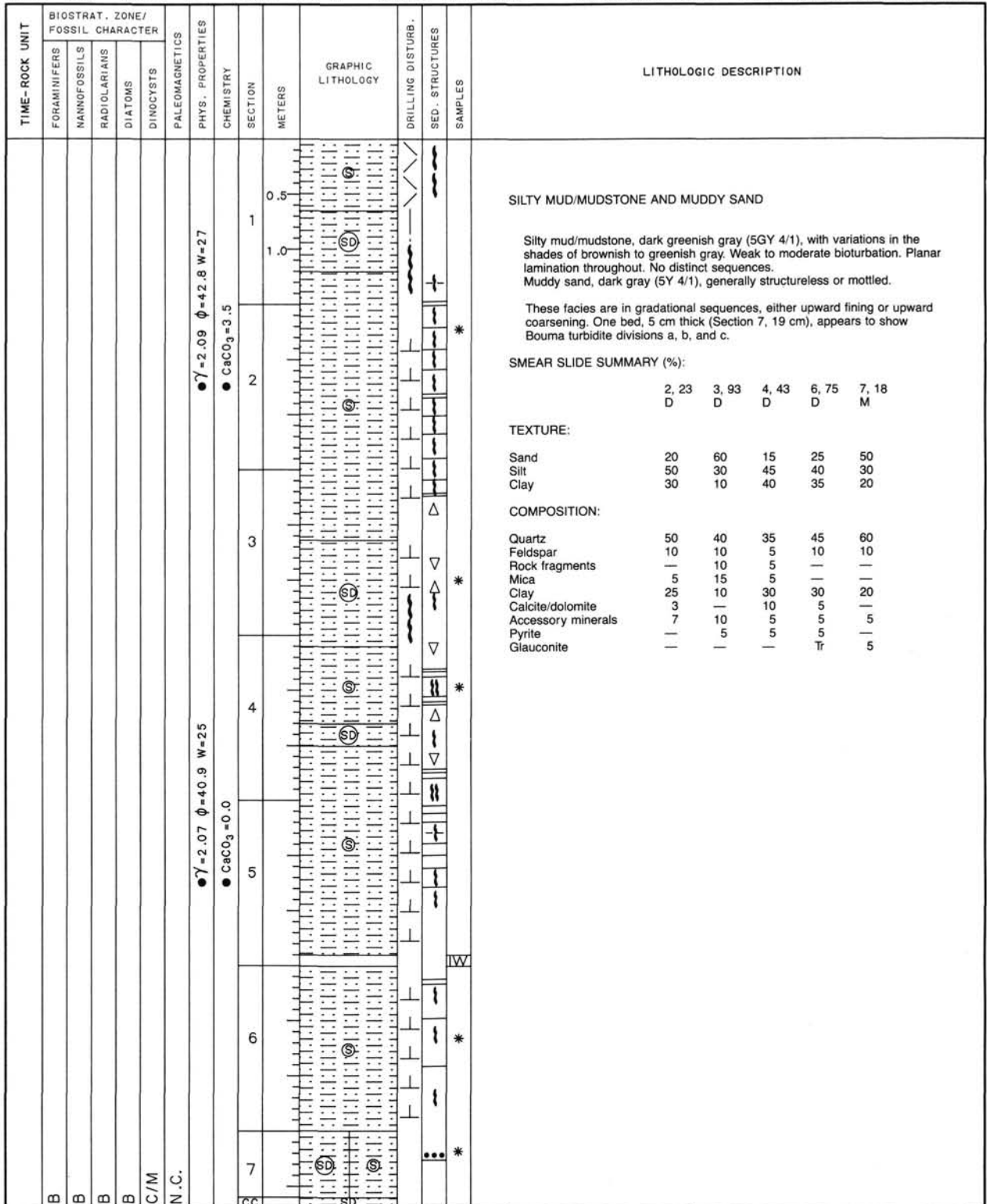


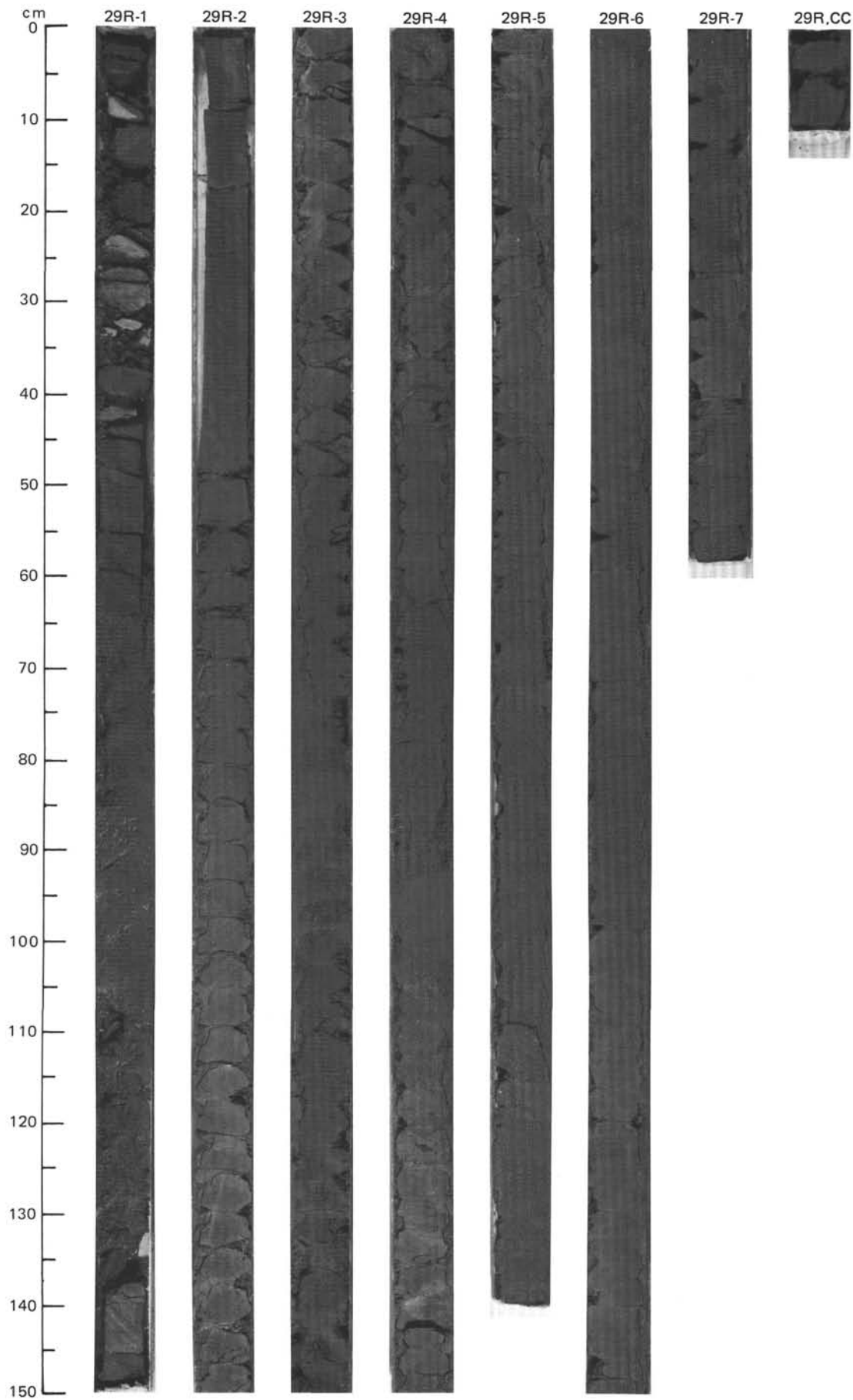


SITE 645 HOLE E CORE 28 R CORED INTERVAL 2683.9-2693.5 mbsl; 676.4-636.0 mbsf

TIME-ROCK UNIT	BIOSTRAT. ZONE/ FOSSIL CHARACTER				PALEOMAGNETICS	PHYS. PROPERTIES	CHEMISTRY	SECTION	METERS	GRAPHIC LITHOLOGY	DRILLING DISTURB.	SED. STRUCTURES	SAMPLES	LITHOLOGIC DESCRIPTION																																	
	FORAMINIFERS	NANNOFOSSILS	RADIOLARIANS	DIATOMS											DINOCYSTS																																
	B				N.C.	<ul style="list-style-type: none"> ● $\gamma = 2.13$ $\phi = 47.5$ $W = 30$ ● $TOC = 1.00$ $CaCO_3 = 0.0$ 	1	0.5	VOID	X				<p>SILTY MUDSTONE AND CLAYEY MUDSTONE</p> <p>Silty mudstone and clayey mudstone, dark greenish gray (5GY 4/1); bioturbated throughout.</p> <p>SMEAR SLIDE SUMMARY (%):</p> <table border="0"> <tr> <td></td> <td>1, 109</td> <td>2, 69</td> </tr> <tr> <td></td> <td>D</td> <td>D</td> </tr> </table> <p>TEXTURE:</p> <table border="0"> <tr> <td>Sand</td> <td>10</td> <td>40</td> </tr> <tr> <td>Silt</td> <td>30</td> <td>35</td> </tr> <tr> <td>Clay</td> <td>60</td> <td>25</td> </tr> </table> <p>COMPOSITION:</p> <table border="0"> <tr> <td>Quartz</td> <td>30</td> <td>70</td> </tr> <tr> <td>Feldspar</td> <td>5</td> <td>10</td> </tr> <tr> <td>Mica</td> <td>Tr</td> <td>1</td> </tr> <tr> <td>Clay</td> <td>55</td> <td>16</td> </tr> <tr> <td>Accessory minerals</td> <td>Tr</td> <td>1</td> </tr> <tr> <td>Pyrite</td> <td>10</td> <td>2</td> </tr> </table>		1, 109	2, 69		D	D	Sand	10	40	Silt	30	35	Clay	60	25	Quartz	30	70	Feldspar	5	10	Mica	Tr	1	Clay	55	16	Accessory minerals	Tr	1	Pyrite	10	2
	1, 109	2, 69																																													
	D	D																																													
Sand	10	40																																													
Silt	30	35																																													
Clay	60	25																																													
Quartz	30	70																																													
Feldspar	5	10																																													
Mica	Tr	1																																													
Clay	55	16																																													
Accessory minerals	Tr	1																																													
Pyrite	10	2																																													
							2	1.0																																							
							CC																																								





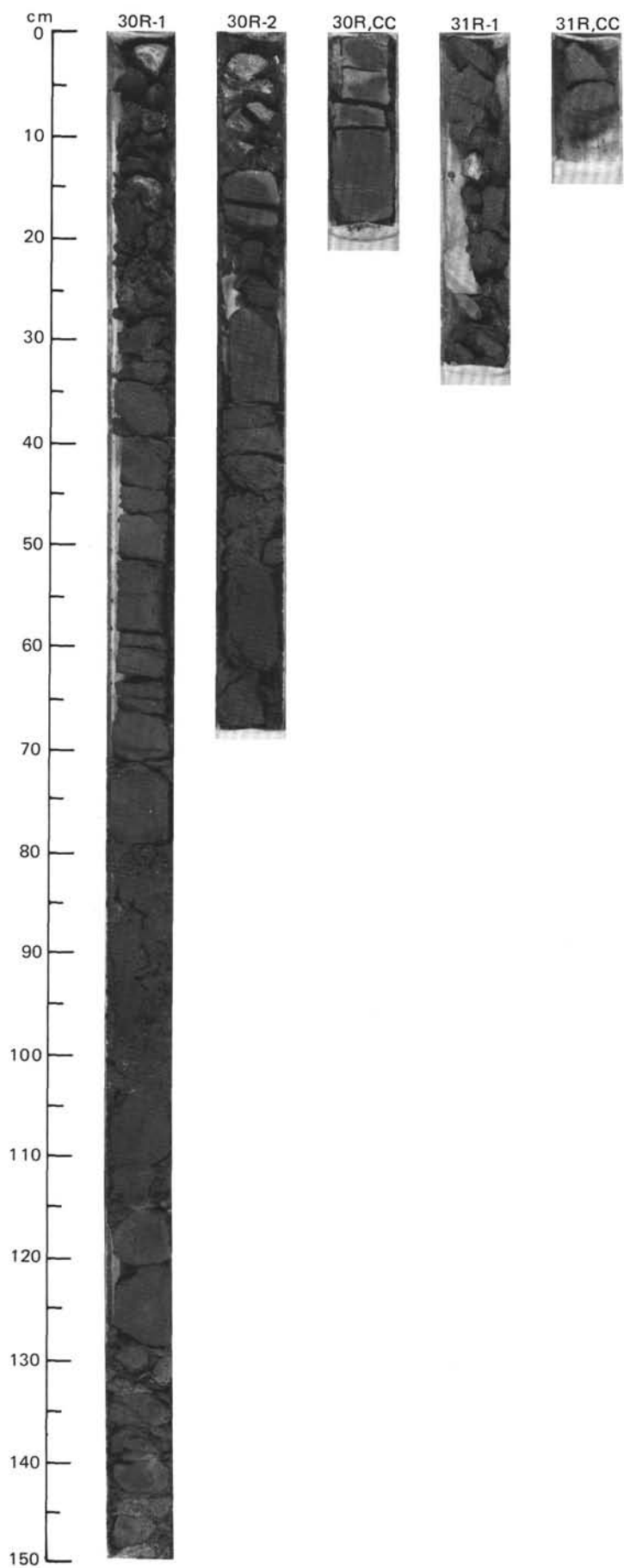


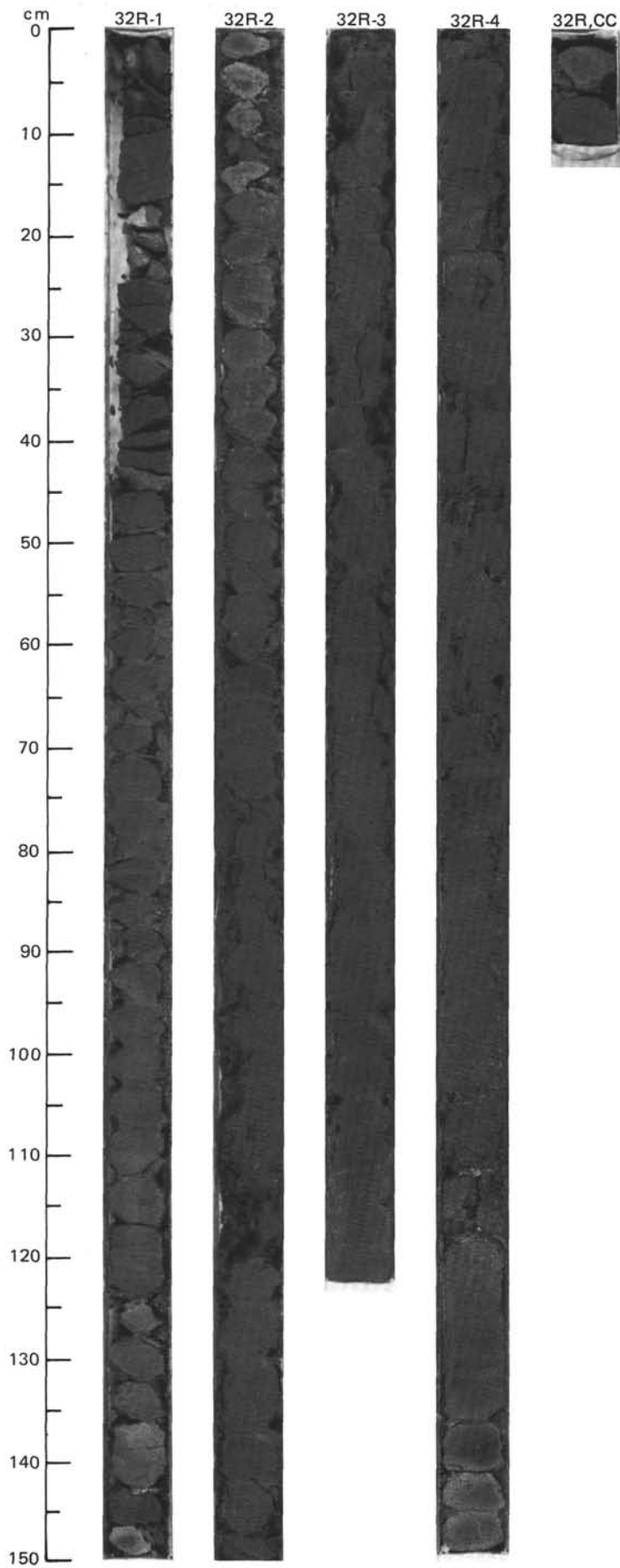
SITE 645 HOLE E CORE 30 R CORED INTERVAL 2703.1-2712.8 mbsl; 695.6-705.3 mbsf

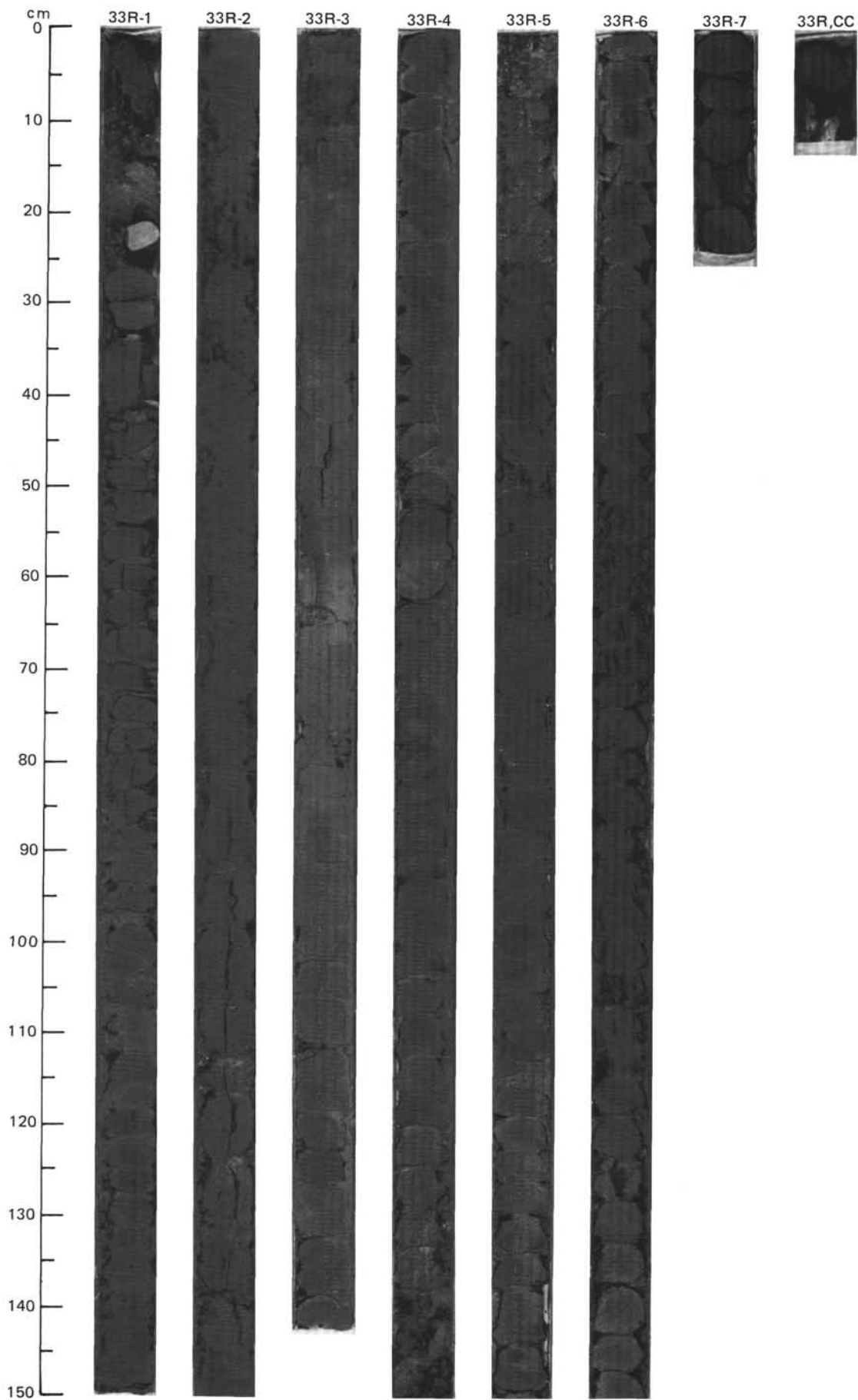
TIME-ROCK UNIT	BIOSTRAT. ZONE/ FOSSIL CHARACTER					PALEOMAGNETICS	PHYS. PROPERTIES	CHEMISTRY	SECTION	METERS	GRAPHIC LITHOLOGY	DRILLING DISTURB.	SED. STRUCTURES	SAMPLES	LITHOLOGIC DESCRIPTION																																							
	FORAMINIFERS	NANNOFOSSILS	RADIOLARIANS	DIATOMS	DINOCYSTS																																																	
	B	B	B	B	R/M	N.C.	$\gamma = 2.05 \phi = 40.8 \text{ W} = 26$	TOC=0.85 CaCO ₃ =4.0	1	0.5 1.0		X		*	<p>SILTY MUD AND MUDDY SAND</p> <p>Silty mud, dark gray (5Y 4/1), weakly bioturbated with very indistinct planar lamination or layering. Muds grade downward into a muddy sand, very dark gray (5Y 3/1), bearing planar laminae and burrows. No sequences are evident.</p> <p>SMEAR SLIDE SUMMARY (%):</p> <table border="0"> <tr> <td></td> <td>1, 76</td> <td>2, 58</td> </tr> <tr> <td>D</td> <td>D</td> <td>D</td> </tr> </table> <p>TEXTURE:</p> <table border="0"> <tr> <td>Sand</td> <td>10</td> <td>50</td> </tr> <tr> <td>Silt</td> <td>50</td> <td>25</td> </tr> <tr> <td>Clay</td> <td>40</td> <td>25</td> </tr> </table> <p>COMPOSITION:</p> <table border="0"> <tr> <td>Quartz</td> <td>30</td> <td>55</td> </tr> <tr> <td>Feldspar</td> <td>5</td> <td>10</td> </tr> <tr> <td>Rock fragments</td> <td>10</td> <td>—</td> </tr> <tr> <td>Mica</td> <td>5</td> <td>5</td> </tr> <tr> <td>Clay</td> <td>40</td> <td>20</td> </tr> <tr> <td>Calcite/dolomite</td> <td>5</td> <td>2</td> </tr> <tr> <td>Accessory minerals</td> <td>5</td> <td>5</td> </tr> <tr> <td>Pyrite</td> <td>Tr</td> <td>3</td> </tr> </table>		1, 76	2, 58	D	D	D	Sand	10	50	Silt	50	25	Clay	40	25	Quartz	30	55	Feldspar	5	10	Rock fragments	10	—	Mica	5	5	Clay	40	20	Calcite/dolomite	5	2	Accessory minerals	5	5	Pyrite	Tr	3
	1, 76	2, 58																																																				
D	D	D																																																				
Sand	10	50																																																				
Silt	50	25																																																				
Clay	40	25																																																				
Quartz	30	55																																																				
Feldspar	5	10																																																				
Rock fragments	10	—																																																				
Mica	5	5																																																				
Clay	40	20																																																				
Calcite/dolomite	5	2																																																				
Accessory minerals	5	5																																																				
Pyrite	Tr	3																																																				

SITE 645 HOLE E CORE 31 R CORED INTERVAL 2712.8-2717.2 mbsl; 705.3-709.7 mbsf

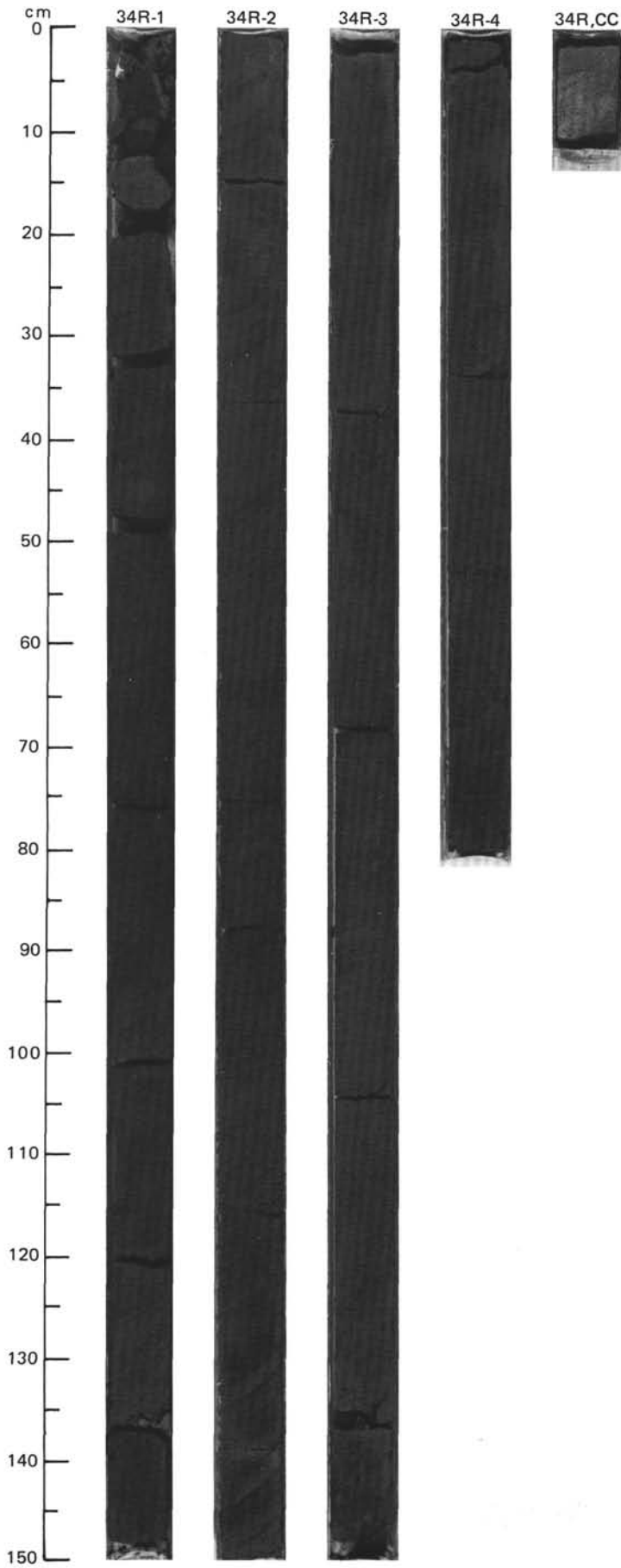
TIME-ROCK UNIT	BIOSTRAT. ZONE/ FOSSIL CHARACTER					PALEOMAGNETICS	PHYS. PROPERTIES	CHEMISTRY	SECTION	METERS	GRAPHIC LITHOLOGY	DRILLING DISTURB.	SED. STRUCTURES	SAMPLES	LITHOLOGIC DESCRIPTION																														
	FORAMINIFERS	NANNOFOSSILS	RADIOLARIANS	DIATOMS	DINOCYSTS																																								
	B	B	B	B		N.C.			1			X		*	<p>CARBONATE CLAYEY MUD</p> <p>Carbonate clayey mud, dark gray (5Y 4/1), with bioturbated laminae. Core is disturbed with drilling breccia. Caved pebbles of gravelly deposits from higher levels in the hole occur at the top of the core.</p> <p>SMEAR SLIDE SUMMARY (%):</p> <table border="0"> <tr> <td></td> <td>1, 17</td> </tr> <tr> <td>D</td> <td>D</td> </tr> </table> <p>TEXTURE:</p> <table border="0"> <tr> <td>Sand</td> <td>20</td> </tr> <tr> <td>Silt</td> <td>30</td> </tr> <tr> <td>Clay</td> <td>50</td> </tr> </table> <p>COMPOSITION:</p> <table border="0"> <tr> <td>Quartz</td> <td>25</td> </tr> <tr> <td>Feldspar</td> <td>7</td> </tr> <tr> <td>Rock fragments</td> <td>Tr</td> </tr> <tr> <td>Mica</td> <td>Tr</td> </tr> <tr> <td>Clay</td> <td>30</td> </tr> <tr> <td>Volcanic glass</td> <td>Tr</td> </tr> <tr> <td>Calcite/dolomite</td> <td>33</td> </tr> <tr> <td>Accessory minerals</td> <td>1</td> </tr> <tr> <td>Pyrite</td> <td>2</td> </tr> <tr> <td>Nannofossils</td> <td>2</td> </tr> </table>		1, 17	D	D	Sand	20	Silt	30	Clay	50	Quartz	25	Feldspar	7	Rock fragments	Tr	Mica	Tr	Clay	30	Volcanic glass	Tr	Calcite/dolomite	33	Accessory minerals	1	Pyrite	2	Nannofossils	2
	1, 17																																												
D	D																																												
Sand	20																																												
Silt	30																																												
Clay	50																																												
Quartz	25																																												
Feldspar	7																																												
Rock fragments	Tr																																												
Mica	Tr																																												
Clay	30																																												
Volcanic glass	Tr																																												
Calcite/dolomite	33																																												
Accessory minerals	1																																												
Pyrite	2																																												
Nannofossils	2																																												

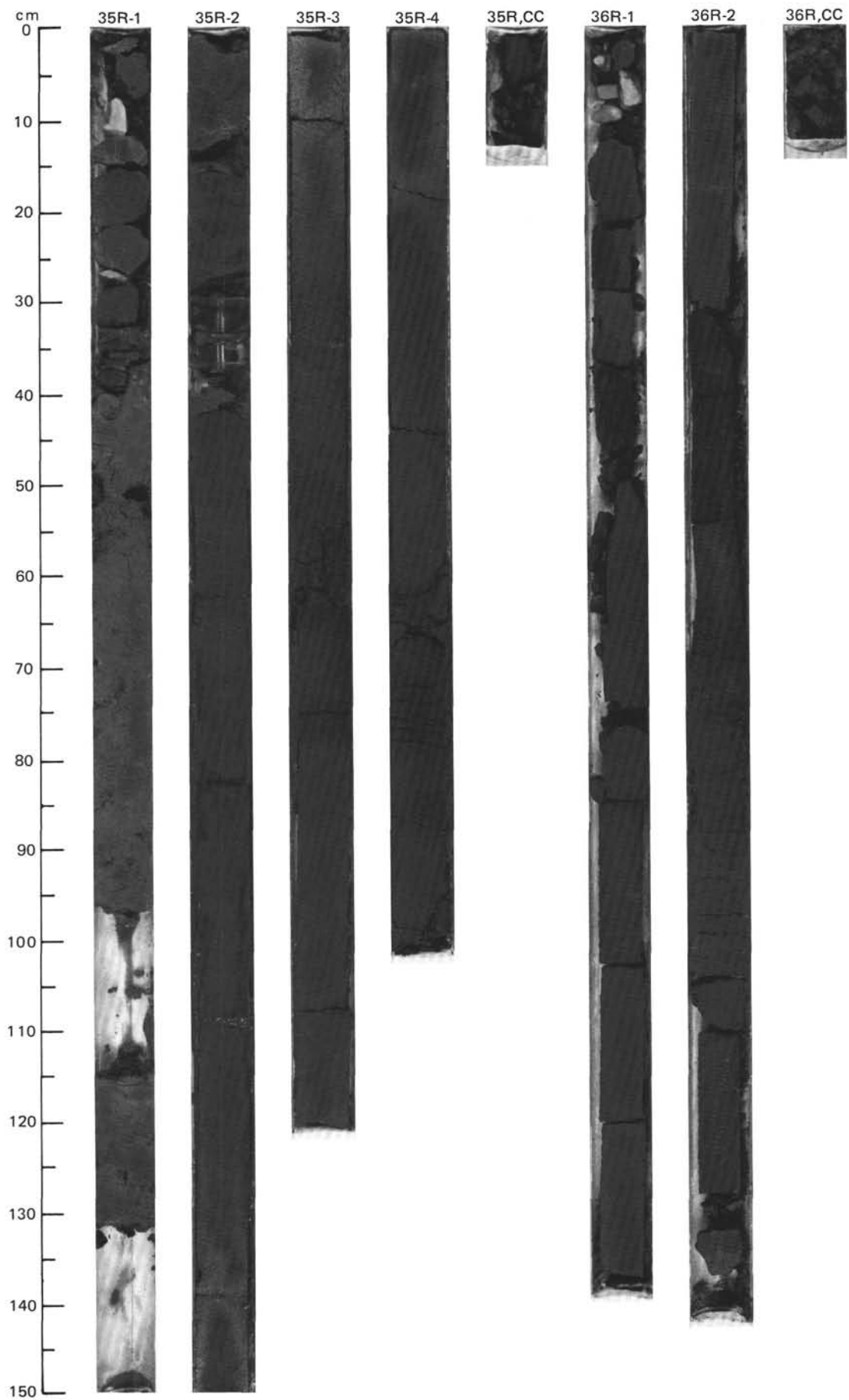


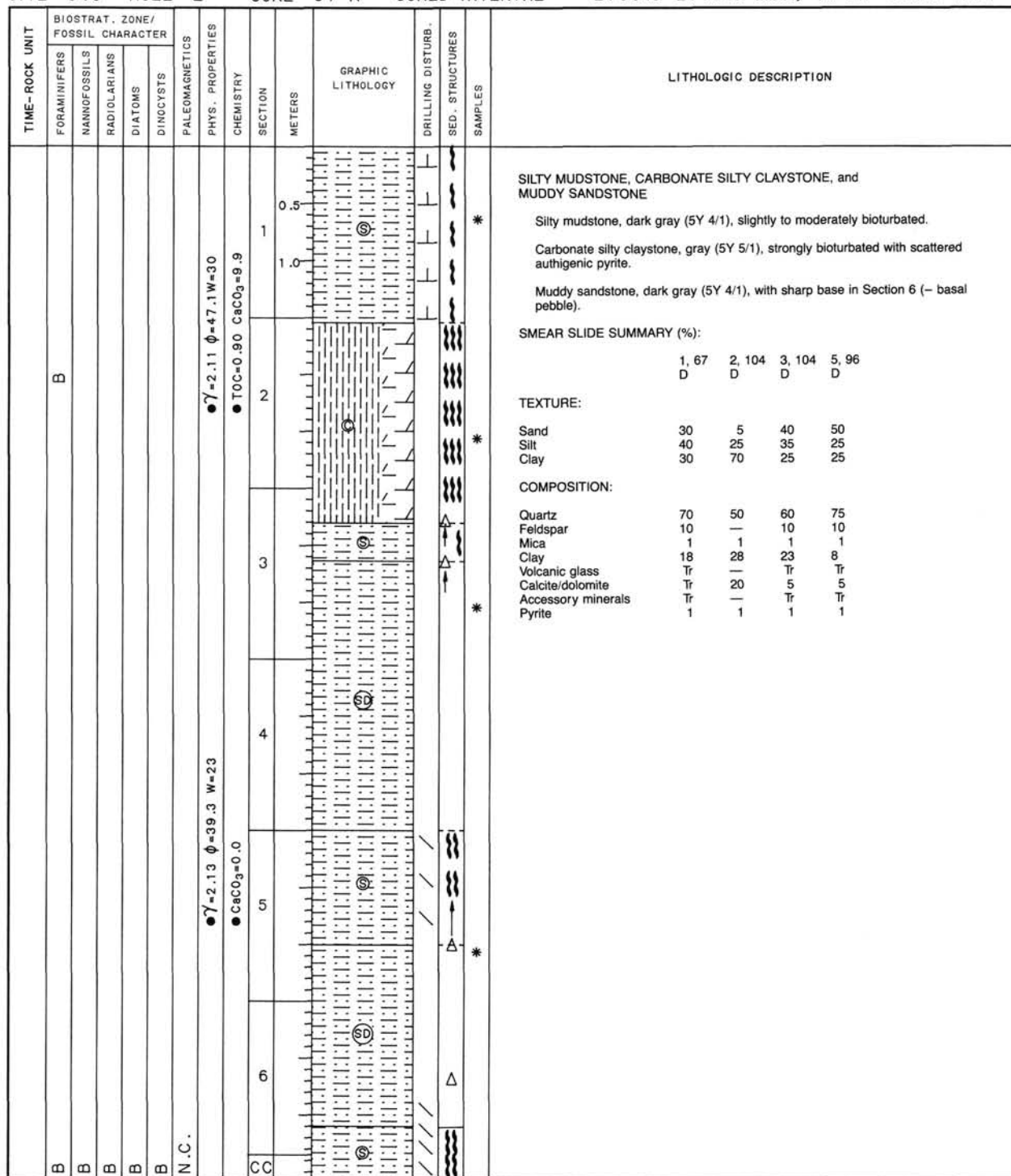


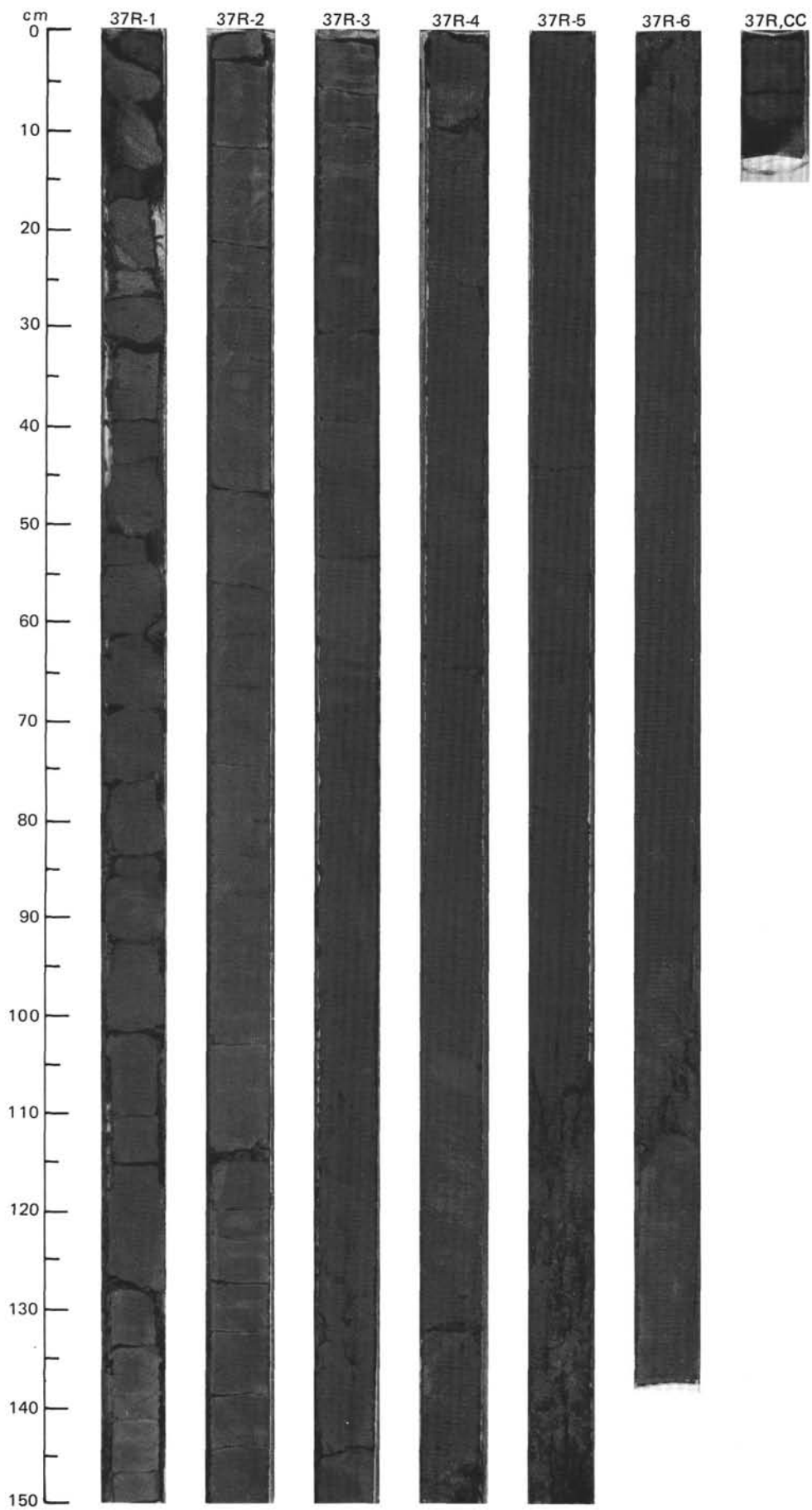


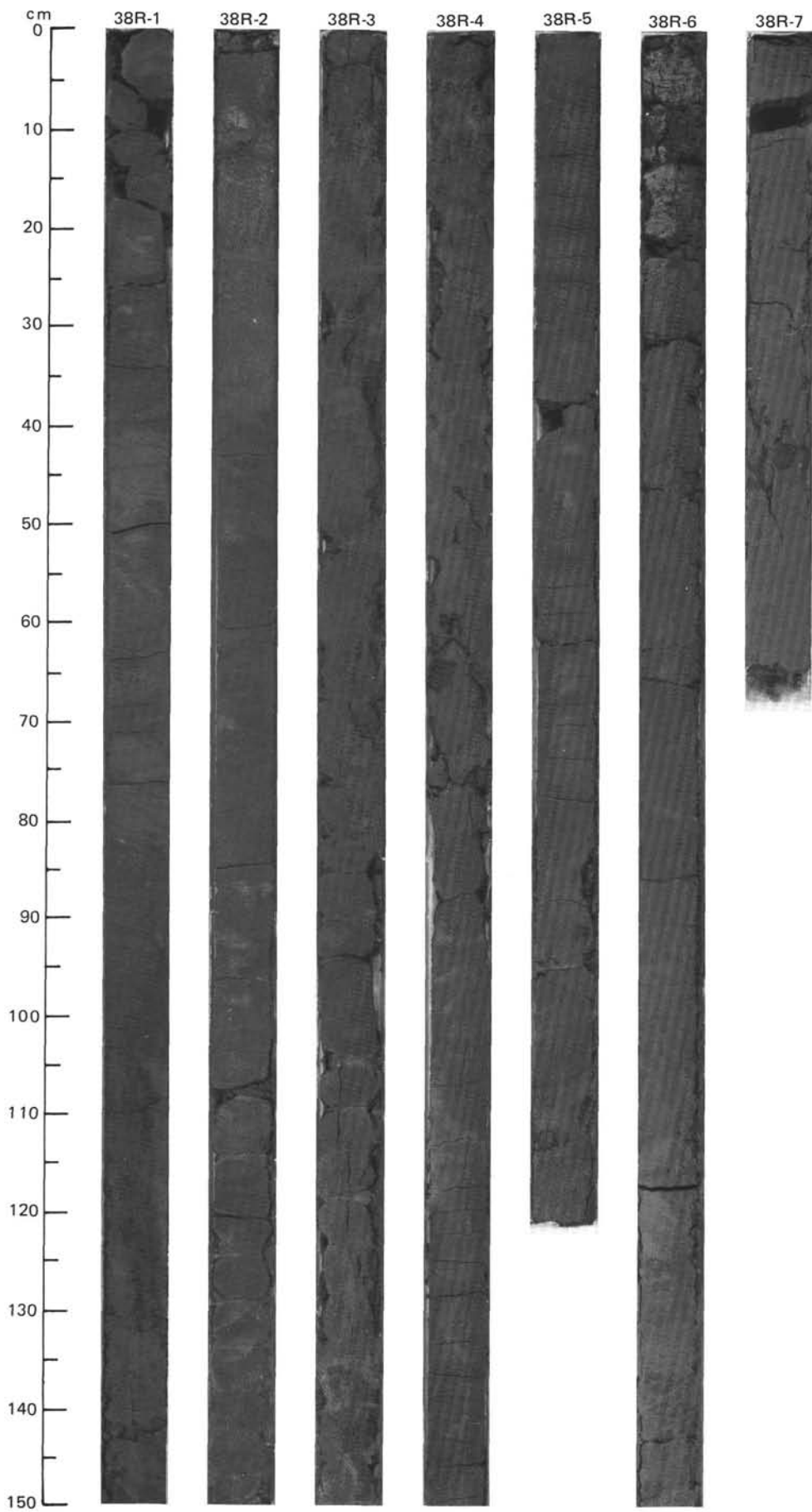
TIME-ROCK UNIT	BIOSTRAT. ZONE/ FOSSIL CHARACTER					PALEOMAGNETICS	PHYS. PROPERTIES	CHEMISTRY	SECTION	METERS	GRAPHIC LITHOLOGY	DRILLING DISTURB.	SED. STRUCTURES	SAMPLES	LITHOLOGIC DESCRIPTION																																																																											
	FORAMINIFERS	NANNOFOSSILS	RADIOLARIANS	DIATOMS	DINOCYSTS																																																																																					
B															<p>MUDDY SANDSTONE AND SILTY MUDSTONE</p> <p>Muddy sandstone and silty mudstone, dark gray (5Y 4/1), with gradational contacts between the two lithologies. Large burrows are locally present. Indistinct planar lamination is more common in the silty muds.</p> <p>SMEAR SLIDE SUMMARY (%):</p> <table border="1"> <tr> <td></td> <td>1, 27</td> <td>2, 21</td> <td>3, 86</td> <td>4, 14</td> </tr> <tr> <td></td> <td>D</td> <td>D</td> <td>M</td> <td>D</td> </tr> </table> <p>TEXTURE:</p> <table border="1"> <tr> <td>Sand</td> <td>50</td> <td>30</td> <td>35</td> <td>50</td> </tr> <tr> <td>Silt</td> <td>30</td> <td>30</td> <td>45</td> <td>15</td> </tr> <tr> <td>Clay</td> <td>20</td> <td>40</td> <td>20</td> <td>30</td> </tr> </table> <p>COMPOSITION:</p> <table border="1"> <tr> <td>Quartz</td> <td>50</td> <td>40</td> <td>50</td> <td>40</td> </tr> <tr> <td>Feldspar</td> <td>10</td> <td>5</td> <td>10</td> <td>10</td> </tr> <tr> <td>Rock fragments</td> <td>5</td> <td>—</td> <td>10</td> <td>—</td> </tr> <tr> <td>Mica</td> <td>5</td> <td>7</td> <td>5</td> <td>5</td> </tr> <tr> <td>Clay</td> <td>25</td> <td>40</td> <td>20</td> <td>25</td> </tr> <tr> <td>Volcanic glass</td> <td>Tr</td> <td>—</td> <td>Tr</td> <td>—</td> </tr> <tr> <td>Calcite/dolomite</td> <td>—</td> <td>3</td> <td>—</td> <td>2</td> </tr> <tr> <td>Accessory minerals</td> <td>5</td> <td>5</td> <td>4</td> <td>6</td> </tr> <tr> <td>Pyrite</td> <td>Tr</td> <td>—</td> <td>1</td> <td>10</td> </tr> <tr> <td>Glauconite</td> <td>—</td> <td>—</td> <td>—</td> <td>2</td> </tr> </table>		1, 27	2, 21	3, 86	4, 14		D	D	M	D	Sand	50	30	35	50	Silt	30	30	45	15	Clay	20	40	20	30	Quartz	50	40	50	40	Feldspar	10	5	10	10	Rock fragments	5	—	10	—	Mica	5	7	5	5	Clay	25	40	20	25	Volcanic glass	Tr	—	Tr	—	Calcite/dolomite	—	3	—	2	Accessory minerals	5	5	4	6	Pyrite	Tr	—	1	10	Glauconite	—	—	—	2
	1, 27	2, 21	3, 86	4, 14																																																																																						
	D	D	M	D																																																																																						
Sand	50	30	35	50																																																																																						
Silt	30	30	45	15																																																																																						
Clay	20	40	20	30																																																																																						
Quartz	50	40	50	40																																																																																						
Feldspar	10	5	10	10																																																																																						
Rock fragments	5	—	10	—																																																																																						
Mica	5	7	5	5																																																																																						
Clay	25	40	20	25																																																																																						
Volcanic glass	Tr	—	Tr	—																																																																																						
Calcite/dolomite	—	3	—	2																																																																																						
Accessory minerals	5	5	4	6																																																																																						
Pyrite	Tr	—	1	10																																																																																						
Glauconite	—	—	—	2																																																																																						
B																																																																																										
B																																																																																										
B																																																																																										
R/M																																																																																										
N.C.																																																																																										
							$\gamma = 2.04$ $\phi = 40.6$ $W = 26$ \bullet $TOC = 0.74$ $CaCO_3 = 0.0$		1	0.5 1.0																																																																																
							$\gamma = 2.10$ $\phi = 37.7$ $W = 27$ \bullet $CaCO_3 = 0.0$		2																																																																																	
									3																																																																																	
									4																																																																																	

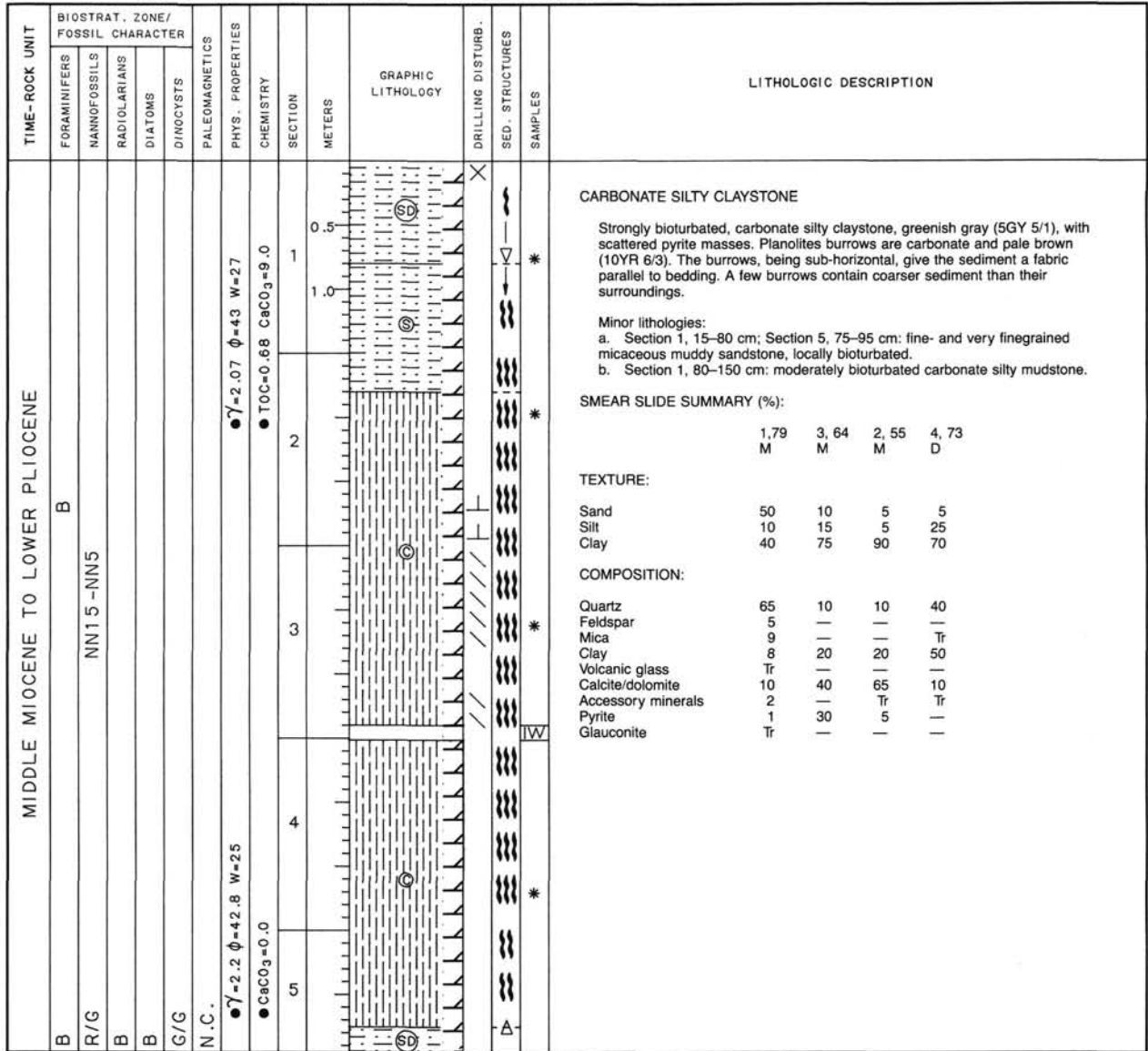


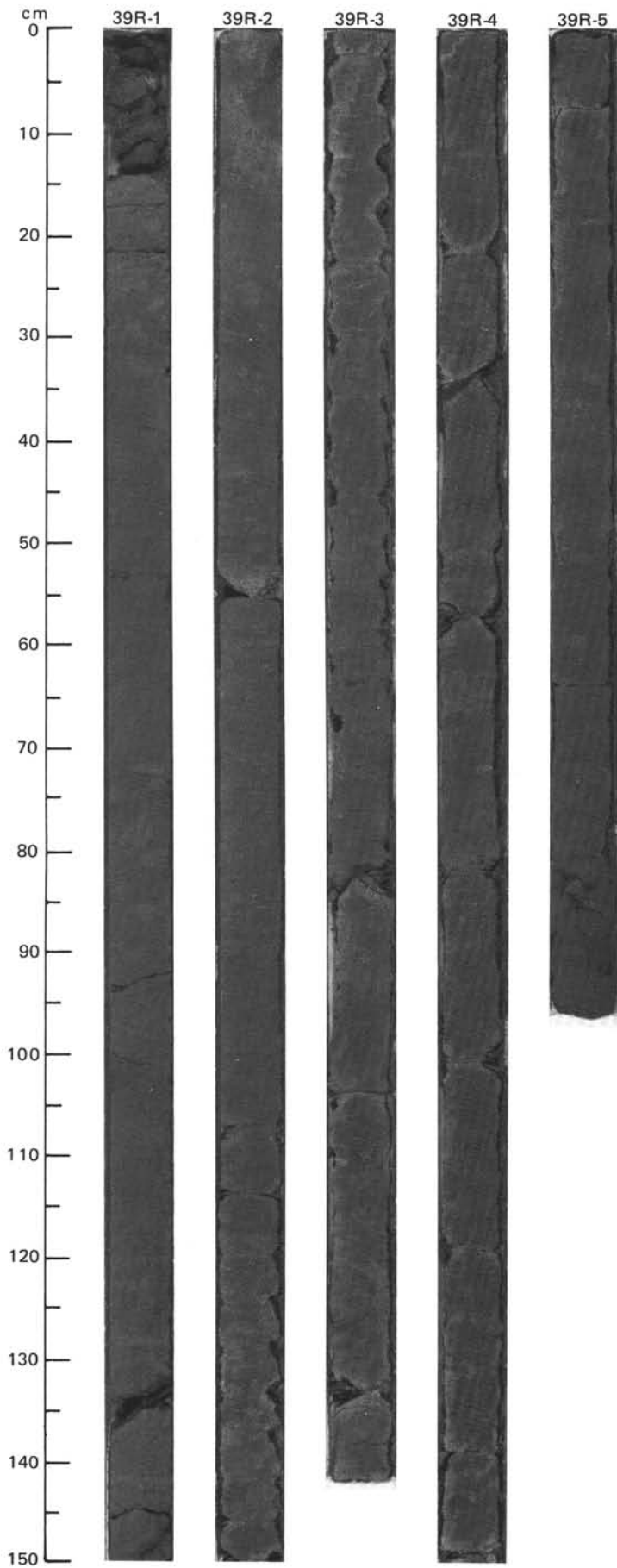


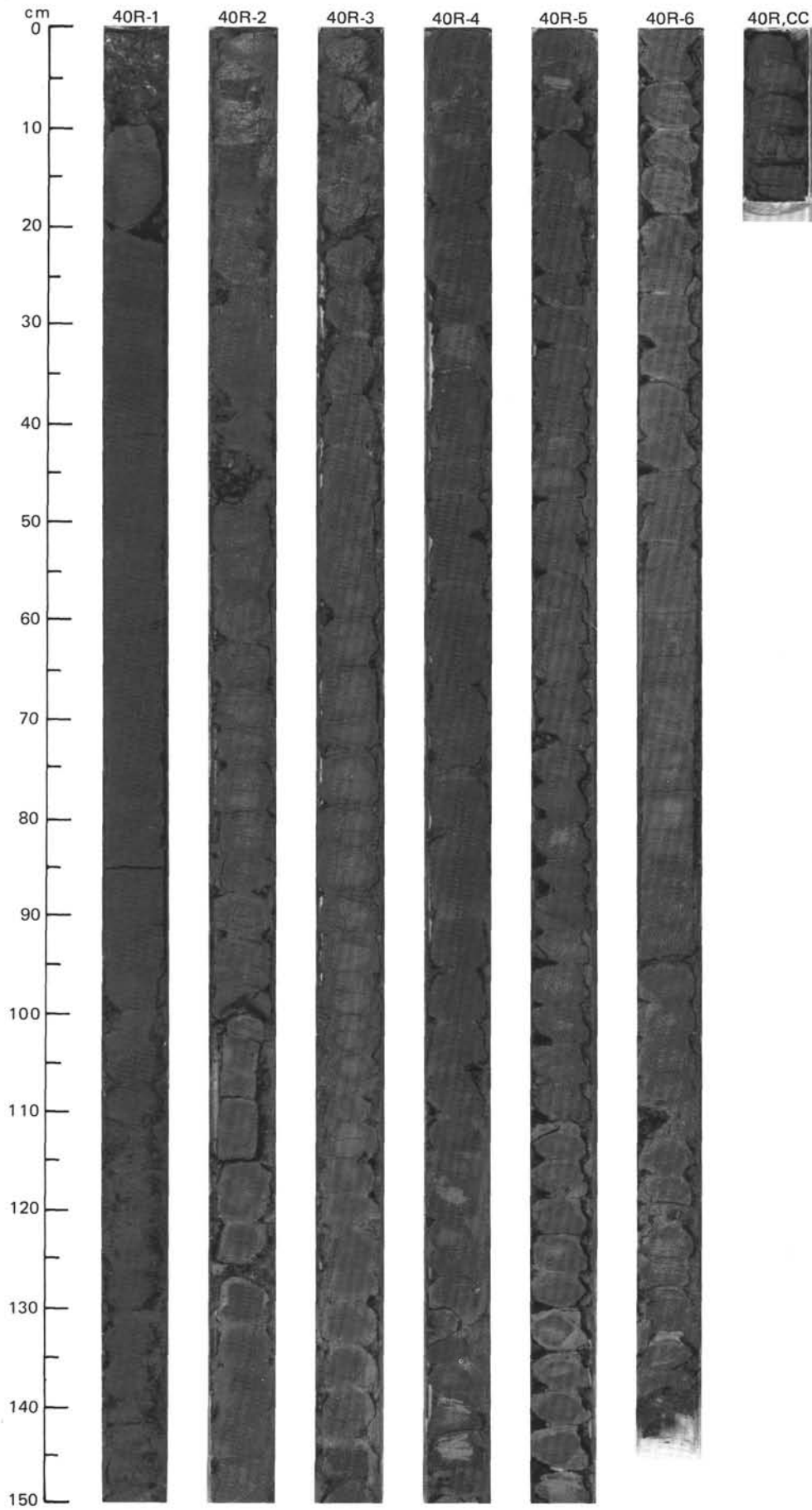






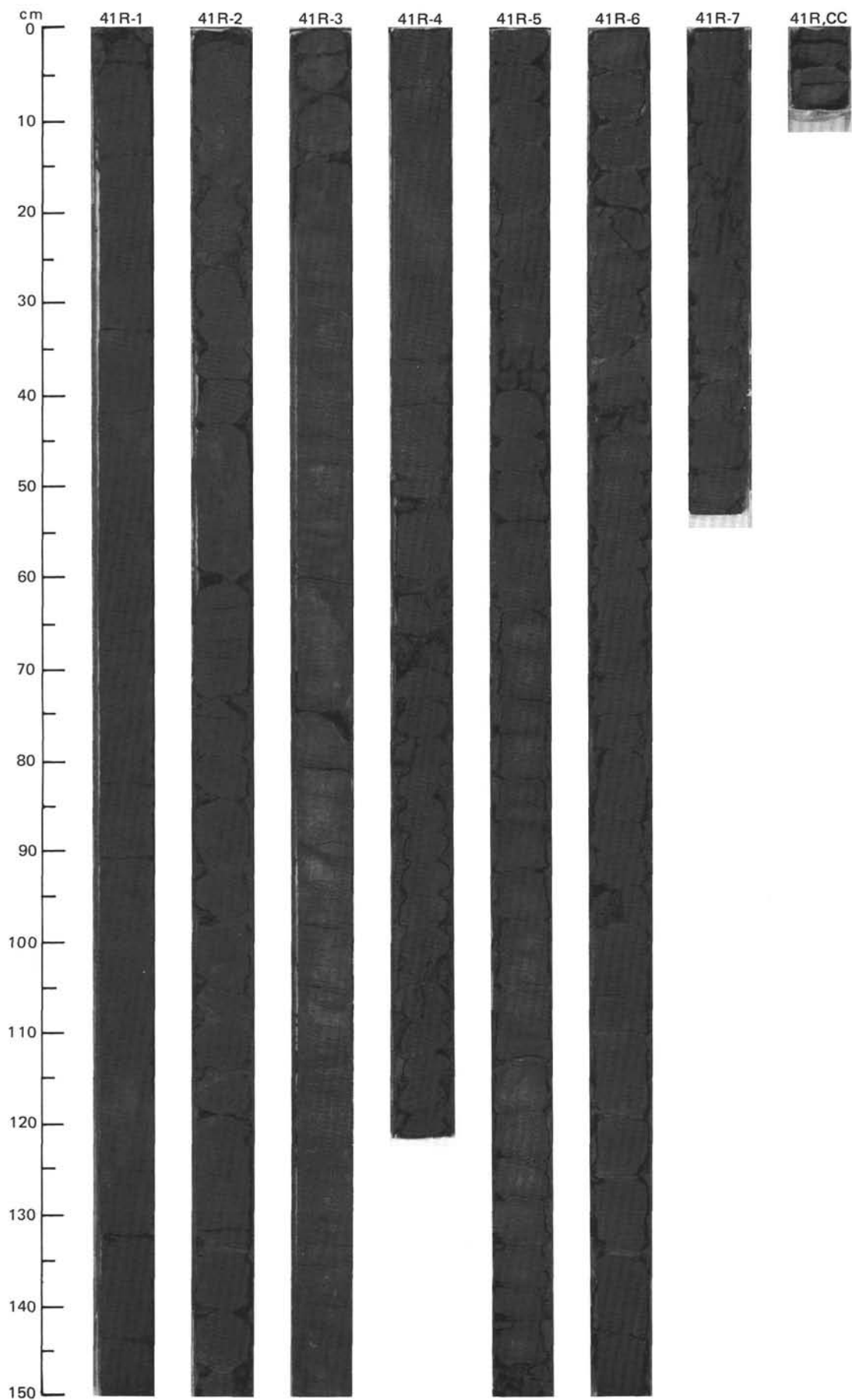


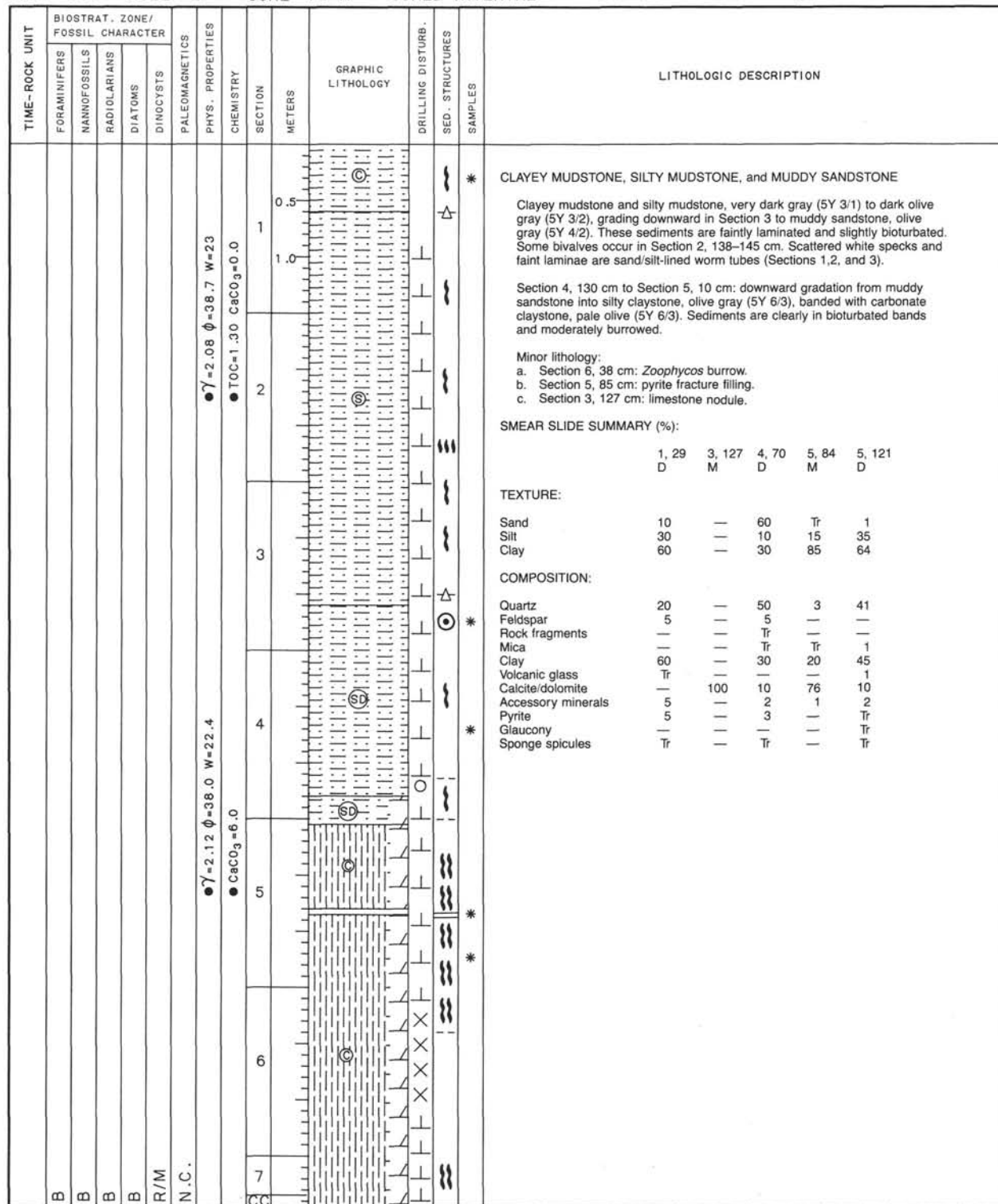


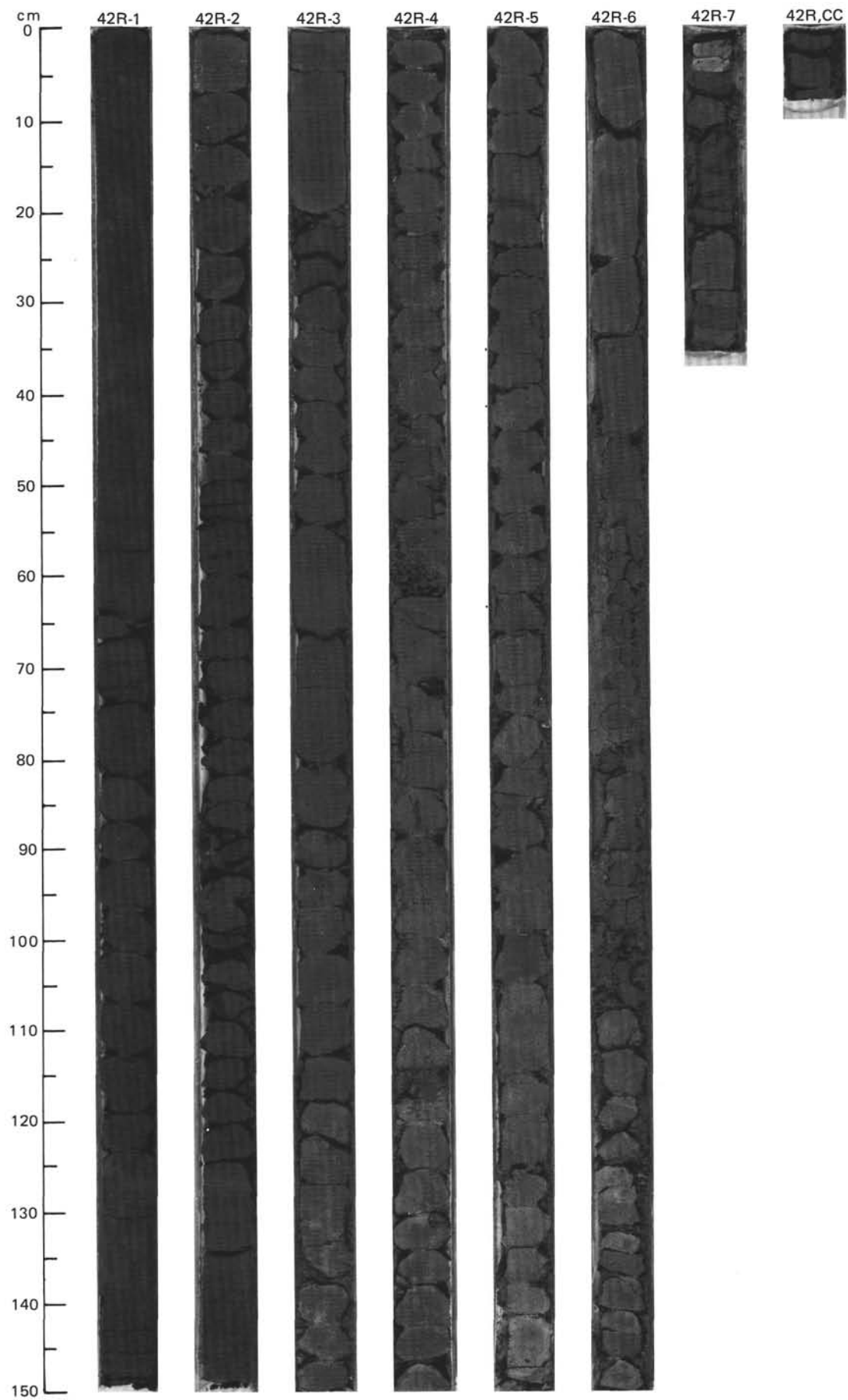


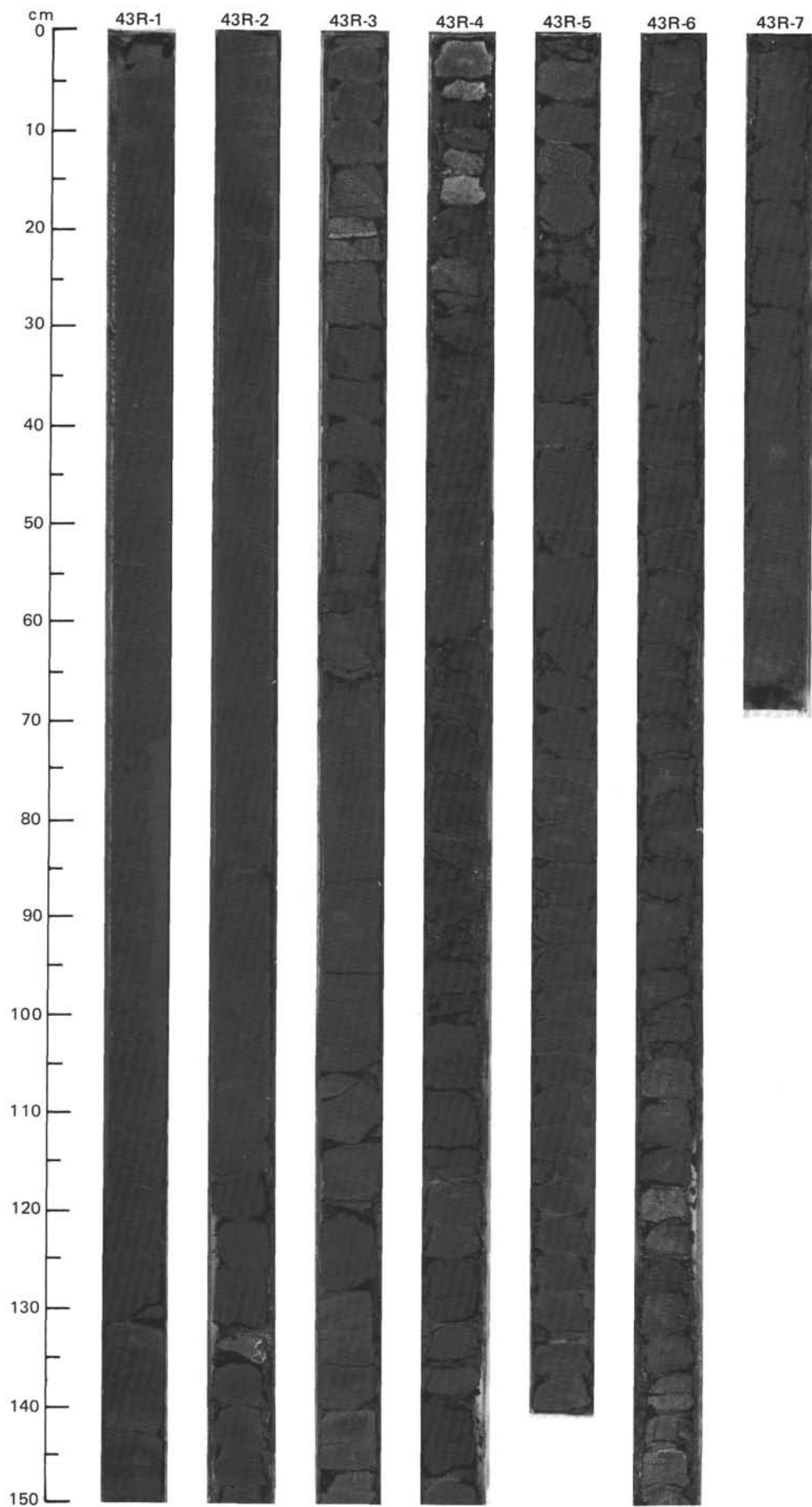
SITE 645 HOLE E CORE 41 R CORED INTERVAL 2799.5-2809.1 mbsf; 792.0 801.6 mbsf

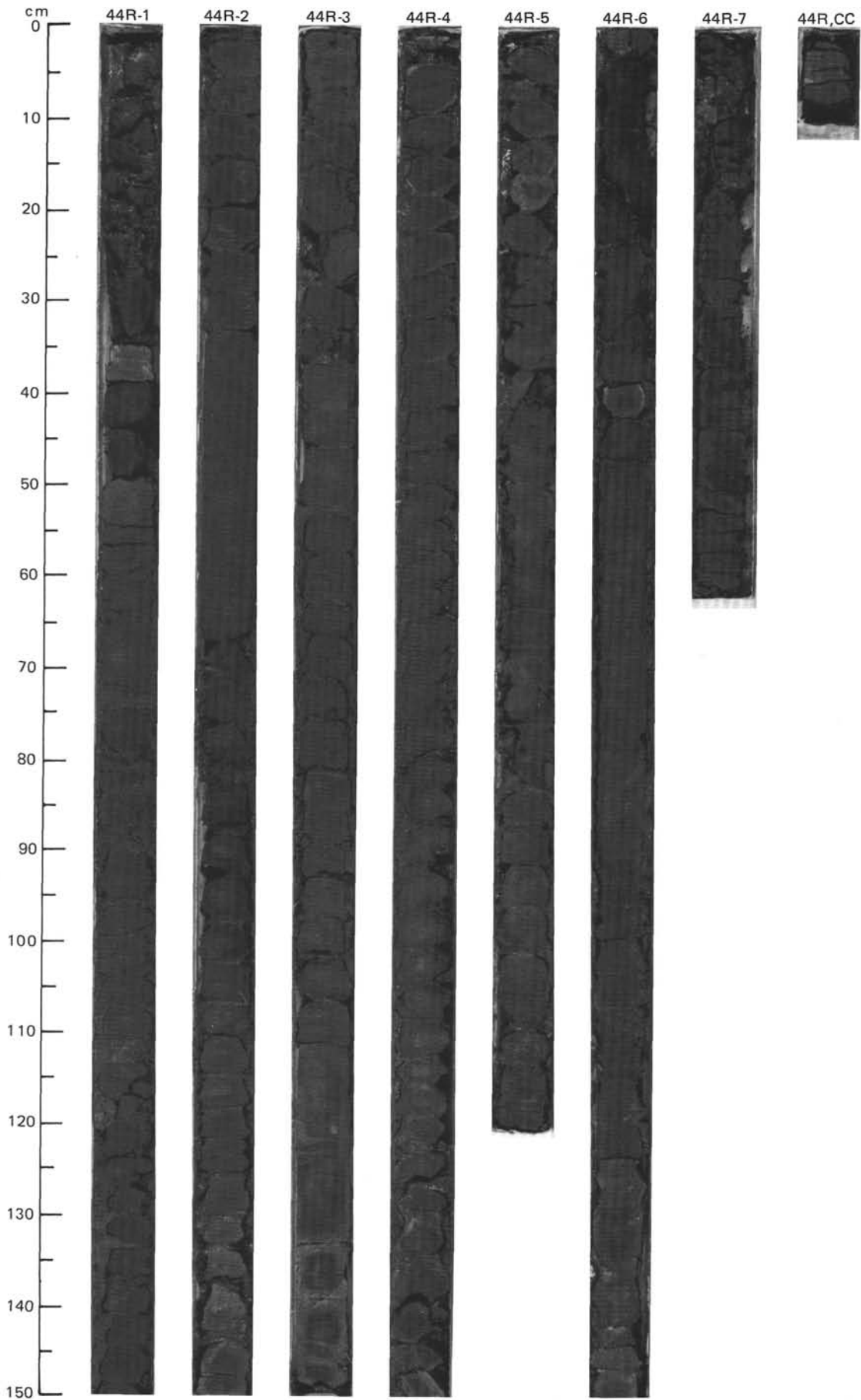
TIME-ROCK UNIT	BIOSTRAT. ZONE/ FOSSIL CHARACTER					CHEMISTRY	SECTION	METERS	GRAPHIC LITHOLOGY	DRILLING DISTURB.	SED. STRUCTURES	SAMPLES	LITHOLOGIC DESCRIPTION																																																				
	FORAMINIFERS	NANNOFOSSILS	RADIOLARIANS	DIATOMS	DINOCYSTS																																																												
B						● $\gamma = 2.14$ $\phi = 38.1$ W=22 ● CaCO ₃ =0	1	0.5 1.0					<p>SILTY and CLAYEY MUDSTONE and MUDDY SANDSTONE</p> <p>Silty and clayey mudstone and muddy sandstone, dark gray (5Y 4/1). Mudstones are faintly bioturbated; sandstones are featureless. Contacts between facies are gradational.</p> <p>Minor lithology: Section 3, 120 cm: One complete shell (gastropod).</p> <p>SMEAR SLIDE SUMMARY (%):</p> <table border="1"> <tr> <td></td> <td>1, 100</td> <td>4, 102</td> <td>5, 105</td> </tr> <tr> <td>D</td> <td>D</td> <td>D</td> <td>D</td> </tr> </table> <p>TEXTURE:</p> <table border="1"> <tr> <td>Sand</td> <td>30</td> <td>40</td> <td>40</td> </tr> <tr> <td>Silt</td> <td>40</td> <td>25</td> <td>35</td> </tr> <tr> <td>Clay</td> <td>30</td> <td>35</td> <td>45</td> </tr> </table> <p>COMPOSITION:</p> <table border="1"> <tr> <td>Quartz</td> <td>55</td> <td>50</td> <td>37</td> </tr> <tr> <td>Feldspar</td> <td>10</td> <td>5</td> <td>7</td> </tr> <tr> <td>Mica</td> <td>1</td> <td>4</td> <td>4</td> </tr> <tr> <td>Clay</td> <td>24</td> <td>25</td> <td>40</td> </tr> <tr> <td>Calcite/dolomite</td> <td>3</td> <td>—</td> <td>—</td> </tr> <tr> <td>Accessory minerals</td> <td>2</td> <td>6</td> <td>4</td> </tr> <tr> <td>Glaucony</td> <td>Tr</td> <td>2</td> <td>—</td> </tr> <tr> <td>Pyrite</td> <td>5</td> <td>8</td> <td>8</td> </tr> </table>		1, 100	4, 102	5, 105	D	D	D	D	Sand	30	40	40	Silt	40	25	35	Clay	30	35	45	Quartz	55	50	37	Feldspar	10	5	7	Mica	1	4	4	Clay	24	25	40	Calcite/dolomite	3	—	—	Accessory minerals	2	6	4	Glaucony	Tr	2	—	Pyrite	5	8	8
	1, 100	4, 102	5, 105																																																														
D	D	D	D																																																														
Sand	30	40	40																																																														
Silt	40	25	35																																																														
Clay	30	35	45																																																														
Quartz	55	50	37																																																														
Feldspar	10	5	7																																																														
Mica	1	4	4																																																														
Clay	24	25	40																																																														
Calcite/dolomite	3	—	—																																																														
Accessory minerals	2	6	4																																																														
Glaucony	Tr	2	—																																																														
Pyrite	5	8	8																																																														
B						● $\gamma = 2.05$ $\phi = 41.9$ W=27 ● CaCO ₃ =9 ● TOC=1.84 CaCO ₃ =0.0	2																																																										
B							3																																																										
R/P							4																																																										
N.C.							5																																																										
							6																																																										
							7																																																										

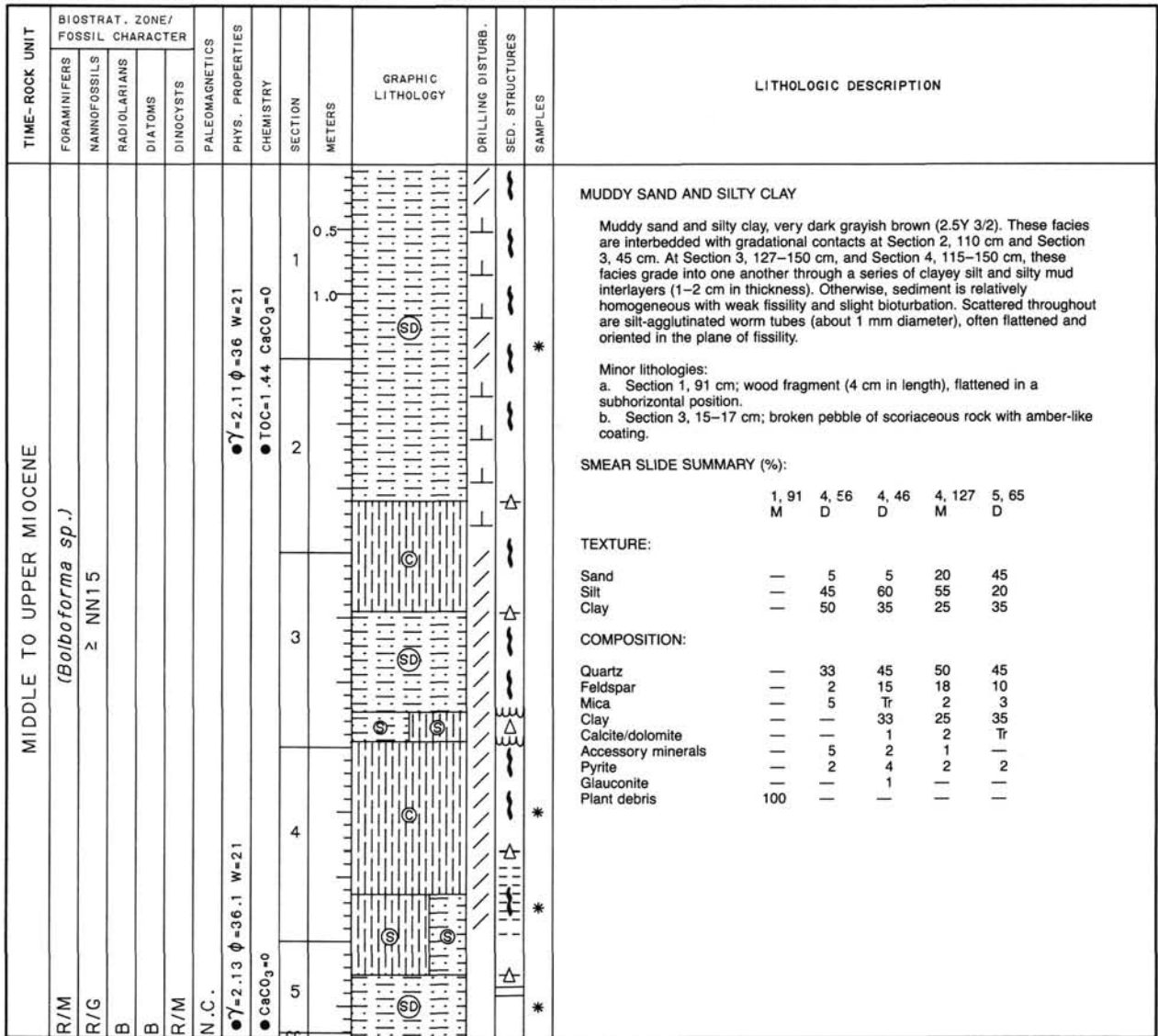


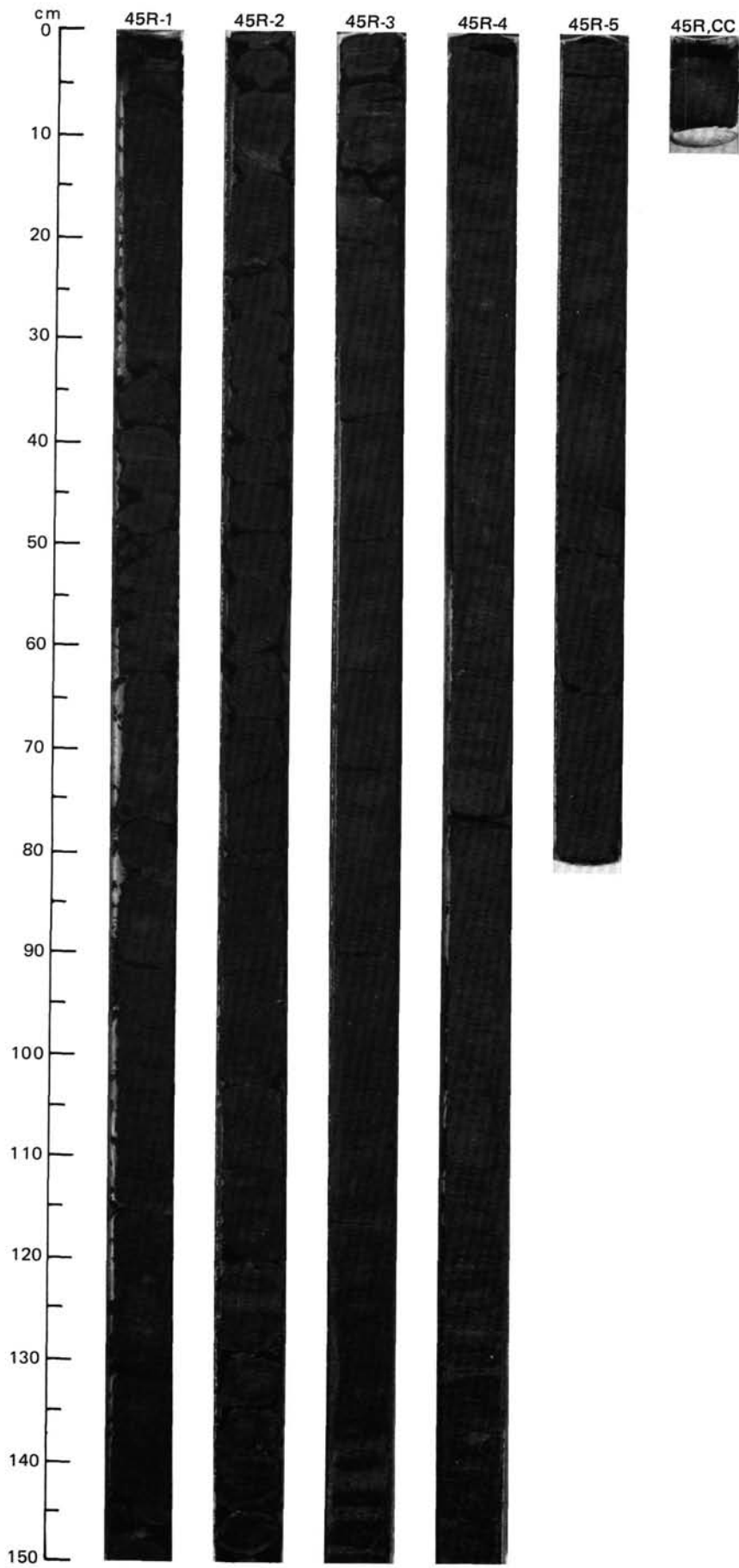


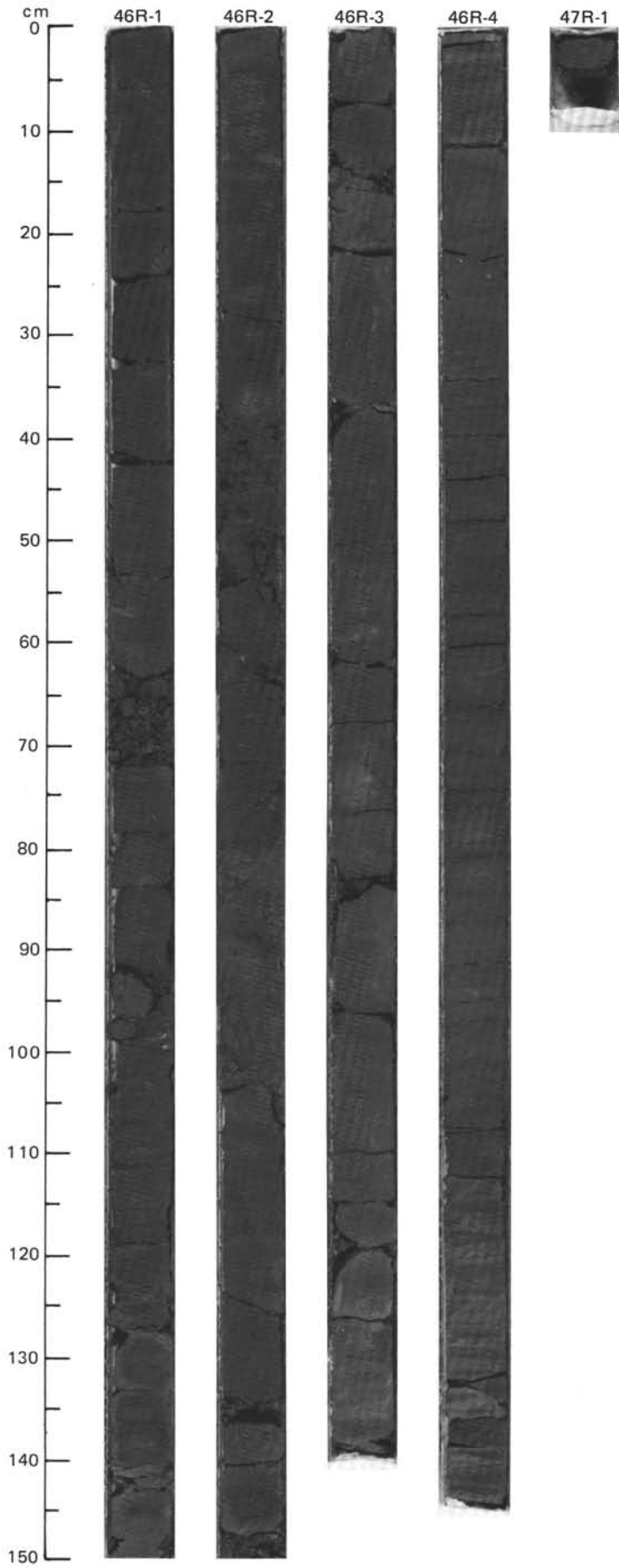


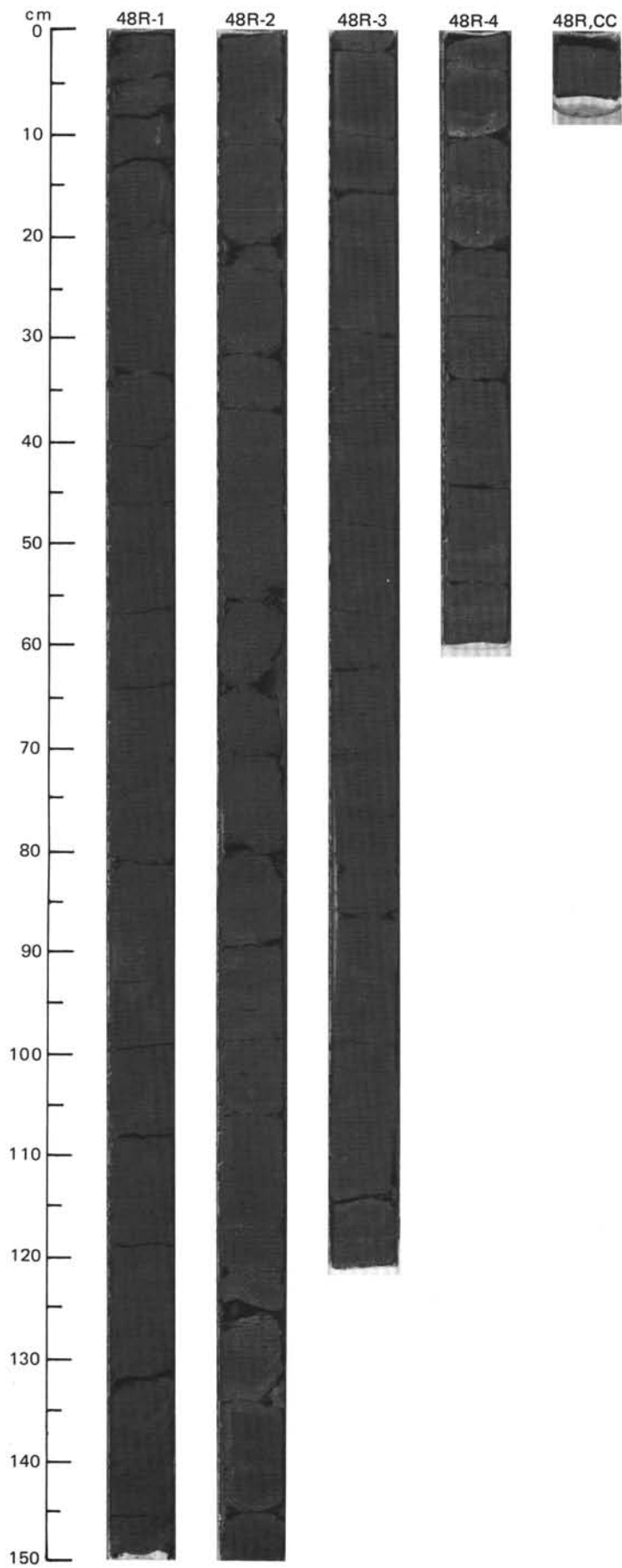


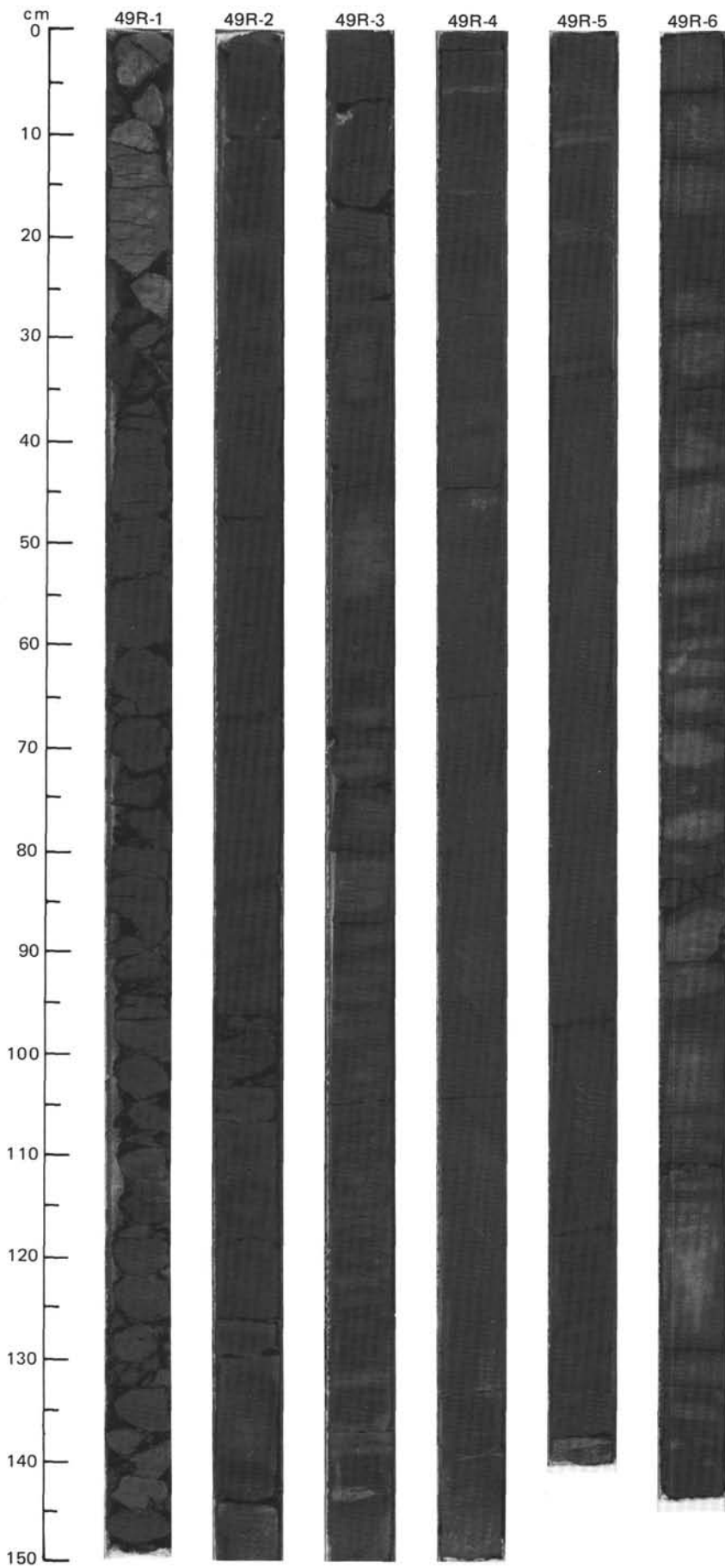


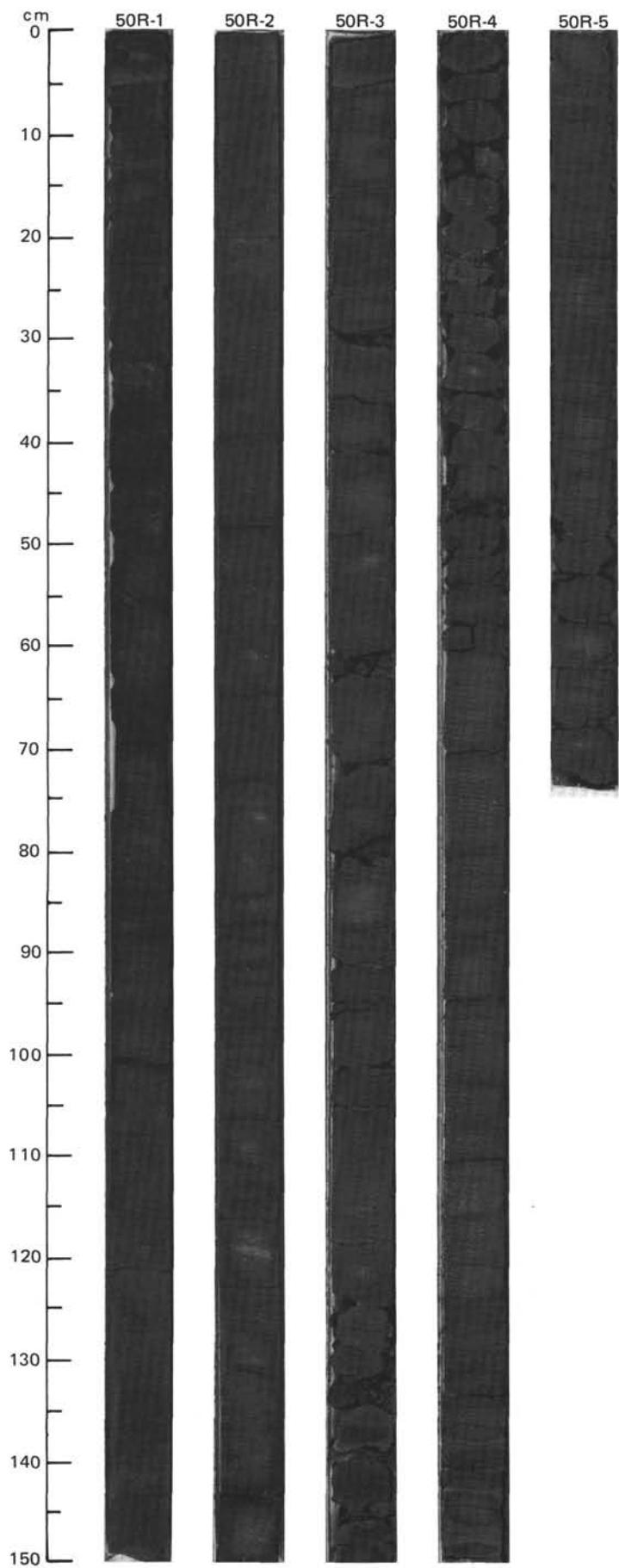


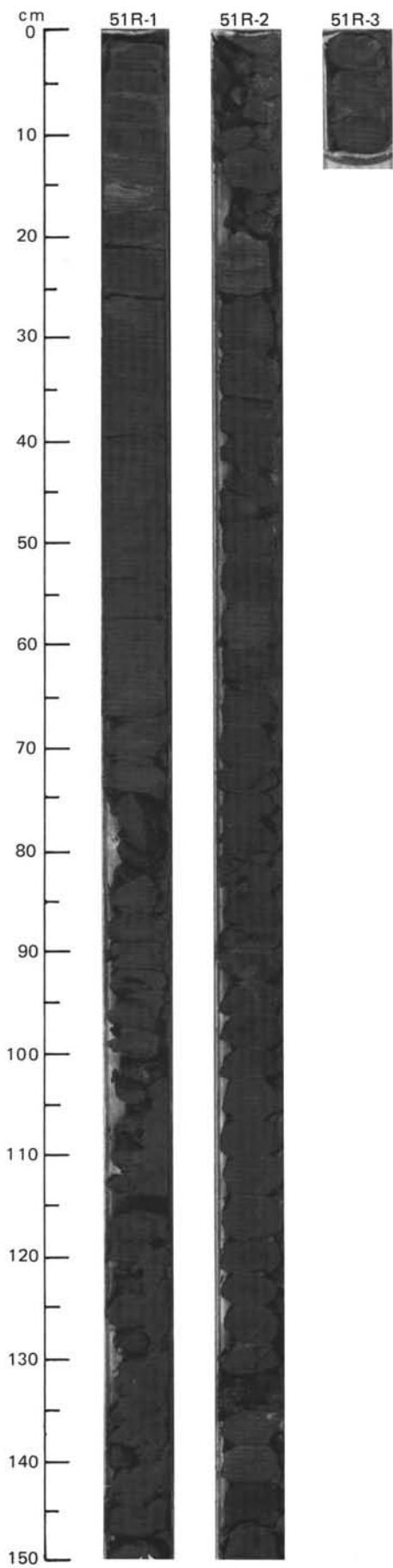




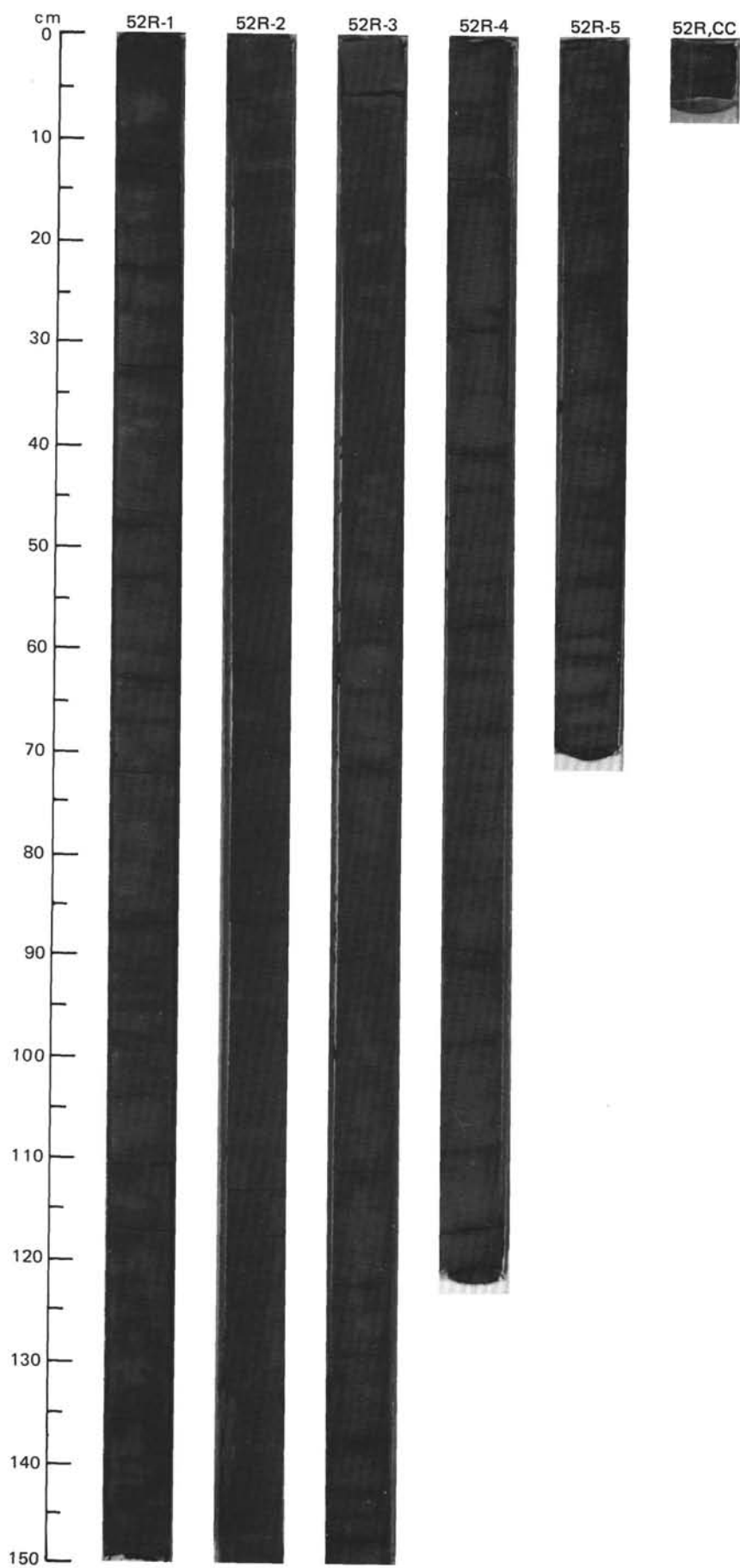




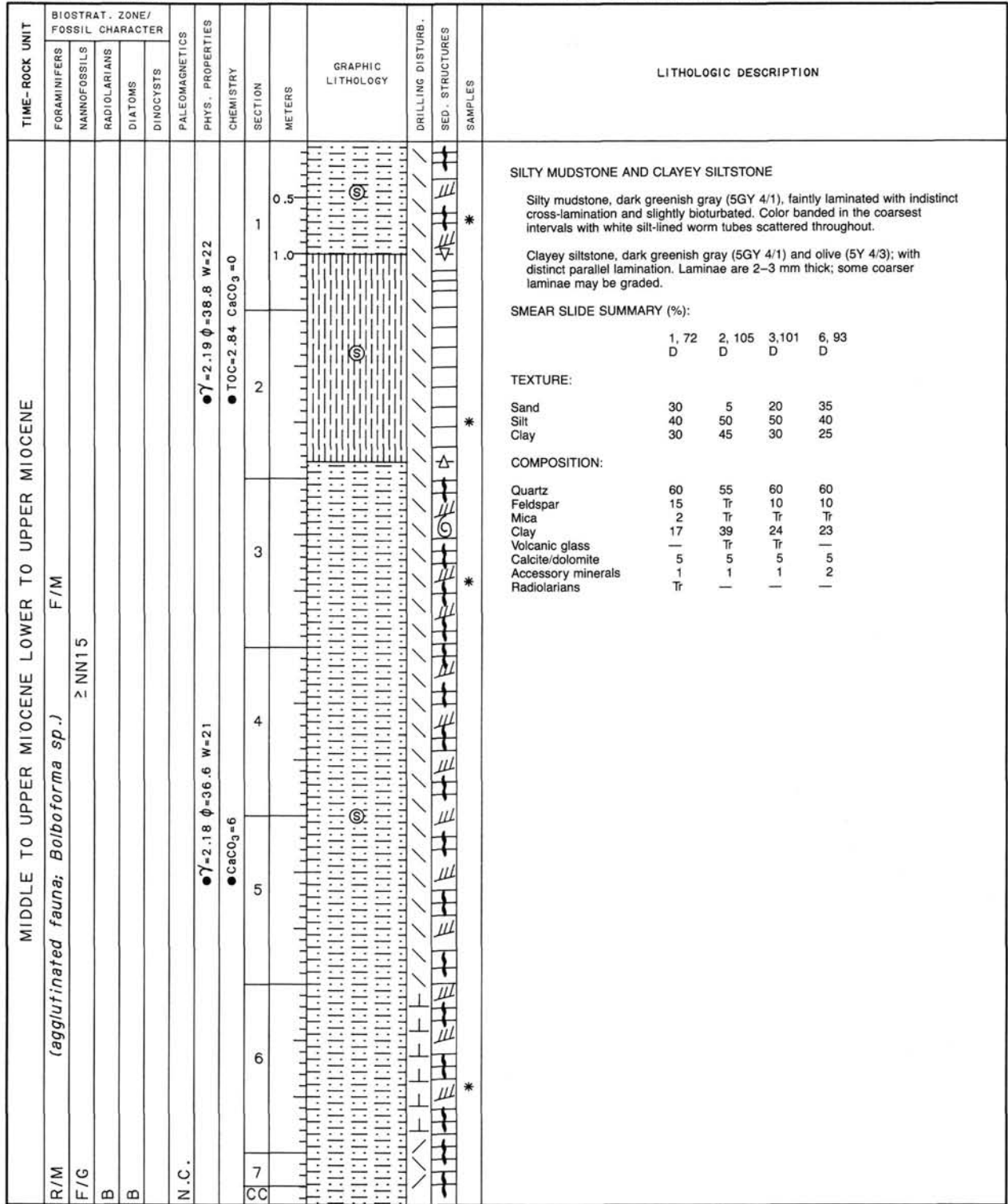


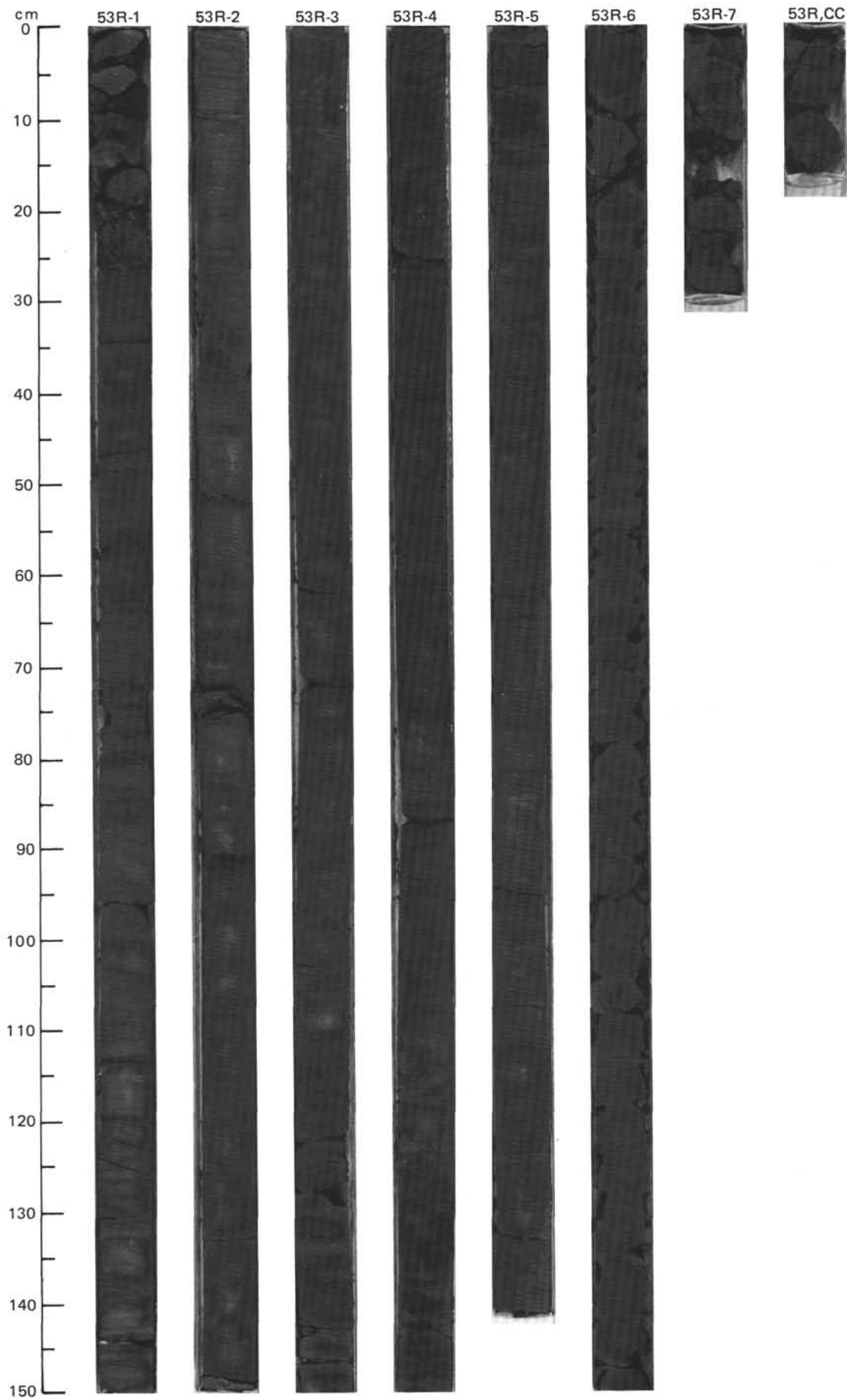


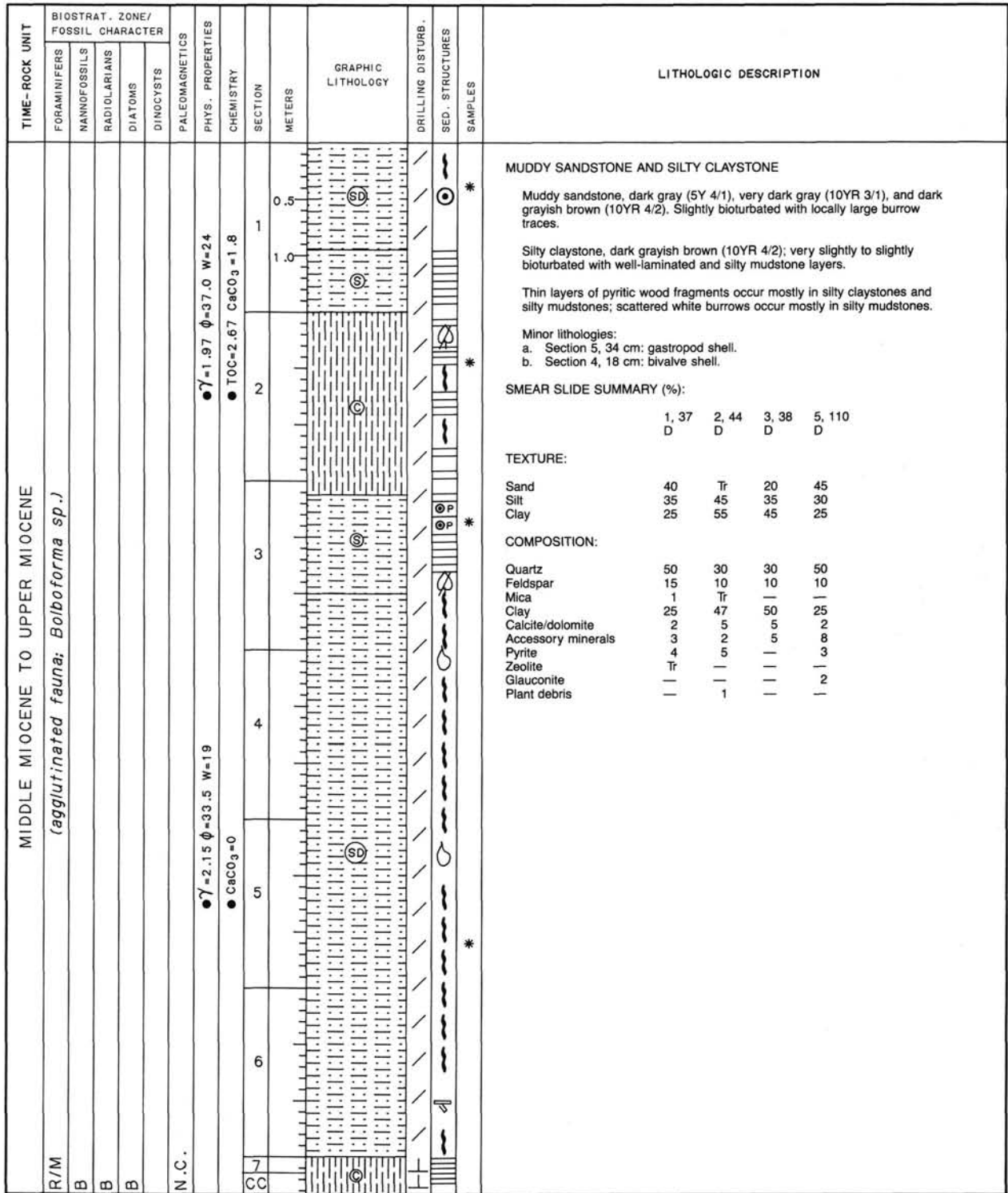
TIME-ROCK UNIT	BIOSTRAT. ZONE/ FOSSIL CHARACTER					PALEOMAGNETICS	PHYS. PROPERTIES	CHEMISTRY	SECTION	METERS	GRAPHIC LITHOLOGY	DRILLING DISTURB.	SED. STRUCTURES	SAMPLES	LITHOLOGIC DESCRIPTION																																																																																										
	FORAMINIFERS	NANNOFOSSILS	RADIOLARIANS	DIATOMS	DINOCTYSTS																																																																																																				
MIDDLE TO UPPER MIOCENE															<p>SILTY CLAYSTONE AND CLAYEY SILTSTONE</p> <p>Silty claystone, dark gray (5Y 4/1), finely laminated, fissile, and only slightly bioturbated. Laminae (about 1 cm thick) are commonly graded from a siltier base, which may be ripple laminated. Textural variation is reflected in a subtle color banding. Rare pyrite.</p> <p>Clayey siltstone, dark gray (5Y 4/1), crudely laminated, generally moderately bioturbated, with local woody debris (black) in Section 4. Laminae may appear graded, but are commonly indistinct.</p> <p>SMEAR SLIDE SUMMARY (%):</p> <table border="1"> <tr> <td></td> <td>1, 80</td> <td>2, 100</td> <td>2, 120</td> <td>3, 88</td> <td>5, 33</td> </tr> <tr> <td></td> <td>D</td> <td>D</td> <td>M</td> <td>D</td> <td>D</td> </tr> </table> <p>TEXTURE:</p> <table border="1"> <tr> <td>Sand</td> <td>8</td> <td>5</td> <td>20</td> <td>5</td> <td>8</td> </tr> <tr> <td>Silt</td> <td>50</td> <td>40</td> <td>50</td> <td>60</td> <td>60</td> </tr> <tr> <td>Clay</td> <td>42</td> <td>55</td> <td>30</td> <td>35</td> <td>32</td> </tr> </table> <p>COMPOSITION:</p> <table border="1"> <tr> <td>Quartz</td> <td>50</td> <td>40</td> <td>35</td> <td>55</td> <td>55</td> </tr> <tr> <td>Feldspar</td> <td>2</td> <td>5</td> <td>4</td> <td>5</td> <td>10</td> </tr> <tr> <td>Mica</td> <td>Tr</td> <td>Tr</td> <td>3</td> <td>Tr</td> <td>Tr</td> </tr> <tr> <td>Clay</td> <td>36</td> <td>44</td> <td>25</td> <td>34</td> <td>28</td> </tr> <tr> <td>Volcanic glass</td> <td>Tr</td> <td>—</td> <td>Tr</td> <td>Tr</td> <td>—</td> </tr> <tr> <td>Calcite/dolomite</td> <td>10</td> <td>10</td> <td>5</td> <td>5</td> <td>5</td> </tr> <tr> <td>Accessory minerals</td> <td>2</td> <td>1</td> <td>1</td> <td>1</td> <td>2</td> </tr> <tr> <td>Pyrite</td> <td>—</td> <td>—</td> <td>27</td> <td>—</td> <td>—</td> </tr> <tr> <td>Diatoms</td> <td>—</td> <td>—</td> <td>Tr</td> <td>—</td> <td>—</td> </tr> <tr> <td>Sponge spicules</td> <td>—</td> <td>—</td> <td>Tr</td> <td>—</td> <td>—</td> </tr> </table>		1, 80	2, 100	2, 120	3, 88	5, 33		D	D	M	D	D	Sand	8	5	20	5	8	Silt	50	40	50	60	60	Clay	42	55	30	35	32	Quartz	50	40	35	55	55	Feldspar	2	5	4	5	10	Mica	Tr	Tr	3	Tr	Tr	Clay	36	44	25	34	28	Volcanic glass	Tr	—	Tr	Tr	—	Calcite/dolomite	10	10	5	5	5	Accessory minerals	2	1	1	1	2	Pyrite	—	—	27	—	—	Diatoms	—	—	Tr	—	—	Sponge spicules	—	—	Tr	—	—
	1, 80	2, 100	2, 120	3, 88	5, 33																																																																																																				
	D	D	M	D	D																																																																																																				
Sand	8	5	20	5	8																																																																																																				
Silt	50	40	50	60	60																																																																																																				
Clay	42	55	30	35	32																																																																																																				
Quartz	50	40	35	55	55																																																																																																				
Feldspar	2	5	4	5	10																																																																																																				
Mica	Tr	Tr	3	Tr	Tr																																																																																																				
Clay	36	44	25	34	28																																																																																																				
Volcanic glass	Tr	—	Tr	Tr	—																																																																																																				
Calcite/dolomite	10	10	5	5	5																																																																																																				
Accessory minerals	2	1	1	1	2																																																																																																				
Pyrite	—	—	27	—	—																																																																																																				
Diatoms	—	—	Tr	—	—																																																																																																				
Sponge spicules	—	—	Tr	—	—																																																																																																				
F/M	<i>(agglutinated fauna; Bolboforma sp.)</i>						● $\gamma = 1.95 \phi = 49.0$ W=35	● CaCO ₃ = 21	1	0.5	(S)			*																																																																																											
B									2	1.0	(C)			*																																																																																											
B									3					*																																																																																											
B									4					*																																																																																											
R/M									5					*																																																																																											
N.C.							● $\gamma = 2.18 \phi = 37.1$ W=21	● TOC = 1.58 CaCO ₃ = 0.38							OG																																																																																										

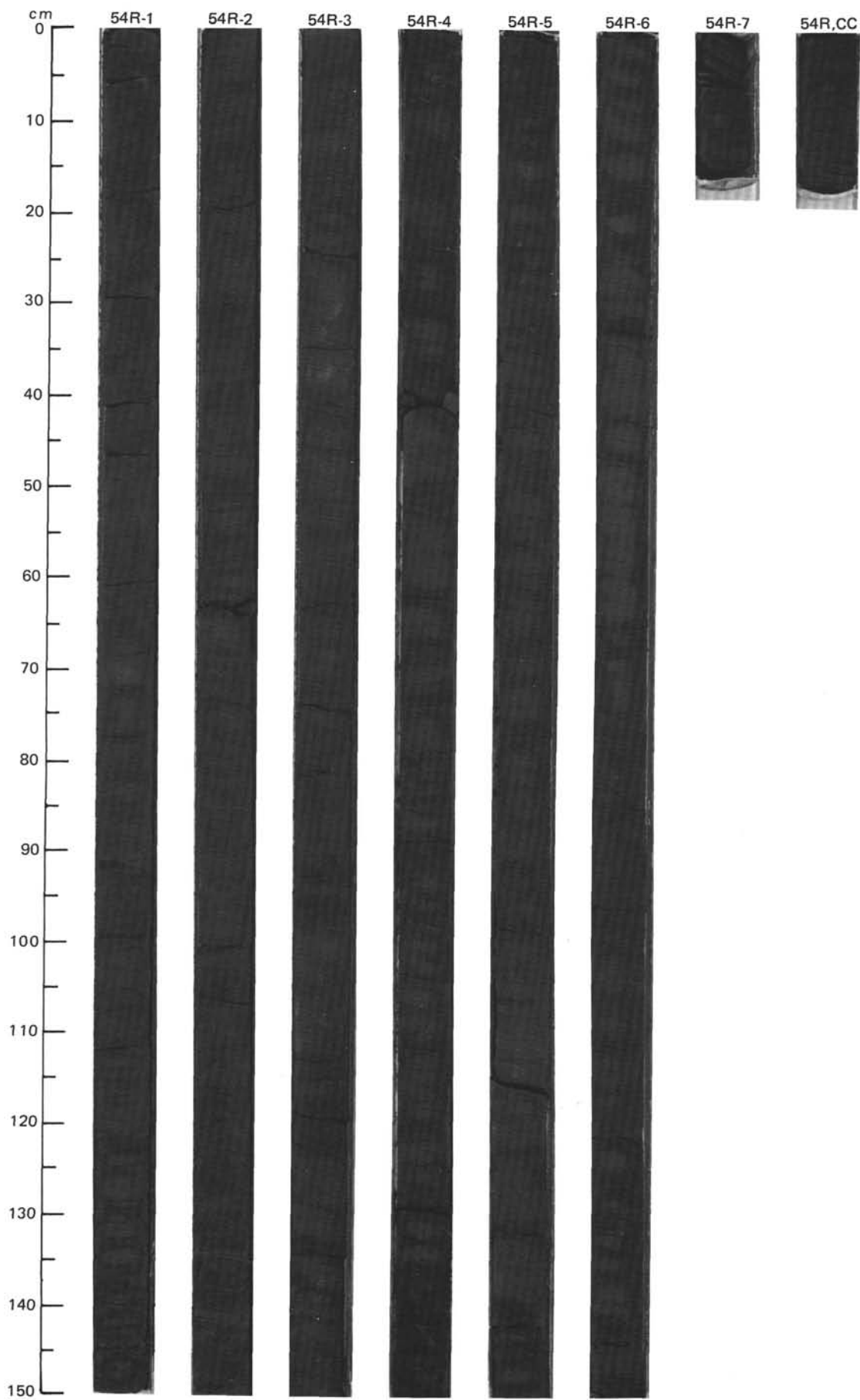


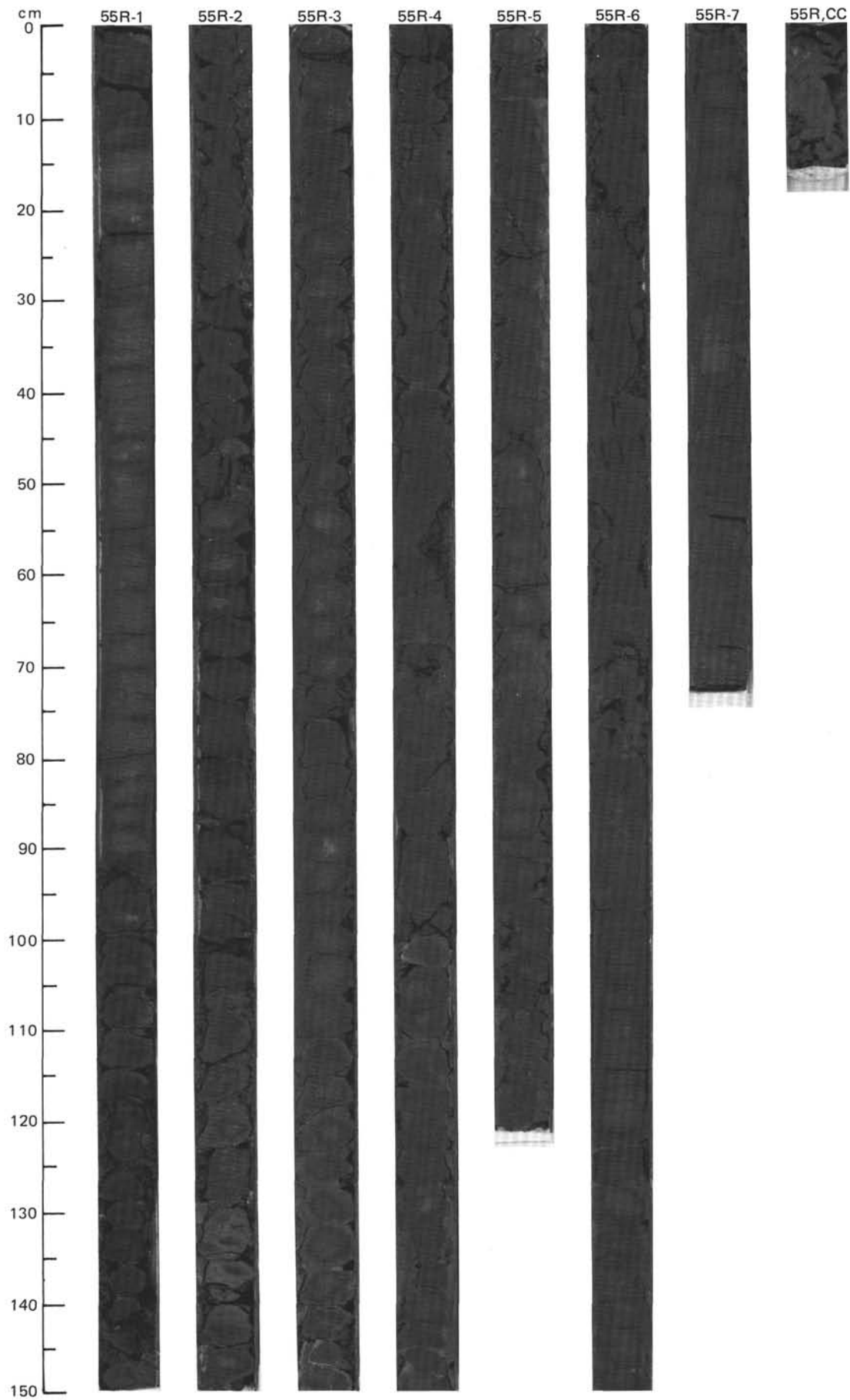
SITE 645 HOLE E CORE 53 R CORED INTERVAL 2905.1-2914.7 mbsl; 897.6-907.2 mbsf

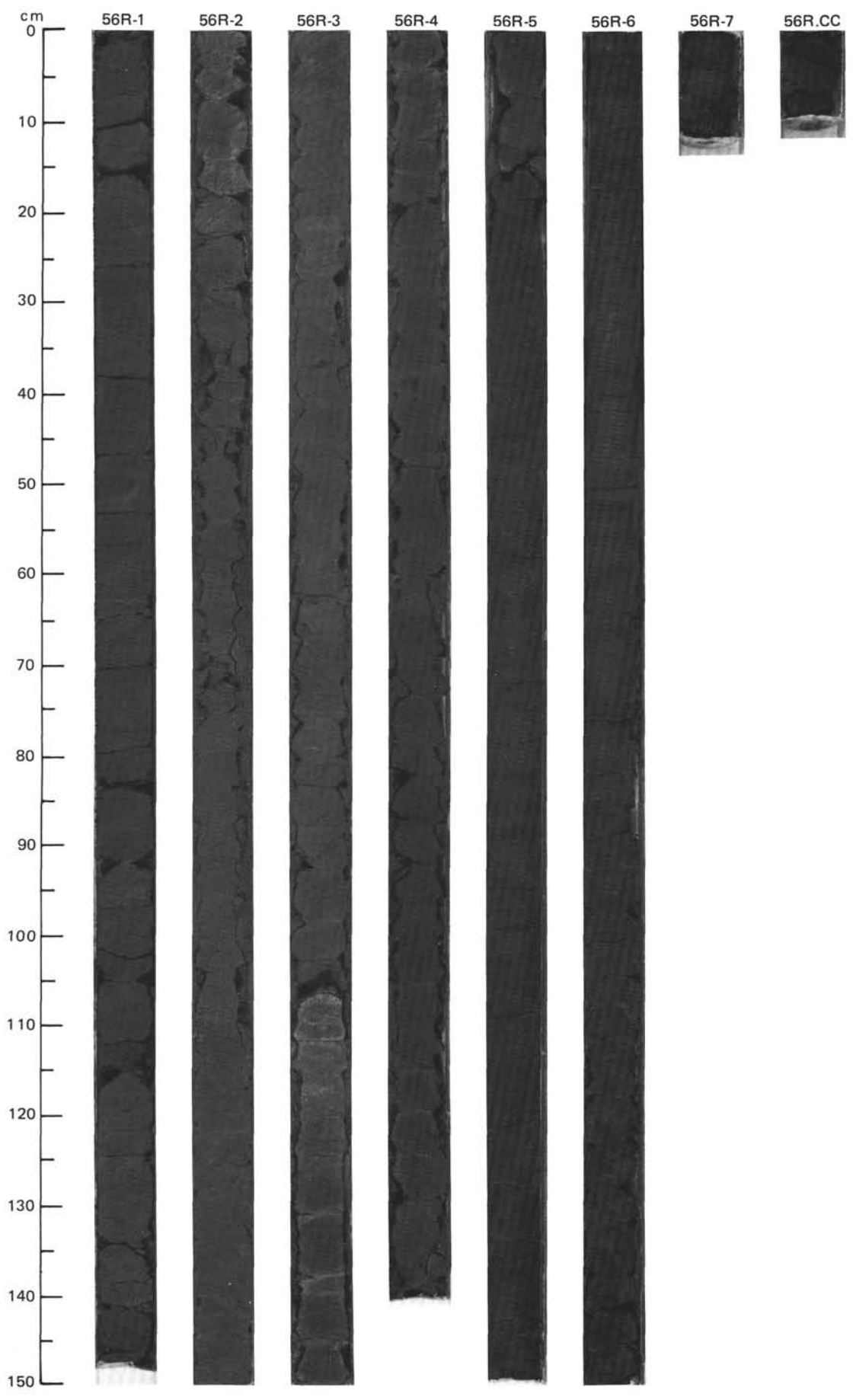


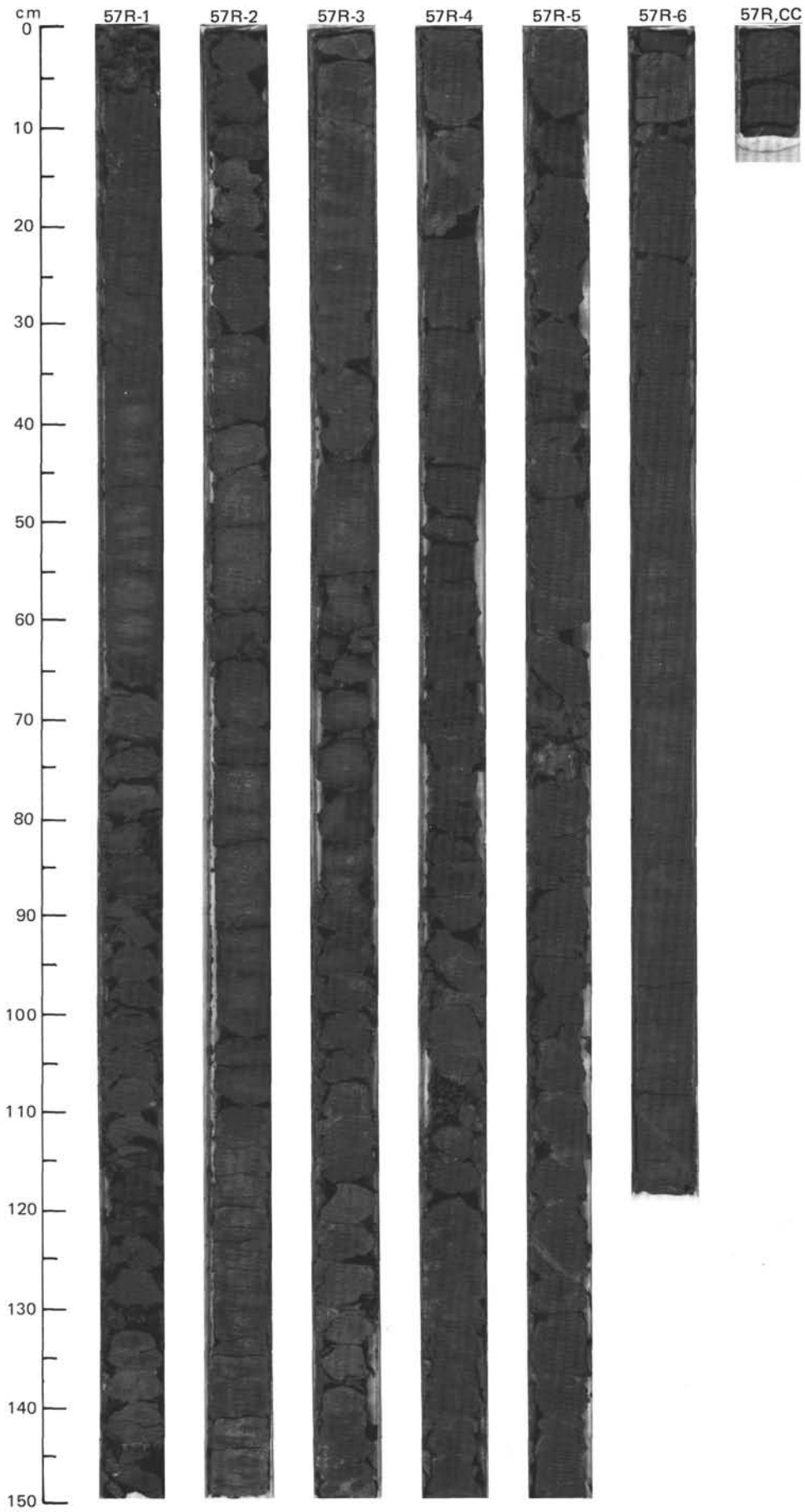


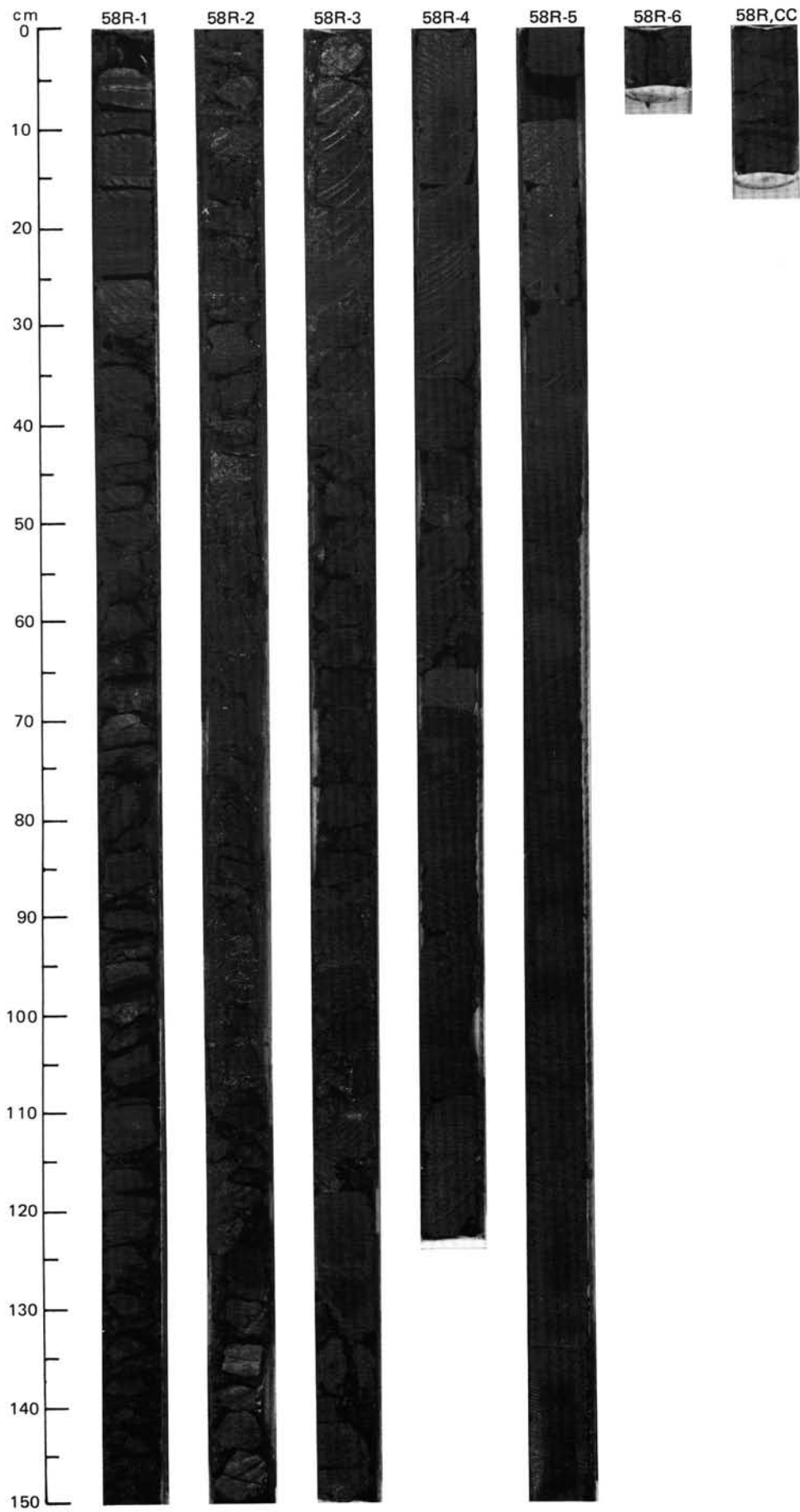


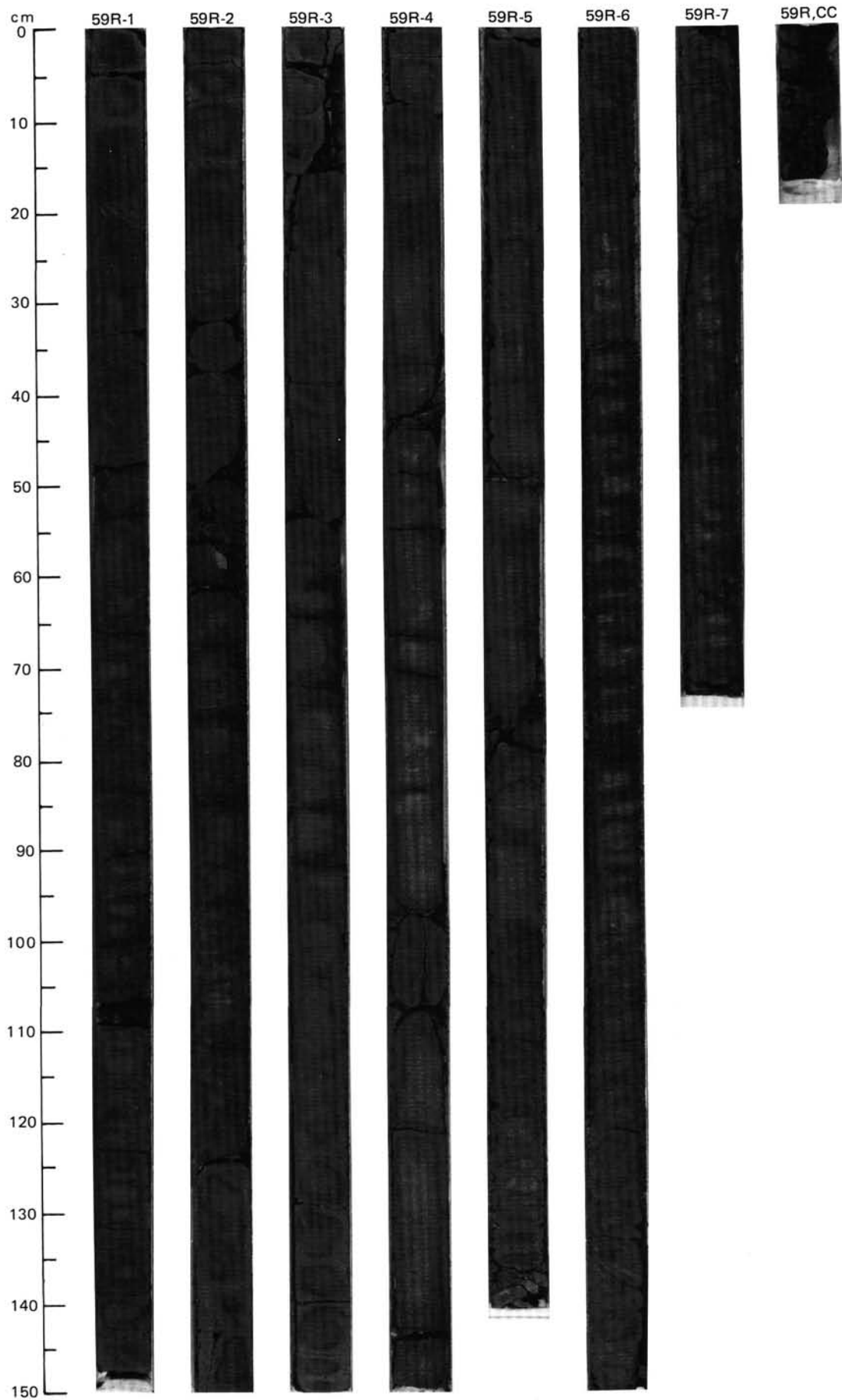


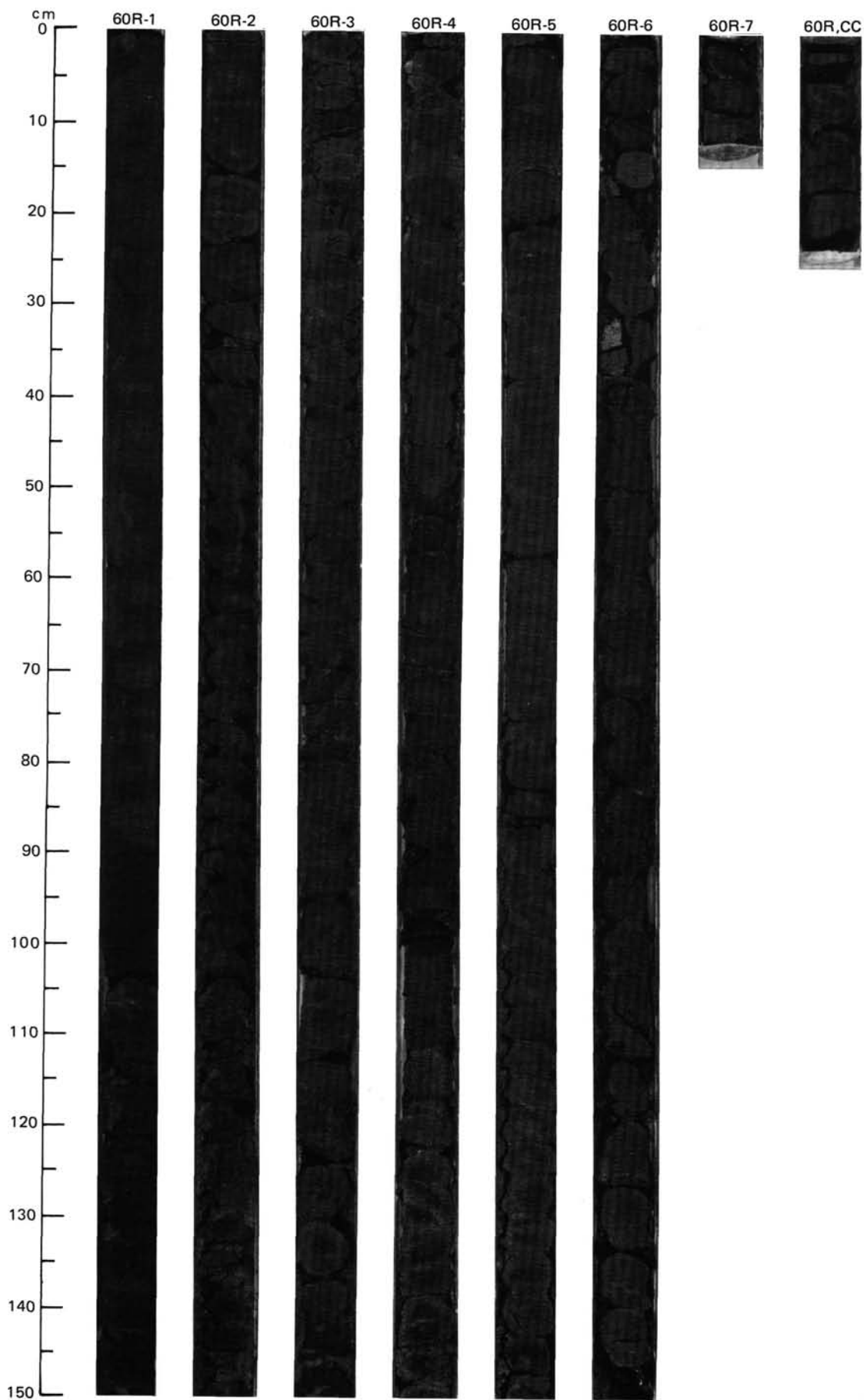


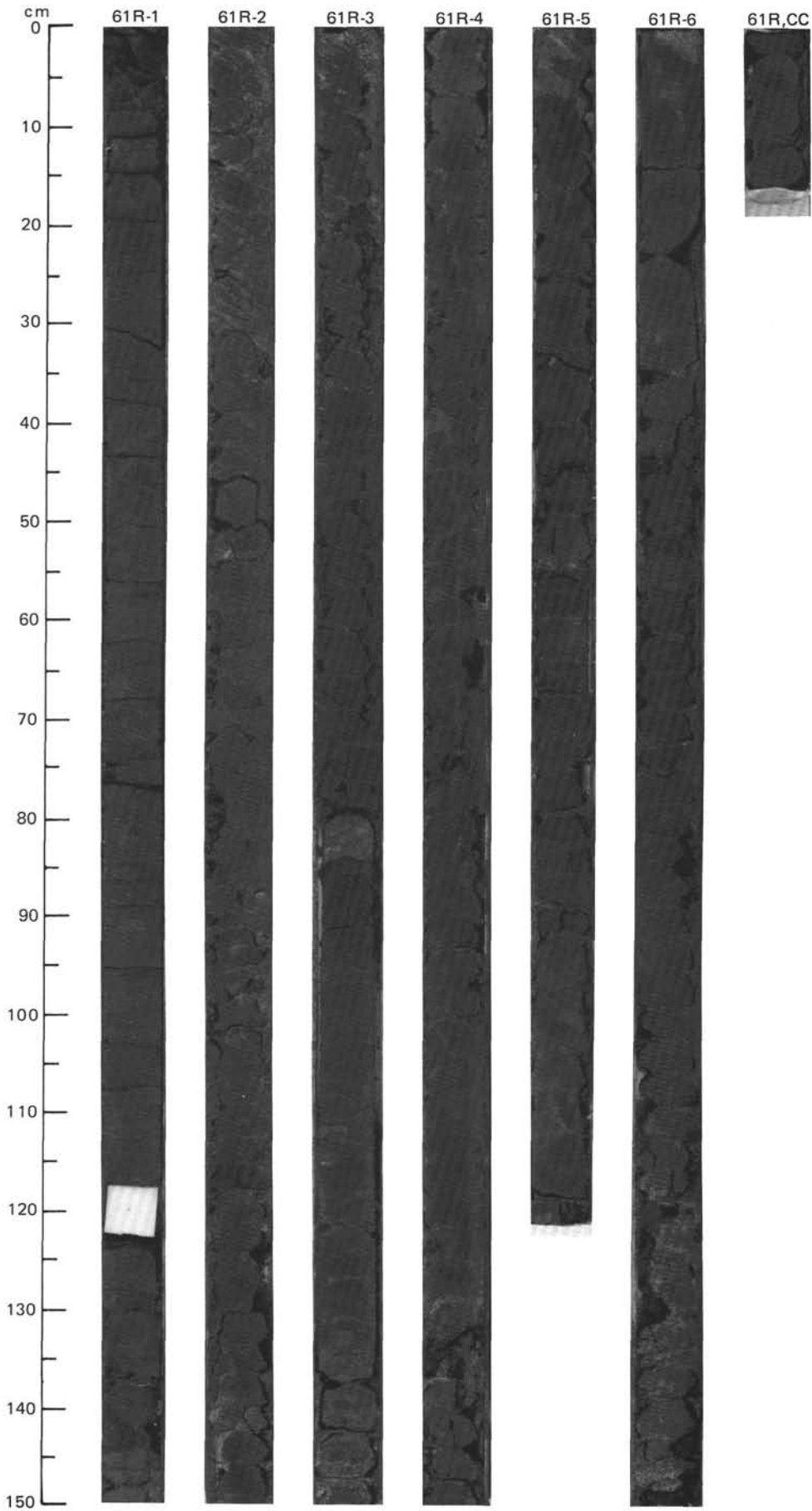






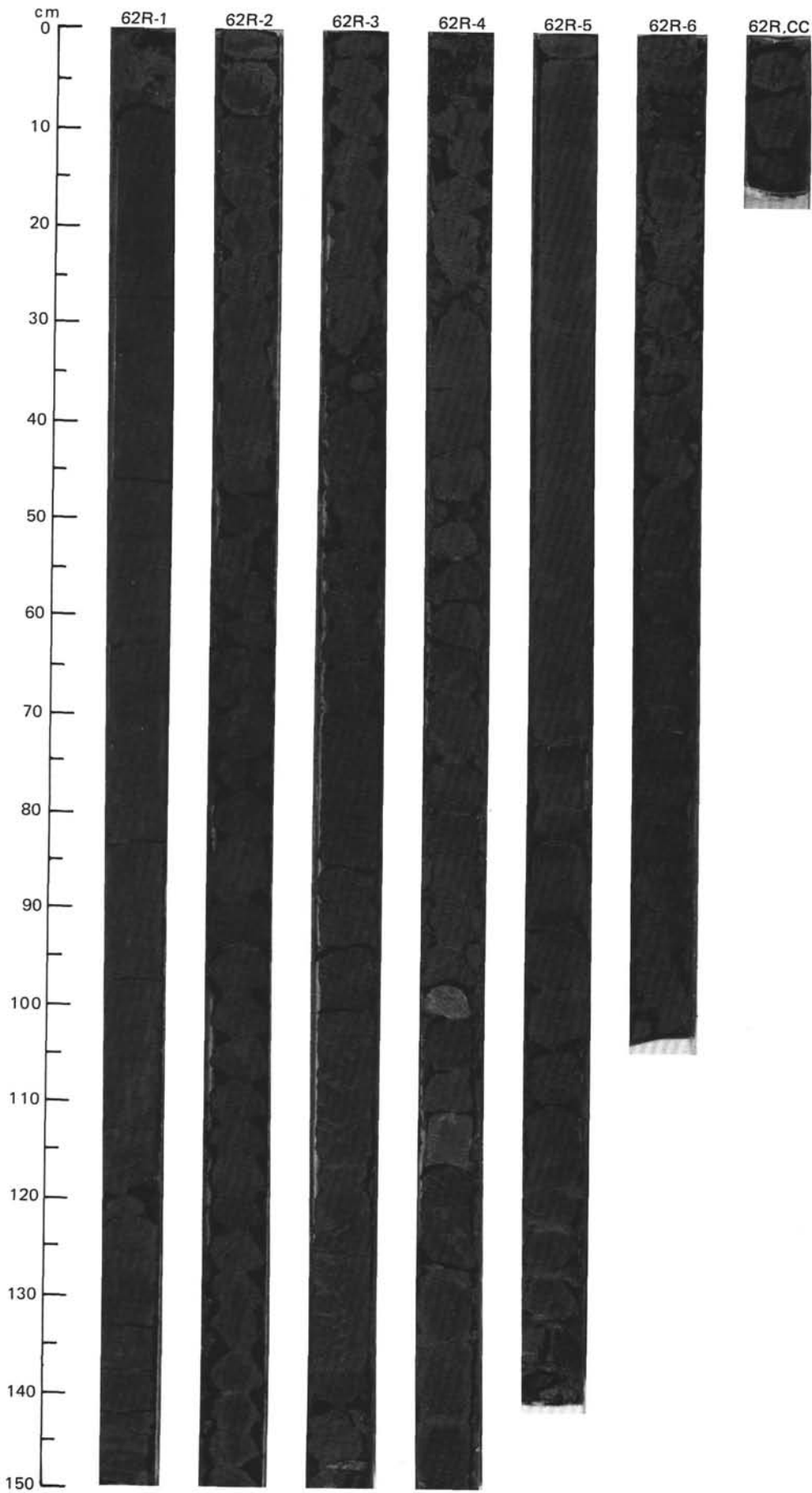


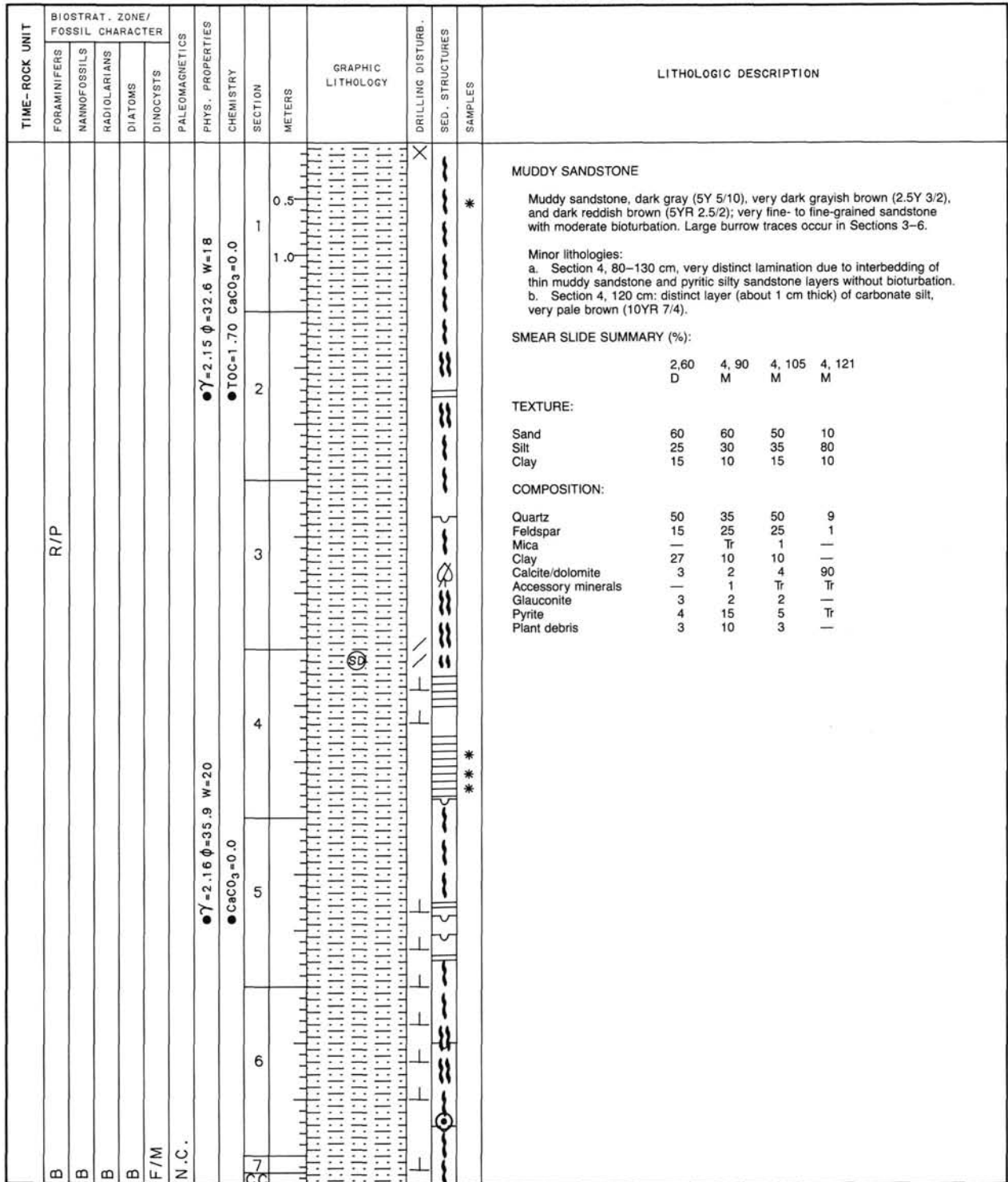


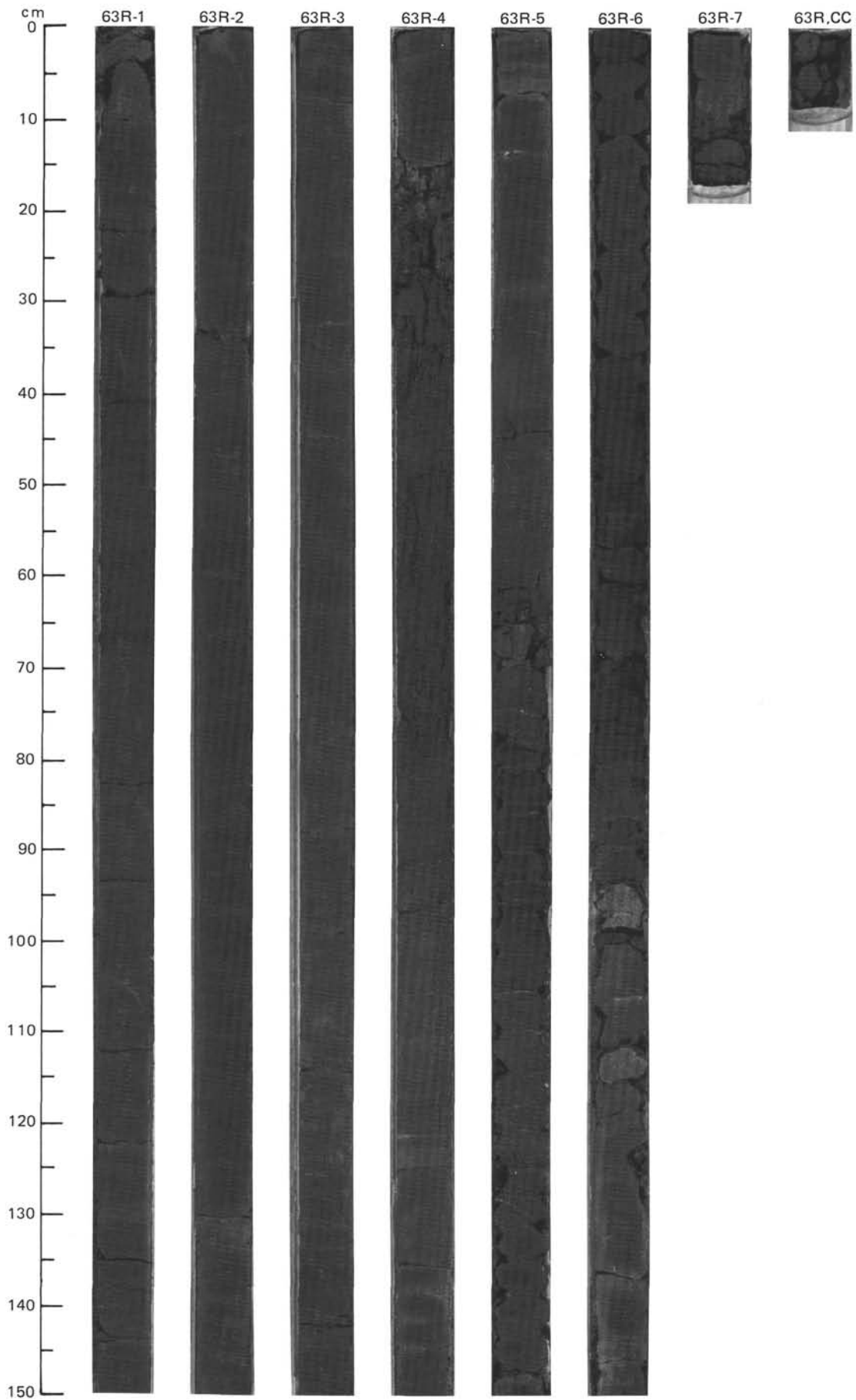


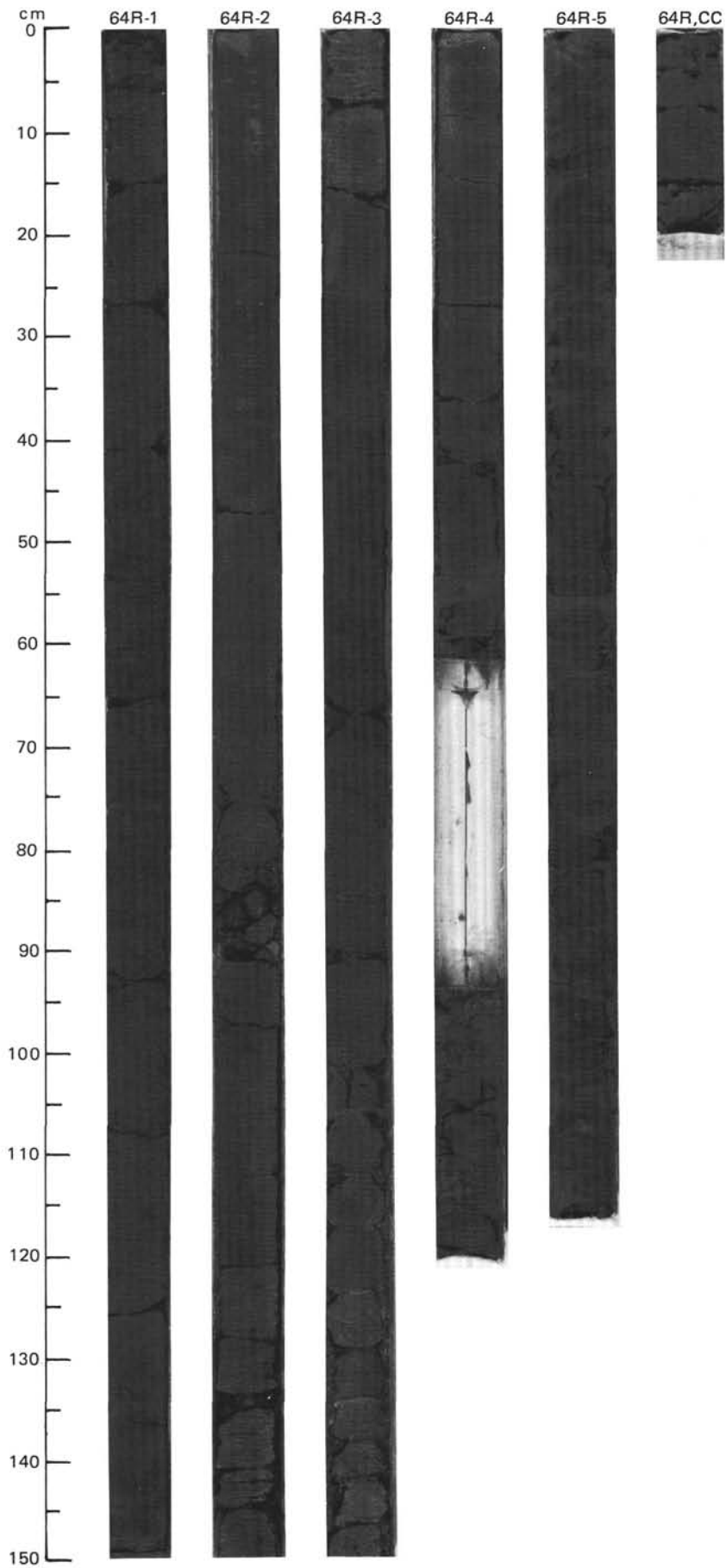
SITE 645 HOLE E CORE 62 R CORED INTERVAL 2992.0-3001.7 mbsl; 984.5-994.2 mbsf

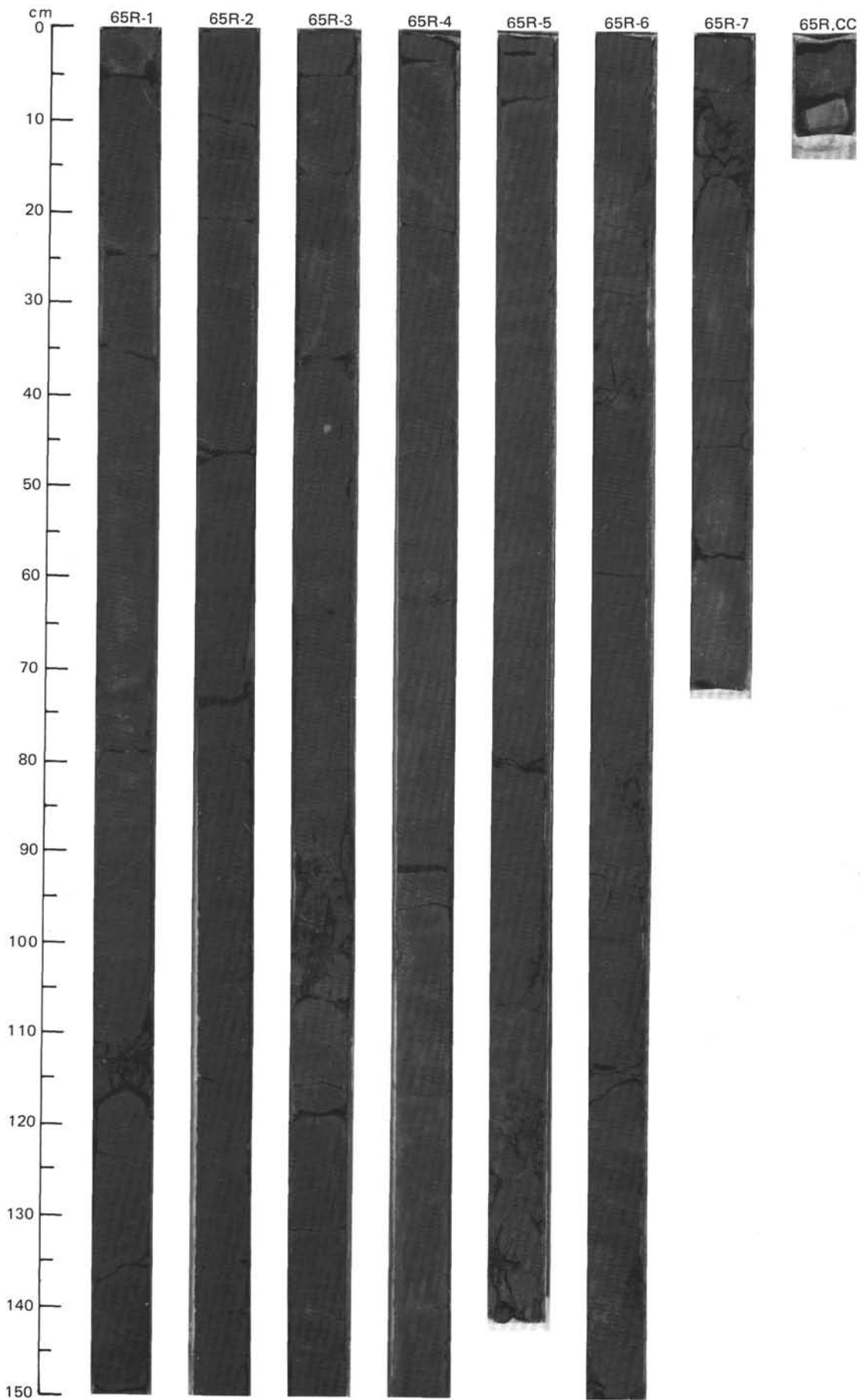
TIME-ROCK UNIT	BIOSTRAT. ZONE/ FOSSIL CHARACTER					PALEOMAGNETICS	PHYS. PROPERTIES	CHEMISTRY	SECTION	METERS	GRAPHIC LITHOLOGY	DRILLING DISTURB.	SED. STRUCTURES	SAMPLES	LITHOLOGIC DESCRIPTION																																							
	FORAMINIFERS	NANNOFOSSILS	RADIOLARIANS	DIATOMS	DINOCTYST																																																	
LOWER TO MIDDLE MIOCENE	R/M									0.5					<p>SILTY MUDSTONE AND MUDDY SANDSTONE</p> <p>Silty mudstone, very dark grayish brown (2.5Y 3/2), with interbedded muddy sandstone, dark olive gray (5Y 3/2). Contacts are gradational; both facies are vaguely laminated and banded with moderate bioturbation and mottling. Scattered throughout are white specks of agglutinated foraminifera and indistinct lenses of sand and silt grains.</p> <p>SMEAR SLIDE SUMMARY (%):</p> <table border="1"> <tr> <td></td> <td>1, 130</td> <td>2, 125</td> </tr> <tr> <td></td> <td>D</td> <td>D</td> </tr> </table> <p>TEXTURE:</p> <table border="1"> <tr> <td>Sand</td> <td>20</td> <td>40</td> </tr> <tr> <td>Silt</td> <td>50</td> <td>30</td> </tr> <tr> <td>Clay</td> <td>30</td> <td>30</td> </tr> </table> <p>COMPOSITION:</p> <table border="1"> <tr> <td>Quartz</td> <td>45</td> <td>45</td> </tr> <tr> <td>Feldspar</td> <td>10</td> <td>10</td> </tr> <tr> <td>Rock fragments</td> <td>—</td> <td>5</td> </tr> <tr> <td>Mica</td> <td>5</td> <td>5</td> </tr> <tr> <td>Clay</td> <td>30</td> <td>30</td> </tr> <tr> <td>Calcite/dolomite</td> <td>Tr</td> <td>—</td> </tr> <tr> <td>Accessory minerals</td> <td>5</td> <td>5</td> </tr> <tr> <td>Pyrite</td> <td>5</td> <td>—</td> </tr> </table>		1, 130	2, 125		D	D	Sand	20	40	Silt	50	30	Clay	30	30	Quartz	45	45	Feldspar	10	10	Rock fragments	—	5	Mica	5	5	Clay	30	30	Calcite/dolomite	Tr	—	Accessory minerals	5	5	Pyrite	5	—
		1, 130	2, 125																																																			
		D	D																																																			
	Sand	20	40																																																			
	Silt	50	30																																																			
	Clay	30	30																																																			
Quartz	45	45																																																				
Feldspar	10	10																																																				
Rock fragments	—	5																																																				
Mica	5	5																																																				
Clay	30	30																																																				
Calcite/dolomite	Tr	—																																																				
Accessory minerals	5	5																																																				
Pyrite	5	—																																																				
	R/G					● $\gamma = 2.14$ $\phi = 35.2$ $W = 20.2$	● $\text{TOC} = 1.11$ $\text{CaCO}_3 = 0.92$	1	1.0																																													
	B							2																																														
	B							3																																														
	N.C.					● $\gamma = 2.15$ $\phi = 35.3$ $W = 20$	● $\text{CaCO}_3 = 1.2$	4																																														
	C							5																																														
								6																																														



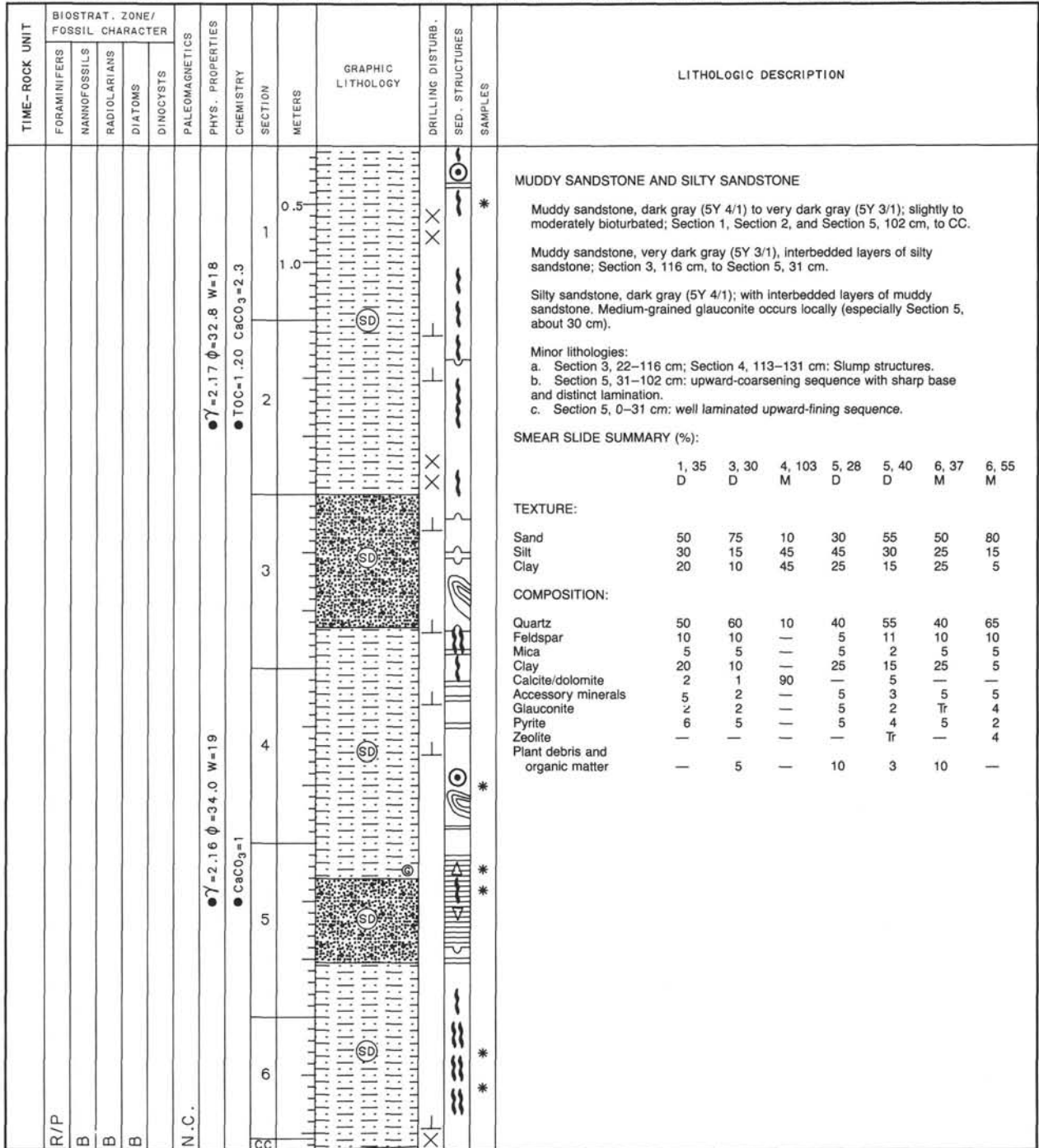


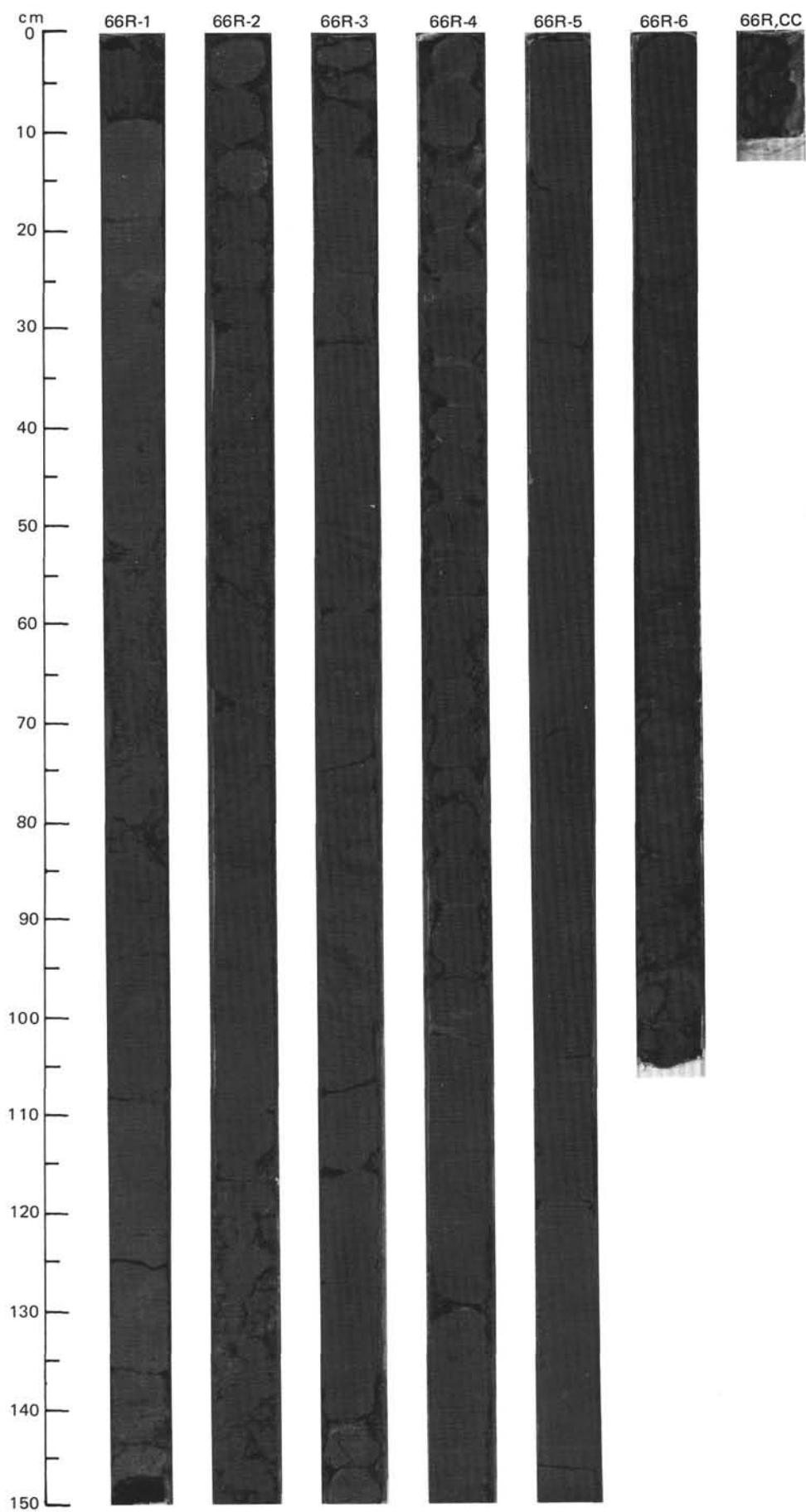


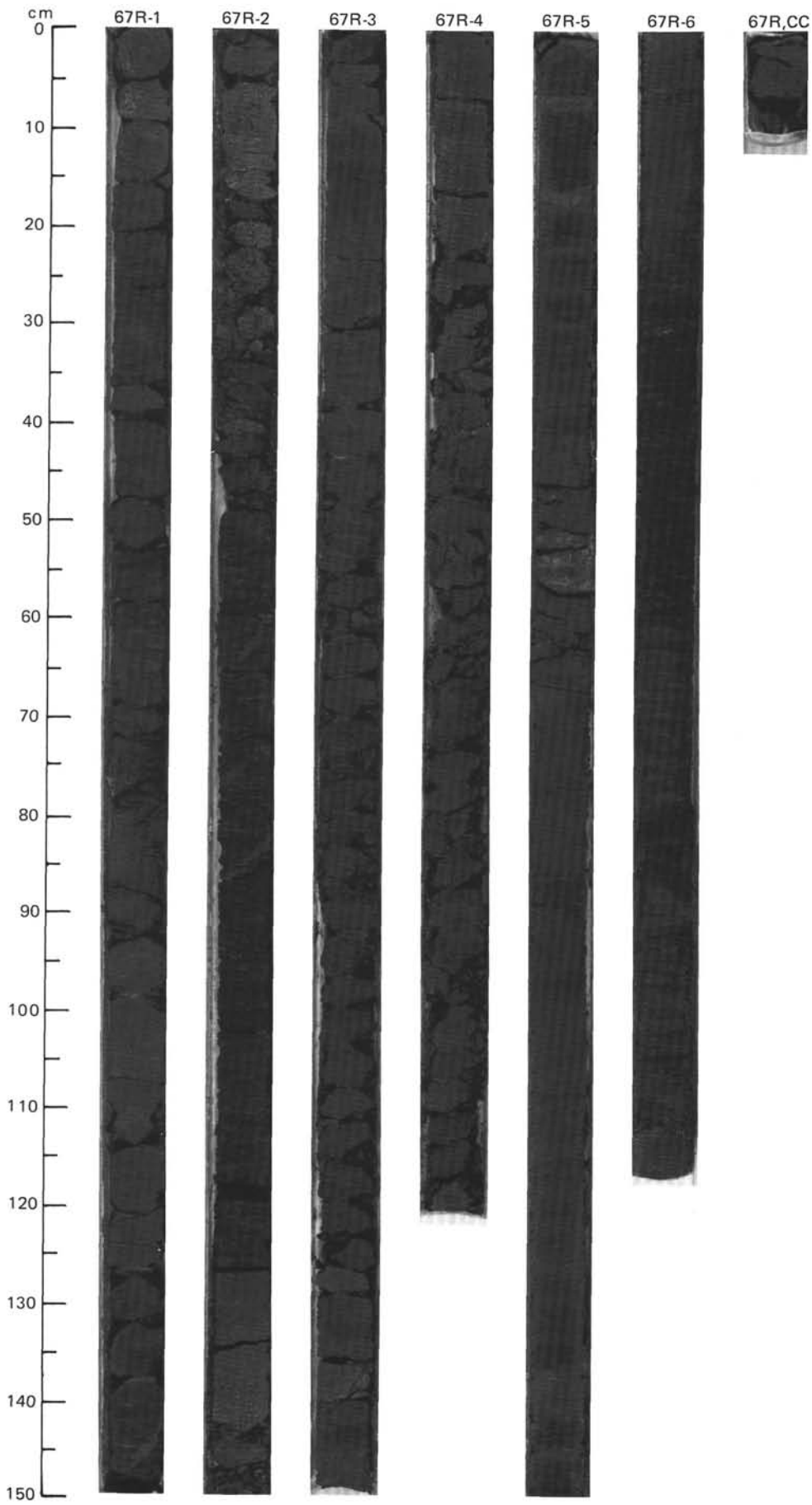




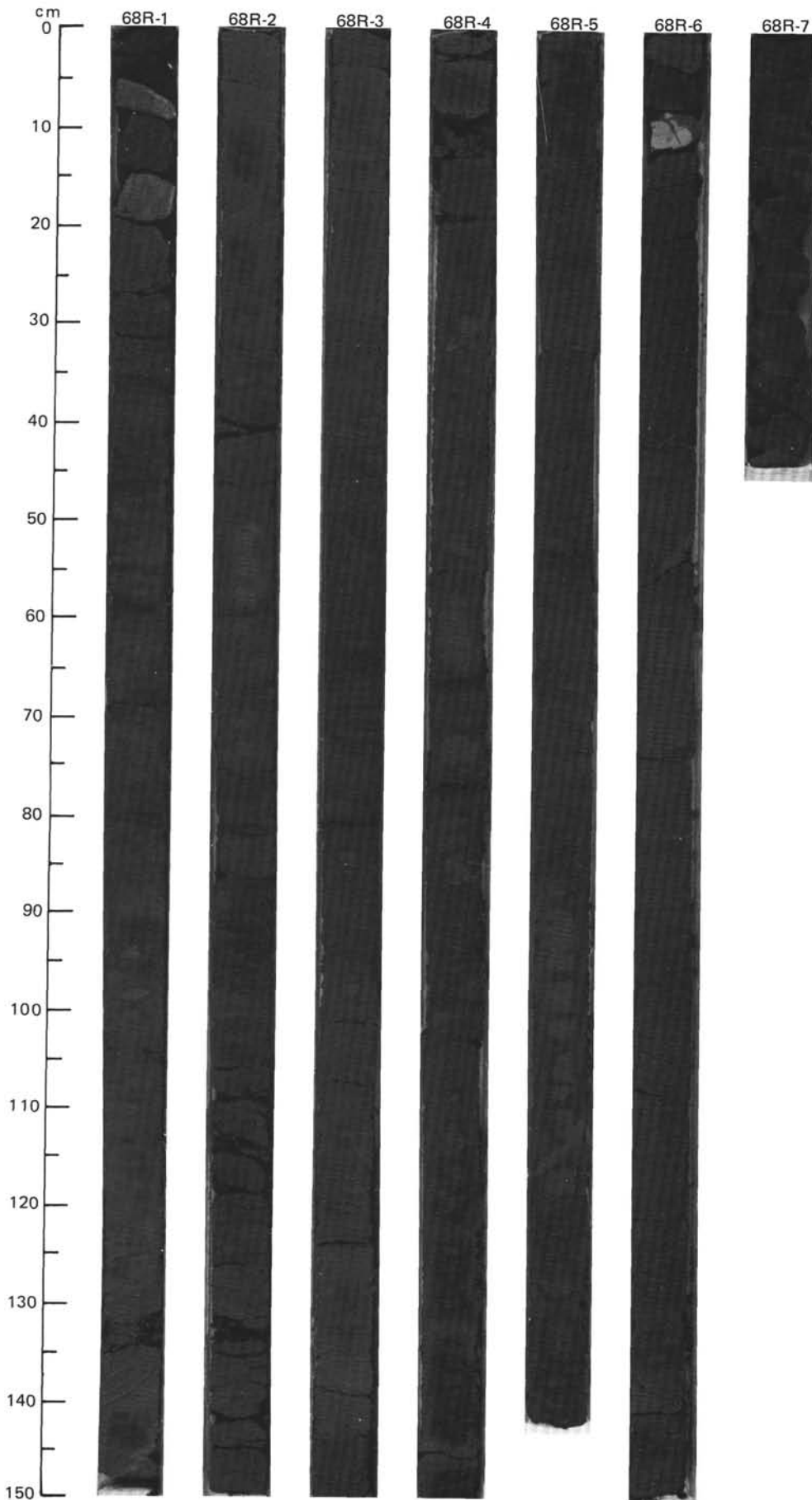
SITE 645 HOLE E CORE 66 R CORED INTERVAL 3031.8-3040.4 mbsl; 1023.3-1032.9 mbsf





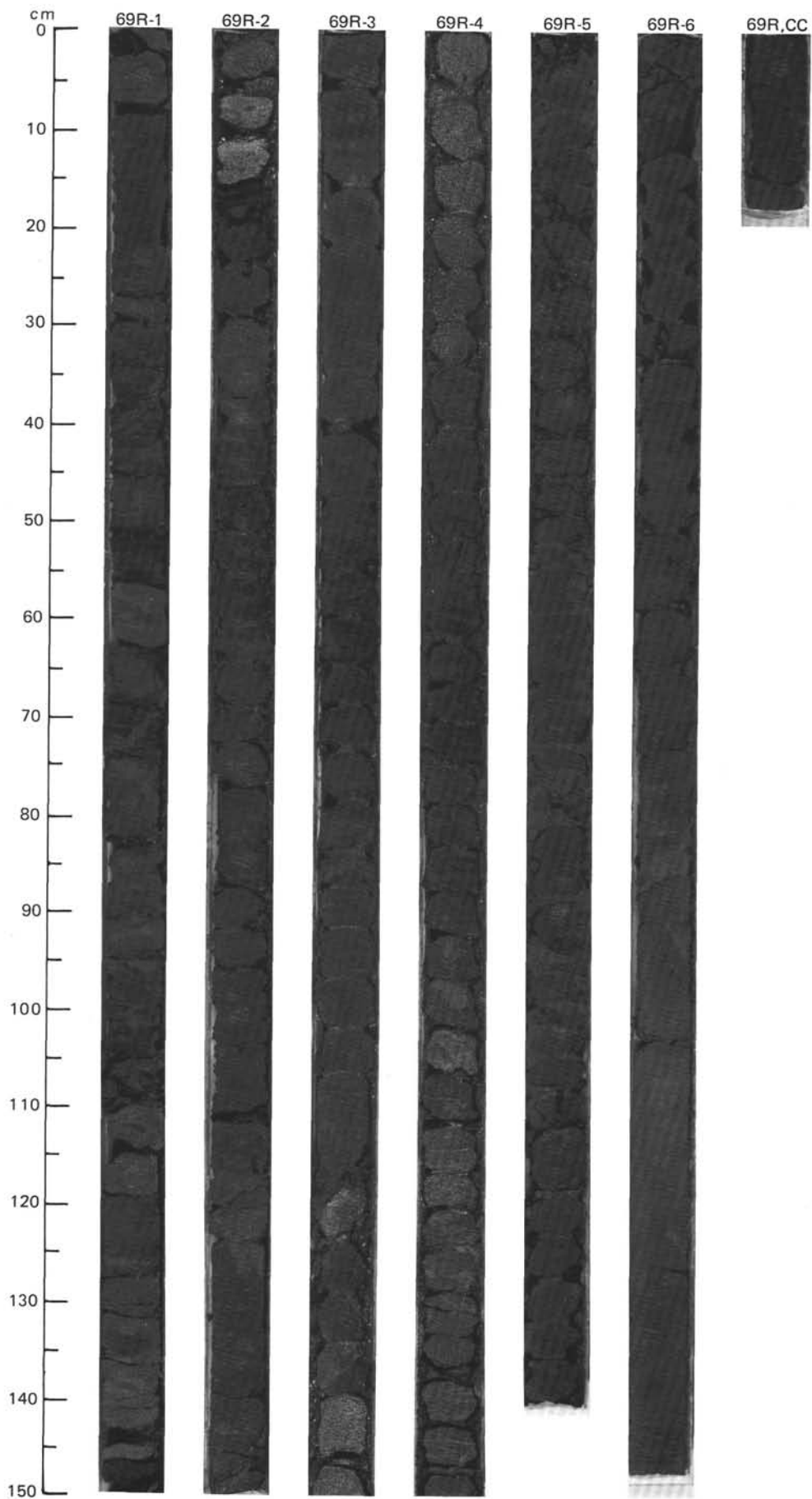


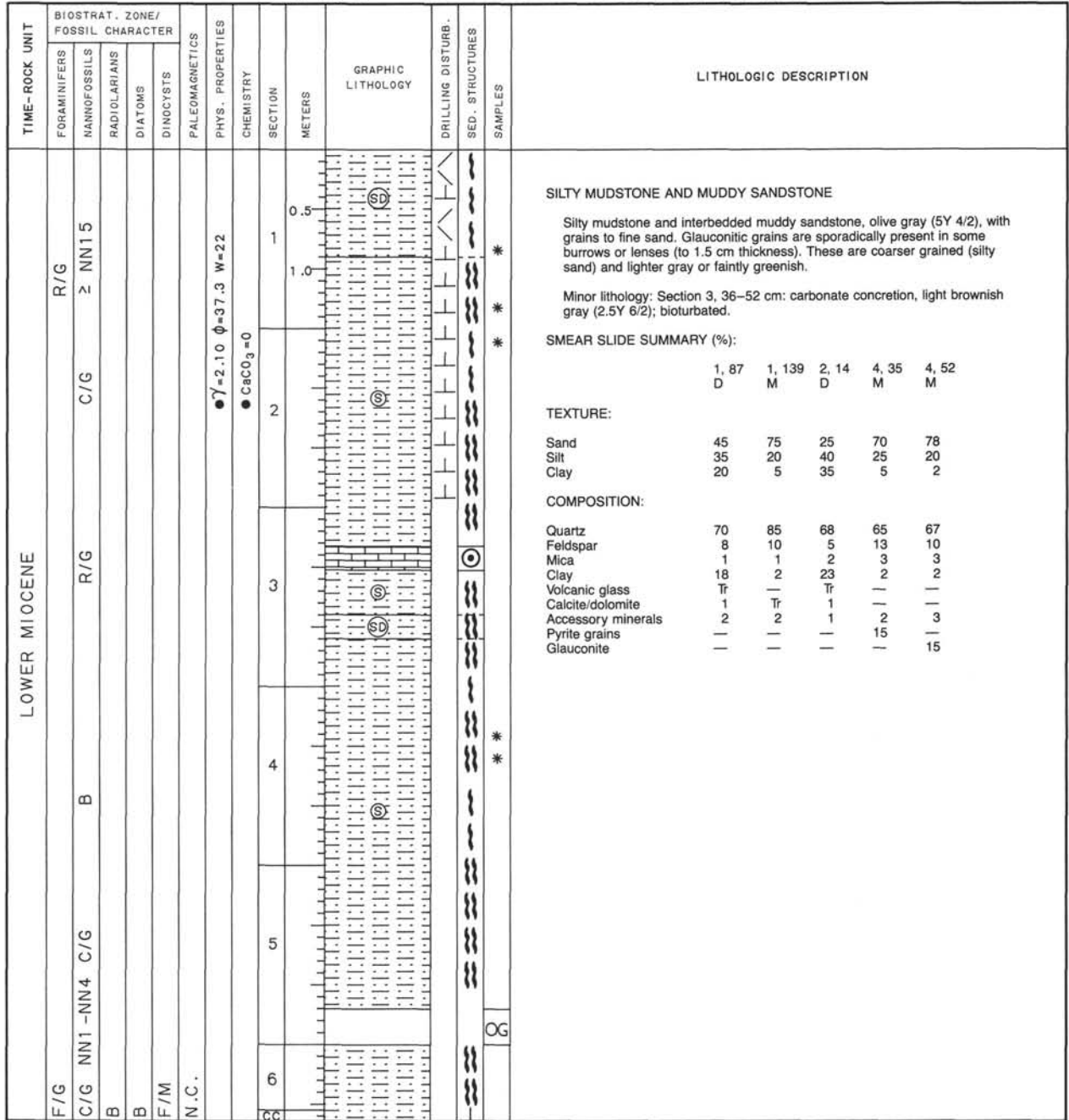
TIME-ROCK UNIT	BIOSTRAT. ZONE/ FOSSIL CHARACTER					PALEOMAGNETICS	PHYS. PROPERTIES	CHEMISTRY	SECTION	METERS	GRAPHIC LITHOLOGY	DRILLING DISTURB.	SED. STRUCTURES	SAMPLES	LITHOLOGIC DESCRIPTION																																																																																																																							
	FORAMINIFERS	NANNOFOSSILS	RADIOLARIANS	DIATOMS	DINOCTYSTS																																																																																																																																	
R/P	F/M						$\gamma = 2.16 \phi = 35.5 W = 20$	TOC=0.82 CaCO ₃ =0.0	1	0.5					<p>SILTY MUDSTONE, CLAYEY SILT, AND SILTY SAND</p> <p>Silty mudstone, olive gray (5Y 4/2); with dark gray laminae of clayey silt (a few mm thick) and lighter gray lenses of silty sand. Burrows, probably <i>Spreiten</i>, occasionally seen as lenses of very fine to fine sand. Interspersed, are more homogeneous areas with less bioturbation. An area of very distinct parallel lamination of silty sand and clayey silt occurs at Section 6, 12-96 cm. Laminae are distinct (about 1-2 mm thick).</p> <p>SMEAR SLIDE SUMMARY (%):</p> <table border="1"> <thead> <tr> <th></th> <th>1, 44</th> <th>1, 107</th> <th>2, 125</th> <th>3, 47</th> <th>4, 86</th> <th>6, 120</th> </tr> <tr> <th></th> <th>M</th> <th>D</th> <th>D</th> <th>M</th> <th>D</th> <th>D</th> </tr> </thead> <tbody> <tr> <td>TEXTURE:</td> <td></td> <td></td> <td></td> <td></td> <td></td> <td></td> </tr> <tr> <td>Sand</td> <td>8</td> <td>35</td> <td>15</td> <td>50</td> <td>15</td> <td>20</td> </tr> <tr> <td>Silt</td> <td>50</td> <td>40</td> <td>50</td> <td>45</td> <td>50</td> <td>50</td> </tr> <tr> <td>Clay</td> <td>42</td> <td>25</td> <td>35</td> <td>5</td> <td>35</td> <td>30</td> </tr> <tr> <td>COMPOSITION:</td> <td></td> <td></td> <td></td> <td></td> <td></td> <td></td> </tr> <tr> <td>Quartz</td> <td>60</td> <td>70</td> <td>65</td> <td>80</td> <td>60</td> <td>40</td> </tr> <tr> <td>Feldspar</td> <td>5</td> <td>10</td> <td>5</td> <td>10</td> <td>5</td> <td>10</td> </tr> <tr> <td>Mica</td> <td>Tr</td> <td>5</td> <td>3</td> <td>5</td> <td>2</td> <td>5</td> </tr> <tr> <td>Clay</td> <td>34</td> <td>10</td> <td>24</td> <td>4</td> <td>29</td> <td>18</td> </tr> <tr> <td>Volcanic glass</td> <td>Tr</td> <td>Tr</td> <td>Tr</td> <td>Tr</td> <td>Tr</td> <td>—</td> </tr> <tr> <td>Calcite/dolomite</td> <td>Tr</td> <td>2</td> <td>2</td> <td>Tr</td> <td>3</td> <td>—</td> </tr> <tr> <td>Accessory minerals</td> <td>1</td> <td>3</td> <td>1</td> <td>1</td> <td>1</td> <td>2</td> </tr> <tr> <td>Glauconite</td> <td>—</td> <td>—</td> <td>—</td> <td>—</td> <td>—</td> <td>5</td> </tr> <tr> <td>Pellets</td> <td>—</td> <td>—</td> <td>—</td> <td>—</td> <td>—</td> <td>20</td> </tr> <tr> <td>Nannofossils</td> <td>—</td> <td>—</td> <td>Tr</td> <td>—</td> <td>Tr</td> <td>—</td> </tr> </tbody> </table>		1, 44	1, 107	2, 125	3, 47	4, 86	6, 120		M	D	D	M	D	D	TEXTURE:							Sand	8	35	15	50	15	20	Silt	50	40	50	45	50	50	Clay	42	25	35	5	35	30	COMPOSITION:							Quartz	60	70	65	80	60	40	Feldspar	5	10	5	10	5	10	Mica	Tr	5	3	5	2	5	Clay	34	10	24	4	29	18	Volcanic glass	Tr	Tr	Tr	Tr	Tr	—	Calcite/dolomite	Tr	2	2	Tr	3	—	Accessory minerals	1	3	1	1	1	2	Glauconite	—	—	—	—	—	5	Pellets	—	—	—	—	—	20	Nannofossils	—	—	Tr	—	Tr	—
	1, 44	1, 107	2, 125	3, 47	4, 86	6, 120																																																																																																																																
	M	D	D	M	D	D																																																																																																																																
TEXTURE:																																																																																																																																						
Sand	8	35	15	50	15	20																																																																																																																																
Silt	50	40	50	45	50	50																																																																																																																																
Clay	42	25	35	5	35	30																																																																																																																																
COMPOSITION:																																																																																																																																						
Quartz	60	70	65	80	60	40																																																																																																																																
Feldspar	5	10	5	10	5	10																																																																																																																																
Mica	Tr	5	3	5	2	5																																																																																																																																
Clay	34	10	24	4	29	18																																																																																																																																
Volcanic glass	Tr	Tr	Tr	Tr	Tr	—																																																																																																																																
Calcite/dolomite	Tr	2	2	Tr	3	—																																																																																																																																
Accessory minerals	1	3	1	1	1	2																																																																																																																																
Glauconite	—	—	—	—	—	5																																																																																																																																
Pellets	—	—	—	—	—	20																																																																																																																																
Nannofossils	—	—	Tr	—	Tr	—																																																																																																																																
B							$\gamma = 2.2 \phi = 33.9 W = 18.8$	CaCO ₃ =0	2	1.0																																																																																																																												
B									3																																																																																																																													
B									4																																																																																																																													
N.C.									5																																																																																																																													
									6																																																																																																																													
									7																																																																																																																													

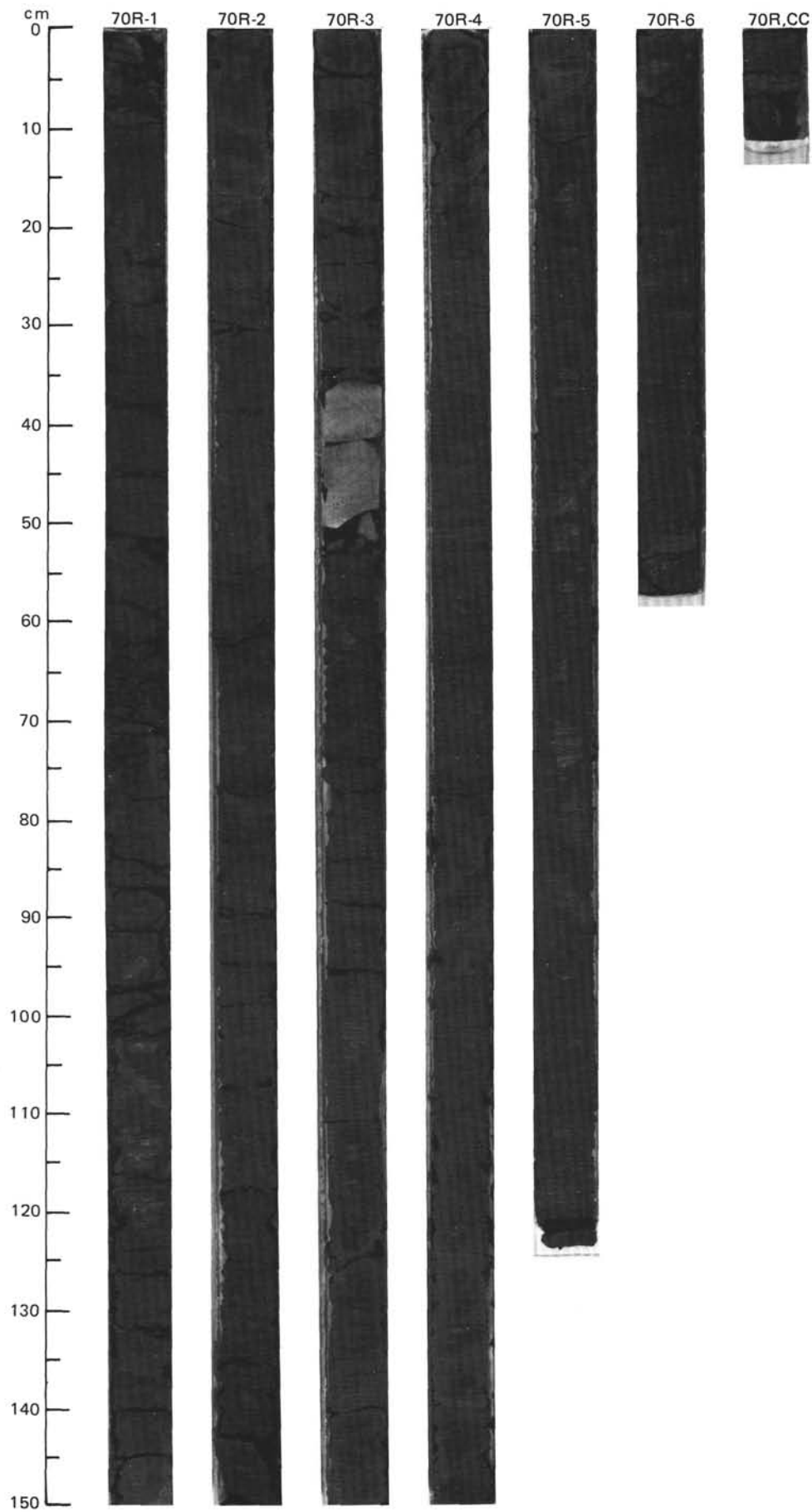


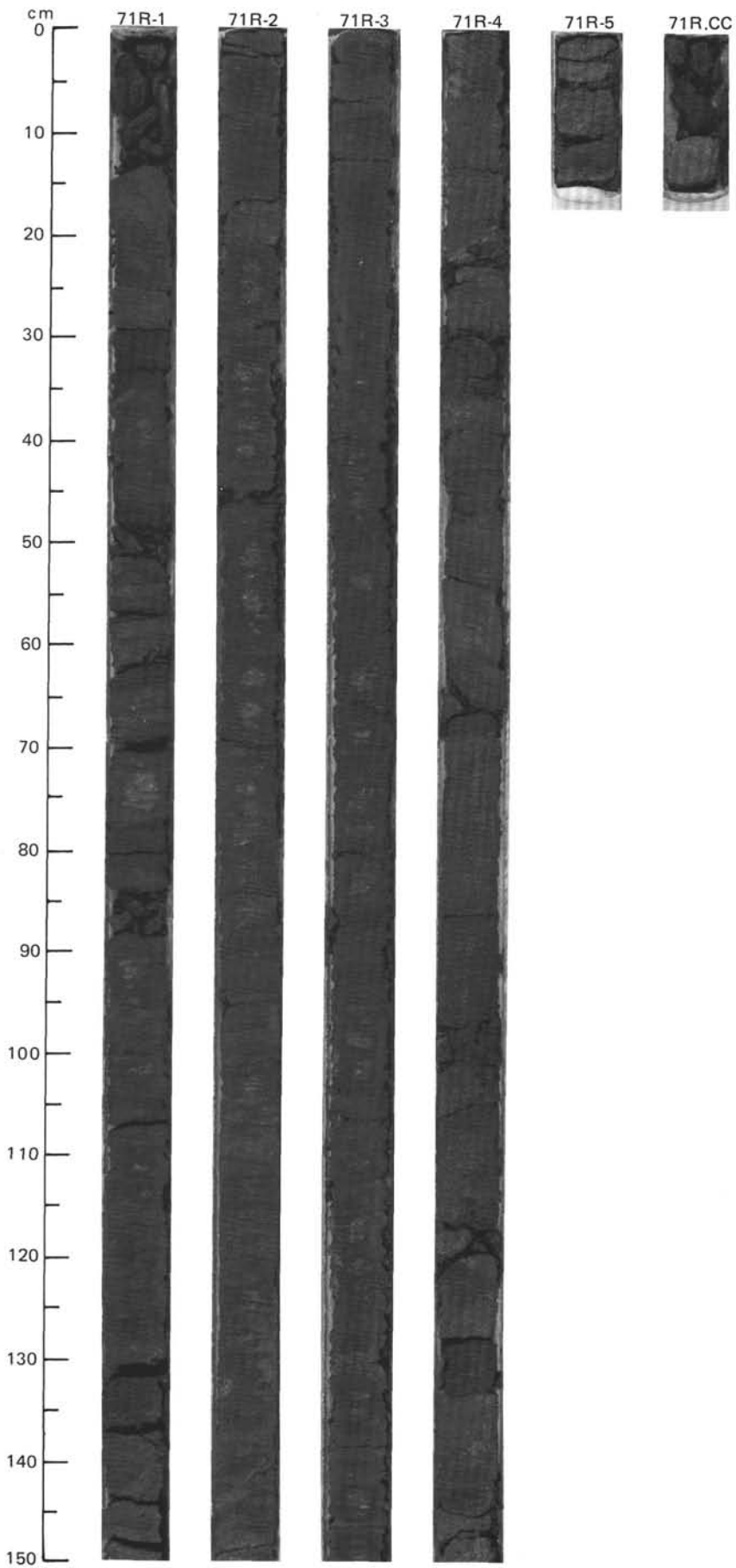
SITE 645 HOLE E CORE 69 R CORED INTERVAL 3059.7-3069.4 mbsl; 1052.2-1061.9 mbsf

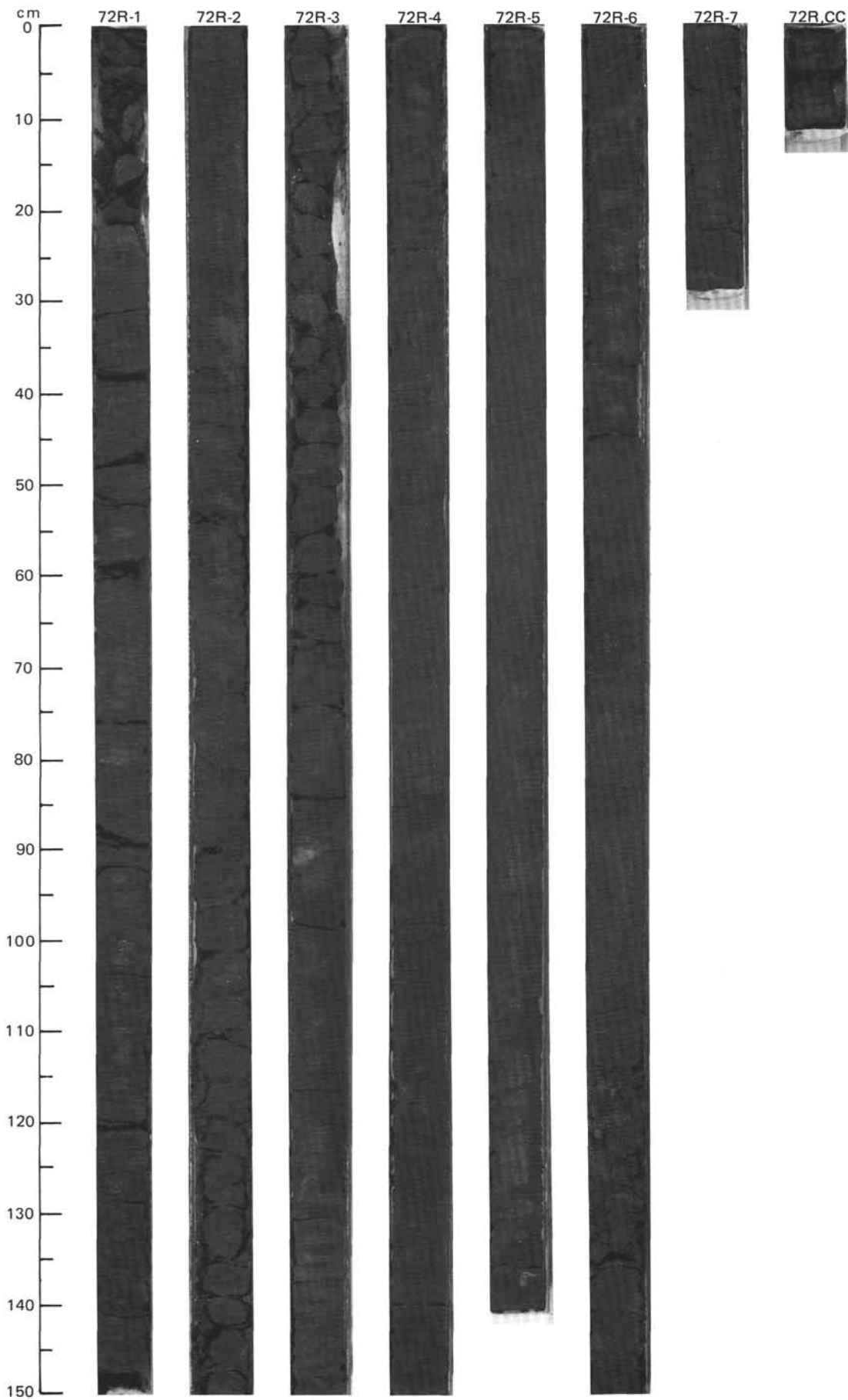
TIME-ROCK UNIT	BIOSTRAT. ZONE/ FOSSIL CHARACTER					PALEOMAGNETICS	PHYS. PROPERTIES	CHEMISTRY	SECTION	METERS	GRAPHIC LITHOLOGY	DRILLING DISTURB.	SED. STRUCTURES	SAMPLES	LITHOLOGIC DESCRIPTION																																																																	
	FORAMINIFERS	NANNOFOSILLS	RADIOLARIANS	DIATOMS	DINOCYSTS																																																																											
B	R/P						● $\gamma = 2.08$ $\phi = 36.7$ $W = 22$	● TOC=0.86 CaCO ₃ = 0.0	1	0.5 1.0					<p>SILTY MUDSTONE AND MUDDY SANDSTONE</p> <p>Silty mudstone, dark gray (10YR 4/1); moderately to intensely bioturbated and less abundant muddy sandstone. Maximum sand size is medium. Both lithologies are characterized by heterogeneous texture, with 1-2 cm lenses and pods of silty sandstone alternating with more silt/clay rich darker laminae. Apparently the lenticular interbedding of coarser and finer layers results solely from bioturbation.</p> <p>Minor lithology: Section 2, 132 cm; Section 5, 85 cm: small grayish green pods containing <10% glauconite.</p> <p>SMEAR SLIDE SUMMARY (%):</p> <table border="1"> <tr> <td></td> <td>1, 87</td> <td>3, 93</td> <td>4, 87</td> <td>5, 60</td> </tr> <tr> <td></td> <td>D</td> <td>D</td> <td>D</td> <td>D</td> </tr> </table> <p>TEXTURE:</p> <table border="1"> <tr> <td>Sand</td> <td>30</td> <td>35</td> <td>50</td> <td>10</td> </tr> <tr> <td>Silt</td> <td>40</td> <td>40</td> <td>45</td> <td>60</td> </tr> <tr> <td>Clay</td> <td>30</td> <td>25</td> <td>5</td> <td>30</td> </tr> </table> <p>COMPOSITION:</p> <table border="1"> <tr> <td>Quartz</td> <td>70</td> <td>70</td> <td>70</td> <td>60</td> </tr> <tr> <td>Feldspar</td> <td>5</td> <td>10</td> <td>10</td> <td>5</td> </tr> <tr> <td>Mica</td> <td>5</td> <td>5</td> <td>10</td> <td>3</td> </tr> <tr> <td>Clay</td> <td>18</td> <td>10</td> <td>4</td> <td>25</td> </tr> <tr> <td>Volcanic glass</td> <td>—</td> <td>—</td> <td>Tr</td> <td>—</td> </tr> <tr> <td>Calcite/dolomite</td> <td>Tr</td> <td>3</td> <td>5</td> <td>Tr</td> </tr> <tr> <td>Accessory minerals</td> <td>2</td> <td>2</td> <td>1</td> <td>1</td> </tr> <tr> <td>Glauconite</td> <td>—</td> <td>—</td> <td>—</td> <td>5</td> </tr> </table>		1, 87	3, 93	4, 87	5, 60		D	D	D	D	Sand	30	35	50	10	Silt	40	40	45	60	Clay	30	25	5	30	Quartz	70	70	70	60	Feldspar	5	10	10	5	Mica	5	5	10	3	Clay	18	10	4	25	Volcanic glass	—	—	Tr	—	Calcite/dolomite	Tr	3	5	Tr	Accessory minerals	2	2	1	1	Glauconite	—	—	—	5
	1, 87	3, 93	4, 87	5, 60																																																																												
	D	D	D	D																																																																												
Sand	30	35	50	10																																																																												
Silt	40	40	45	60																																																																												
Clay	30	25	5	30																																																																												
Quartz	70	70	70	60																																																																												
Feldspar	5	10	10	5																																																																												
Mica	5	5	10	3																																																																												
Clay	18	10	4	25																																																																												
Volcanic glass	—	—	Tr	—																																																																												
Calcite/dolomite	Tr	3	5	Tr																																																																												
Accessory minerals	2	2	1	1																																																																												
Glauconite	—	—	—	5																																																																												
R/G						● $\gamma = 2.18$ $\phi = 37.6$ $W = 21$	● TOC=0.8 CaCO ₃ = 0	2																																																																								
B									3																																																																							
B									4																																																																							
F/M									5																																																																							
N.C.									6																																																																							
CC																																																																																

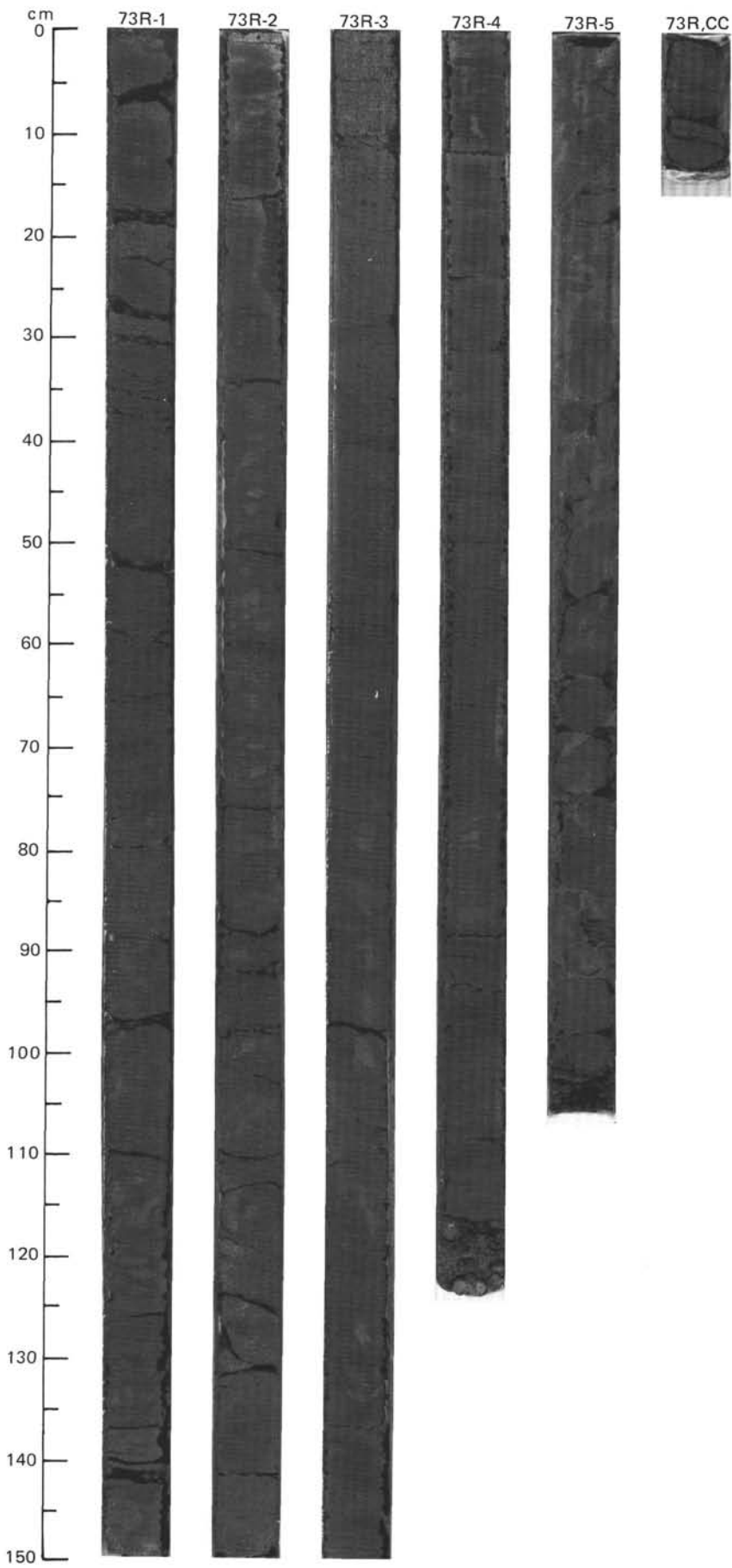


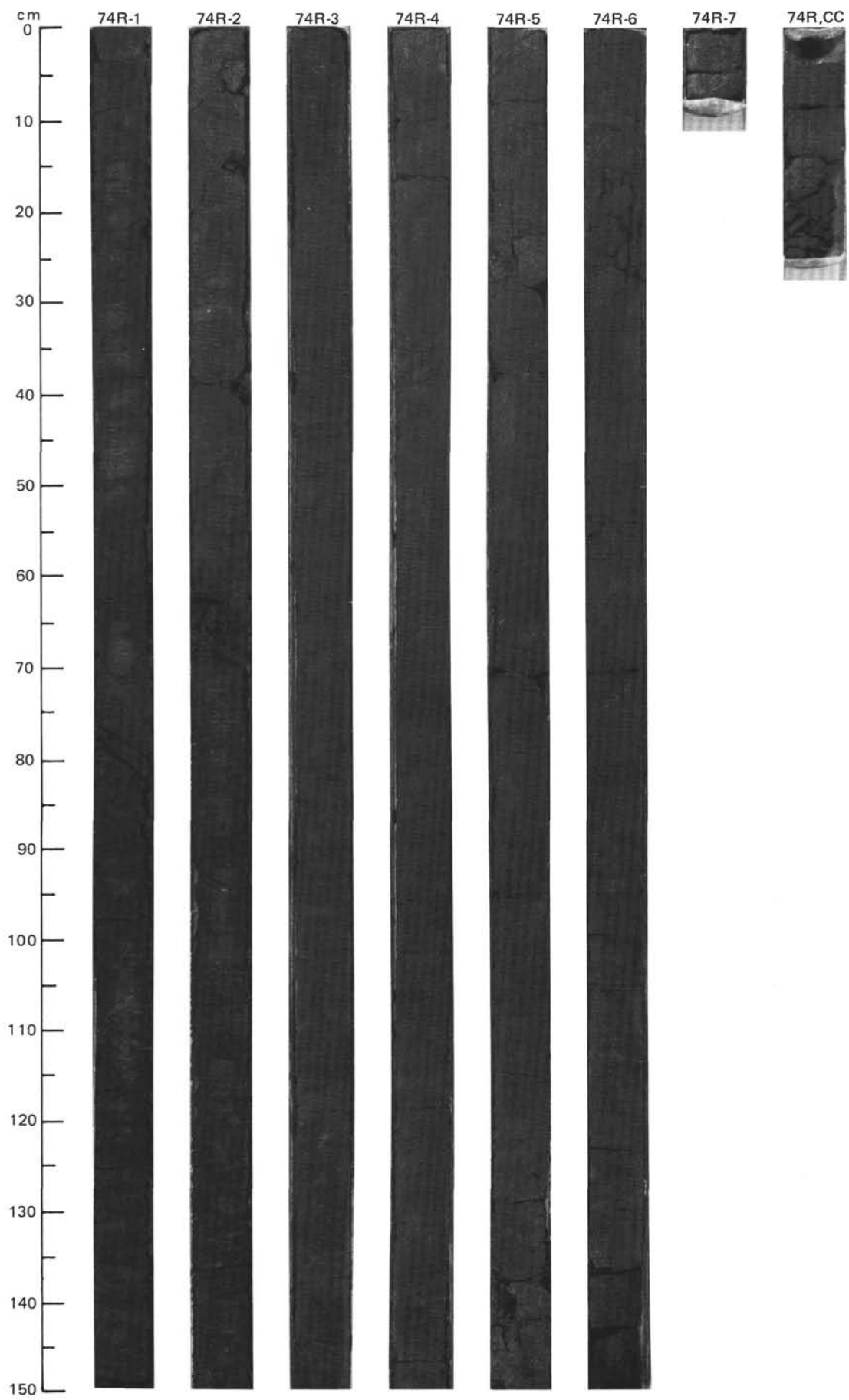


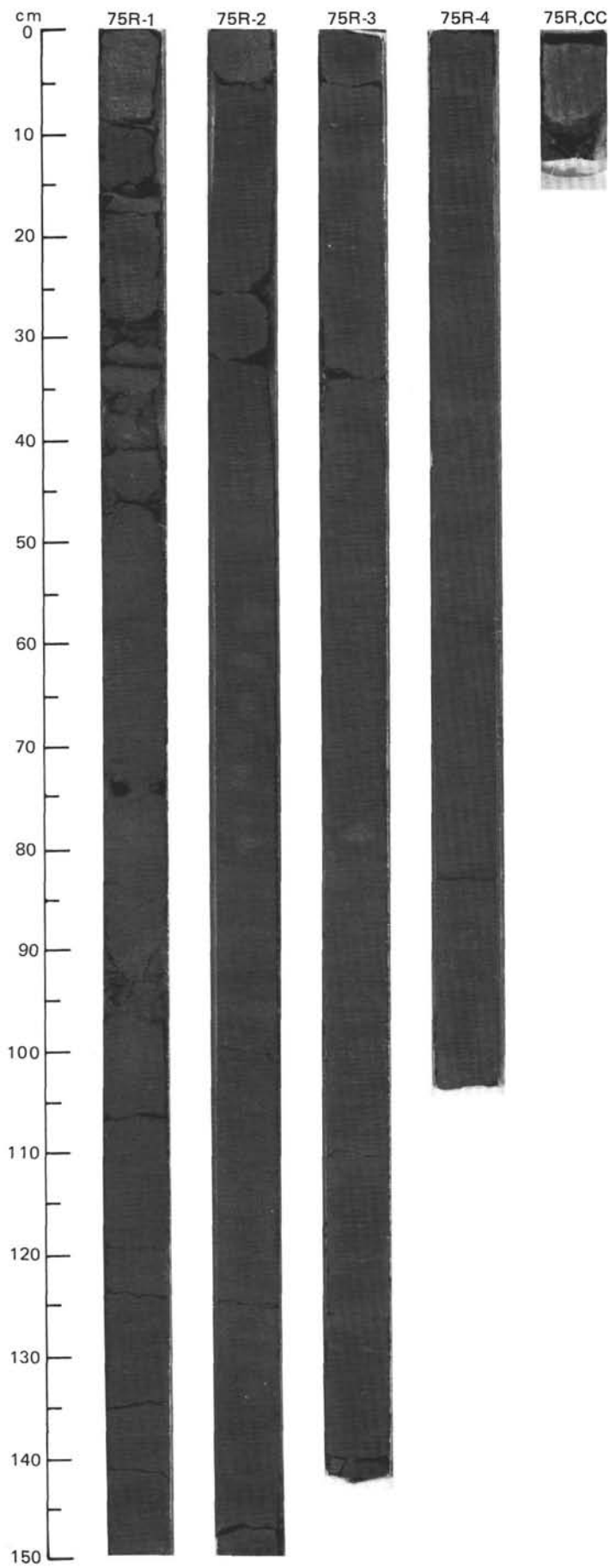


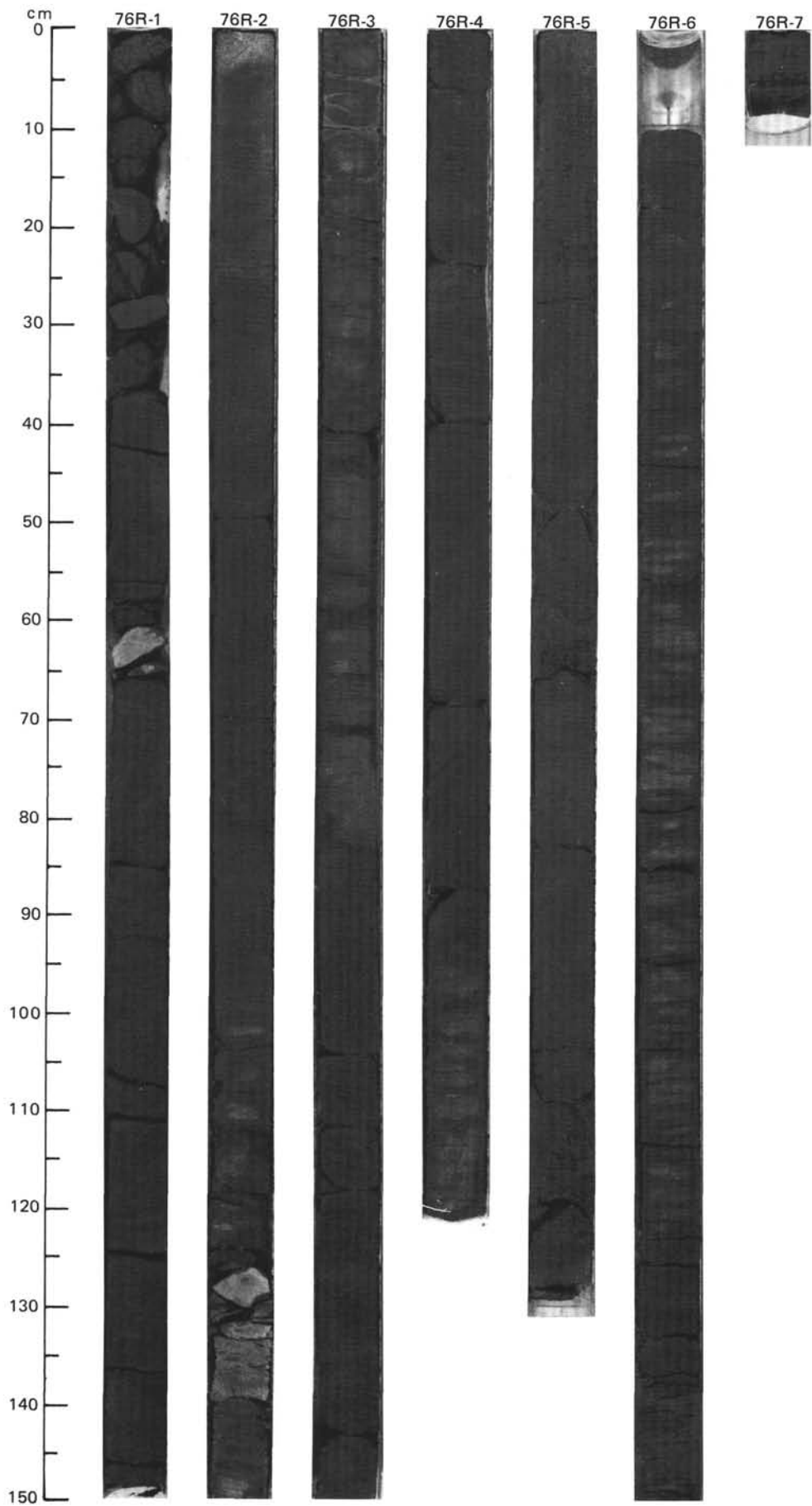


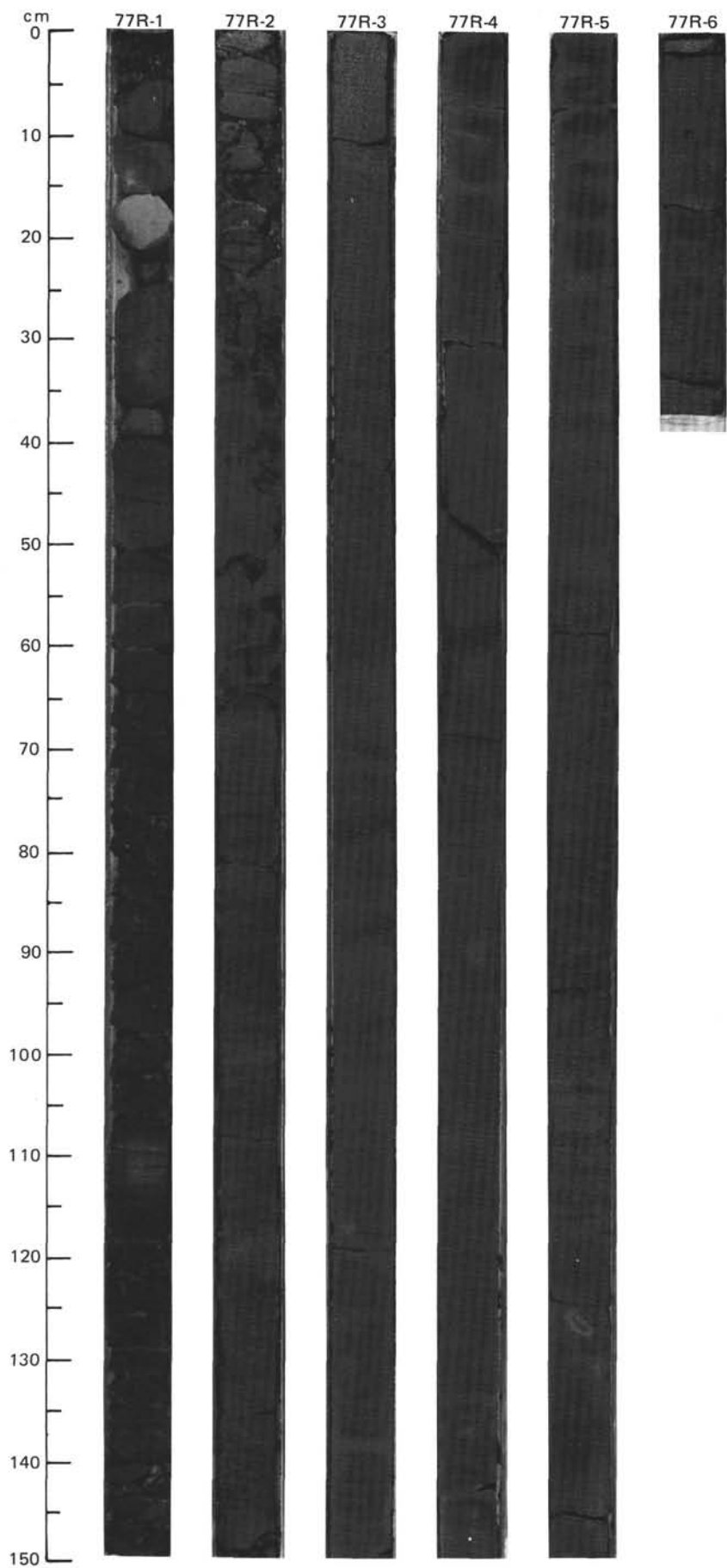


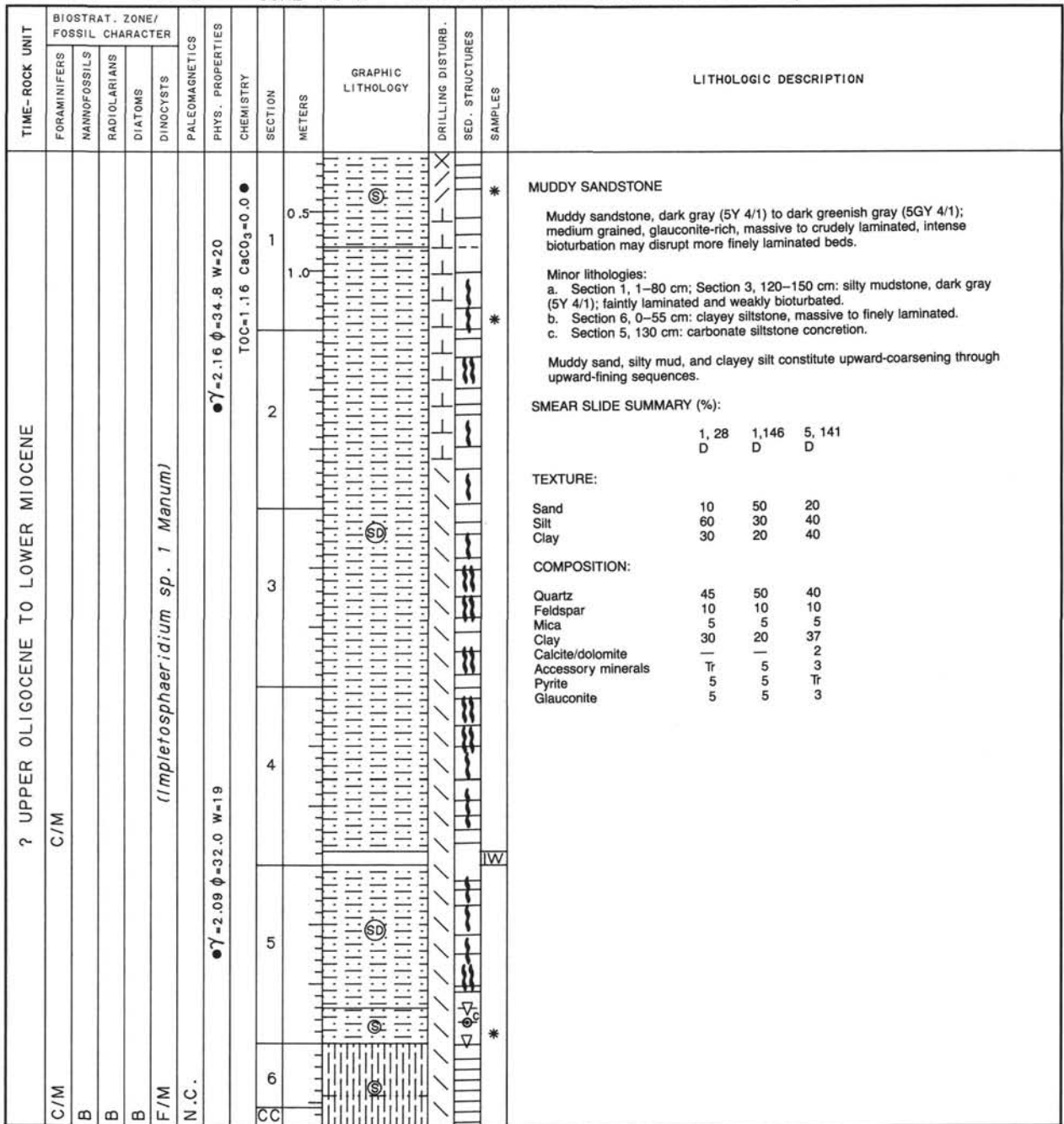


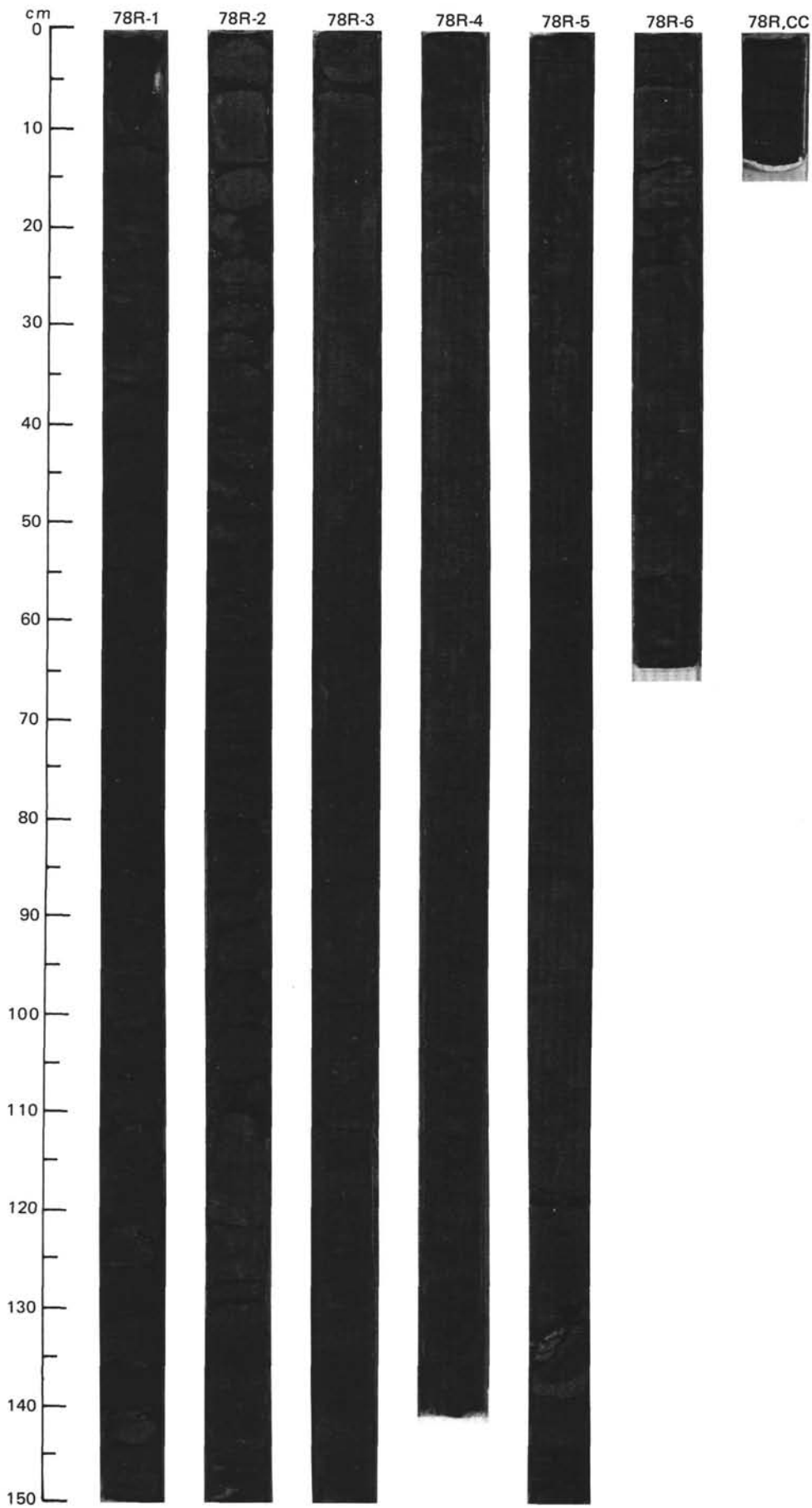


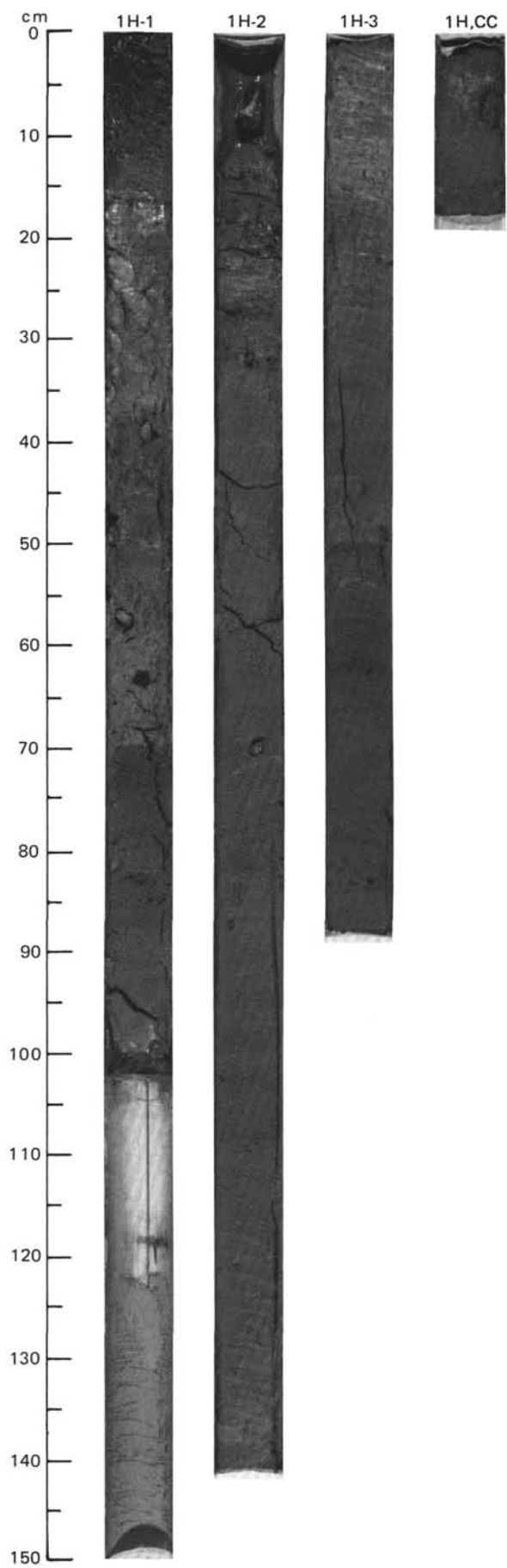




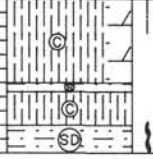


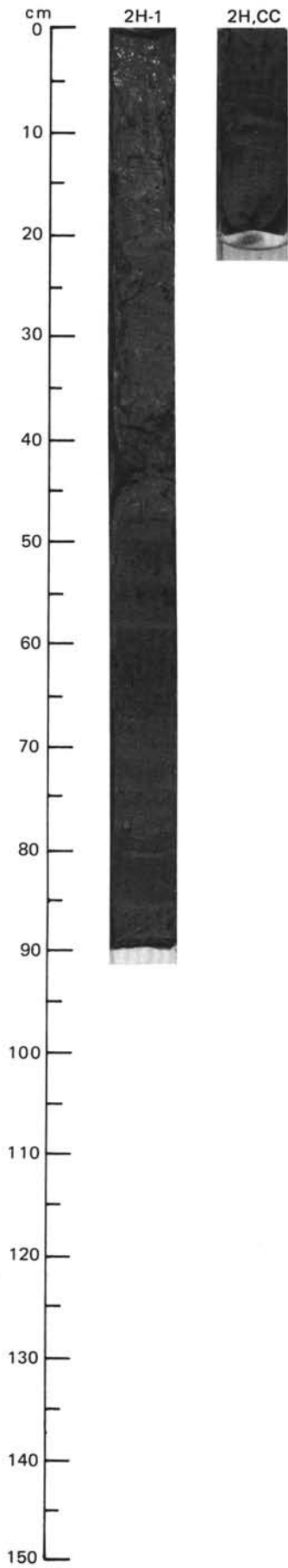


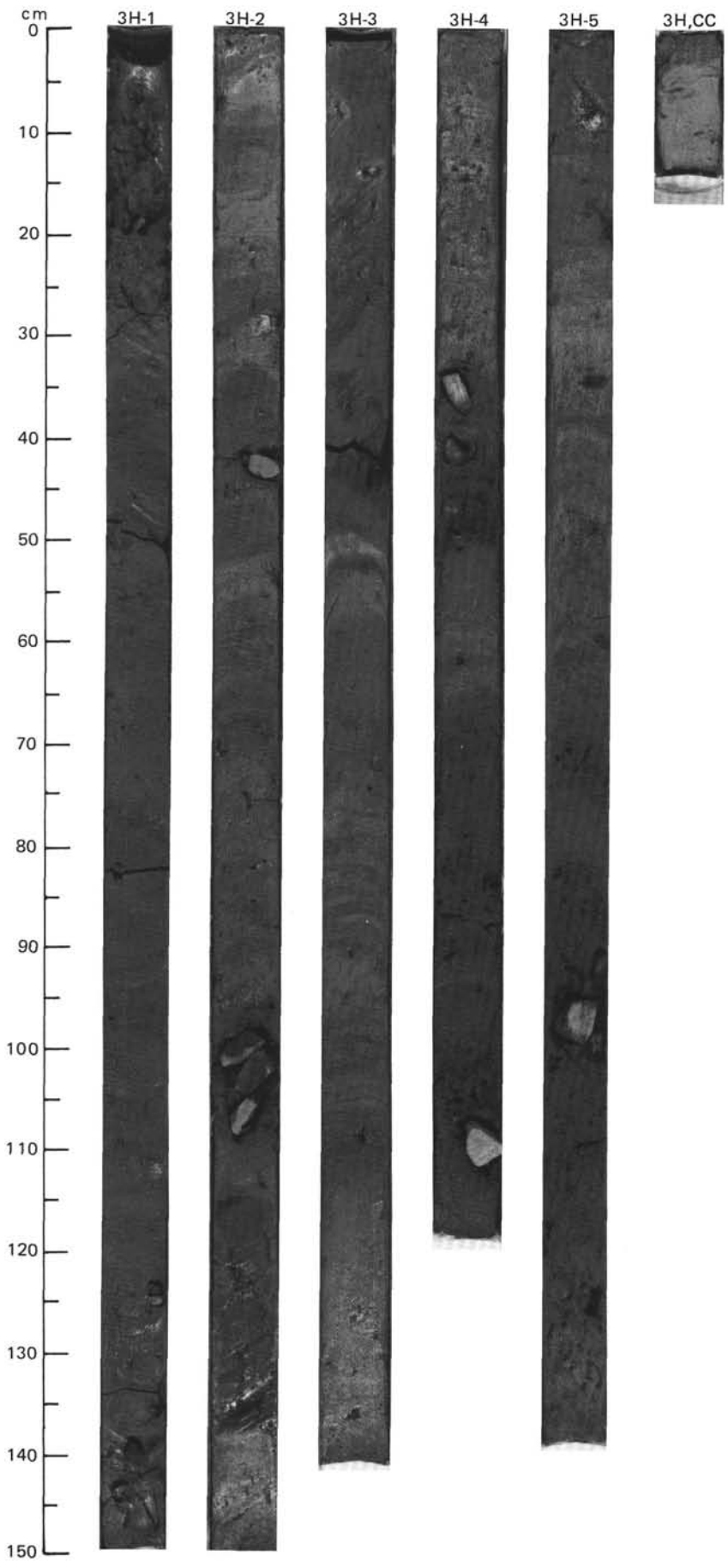




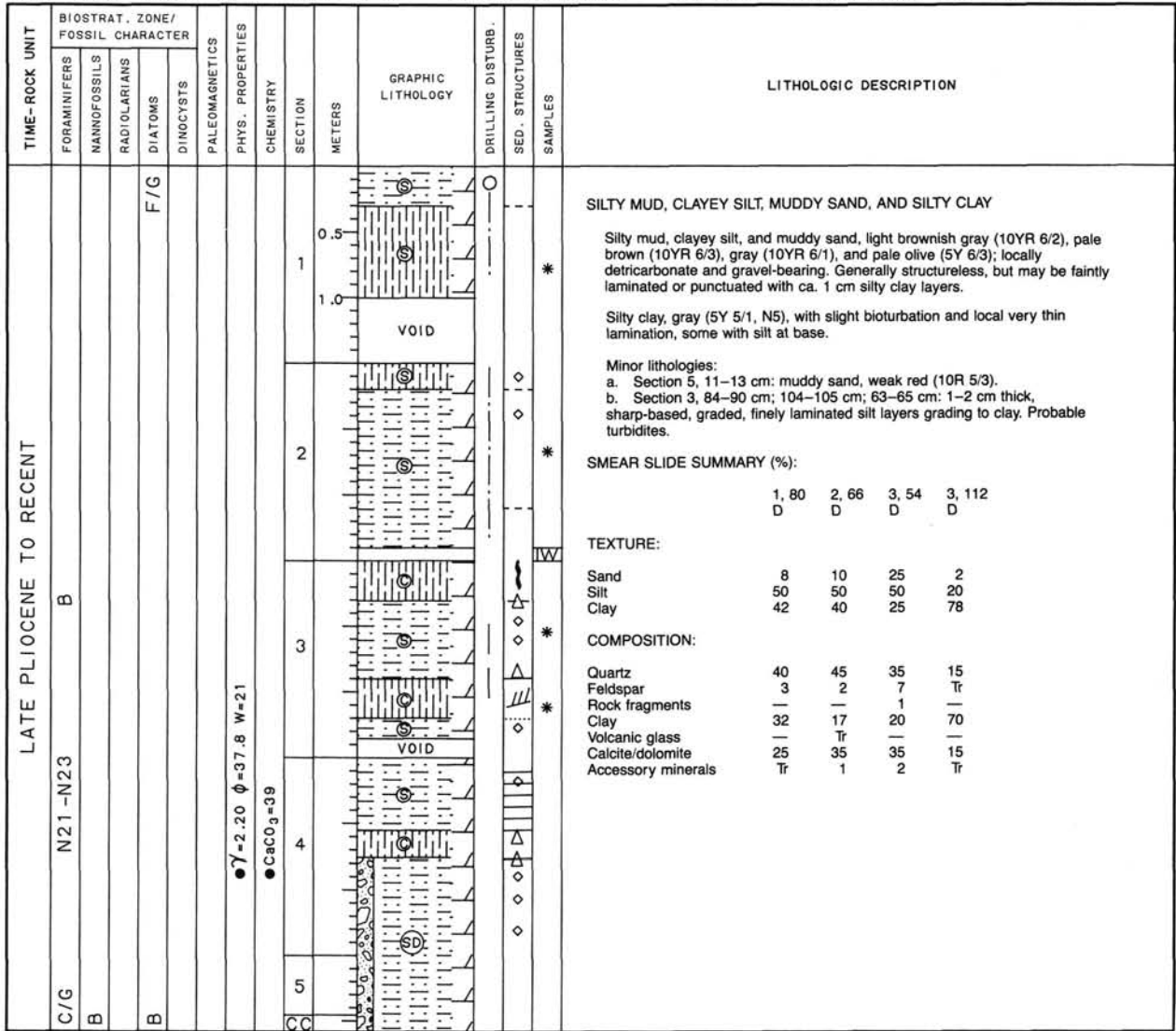
SITE 645 HOLE F CORE 2 H CORED INTERVAL 2012.3-2021.8 mbsf; 4.0-13.5 mbsf

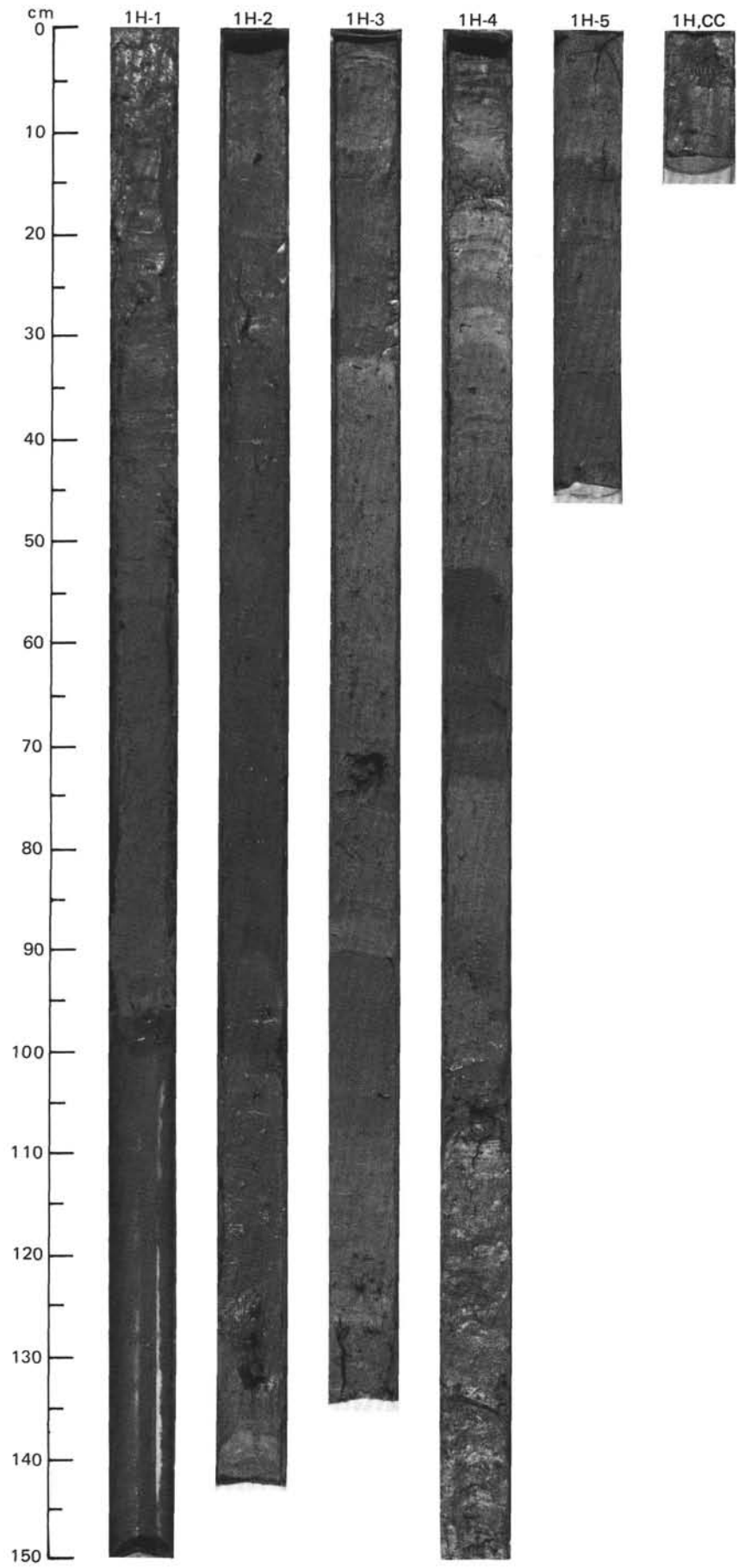
TIME-ROCK UNIT	BIOSTRAT. ZONE/ FOSSIL CHARACTER				PALEOMAGNETICS	PHYS. PROPERTIES	CHEMISTRY	SECTION	METERS	GRAPHIC LITHOLOGY	DRILLING DISTURB.	SED. STRUCTURES	SAMPLES	LITHOLOGIC DESCRIPTION																																																
	FORAMINIFERS	NANNOFOSSILS	RADIOLARIANS	DIATOMS											DINOCYSTS																																															
LATE-PLIOCENE-RECENT	N21-N23	C/G	B	B	B				1 0.5 CC				*	<p>DETRICARBONATE SILTY CLAY, FE-OXIDE-BEARING DETRICARBONATE SILTY MUD, AND SILTY CLAY</p> <p>Detriticarbonate silty clay, grayish brown (10YR 5/2); grading downward, through a Fe-oxide-bearing detriticarbonate silty mud, weak red (10R 4/3); into a silty clay, gray (N 5/1). The lowermost part of the core (Section 1, 72 cm-CC) consists of silty clay and detriticarbonate silty clay intercalated in cm-scale layers. These grade downward to an indistinctly color-banded muddy sand, dark gray (5Y 4/1) in the upper 10 cm of CC.</p> <p>SMEAR SLIDE SUMMARY (%):</p> <table border="1"> <tr> <td></td> <td>1, 25</td> <td>1, 62</td> <td>1, 82</td> </tr> <tr> <td></td> <td>D</td> <td>M</td> <td>D</td> </tr> </table> <p>TEXTURE:</p> <table border="1"> <tr> <td>Sand</td> <td>2</td> <td>20</td> <td>5</td> </tr> <tr> <td>Silt</td> <td>40</td> <td>45</td> <td>45</td> </tr> <tr> <td>Clay</td> <td>58</td> <td>35</td> <td>50</td> </tr> </table> <p>COMPOSITION:</p> <table border="1"> <tr> <td>Quartz</td> <td>22</td> <td>25</td> <td>40</td> </tr> <tr> <td>Feldspar</td> <td>2</td> <td>5</td> <td>7</td> </tr> <tr> <td>Clay</td> <td>35</td> <td>40</td> <td>40</td> </tr> <tr> <td>Calcite/dolomite</td> <td>40</td> <td>30</td> <td>10</td> </tr> <tr> <td>Accessory minerals</td> <td>1</td> <td>Tr</td> <td>2</td> </tr> <tr> <td>Pyrite</td> <td>1</td> <td>—</td> <td>1</td> </tr> <tr> <td>Foraminifers</td> <td>Tr</td> <td>—</td> <td>—</td> </tr> </table>		1, 25	1, 62	1, 82		D	M	D	Sand	2	20	5	Silt	40	45	45	Clay	58	35	50	Quartz	22	25	40	Feldspar	2	5	7	Clay	35	40	40	Calcite/dolomite	40	30	10	Accessory minerals	1	Tr	2	Pyrite	1	—	1	Foraminifers	Tr	—	—
	1, 25	1, 62	1, 82																																																											
	D	M	D																																																											
Sand	2	20	5																																																											
Silt	40	45	45																																																											
Clay	58	35	50																																																											
Quartz	22	25	40																																																											
Feldspar	2	5	7																																																											
Clay	35	40	40																																																											
Calcite/dolomite	40	30	10																																																											
Accessory minerals	1	Tr	2																																																											
Pyrite	1	—	1																																																											
Foraminifers	Tr	—	—																																																											



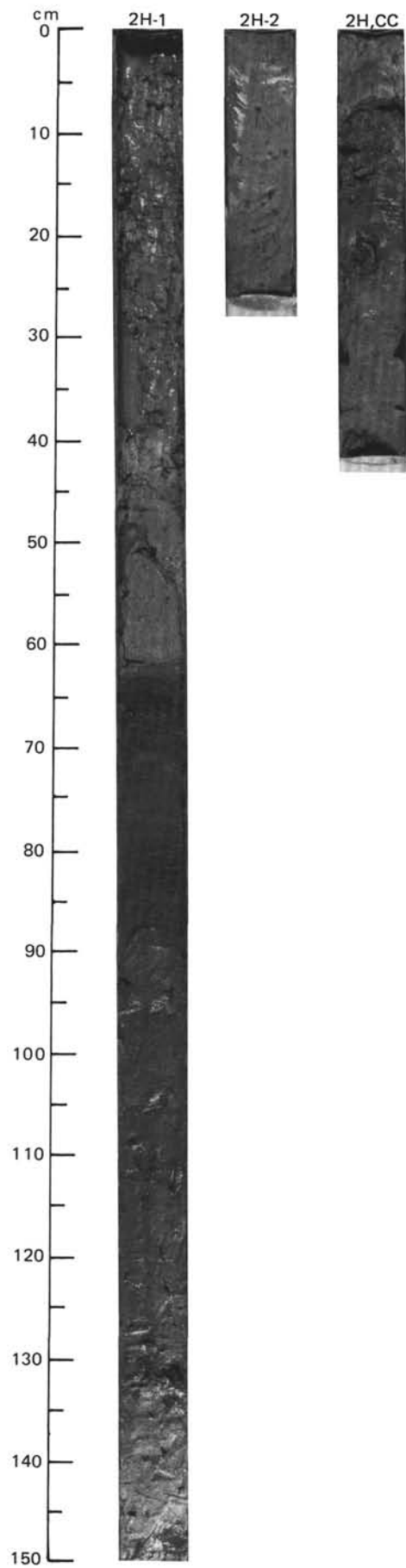


SITE 645 HOLE G CORE 1 H CORED INTERVAL 2009.3-2014.8 mbsl; 1.0-7.5 mbsf

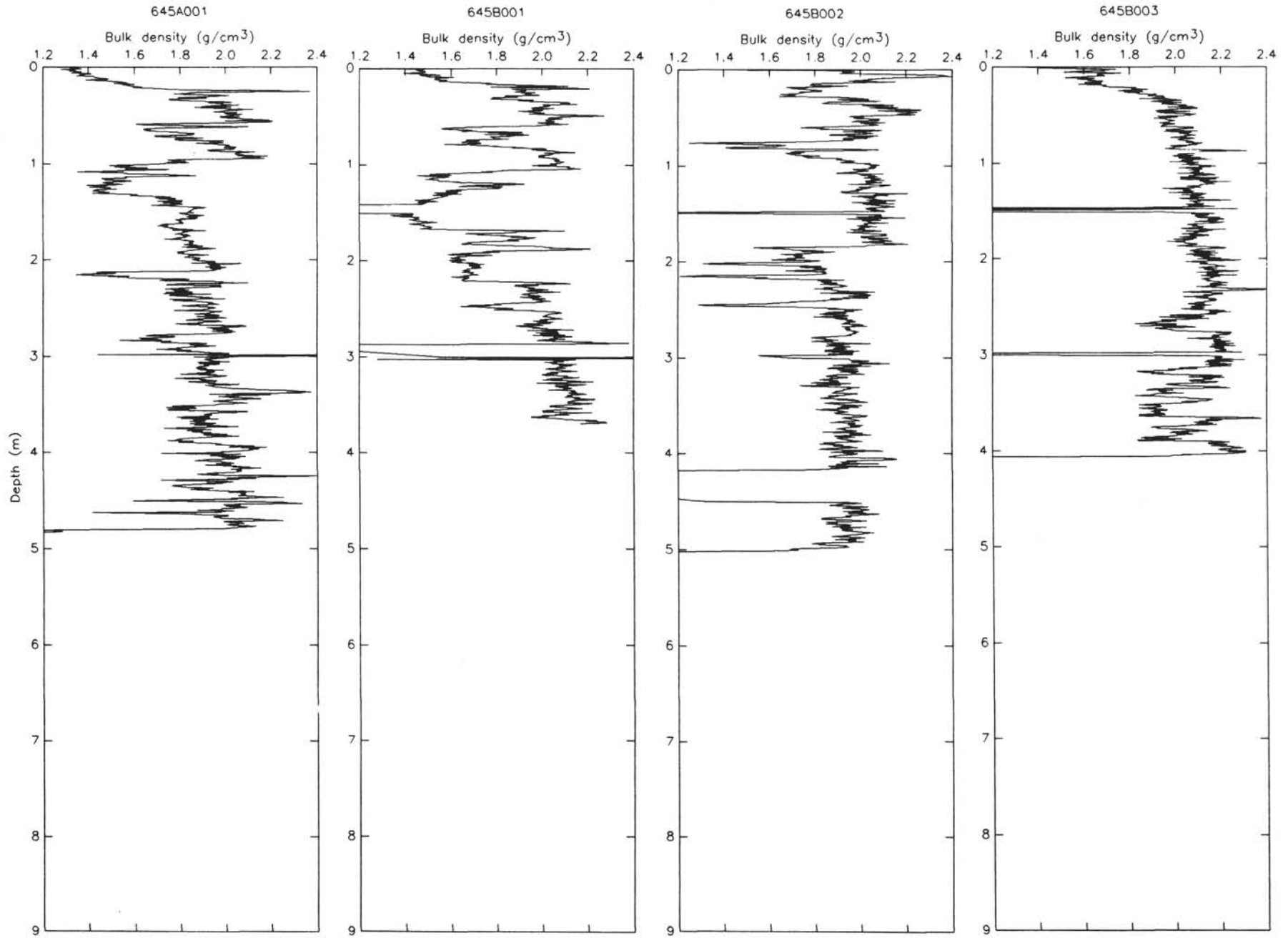




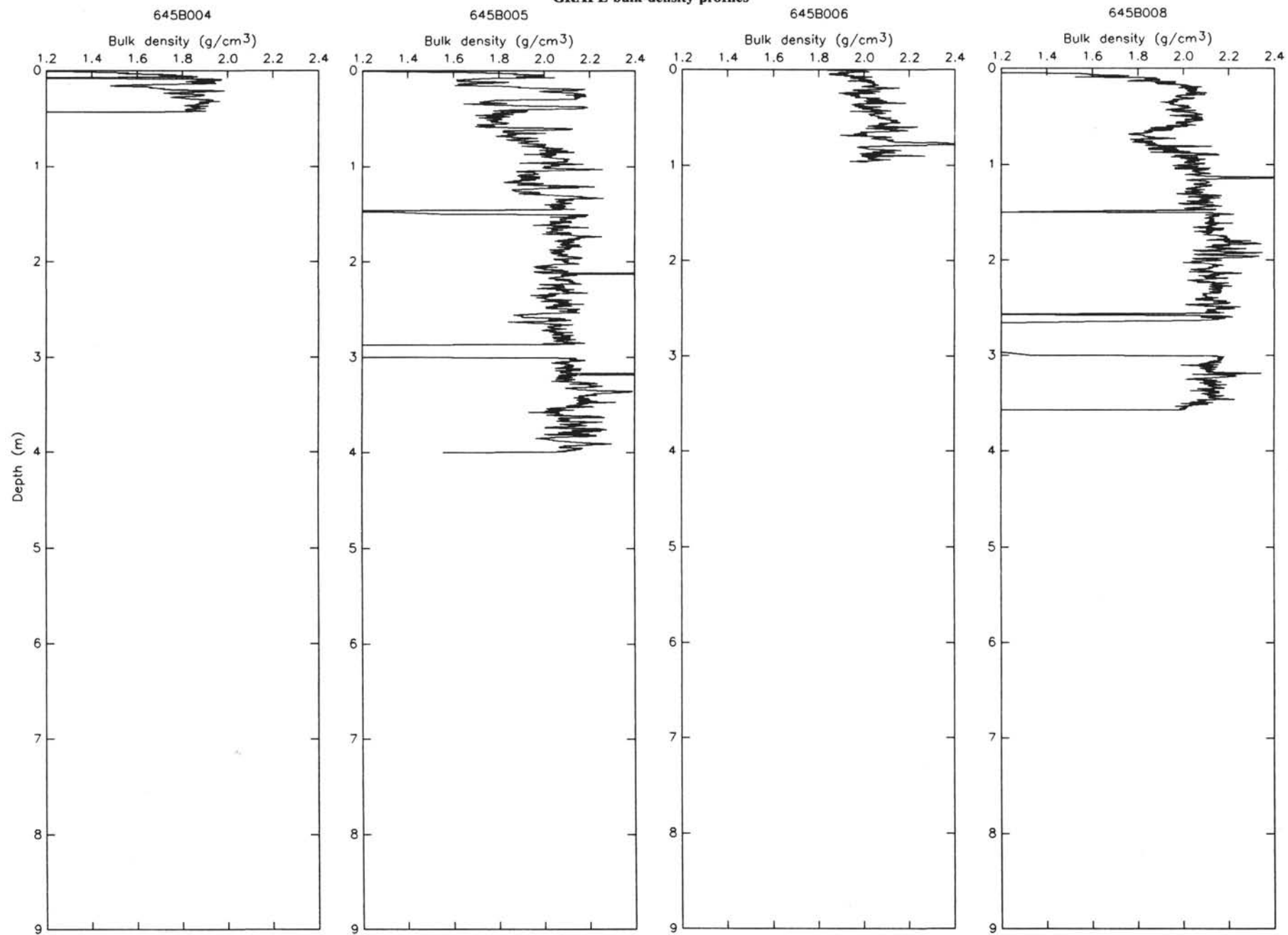
TIME-ROCK UNIT	BIOSTRAT. ZONE/ FOSSIL CHARACTER					PALEOMAGNETICS	PHYS. PROPERTIES	CHEMISTRY	SECTION	METERS	GRAPHIC LITHOLOGY	DRILLING DISTURB.	SED. STRUCTURES	SAMPLES	LITHOLOGIC DESCRIPTION																																												
	FORAMINIFERS	NANNOFOSSILS	RADIOLARIANS	DIATOMS	DINOCTYSTS																																																						
									1	0.5			*		<p>DETRICARBONATE SILTY MUD AND SILTY MUD</p> <p>Detriticarbonate silty mud, without lamination and distinct color banding. Poorly sorted, with scattered granules and pebbles. Section 1, 0-60 cm: light brownish gray (10YR 6/2). Section 1, 116-126 cm; 131-150 cm; Section 2, 0-27 cm; CC, 0-8 cm: yellowish brown (10YR 5/4). Section 1, 83-116 cm: grayish brown (10YR 5/2).</p> <p>Silty mud, with scattered granules and pebbles, some intervals laminated and color banded. Poorly sorted. Section 1, 61-83 cm, CC, 16-24 cm: dark gray (5Y 4/1). Section 1, 126-131 cm: dark gray (10YR 4/1).</p> <p>Minor lithology: Section 2, 8-16 cm: detriticarbonate clayey sand, gray (5Y 5/1); coarse to very coarse sand with fine fraction almost entirely composed of carbonate. Poorly sorted.</p> <p>SMEAR SLIDE SUMMARY (%):</p> <table border="0"> <tr> <td></td> <td>1, 55</td> <td>1, 122</td> <td>CC, 10</td> </tr> <tr> <td></td> <td>D</td> <td>D</td> <td>M</td> </tr> </table> <p>TEXTURE:</p> <table border="0"> <tr> <td>Sand</td> <td>15</td> <td>10</td> <td>60</td> </tr> <tr> <td>Silt</td> <td>50</td> <td>60</td> <td>5</td> </tr> <tr> <td>Clay</td> <td>35</td> <td>30</td> <td>35</td> </tr> </table> <p>COMPOSITION:</p> <table border="0"> <tr> <td>Quartz</td> <td>30</td> <td>40</td> <td>65</td> </tr> <tr> <td>Feldspar</td> <td>—</td> <td>2</td> <td>Tr</td> </tr> <tr> <td>Clay</td> <td>20</td> <td>18</td> <td>5</td> </tr> <tr> <td>Volcanic glass</td> <td>—</td> <td>Tr</td> <td>—</td> </tr> <tr> <td>Calcite/dolomite</td> <td>50</td> <td>40</td> <td>30</td> </tr> <tr> <td>Accessory minerals</td> <td>Tr</td> <td>Tr</td> <td>Tr</td> </tr> </table>		1, 55	1, 122	CC, 10		D	D	M	Sand	15	10	60	Silt	50	60	5	Clay	35	30	35	Quartz	30	40	65	Feldspar	—	2	Tr	Clay	20	18	5	Volcanic glass	—	Tr	—	Calcite/dolomite	50	40	30	Accessory minerals	Tr	Tr	Tr
	1, 55	1, 122	CC, 10																																																								
	D	D	M																																																								
Sand	15	10	60																																																								
Silt	50	60	5																																																								
Clay	35	30	35																																																								
Quartz	30	40	65																																																								
Feldspar	—	2	Tr																																																								
Clay	20	18	5																																																								
Volcanic glass	—	Tr	—																																																								
Calcite/dolomite	50	40	30																																																								
Accessory minerals	Tr	Tr	Tr																																																								
									2				*																																														
									CC				*																																														
													*																																														



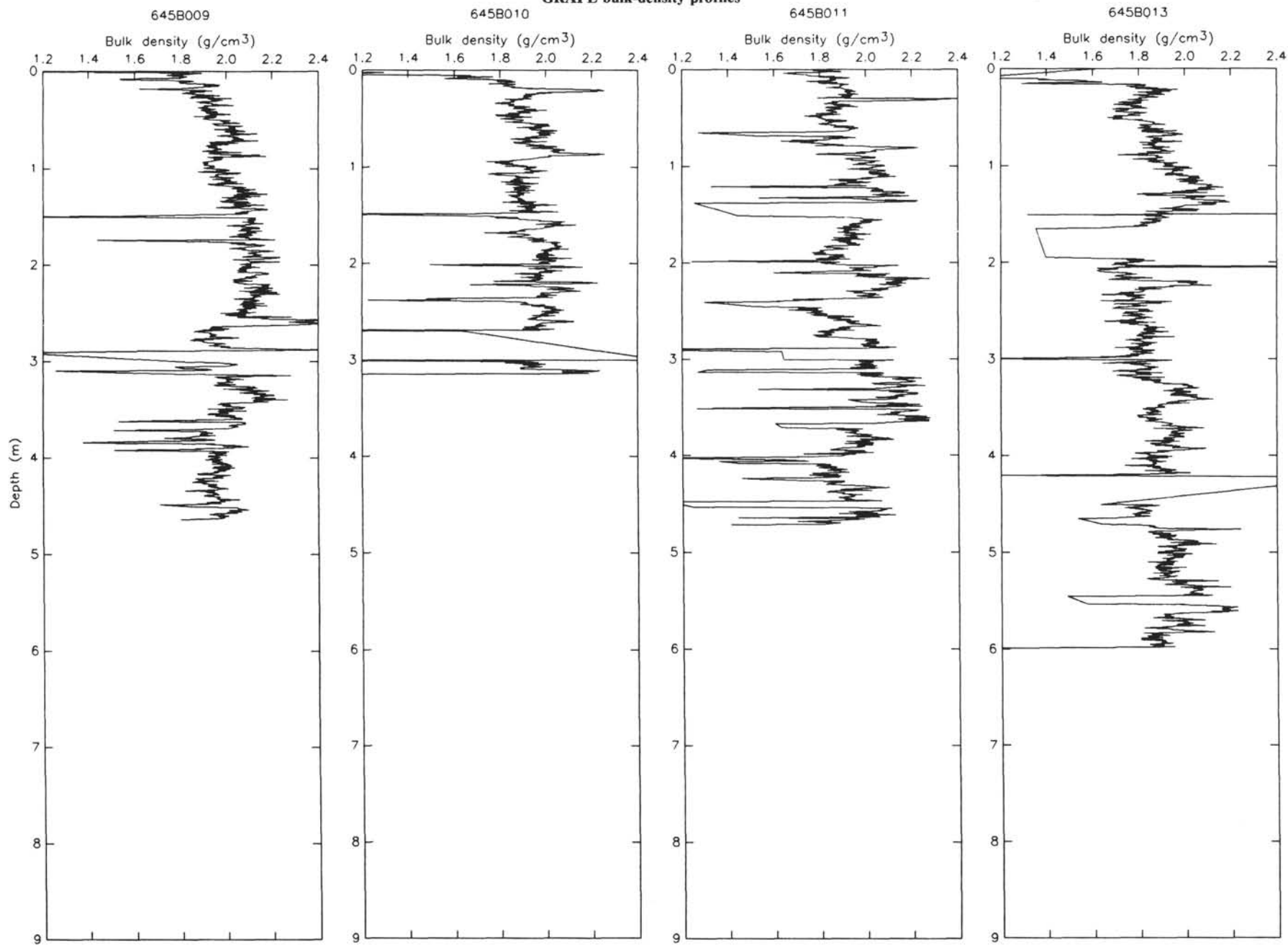
GRAPE bulk-density profiles



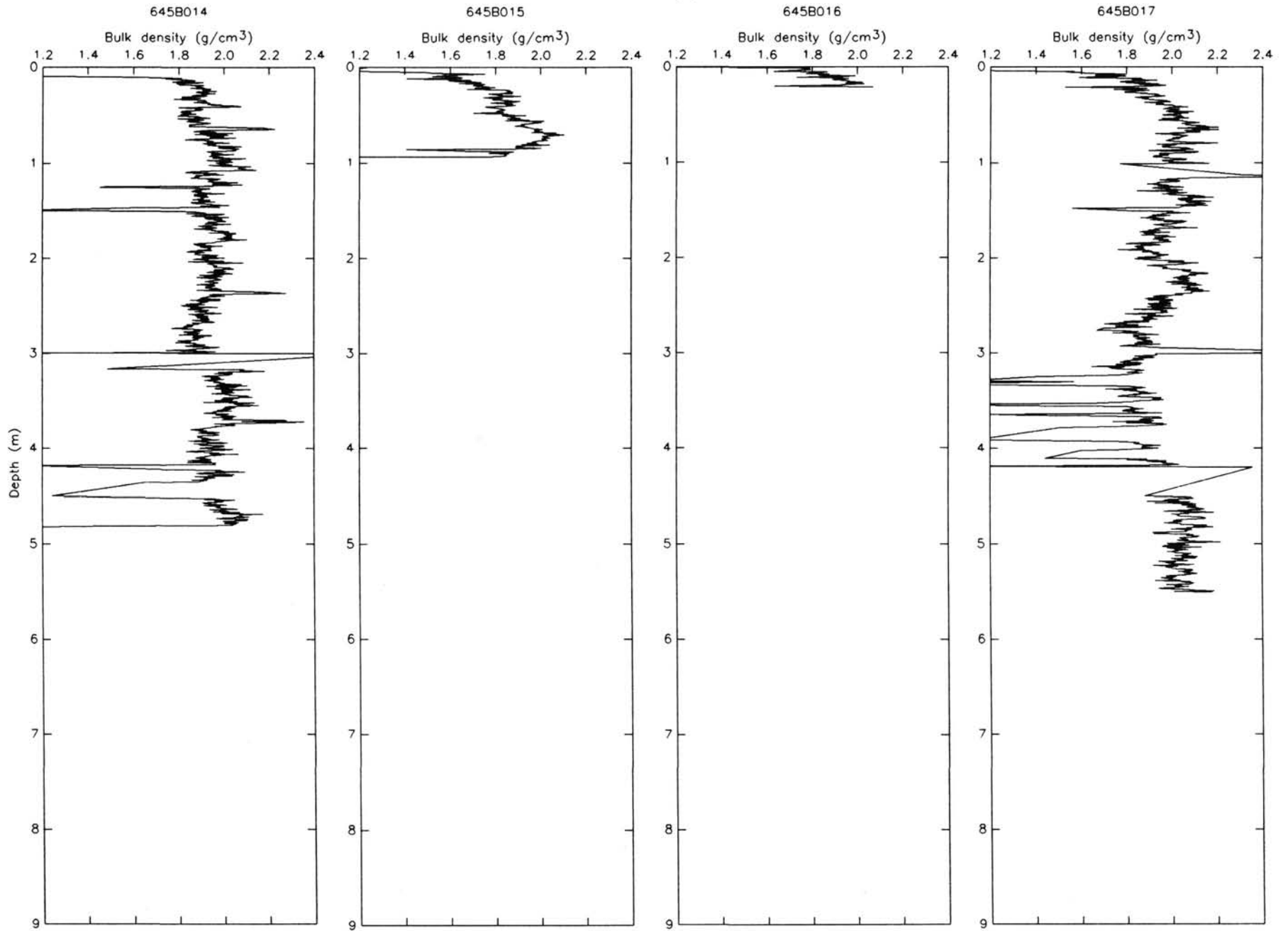
GRAPE bulk-density profiles



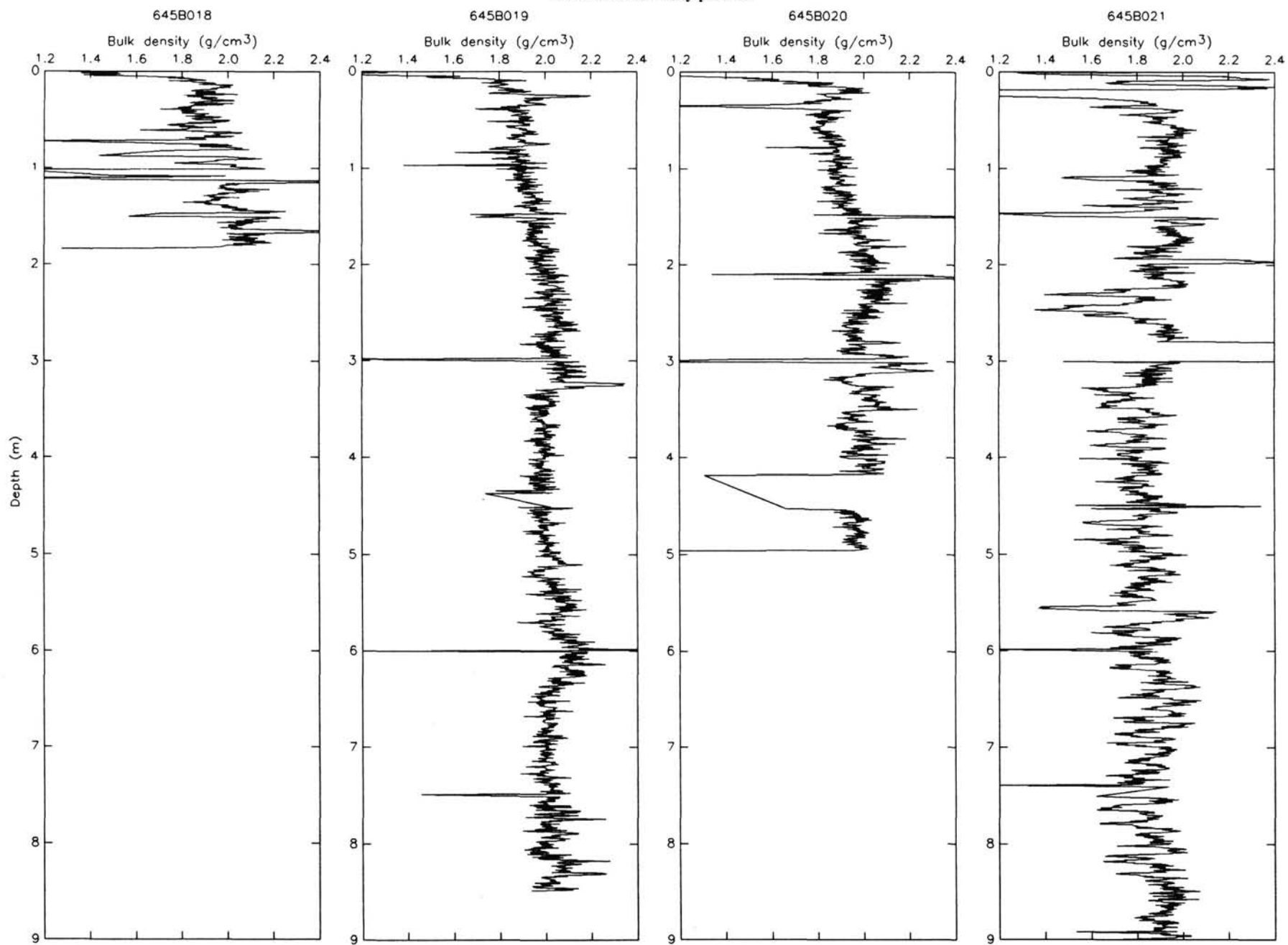
GRAPE bulk-density profiles



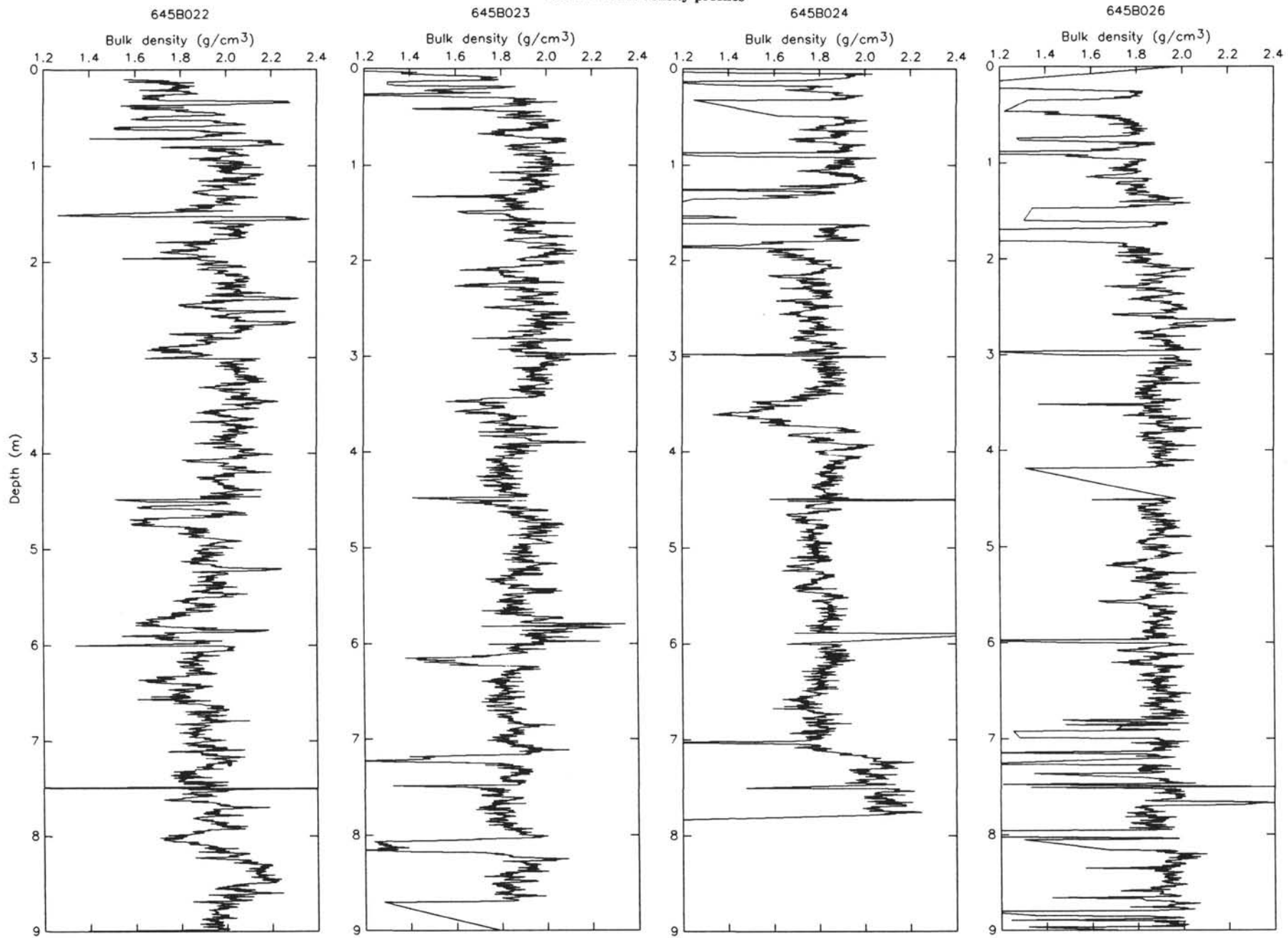
GRAPE bulk-density profiles



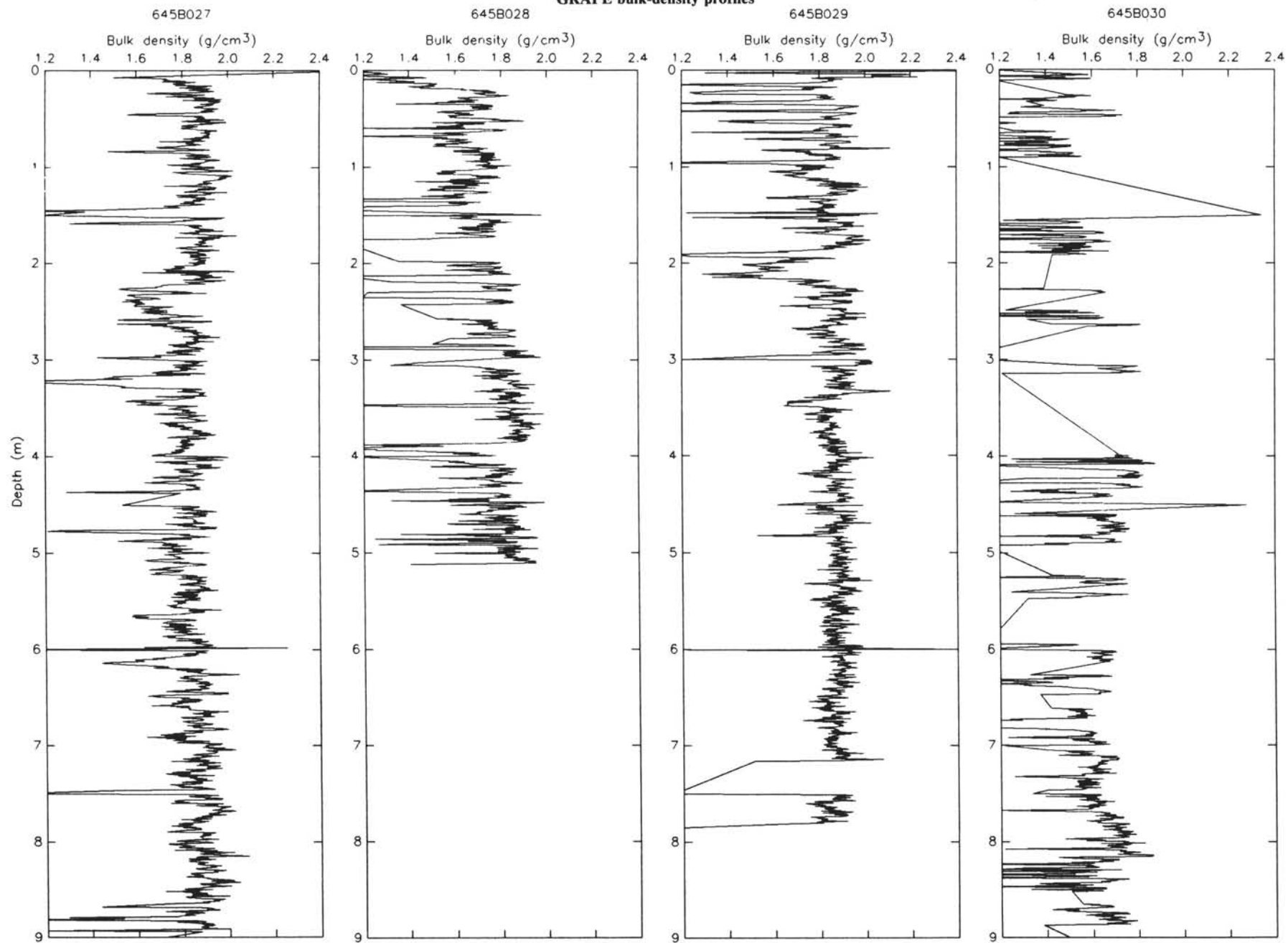
GRAPE bulk-density profiles



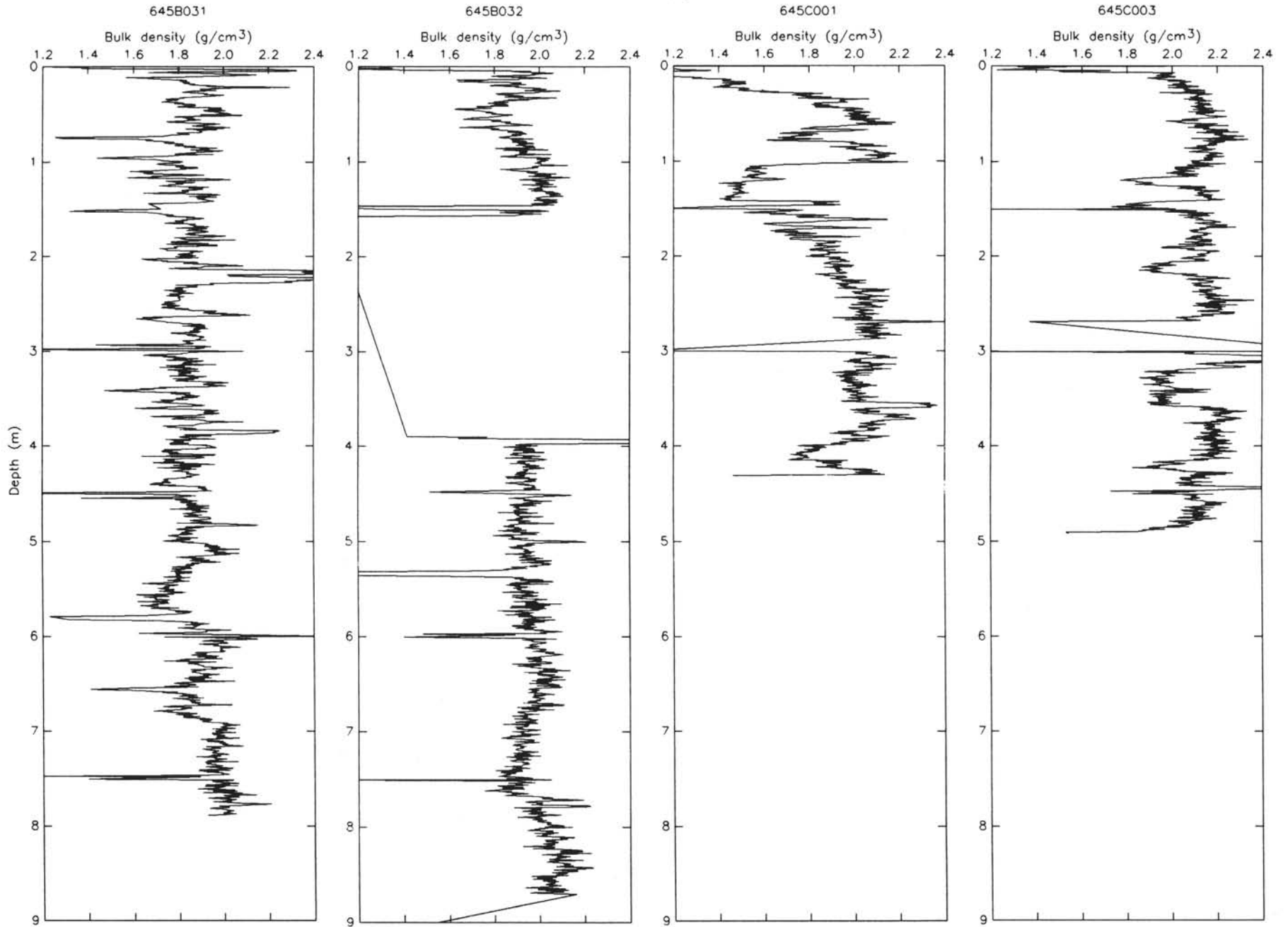
GRAPE bulk-density profiles



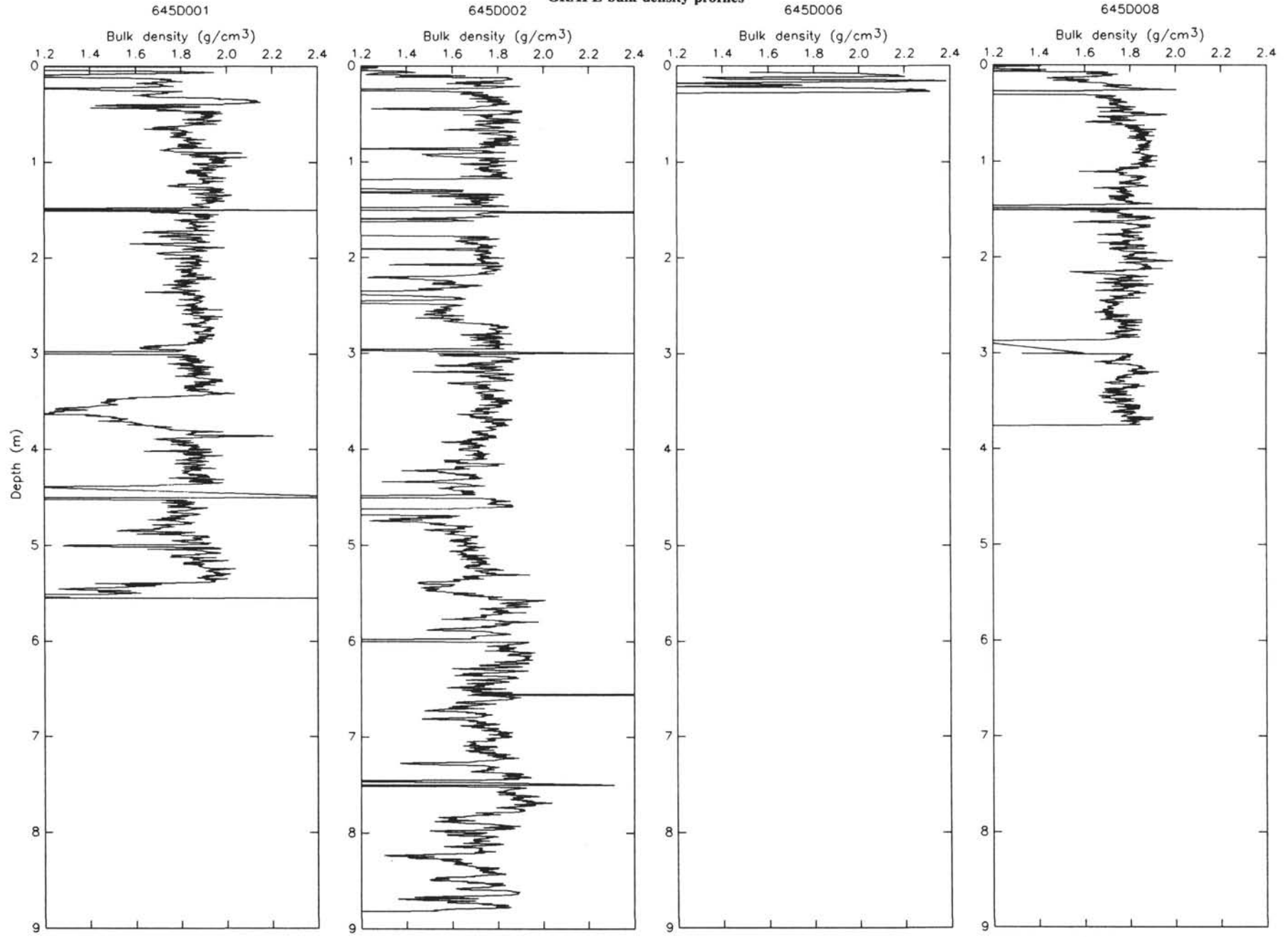
GRAPE bulk-density profiles



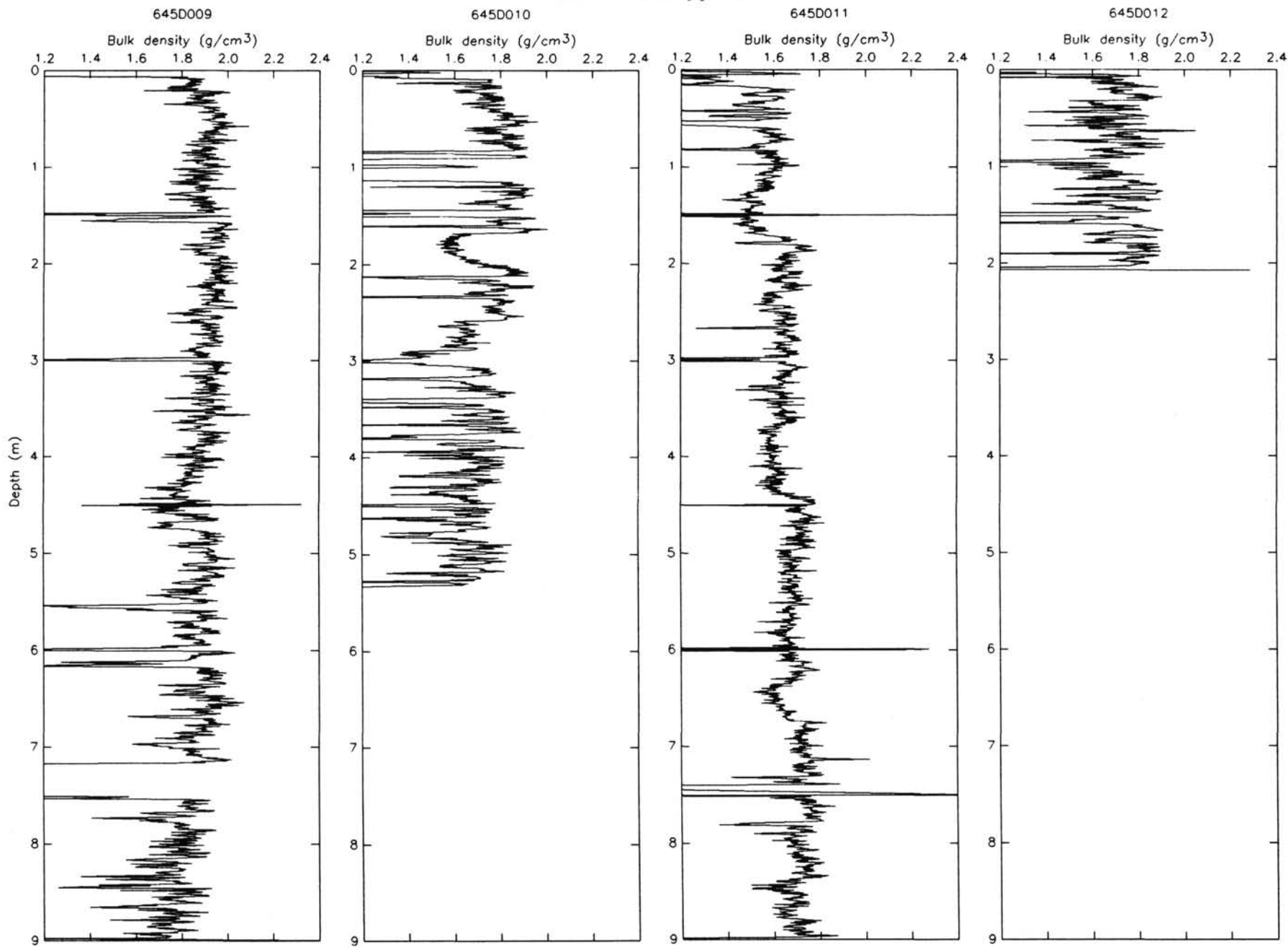
GRAPE bulk-density profiles



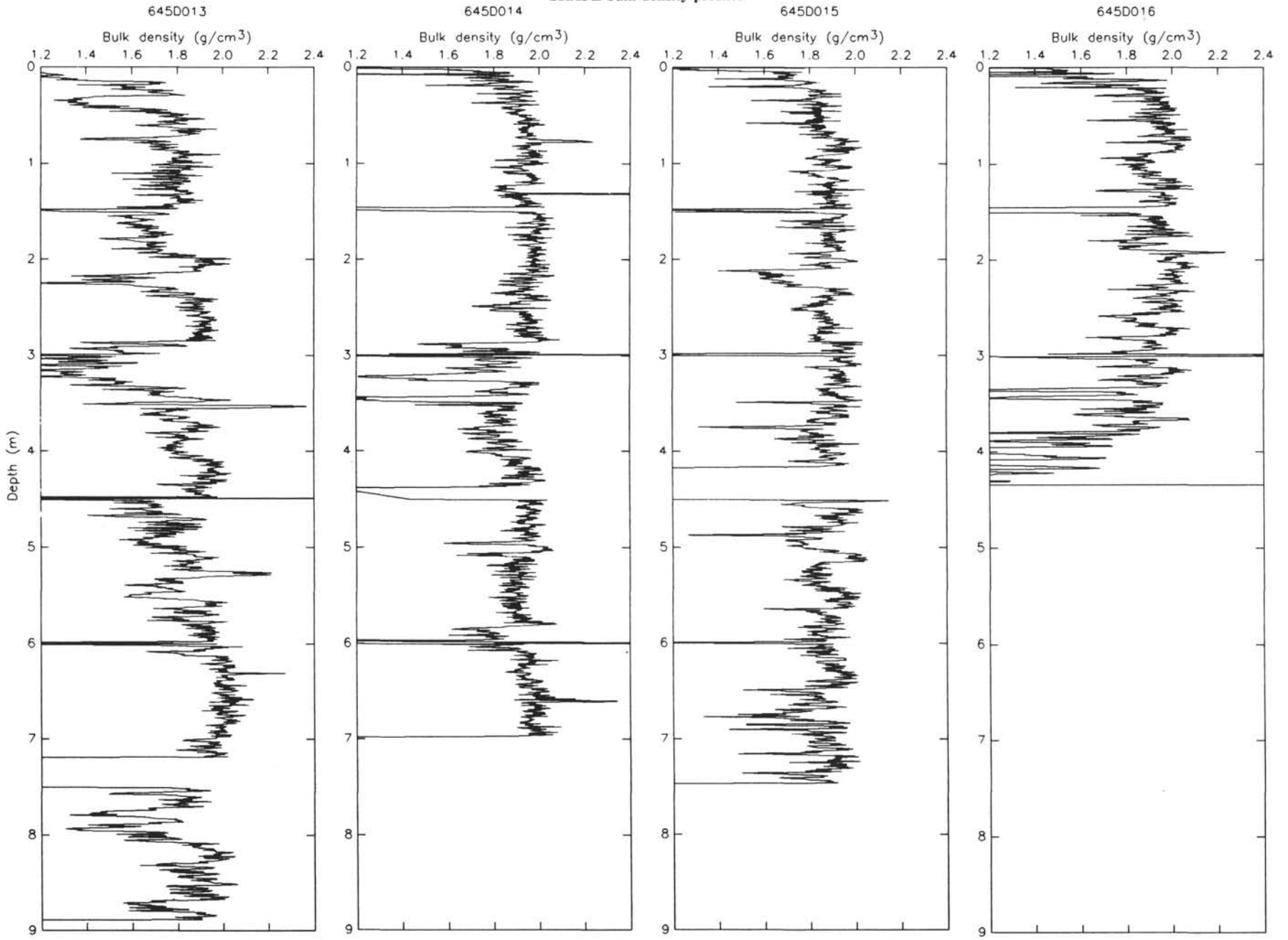
GRAPE bulk-density profiles



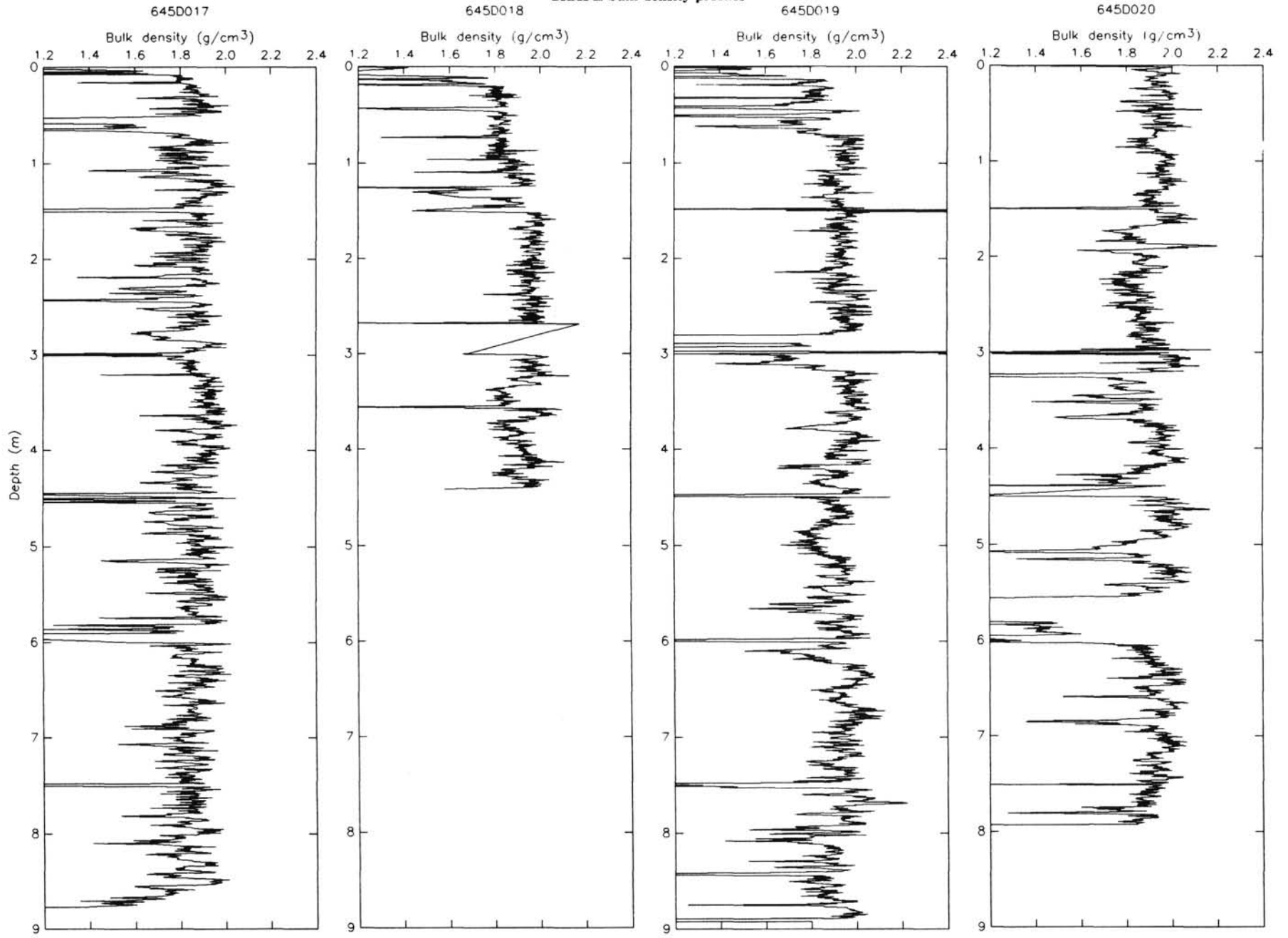
GRAPE bulk-density profiles



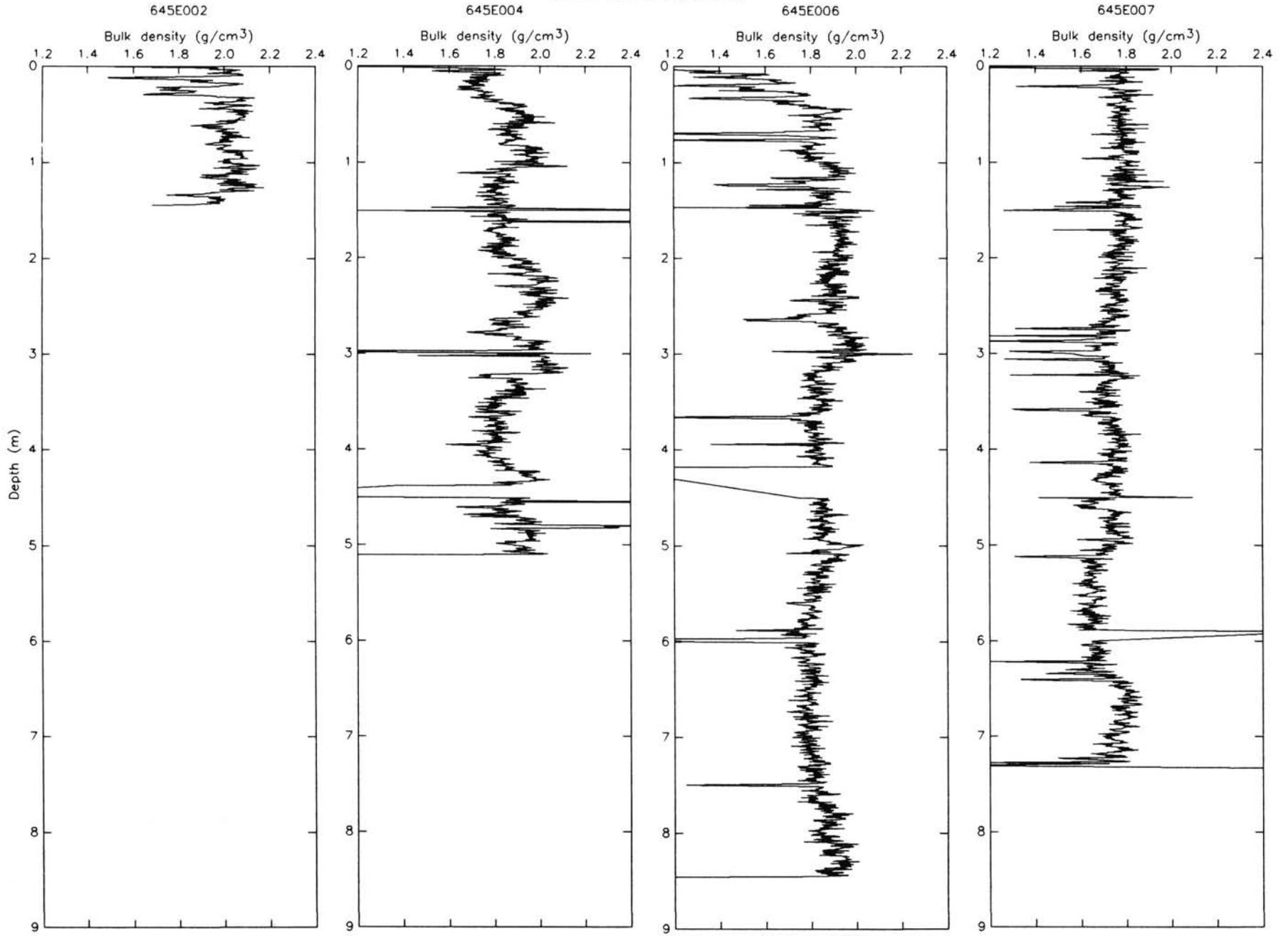
GRAPE bulk-density profiles



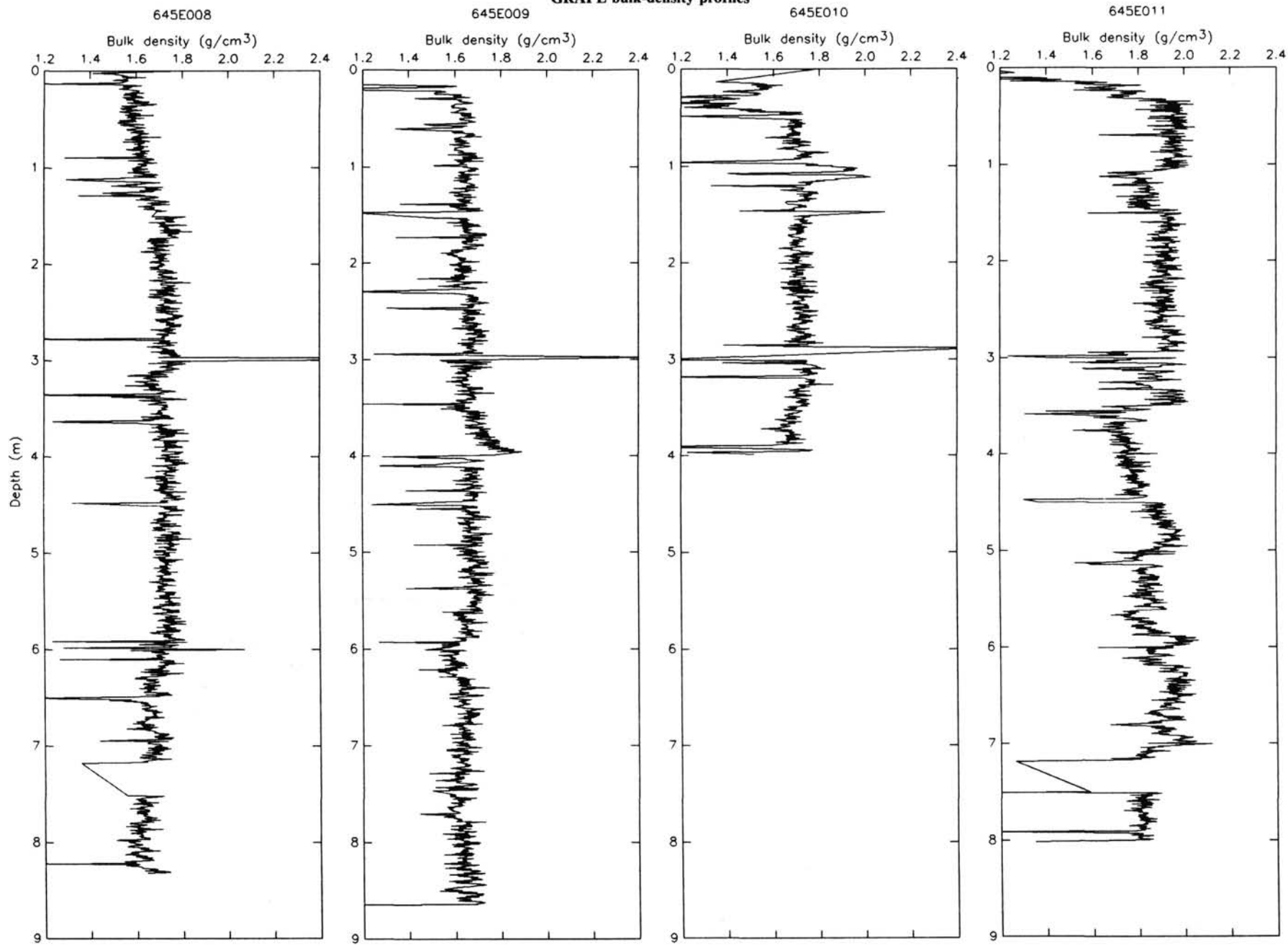
GRAPE bulk-density profiles



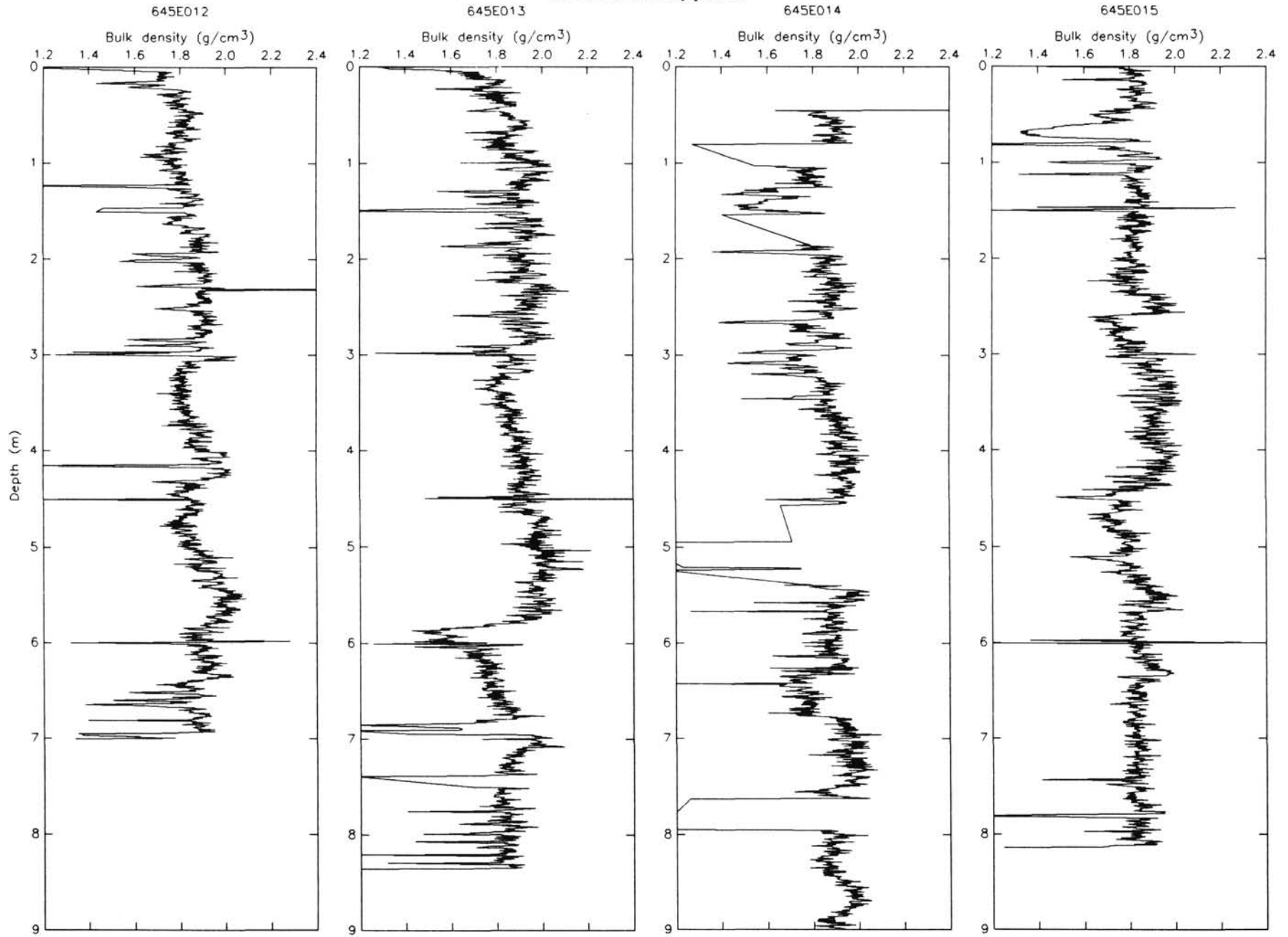
GRAPE bulk-density profiles



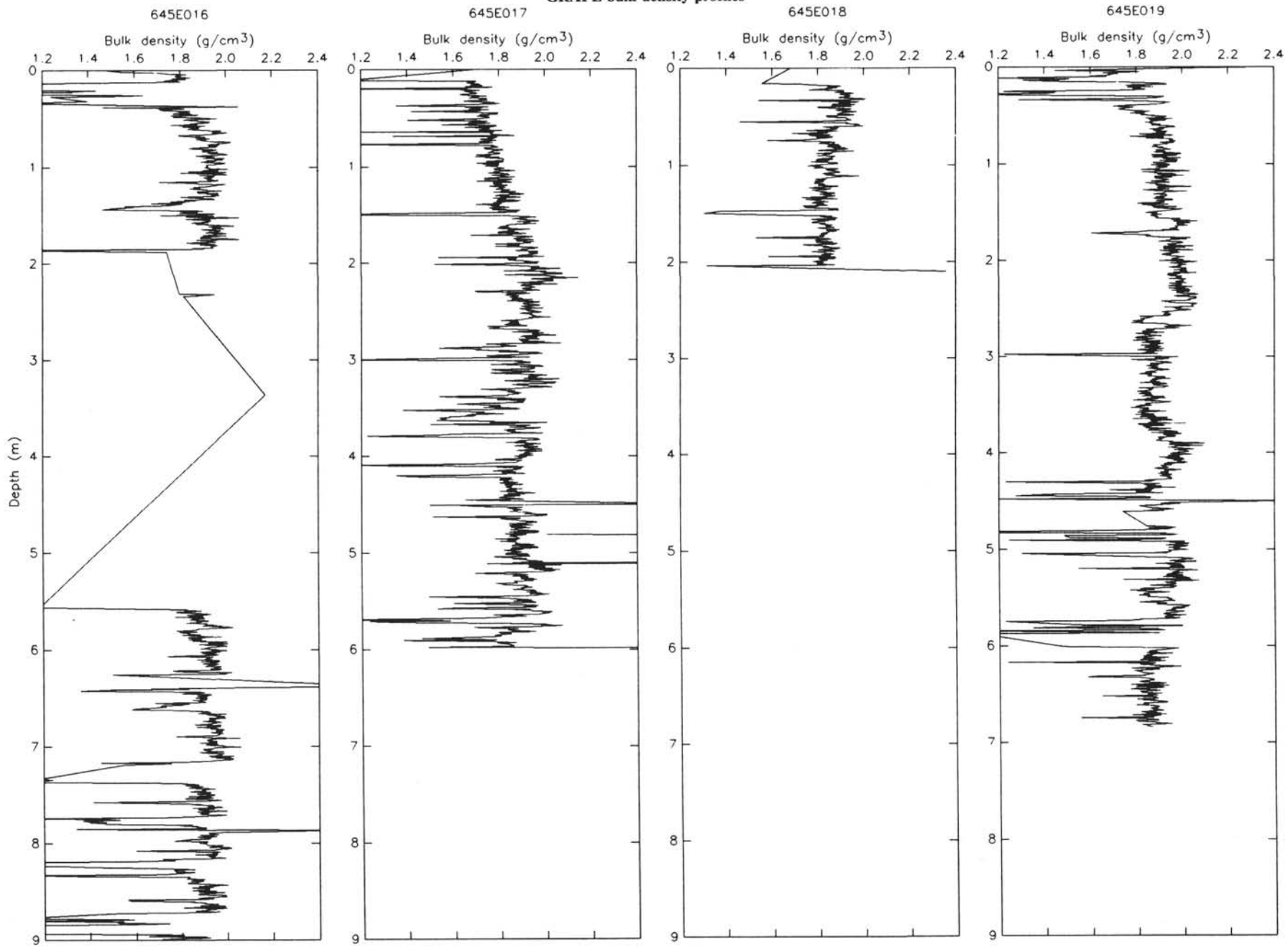
GRAPE bulk-density profiles



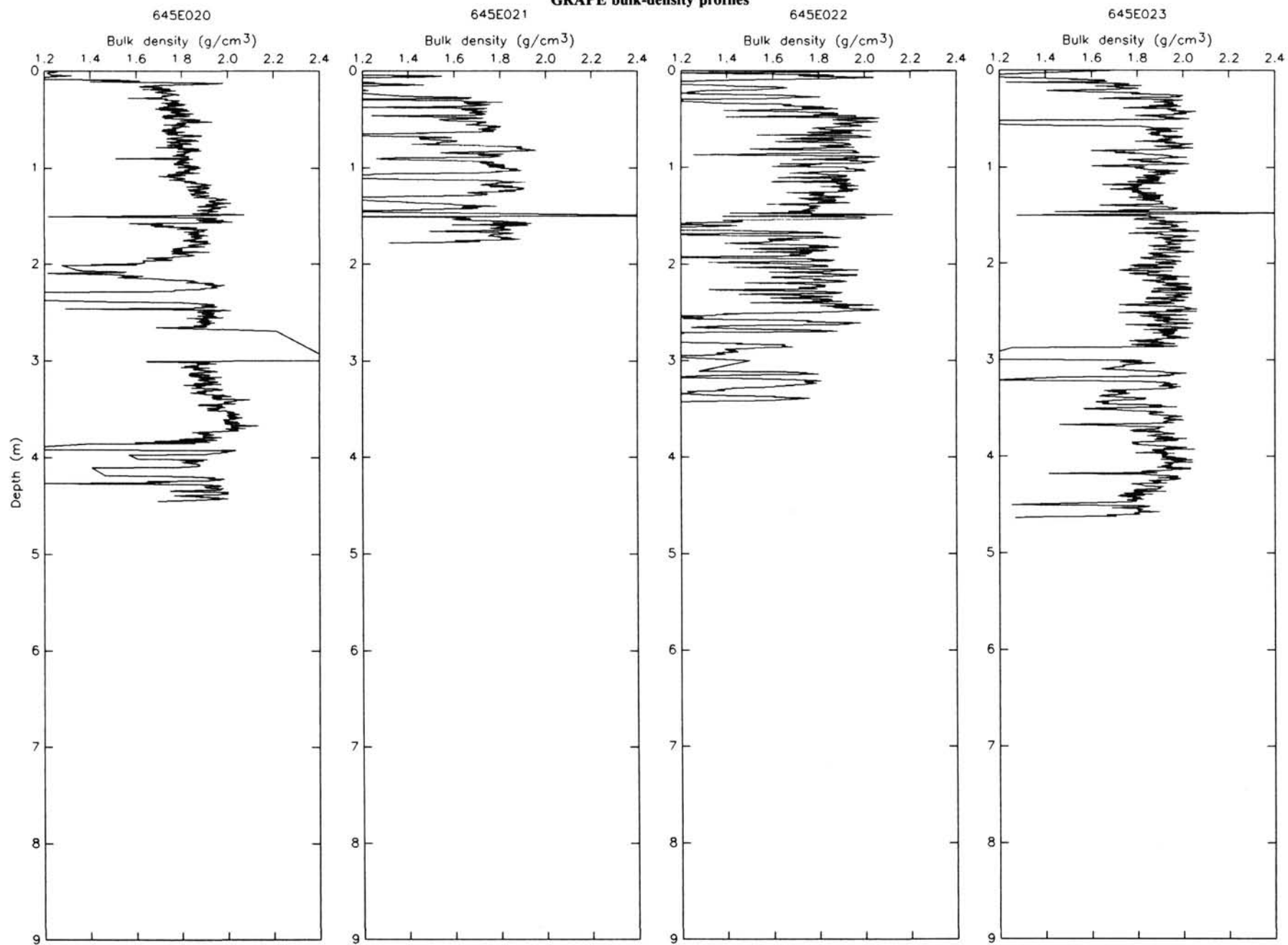
GRAPE bulk-density profiles



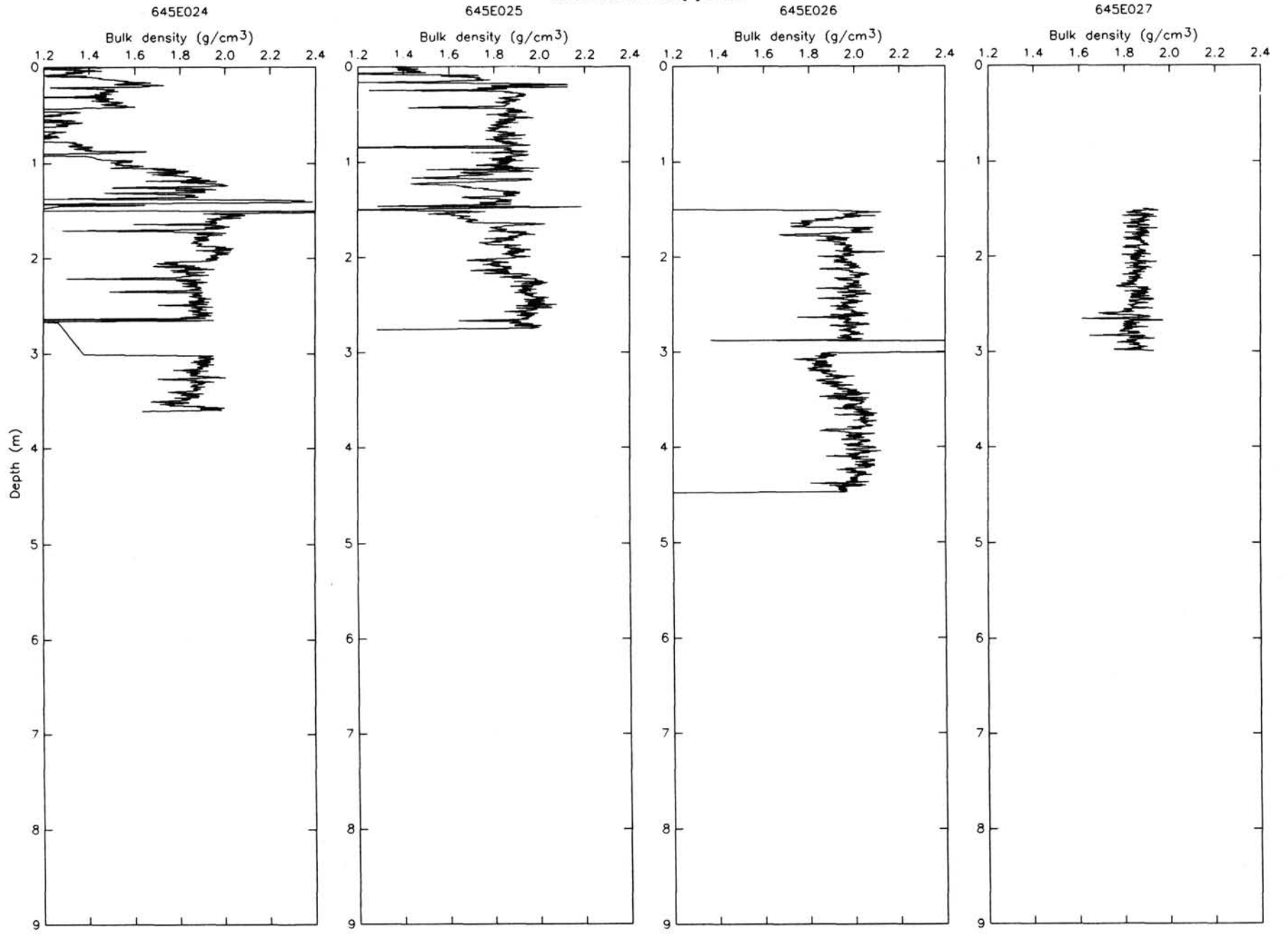
GRAPE bulk-density profiles



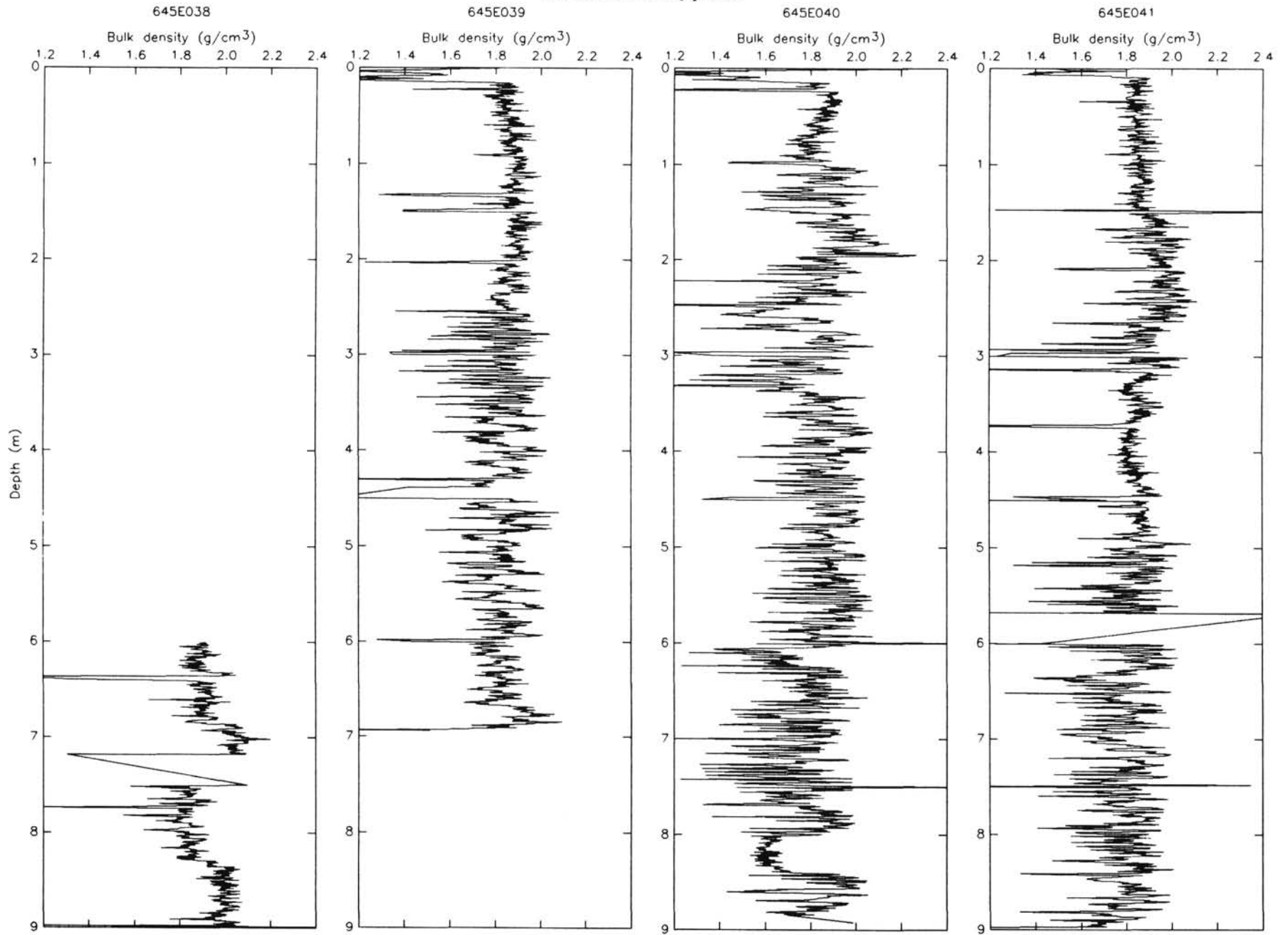
GRAPE bulk-density profiles



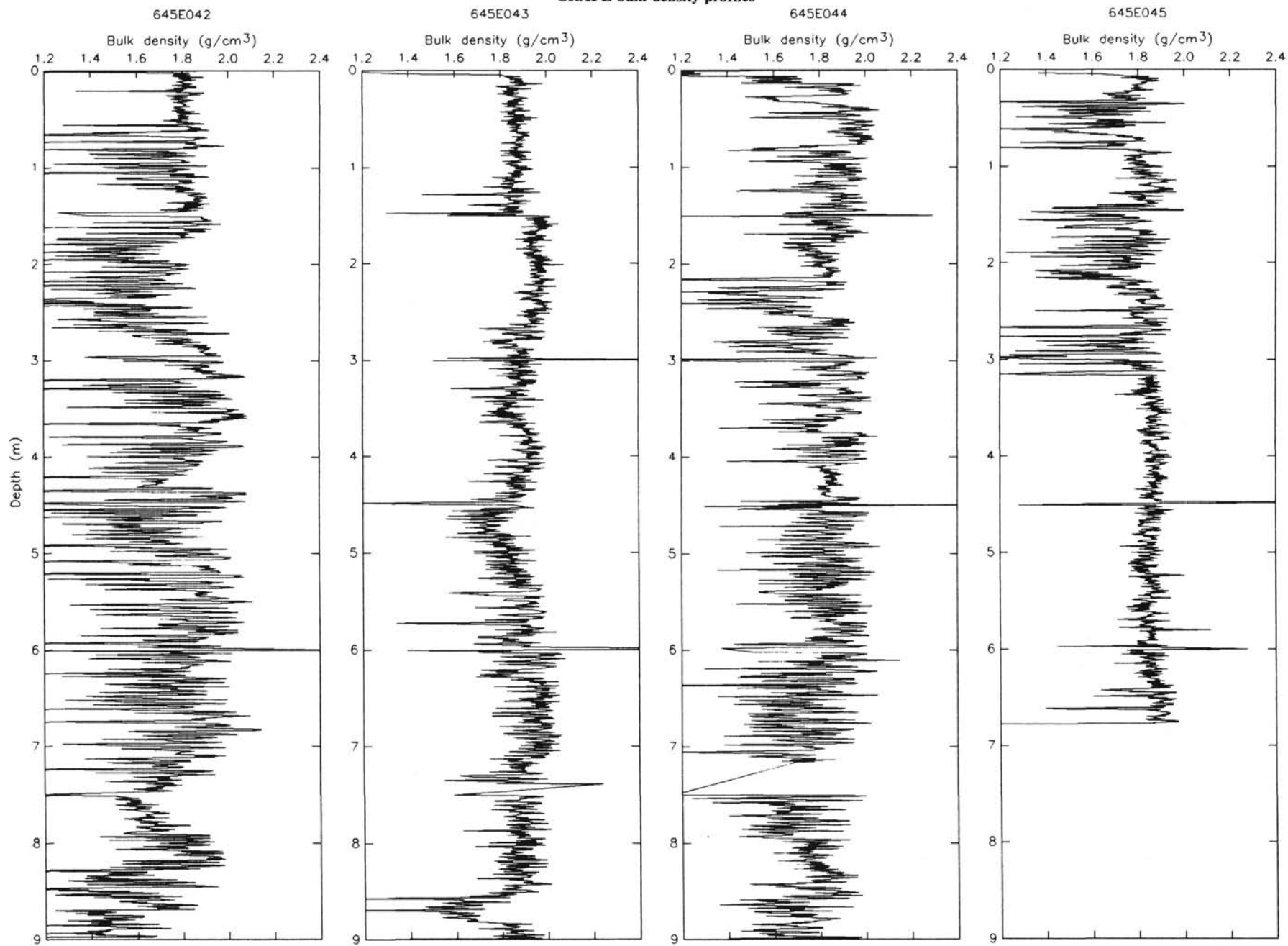
GRAPE bulk-density profiles



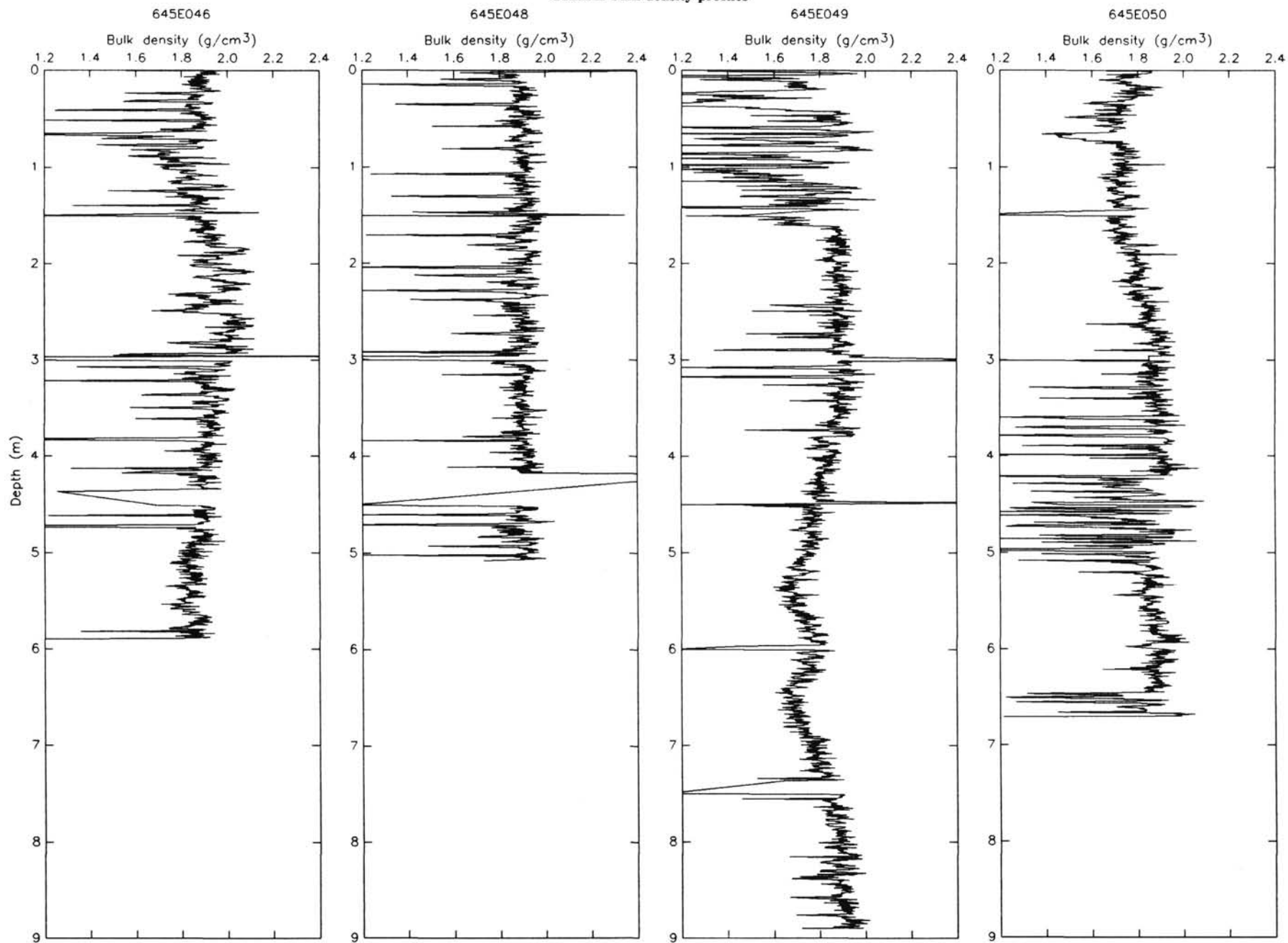
GRAPE bulk-density profiles



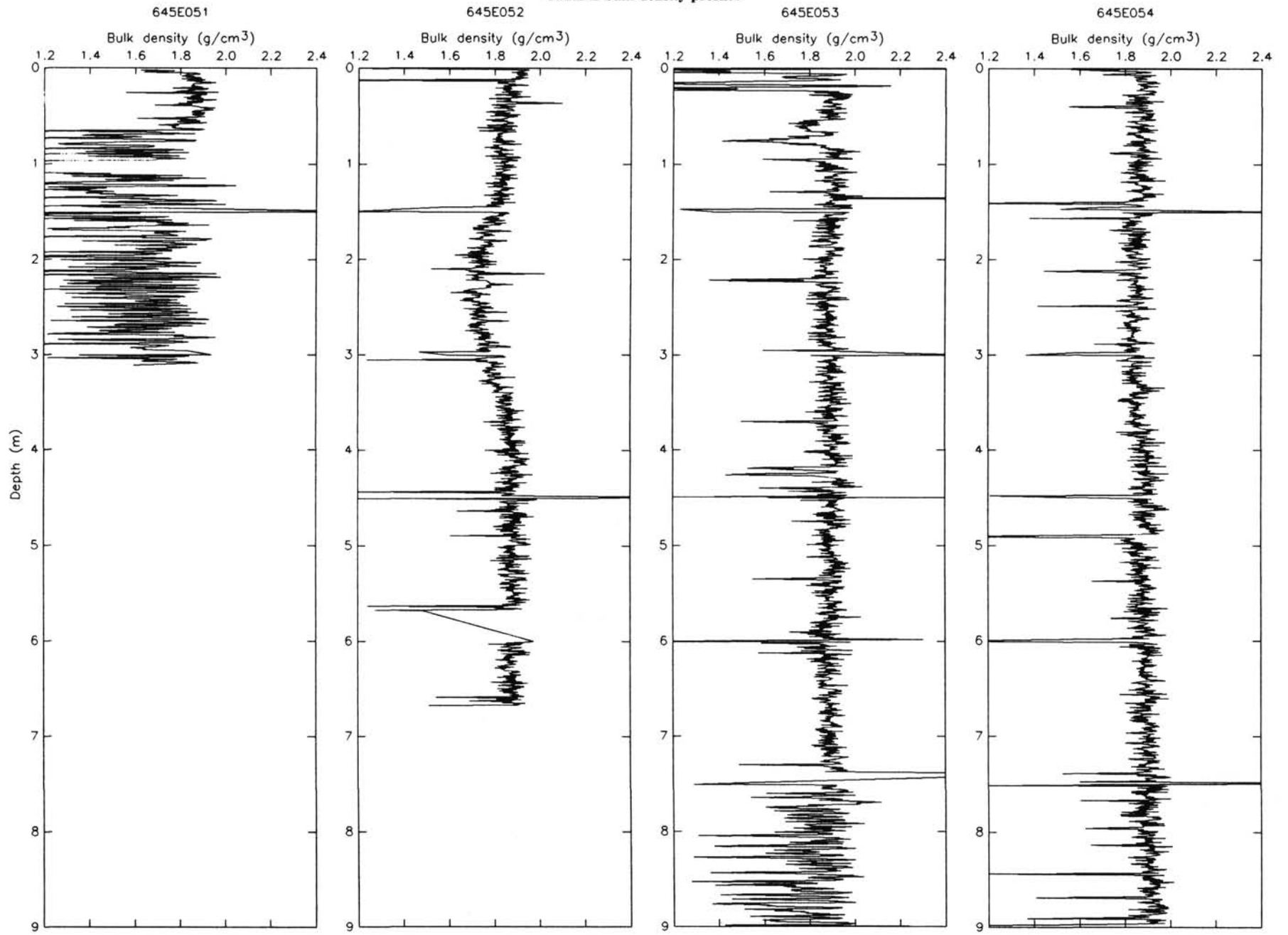
GRAPE bulk-density profiles



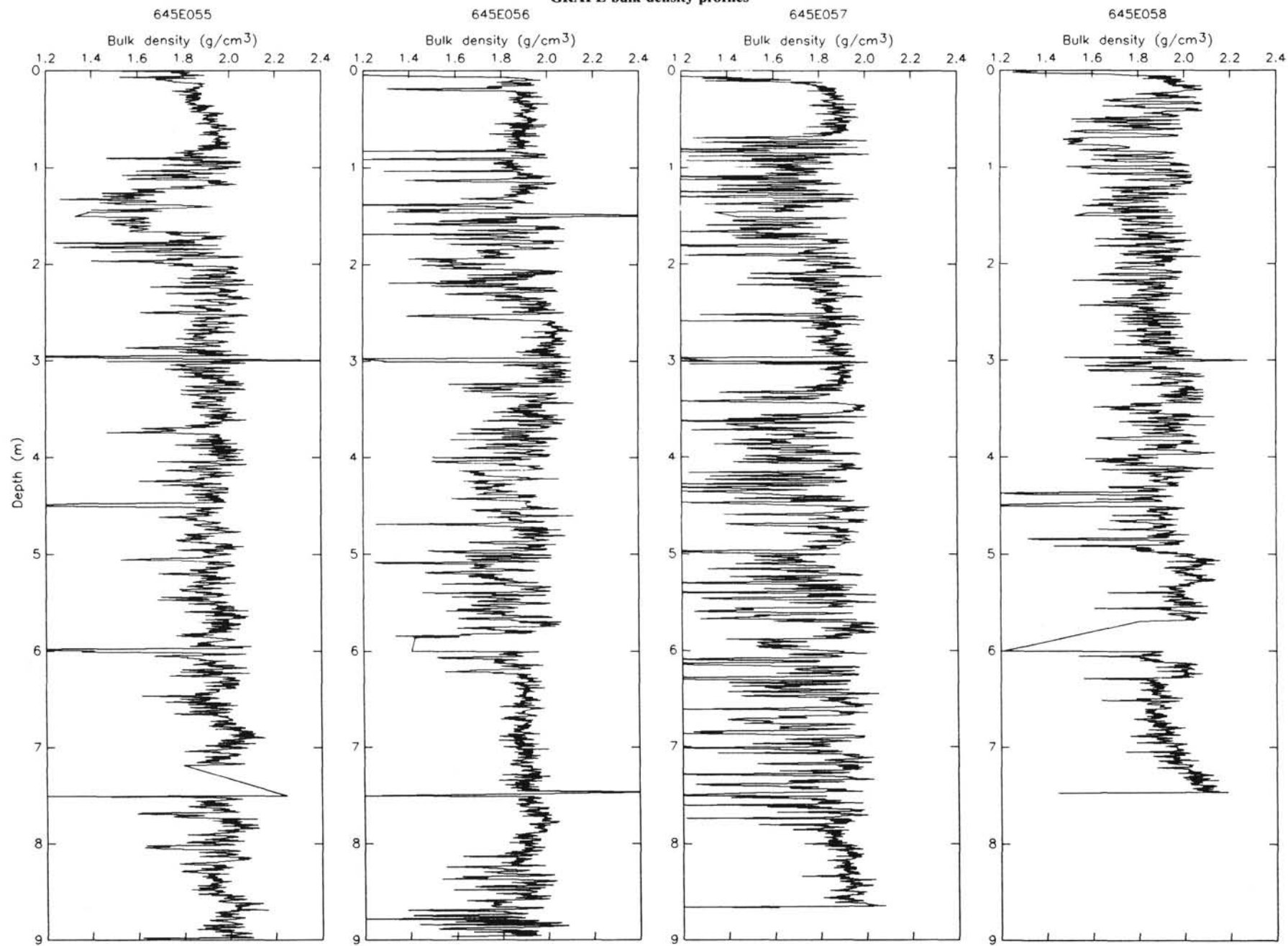
GRAPE bulk-density profiles



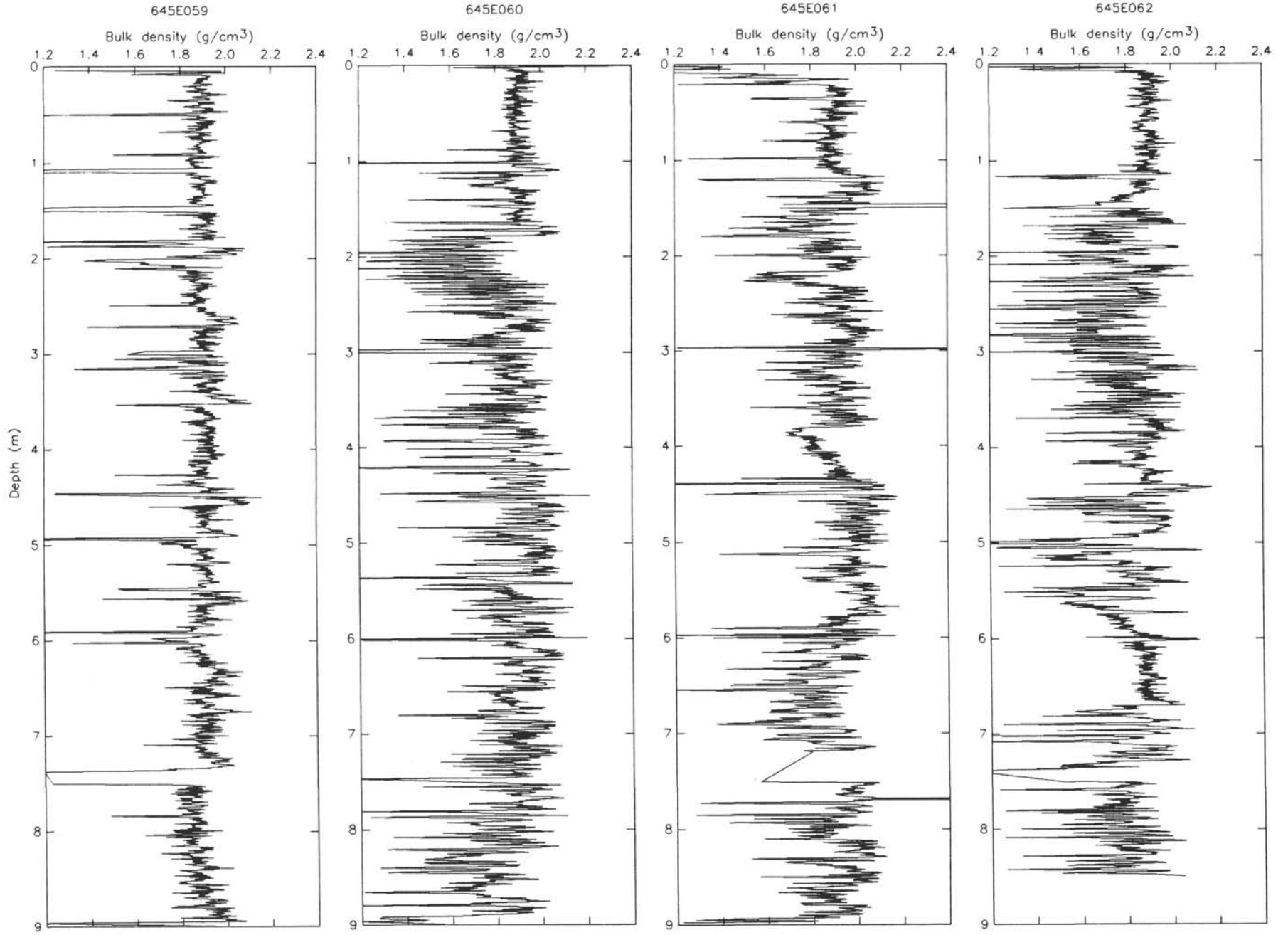
GRAPE bulk-density profiles



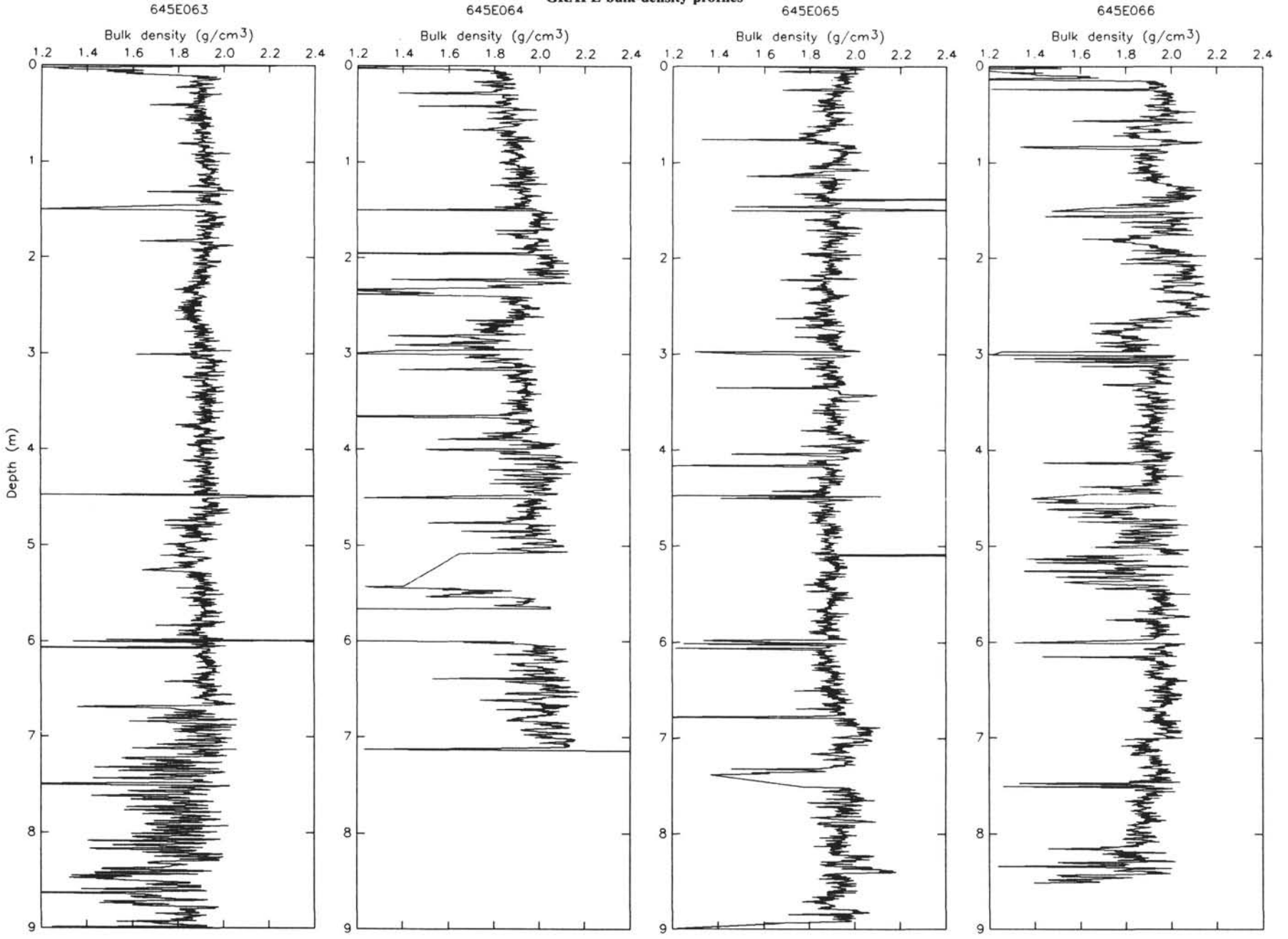
GRAPE bulk-density profiles



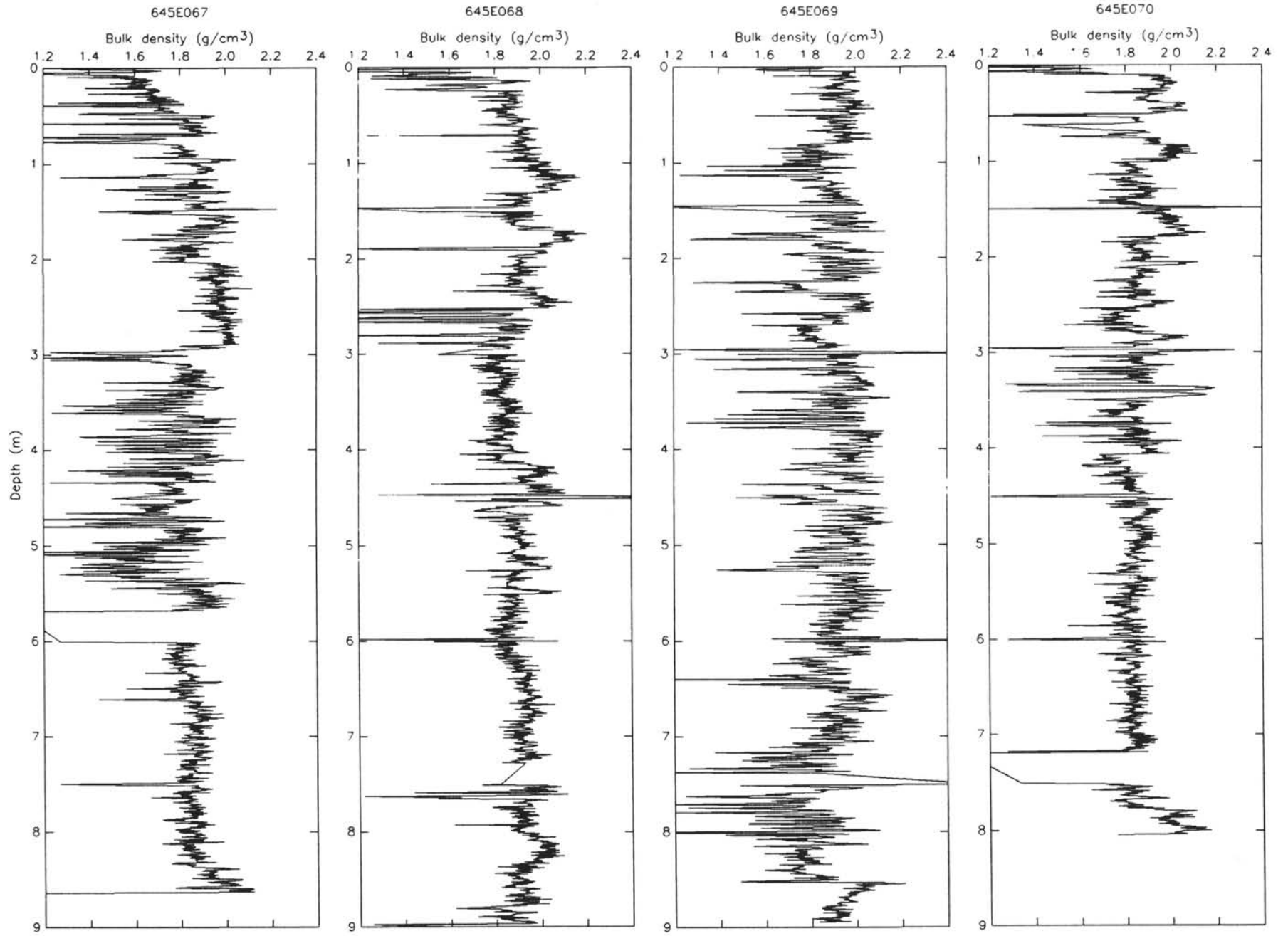
GRAPE bulk-density profiles



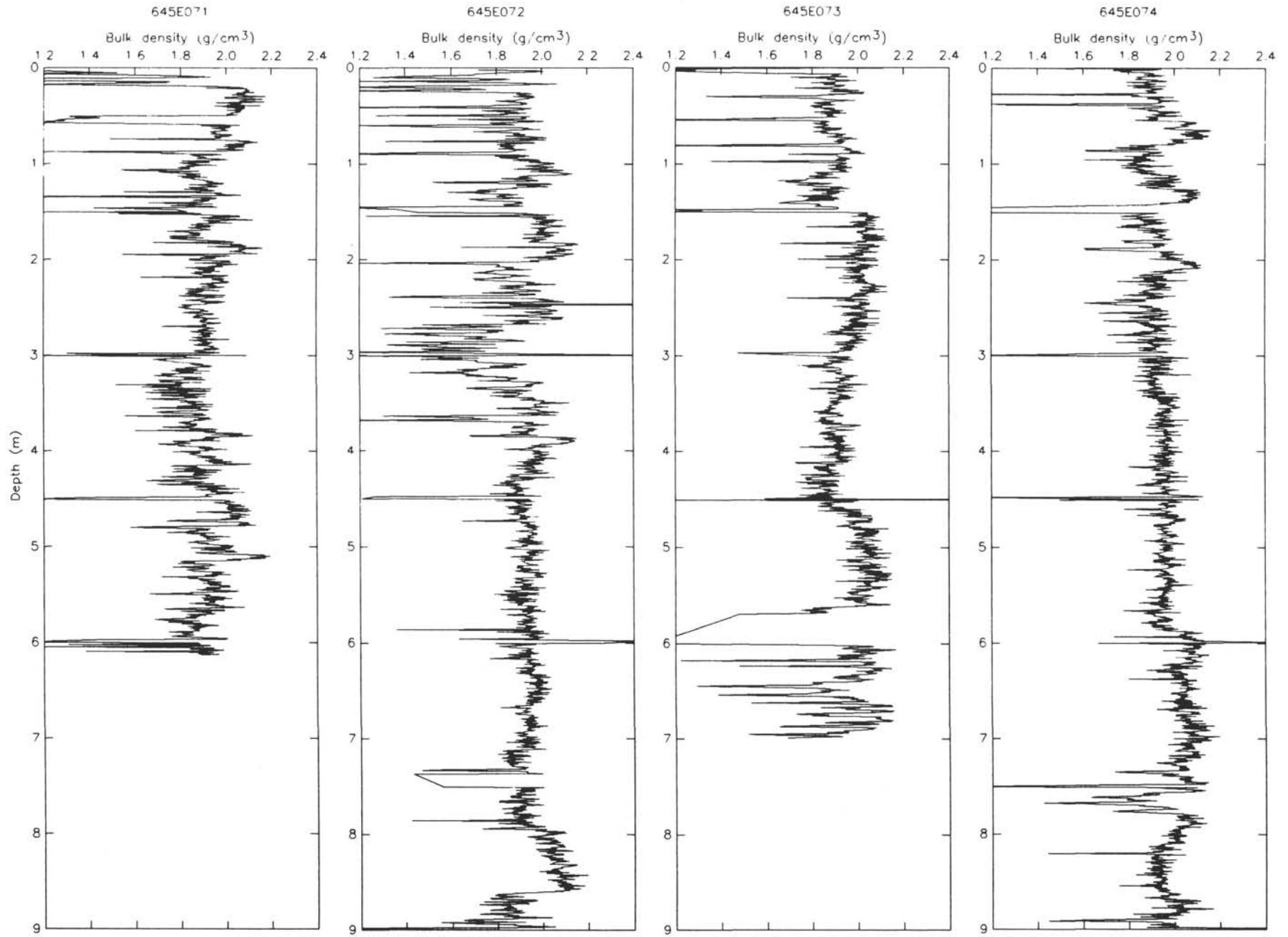
GRAPE bulk-density profiles



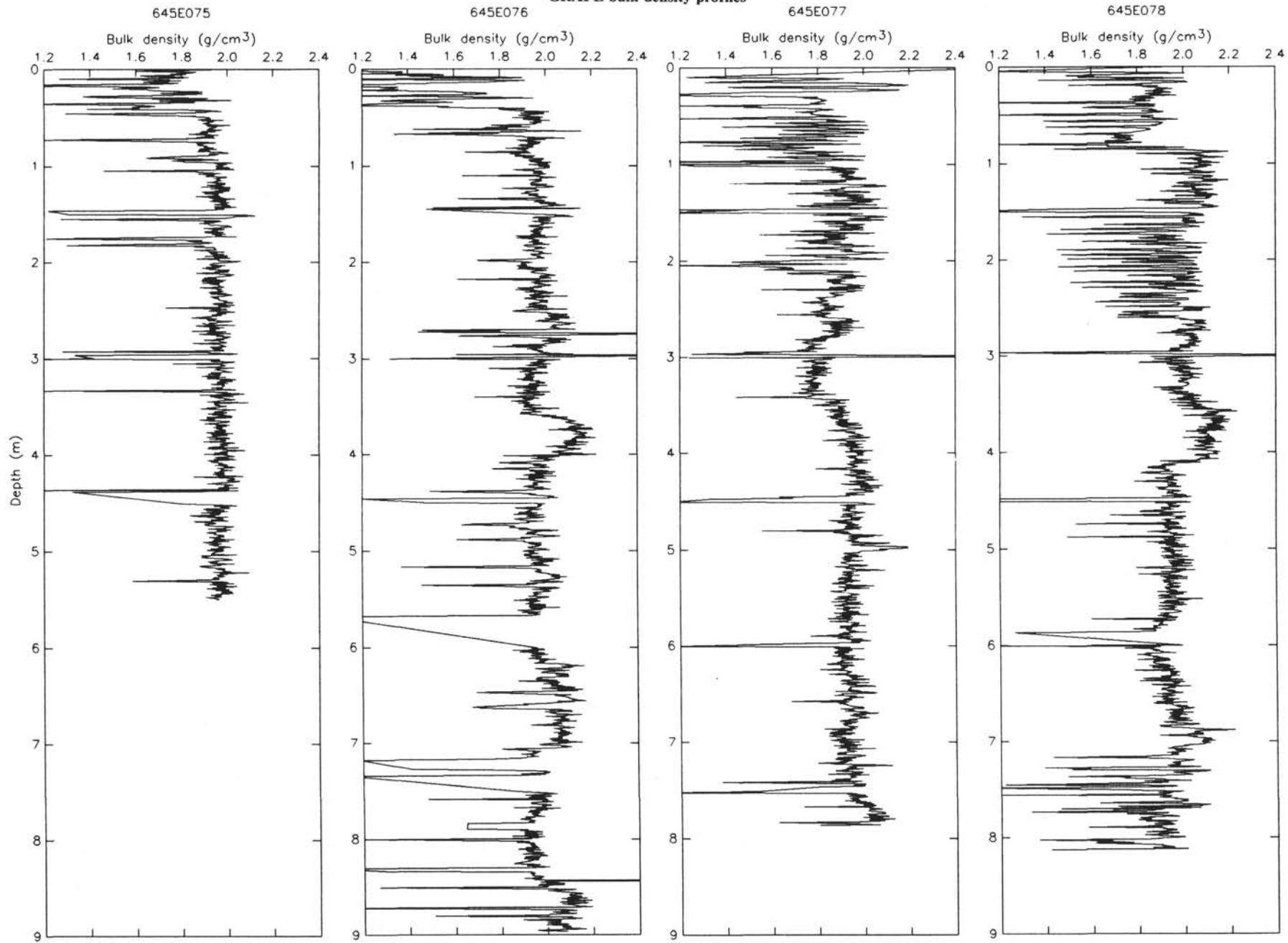
GRAPE bulk-density profiles



GRAPE bulk-density profiles



GRAPE bulk-density profiles



GRAPE bulk-density profiles

